

Purinergic pharmacology, volume II

Edited by

Francisco Ciruela
and Kenneth. A. Jacobson

Published in

Frontiers in Pharmacology



FRONTIERS EBOOK COPYRIGHT STATEMENT

The copyright in the text of individual articles in this ebook is the property of their respective authors or their respective institutions or funders. The copyright in graphics and images within each article may be subject to copyright of other parties. In both cases this is subject to a license granted to Frontiers.

The compilation of articles constituting this ebook is the property of Frontiers.

Each article within this ebook, and the ebook itself, are published under the most recent version of the Creative Commons CC-BY licence. The version current at the date of publication of this ebook is CC-BY 4.0. If the CC-BY licence is updated, the licence granted by Frontiers is automatically updated to the new version.

When exercising any right under the CC-BY licence, Frontiers must be attributed as the original publisher of the article or ebook, as applicable.

Authors have the responsibility of ensuring that any graphics or other materials which are the property of others may be included in the CC-BY licence, but this should be checked before relying on the CC-BY licence to reproduce those materials. Any copyright notices relating to those materials must be complied with.

Copyright and source acknowledgement notices may not be removed and must be displayed in any copy, derivative work or partial copy which includes the elements in question.

All copyright, and all rights therein, are protected by national and international copyright laws. The above represents a summary only. For further information please read Frontiers' Conditions for Website Use and Copyright Statement, and the applicable CC-BY licence.

ISSN 1664-8714
ISBN 978-2-8325-2575-3
DOI 10.3389/978-2-8325-2575-3

About Frontiers

Frontiers is more than just an open access publisher of scholarly articles: it is a pioneering approach to the world of academia, radically improving the way scholarly research is managed. The grand vision of Frontiers is a world where all people have an equal opportunity to seek, share and generate knowledge. Frontiers provides immediate and permanent online open access to all its publications, but this alone is not enough to realize our grand goals.

Frontiers journal series

The Frontiers journal series is a multi-tier and interdisciplinary set of open-access, online journals, promising a paradigm shift from the current review, selection and dissemination processes in academic publishing. All Frontiers journals are driven by researchers for researchers; therefore, they constitute a service to the scholarly community. At the same time, the *Frontiers journal series* operates on a revolutionary invention, the tiered publishing system, initially addressing specific communities of scholars, and gradually climbing up to broader public understanding, thus serving the interests of the lay society, too.

Dedication to quality

Each Frontiers article is a landmark of the highest quality, thanks to genuinely collaborative interactions between authors and review editors, who include some of the world's best academicians. Research must be certified by peers before entering a stream of knowledge that may eventually reach the public - and shape society; therefore, Frontiers only applies the most rigorous and unbiased reviews. Frontiers revolutionizes research publishing by freely delivering the most outstanding research, evaluated with no bias from both the academic and social point of view. By applying the most advanced information technologies, Frontiers is catapulting scholarly publishing into a new generation.

What are Frontiers Research Topics?

Frontiers Research Topics are very popular trademarks of the *Frontiers journals series*: they are collections of at least ten articles, all centered on a particular subject. With their unique mix of varied contributions from Original Research to Review Articles, Frontiers Research Topics unify the most influential researchers, the latest key findings and historical advances in a hot research area.

Find out more on how to host your own Frontiers Research Topic or contribute to one as an author by contacting the Frontiers editorial office: frontiersin.org/about/contact

Purinergic pharmacology, volume II

Topic editors

Francisco Ciruela — University of Barcelona, Spain

Kenneth. A. Jacobson — National Institutes of Health (NIH), United States

Citation

Ciruela, F., Jacobson, K. A., eds. (2023). *Purinergic pharmacology, volume II*.
Lausanne: Frontiers Media SA. doi: 10.3389/978-2-8325-2575-3

Table of contents

- 05 **Editorial: Purinergic pharmacology, Volume II**
Francisco Ciruela and Kenneth A. Jacobson
- 08 **Adenosine-A_{2A} Receptor Signaling Plays a Crucial Role in Sudden Unexpected Death in Epilepsy**
Hai-Ying Shen, Sadie B. Baer, Raey Gesese, John M. Cook, Landen Weltha, Shayla Q. Coffman, Jie Wu, Jiang-Fan Chen, Ming Gao and Teng Ji
- 21 **UTP Regulates the Cardioprotective Action of Transplanted Stem Cells Derived From Mouse Cardiac Adipose Tissue**
Esteban Diaz Villamil, Lucas De Roeck, Marion Vanorlé and Didier Communi
- 34 **Machine Learning for Discovery of New ADORA Modulators**
Ana C. Puhl, Zhan-Guo Gao, Kenneth A. Jacobson and Sean Ekins
- 43 **Alternative adenosine Receptor activation: The netrin-Adora2b link**
Xiaoyi Yuan, Tingting Mills, Marie-Francoise Doursout, Scott E. Evans, Marcos F. Vidal Melo and Holger K. Eltzschig
- 59 **ATP indirectly stimulates hippocampal CA1 and CA3 pyramidal neurons *via* the activation of neighboring P2X7 receptor-bearing astrocytes and NG2 glial cells, respectively**
Ying Zhang, Hai-Yan Yin, Patrizia Rubini, Peter Illes and Yong Tang
- 75 **Guanine inhibits the growth of human glioma and melanoma cell lines by interacting with GPR23**
Roberta Garozzo, Mariachiara Zuccarini, Patricia Giuliani, Valentina Di Liberto, Giuseppa Mudò, Francesco Caciagli, Renata Ciccarelli, Francisco Ciruela, Patrizia Di Iorio and Daniele F. Condorelli
- 90 **Update on the recent development of allosteric modulators for adenosine receptors and their therapeutic applications**
Silvia Pasquini, Chiara Contri, Martina Cappello, Pier Andrea Borea, Katia Varani and Fabrizio Vincenzi
- 101 **Effective targeting of microglial P2X7 following intracerebroventricular delivery of nanobodies and nanobody-encoding AAVs**
Carolina Pinto-Espinoza, Charlotte Guillou, Björn Rissiek, Maximilian Wilmes, Ehsan Javidi, Nicole Schwarz, Marten Junge, Friedrich Haag, Nastassia Liaukouskaya, Nicola Wanner, Annette Nicke, Catelijne Stortelers, Yossan-Var Tan, Sahil Adriouch, Tim Magnus and Friedrich Koch-Nolte
- 118 **Origin, distribution, and function of three frequent coding polymorphisms in the gene for the human P2X7 ion channel**
Waldemar Schäfer, Tobias Stähler, Carolina Pinto Espinoza, Welbeck Danquah, Jan Hendrik Knop, Björn Rissiek, Friedrich Haag and Friedrich Koch-Nolte

- 131 **Loss-of-function N178T variant of the human P2Y₄ receptor is associated with decreased severity of coronary artery disease and improved glucose homeostasis**
Michael Horckmans, Esteban Díaz Villamil, Céline Verdier, Henrik Laurell, Jean-Bernard Ruidavets, Lucas De Roeck, Guillaume Combes, Laurent O. Martinez and Didier Communi
- 143 **Identification of a novel P2X7 antagonist using structure-based virtual screening**
Gaia Pasqualetto, Marika Zuanon, Andrea Brancale and Mark T. Young
- 160 **Nanomolar clodronate induces adenosine accumulation in the perfused rat mesenteric bed and mesentery-derived endothelial cells**
M. Verónica Donoso, Felipe Hernández, Rafael Barra and J. Pablo Huidobro-Toro
- 176 **Identification of the molecular determinants of antagonist potency in the allosteric binding pocket of human P2X4**
Gaia Pasqualetto, Marika Zuanon, Andrea Brancale and Mark T. Young



OPEN ACCESS

EDITED BY

Filippo Drago,
University of Catania, Italy

REVIEWED BY

Peter Illes,
Leipzig University, Germany
Samuel J. Fountain,
University of East Anglia, United Kingdom
Vera Ralevic,
University of Nottingham,
United Kingdom

*CORRESPONDENCE

Francisco Ciruela,
✉ fciruela@ub.edu

RECEIVED 04 April 2023

ACCEPTED 09 May 2023

PUBLISHED 16 May 2023

CITATION

Ciruela F and Jacobson KA (2023),
Editorial: Purinergic pharmacology,
Volume II.
Front. Pharmacol. 14:1200187.
doi: 10.3389/fphar.2023.1200187

COPYRIGHT

© 2023 Ciruela and Jacobson. This is an open-access article distributed under the terms of the [Creative Commons Attribution License \(CC BY\)](#). The use, distribution or reproduction in other forums is permitted, provided the original author(s) and the copyright owner(s) are credited and that the original publication in this journal is cited, in accordance with accepted academic practice. No use, distribution or reproduction is permitted which does not comply with these terms.

Editorial: Purinergic pharmacology, Volume II

Francisco Ciruela^{1,2*} and Kenneth A. Jacobson³

¹Pharmacology Unit, Department of Pathology and Experimental Therapeutics, School of Medicine and Health Sciences, Institute of Neurosciences, University of Barcelona, Llobregat, Spain,

²Neuropharmacology and Pain Group, Neuroscience Program, Bellvitge Biomedical Research Institute, Llobregat, Spain, ³Molecular Recognition Section, Laboratory of Bioorganic Chemistry, National Institute of Diabetes and Digestive and Kidney Diseases, National Institutes of Health, Bethesda, MD, United States

KEYWORDS

ATP, G protein-coupled purinergic receptors, adenosine, purinergic signalling, adenosine transport, purinergic pathophysiology, ligand-gated ion channels, guanosine

Editorial on the Research Topic Purinergic pharmacology, Volume II

Extracellular purine nucleotides and nucleosides serve as crucial signalling molecules, acting as neurotransmitters and neuromodulators. Tightly regulated extracellular levels of adenosine 5'-triphosphate (ATP) and adenosine, which are controlled by various enzymes and transporters, activate a variety of purinergic receptors. These receptors, which appear early in evolution, are among the most abundant receptors in living organisms and regulate numerous physiological processes, making them attractive therapeutic targets for a wide range of diseases. While P1 (adenosine) receptors are selective for adenosine, the breakdown product of ATP, P2 receptors respond to purine and pyrimidine nucleotides. Importantly, purinergic receptors, including both G protein-coupled receptors (ARs and P2YRs) and ligand-gated ion channel receptors (P2XRs), are involved in a multitude of neuronal and non-neuronal mechanisms, such as pain, immune responses, exocrine and endocrine secretion, platelet aggregation, endothelium-mediated vasodilatation, and inflammation. However, since purinergic receptors are widely distributed throughout the body, it is challenging to develop drugs that selectively target specific receptor subtypes without causing unwanted side effects. Additionally, extracellular levels of purines and pyrimidines can also vary greatly, leading to the simultaneous activation of different purinergic receptors in response to oscillating concentrations of endogenous purines. Consequently, through these different subtypes of P1 and P2 receptors, cells integrate extracellular purine responses, harmonising short- and long-term purinergic signalling. Therefore, the selectivity of drugs is a crucial goal in the field of purinergic pharmacology. For decades, medicinal chemists have been developing potent and selective synthetic agonists and antagonists for purinergic receptors, as well as allosteric modulators that allow for event-responsive and temporally specific manipulation of the endogenous purinergic system. Additionally, modulation of the metabolism and uptake of extracellular purine nucleotides and nucleosides can also regulate purinergic processes. Overall, the field of purinergic pharmacology is rapidly expanding and presents exciting opportunities for pharmacotherapeutic development.

In this Research Topic that follows an earlier volume on the same Research Topic (Ciruela and Jacobson), an overview of purinergic pharmacology is provided through 13 articles written by 82 authors. This comprehensive compilation contains 1 minireview, 1 review, 1 brief research report, and 10 original research articles. The

minireview provides an update on the recent development of allosteric modulators for adenosine receptors and their therapeutic applications (Pasquini et al.). The authors highlight that allosteric modulators of ARs may evolve into valuable pharmacological tools that can overcome the limitations of orthosteric ligands. Thus, while several allosteric modulators have been identified for A₁R and A₃R, with some promising results in preclinical settings, the discovery of allosteric modulators for A₂R and A_{2B}R has been less successful, although current findings are still encouraging. Despite the promising results, no AR allosteric modulator has yet advanced to clinical trials, highlighting the considerable challenges involved in the discovery and development of this class of compounds. Adenosine signalling is known to be upregulated during periods of restricted oxygen availability, such as those experienced during ischemic events or inflammatory conditions. Yuan et al. elegantly review the molecular connection between netrin-1 and A_{2B}R and summarise relevant research on their interaction within the context of tissue inflammation (Yuan et al.). It is suggested that netrin-1 may serve as an endogenous anti-inflammatory agent during organ injury by enhancing the adenosine-A_{2B}R axis, which has anti-inflammatory properties.

The Research Topic contains a series of original research articles covering important aspects of purinergic pharmacology. A brief research report article shows the use of machine learning models to find ligands for the different AR subtypes (Puhl et al.). The authors have made an interesting discovery by identifying three new modulators for ARs (crisaborole, febusostat, and paroxetine) that are structurally different from previously known compounds targeting ARs. These medications, in some cases suggesting noncanonical interaction with ARs, could potentially be repurposed for adenosine-related diseases. Five articles revolve around P2XR, with particular attention paid to P2X₇R. These articles explore various aspects such as structural studies, analysis of frequent coding polymorphisms, and physiological evaluations, indicating the considerable interest in P2X₇R. Molecular determinants of antagonist potency in the allosteric binding pocket of human P2X₄R were identified (Pasqualeto et al.). Therefore, through a combination of molecular docking, mutagenesis, and functional assay, they demonstrate the likely binding pocket for the allosteric antagonist BX430, a potent allosteric P2X₄R receptor antagonist, to human P2X₄R. Interestingly, the importance of the amino acid residue Ile312 for the receptor sensitivity to BX430 is confirmed. These findings have immense potential to aid in the design and development of potent allosteric P2X₄R antagonists. In an associated article, the same group identified a novel P2X₇R antagonist using structure-based virtual screening (Pasqualeto et al.). This study conducted virtual screening using a molecular model of human P2X₄R based on the crystal structure of *Danio rerio* P2X₄R. From a library of 300,000 drug-like compounds, none of these compounds displayed a significant antagonist effect in P2X₄R. However, when the same set of compounds was tested against human P2X₇, one compound (GP-25) showed partial antagonistic activity. Next, in a separate article on the Research Topic, effective antagonism of microglial P2X₇R is accomplished using nanobodies and nanobody-encoding adeno-associated

virus (Pinto-Espinoza et al.). The results obtained in this study offer novel and in-depth information on optimal conditions, including route, dose, and administration time, for effective nanobody-mediated receptor targeting of microglia. Thus, the potential of nanobodies as a promising new therapeutic strategy for the treatment of sterile brain inflammation is highlighted. The existence of P2X₇R in CNS neurones is a matter of ongoing debate. While some argue that only non-neuronal cells bear this receptor type and indirectly signal to neighbouring neurons, others propose that CNS neurons themselves possess these receptors. Additional aspects of this hypothesis are explored (Zhang et al.). Using genetic deletion of P2X₇R specifically in astrocytes, oligodendrocytes, and microglia, and then recording current responses in neurons to 2'-(3')-O-(4-benzoylbenzoyl)-ATP (Bz-ATP), a P2X₇R agonist, the authors demonstrate that pyramidal neurons of mouse CA1 and CA3 did not possess P2X₇R, but were indirectly modulated by astrocytic and oligodendrocytic P2X₇R, respectively. Finally, the origin, distribution, and function of three frequent coding polymorphisms in the gene for the human P2X₇R ion channel were evaluated (Schäfer et al.). The human P2RX₇R gene has multiple single nucleotide polymorphisms (SNPs) but unlike other P2XR family members, non-synonymous SNPs in P2X₇R are prevalent. Three of these SNPs have a frequency of more than 25% and impact the extracellular head domain of P2X₇R (155 Y/H), the lower body (270 R/H), and the tail in the second transmembrane domain (348 T/A). The authors contribute to a deeper understanding of how the structure of P2X₇R influences receptor function and highlight the importance of incorporating P2X₇R variants into the design of clinical trials targeting this receptor.

There are eight known subtypes of P2YR, each of which has a different ligand specificity and signalling pathway. The potential role of P2Y₂R in the cardioprotective effects of transplanted undifferentiated cardiac adipose derived stem cells (cADSC) was examined in a mouse model of myocardial infarction (Diaz Villamil et al.). Their findings suggest that P2Y₂R serves as a crucial regulator of the therapeutic use of undifferentiated cADSC for the treatment of cardiac ischemia. This new insight could help optimise the development of cardiac repair cell therapies, potentially improving patient outcomes. In a separate article, the potential association between P2Y₄R mutations and the severity of coronary artery disease (CAD) is studied in a population study involving 50 patients diagnosed with (CAD) and 50 age-matched control individuals (Horckmans et al.). Accordingly, the authors focus on a polymorphism in the coding region (rs3745601) that results in the replacement of asparagine at residue 178 with threonine (N178T) located in the P2Y₄R second extracellular loop. The N178T variant represents a loss-of-function of the receptor that is associated with less severe coronary artery atherosclerosis and lower fasting plasma glucose in coronary patients.

Another article investigated the impact of bisphosphonate clodronate, which has been suggested to act as a potent vesicular nucleotide transporter (VNUT) blocker *in vitro*, on the spontaneous and/or electrically evoked release of ATP/metabolites and noradrenaline from the perivascular nerve terminals in the mesentery sympathetic nervous system

(Donoso et al.). Surprisingly, the authors demonstrate that clodronate inhibits adenosine deaminase activity in isolated endothelial cells as in a crude extract preparation, a finding that may explain the accumulation of adenosine after clodronate mesentery perfusion. Subsequently, the role of $A_{2A}R$ signalling in sudden unexpected death in epilepsy (SUDEP) is evaluated (Shen et al.). The article introduces a novel animal model of SUDEP using a combined paradigm of intrahippocampal and intraperitoneal administration of kainic acid (KA) in mice with genetically modified adenosine kinase (ADK) knockdown ($Adk^{+/-}$), which exhibit reduced ADK in the brain. Through this model, the authors identified a critical role for $A_{2A}R$ in the nucleus tractus solitarius in the pathophysiology of SUDEP, highlighting $A_{2A}R$ as a potential therapeutic target to prevent the risk of SUDEP. Guanine-based purines (GBPs) exert numerous biological effects in the central nervous system through putative membrane receptors, the existence of which is still elusive. To shed light on this question, Garozzo et al. conducted a screening of orphan and poorly characterized G protein-coupled receptors (GPRs) expressed in glioma cells, where GBPs showed an antiproliferative effect. Among the GPRs tested, GPR23, also known as the lysophosphatidic acid 4 receptor, was found to counteract the growth inhibition caused by GBPs in U87 cells (Garozzo et al.). These data indicate the involvement of GPR23 in modulating guanine responses in tumour cell lines.

In general, this Research Topic explores in detail the wide-ranging physiological functions of purines and the underlying structural and mechanistic basis of purinergic signalling. It holds significant promise for the development of innovative therapies for both chronic and acute diseases, while posing a challenge to achieving drug selectivity. The potential to translate basic purinergic knowledge into clinical opportunities is enormous, and further exploration of this field could lead to exciting breakthroughs in pharmacotherapy.

Author contributions

All authors listed have made a substantial, direct, and intellectual contribution to the work and approved it for publication.

Acknowledgments

We would like to thank all authors for their highly valuable contribution. Also, we would like to acknowledge the work of reviewers whose constructive input contributed to improving the quality of the articles. Finally, we would like to acknowledge the support of FEDER/Ministerio de Ciencia, Innovación y Universidades-Agencia Estatal de Investigación (PID2020-118511RB-I00), the Catalan government (2021 SGR 00698) to FC and NIDDK Intramural Research Program (ZIADK031117) to KJ. We thank Centres de Recerca de Catalunya (CERCA) Programme/Generalitat de Catalunya for IDIBELL institutional support and Maria de Maeztu MDM-2017-0729 to Institut de Neurociències, Universitat de Barcelona.

Conflict of interest

The authors declare that the research was conducted in the absence of any commercial or financial relationships that could be construed as a potential conflict of interest.

Publisher's note

All claims expressed in this article are solely those of the authors and do not necessarily represent those of their affiliated organizations, or those of the publisher, the editors and the reviewers. Any product that may be evaluated in this article, or claim that may be made by its manufacturer, is not guaranteed or endorsed by the publisher.



Adenosine-A_{2A} Receptor Signaling Plays a Crucial Role in Sudden Unexpected Death in Epilepsy

Hai-Ying Shen^{1*}, Sadie B. Baer¹, Raey Gesese¹, John M. Cook¹, Landen Weltha¹, Shayla Q. Coffman¹, Jie Wu², Jiang-Fan Chen³, Ming Gao² and Teng Ji⁴

¹Department of Neuroscience, Legacy Research Institute, Portland, OR, United States, ²Department of Neurobiology, Barrow Neurological Institute, St. Joseph's Hospital and Medical Center, Phoenix, AZ, United States, ³Molecular Neuropharmacology Laboratory, School of Optometry and Ophthalmology and Eye Hospital, Wenzhou Medical University, Wenzhou, China, ⁴Department of Pediatric Neurology, Randall Children's Hospital, Legacy Emanuel Medical Center, Portland, OR, United States

OPEN ACCESS

Edited by:

Francisco Ciruela,
University of Barcelona, Spain

Reviewed by:

Rodrigo A. Cunha,
University of Coimbra, Portugal
Anna Maria Pugliese,
University of Florence, Italy

*Correspondence:

Hai-Ying Shen
hshen@downneurobiology.org

Specialty section:

This article was submitted to
Experimental Pharmacology and Drug
Discovery,
a section of the journal
Frontiers in Pharmacology

Received: 01 April 2022

Accepted: 16 May 2022

Published: 09 June 2022

Citation:

Shen H-Y, Baer SB, Gesese R,
Cook JM, Weltha L, Coffman SQ,
Wu J, Chen J-F, Gao M and Ji T (2022)
Adenosine-A_{2A} Receptor Signaling
Plays a Crucial Role in Sudden
Unexpected Death in Epilepsy.
Front. Pharmacol. 13:910535.
doi: 10.3389/fphar.2022.910535

Adenosinergic activities are suggested to participate in SUDEP pathophysiology; this study aimed to evaluate the adenosine hypothesis of SUDEP and specifically the role of adenosine A_{2A} receptor (A_{2A}R) in the development of a SUDEP mouse model with relevant clinical features. Using a combined paradigm of intrahippocampal and intraperitoneal administration of kainic acid (KA), we developed a boosted-KA model of SUDEP in genetically modified adenosine kinase (ADK) knockdown (Adk^{+/-}) mice, which has reduced ADK in the brain. Seizure activity was monitored using video-EEG methods, and *in vivo* recording of local field potential (LFP) was used to evaluate neuronal activity within the nucleus tractus solitarius (NTS). Our boosted-KA model of SUDEP was characterized by a delayed, postictal sudden death in epileptic mice. We demonstrated a higher incidence of SUDEP in Adk^{+/-} mice (34.8%) vs. WT (8.0%), and the ADK inhibitor, 5-Iodotubercidin, further increased SUDEP in Adk^{+/-} mice (46.7%). We revealed that the NTS level of ADK was significantly increased in epileptic WT, but not in epileptic Adk^{+/-} mutants, while the A_{2A}R level in NTS was increased in epileptic (WT and Adk^{+/-}) mice vs. non-epileptic controls. The A_{2A}R antagonist, SCH58261, significantly reduced SUDEP events in Adk^{+/-} mice. LFP data showed that SCH58261 partially restored KA injection-induced suppression of gamma oscillation in the NTS of epileptic WT mice, whereas SCH58261 increased theta and beta oscillations in Adk^{+/-} mutants after KA injection, albeit with no change in gamma oscillations. These LFP findings suggest that SCH58261 and KA induced changes in local neuronal activities in the NTS of epileptic mice. We revealed a crucial role for NTS A_{2A}R in SUDEP pathophysiology suggesting A_{2A}R as a potential therapeutic target for SUDEP risk prevention.

Keywords: adenosine A_{2A} receptor, NTS, nucleus tractus solitarius, brainstem, SUDEP (sudden unexplained death in epilepsy), local field potential, adenosine kinase

INTRODUCTION

SUDEP is the leading cause of death in individuals with epilepsy, and as yet, no pharmacological intervention is available (Surges et al., 2009; Devinsky et al., 2016; Maguire et al., 2016). Although the mechanisms underlying SUDEP remain elusive, brainstem-related central apnea and cardiac arrest are considered two characteristic hallmarks (Stöllberger and Finsterer, 2004; Hirsch, 2010; Shorvon

and Tomson, 2011). Animal models of SUDEP currently remain limited (Devinsky et al., 2016; Pansani et al., 2016; Li and Buchanan, 2019) in representing key features of clinical SUDEP cases, (i.e., the chronic nature of epilepsy and the preceding convulsive seizures), which in turn, impedes efforts in investigating SUDEP mechanisms.

The adenosinergic system has been proposed as one of the potential mechanisms for the pathophysiological development of SUDEP (Shen et al., 2010; Massey et al., 2014; Devinsky et al., 2016; Faingold et al., 2016; Kommajosyula et al., 2016; Ashraf et al., 2021). Findings from animal studies and clinical evidence also suggest a complexity of adenosinergic adaptations in epilepsy and SUDEP, including changes in adenosine metabolism and adenosine receptors (ARs). For instance, adenosine A_1 and A_{2A} receptors (A_1 R and A_{2A} R) are identified to express on synapses in limbic cortical areas (Tetzlaff et al., 1987; Rebola et al., 2003a; Rebola et al., 2005a; Rebola et al., 2005b); an increased A_{2A} R density and a decreased A_1 R density are shown at excitatory terminals of different limbic areas from animal models of epilepsy and patients with epilepsy (Rebola et al., 2003b; Rebola et al., 2005c; He et al., 2020). The disrupted adenosinergic system, e.g., altered densities of A_1 R, A_{2A} R, and the adenosine metabolic enzyme, adenosine kinase (ADK) were also seen in different brain areas in patients with temporal lobe epilepsy (TLE) and correlated to SUDEP risk (Patodia et al., 2020). Thus, further characterization of brain area-dependent changes is warranted to reveal the complexity of adenosine and A_{2A} R-mediated regulation actions in SUDEP. During seizure events, adenosine is increased by tremendous consumption of ATP, and sequentially, increased adenosine alters neurotransmission in the brain and acts as a potent endogenous anticonvulsant to terminate seizures (During and Spencer, 1992; Dunwiddie and Masino, 2001). This anticonvulsive effect is mainly due to A_1 Rs-mediated inhibition of excitatory neurotransmissions (Dunwiddie and Masino, 2001). However, seizure-induced increases of extracellular adenosine can also broadly affect brain regions outside the primary seizure origins to exert a wide spectrum of actions through dominantly distributed A_1 Rs in the hippocampus, cerebral cortex, and cerebellum and enriched A_{2A} Rs in the striatum, nucleus accumbens, and brainstem (Fredholm et al., 2001; Sebastião and Ribeiro, 2009). Indeed, adenosine actions in the brainstem contribute to the central regulation of cardiorespiratory functions (Barraco and Janusz, 1989; Phillis et al., 1997) that are proposed to play a crucial role in SUDEP events (Hirsch, 2010; Massey et al., 2014; Devinsky et al., 2016). Since NTS is a critical hub for cardiorespiratory regulation, manipulation of A_{2A} Rs and A_1 Rs in the NTS affects cardiac and respiratory functions (Minic et al., 2015). Specifically, activation of A_{2A} Rs can alter GABAergic neuron activity (Wilson et al., 2004; Minic et al., 2015) and overactivation of A_{2A} R was associated with increased mortality in mice with febrile seizures (Fukuda et al., 2012). These findings indicate an important role of A_{2A} Rs and the brainstem in SUDEP pathophysiology.

The metabolic clearance of extracellular adenosine is important for limiting the activation of adenosine receptors and seizure-related death. Clinical studies showed upregulated

ADK densities in the brains of TLE patients (Aronica et al., 2011). We previously demonstrated that inhibition of ADK led to increased sudden deaths in mice with acute seizures (Shen et al., 2010), indicating that adenosine removal is essential for the brain to respond to the seizure-induced adenosine surge in the seizing brain to maintain balanced adenosinergic activities, i.e., as an endogenous anticonvulsant affecting seizure risk. Of note, seizure-induced increases of extracellular adenosine were reported in patients with intractable epilepsy (During and Spencer, 1992), and importantly, patients with uncontrolled or refractory seizures are associated with a high risk of SUDEP (Sperling, 2001; Devinsky et al., 2016).

Taken together, we hypothesized that in the brainstem chronic seizure-induced adenosine surges, in combination with abnormal metabolic adenosine removal, may cause fatal overactivation of A_{2A} R and result in cardiorespiratory dysfunctions and increased risk of SUDEP. The present study aimed to evaluate whether targeting A_{2A} R activity can reduce SUDEP risk. To accomplish this objective, we developed a new SUDEP mouse model with relevant clinical features, using a boosted-KA administration paradigm, and we investigated the vulnerability of SUDEP phenotype in mutant $Adk^{+/-}$ mouse (Boison et al., 2002; Palchykova et al., 2010) that was characterized by a ~50% decrease in ADK and thus impaired adenosine clearance.

MATERIALS AND METHODS

Animals and Pharmacological Reagents

All animal procedures were conducted in accordance with protocols approved by the Institutional Animal Care and Use Committee of the Legacy Research Institute (LRI, No. 120–2018, 114–2020, and 120–2021) and Barrow Neurological Institute (BNI, No. 366) consistent with the principles outlined by the National Institutes of Health. $Adk^{+/-}$ mutants (Boison et al., 2002; Palchykova et al., 2010) and their wild-type (WT) littermates were bred at the LRI (Portland, OR, United States). Adult male mice (bodyweight of 26–30 g) were used for the experiments, which were housed in a temperature- and humidity-controlled room with a 12-h light/dark cycle (lights on at 7:00 a.m.) throughout the experimental period. The reagents used in this study were commercially purchased: Kainic acid (KA, 0222, Tocris), 5-Iodotubercidin (5-ITU, 1745, Tocris), SCH58261 (S4568, Sigma).

Boosted Kainic Acid Model of SUDEP

To develop a SUDEP model with clinically relevant features, we designed a boosted-KA administration paradigm that consists of an intrahippocampal KA (IHKA) injection followed by a single systemic KA (SKA) intraperitoneal (i.p.) injection (**Figure 1A**). Specifically, 1) for generating chronic epilepsy, adult male $Adk^{+/-}$ and WT mice were subjected to unilateral IHKA (400 ng KA in 200 nl 0.9% saline—a dose used in our previous studies to establish chronic seizures (Shen et al., 2015)) or intrahippocampal injection of 200 nl saline (as sham control) into the right hemisphere, using coordinates (to Bregma): AP = –2.00 mm; ML = \pm 1.25 mm; DV = –1.70 mm from procedures

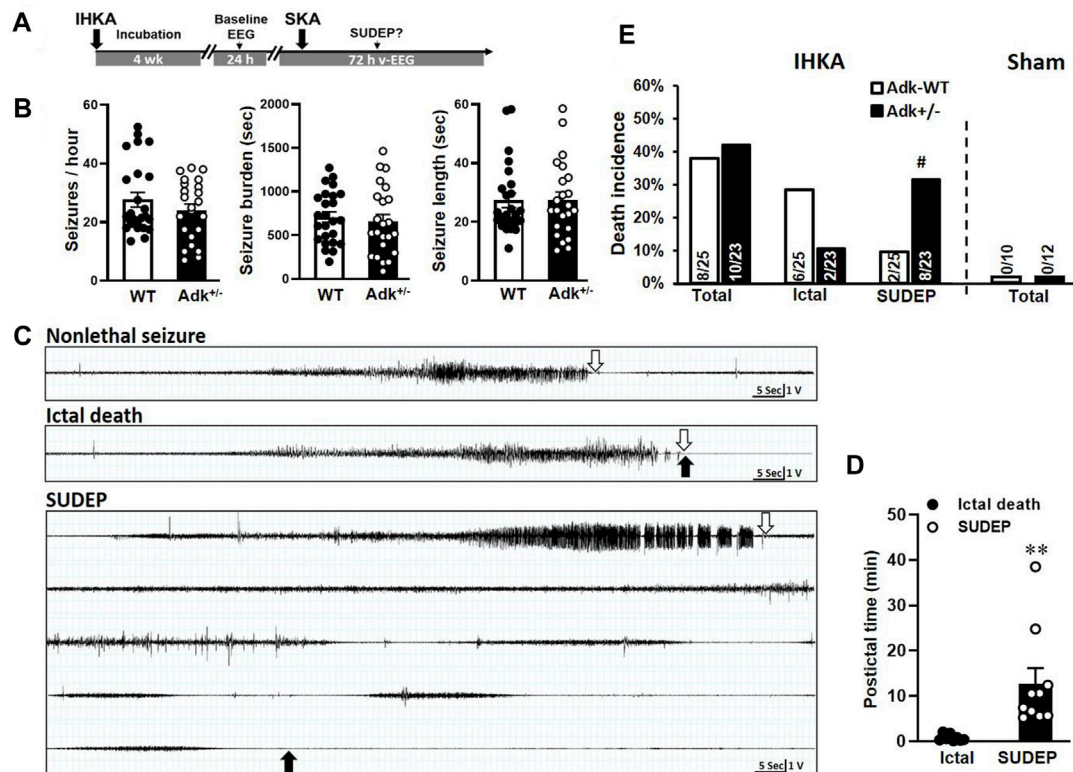


FIGURE 1 | Boosted kainic acid (KA) model of SUDEP. **(A)** Boosted KA administration paradigm that consists of an intrahippocampal KA (IHKA) injection followed by a single systemic KA (SKA) intraperitoneal (i.p.) injection. **(B)** Baseline EEG evaluation of Adk^{+/-} mice and their WT littermates at 4 weeks after IHKA injection. **(C)** Representative EEG traces of non-lethal seizure (upper panel), ictal death (middle panel), and SUDEP event (lower panel). Open arrows indicate the stop points of seizures; solid arrows indicate the point of death occurrence. **(D)** The postictal period from the end of the seizure until the death occurred. **(E)** Rates of ictal death, SUDEP, and total mortality in mice received IHKA injection (IHKA) or vehicle control (Sham). Data are mean ± SEM. #*p* < 0.05 vs. SUDEP in Adk-WT, Fisher's exact test, two-sided; ***p* < 0.01 vs. ictal death, unpaired *t*-test.

published previously (Shen et al., 2015). Ten days after the IHKA or vehicle injection, mice were implanted with bipolar coated stainless steel electrodes (80 μm in diameter; Plastics One) into the right hippocampus using the same coordinates as the IHKA injection (Shen et al., 2015). Animals were maintained in a group in their housing cage throughout the experiment period, except for the v-EEG monitoring period in which the mice were single-housed. 2) For triggering convulsive seizures and possible postictal SUDEP phenotype, one single SKA injection (15 mg/kg, i. p.—a dose that is not expectable to trigger convulsions in naïve mice) was given to the epileptic mice that received IHKA injection 6–8 weeks prior. Then, animals underwent a block of 72-h v-EEG recording for evaluation of possible SUDEP phenotype, and EEG seizure activities were also determined and analyzed (see next section).

Video-Electroencephalogram Recording and Analysis

The video-electroencephalogram (v-EEG) was performed according to previously published methods (Shen et al., 2015). Mice were singly housed while tethered for the acquisition of the EEG recordings. Four weeks after IHKA injection, each mouse

was subjected to a baseline EEG evaluation of an epileptic phenotype with a block of 24-h EEG monitoring and recording (P511/P122 Grass Instruments, Astro-Med, West Warwick, RI). Electrical brain activity was digitized (ML880 PowerLab 16/30; AD Instruments, Colorado Springs, CO) and quantification of EEG seizure activity was determined as in our previous work (Shen et al., 2015). For evaluation of possible SUDEP phenotype and pharmacological pretreatment on SUDEP risk, animals underwent a block of 72-h v-EEG recording, starting prior to the pretreatment of A_{2A}R antagonist, SCH58261 (3 mg/kg), ADK inhibitor, 5-ITU (2 mg/kg), or vehicle (1.5% DMSO in saline) i. p. and lasting for 72 h. EEG seizure activities were determined and analyzed as aforementioned.

Immunohistochemistry

For immunohistochemistry assessment of chronic epilepsy-induced biochemistry changes, a set of mice (*n* = 22) was sacrificed 6 weeks post-IHKA or vehicle injection after completion of EEG evaluation but without receiving systemic KA injection. Mice were transcardially perfused with 4% formaldehyde; the dissected brains were postfixed in 4% formaldehyde and cryoprotected in 30% sucrose PBS solution before sectioning into 30 μm sagittal sections using a cryostat (VT

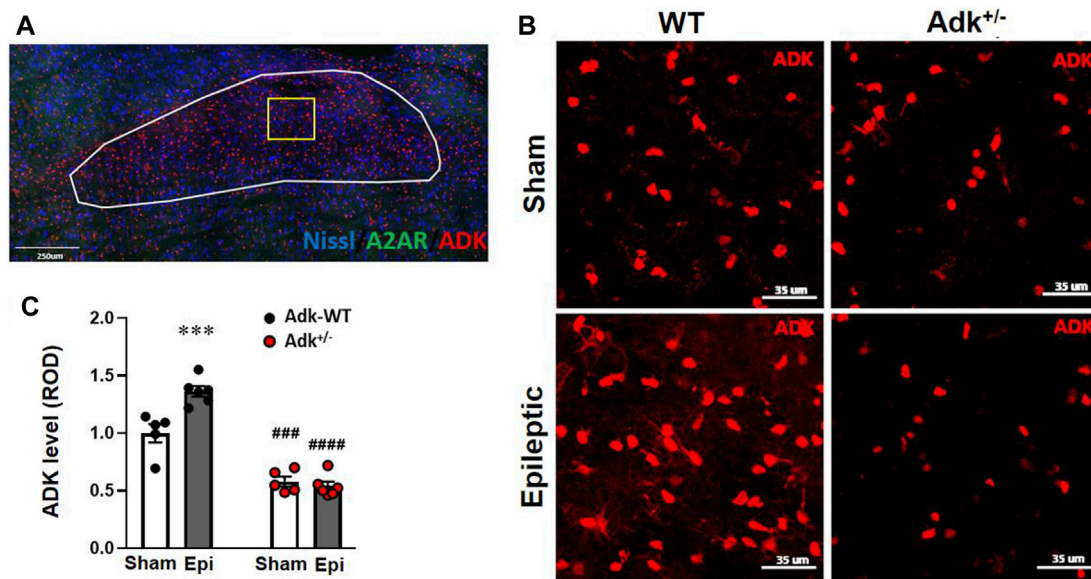


FIGURE 2 | ADK changes in the NTS of IHKA modeled epileptic mice. **(A)** Representative immunofluorescence (IF) image and an indication of selection of NTS region. **(B)** Representative images of IF staining for ADK in the NTS of IHKA modeled epileptic mice (Epileptic) vs. sham controls (Sham). **(C)** Quantitative analysis of the NTS expression levels of ADK (presented as relative optical density, ROD) in IHKA modeled epileptic (Epi) mice vs. sham controls (Sham). Data are mean \pm SEM. *** p < 0.001 vs. sham controls of same genotype; ### p < 0.001 vs. WT sham controls; #### p < 0.0001 vs. WT epileptics; unpaired t -test. Scale bar = 35 μ m.

1000 S, Leica, Bannockburn) (Shen et al., 2015). For staining, tissue sections were pretreated with citrate buffer at 80°C for 30 min; then blocked in goat blocking buffer (GBB, containing 2% goat serum, 0.05% Triton X-100 and 1% BSA) for 1 h and incubated at 1% sodium tetraborate for 30 min at room temperature. Pretreated sections were then incubated at 4°C for 48 h in GBB containing corresponding primary antibodies with the indicated dilution: ADK (A304-280A, Bethy Labs, 1:1,000), A_{2A}R (A2A-GP-Af1000, Frontier Institute, 1:100), or cAMP (MAB2146, R&D Systems, 1:200); followed by incubation of corresponding secondary antibodies: Goat anti-guinea pig IgG H&L, Alexa Fluor 488 (A11073, Thermo, 1:500), Donkey anti-rabbit IgG H&L, Alexa Fluor 555 (A-31572, Thermo, 1:1,000), Donkey anti-mouse IgG H&L, Alexa Fluor 647 (ab150107, Abcam, 1:500), or NeuroTrace 435/455 Blue Fluorescent Nissl Stain (N21479, Thermo, 1:1,000), for 90 min at room temperature. Sections were then washed and mounted on slides. Once dried, sections were cover-slipped with Vectashield Antifade Mounting Medium (H-1000) for fluorescence microscopy observation on a Leica TCS SPE confocal laser-scanning microscope (LAS X 3.1.2.16221). Three independent sections were stained for each method. All sections were processed in parallel using identical solutions and incubation times, while stain slices without either primary or secondary antibodies were used for controls.

Image Quantification of Densitometry

High-resolution digital images were acquired under identical conditions using the LasX software system (Leica, Buffalo Grove, IL, United States). Fluorescence intensity analysis was performed using Leica Application Suite analysis software (Leica,

Buffalo Grove, IL) or ImageJ software (ImageJ, US. National Institutes of Health, Bethesda, MD; ImageJ.nih.gov/ij/). All image processing was applied identically across experimental groups. The NTS region was selected as shown in Figure 2A, and immunoreactive material was measured in the same designated area of NTS for each sample and expressed as relative optical density (ROD) by area. Three levels were measured for each mouse, and data analysis is expressed as the mean \pm SEM of ROD. The average levels in treatment groups were normalized according to that in the corresponding control group (as baseline).

Electrophysiology Recording of Local Field Potential in the NTS

In vivo LFP in the NTS was recorded with similar procedures as our previous work (Gao et al., 2007) using the below coordinates (to Bregma): AP = -7.35 mm; ML = 0.20 mm; DV = 4.50 mm, with animals under anesthesia (isoflurane; induction 3.0%, maintenance 1.5%). For LFP recordings, the signals were collected by tetrodes and amplified by a 16-channel amplifier (Plexon DigiAmp; bandpass filtered at 0.1–300 Hz, 2,000 \times gain, sampled at 2 k Hz). First, a baseline LFP was recorded for 30 min, then mice received pretreatment of SCH58261 (3 mg/kg, i. p.) or 0.9% saline (0.3 ml, i. p.) as control with continued recording; 30 min later mice were given a single KA dose (15 mg/kg, i. p.) and recording was continued for another 30 min. For LFP analysis, the raw data of the 2 min prior to the onset of drug administration were selected as representing ongoing LFP activity. A time-frequency transformation was performed (Hanning window; FFT size, 256) with NeuroExplorer, and

the spectral power was calculated for each frequency resolution. The spectral power from all frequencies included within the bandwidth was averaged. LFP signals were divided into different frequency bands: theta (2–12 Hz), beta (15–35 Hz), and gamma (36–95 Hz).

Statistical Analyses

All data were analyzed using GraphPad Prism software. The quantitative data are presented as mean \pm SEM and were analyzed using one-way ANOVA, two-way ANOVA, or *t*-tests, as appropriate. The categorical data were analyzed using Fisher's exact test or Chi-square test, as appropriate. A *p*-value < 0.05 was considered significant.

RESULTS

Establishment of a Boosted KA Mouse Model of SUDEP

We established a new SUDEP model using a boosted-KA paradigm (**Figure 1A**) and tested the vulnerability of SUDEP risk in Adk^{+/-} mutants that have approximately 50% reduction in ADK protein level in the brain and compromised ability to metabolize adenosine (Boison et al., 2002; Palchykova et al., 2010). This model consists of two phases - chronic epilepsy modeled by IHKA injection (400 ng) and a potential phenotypic SUDEP (i.e., delayed postictal sudden death) event triggered by a single SKA (15 mg/kg) challenge (**Figure 1A**). We first assessed the epileptic features between Adk^{+/-} and WT mice at 4 weeks post-IHKA (or vehicle) injections as a baseline EEG evaluation. No EEG seizures were observed in sham control animals with the intrahippocampal injection of saline (WT *n* = 10 and Adk^{+/-} *n* = 12), whereas spontaneous recurrent electrographic seizures were developed in IHKA-injected WT mice and Adk^{+/-} mutants. There was no significant difference in seizure-onset frequencies (*p* = 0.2778), seizure burden (i.e., total duration of seizure activity, *p* = 0.5995), and average length of seizures (*p* = 0.9687), between IHKA-injected Adk^{+/-} vs. WT mice (*n* = 23–25 per genotype, unpaired *t*-test, two-tailed) (**Figure 1B**).

After baseline EEG evaluations, mice were subjected to SKA (15 mg/kg, i. p.) to trigger possible SUDEP events. The v-EEG monitoring data showed SKA injection-induced convulsive seizures in all the epileptic animals, which eventually resulted in two outcomes: non-lethal seizures or lethal seizures (**Figure 1C**). Importantly, v-EEG monitoring demonstrated two distinctive phenotypes of lethal seizures: 1) ictal death - which occurred immediately after the end of SKA-induced seizures (**Figure 1C**, middle panel), or 2) delayed postictal death (aka, SUDEP event (Ryvlin et al., 2013)) - defined as a sudden death that occurred without coexisting behavioral and/or electrographic EEG seizures (based on v-EEG monitoring) for more than 5 min (**Figure 1C**, lower panel). In contrast, SKA (15 mg/kg, i. p.) did not trigger any death in non-epileptic sham control mice without prior IHKA (but intrahippocampal saline) injection, regardless of their genotypes (*n* = 10–12 per genotype) (**Figure 1E**, right panel). The v-EEG analysis showed that the

SUDEP events occurred in a period of 12.73 ± 3.40 min after the last v-EEG-recorded seizure (**Figure 1D**), with the longest seizure-free period prior to a SUDEP event being 38.5 min. The periods from last seizure to death occurrence were significantly different between defined ictal deaths vs. SUDEP events (*p* = 0.0067, unpaired *t*-test, *n* = 8–10/phenotype) (**Figure 1D**). Remarkably, the occurrences of SUDEP events in epileptic Adk^{+/-} mutants (34.8%, 8/23) was significantly higher than epileptic WT mice (8.0%, 2/25, *p* = 0.0335, Fisher's exact test, two-sided), whereas the ictal seizure death rate was not significantly different between Adk^{+/-} mutants (8.7%, 2/23) and WT mice (24.0%, 6/25) (*p* = 0.2487, Fisher's exact test, two-sided), and the seizure-related total mortality was not significantly different between Adk^{+/-} mutants (43.5%, 10/23) and WT mice (32.0%, 8/25) (*p* = 0.5524, Fisher's exact test, two-sided) (**Figure 1E**, left panel). This suggests that Adk^{+/-} mice, with impaired adenosine removal, are more vulnerable to SUDEP risk.

Chronic Epilepsy-Induced Adenosinergic Changes in the Brainstem of Mice

To understand the underlying mechanisms of chronic epilepsy-associated SUDEP, we evaluated the molecular changes related to adenosinergic activity with immunofluorescence staining of ADK, A_{2A}R, and cAMP in the NTS. The NTS level of ADK (**Figures 2B,C**) was altered by Adk mutation and IHKA-modeled epilepsy (genotype factor, *p* < 0.0001 $F_{(1,18)} = 189.2$; modeling factor, *p* = 0.0012, $F_{(1,18)} = 14.69$; interaction, *p* = 0.002, $F_{(1,18)} = 22.21$; two-way ANOVA, *n* = 5–6 per group). Specifically, the basal NTS level of ADK in sham Adk^{+/-} mutants was lower than sham WT mice (*p* < 0.0002), at 57.9% of the level of sham WT mice (**Figures 2B,C**). The epileptic WT mice had significantly (36.5%) increased NTS ADK vs. sham WT mice (*p* = 0.0006, unpaired *t*-test). Of note, epileptic Adk^{+/-} mutants showed no increase in NTS ADK level vs. sham mutants (*p* = 0.9514, unpaired *t*-test), whereas NTS ADK level in epileptic Adk^{+/-} mutants was significantly lower vs. epileptic WT mice (*p* < 0.0001, unpaired *t*-test) (**Figures 2B,C**). This suggests an epilepsy-induced compensatory increase of ADK in the NTS of WT mice whereas Adk^{+/-} mice were devoid of this change. Furthermore, NTS A_{2A}R level was altered by IHKA epilepsy vs. sham controls (*p* < 0.0001, $F_{(1,18)} = 166.5$, modeling factor, two-way ANOVA, *n* = 5–6 per group), in both epileptic Adk^{+/-} and WT mice vs. their corresponding sham controls (*p* < 0.0001 and *p* < 0.0001, unpaired *t*-test) (**Figures 3A,B**). These indicate an epilepsy-induced adaptive A_{2A}R increase in the NTS of both genotypes, regardless of ADK levels.

To further explore A_{2A}R activation-related changes, we evaluated cAMP in the NTS (**Figure 3C**). IHKA-modeled epilepsy significantly increased NTS cAMP levels (*p* < 0.0001, $F_{(1,18)} = 32.17$, treatment effect, two-way ANOVA, *n* = 5–6 per group) without a difference between genotypes (*p* = 0.4676, $F_{(1,18)} = 0.5506$, two-way ANOVA) (**Figure 3D**). Specifically, NTS cAMP levels were increased in both epileptic WT mice and Adk^{+/-} mutant vs. their corresponding non-epileptic sham controls (*p* = 0.0022, *p* = 0.0080, *t*-test, *n* = 5–6 per group) (**Figure 3D**), which was in line with the changing pattern of A_{2A}R in the NTS

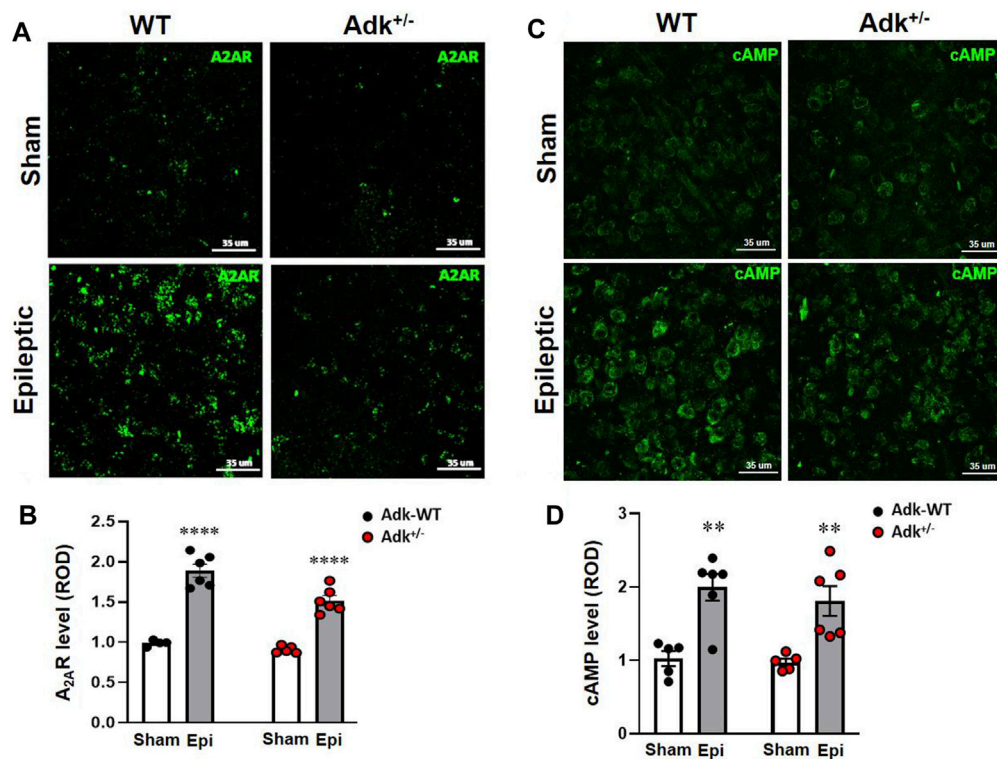


FIGURE 3 | Changes of A_{2A}R and cAMP in the NTS of IHKA modeled epileptic mice. Representative images of IF staining for A_{2A}R (A) and cAMP (C) in the NTS of IHKA modeled epileptic mice (Epileptic) vs. sham controls (Sham). Quantitative analysis of the NTS densities of A_{2A}R (B) and cAMP (D) (presented as relative optical density, ROD) in IHKA modeled epileptic (Epi) mice vs. sham controls (Sham). Data are mean ± SEM. ***p* < 0.01 and *****p* < 0.0001, vs. sham controls within same genotype, unpaired *t*-test. Scale bar = 35 μm.

(Figure 3B). Together, these biochemistry findings revealed that chronic epilepsy resulted in increased ADK levels for the removal of excessive adenosine, and increased A_{2A}R activities were in line with increased cAMP in the NTS.

Blockade of A_{2A}R Activation Reduced the SUDEP Risk in Epileptic Mice

Having demonstrated perturbations in the adenosinergic pathway in the NTS induced by epilepsy, we further explored whether the increased A_{2A}R activity contributes to the risk of SUDEP events. We tested if suppressing A_{2A}R activity, with A_{2A}R antagonist SCH58261, can reduce the risk of SUDEP and whether ADK inhibition can exacerbate SUDEP risk. A cohort of epileptic Adk^{+/-} mutants and WT mice was generated by IHKA-injection and confirmed via EEG evaluation for their baseline epileptic features (Figure 4A). They then were randomly assigned to three groups to receive pretreatment of SCH58261 (3 mg/kg, i. p., *n* = 11–12), 5-ITU (2 mg/kg, i. p., *n* = 15), or vehicle (*n* = 17); and 30 min later each mouse was given a single injection of SKA (15 mg/kg, i. p.) followed by v-EEG monitoring for 72 h (Figure 4A). Figure 4B demonstrates the epileptic features of each group of mice at 4 weeks post-IHKA injections as their baseline EEG evaluation. There was no significant difference in seizure-onset frequencies between groups (*n* = 11–17 per group) (*p* = 0.7769, *F*_(2, 81) =

0.2532, two-way ANOVA) or between genotypes (*p* = 0.9867 *F*_(1, 81) = 0.0002, genotype effect, two-way ANOVA) (Figure 4B, upper panel); no significant difference was observed in seizure burden between groups (*p* = 0.8933, *F*_(2, 81) = 0.1130, two-way ANOVA) or between genotypes (*p* = 0.2321, *F*_(1, 81) = 1.450, genotype effect, two-way ANOVA) (Figure 4B, middle panel); also no difference was shown in average seizure length across groups (*p* = 0.5270, *F*_(2, 81) = 0.6456) and genotypes (*p* = 0.1338, *F*_(1, 81) = 2.294) (Figure 4B, lower panel).

The v-EEG analysis showed that the SUDEP occurrences increased in 5-ITU pretreatment (46.7%, 7/15), whereas SCH58261-pretreatment drastically reduced SUDEP events (0%, 0/11) in Adk^{+/-} mutants vs. vehicle-pretreated controls (29.4%, 5/17) (*X*²_(2, N=43) = 6.901, *p* = 0.0317). The SCH58261-pretreatment also reduced SUDEP events in WT mice (0%, 0/11), but 5-ITU pretreatment did not significantly increase SUDEP onset vs. vehicle pretreated WT mice (*X*²_(2, N=44) = 1.904, *p* = 0.3860) (Figure 4C). These findings indicate that A_{2A}R overactivation could contribute to increased SUDEP risk, and A_{2A}R blockade efficiently reduced the SUDEP risk. Retrospective analysis of their baseline EEG showed that no significant differences were found in seizure onset frequencies among mice of survival, ictal death, and SUDEP groups that received different treatments (*F*_(5,10) = 1.799, *p* = 0.2007, one-way ANOVA) (Figure 4D). This suggests that the baseline epileptic

phenotype was not linked to their seizure-related death phenotypes.

A_{2A}R Blockade Disinhibits Seizure-suppressed Coordination of Activity in the NTS

To mechanistically dissect the A_{2A}R effects on the coordination of activity in the NTS, SCH58261 or saline (as control) was administered 30 min prior to KA injection in a separated cohort of IHKA-modeled Adk^{+/-} and WT mice (n = 4–6 per group), and LFP of NTS was recorded to reflect the neural activity of the assembly of cells surrounding the recording site (Bantikyan et al., 2009). We compared the LFP signals in epileptic Adk^{+/-} and WT mice following pretreatment with saline or SCH58261, and afterward with KA injections (Figure 5). The raw LFP signals were divided into three frequency bands, i.e., theta, 2–12 Hz; beta, 15–35 Hz; gamma, 36–95 Hz (Figure 5A). The heat map of the power spectrum of LFP signals shows an overt continuous reduced gamma response after KA in WT mice with saline pretreatment (Figure 5B). Analysis of averaged power spectrums between the genotypes demonstrated that the baseline oscillation power of gamma was significantly lower

in Adk^{+/-} mice vs. WT (p = 0.0037, unpaired t-test) while their baseline theta or beta powers were not different (p = 0.8656 and p = 0.9081, unpaired t-test, n = 5–6 per group) (Figure 5C).

Further analysis showed that the saline- or SCH58261-pretreatment *per se* did not cause LFP power changes in theta (F_(2,9) = 1.801, p = 0.2189), beta (F_(2,9) = 1.017, p = 0.3997), or gamma (F_(2,9) = 0.0742, p = 0.9290, one-way ANOVA) band vs. baselines (Figure 5E). KA injection following saline pretreatment decreased the gamma oscillation in WT (F_(2,6) = 9.504, p = 0.0138, one-way ANOVA; p = 0.0077 vs. saline, p = 0.0115 vs. baseline, paired t-test), but the reduction of gamma oscillation was not seen when following SCH58261 pretreatment (F_(2,6) = 3.057, p = 0.1215, one-way ANOVA; p = 0.0967 vs. SCH58261, p = 0.0328 vs. baseline, paired t-test), suggesting that SCH58261 partially blocked the KA suppression on gamma. The inferred role of A_{2A}R is similar to that previously reported (Pietersen et al., 2009), although in this previous study kainate enhanced cortical gamma power. Also, while the baseline power of gamma oscillation in Adk^{+/-} mutants was significantly lower than WT (Figure 5D), no gamma power change resulted after KA injection following saline pretreatment (F_(2,10) = 0.0021, p = 0.9979, one-way ANOVA; p = 0.9509 vs. saline, p = 0.9649 vs. baseline,

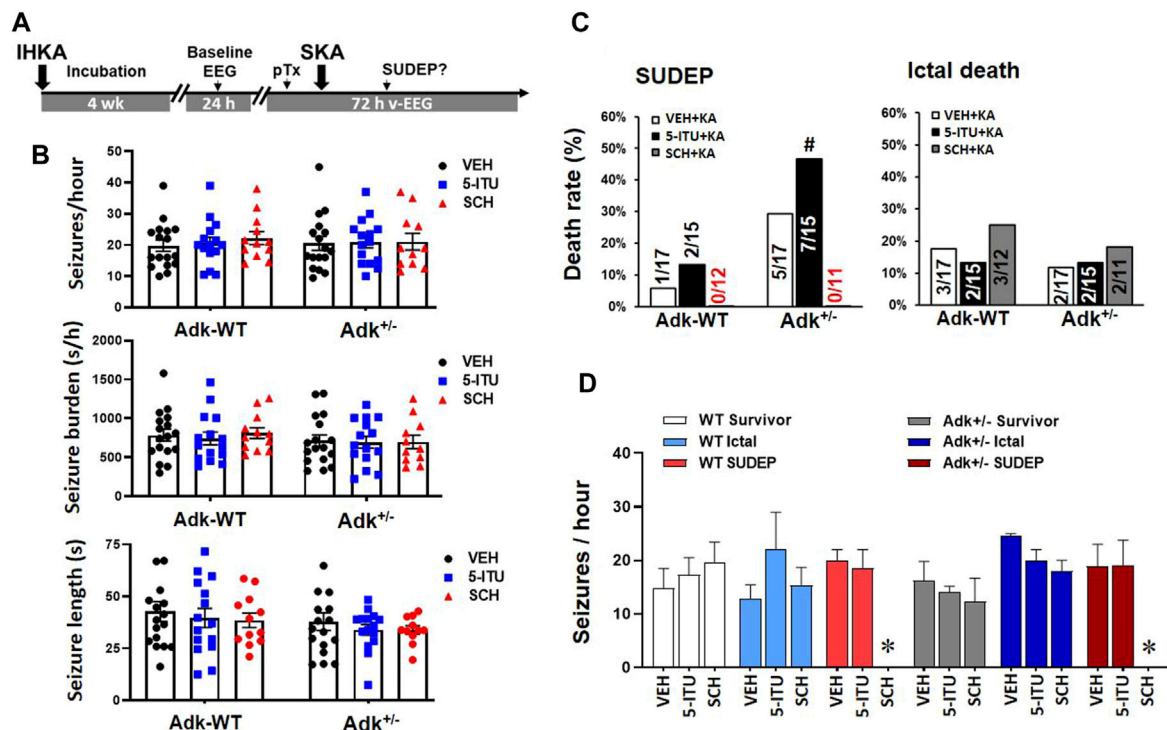
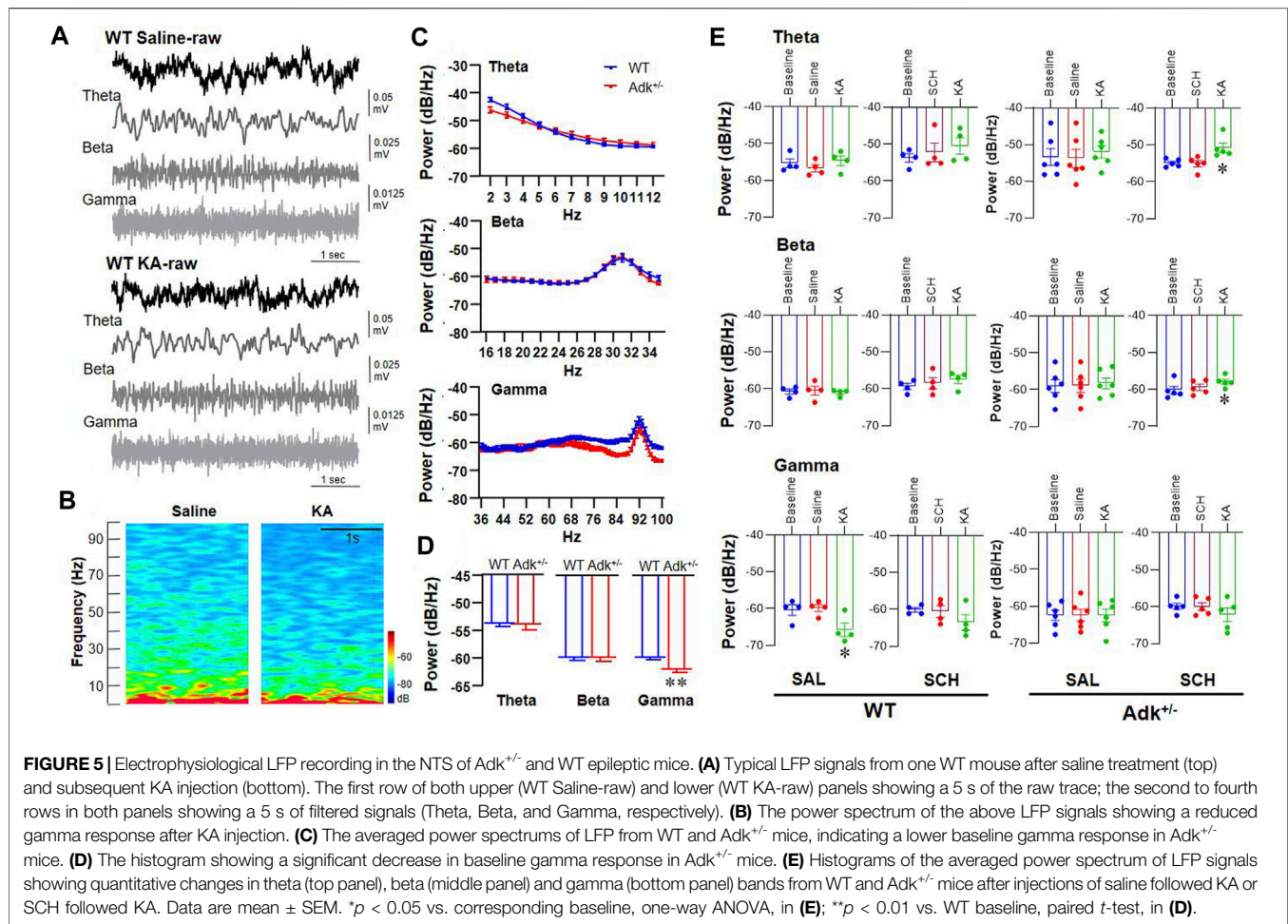


FIGURE 4 | A_{2A}R antagonist SCH58261 reduced SUDEP occurrence in epileptic mice. **(A)** The paradigm of pharmacological pretreatment (pTx) in the boosted KA model of SUDEP. **(B)** EEG validation of epileptic phenotypes in each group of Adk^{+/-} mice and their littermates (Adk-WT) at 4 weeks after IHKA injection, prior to the experimental SKA (15 mg/kg, i. p.) injections. **(C)** Rates of ictal death, SUDEP, and total mortality among groups with pretreatment of i. p. injection of vehicle (VEH), 5-lodotubercidin (5-ITU, 2 mg/kg), and SCH58261 (SCH, 3 mg/kg). **(D)** Baseline EEG evaluation of seizure onset frequencies (seizure/hour) in mice grouped as survivors, ictal death, and SUDEP, with different pretreatments of a VEH, 5-ITU, or SCH. * Indicating zero animals with SUDEP existing in the marked (SCH) group. #p < 0.05 vs. same treatment group in Adk-WT mice, Chi-square test.



paired *t*-test) (**Figure 5E**, lower panel). Similarly, no KA-induced changes in theta ($F_{(2, 10)} = 0.6913$, $p = 0.5234$) or beta ($F_{(2, 10)} = 0.3417$, $p = 0.7185$, one-way ANOVA) were found in Adk^{+/-} mice when following saline pretreatment. Remarkably, the SCH58261 pretreatment significantly increased the theta ($F_{(2, 8)} = 8.959$, $p = 0.0091$, one-way ANOVA; $p = 0.0056$, paired *t*-test) and beta powers ($F_{(2, 8)} = 5.452$, $p = 0.0321$, one-way ANOVA; $p = 0.0119$, paired *t*-test) in Adk^{+/-} mice post-KA injection (**Figure 5E**, upper and middle panels). Together, we demonstrated the differential effects of KA-induced LFP power changes and SCH58261 manipulation on KA effects between WT and Adk^{+/-} mice.

DISCUSSION

While the mechanisms of SUDEP remain elusive (Stöllberger and Finsterer, 2004; Hirsch, 2010; Shorvon and Tomson, 2011), studies suggested that abnormalities in the adenosinergic system may play an important role in SUDEP events (Shen et al., 2010; Boison, 2012; Devinsky et al., 2016). We hypothesized that repeated seizure-induced adenosine increases in the brainstem can result in potentially fatal

overactivation of A_{2A}R while decreased ADK can exacerbate fatality. We developed a new SUDEP model characterized by a delayed postictal death phenotype in mice with chronic epilepsy. Our findings suggest an enhanced A_{2A}R activity in the NTS of epileptic mice - while LFP alteration can result from a local modulation by A_{2A}R and/or potentially by a long-distance network effect triggered by A_{2A}R in different brain regions - and provide experimental evidence supporting A_{2A}R as a therapeutic target for SUDEP prevention. To better understand the role of A_{2A}R in SUDEP and its therapeutic potential, the following aspects warrant further discussion.

SUDEP Animal Models and Clinically Relevant Phenotypes

The unmet need in developing pharmacological preventative therapies against SUDEP was not only due to inadequate understanding of SUDEP mechanisms (Hirsch, 2010; Shorvon and Tomson, 2011; Stöllberger and Finsterer, 2004) but also was compromised by limitations of available SUDEP animal models (Surges et al., 2009; Devinsky et al., 2016; Pansani et al., 2016). Of the previous animal models used for SUDEP research, most carry genetic mutations that mimic several major clinical conditions

related to sudden death (e.g., cardiac arrhythmia, arrest, and coincidence of seizures) (Massey et al., 2014; Scheffer and Nabbout, 2019; Tu et al., 2011). Also, there is a lack of data in systematically characterizing the types of death (such as ictal death vs. delayed postictal death). These include rodents with mutations in the *SCN1A* gene (mimics Dravet syndrome) (Scheffer and Nabbout, 2019), *SCN5A* gene (mimics Brugada syndrome), *KCNH2*, *KCNQ1* genes (mimics Long QT syndrome), etc. (Tu et al., 2011). These genetic mutations could be potential causes of SUDEP; however, while they can result in pathophysiological changes, e.g., prolonged cardiac action potential, ventricular tachycardia, syncope, and sudden death, these genetic deficits were rarely reported in clinical SUDEP cases or patients with TLE—the most common form of epilepsy involved in SUDEP cases (Massey et al., 2014; Patodia et al., 2020; Devinsky, 2011). Facing these limitations, we developed a new SUDEP mouse model using a boosted-KA paradigm that mimics major, clinically relevant features of SUDEP cases, including: 1) a chronic nature of spontaneous seizures (Figure 1B) (Shen et al., 2015); and 2) a delayed postictal death phenotype - i.e., SUDEP event - one of the central revelations of the MORTEMUS study (Ryvlin et al., 2013), dissociated from prior convulsive and/or electrographic seizures (Figure 1C). Notably, the average latency to the SUDEP event is substantially longer than the delay seen in most (but not all) epilepsy patients reported in the MORTEMUS study (Ryvlin et al., 2013). A limitation of this study is the need for cardiopulmonary monitoring, which should be undertaken in future studies to fully characterize this model. It may be of interest to note that the adenosine modulation system also has direct cardiorespiratory effects which are affected in the global genetic and pharmacological manipulation attempted in this study. Additionally, future work could optimize our paradigm. For example, we utilized 15 mg/kg KA to trigger behavior seizures in epileptic mice; a lower KA dose may achieve a less severe behavioral seizure phenotype, while still triggering a SUDEP event in epileptic animals, resulting in a longer postictal period before SUDEP occurrence. These models have the potential for better characterization of adenosinergic changes in other brain regions in SUDEP, e.g., hippocampus, cortex, and other brainstem nuclei. Nevertheless, this adenosinergic SUDEP mouse model provides a novel tool for the SUDEP research field while it warrants continued optimization. The biological sex variable should also be investigated and addressed in future studies.

Disturbances in the Adenosinergic Signaling Pathway Resulted in SUDEP

Adenosinergic activities are tightly linked to the etiological and pathophysiological outcomes of seizures and epilepsy (Ashraf et al., 2021; Faingold et al., 2016; Kommajosyula et al., 2016; Masino et al., 2014; O'Brien, 1988; Shen et al., 2014). Acute and chronic seizures can trigger repeated adenosine surges and increase adenosine tone in the brain, which can act as an endogenous anticonvulsant and also reset neuron network stability by affecting neurotransmission at the synapse

(Masino et al., 2014; O'Brien, 1988). It is increasingly established that two main systems are contributing to the extracellular adenosine that engages the adenosine modulation system in the brain: the activity of equilibrative nucleoside transporters (ENTs) and of ADK mostly associated with a global A₁R function and CD73-mediated formation of ATP-derived adenosine tightly associated with A_{2A}R activation (Cunha, 2016). Seizure-induced adenosine surges can result in changes in ADK (Aronica et al., 2011), which together with adaptive alterations of the density and activity of adenosine receptors (He et al., 2020; Rebola et al., 2005c) maintain balanced adenosine activities in epileptic sites. Despite *Adk*^{+/-} mutants having reduced endogenous brain ADK, intriguingly, no overt genotype effect of *Adk*^{+/-} mutants was observed in IHKA-induced chronic seizures (Figure 1B). This could be attributed to potential adaptations of mutants to genetic knockdown of ADK during their development, or it could be masked by undetermined compensatory changes in the adenosinergic pathway: changes in additional adenosine metabolic pathways, e.g., adenosine deaminase (to process adenosine into inosine and then into hypoxanthine), and/or changes in adenosine receptors in the hippocampus of *Adk*^{+/-} mutants. These potential changes may separately and/or synergistically affect the seizure phenotypes in *Adk*^{+/-} mice. The complexity and seeming discrepancy of the relationship between the ADK/adenosine and seizure phenotypes were also shown in the Sandau et al. study with similar ADK deletion in the hippocampus (Sandau et al., 2016), in which the *Adk*^{Δbrain} mice (i.e., *Nestin-Cre*^{+/-}:*Adk*^{fl/fl} mice) were used with the characterized conditional *Adk* gene deletion, which caused brain-wide ADK deficiency and increased synaptic adenosine levels. However, *Adk*^{Δbrain} mice surprisingly showed an increase in spontaneous seizures and susceptibility to seizure induction compared to their WT littermates (Sandau et al., 2016). The findings from *Adk*^{Δbrain} mice and our *Adk*^{+/-} mutants indicated a complexity between ADK/adenosine and seizure (onset) phenotypes, which is also a suggestive indication supporting the contention that studying only ADK as a controller of the adenosine levels may well be inadequate. The work of Sandau et al. (2016) did not consider the possibility that changes in ATP release and ect-nucleotidase activity might have occurred in the tested *Adk* transgenic mice. Nevertheless, whether genetic ADK knockdown can yield possible preconditioning effects against the development of epilepsy warrants additional evaluation.

In the brainstem, we demonstrated that chronic seizures led to a compensatory increase in NTS ADK (of WT mice), an area outside the hippocampal seizure origin; epileptic *Adk*^{+/-} mice did not experience any ADK level increases, which may have contributed to their increased death rates. The NTS level of A_{2A}Rs was enhanced in epileptic mice along with increased cAMP, suggesting an increased output of A_{2A}R activation. Notably, in epileptic *Adk*^{+/-} mice, the combination of impaired adenosine removal potential with increased A_{2A}Rs in the NTS could result in lethal suppression on cardiorespiratory reflexes of

chemo- and baroreceptors inputs (Wilson et al., 2004; Zoccal et al., 2014; Minic et al., 2015). Mechanistically, A_{2A}Rs can alter GABAergic activities in several aspects: 1) A_{2A}R controls the depolarization-evoked GABA release in synaptosomes in the hippocampus (Cunha and Ribeiro, 2000) and striatum (Kirk and Richardson, 1994); 2) A_{2A}R controls the activity of GABAergic interneurons, increasing synchronization in hippocampal networks (Rombo et al., 2015) and most evidently controlling adaptive plastic changes in GABAergic synapses in the prefrontal cortex (Kerkhofs et al., 2018); 3) previous studies in different animal models of epilepsy suggested that the neuroprotection afforded by A_{2A}R blockade might involve a rebalance of GABAergic transmission (Seo et al., 2020); 4) A_{2A}R are critical mediators of the stability of GABAergic synapses (Gomez-Castro et al., 2021). Thus, overactivation of A_{2A}Rs in the NTS can attenuate depolarization-evoked GABA release (Saransaari and Oja, 2005) and affect oscillations of GABAergic interneurons (Buzsáki and Wang, 2012). Meanwhile, it has been shown that A_{2A}R is located in glutamatergic synapses (Rebola et al., 2005b) acting as a controller of plasticity processes at glutamatergic synapses, either in the hippocampus (Costenla et al., 2011), dorsal or ventral (Reis et al., 2019) hippocampus, the striatum (Shen et al., 2008; Li et al., 2015), the amygdala (Simões et al., 2016), or the prefrontal cortex (Kerkhofs et al., 2018). Overactivated A_{2A}R may also lead to altered synaptic glutamatergic activities in NTS neurons.

Remarkably, A_{2A}R antagonist SCH58261 disinhibited KA-induced continuous suppression in gamma oscillation and enhanced theta and beta oscillations in anesthesia preparation (Figure 5E), likely preventing the lethal suppression of NTS neuronal activity during and after seizures (Kuo et al., 2016). Theta, beta, and gamma oscillations not only represent activity changes of local neurons in the recorded area but also activities from specific brain circuits of information flow (Massimini et al., 2004). Our study demonstrated that under chronic epileptic condition, KA and/or acute seizure tends to decrease the slow-wave synchrony, suggesting decreased communications between brain regions. SCH58261 pretreatment can restore KA-induced inhibition on slow waves, indicating the disinhibition is mainly mediated by A_{2A}R activation. In the mammalian cortex, neural communication is organized by 30–100 Hz gamma oscillation, with gamma frequency related to processing speed in neural networks (Insel et al., 2012). Furthermore, this fast band typically requires interplay between excitatory and inhibitory transmission (Buzsáki et al., 2012). However, we need to bear in mind that though LFP recorded from the anesthetized animal has been accepted in epilepsy studies (Williams et al., 2016; Wenzel et al., 2017) to reflect synchronous activities of neuronal assemblies, the anesthetized states might mask changes in seizure activity, respiration, and potential neurobehavioral outcomes. The LFP findings aimed to mechanistically demonstrate the local neuronal activities in the NTS, linked to IHKA-induced chronic epilepsy and/or affected by adenosine-A_{2A}R activities.

In the NTS, neurons are segregated into neuronal clusters, which receive distinct cardiorespiratory afferents and regulate their function by regulating NMDAR- and GABAAR-mediated

excitatory/inhibitory synaptic plasticity (Bantikyan et al., 2009). We propose that, in ADK^{+/-} mice, the inhibitory transmission may predominate in the NTS because of its impaired capacity to remove the endogenous adenosine, which may lead to a potential tonic suppression of cardiorespiratory function, and a higher vulnerability to SUDEP risk. As such, the additional KA injection can cause a higher sudden death rate in ADK^{+/-} mice. While the cell type- and/or neurotransmitter-dependent actions of A_{2A}R in the NTS warrant further characterization to reveal the complexity of A_{2A}R-mediated regulation in NTS circuits, a report from Derera et al (2017) supports the role of A_{2A}R in the NTS in an increased risk of cardiorespiratory dysfunction and sudden death in TLE patients (Derera et al., 2017). Enhanced A_{2A}R signaling may not be limited to NTS; it may affect other autonomic brainstem structures that potentially contribute to SUDEP. Our findings indicate a crucial role of A_{2A}R in the pathophysiology of SUDEP and suggest that antagonism of A_{2A}R may be a therapeutic strategy for SUDEP prevention.

Adenosinergic Intervention—do the Timing and Subtype of Receptor Matter?

With a broader consideration, seizures also trigger a release of ATP (Wieraszko et al., 1989; Augusto et al., 2021) and an increased extracellular catabolism of ATP into adenosine (Bonan et al., 2000; Bruno et al., 2003; Nicolaidis et al., 2005), which sustains A_{2A}R activation (Augusto et al., 2013; Carmo et al., 2019; Gonçalves et al., 2019; Alçada-Morais et al., 2021; Augusto et al., 2021) that is critically associated with seizure-induced neurodegeneration (Cognato et al., 2010; Canas et al., 2018; Augusto et al., 2021). This evidence is of key importance to understand the role of A_{2A}R and the limitations in studying only the relation between ADK and adenosine neuromodulation without considering the whole limb of ATP release and ectonucleotidase activity selectively associated with A_{2A}R activation (Augusto et al., 2013; Carmo et al., 2019; Gonçalves et al., 2019; Alçada-Morais et al., 2021; Augusto et al., 2021). Strangely, it has never been tested if decreased ADK results in aberrantly increased ATP release upon neuronal activation.

Further, due to the complexity of the adenosinergic actions in the CNS and diverse and wide distributions of A₁R and A_{2A}R across brain regions (O'Brien, 1988; Chen et al., 2014; Fredholm et al., 2005; Chen et al., 2013), the application of adenosinergic interventions to prevent SUDEP deserves deeper discussion. In the hippocampus, A₁R suppresses the ictal firing of excitatory neurons; conversely, hippocampal A_{2A}R activation is proconvulsant and proseizure (Zeraati et al., 2006; El Yacoubi et al., 2009). Clinical findings revealed upregulated hippocampal A_{2A}Rs in patients with TLE, which supports the notion of applying A_{2A}R antagonists without exacerbating epileptic seizures. In the brainstem, a working hypothesis is that A_{2A}R activation leads to suppression of GABAergic inhibitory neurons and their mediated cardiorespiratory functions, whereas A₁R activation promotes opposite effects (Phillis et al., 1997). These diverse effects of A_{2A}R vs. A₁R limit the potential application of the widely used, non-selective adenosine receptor antagonist, caffeine. Indeed, the cause-and-effect relationship between caffeine and epileptic seizures has

long been debated (Kaufman and Sachdeo, 2003; Samsonsen et al., 2013) and was recently reviewed (Tescarollo et al., 2020) with due care to distinguish the effects of acutely administered caffeine compared to the ‘chronic’ consumption of caffeine, the latter attenuating epileptic-like phenotypes. Rather, specific antagonism of A_{2A}R can reduce the adenosine surge-related brainstem suppression, while avoiding interference with A₁R-mediated anticonvulsive actions. Last but not least, antiepileptic drug-resistant/refractory patients are linked to a high risk of SUDEP, while having tonic-clonic seizures is considered the greatest risk factor (Annegers and Coan, 1999). With the recent FDA approval of the A_{2A}R antagonist istradefylline for PD treatment (Chen and Cunha, 2020), our results indicate istradefylline should be examined for repurposing for epileptic patients at risk of SUDEP. Together, A_{2A}R antagonists may be a potential add-on anti-SUDEP approach. This approach may provide an important reduction of SUDEP with a remaining question as to the suppression of seizures.

DATA AVAILABILITY STATEMENT

The raw data supporting the conclusions of this article will be made available by the authors, without undue reservation.

ETHICS STATEMENT

The animal study was reviewed and approved by the Legacy Research Institute and Barrow Neurological Institute.

REFERENCES

- Alçada-Morais, S., Gonçalves, N., Moreno-Juan, V., Andres, B., Ferreira, S., Marques, J. M., et al. (2021). Adenosine A_{2A} Receptors Contribute to the Radial Migration of Cortical Projection Neurons through the Regulation of Neuronal Polarization and Axon Formation. *Cereb. Cortex* 31, 5652–5663. doi:10.1093/cercor/bhab188
- Annegers, J. F., and Coan, S. P. (1999). SUDEP: Overview of Definitions and Review of Incidence Data. *Seizure* 8, 347–352. doi:10.1053/seiz.1999.0306
- Aronica, E., Zurolo, E., Iyer, A., de Groot, M., Anink, J., Carbonell, C., et al. (2011). Upregulation of Adenosine Kinase in Astrocytes in Experimental and Human Temporal Lobe Epilepsy. *Epilepsia* 52, 1645–1655. doi:10.1111/j.1528-1167.2011.03115.x
- Ashraf, O., Huynh, T., Purnell, B. S., Murugan, M., Fedele, D. E., Chitravanshi, V., et al. (2021). Suppression of Phrenic Nerve Activity as a Potential Predictor of Imminent Sudden Unexpected Death in Epilepsy (SUDEP). *Neuropharmacology* 184, 108405. doi:10.1016/j.neuropharm.2020.108405
- Augusto, E., Matos, M., Sévigny, J., El-Tayeb, A., Bynoe, M. S., Müller, C. E., et al. (2013). Ecto-5'-nucleotidase (CD73)-Mediated Formation of Adenosine Is Critical for the Striatal Adenosine A_{2A} Receptor Functions. *J. Neurosci.* 33, 11390–11399. doi:10.1523/JNEUROSCI.5817-12.2013
- Augusto, E., Gonçalves, F. Q., Real, J. E., Silva, H. B., Pochmann, D., Silva, T. S., et al. (2021). Increased ATP Release and CD73-Mediated Adenosine A_{2A} Receptor Activation Mediate Convulsion-Associated Neuronal Damage and Hippocampal Dysfunction. *Neurobiol. Dis.* 157, 105441. doi:10.1016/j.nbd.2021.105441
- Bantkayan, A., Song, G., Feinberg-Zadek, P., and Poon, C. S. (2009). Intrinsic and Synaptic Long-Term Depression of NTS Relay of Nociceptin- and Capsaicin-Sensitive Cardiopulmonary Afferents Hyperactivity. *Pflugers Arch.* 457, 1147–1159. doi:10.1007/s00424-008-0571-9

AUTHOR CONTRIBUTIONS

SB, RG, and JC performed research and analyzed data; LW and SC performed research, MG performed research, analyzed data, and wrote the paper; JW and J-FC contributed unpublished reagents/analytic tools and edited the paper; TJ designed research and analyzed data; H-YS designed and performed research, analyzed data, and wrote the paper.

FUNDING

The research was supported by grants from the Good Samaritan Foundation of Legacy Health.

ACKNOWLEDGMENTS

The authors wish to thank Danielle Osborne and Joseph Frascella for their discussion and intellectual contribution.

SUPPLEMENTARY MATERIAL

The Supplementary Material for this article can be found online at: <https://www.frontiersin.org/articles/10.3389/fphar.2022.910535/full#supplementary-material>

- Barraco, R. A., and Janusz, C. A. (1989). Respiratory Effects of 5'-ethylcarboxamidoadenosine, an Analog of Adenosine, Following Microinjections into the Nucleus Tractus Solitarius of Rats. *Brain Res.* 480, 360–364. doi:10.1016/0006-8993(89)90208-4
- Boison, D., Scheurer, L., Zumsteg, V., Rüllicke, T., Litynski, P., Fowler, B., et al. (2002). Neonatal Hepatic Steatosis by Disruption of the Adenosine Kinase Gene. *Proc. Natl. Acad. Sci. U. S. A.* 99, 6985–6990. doi:10.1073/pnas.092642899
- Boison, D. (2012). Adenosine Dysfunction in Epilepsy. *Glia* 60, 1234–1243. doi:10.1002/glia.22285
- Bonan, C. D., Walz, R., Pereira, G. S., Worm, P. V., Battastini, A. M., Cavalheiro, E. A., et al. (2000). Changes in Synaptosomal Ectonucleotidase Activities in Two Rat Models of Temporal Lobe Epilepsy. *Epilepsy Res.* 39, 229–238. doi:10.1016/s0920-1211(00)00095-4
- Bruno, A. N., Oses, J. P., Amaral, O., Coitinho, A., Bonan, C. D., Battastini, A. M., et al. (2003). Changes in Nucleotide Hydrolysis in Rat Blood Serum Induced by Pentylentetrazol-Kindling. *Brain Res. Mol. Brain Res.* 114, 140–145. doi:10.1016/s0169-328x(03)00168-2
- Buzsáki, G., and Wang, X. J. (2012). Mechanisms of Gamma Oscillations. *Annu. Rev. Neurosci.* 35, 203–225. doi:10.1146/annurev-neuro-062111-150444
- Buzsáki, G., Anastassiou, C. A., and Koch, C. (2012). The Origin of Extracellular Fields and Currents—EEG, ECoG, LFP and Spikes. *Nat. Rev. Neurosci.* 13, 407–420. doi:10.1038/nrn3241
- Canas, P. M., Porciúncula, L. O., Simões, A. P., Augusto, E., Silva, H. B., Machado, N. J., et al. (2018). Neuronal Adenosine A_{2A} Receptors Are Critical Mediators of Neurodegeneration Triggered by Convulsions. *eNeuro* 5, ENEURO.0385-18.2018. doi:10.1523/ENEURO.0385-18.2018
- Carmo, M., Gonçalves, F. Q., Canas, P. M., Oses, J. P., Fernandes, F. D., Duarte, F. V., et al. (2019). Enhanced ATP Release and CD73-Mediated Adenosine Formation Sustain Adenosine A_{2A} Receptor Over-activation in a Rat Model of Parkinson's Disease. *Br. J. Pharmacol.* 176, 3666–3680. doi:10.1111/bph.14771

- Chen, J. F., and Cunha, R. A. (2020). The Belated US FDA Approval of the Adenosine A_{2A} Receptor Antagonist Istradefylline for Treatment of Parkinson's Disease. *Purinergic Signal* 16, 167–174. doi:10.1007/s11302-020-09694-2
- Chen, J. F., Eltzschig, H. K., and Fredholm, B. B. (2013). Adenosine Receptors as Drug Targets-What Are the Challenges? *Nat. Rev. Drug Discov.* 12, 265–286. doi:10.1038/nrd3955
- Chen, J. F., Lee, C. F., and Chern, Y. (2014). Adenosine Receptor Neurobiology: Overview. *Int. Rev. Neurobiol.* 119, 1–49. doi:10.1016/B978-0-12-801022-8.00001-5
- Cognato, G. P., Agostinho, P. M., Hockemeyer, J., Müller, C. E., Souza, D. O., and Cunha, R. A. (2010). Caffeine and an Adenosine A(2A) Receptor Antagonist Prevent Memory Impairment and Synaptotoxicity in Adult Rats Triggered by a Convulsive Episode in Early Life. *J. Neurochem.* 112, 453–462. doi:10.1111/j.1471-4159.2009.06465.x
- Costenla, A. R., Diógenes, M. J., Canas, P. M., Rodrigues, R. J., Nogueira, C., Maroco, J., et al. (2011). Enhanced Role of Adenosine A(2A) Receptors in the Modulation of LTP in the Rat hippocampus upon Ageing. *Eur. J. Neurosci.* 34, 12–21. doi:10.1111/j.1460-9568.2011.07719.x
- Cunha, R. A., and Ribeiro, J. A. (2000). Purinergic Modulation of [(3)H]GABA Release from Rat Hippocampal Nerve Terminals. *Neuropharmacology* 39, 1156–1167. doi:10.1016/S0028-3908(99)00237-3
- Cunha, R. A. (2016). How Does Adenosine Control Neuronal Dysfunction and Neurodegeneration? *J. Neurochem.* 139, 1019–1055. doi:10.1111/jnc.13724
- Derera, I. D., Delisle, B. P., and Smith, B. N. (2017). Functional Neuroplasticity in the Nucleus Tractus Solitarius and Increased Risk of Sudden Death in Mice with Acquired Temporal Lobe Epilepsy. *eNeuro* 4, ENEURO.0319-17.2017. doi:10.1523/ENEURO.0319-17.2017
- Devinsky, O., Hesdorffer, D. C., Thurman, D. J., Lhatoo, S., and Richerson, G. (2016). Sudden Unexpected Death in Epilepsy: Epidemiology, Mechanisms, and Prevention. *Lancet Neurol.* 15, 1075–1088. doi:10.1016/S1474-4422(16)30158-2
- Devinsky, O. (2011). Sudden, Unexpected Death in Epilepsy. *N. Engl. J. Med.* 365, 1801–1811. doi:10.1056/NEJMra1010481
- Dunwiddie, T. V., and Masino, S. A. (2001). The Role and Regulation of Adenosine in the Central Nervous System. *Annu. Rev. Neurosci.* 24, 31–55. doi:10.1146/annurev.neuro.24.1.31
- During, M. J., and Spencer, D. D. (1992). Adenosine: a Potential Mediator of Seizure Arrest and Postictal Refractoriness. *Ann. Neurol.* 32, 618–624. doi:10.1002/ana.410320504
- El Yacoubi, M., Ledent, C., Parmentier, M., Costentin, J., and Vaugeois, J. M. (2009). Adenosine A_{2A} Receptor Deficient Mice Are Partially Resistant to Limbic Seizures. *Naunyn Schmiedeb. Arch. Pharmacol.* 380, 223–232. doi:10.1007/s00210-009-0426-8
- Faingold, C. L., Randall, M., and Kommajosyula, S. P. (2016). Susceptibility to Seizure-Induced Sudden Death in DBA/2 Mice Is Altered by Adenosine. *Epilepsy Res.* 124, 49–54. doi:10.1016/j.eplepsyres.2016.05.007
- Fredholm, B. B., IJzerman, A. P., Jacobson, K. A., Klotz, K. N., and Linden, J. (2001). International Union of Pharmacology. XXV. Nomenclature and Classification of Adenosine Receptors. *Pharmacol. Rev.* 53, 527–552.
- Fredholm, B. B., Chen, J. F., Masino, S. A., and Vaugeois, J. M. (2005). Actions of Adenosine at its Receptors in the CNS: Insights from Knockouts and Drugs. *Annu. Rev. Pharmacol. Toxicol.* 45, 385–412. doi:10.1146/annurev.pharmtox.45.120403.095731
- Fukuda, M., Suzuki, Y., Hino, H., and Ishii, E. (2012). Over-activation of Adenosine A(2A) Receptors and Sudden Unexpected Death in Epilepsy. *Epilepsy Behav.* 23, 387–388. doi:10.1016/j.yebeh.2011.12.022
- Gao, M., Liu, C. L., Yang, S., Jin, G. Z., Bunney, B. S., and Shi, W. X. (2007). Functional Coupling between the Prefrontal Cortex and Dopamine Neurons in the Ventral Tegmental Area. *J. Neurosci.* 27, 5414–5421. doi:10.1523/JNEUROSCI.1318-04.2004
- Gomez-Castro, F., Zappettini, S., Pressey, J. C., Silva, C. G., Russeau, M., Gervasi, N., et al. (2021). Convergence of Adenosine and GABA Signaling for Synapse Stabilization during Development. *Science* 374, eabk2055. doi:10.1126/science.abk2055
- Gonçalves, F. Q., Lopes, J. P., Silva, H. B., Lemos, C., Silva, A. C., Gonçalves, N., et al. (2019). Synaptic and Memory Dysfunction in a β -amyloid Model of Early Alzheimer's Disease Depends on Increased Formation of ATP-Derived Extracellular Adenosine. *Neurobiol. Dis.* 132, 104570. doi:10.1016/j.nbd.2019.104570
- He, X., Chen, F., Zhang, Y., Gao, Q., Guan, Y., Wang, J., et al. (2020). Upregulation of Adenosine A_{2A} Receptor and Downregulation of GLT1 Is Associated with Neuronal Cell Death in Rasmussen's Encephalitis. *Brain Pathol.* 30, 246–260. doi:10.1111/bpa.12770
- Hirsch, L. J. (2010). Is Sudden Unexpected Death in Epilepsy Due to Postictal Brain Shutdown? *Ann. Neurol.* 68, 773–775. doi:10.1002/ana.22242
- Insel, N., Patron, L. A., Hoang, L. T., Nematollahi, S., Schimanski, L. A., Lipa, P., et al. (2012). Reduced Gamma Frequency in the Medial Frontal Cortex of Aged Rats during Behavior and Rest: Implications for Age-Related Behavioral Slowing. *J. Neurosci.* 32, 16331–16344. doi:10.1523/JNEUROSCI.1577-12.2012
- Kaufman, K. R., and Sachdeo, R. C. (2003). Caffeinated Beverages and Decreased Seizure Control. *Seizure* 12, 519–521. doi:10.1016/S1059-1311(03)00048-7
- Kerkhofs, A., Canas, P. M., Timmerman, A. J., Heistek, T. S., Real, J. I., Xavier, C., et al. (2018). Adenosine A_{2A} Receptors Control Glutamatergic Synaptic Plasticity in Fast Spiking Interneurons of the Prefrontal Cortex. *Front. Pharmacol.* 9, 133. doi:10.3389/fphar.2018.00133
- Kirk, I. P., and Richardson, P. J. (1994). Adenosine A_{2A} Receptor-Mediated Modulation of Striatal [3H]GABA and [3H]acetylcholine Release. *J. Neurochem.* 62, 960–966. doi:10.1046/j.1471-4159.1994.62030960.x
- Kommajosyula, S. P., Randall, M. E., and Faingold, C. L. (2016). Inhibition of Adenosine Metabolism Induces Changes in Post-ictal Depression, Respiration, and Mortality in Genetically Epilepsy Prone Rats. *Epilepsy Res.* 119, 13–19. doi:10.1016/j.eplepsyres.2015.11.001
- Kuo, J., Zhao, W., Li, C. S., Kennedy, J. D., and Seyal, M. (2016). Postictal Immobility and Generalized EEG Suppression Are Associated with the Severity of Respiratory Dysfunction. *Epilepsia* 57, 412–417. doi:10.1111/epi.13312
- Li, R., and Buchanan, G. F. (2019). Scurrying to Understand Sudden Expected Death in Epilepsy: Insights From Animal Models. *Epilepsy Curr.* 19, 390–396. doi:10.1177/1535759719874787
- Li, W., Silva, H. B., Real, J., Wang, Y. M., Rial, D., Li, P., et al. (2015). Inactivation of Adenosine A_{2A} Receptors Reverses Working Memory Deficits at Early Stages of Huntington's Disease Models. *Neurobiol. Dis.* 79, 70–80. doi:10.1016/j.nbd.2015.03.030
- Maguire, M. J., Jackson, C. F., Marson, A. G., and Nolan, S. J. (2016). Treatments for the Prevention of Sudden Unexpected Death in Epilepsy (SUDEP). *Cochrane Database Syst. Rev.* 7, CD011792. doi:10.1002/14651858.CD011792.pub2
- Masino, S. A., Kawamura, M., Jr., and Ruskin, D. N. (2014). Adenosine Receptors and Epilepsy: Current Evidence and Future Potential. *Int. Rev. Neurobiol.* 119, 233–255. doi:10.1016/B978-0-12-801022-8.00011-8
- Massey, C. A., Sowers, L. P., Dlouhy, B. J., and Richerson, G. B. (2014). Mechanisms of Sudden Unexpected Death in Epilepsy: The Pathway to Prevention. *Nat. Rev. Neurol.* 10, 271–282. doi:10.1038/nrneurol.2014.64
- Massimini, M., Huber, R., Ferrarelli, F., Hill, S., and Tononi, G. (2004). The Sleep Slow Oscillation as a Traveling Wave. *J. Neurosci.* 24, 6862–6870. doi:10.1523/JNEUROSCI.1318-04.2004
- Minic, Z., O'Leary, D. S., and Scislo, T. J. (2015). NTS Adenosine A_{2A} Receptors Inhibit the Cardiopulmonary Chemoreflex Control of Regional Sympathetic Outputs via a GABAergic Mechanism. *Am. J. Physiol. Heart Circ. Physiol.* 309, H185–H197. doi:10.1152/ajpheart.00838.2014
- Nicolaidis, R., Bruno, A. N., Sarkis, J. J., and Souza, D. O. (2005). Increase of Adenine Nucleotide Hydrolysis in Rat Hippocampal Slices after Seizures Induced by Quinolinic Acid. *Neurochem. Res.* 30, 385–390. doi:10.1007/s11064-005-2613-4
- O'Brien, D. R. (1988). The Adenosine Hypothesis of Epilepsy. *Med. Hypotheses* 27, 281–284. doi:10.1016/0306-9877(88)90007-2
- Palchykova, S., Winsky-Sommerer, R., Shen, H. Y., Boison, D., Gerling, A., and Tobler, I. (2010). Manipulation of Adenosine Kinase Affects Sleep Regulation in Mice. *J. Neurosci.* 30, 13157–13165. doi:10.1523/JNEUROSCI.1359-10.2010
- Pansani, A. P., Colugnati, D. B., Scorza, C. A., de Almeida, A. C., Cavalheiro, E. A., and Scorza, F. A. (2016). Furthering Our Understanding of SUDEP: The Role of Animal Models. *Expert Rev. Neurother.* 16, 561–572. doi:10.1586/14737175.2016.1169925
- Patodia, S., Paradiso, B., Garcia, M., Ellis, M., Diehl, B., Thom, M., et al. (2020). Adenosine Kinase and Adenosine Receptors A₁ R and A_{2A} R in Temporal Lobe

- Epilepsy and Hippocampal Sclerosis and Association with Risk Factors for SUDEP. *Epilepsia* 61, 787–797. doi:10.1111/epi.16487
- Phillis, J. W., Scislo, T. J., and O'Leary, D. S. (1997). Purines and the Nucleus Tractus Solitarius: Effects on Cardiovascular and Respiratory Function. *Clin. Exp. Pharmacol. Physiol.* 24, 738–742. doi:10.1111/j.1440-1681.1997.tb02124.x
- Pietersen, A. N., Lancaster, D. M., Patel, N., Hamilton, J. B., and Vreugdenhil, M. (2009). Modulation of Gamma Oscillations by Endogenous Adenosine through A1 and A2A Receptors in the Mouse hippocampus. *Neuropharmacology* 56, 481–492. doi:10.1016/j.neuropharm.2008.10.001
- Rebola, N., Pinheiro, P. C., Oliveira, C. R., Malva, J. O., and Cunha, R. A. (2003). Subcellular Localization of Adenosine A(1) Receptors in Nerve Terminals and Synapses of the Rat hippocampus. *Brain Res.* 987, 49–58. doi:10.1016/s0006-8993(03)03247-5
- Rebola, N., Coelho, J. E., Costenla, A. R., Lopes, L. V., Parada, A., Oliveira, C. R., et al. (2003). Decrease of Adenosine A1 Receptor Density and of Adenosine Neuromodulation in the hippocampus of Kindled Rats. *Eur. J. Neurosci.* 18, 820–828. doi:10.1046/j.1460-9568.2003.02815.x
- Rebola, N., Canas, P. M., Oliveira, C. R., and Cunha, R. A. (2005). Different Synaptic and Subsynaptic Localization of Adenosine A2A Receptors in the hippocampus and Striatum of the Rat. *Neuroscience* 132, 893–903. doi:10.1016/j.neuroscience.2005.01.014
- Rebola, N., Rodrigues, R. J., Lopes, L. V., Richardson, P. J., Oliveira, C. R., and Cunha, R. A. (2005). Adenosine A1 and A2A Receptors Are Co-expressed in Pyramidal Neurons and Co-localized in Glutamatergic Nerve Terminals of the Rat hippocampus. *Neuroscience* 133, 79–83. doi:10.1016/j.neuroscience.2005.01.054
- Rebola, N., Porciúncula, L. O., Lopes, L. V., Oliveira, C. R., Soares-da-Silva, P., and Cunha, R. A. (2005). Long-term Effect of Convulsive Behavior on the Density of Adenosine A1 and A2A Receptors in the Rat Cerebral Cortex. *Epilepsia* 46 Suppl 5, 159–165. doi:10.1111/j.1528-1167.2005.01026.x
- Reis, S. L., Silva, H. B., Almeida, M., Cunha, R. A., Simões, A. P., and Canas, P. M. (2019). Adenosine A1 and A2A Receptors Differently Control Synaptic Plasticity in the Mouse Dorsal and Ventral hippocampus. *J. Neurochem.* 151, 227–237. doi:10.1111/jnc.14816
- Rombo, D. M., Newton, K., Nissen, W., Badurek, S., Horn, J. M., Minichiello, L., et al. (2015). Synaptic Mechanisms of Adenosine A2A Receptor-Mediated Hyperexcitability in the hippocampus. *Hippocampus* 25, 566–580. doi:10.1002/hipo.22392
- Ryvlin, P., Nashef, L., Lhatoo, S. D., Bateman, L. M., Bird, J., Bleasel, A., et al. (2013). Incidence and Mechanisms of Cardiorespiratory Arrests in Epilepsy Monitoring Units (MORTEMUS): a Retrospective Study. *Lancet Neurol.* 12, 966–977. doi:10.1016/S1474-4422(13)70214-X
- Samsonsen, C., Bräthen, G., Reimers, A., Helde, G., and Brodtkorb, E. (2013). Is Dietary Caffeine Involved in Seizure Precipitation? *Epilepsy Behav.* 28, 147–150. doi:10.1016/j.jybeh.2013.05.003
- Sandau, U. S., Colino-Oliveira, M., Jones, A., Saleumvong, B., Coffman, S. Q., Liu, L., et al. (2016). Adenosine Kinase Deficiency in the Brain Results in Maladaptive Synaptic Plasticity. *J. Neurosci.* 36, 12117–12128. doi:10.1523/JNEUROSCI.2146-16.2016
- Saransaari, P., and Oja, S. S. (2005). GABA Release Modified by Adenosine Receptors in Mouse Hippocampal Slices under Normal and Ischemic Conditions. *Neurochem. Res.* 30, 467–473. doi:10.1007/s11064-005-2682-4
- Scheffer, I. E., and Nabhout, R. (2019). SCN1A-related Phenotypes: Epilepsy and beyond. *Epilepsia* 60 Suppl 3, S17–S24. doi:10.1111/epi.16386
- Sebastião, A. M., and Ribeiro, J. A. (2009). Adenosine Receptors and the Central Nervous System. *Handb. Exp. Pharmacol.* 193, 471–534. doi:10.1007/978-3-540-89615-9_16
- Seo, S., Song, Y., Gu, S. M., Min, H. K., Hong, J. T., Cha, H. J., et al. (2020). D-limonene Inhibits Pentylenetetrazole-Induced Seizure via Adenosine A2A Receptor Modulation on GABAergic Neuronal Activity. *Int. J. Mol. Sci.* 21. doi:10.3390/ijms21239277
- Shen, H. Y., Coelho, J. E., Ohtsuka, N., Canas, P. M., Day, Y. J., Huang, Q. Y., et al. (2008). A Critical Role of the Adenosine A2A Receptor in Extrastriatal Neurons in Modulating Psychomotor Activity as Revealed by Opposite Phenotypes of Striatum and Forebrain A2A Receptor Knock-Outs. *J. Neurosci.* 28, 2970–2975. doi:10.1523/JNEUROSCI.5255-07.2008
- Shen, H. Y., Li, T., and Boison, D. (2010). A Novel Mouse Model for Sudden Unexpected Death in Epilepsy (SUDEP): Role of Impaired Adenosine Clearance. *Epilepsia* 51, 465–468. doi:10.1111/j.1528-1167.2009.02248.x
- Shen, H. Y., Sun, H., Hanthorn, M. M., Zhi, Z., Lan, J. Q., Poulsen, D. J., et al. (2014). Overexpression of Adenosine Kinase in Cortical Astrocytes and Focal Neocortical Epilepsy in Mice. *J. Neurosurg.* 120, 628–638. doi:10.3171/2013.10.JNS13918
- Shen, H. Y., van Vliet, E. A., Bright, K. A., Hanthorn, M., Lytle, N. K., Gorter, J., et al. (2015). Glycine Transporter 1 Is a Target for the Treatment of Epilepsy. *Neuropharmacology* 99, 554–565. doi:10.1016/j.neuropharm.2015.08.031
- Shorvon, S., and Tomson, T. (2011). Sudden Unexpected Death in Epilepsy. *Lancet* 378, 2028–2038. doi:10.1016/S0140-6736(11)60176-1
- Simões, A. P., Machado, N. J., Gonçalves, N., Kaster, M. P., Simões, A. T., Nunes, A., et al. (2016). Adenosine A2A Receptors in the Amygdala Control Synaptic Plasticity and Contextual Fear Memory. *Neuropsychopharmacology* 41, 2862–2871. doi:10.1038/npp.2016.98
- Sperling, M. R. (2001). Sudden Unexplained Death in Epilepsy. *Epilepsy Curr.* 1, 21–23. doi:10.1046/j.1535-7597.2001.00012.x
- Stöllberger, C., and Finsterer, J. (2004). Cardiorespiratory Findings in Sudden Unexplained/unexpected Death in Epilepsy (SUDEP). *Epilepsy Res.* 59, 51–60. doi:10.1016/j.eplepsyres.2004.03.008
- Surges, R., Thijs, R. D., Tan, H. L., and Sander, J. W. (2009). Sudden Unexpected Death in Epilepsy: Risk Factors and Potential Pathomechanisms. *Nat. Rev. Neurol.* 5, 492–504. doi:10.1038/nrneurol.2009.118
- Tescarollo, F. C., Rombo, D. M., DeLiberto, L. K., Fedele, D. E., Alharfoush, E., Tomé, Á. R., et al. (2020). Role of Adenosine in Epilepsy and Seizures. *J. Caffeine Adenosine Res.* 10, 45–60. doi:10.1089/caff.2019.0022
- Tetzlaff, W., Schubert, P., and Kreutzberg, G. W. (1987). Synaptic and Extrasynaptic Localization of Adenosine Binding Sites in the Rat hippocampus. *Neuroscience* 21, 869–875. doi:10.1016/0306-4522(87)90043-1
- Tu, E., Bagnall, R. D., Duflou, J., and Semsarian, C. (2011). Post-mortem Review and Genetic Analysis of Sudden Unexpected Death in Epilepsy (SUDEP) Cases. *Brain Pathol.* 21, 201–208. doi:10.1111/j.1750-3639.2010.00438.x
- Wenzel, M., Hamm, J. P., Peterka, D. S., and Yuste, R. (2017). Reliable and Elastic Propagation of Cortical Seizures *In Vivo*. *Cell Rep.* 19, 2681–2693. doi:10.1016/j.celrep.2017.05.090
- Wieraszko, A., Goldsmith, G., and Seyfried, T. N. (1989). Stimulation-dependent Release of Adenosine Triphosphate from Hippocampal Slices. *Brain Res.* 485, 244–250. doi:10.1016/0006-8993(89)90567-2
- Williams, A. J., Zhou, C., and Sun, Q. Q. (2016). Enhanced Burst-Suppression and Disruption of Local Field Potential Synchrony in a Mouse Model of Focal Cortical Dysplasia Exhibiting Spike-Wave Seizures. *Front. Neural Circuits* 10, 93. doi:10.3389/fncir.2016.00093
- Wilson, C. G., Martin, R. J., Jaber, M., Abu-Shaweeh, J., Jafri, A., Haxhiu, M. A., et al. (2004). Adenosine A2A Receptors Interact with GABAergic Pathways to Modulate Respiration in Neonatal Piglets. *Respir. Physiol. Neurobiol.* 141, 201–211. doi:10.1016/j.resp.2004.04.012
- Zeraati, M., Mirnajafi-Zadeh, J., Fathollahi, Y., Namvar, S., and Rezvani, M. E. (2006). Adenosine A1 and A2A Receptors of Hippocampal CA1 Region Have Opposite Effects on Piriform Cortex Kindled Seizures in Rats. *Seizure* 15, 41–48. doi:10.1016/j.seizure.2005.10.006
- Zoccal, D. B., Furuya, W. I., Bassi, M., Colombari, D. S., and Colombari, E. (2014). The Nucleus of the Solitary Tract and the Coordination of Respiratory and Sympathetic Activities. *Front. Physiol.* 5, 238. doi:10.3389/fphys.2014.00238

Conflict of Interest: The authors declare that the research was conducted in the absence of any commercial or financial relationships that could be construed as a potential conflict of interest.

Publisher's Note: All claims expressed in this article are solely those of the authors and do not necessarily represent those of their affiliated organizations, or those of the publisher, the editors and the reviewers. Any product that may be evaluated in this article, or claim that may be made by its manufacturer, is not guaranteed or endorsed by the publisher.

Copyright © 2022 Shen, Baer, Gesese, Cook, Weltha, Coffman, Wu, Chen, Gao and Ji. This is an open-access article distributed under the terms of the Creative Commons Attribution License (CC BY). The use, distribution or reproduction in other forums is permitted, provided the original author(s) and the copyright owner(s) are credited and that the original publication in this journal is cited, in accordance with accepted academic practice. No use, distribution or reproduction is permitted which does not comply with these terms.



UTP Regulates the Cardioprotective Action of Transplanted Stem Cells Derived From Mouse Cardiac Adipose Tissue

Esteban Diaz Villamil, Lucas De Roeck, Marion Vanorlé and Didier Communi*

Institute of Interdisciplinary Research, IRIBHM, Université Libre de Bruxelles, Brussels, Belgium

OPEN ACCESS

Edited by:

Francisco Ciruela,
University of Barcelona, Spain

Reviewed by:

Paulo Correia-De-Sá,
University of Porto, Portugal
Mariachiara Zuccarini,
University of Studies G. d'Annunzio
Chieti and Pescara, Italy

*Correspondence:

Didier Communi
didier.communi@ulb.be,
orcid.org/0000-0003-1050-1493

Specialty section:

This article was submitted to
Experimental Pharmacology and Drug
Discovery,
a section of the journal
Frontiers in Pharmacology

Received: 28 March 2022

Accepted: 20 May 2022

Published: 15 June 2022

Citation:

Diaz Villamil E, De Roeck L, Vanorlé M
and Communi D (2022) UTP Regulates
the Cardioprotective Action of
Transplanted Stem Cells Derived From
Mouse Cardiac Adipose Tissue.
Front. Pharmacol. 13:906173.
doi: 10.3389/fphar.2022.906173

Adipose tissue is a source of stem cells with a high potential of differentiation for cell-based regenerative therapies. We previously identified mouse P2Y₂, an ATP and UTP nucleotide receptor, as a regulator of adipogenic and endothelial differentiation of cardiac adipose-derived stem cells (cADSC). We investigated here the potential involvement of P2Y₂ receptor in the cardioprotective action of undifferentiated cADSC transplantation in mouse ischemic heart. Transplantation of cADSC was realized in the periphery of the infarcted zone of ischemic heart, 3 days after left anterior descending artery ligation. A strong reduction of collagen stained area was observed 14 days after cADSC injection, compared to PBS injection. Interestingly, loss of P2Y₂ expression totally inhibits the ability of transplanted cADSC to reduce cardiac fibrosis. A detailed gene ontology enrichment analysis was realized by comparing RNA-sequencing data obtained for UTP-treated wild type cADSC and UTP-treated P2Y₂-null cADSC. We identified UTP target genes linked to extracellular matrix organization such as matrix metalloproteinases and various collagen types, UTP target genes related to macrophage chemotaxis and differentiation into pro-fibrotic foam cells, and a significant number of UTP target genes linked to angiogenesis regulation. More particularly, we showed that UTP regulated the secretion of CCL5, CXCL5, and CCL12 chemokines and serum amyloid apolipoprotein 3, in the supernatants of UTP-treated cADSC. Interestingly, CCL5 is reported as a key factor in post-infarction heart failure and in the reparative and angiogenic action of transplanted ADSC on ischemic tissue. We investigated then if a UTP-pretreatment of cADSC amplifies their effect on cardiac revascularization in mouse ischemic heart. Transplantation of cADSC was able to increase peri-infarct capillary density, 14 days after their injection. This beneficial effect on cardiac revascularization was enhanced by a UTP-pretreatment of cADSC before their transplantation, and not observed using P2Y₂-null cADSC. Our data support that the efficacy of transplanted cADSC can be regulated by the release of inflammatory mediators such as extracellular nucleotides in the ischemic site. The present study highlights the P2Y₂ receptor as a regulator of cADSC cardioprotective action, and as a potential target for the therapeutic use of undifferentiated cADSC in post-ischemic cardiac ischemia.

Keywords: P2Y receptors, adipose-derived adult stem cells, cardiac ischemia, extracellular nucleotides, cardioprotection

INTRODUCTION

Adipose-derived stem cells (ADSC) are now recognized as an ideal source for therapeutic applications due to their multidifferentiation capacity and low immunogenicity (Schenke-Layland et al., 2009). ADSC implanted in the myocardium after ischemic injury produce and release pro-angiogenic, anti-apoptotic and anti-inflammatory cytokines and growth factors (Lévy et al., 2013; Zhao et al., 2017).

The therapeutic effects of ADSC are caused more by their secretory potential than by their cardiac differentiation capacity and direct integration into damaged tissue (Gnecchi et al., 2008). It is thus essential to elucidate the paracrine mechanisms underlying tissue repair and regeneration after ADSC transplantation. Pretreatment of ADSC before transplantation with specific factors constitutes a major approach to improve ADSC cardioprotective therapeutic effects (Stubbs et al., 2012; Zhu et al., 2015). Nevertheless the optimization of the cardioprotective abilities of transplanted ADSC in myocardial infarction treatment remains a major issue. ADSC isolated from cardiac adipose tissue display a better potential to differentiate into multiple cardiovascular cells including cardiomyocytes, endothelial cells, and vascular smooth muscle cells *in vitro* than stem cells derived from other fat depots such as subcutaneous and visceral adipose tissues (Nagata et al., 2016).

Therapeutic treatments for myocardial infarction display a limited success in preventing the progression of left ventricular remodeling, which results in only a partial restoration of cardiac function (Zhu et al., 2015; Zhao et al., 2017). Many research studies and clinical trials have highlighted the ability of ADSC injection to reduce myocardial infarction, promote post-ischemic vascularization and improve cardiac function (Yang et al., 2013; Chen et al., 2014). The use of ADSC has reinforced the idea that stem cell transplantation is still a promising strategy of therapeutic revascularization developed for patients with myocardial infarction (MI) (Cai et al., 2009). The regulation of cardiac fibrosis as well as revascularization and restoration of blood flow are the basis of the used therapeutic interventions to myocardial ischemia. Therapy based on the use of adipose-derived stem cells has already been performed for tissue regeneration and revascularization. Their paracrine actions include pro-angiogenic and anti-apoptotic effects through the secretion of various cytokines (Nagata et al., 2016) and their efficacy has been already tested in clinical trials (Cai et al., 2009; Chen et al., 2014).

An important release of extracellular nucleotides by cardiomyocytes and cardiac endothelial cells has been reported during myocardial ischemia (Dutta et al., 2004) and could modulate the inflammatory and fibrotic response within the infarcted area. P2Y₂ receptor is an ubiquitously expressed ATP/UTP G-protein-coupled nucleotide receptor coupled to the phosphoinositide pathway (Lustig et al., 1993). P2Y₂ activation significantly reduces cardiomyocyte death induced by hypoxia and UTP administration to rats reduces infarct size (Yitzhaki et al., 2005). We demonstrated previously that loss of P2Y₄ receptor, another ATP/UTP nucleotide receptor, is associated with a protection against infarction and a decrease in

cardiac inflammation, fibrosis and permeability (Horckmans et al., 2015). Purinergic receptors are considered as key regulators of proliferation, differentiation, cell death, and engraftment of diverse stem cells (Glaser et al., 2012; Zippel et al., 2012; Kaebisch et al., 2015). We demonstrated the differential involvement of P2Y₂ and P2Y₄ receptors on adipogenic differentiation of mouse cardiac adipose-derived stem cells (cADSC) (Lemaire et al., 2017; Negri et al., 2019). More recently, we showed that UTP is a regulator of endothelial differentiation and angiogenic properties of cADSC (Vanorlé et al., 2021).

Therapeutic applications based on ADSC preconditioning with extracellular nucleotides may provide a new advance for cardiac tissue repair. In the present study, we investigated the potential role of P2Y₂ receptor in the cardioprotective action of transplanted undifferentiated cADSC in an *in vivo* model of mouse myocardial infarction.

METHODS

Animals

P2Y₂ knockout (KO) CD1/C57BL/6J mice were a kind gift from Dr. B. Koller (University of North Carolina, Chapel Hill, United States) (Homolya et al., 1999). 12- to 16-week-old male and female wild type (WT) and P2Y₂ KO mice were used randomly for cADSC isolation and ischemia experiments.

cADSC Isolation and Culture

cADSC were isolated from the stromal vascular fraction of wild type (WT) and P2Y₂ KO mouse cardiac adipose tissue and their purity was checked by flow cytometry as previously described (Nagata et al., 2016). The cardiac adipose tissue, located between the visceral pericardium and the epicardium (including epi- and pericardic fat depots) was freshly harvested. Adipose tissue was washed in phosphate-buffered saline (PBS) and minced, followed by a digestion in collagenase A (2.5 g/L) at 37°C for 45 min. The digested tissue was filtered through a 100 µm cell strainer (Corning) and centrifuged at 500 g for 5 min. The supernatant containing adipocytes and debris was discarded. A red blood cell lysis was performed on the pelleted cells by an osmotic shock using ammonium-chloride-potassium (ACK) lysing buffer containing 0.15 M ammonium chloride, 0.01 M potassium bicarbonate and 0.0001 M disodium EDTA. After a last centrifugation at 500 g for 5 min, the resultant pellet, named the stromal vascular fraction, was suspended in Dulbecco's modified Eagle's medium (DMEM, Gibco) supplemented with 10% fetal bovine serum and 1% penicillin-streptomycin, plated at a density of 5×10^4 per cm² and incubated at 37°C in a humidified 95% O₂/5% CO₂ atmosphere. cADSC were selected by their high plastic adhesion, non-adherent cells were removed after 24 h, and the culture medium was subsequently replaced every 2 days. The cADSC cultures were not stimulated or stimulated daily with UTP (100 µM) for 7 days in the DMEM medium described above. A fraction of cADSC was used to check their purity before transplantation by flow cytometry using CD90, C105, and CD44 markers, as previously described (Nagata et al., 2016).

Myocardial Infarction Model and Intra-Myocardial cADSC Injection

WT mice were anesthetized with a mixture of Dormazolam (midazolam, 5 mg/kg), Domitor (medetomidine hydrochloride, 0.5 mg/kg) and Fentadon (fentanyl, 0.05 mg/kg), intubated and mechanically ventilated (rate 130 stroke/min, tidal volume 0.13 ml). Optical magnification loop was used for better visualization of the operation field. A left side thoracotomy was performed between the third and the fourth rib, and the pericardium was incised. Once the heart was exposed, MI was induced by the permanent ligation of the left anterior descending artery (LAD) proximal to its bifurcation from the main stem. Successful performance of coronary occlusion was confirmed by blanching of the myocardium distal to the coronary ligation. The thoracic incision was then closed with a 5-0 silk suture at the muscle tissue and a 7-0 silk suture at the skin. An antagonist cocktail of Naloxon (naloxone hydrochloride, 1.2 mg/kg), Anexate (flumazenil, 0.5 mg/kg) and Atipam (atipamezole hydrochloride, 2.5 mg/kg) was finally administered to the mice to reverse the general anesthesia. An intraperitoneal injection of Temgesic (buprenorphine, 0.3 mg/kg) was administered after the surgery and the next morning. Three days after LAD, mice underwent a second thoracotomy, as described above. This was followed by intramyocardial cADSC injections. Briefly, cADSC cultured in DMEM for 7 days, untreated or stimulated daily with UTP (100 μ M), were detached with trypsin/EDTA and resuspended in PBS. These cells were then injected at a concentration of 10^4 cells/ μ l at 3 different sites along the infarct border zone with a final volume of 10 μ l at each site (3×10^5 cells/heart). Sham/control group mice underwent the same experimental procedure excepted that they were subjected only to PBS injection. 14 days after injection, hearts were perfused with PAF 4%, collected, fixed in PAF 4%, and either immersed in isopropanol 70% and embedded in paraffin or immersed in a 10%, 20%, and finally a 30% sucrose solution and embedded in Tissue-Tek OCT compound (Sakura Finetek) and frozen at -80°C .

Quantification of Fibrosis Area in Ischemic Hearts

Paraffin cross-sections (8 μ m) of infarcted hearts were cut, fixed in Bouin's solution (Sigma-Aldrich) and stained with Masson's trichrome (Sigma-Aldrich), according to the manufacturer's protocol. Sections were counterstained with hematoxyline and mounted. Images of whole hearts were acquired with NanoZoomer-SQ (Hamamatsu) at 0.23 μ m/pixel. Fibrosis was quantified as the relative area of the blue staining (collagen) on five sections per ischemic heart compared to the left ventricle surface, using ImageJ software.

Quantification of Vascular Density in Ischemic Hearts

The vascularity of the ischemic myocardium was assessed by staining with specific markers recognizing the presence of

capillaries and arterioles. Briefly, 8 μ m-thick heart cryosections were stained with an anti-isolectin B4 antibody—Alexa Fluor™ 647 conjugate (1/400 ON at 4°C) (Invitrogen, Merelbeke, Belgium), an anti- α -smooth muscle actin antibody—Cy3™ conjugate (1/400 1 h at RT) (Sigma-Aldrich, St. Louis, MO, United States) and Hoechst (1/2000 1 min at RT) (Thermo Scientific, Merelbeke, Belgium). The area of the infarct border zone was determined as the 0.5 mm region of histologically intact myocardium surrounding the infarct-related fibrocellular region. Capillary and arteriole density was quantified in this peri-infarct myocardium. The final data were expressed as the number of capillaries or arterioles ($<20 \mu$ m in diameter) per square millimeter, the percentage is referring to the ratio between control condition (PBS injection) and cADSC injection conditions. These analyses were performed using ImageJ software by examining 30 counting surfaces/field for capillary and arteriole density on a total of five sections per heart, at $\times 10$ magnification, in a blinded fashion. Sections were counterstained with Hoechst to visualize the entire population of cell nuclei within each myocardial section.

Image Acquisition of Transplanted Ischemic Hearts

Images were acquired at LiMiF (Université Libre de Bruxelles, Faculté de Médecine, Bruxelles, Belgique), on an Axio Observer Z1 inverted microscope (Zeiss) equipped with a Zeiss Axiocam 702 mono camera using a EC Plan NeoFluar $\times 10/0.3$ dry objective (Zeiss). The microscope is equipped with an HBO 100 light source. Three channels were recorded with narrow band-pass filter sets (Zeiss) #49 (ex. 335–383 nm, em. 420–470 nm), #43 (ex. 538–562 nm, em. 570–640 nm), and #50 (ex. 625–655 nm, em. 665–715 nm) used to visualize blue, red and far-red fluorochromes, respectively. Images of 2.3 pixels (Axiocam 702 m) were acquired and recorded as 16-bit czi files. The field of view is defined by the $\times 10$ objective resulting in 1.13 mm by 712.58 micron images. The pixel scaling results in 0.586 micron by 0.586 micron. Settings were kept identical for all conditions. Single plane images were displayed using Zen (Blue Edition) software (Zeiss) and exported as uncompressed TIF images.

RNA-Sequencing Experiments

RNA-sequencing experiments were performed on WT or P2Y₂ KO cADSCs cultured in DMEM for 7 days, untreated or treated every 24 h with UTP (100 μ M). RNA was extracted using the RNeasy Mini Kit (Qiagen) after cell lysis using TRI Reagent Solution (Invitrogen). 1 μ g/50 μ l of RNA was engaged and the quality was checked using a Bioanalyzer 2100 (Agilent technologies). RNA-sequencing experiments were performed on two different pools of RNA from two cADSC cultures per condition. Complementary DNA (cDNA) libraries were obtained using the TruSeq Stranded mRNA Library Prep kit (NuGen) following manufacturer recommendations. The multiplex libraries (18 pM) were loaded on flow cells and sequences were produced using a HiSeq PE Cluster Kit v4 and TruSeq SBS Kit v3-HS from a HiSeq 1500 (Illumina). Approximately 25

TABLE 1 | Specific primers for UTP target genes, P2Y receptor genes and Rpl32 gene. Specific primers for UTP target genes Ccl5, Cxcl5, Ccl12, and Saa3, and for P2ry2 and P2ry4 receptor genes, were used in qPCR experiments and normalized to Rpl32 mRNA level.

Gene	Forward primer sequence	Reverse primer sequence
Ccl5	5'-GCTGCTTTGCCTACCTCTCC-3'	5'-TCGAGTGACAAACACGACTGC-3'
Cxcl5	5'-CCTCCTTCTGGTTTTTCAGTTTAGC-3'	5'-GCATTCTGTTGCTGTTACAGCTG-3'
Ccl12	5'-AGTCCTCAGGTATTGGCTGG-3'	5'-CTTCCGGACGTGAATCTTCT-3'
Saa3	5'-GTTGACAGCCAAAGATGGGT-3'	5'-CCCGAGCATGGAAGTATTG-3'
P2ry2	5'-AGCCCTTGTACTGCGCAAAC-3'	5'-GAAGATATAGAGGCCACGACGTT-3'
P2ry4	5'-GCCCAAGTTCTGGAGATGGTG-3'	5'-GGTGGTTCATTGGCATTGG-3'
Rpl32	5'-GCACCAAGTCAGACCGATAT-3'	5'-CAGGATCTGGCCCTTGAAC-3'

million paired-end reads per sample were mapped against the mouse reference genome (GRCm38.p4/mm10) using STAR software to generate read alignments for each sample. Annotations Mus_musculus GRC38.87.gtf were obtained from ftp.Ensembl.org. After transcripts assembling, gene level counts were obtained using HTSeq.

A gene enrichment analysis was performed with DAVID software on the RNA-sequencing data to determine which biological processes were enriched for differentially expressed genes. Only genes with CPM > 0.5 and a fold change >2 or <0.5 were considered. The modified Fisher Exact *p*-value or EASE score was reported by the software and indicated as logarithmic *p*-value.

Quantitative Reverse-Transcription Polymerase Chain Reaction

Total mRNA was extracted from cADSC, cultured for 7 days in DMEM and untreated or treated daily with UTP (100 μ M), as described above. RNA samples were eluted with RNase-Free water and RNA concentration was quantified by NanoDrop. Reverse transcription was performed with 500 ng mRNA, 0.5 μ l random hexamers, 1 μ l dNTPs (10 mM), 4 μ l \times 5 First Strand Buffer (250 mM Tris-HCl, pH 8.3, 375 mM KCl, 15 mM MgCl₂), 2 μ l DTT (0.1 M), 1 μ l RNaseOUT ribonuclease inhibitor (40 U/ μ l), 1 μ l SuperScript II reverse transcriptase (200 U/ μ l) and RNase-Free water up to a volume of 20 μ l. Samples were incubated at 42°C for 50 min to synthesize cDNA and at 70°C for 10 min to stop the reaction. Quantitative polymerase chain reaction (qPCR) experiments were performed using 5 ng cDNA, specific primers (5 μ M) for UTP target genes and P2Y receptors, 2x KAPA SYBR FAST qPCR Master Mix [KAPA SYBR FAST DNA Polymerase, reaction buffer, dNTPs, SYBR Green I dye, and MgCl₂ (2.5 mM)], 50x KAPA SYBR FAST ROX Low and RNase-Free water up to a 20 μ l volume on a 7500 Fast Real-Time PCR System (Applied Biosystems). Expression values for each gene were normalized to the expression of the housekeeping gene Rpl32. Results were expressed as $2^{-\Delta\Delta C_t}$. The specific primers for Ccl5, Cxcl5, Ccl12, Saa3, and Rpl32 genes and for P2ry2 and P2ry4 genes are shown in **Table 1**.

ELISA Experiments

Supernatants from cADSC cultured in DMEM for 7 days, untreated or treated daily with UTP (100 μ M), were collected. CCL5, CXCL5, CCL12, and SAA3 protein levels were quantified

by ELISA following the manufacturer's procedure (R&D Systems). Total proteins were quantified using Pierce™ 660 nm Protein Assay Reagent (Thermo Scientific) supplemented with Ionic Detergent Compatibility Reagent (Thermo Scientific) to normalize ELISA results.

Statistical Analysis

All data are expressed as mean \pm SEM, and statistical analysis was performed with Prism Software (version 6; GraphPad, San Diego, CA, United States). Endpoint comparisons between 2 groups were performed using unpaired 2-tailed Student's *t*-test. For multiple comparisons, false discovery rate according Benjamini-Hochberg was applied to control for type I false positive errors, FDR was set to 0.05. For parallel repeated-measures studies, 2-way ANOVA was used with Bonferroni post-hoc evaluation to determine the significance for individual time points. A 2-tailed *p* < 0.05 was considered as significant.

RESULTS

Role of P2Y₂ Receptor in the Ability of Transplanted cADSC to Reduce Post-ischemic Cardiac Fibrosis

Stromal cells were isolated from cardiac adipose tissue of WT and P2Y₂ KO mice. Non-adherent cells were removed 24 h after the plastic adherence step. Flow cytometry experiments were performed with adherent stromal cells using CD90, CD105, and CD44 as markers of mesenchymal stem cells, and CD26 as fibroblast marker. More than 90% of isolated cells were CD90⁺ CD105⁺ CD44⁺ CD26⁻, and they were cultured for 7 days in proliferation medium (data not shown). These cADSC were then counted for intramyocardial injections (3 \times 10⁵ μ l containing 10⁵ cells each). LAD ligation was performed on WT mice and intramyocardial injections of PBS (control), WT cADSC and P2Y₂ KO cADSC were performed in the peri-infarct border zone, 3 days after LAD ligation. 14 days after injection, hearts were harvested and embedded in paraffin for further analysis.

Five heart sections per transplanted ischemic heart were stained with Masson's trichrome to evaluate cardiac fibrosis. Fibrosis was quantified by calculating the area stained blue, expressed as a percentage of the left ventricle's total area (**Figures 1A,B**). We observed a strong reduction of cardiac

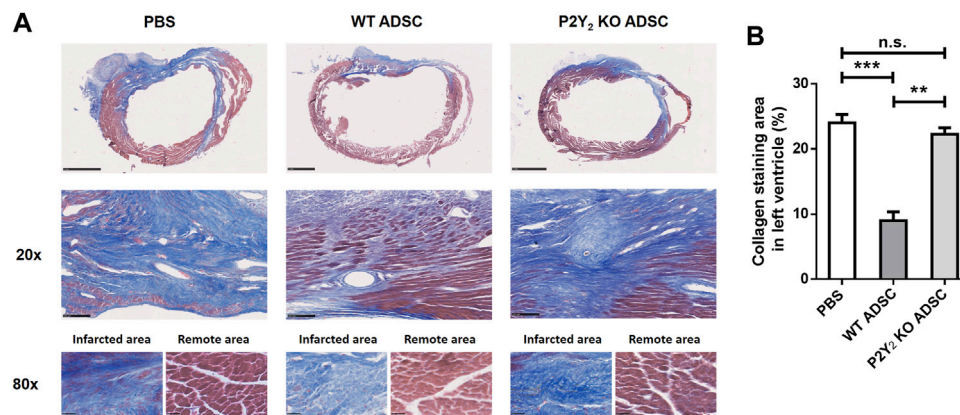


FIGURE 1 | Role of P2Y₂ receptor in the transplanted cADSC ability to reduce post-ischemic cardiac fibrosis. **(A)** Representative Masson's trichrome staining of cardiac fibrosis in transplanted ischemic hearts. PBS, WT cADSC or P2Y₂ KO cADSC were injected in the peri-infarct zone of ischemic hearts, 3 days after LAD ligation. 14 days after injection, images of Masson's trichrome staining (in blue) in ischemic hearts were obtained for total heart (scale bar represents 1 mm), at ×20 magnification for the fibrotic area (scale bar represents 100 μm) and at ×80 magnification inside the infarcted and remote area regions (scale bar represents 25 μm) **(B)**. Quantification of fibrosis area normalized to total left ventricle area in ischemic hearts, 14 days after injection of PBS, WT cADSC or P2Y₂ KO cADSC. Fibrosis area was quantified as the relative surface of collagen blue staining on five sections per ischemic heart, quantified by color image analyzer ImageJ in left ventricle (LV) and expressed as percentages of total LV surface ($n = 3-5$). Data represent mean ± SEM. * $p < 0.05$; ** $p < 0.01$; *** $p < 0.001$, n.s., not significant.

fibrosis in ischemic heart transplanted with WT cADSC compared to mice injected with PBS. Collagen stained area was reduced from $24.0 \pm 1.3\%$ of left ventricle area in PBS-injected hearts to $9.0 \pm 1.3\%$ of left ventricle area in WT cADSC-injected hearts (decrease of $62.5 \pm 8.5\%$; mean ± SEM; ***: $p < 0.001$) (**Figure 1A**). Very interestingly this cardiac fibrosis reduction was not observed after transplantation of cADSC isolated from P2Y₂ KO mice (**Figures 1A,B**). Effectively collagen stained area observed in PBS-injected ischemic mice ($24.0 \pm 1.3\%$; mean ± SEM), was comparable after P2Y₂ KO cADSC transplantation ($22.3 \pm 1.0\%$; mean ± SEM). We observed comparable collagen blue staining for the fibrotic area of ischemic hearts injected with P2Y₂ KO cADSC and PBS-injected ischemic hearts (**Figure 1A**, ×20 magnification). Collagen stainings are shown inside the fibrotic and remote areas of ischemic hearts injected with PBS, WT cADSCs or P2Y₂ KO cADSC (**Figure 1A**, ×80 magnification).

The inhibitory effect of undifferentiated cADSC transplantation on post-ischemic cardiac fibrosis is thus dependent on their P2Y₂ receptor expression. Reduced cardiac fibrosis was observed without any required pretreatment of cADSC. The release of endogenous extracellular nucleotides currently observed during ischemia could thus regulate the cardioprotective action of transplanted cADSC through activation of P2Y₂ receptors expressed at their surface.

Identification of UTP Target Genes in Mouse cADSC

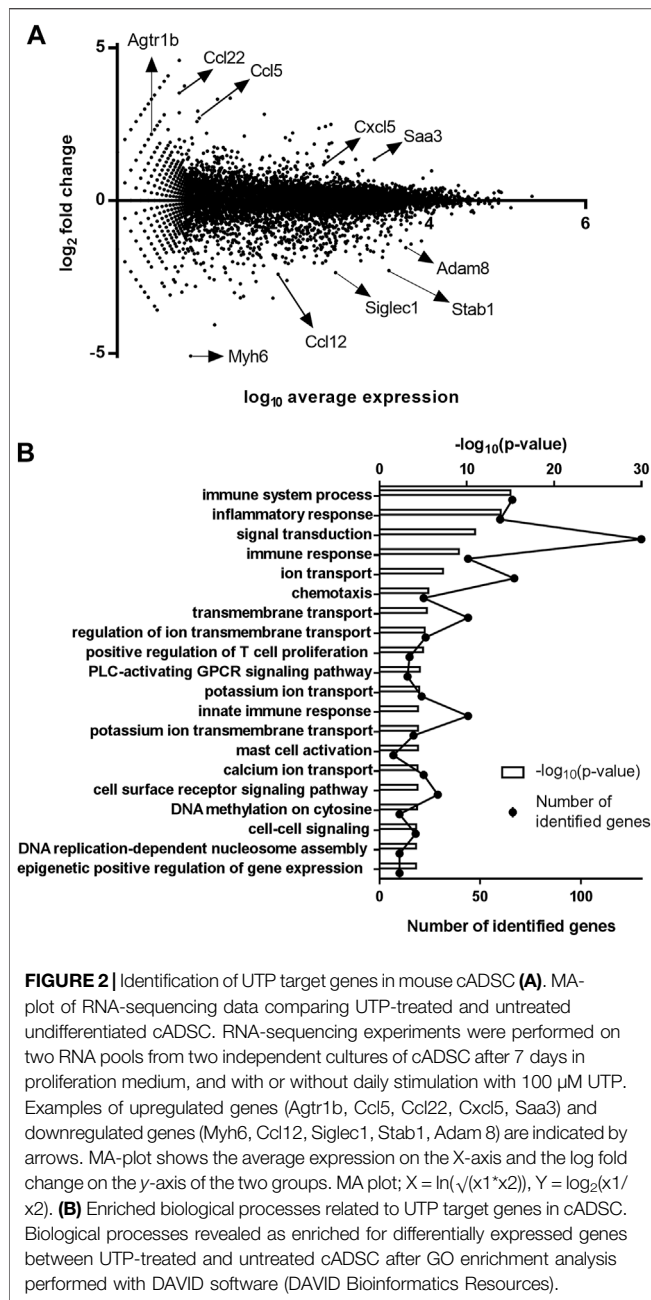
RNA-sequencing experiments were assessed on undifferentiated cADSC cells, unstimulated or treated daily with UTP (100 μM) during 7 days of culture in proliferation medium. RNA samples were extracted from two different cADSC cultures per condition and pooled for RNA-sequencing experiments. Among the 1,359

differentially regulated genes, 598 genes were upregulated by UTP (fold change > 2) and 761 were downregulated by UTP (fold change < 0.5). MA-plot representation provides an overview of regulated-gene distribution within two-sample comparison (**Figure 2A**). We observed inter alia upregulation of Ccl5, Ccl22, Cxcl5, and downregulation of Ccl12 chemokine genes by UTP in ADSC (**Figure 2A**). A gene ontology (GO) enrichment analysis with DAVID software on the RNA-sequencing data obtained from UTP-treated ADSC versus untreated ADSC revealed that several biological processes linked to innate immune response, inflammation, as well as signal/receptor transduction and transmembrane/ion transport were enriched (**Figure 2B**). The modified Fisher Exact p -value or EASE score was reported by the software and indicated as logarithmic p -value.

Detailed Analysis of Genes Regulated by UTP Through P2Y₂ Receptor Activation in Mouse cADSC

We have previously demonstrated differential involvement of both mouse P2Y₂ and P2Y₄ receptors for UTP and ATP, in cADSC adipogenic differentiation thanks to P2Y₂ and P2Y₄ knockout mice (Lemaire et al., 2017; Negri et al., 2019). The absence of a clear detection of membrane-bound P2Y₂ receptors remains a limitation. Our use of mouse monoclonal anti-P2Y₂ antibody (H-5) from Santa Cruz Biotechnology (sc-518121) at 1:500 dilution was previously unsuccessful in mouse cADSC (data not shown). A comparable weak staining of cADSC was obtained with phycoerythrin-conjugated m-IgGκ secondary antibody alone (sc-516141; Santa Cruz Biotechnology) (data not shown).

We decided to compare UTP-regulated genes in WT and P2Y₂ KO cADSC to identify more precisely genes and associated-biological processes specific of P2Y₂ activation in these cells,



and potentially linked to our cardiac fibrosis data using WT and P2Y₂ KO ADSC (Figure 1). UTP is used as a stimulating agent instead of ATP to avoid regulation of genes related to ADP or adenosine receptor activation after ATP degradation. We have not detected expression of P2Y₆ UDP receptor in cADSC (data not shown). A UTP-treatment during 7 days with UTP would thus activate only P2Y₂ and P2Y₄ receptors in cADSC.

RNA-sequencing experiments were performed using P2Y₂ KO cADSC, unstimulated or treated daily with UTP (100 μ M). UTP gene expression profile was compared in both WT and P2Y₂ KO cADSC, only genes with CPM >0.5 and a fold change >2 or <0.5 being considered. Among the 1,359 regulated genes identified in WT

cADSC (Figure 2A), we observed that 977 genes were no more regulated in P2Y₂ KO cADSC whereas 382 genes were still regulated by UTP in P2Y₂ KO cADSC. A detailed GO enrichment analysis was made for these 977 UTP target genes only identified in WT ADSC and not in P2Y₂ KO ADSC (Figure 3A). Besides the important number of genes involved in immune and inflammatory responses, GO analysis revealed enriched biological processes linked to multicellular organism development, cell differentiation and adhesion, angiogenesis and response to hypoxia (Figure 3A). Table 2 shows UTP target genes linked to processes moderately enriched but potentially related to our model of cardiac ischemia. Among the 977 UTP target genes, we identified genes linked to extracellular matrix organization and collagen catabolic process such as matrix metalloproteinases Mmp1b, Mmp9, and Mmp25 and collagen types Col10a1, Col17a1, and Col25a1, and genes related to macrophage chemotaxis such as Ccr7 chemokine receptor and colony-stimulating factor 1 receptor (Csflr) (Table 2). We also identified UTP target genes involved in macrophage differentiation into pro-fibrotic foam cell such as Csf2, macrophage scavenger receptor Msr1 and apolipoprotein B (ApoB), as well as genes linked to response to hypoxia such as Agtr1b, purinergic receptor P2X₂, adenosine A1 receptors and uncoupling protein Ucp3 (Table 2). Interestingly, we identified a significant number of UTP target genes linked to angiogenesis regulation such as Wnt7a, Ramp3, Mmp9, Nos3, and Adam8 (Table 2).

UTP Induces CCL5, CXCL5 and SAA3 Secretion and Inhibits CCL12 Secretion by cADSC

Among all the UTP-regulated genes, we studied further the up-regulation of three pro-angiogenic genes, Ccl5, Cxcl5, and Saa3, and the down-regulation of the pro-fibrotic chemokine Ccl12. We confirmed up-regulation of Ccl5, Cxcl5, and Saa3, and downregulation of Ccl12 mRNAs in response to UTP in cADSC by qPCR experiments (Figure 3B). CCL5, CXCL5, CCL12, and SAA3 protein levels were quantified by ELISA in the supernatants of UTP-treated or untreated undifferentiated cADSC. We observed that UTP treatment increased the release of CCL5, CXCL5, and SAA3, and decreased the release of CCL12 by cADSC (Figure 3C).

SAA3 is a key inflammatory adipocyte-derived factor which is the murine ortholog of human serum amyloid A promoting angiogenesis in many diseases. (Lv et al., 2016; Tannock et al., 2018) Interestingly, CCL5 chemokine was previously reported as a major regulator of ADSC migration and post-ischemic reparative capacities. (Kauts et al., 2013; Kimura et al., 2014) UTP-mediated release of CCL5, CXCL5, and SAA3 by cADSC, as well as the consistent number of UTP-regulated genes involved in angiogenesis regulation (Table 2), led us to investigate the potential action of UTP-treated cADSC transplantation on cardiac revascularization.

Effect of Transplanted UTP-Treated cADSC on Post-ischemic Cardiac Revascularization

WT and P2Y₂ KO cADSC were cultured without or with daily stimulation of UTP (100 μ M) for 7 days in proliferation medium.

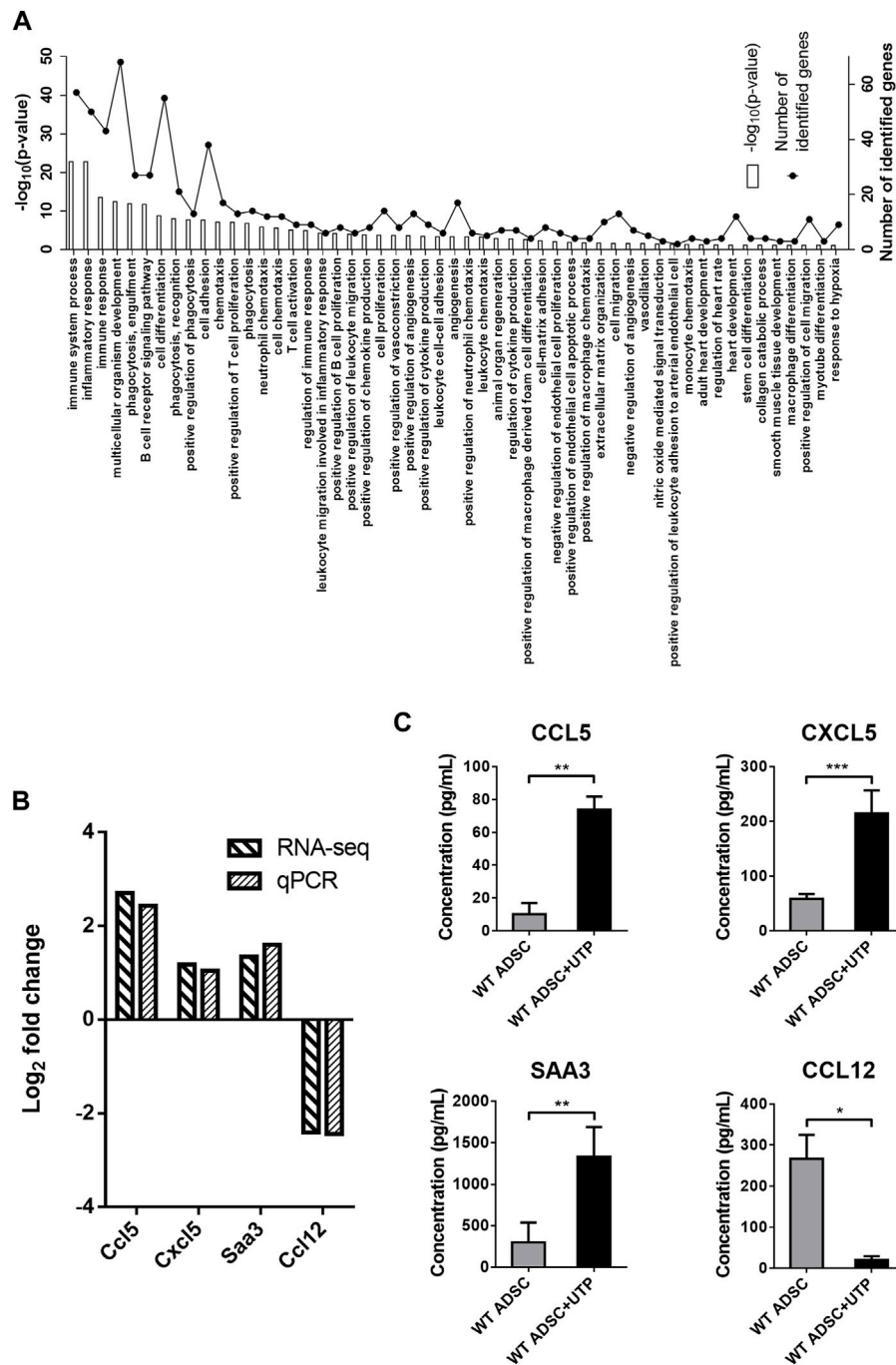


FIGURE 3 | Detailed analysis of genes regulated by UTP through P2Y₂ receptor activation in cADSC. **(A)** Enriched biological processes related to UTP target genes after comparison of RNA-sequencing data in WT and P2Y₂ KO cADSC. RNA-sequencing experiments were performed on two RNA pools from two independent cultures of WT and P2Y₂ KO cADSC after 7 days in proliferation medium and daily stimulated or not with 100 μ M UTP. Comparison of RNA-sequencing data identified 977 genes regulated by UTP only in WT ADSC and not in P2Y₂ KO cADSC. GO detailed analysis revealed various enriched biological processes related to the 977 UTP target genes. **(B)** Confirmation of specific UTP target genes by qPCR experiments. Ccl5, Cxcl5, and Saa3 mRNAs are upregulated, and Ccl12 mRNA is downregulated, in UTP-treated versus untreated cADSC in RNA-sequencing and qPCR experiments. Quantification of Ccl5, Cxcl5, Saa3, and Ccl12 mRNA level was performed by qPCR in at least six independent cADSC cultures and normalized to Rpl32 mRNA level. **(C)** UTP increases CCL5, CXCL5, and SAA3 release, and inhibits CCL12 release by cADSC. CCL5, CXCL5, SAA3, and CCL12 protein level was measured in the supernatants of cADSC cultures after 7 days in proliferation medium with or without daily stimulation with UTP 100 μ M. ELISA data were obtained for six to nine independent cADSC cultures. Values represent mean \pm SEM. * $p < 0.05$, ** $p < 0.01$ and *** $p < 0.001$.

TABLE 2 | Selection of genes regulated by UTP through P2Y₂ receptor activation in cADSC. RNA-sequencing data comparison of UTP target genes in WT and P2Y₂ KO cADSC, revealed 977 genes regulated by UTP only in WT ADSC and not in P2Y₂ KO cADSC. Several processes and associated UTP target genes potentially linked to the studied model of cardiac ischemia, were identified after a detailed GO analysis.

Gene symbol	Gene name	Ratio
UTP-regulated genes involved in extracellular matrix organization and collagen catabolic process		
Col17a1	Collagen type XVII. alpha 1 (Col17a1)	3.38
Mmp9	Matrix metalloproteinase 9 (Mmp9)	2.76
Col25a1	Collagen type XXV. alpha 1 (Col25a1)	2.00
Mmp1b	Matrix metalloproteinase 1b (interstitial collagenase) (Mmp1b)	2.00
Prtn3	proteinase 3 (Prtn3)	0.50
Adams19	A disintegrin-like and metalloproteinase (reprolysin type) with thrombospondin type 1 motif. 19 (Adams19)	0.48
Tgfb1	Transforming growth factor. beta induced (Tgfb1)	0.43
Mmp25	Matrix metalloproteinase 25 (Mmp25)	0.43
Tnf	Tumor necrosis factor (Tnf)	0.43
Col10a1	Collagen type X. alpha 1 (Col10a1)	0.19
Rxfp1	Relaxin/insulin-like family peptide receptor 1 (Rxfp1)	0.17
UTP-regulated genes involved in macrophage chemotaxis and macrophage-derived foam cell differentiation		
Csf2	Colony stimulating factor 2 (granulocyte-macrophage) (Csf2)	2.00
Apob	Apolipoprotein B (Apob)	2.00
Cebpe	CCAAT/enhancer binding protein (C/EBP). epsilon (Cebpe)	0.50
Spib	Spi-B transcription factor (Spi-1/PU.1 related) (Spib)	0.50
Pla2g5	Phospholipase A2. group V (Pla2g5)	0.50
Msr1	Macrophage scavenger receptor 1 (Msr1)	0.37
Csf1r	Colony stimulating factor 1 receptor (Csf1r)	0.37
C3ar1	Complement component 3a receptor 1 (C3ar1)	0.32
Ccr7	Chemokine (C-C motif) receptor 7 (Ccr7)	0.31
C5ar1	Complement component 5a receptor 1 (C5ar1)	0.26
UTP-regulated genes involved in the response to hypoxia		
Agtr1b	Angiotensin II receptor. type 1b (Agtr1b)	4.50
P2rx2	Purinergic receptor P2X. ligand-gated ion channel. 2 (P2rx2)	3.33
Chma4	Cholinergic receptor. nicotinic. alpha polypeptide 4 (Chma4)	2.78
Ascl2	Achaete-scute family bHLH transcription factor 2 (Ascl2)	2.00
Trh	Thyrotropin releasing hormone (Trh)	2.00
Ucp3	Uncoupling protein 3 (mitochondrial. proton carrier) (Ucp3)	2.00
Casp1	Caspase 1 (Casp1)	0.47
Adora1	Adenosine A1 receptor (Adora1)	0.44
Myb	Myeloblastosis oncogene (Myb)	0.42
UTP-regulated genes involved in the regulation of angiogenesis		
Wnt7a	Wingless-type MMTV integration site family. member 7A (Wnt7a)	4.14
Ramp3	Receptor (calcitonin) activity modifying protein 3 (Ramp3)	2.92
Mmp9	Matrix metalloproteinase 9 (Mmp9)	2.76
Nos3	Nitric oxide synthase 3. endothelial cell (Nos3)	2.07
Cnmd	Chondromodulin (Cnmd)	2.00
Il17f	Interleukin 17F (Il17f)	2.00
Nrxn3	Neurexin III (Nrxn3)	0.50
Shh	Sonic hedgehog (Shh)	0.50
Arhgap22	Rho GTPase activating protein 22 (Arhgap22)	0.49
Pik3r6	Phosphoinositide-3-kinase regulatory subunit 5 (Pik3r6)	0.47
Lepr	Leptin receptor (Lepr)	0.45
Hhex	Hematopoietically expressed homeobox (Hhex)	0.45
Cxcr3	Chemokine (C-X-C motif) receptor 3 (Cxcr3)	0.44
Plxdc1	Plexin domain containing 1 (Plxdc1)	0.44
Alox5	Arachidonate 5-lipoxygenase (Alox5)	0.43
Tgfb1	Transforming growth factor. beta induced (Tgfb1)	0.43
Tal1	T cell acute lymphocytic leukemia 1 (Tal1)	0.43
Cysltr1	Cysteinyl leukotriene receptor 1 (Cysltr1)	0.42
Cx3cr1	Chemokine (C-X3-C motif) receptor 1 (Cx3cr1)	0.41
Cysltr2	Cysteinyl leukotriene receptor 2 (Cysltr2)	0.40
Vav3	Vav 3 oncogene (Vav3)	0.39
Cd40	CD40 antigen (Cd40)	0.35
Adam8	A disintegrin and metalloproteinase domain 8 (Adam8)	0.34

(Continued on following page)

TABLE 2 | (Continued) Selection of genes regulated by UTP through P2Y₂ receptor activation in cADSC. RNA-sequencing data comparison of UTP target genes in WT and P2Y₂ KO cADSC, revealed 977 genes regulated by UTP only in WT ADSC and not in P2Y₂ KO cADSC. Several processes and associated UTP target genes potentially linked to the studied model of cardiac ischemia, were identified after a detailed GO analysis.

Gene symbol	Gene name	Ratio
Mir27b	microRNA 27b (Mir27b)	0.33
C3ar1	Complement component 3a receptor 1 (C3ar1)	0.32
Pik3cg	Phosphatidylinositol-4,5-bisphosphate 3-kinase catalytic subunit gamma (Pik3cg)	0.32
C5ar1	Complement component 5a receptor 1 (C5ar1)	0.26
Angptl3	Angiopoietin-like 3 (Angptl3)	0.25
C6	Complement component 6 (C6)	0.25
Thbs4	Thrombospondin 4 (Thbs4)	0.25
Ccl12	Chemokine (C-C motif) ligand 12 (Ccl12)	0.19

Flow cytometry experiments revealed a comparable amount, between 92% and 95%, of CD90⁺ CD105⁺ CD44⁺ CD26⁻ cells in all the cell cultures (data not shown). We have performed qPCR experiments to quantify P2Y₂ and P2Y₄ mRNA in wild type cADSC, after stimulation or not with 100 μ M during 7 days (**Figure 4A**). We observed a high level of expression of P2Y₂ mRNAs compared to weakly detected P2Y₄ receptor mRNAs, in cADSC after 7 days of culture in the proliferation medium (**Figure 4A**). We also observed that sustained stimulation with 100 μ M UTP during 7 days did not induce down-regulation of P2Y₂ receptor mRNAs (**Figure 4A**).

Intramyocardial injections of PBS (control), untreated WT or P2Y₂ KO cADSC, and UTP-treated WT or P2Y₂ KO cADSC were performed in ischemic mice, 3 days after LAD ligation. Immunofluorescent stainings using anti-isolectin B4 and anti- α -SMA antibodies were performed on heart sections, 14 days after cADSC injection, to quantify capillary and arteriole density respectively, in infarct border zone at different levels of the ischemic heart (**Figure 4B**). Analysis of peri-infarct microvasculature 14 days after cADSC injection revealed a higher capillary density in heart transplanted with untreated cADSC compared to PBS-injected mice (increase of $15.2 \pm 2.8\%$; mean \pm SEM; ***: $p < 0.001$) (**Figures 4C,D**). Capillary density was even more enhanced in heart transplanted with UTP-treated cADSC compared to PBS-injected mice (increase of $27.2 \pm 4.2\%$; mean \pm SEM; ***: $p < 0.001$) (**Figure 4D**). Interestingly, capillary density was similar in P2Y₂ KO cADSC-transplanted mice and in PBS-injected mice (**Figure 4D**). Moreover, the effect of UTP treatment on the capacity of cADSC to increase capillary density, was not observed using UTP-treated P2Y₂ KO cADSC (**Figure 4D**). No significant effect of UTP-treated or untreated ADSC transplantation was observed on arteriole density, defined by the number of α -SMA positive vessels with a diameter $< 20 \mu$ m (**Figures 4E,F**).

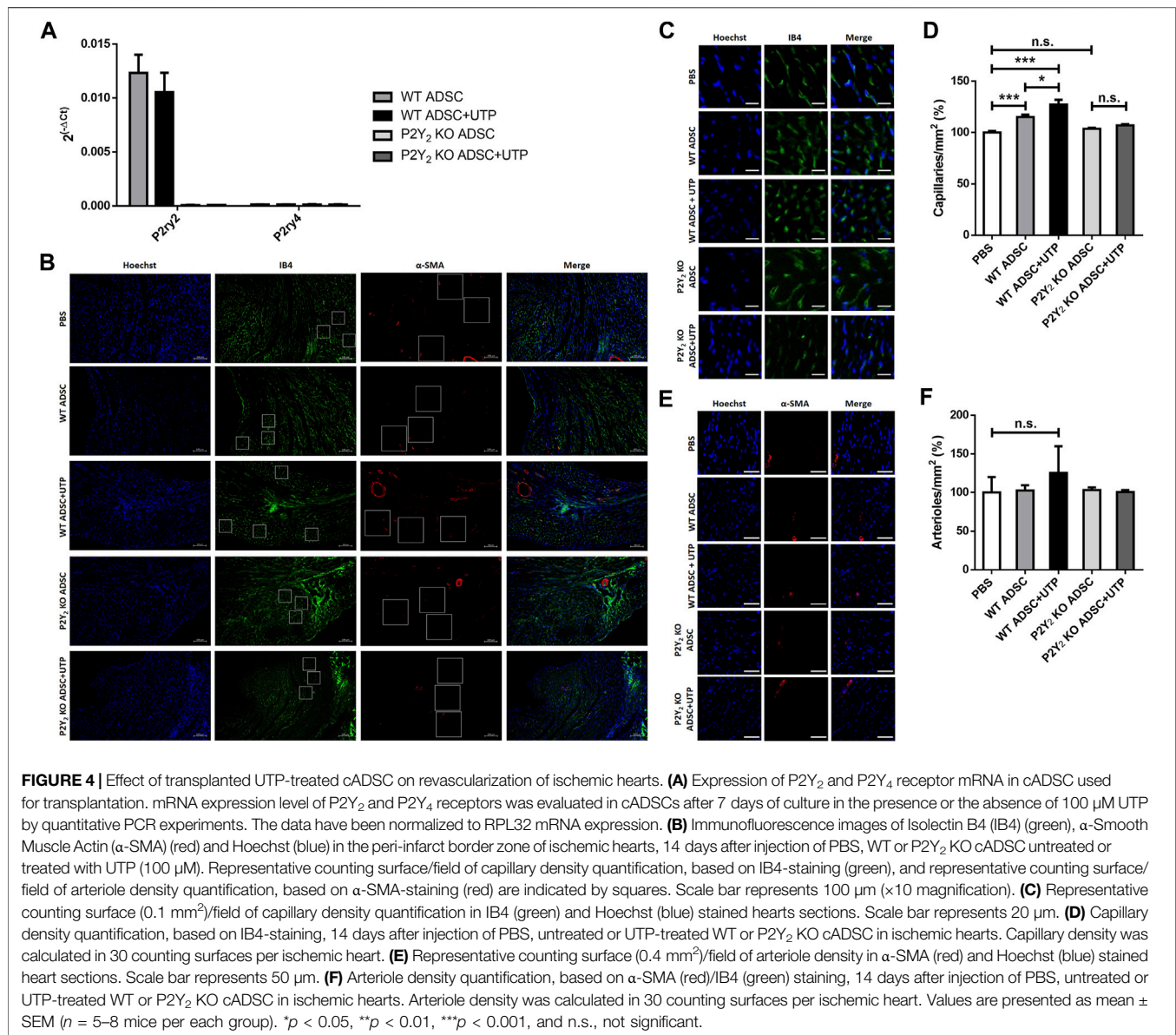
DISCUSSION

Therapeutic strategies contributing to myocardial repair by regulating cardiac fibrosis and revascularization still need to be improved. Early reperfusion by restoration of blood flow is the way to heal the ischemic myocardium by limiting infarct size and improving clinical outcomes (Zhao et al., 2017). Multiple challenges have to be solved to establish a routine clinical use of ADSC-based cell therapy. The regulatory function of cardiac adipose tissue in cardioprotection represents a major interest by

its proximity to the myocardium. Despite its limited size, cardiac adipose tissue was described as an ideal source of therapeutically effective ADSC for cardiac regeneration (Nagata et al., 2016). cADSC have a higher proliferation activity *in vitro* than ADSC isolated from other sources, such as visceral, subcutaneous and subscapular adipose tissues (Nagata et al., 2016). Systemic transfusion of cADSC in ischemic mice leads to the highest cardiac functional recovery after myocardial infarction, compared to other types of ADSC (Nagata et al., 2016).

We have previously demonstrated that UTP regulates the endothelial differentiation and the angiogenic effects of cADSC (Vanorlé et al., 2021). This previous work was exclusively based on the use of UTP-treated cADSC differentiated into endothelial cells, to regulate post-ischemic revascularization (Vanorlé et al., 2021). The present study investigates the potential involvement of P2Y₂ on the beneficial effects of undifferentiated cADSC injection on post-ischemic cardiac fibrosis and revascularization. Undifferentiated cADSC were used here to study the consequence of their injection into mouse ischemic heart without any orientation into a specific cell lineage. Their effect on both post-ischemic cardiac fibrosis and revascularization was observed without a required pretreatment of cADSC with extracellular nucleotides. Interestingly, the inhibitory effect of undifferentiated cADSC transplantation on cardiac fibrosis was no more observed using P2Y₂ KO cADSC. The release of endogenous extracellular nucleotides on the ischemic site could thus contribute to regulate the cardioprotective action of transplanted cADSC through activation of P2Y₂ receptors expressed at their surface.

RNA-sequencing experiments revealed a gene expression profile very different in UTP-treated undifferentiated cADSC, than the one we had previously reported in UTP-treated cADSC differentiated into endothelial cells (Vanorlé et al., 2021). We have previously demonstrated differential involvement of both P2Y₂ and P2Y₄ receptors in cADSC adipogenic differentiation (Lemaire et al., 2017; Negri et al., 2019). We compared here UTP-regulated genes in WT and P2Y₂ KO cADSCs to discriminate genes and associated-biological processes specific of P2Y₂ activation in these cells. Detailed gene profiling analysis revealed UTP-regulated genes linked to extracellular matrix organization and collagen catabolism such as matrix metalloproteinases and many collagen types, and UTP-regulated genes related to macrophage chemotaxis and foam



cell differentiation. We also demonstrated UTP-mediated inhibition of CCL12 release by ADSC. CCL12 is a pro-fibrotic chemokine that generates an unfavorable cardiac healing environment (DeLeon-Pennell et al., 2017). The inhibition of CCL12 release by extracellular nucleotides present on the ischemic site could contribute to ADSC inhibitory action on cardiac fibrosis, and ameliorate cardiac repair. Ccl22 was also identified as a UTP target gene in ADSC in our RNA-sequencing experiments. CCL22 is involved in CCR4-mediated cardiac cell migration (Safa et al., 2016) and CCL22/CCR4 polymorphisms have been associated to patients diagnosed with myocardial infarction (Noori et al., 2018).

Interestingly, a significant number of UTP-regulated genes in ADSC are linked to angiogenesis regulation. More precisely, we showed that UTP increased pro-angiogenic Ccl5, Cxcl5, and Saa3 mRNAs by qPCR experiments, and the release of CCL5, CXCL5,

and SAA3 in the supernatants of undifferentiated ADSC. The release of CCL5/RANTES by cADSC in response to UTP was particularly interesting. CCL5 is an angiogenic chemokine, and CCL5/CCR5 axis is notably involved in VEGF-mediated tumor angiogenesis (Wang et al., 2015). CCL5 was also reported to stimulate multipotency, migration and post-ischemic reparative capacities of ADSC (Kimura et al., 2014). The fact that transplanted ADSC have higher repair capacities of the ischemic tissue than bone marrow or dental tissue mesenchymal cells was associated to their higher secretion of CCL5 chemokine (Kimura et al., 2014). ADSC were the most effective stem cells to increase microvessel formation and ADSC lacking CCL5 expression were no more able to restore blood flow in the ischemic limb model (Kimura et al., 2014).

A high expression of P2Y₂ receptor mRNAs was detected in unstimulated and UTP-treated cADSC used for

transplantation, compared to low P2Y₄ receptor mRNA expression. P2Y₄ receptor is involved in cADSC adipogenic differentiation (Lemaire et al., 2017) but its expression in these cells was effectively very low after 7 days of culture in the proliferation medium. We used UTP instead of ATP to prestimulate cADSC to avoid ADP or adenosine receptor activation due to ATP degradation. We confirmed that prolonged UTP stimulation during 7 days did not induce P2Y₂ receptor desensitization before transplantation. Quantification of capillary and arteriole density in the ischemic border zone revealed that, 14 days after intramyocardial transplantation of WT cADSC, a higher capillary density was found around the necrotic zone. This effect was enhanced by a pretreatment of cADSC with UTP before transplantation. Interestingly this positive effect on post-ischemic revascularization was lost using P2Y₂ KO cADSC. These data showed that the orientation of cADSC differentiation into endothelial cells was not necessary to have an effect of their transplantation on post-ischemic revascularization and highlight the importance of P2Y₂ expression in their capacity to increase capillary density.

Extracellular nucleotide-mediated CCL5 secretion by cADSC in the ischemic heart could contribute to their beneficial action on cardiac revascularization and fibrosis after transplantation. Neutralizing anti-CCL5 antibodies have provided a therapeutic benefit in a mouse model of chronic cardiac ischemia (Montecucco et al., 2012). Nevertheless targeting CCR5 was not always effective in cardiovascular treatments because CCL5/CCR5 facilitates progenitor cell recruitment and promotes vascular endothelial cell repair (Zhang et al., 2020). CCR5 signaling is reported to suppress inflammation and reduce adverse remodeling of the infarcted heart (Dobaczewski et al., 2010).

A P2Y₂-mediated cardioprotective effect of UTP injection was described in ischemic mice. Cohen et al. (2011) described that UTP injection reduces infarct size and improves cardiac function after myocardial infarct in mice through P2Y₂ activation of cardiomyocytes (Cohen et al., 2011). Therapeutic use of UTP intramyocardial injection is problematic, knowing its rapid degradation and the ubiquitous expression of P2Y₂ receptor, accompanied by multiple side effects on cardiac and immune cells. The activation of P2Y₂ receptors and its target proteins in cADSC before their transplantation would be an appropriate way to amplify their beneficial effects and ameliorate post-ischemic cardiac response. This therapeutic approach would avoid the problems inherent to intramyocardial injection of extracellular nucleotides which are due to their rapid metabolism and ubiquitous receptor expression.

Injected stem cells are known to be rapidly eliminated after their injection in the ischemic heart, limiting strongly their possible integration into the fibrotic area or in newly formed capillaries (Schenke-Layland et al., 2009; Zhao et al., 2017; Vanorlé et al., 2021). The restricted engraftment of intramyocardial transplanted stem cells points out the importance of their paracrine effects (Patel and Zhang, 2014).

A lot of inflammatory mediators including extracellular nucleotides, chemokines and angiogenic factors, are released in the infarct zone and can modulate the action of injected cADSC. Extracellular nucleotides could contribute to the regulation of cADSC paracrine signals, such as the secretion of pro-angiogenic chemokines and other target proteins identified in our RNA-sequencing experiments. The supernatant of cADSC is removed for cell counting before injection in the ischemic heart, but their pretreatment with UTP changes their gene expression profile and amplifies their effects on cardiac revascularization. Strategies using stem cell preconditioning are known to improve their paracrine ability to release cardioprotective factors (Baraniak and McDevitt, 2010). The identification of UTP target genes in cADSC involved in cardiac angiogenesis and fibrosis, is very promising and needs further investigation to define all the involved mechanisms.

Altogether, our data indicate that the activation of nucleotide receptors on the surface of cADSC exerts a prevalent action on their cardioprotective abilities. The present study defines P2Y₂ receptor as a key regulator of the therapeutic use of undifferentiated cADSC against cardiac ischemia, and provides a novel insight for the optimization of cardiac repair cell therapies.

DATA AVAILABILITY STATEMENT

The datasets presented in this study can be found in online repositories. The names of the repository/repositories and accession number(s) can be found below: <https://www.ncbi.nlm.nih.gov/geo/query/acc.cgi?acc=GSE201055>.

ETHICS STATEMENT

This study was conducted in accordance with the Belgian, European and international guidelines for the care and use of laboratory animals. All animal work has been conducted in accordance with the European Community guidelines for the care and use of laboratory animals and approved by the Ethics committee of the Free University of Brussels (CEBEA, commission d'éthique du bien-être animal) (current approved protocols 2019/659N and 2019/714N).

AUTHOR CONTRIBUTIONS

DC designed and funded this study; DC and EDV wrote the manuscript and analyzed the experimental data; EDV, LDR, and MV performed the experimental work.

FUNDING

This work was supported by Research Project and Research Credit of the Fonds National de la Recherche Scientifique (F.N.R.S.), Communauté Française de Belgique (J.0060.18 CDR

grant), by Fonds pour la Chirurgie Cardiaque, by an ATIMI (Attract Brains for Brussels, Belgium) grants of Innoviris Brussels (2019-BFB-106 ATIMI grant), by the Fund Lokumo, King Baudouin Foundation, Belgium (2017-B7131100-207336 grant), by the Fonds et Crédit d'Encouragement à la Recherche (F.E.R., C.E.R.) from the Free University of Brussels (U.L.B.), Belgium. E. Diaz Villamil and M. Vanorlé are supported by the F.R.I.A., Fonds National de la Recherche Scientifique, Communauté Française de Belgique, Belgium. L. De Roeck is supported by U.L.B., Belgium. D. Communi is Senior Research Associate of the Fonds National de la Recherche Scientifique,

Communauté Française de Belgique, Belgium. The funders had no role in study design, data collection and analysis, decision to publish, or preparation of the manuscript.

ACKNOWLEDGMENTS

The authors thank Michael Horckmans and Frédérick Libert for technical advice related to, respectively, ischemia and RNA-sequencing experiments.

REFERENCES

- Baraniak, P. R., and McDevitt, T. C. (2010). Stem Cell Paracrine Actions and Tissue Regeneration. *Regen. Med.* 5, 121–143. doi:10.2217/rme.09.74
- Cai, L., Johnstone, B. H., Cook, T. G., Tan, J., Fishbein, M. C., Chen, P. S., et al. (2009). IFATS Collection: Human Adipose Tissue-Derived Stem Cells Induce Angiogenesis and Nerve Sprouting Following Myocardial Infarction, in Conjunction with Potent Preservation of Cardiac Function. *Stem Cells* 27, 230–237. doi:10.1634/stemcells.2008-0273
- Chen, L., Qin, F., Ge, M., Shu, Q., and Xu, J. (2014). Application of Adipose-Derived Stem Cells in Heart Disease. *J. Cardiovasc. Transl. Res.* 7, 651–663. doi:10.1007/s12265-014-9585-1
- Cohen, R., Shainberg, A., Hochhauser, E., Cheporko, Y., Tobar, A., Birk, E., et al. (2011). UTP Reduces Infarct Size and Improves Mice Heart Function after Myocardial Infarct via P2Y2 Receptor. *Biochem. Pharmacol.* 82, 1126–1133. doi:10.1016/j.bcp.2011.07.094
- DeLeon-Pennell, K. Y., Iyer, R. P., Ero, O. K., Cates, C. A., Flynn, E. R., Cannon, P. L., et al. (2017). Periodontal-induced Chronic Inflammation Triggers Macrophage Secretion of CCL12 to Inhibit Fibroblast-Mediated Cardiac Wound Healing. *JCI Insight* 2, e94207. doi:10.1172/jci.insight.94207
- Dobaczewski, M., Xia, Y., Bujak, M., Gonzalez-Quesada, C., and Frangogiannis, N. G. (2010). CCR5 Signaling Suppresses Inflammation and Reduces Adverse Remodeling of the Infarcted Heart, Mediating Recruitment of Regulatory T Cells. *Am. J. Pathol.* 176 (5), 2177–2187. doi:10.2353/ajpath.2010.090759
- Dutta, A. K., Sabirov, R. Z., Uramoto, H., and Okada, Y. (2004). Role of ATP-Conductive Anion Channel in ATP Release from Neonatal Rat Cardiomyocytes in Ischaemic or Hypoxic Conditions: ATP-Conductive Channel in Ischaemic Cardiomyocytes. *J. Physiol.* 559, 799–812. doi:10.1113/jphysiol.2004.069245
- Glaser, T., Cappellari, A. R., Pillat, M. M., Iser, I. C., Wink, M. R., Battastini, A. M., et al. (2012). Perspectives of Purinergic Signaling in Stem Cell Differentiation and Tissue Regeneration. *Purinergic Signal* 8, 523–537. doi:10.1007/s11302-011-9282-3
- Gnecchi, M., Zhang, Z., Ni, A., and Dzau, V. J. (2008). Paracrine Mechanisms in Adult Stem Cell Signaling and Therapy. *Circ. Res.* 103, 1204–1219. doi:10.1161/CIRCRESAHA.108.176826
- Homolya, L., Watt, W. C., Lazarowski, E. R., Koller, B. H., and Boucher, R. C. (1999). Nucleotide-regulated Calcium Signaling in Lung Fibroblasts and Epithelial Cells from Normal and P2Y(2) Receptor (-/-) Mice. *J. Biol. Chem.* 274, 26454–26460. doi:10.1074/jbc.274.37.26454
- Horckmans, M., Esfahani, H., Beauloye, C., Clouet, S., di Pietrantonio, L., Robaye, B., et al. (2015). Loss of Mouse P2Y4 Nucleotide Receptor Protects against Myocardial Infarction through Endothelin-1 Downregulation. *J. Immunol.* 194 (4), 1874–1881. doi:10.4049/jimmunol.1401364
- Kaebisch, C., Schipper, D., Babczyk, P., and Tobiasch, E. (2015). The Role of Purinergic Receptors in Stem Cell Differentiation. *Comput. Struct. Biotechnol. J.* 13, 75–84. doi:10.1016/j.csbj.2014.11.003
- Kauts, M. L., Pihelgas, S., Orro, K., Neuman, T., and Piirsoo, A. (2013). CCL5/CCR1 axis Regulates Multipotency of Human Adipose Tissue Derived Stromal Cells. *Stem Cell Res.* 10, 166–178. doi:10.1016/j.scr.2012.11.004
- Kimura, K., Nagano, M., Salazar, G., Yamashita, T., Tsuboi, I., Mishima, H., et al. (2014). The Role of CCL5 in the Ability of Adipose Tissue-Derived Mesenchymal Stem Cells to Support Repair of Ischemic Regions. *Stem Cells Dev.* 23 (5), 488–501. doi:10.1089/scd.2013.0307
- Lemaire, A., Vanorlé, M., Horckmans, M., di Pietrantonio, L., Clouet, S., Robaye, B., et al. (2017). Mouse P2Y4 Nucleotide Receptor is a Negative Regulator of Cardiac Adipose-Derived Stem Cell Differentiation and Cardiac Fat Formation. *Stem Cells Dev.* 26 (5), 363–373. doi:10.1089/scd.2016.0166
- Lévy, B., Smadja, D., and Silvestre, J.-S. (2013). *Ischémie tissulaire et régénération vasculaire: Mécanismes moléculaires et cellulaires, perspectives thérapeutiques*. Arcueil, France: John Libbey Eurotext.
- Lustig, K. D., Shiau, A. K., Brake, A. J., and Julius, D. (1993). Expression Cloning of an ATP Receptor from Mouse Neuroblastoma Cells. *Proc. Natl. Acad. Sci. U. S. A.* 90, 5113–5117. doi:10.1073/pnas.90.11.5113
- Lv, M., Xia, Y. F., Li, B., Liu, H., Pan, J. Y., Li, B. B., et al. (2016). Serum Amyloid A Stimulates Vascular Endothelial Growth Factor Receptor 2 Expression and Angiogenesis. *J. Physiol. Biochem.* 72, 71–81. doi:10.1007/s13105-015-0462-4
- Montecucco, F., Brauner-Reuther, V., Lenglet, S., Delattre, B. M., Pelli, G., Buatois, V., et al. (2012). CC Chemokine CCL5 Plays a Central Role Impacting Infarct Size and Post-infarction Heart Failure in Mice. *Eur. Heart J.* 33, 1964–1974. doi:10.1093/eurheartj/ehr127
- Nagata, H., Ii, M., Kohbayashi, E., Hoshiga, M., Hanafusa, T., and Asahi, M. (2016). Cardiac Adipose-Derived Stem Cells Exhibit High Differentiation Potential to Cardiovascular Cells in C57BL/6 Mice. *Stem Cells Transl. Med.* 5, 141–151. doi:10.5966/sctm.2015-0083
- Negri, I., Diaz Villamil, E., De Roeck, L., Communi, D., and Horckmans, M. (2019). P2Y2 Nucleotide Receptor is a Regulator of the Formation of Cardiac Adipose Tissue and its Fat-Associated Lymphoid Clusters. *Stem Cells Dev.* 29 (2), 100–109. doi:10.1089/scd.2019.0200
- Noori, F., Naeimi, S., Zibaenezhad, M. J., and Gharemirshamlu, F. R. (2018). CCL22 and CCR4 Gene Polymorphisms in Myocardial Infarction: Risk Assessment of Rs4359426 and Rs2228428 in Iranian Population. *Clin. Lab.* 64 (6), 907–913. doi:10.7754/Clin.Lab.2018.171106
- Patel, N. G., and Zhang, G. (2014). Stacked Stem Cell Sheets Enhance Cell-Matrix Interactions. *Organogenesis* 10, 170–176. doi:10.4161/org.28990
- Safa, A., Rashidinejad, H. R., Khalili, M., Dabiri, S., Nemat, M., Mohammadi, M. M., et al. (2016). Higher Circulating Levels of Chemokines CXCL10, CCL20 and CCL22 in Patients with Ischemic Heart Disease. *Cytokine* 83, 147–157. doi:10.1016/j.cyt.2016.04.006
- Schenke-Layland, K., Strem, B. M., Jordan, M. C., DeMedio, M. T., Hedrick, M. H., Roos, K. P., et al. (2009). Adipose Tissue-Derived Cells Improve Cardiac Function Following Myocardial Infarction. *J. Surg. Res.* 153, 217–223. doi:10.1016/j.jss.2008.03.019
- Stubbs, S. L., Hsiao, S. T., Peshavariya, H. M., Lim, S. Y., Disting, G. J., and Dilley, R. J. (2012). Hypoxic Preconditioning Enhances Survival of Human Adipose-Derived Stem Cells and Conditions Endothelial Cells *In Vitro*. *Stem Cells Dev.* 21, 1887–1896. doi:10.1089/scd.2011.0289
- Tannock, L. R., De Beer, M. C., Ji, A., Shridas, P., Noffsinger, V. P., den Hartigh, L., et al. (2018). Serum Amyloid A3 is a High Density Lipoprotein-Associated Acute-phase Protein. *J. Lipid Res.* 59, 339–347. doi:10.1194/jlr.M080887
- Vanorlé, M., Lemaire, A., di Pietrantonio, L., Horckmans, M., and Communi, D. (2021). UTP is a Regulator of *In Vitro* and *In Vivo* Angiogenic Properties of Cardiac Adipose-Derived Stem Cells. *Purinergic Signal* 17, 681–691. doi:10.1007/s11302-021-09812-8
- Wang, S. W., Liu, S. C., Sun, H. L., Huang, T. Y., Chan, C. H., Yang, C. Y., et al. (2015). CCL5/CCR5 axis Induces Vascular Endothelial Growth Factor-

- Mediated Tumor Angiogenesis in Human Osteosarcoma Microenvironment. *Carcinogenesis* 36 (1), 104–114. doi:10.1093/carcin/bgu218
- Yang, D., Wang, W., Li, L., Peng, Y., Chen, P., Huang, H., et al. (2013). The Relative Contribution of Paracrine Effect versus Direct Differentiation on Adipose-Derived Stem Cell Transplantation Mediated Cardiac Repair. *PLoS One* 8 (3), e59020. doi:10.1371/journal.pone.0059020
- Yitzhaki, S., Shneyvays, V., Jacobson, K. A., and Shainberg, A. (2005). Involvement of Uracil Nucleotides in Protection of Cardiomyocytes from Hypoxic Stress. *Biochem. Pharmacol.* 69, 1215–1223. doi:10.1016/j.bcp.2005.01.018
- Zhang, Z., Wang, Q., Yao, J., Zhou, X., Zhao, J., Zhang, X., et al. (2020). Chemokine Receptor 5, a Double-Edged Sword in Metabolic Syndrome and Cardiovascular Disease. *Front. Pharmacol.* 11, 146. doi:10.3389/fphar.2020.00146
- Zhao, L., Johnson, T., and Liu, D. (2017). Therapeutic Angiogenesis of Adipose-Derived Stem Cells for Ischemic Diseases. *Stem Cell Res. Ther.* 8 (1), 125. doi:10.1186/s13287-017-0578-2
- Zhu, P., Liu, J., Shi, J., Zhou, Q., Liu, J., Zhang, X., et al. (2015). Melatonin Protects ADSCs from ROS and Enhances Their Therapeutic Potency in a Rat Model of Myocardial Infarction. *J. Cell. Mol. Med.* 19, 2232–2243. doi:10.1111/jcmm.12610
- Zippel, N., Limbach, C. A., Ratajski, N., Urban, C., Luparello, C., Pansky, A., et al. (2012). Purinergic Receptors Influence the Differentiation of Human Mesenchymal Stem Cells. *Stem Cells Dev.* 21, 884–900. doi:10.1089/scd.2010.0576
- Conflict of Interest:** The authors declare that the research was conducted in the absence of any commercial or financial relationships that could be construed as a potential conflict of interest.
- Publisher's Note:** All claims expressed in this article are solely those of the authors and do not necessarily represent those of their affiliated organizations, or those of the publisher, the editors and the reviewers. Any product that may be evaluated in this article, or claim that may be made by its manufacturer, is not guaranteed or endorsed by the publisher.
- Copyright © 2022 Diaz Villamil, De Roock, Vanorlé and Communi. This is an open-access article distributed under the terms of the Creative Commons Attribution License (CC BY). The use, distribution or reproduction in other forums is permitted, provided the original author(s) and the copyright owner(s) are credited and that the original publication in this journal is cited, in accordance with accepted academic practice. No use, distribution or reproduction is permitted which does not comply with these terms.



Machine Learning for Discovery of New ADORA Modulators

Ana C. Puhl^{1*}, Zhan-Guo Gao², Kenneth A. Jacobson² and Sean Ekins^{1*}

¹Collaborations Pharmaceuticals, Inc., Raleigh, NC, United States, ²Molecular Recognition Section, Laboratory of Bioorganic Chemistry, National Institute of Diabetes and Digestive and Kidney Diseases, National Institutes of Health, Bethesda, MD, United States

OPEN ACCESS

Edited by:

Yuhei Nishimura,
Mie University, Japan

Reviewed by:

Yinglong Miao,
University of Kansas, United States
Giuseppe Deganutti,
Coventry University, United Kingdom
John A. Allen,
University of Texas Medical Branch at
Galveston, United States

*Correspondence:

Ana C. Puhl
ana@collaborationspharma.com
Sean Ekins
sean@collaborationspharma.com

Specialty section:

This article was submitted to
Experimental Pharmacology and Drug
Discovery,
a section of the journal
Frontiers in Pharmacology

Received: 14 April 2022

Accepted: 30 May 2022

Published: 22 June 2022

Citation:

Puhl AC, Gao Z-G, Jacobson KA and
Ekins S (2022) Machine Learning for
Discovery of New ADORA Modulators.
Front. Pharmacol. 13:920643.
doi: 10.3389/fphar.2022.920643

Adenosine (ADO) is an extracellular signaling molecule generated locally under conditions that produce ischemia, hypoxia, or inflammation. It is involved in modulating a range of physiological functions throughout the brain and periphery through the membrane-bound G protein-coupled receptors, called adenosine receptors (ARs) A₁AR, A_{2A}AR, A_{2B}AR, and A₃AR. These are therefore important targets for neurological, cardiovascular, inflammatory, and autoimmune diseases and are the subject of drug development directed toward the cyclic adenosine monophosphate and other signaling pathways. Initially using public data for A₁AR agonists we generated and validated a Bayesian machine learning model (Receiver Operator Characteristic of 0.87) that we used to identify molecules for testing. Three selected molecules, crisaborole, febuxostat and paroxetine, showed initial activity *in vitro* using the HEK293 A₁AR Nomad cell line. However, radioligand binding, β -arrestin assay and calcium influx assay did not confirm this A₁AR activity. Nevertheless, several other AR activities were identified. Febuxostat and paroxetine both inhibited orthosteric radioligand binding in the μ M range for A_{2A}AR and A₃AR. In HEK293 cells expressing the human A_{2A}AR, stimulation of cAMP was observed for crisaborole (EC₅₀ 2.8 μ M) and paroxetine (EC₅₀ 14 μ M), but not for febuxostat. Crisaborole also increased cAMP accumulation in A_{2B}AR-expressing HEK293 cells, but it was weaker than at the A_{2A}AR. At the human A₃AR, paroxetine did not show any agonist activity at 100 μ M, although it displayed binding with a K_i value of 14.5 μ M, suggesting antagonist activity. We have now identified novel modulators of A_{2A}AR, A_{2B}AR and A₃AR subtypes that are clinically used for other therapeutic indications, and which are structurally distinct from previously reported tool compounds or drugs.

Keywords: ADORA, crisaborole, febuxostat, paroxetine, machine learning, adenosine receptor

Abbreviations: ADO, Adenosine; ARs, Adenosine receptors; A₁AR, Adenosine receptor A1; A_{2A}AR, Adenosine receptor A2A; A_{2B}AR, Adenosine receptor A2B; A₃AR, Adenosine receptor A3; GPCR, G protein-coupled receptor; cAMP, cyclic adenosine monophosphate; AC, adenylate cyclase; NECA, adenosine-5'-N-ethyluronamide; CPA, N6-cyclopentyladenosine; PDE4, phosphodiesterase 4; D₂R, dopamine D2 receptors.

INTRODUCTION

Adenosine (ADO) is an extracellular signaling molecule generated locally under conditions that produce ischemia, hypoxia, or inflammation and is involved in modulating a range of physiological functions throughout the brain and periphery by activating membrane-bound G protein-coupled receptors (GPCRs) (Borea et al., 2018). There are four subtypes of adenosine receptors (A_1 AR, A_{2A} AR, A_{2B} AR, and A_3 AR), which are the subject of vigorous drug development directed toward the cyclic adenosine monophosphate (cAMP) and other signaling pathways (Borea et al., 2016; Borea et al., 2018; Jacobson et al., 2019; Effendi et al., 2020). Adenosine receptors (ARs) were first classified according to their differential coupling to adenylate cyclase (AC) to regulate cAMP levels (Borea et al., 2018). Adenosine induces various biological effects associated with each adenosine receptor on the membrane surface of specific cells or tissues (Borea et al., 2018). Based upon sequence similarity and G protein-coupling specificity, A_1 AR and A_3 AR share 49% sequence identity and preferentially couple to Gai/o to inhibit AC (Effendi et al., 2020), which subsequently inhibits presynaptic glutamate release (Ciruela et al., 2006; Effendi et al., 2020). In contrast, A_{2A} AR and A_{2B} AR receptors, which are ~59% identical and couple to Gas, are able to stimulate AC (Cheng et al., 2017) increasing levels of cAMP (Wardas, 2002). A_1 AR and A_{2A} AR receptors possess high affinity for ADO, while A_{2B} AR and A_3 AR receptors show relatively lower affinity. A_1 AR has been found to be widely distributed throughout the body. In the brain, it slows metabolic activity by a combination of actions. At neuronal synapses, it reduces synaptic vesicle release. A_1 AR is implicated in sleep promotion by inhibiting wake-promoting cholinergic neurons in the basal forebrain (Elmenhorst et al., 2007). A_1 AR is also present in smooth muscle throughout the vascular system (Fredholm et al., 2001; Tawfik et al., 2005). A_1 AR has antiseizure activity and contributes to neuroprotection in models of neurodegeneration (Effendi et al., 2020). A_1 AR activation under hypoxic conditions leads to inhibition of presynaptic Ca^{2+} influx-related release of transmitters (Wu and Saggau, 1997) such as dopamine, acetylcholine, GABA, and, especially, glutamate, to generate neuroprotection (Stone et al., 2009).

A_{2A} AR has been linked to the anti-inflammatory effects of adenosine. Activation of A_{2A} AR reduces immune cell migration and produces tissue protection from ischemia/reperfusion injury (Okusa et al., 1999; Ohta and Sitkovsky, 2001). In contrast to other adenosine receptors, A_{2B} AR, shows upregulated expression in many pathological conditions, such as inflammation, cancer and hypoxia (Borea et al., 2016; Cekic and Linden, 2016; Gao and Jacobson, 2019). It interacts with Gs to induce the PKA signaling to increase cAMP and can trigger signaling transduction to elevate intracellular Ca^{+2} levels (Effendi et al., 2020). Activation of A_{2B} AR in mast cells might be useful in the treatment of asthma (Gao and Jacobson, 2017). A_3 AR is widespread with abundant expression in the lung and liver, and its activation reduces inflammation and chronic neuropathic pain (Jacobson et al.,

2019). A_3 AR coupled to Gi proteins inhibits AC, decreases cAMP accumulation and PKA activity, while A_3 AR also increases Ca^{2+} levels and modulates PKC activity (Baraldi et al., 2012; Borea et al., 2018).

ARs are therefore important targets for neurological, cardiovascular, inflammatory, and autoimmune diseases (Borea et al., 2016; Borea et al., 2018). In addition, selective ligands are available for the different AR subtypes, which increase the chances to achieve spatially-specific modulation, representing a pharmacological opportunity to control addictive psychostimulant consumption, among many other health problems (Ballesteros-Yáñez et al., 2017). Initially, we used machine learning models to find agonists of A_1 AR and further expanded the testing against other subtypes, and we have identified novel AR modulators that are structurally distinct from previously reported tool compounds or drugs in clinical trials for targeting ADO receptors (Jacobson et al., 2019).

METHODS

Reagents

All test compounds were purchased from MedChemExpress (MCE, Monmouth Junction, NJ).

Machine Learning

Initially, an A_1 AR model was built with data reported in ChEMBL (Gaulton et al., 2017) (target 262). Assay Central[®] was used to build the model using EC₅₀ values, and non-druglike compounds such as Zn^{2+} (ChEMBL1201279), $Li^+ Cl^-$ (ChEMBL69710), and Li^+ (ChEMBL1234004) were removed to increase the performance of the model. The ChEMBL compounds for ADORA1 consisted of 430 compounds with EC₅₀ values, and the corresponding Bayesian model was built using Assay Central[®]. Assay Central[®] has been used by our group in various drug discovery projects (Hernandez et al., 2018; Lane et al., 2018; Russo et al., 2018; Sandoval et al., 2018; Ekins et al., 2019a; Anantpadma et al., 2019; Ekins et al., 2019b; Dalecki et al., 2019; Wang et al., 2019; Ekins et al., 2020); its use as well as clarification on the applicability of the model statistics have been previously described. Metrics such as Receiver Operator Characteristic (ROC), Recall, Precision, F1 Score, Cohen's Kappa and Matthew's Correlation Coefficient are generated from internal five-fold cross-validation of the model. To maximize these internal performance statistics, the software can select a reasonable activity threshold, and generate predictions as well as applicability scores for any desired compound. Higher prediction scores are desirable as scores higher than 0.5 are assigned to active compounds (inhibitors). Higher applicability scores are also desirable as they ensure the representation of a given drug in the training set (Clark et al., 2015). The activity threshold for this external dataset was set to 100 nM, and Assay Central[™] was used to generate the model performance metrics.

We have also used our updated Assay Central[®] software which now uses multiple classification algorithms described previously (Lane et al., 2018) as well as multiple regression algorithms

including adaboost, Bayesian, elastic net, K-nearest neighbors (knn), random forest, support vector machine and XGboost. We have further curated data available from ChEMBL for not only A₁AR (ChEMBL226) but also A_{2A}AR (ChEMBL251), A_{2B}AR (ChEMBL255) and A₃AR (ChEMBL256L). The data on ChEMBL comprise a diverse set of molecules and may comprise both full agonists and positive allosteric modulators (PAMs). For classification models the cut-off was set to 100 nM. 5-fold cross validation was performed for all algorithms except deep learning, which used the removal of 20% of the training set, in a stratified manner, and these were used as external test sets for models trained on the remainder of the data.

A₁AR-cAMP Assay

This assay was performed using the screening services of Innoprot (Bizkaia, Spain). For screening of the initial compounds predicted by machine learning models to activate A₁AR receptor, we used the HEK293 A₁AR Nomad cell line, which consists of HEK293 cells stably expressing human A₁AR with no tag. This cell line has been designed to assay compounds or analyze their capability to modulate the A₁AR. When the agonist binds to A₁AR in this engineered cell line a G_o protein is activated, which in turn, triggers a cellular response mediated by cAMP inhibition. This cellular response can be measured by quantifying the increase in fluorescence intensity and its cellular distribution. An agonist assay was performed for 29 compounds (predicted to be active by the machine learning model) in the human recombinant HEK293 A₁AR Nomad cell line using a fluorescence-based assay. An agonist effect of the compounds was measured by quantifying the changes in the fluorescence emission cAMP Nomad biosensor, this elevation of fluorescence was analyzed using a plate reader Synergy 2 (Biotek, Winooski, VT). The error bars represent the standard deviation among the three replicate wells. The 29 compounds were tested at 10 μ M using nonselective AR agonist adenosine-5'-N-ethyluronamide (NECA) at 10 μ M as a reference.

Radioligand Binding Assays

HEK293 cells stably expressing the human A₁AR, A_{2A}AR, A₃AR were cultured in DMEM supplemented with 10% fetal bovine serum, 100 Units/ml penicillin, 100 μ g/ml streptomycin, and 2 μ mol/ml glutamine. To prepare cell membranes, cells were detached from culture plates by scraping into cold PBS and centrifuged at 250 g for 5 min. The pellets were resuspended in ice-cold PBS buffer (pH 7.4) and then homogenized. After homogenization and suspension, cells were centrifuged at 1,000 g for 10 min, and the pellet was discarded. The suspension was then re-centrifuged at 20,000 g for 60 min at 4°C. The pellets were resuspended in buffer containing 3 Units/ml adenosine deaminase (Worthington Biochemical, Lakewood, NJ) and incubated at 37°C for 30 min. The aliquots of membrane preparations were stored at -80°C until the binding experiments. For displacement binding assays, membrane preparations (20 μ g proteins/tube) were incubated at 25°C for 60 min with a final concentration of [³H]DPCPX (0.5 nM), [³H]ZM241385 (1.0 nM), [³H]DPCPX (5.0 nM) and [¹²⁵I]I-AB-MECA (0.1 nM) for A₁AR, A_{2A}AR, A₃AR, respectively, in a mixture containing

50 μ l of increasing concentrations of a test ligand in a total assay volume of 200 μ l of 50 mM Tris HCl, pH 7.4, containing 10 mM MgCl₂. Nonspecific binding was determined using 100 μ M of XAC. The reaction was terminated by filtration with GF/B filters using a Brandel (Gaithersburg, MD) 24-channel harvester. Filters were placed in scintillation vials containing 5 ml of Hydrofluor scintillation buffer (National Diagnostics, Atlanta, GA) and counted using a Tricarb 2810TR liquid scintillation counter (PerkinElmer, Waltham, MA).

cAMP Assay in AR-Expressing HEK293 Cells

HEK293 cells were grown in 96-well plates in DMEM supplemented with 10% fetal bovine serum, 100 Units/ml penicillin, 100 μ g/ml streptomycin, and 2 μ mol/ml glutamine. After overnight growth, cells were treated with assay buffer containing phosphodiesterase (PDE) inhibitor rolipram (10 μ M), and adenosine deaminase (3 units/ml) for 30 min (for A₁AR, A_{2A}AR and A₃AR assays PSB603 (8-[4-[4-(4-chlorophenyl)piperazine-1-sulfonyl]phenyl]-1-propylxanthine, 1 μ M, was included to block the endogenous A_{2B}AR) followed by addition of agonists and a 20 min incubation. For A₁AR and A₃AR, after incubation with agonists for 20 min, forskolin (10 μ M) was added and the mixture incubated for an additional 15 min. The reaction was terminated upon removal of the supernatant and addition of 100 μ l Tween-20 (0.3%). Intracellular cAMP levels were measured with an ALPHAScreen cAMP assay kit as instructed by the manufacturer (PerkinElmer).

A₁AR-bla U2OS-Agonist Screen

This assay was performed using the screening services of Thermo Fisher (Waltham, MA). A₁AR-bla U2OS cells are thawed and resuspended in Assay Media (Freestyle media) to a concentration of 312,500 cells/ml. 32 μ l of cell suspension (10,000 cells) was added to each well of a 384-well TC-Treated assay plate. Cells in Assay Media were incubated for 16–24 h in the plate at 37°C/5% CO₂ in a humidified incubator. 4 μ l aliquots of a 10X serial dilution of NECA (control agonist starting concentration, 500 nM) or compounds were added to appropriate wells of the plate. 4 μ l of Assay Media was added to all wells to bring the final assay volume to 40 μ l. The plate was incubated for 5 h at 37°C/5% CO₂ in a humidified incubator. 8 μ l of 1 μ M substrate + Solution D Loading Solution was added to each well and the plate was incubated for 2 h at room temperature. The plate was read on a fluorescence plate reader.

PathHunter® β -Arrestin Assays

This assay was performed using the screening services of Eurofins (Luxembourg). The PathHunter® β -Arrestin assay monitors the activation of a A₁AR in a homogenous, non-imaging assay format using a technology developed by DiscoverX called Enzyme Fragment Complementation (EFC) with β -galactosidase (β -Gal) as the functional reporter. The enzyme is split into two inactive complementary portions (EA for Enzyme Acceptor and PK for ProLink) expressed as fusion proteins in the cell. EA is

fused to β -Arrestin and PK is fused to the A_1 AR. When the A_1 AR is activated and β -Arrestin is recruited to the receptor, ED and EA complementation occurs, restoring β -Gal activity which is measured using chemiluminescent PathHunter® Detection Reagents. PathHunter cell lines were expanded from freezer stocks according to standard procedures. Cells were seeded in a total volume of 20 μ l into white walled, 384-well microplates and incubated at 37°C for the appropriate time prior to testing. For agonist determination, cells were incubated with sample to induce response. Intermediate dilution of sample stocks was performed to generate 5X sample in assay buffer. 5 μ l of 5X sample was added to cells and incubated at 37°C or room temperature for 90–180 min. Vehicle concentration was 1%. Assay signal was generated through a single addition of 12.5 or 15 μ l (50% v/v) of PathHunter Detection reagent cocktail, followed by a 1 h incubation at room temperature. Microplates were read following signal generation with a PerkinElmer Envision™ instrument for chemiluminescent signal detection. Compound activity was analyzed using CBIS data analysis suite (ChemInnovation, San Diego, CA). For agonist mode assays, percentage activity was calculated using the following formula: % Activity = 100% \times (mean RLU of test sample–mean RLU of vehicle control)/(mean MAX control ligand–mean RLU of vehicle control).

A_1 AR–Calcium Influx Assay

This assay was performed using the screening services of Eurofins. Evaluation of the agonist activity of compounds at the human A_1 receptor expressed in BA/F3 cells was determined by measuring their effect on cytosolic Ca^{2+} ion mobilization using a fluorimetric detection method. The cells were suspended in HBSS buffer (Invitrogen) complemented with 20 mM Hepes and then distributed in microplates at a density of 5×10^4 cells/well. The fluorescent probe (Fluo8, AAT Bioquest, San Francisco, CA) mixed with probenidol in HBSS buffer (Invitrogen) complemented with 20 mM Hepes (Millipore, Burlington, MA) (pH 7.4) was then added into each well and equilibrated with the cells for 60 min at 30°C. Thereafter, the assay plates were positioned in a microplate reader (FlipR Tetra, Molecular Devices, San Jose, CA), which was used for the addition of the test compound, reference agonist or HBSS buffer (basal control), and for the measurements of changes in fluorescence intensity that varies proportionally to the free cytosolic Ca^{2+} ion concentration. For stimulated control measurements, N^6 -cyclopentyladenosine (CPA) at 0.25 μ M was added in separate assay wells. The results were expressed as a percent of the control response to CPA at 0.25 μ M. The standard reference agonist was CPA, which was tested in each experiment at several concentrations to generate a concentration-response curve from which its EC_{50} value was calculated.

RESULTS

Machine Learning

Assay Central® (Clark and Ekins, 2015; Clark et al., 2015) is our in-house software that was used to curate the published A_1 AR data, build and validate machine learning models then enable predictions

for molecules. This software has been previously used to build Bayesian machine learning models that generate predictions in toxicological and drug discovery projects (Lane et al., 2018; Russo et al., 2018; Zorn et al., 2019). The interpretation of the model metrics as well as the prediction and applicability scores have been described in detailed in previously published work (Clark et al., 2015; Lane et al., 2018; Russo et al., 2018; Zorn et al., 2019). While our Assay Central® software can select a reasonable threshold, 100 nM was set for the original A_1 AR Bayesian model (and subsequent models derived with additional algorithms). Compounds with an EC_{50} lower than this threshold were considered active, and those above were considered inactive. The initial Bayesian model for A_1 AR agonists using literature data (Figure 1A), demonstrated a five-fold cross-validation ROC of 0.87, which is excellent. This model was then used to predict the SuperDrug library (Siramshetty et al., 2018) and our in-house library of compounds (predominantly consisting of FDA approved drugs and other compounds of interest), and 30 compounds were initially selected for testing for agonist activity in the A_1 AR cAMP assay (Supplementary Table S1).

Subsequently we have also built classification and regression models using our latest version of the Assay Central software for A_1 AR, A_{2A} AR, A_{2B} AR and A_3 AR (Supplementary Figures S1–S4). The classification machine learning models (100 nM cutoff) all had good 5-fold cross-validation statistics, and we have additionally generated regression models that can be used for scoring and selecting new compounds for testing in future. We used these additional models to predict activity of the hits selected from our initial models (Supplementary Table S2).

A_1 AR Assays

The initially selected 29 molecules were tested using the HEK293 A_1 AR Nomad cell line stably expressing human protein with no tag (Figure 1B). Activation of A_1 AR by an agonist engages $G_{i1/2/3}$ or G_o protein to inhibit adenylate cyclase and, therefore, decreases the cAMP concentration. Compounds were tested at 10 μ M using NECA at 10 μ M as the reference agonist. The fluorescence intensity was normalized to NECA at 10 μ M and vehicle (DMSO) alone, which were considered 100% and 0%, respectively. The normalized results showed that febuxostat, BAY11-7082 ((E)-3-(4-methylphenylsulfonyl)-2-propenenitrile) and crisaborole showed a normalized activity with respect to the positive control of 94.53%, 95.74% and 98.52%, respectively (Figure 1B). Additionally, tilorone hydrochloride and paroxetine hydrochloride showed a normalized activity with respect to the positive control of 55.9 % and 68.0%, respectively (Figure 1B). Other compounds predicted computationally by Assay Central showed an activity of less than 50% at the concentration tested. We therefore conducted additional assays with crisaborole, febuxostat and paroxetine using radioligand binding assays and measured dose response curves in the HEK293 A_1 AR assay using ALPHAScreen (Perkin Elmer) assay, as described below.

Radioligand Binding

The first step toward activation involves receptor binding. Thus, we have measured the inhibition of the binding of standard AR radioligands at the orthosteric site of three AR subtypes (Table 1).

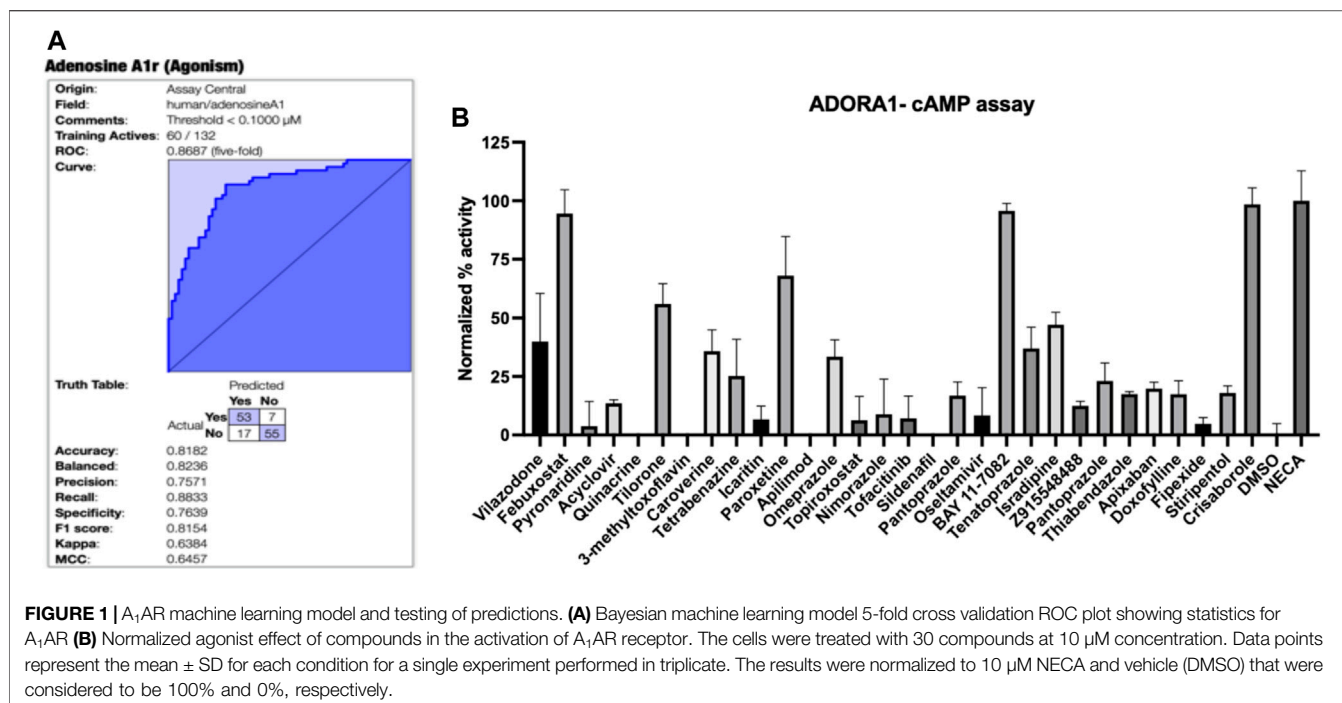


FIGURE 1 | A_1 AR machine learning model and testing of predictions. **(A)** Bayesian machine learning model 5-fold cross validation ROC plot showing statistics for A_1 AR **(B)** Normalized agonist effect of compounds in the activation of A_1 AR receptor. The cells were treated with 30 compounds at 10 μM concentration. Data points represent the mean \pm SD for each condition for a single experiment performed in triplicate. The results were normalized to 10 μM NECA and vehicle (DMSO) that were considered to be 100% and 0%, respectively.

TABLE 1 | Inhibition of specific binding at all four ARs (% inhibition at 100 μM of the radioligand shown, or K_i (μM)).^a

Molecule	A_1 ($[^3\text{H}]\text{DPCPX}$)	A_{2A} ($[^3\text{H}]\text{ZM241385}$)	A_{2B} ($[^3\text{H}]\text{DPCPX}$)	A_3 ($[^{125}\text{I}]\text{I-AB-MECA}$)
Crisaborole	36.9 \pm 3.4%	31.2 \pm 5.6%	<10%	28.8 \pm 16.3%
Febuxostat	29.8 \pm 5.2%	22.9 \pm 4.3 μM	<10%	67.3 \pm 45.7 μM
Paroxetine	9.1 \pm 3.9%	40.4 \pm 9.8 μM	<10%	14.5 \pm 9.7 μM

^aData are expressed as mean \pm standard error from three independent experiments. Experimental procedures are described in Methods.

TABLE 2 | Summary table of *in vitro* data for compounds tested against adenosine receptors.

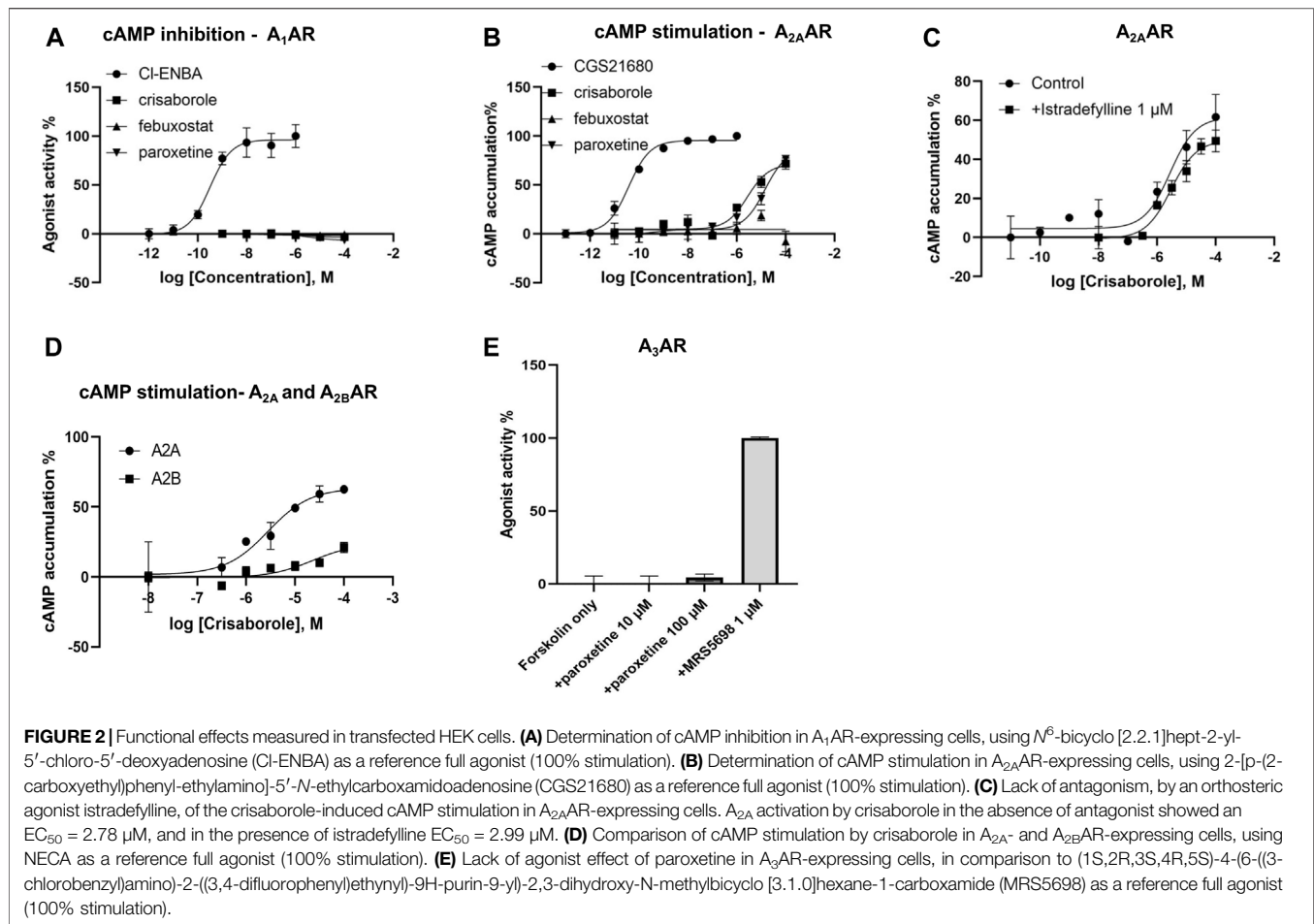
Adenosine receptor	Binds with	Adenosine	Adenylate cyclase/cAMP	Crisaborole cAMP	Febuxostat cAMP	Paroxetine cAMP
A_1 AR	Gi	High affinity	Inhibition/Decrease	Not active	Not active	Not active
A_{2A} AR	Gs	High affinity	Stimulate/Increase	Active E_{max} = 67%	Not active	Active E_{max} = 69%
A_{2B} AR	Gs	Low affinity	Stimulate/Increase	E_{max} = 17%	N/A	N/A
A_3 AR	Gi	High affinity	Inhibition/Decrease	N/A	N/A	Not active

No significant binding inhibition was observed at 100 μM for the three compounds at the human A_1 AR or human A_{2B} AR or by crisaborole at human A_{2A} AR and A_3 ARs. However, febuxostat and paroxetine both inhibited orthosteric radioligand binding in the μM range for A_{2A} AR and A_3 AR.

Functional Activity on cAMP Levels in Transfected HEK Cells

Functional activity on cAMP levels in transfected HEK cells was determined for the three hit compounds. No A_1 AR agonist activity was observed (**Figure 2**). In HEK cells expressing the human A_{2A} AR, stimulation of cAMP was observed for

crisaborole (EC_{50} 2.8 μM) and paroxetine (EC_{50} 14 μM), but not for febuxostat. We did not measure A_{2B} AR and A_3 AR effects of febuxostat in the cAMP cell assays. However, crisaborole is not an orthosteric A_{2A} AR agonist, because it did not inhibit binding. Istradefylline, an A_{2A} AR antagonist, only minimally affected crisaborole's effect, suggesting a mechanism of crisaborole-induced cAMP accumulation that is different from standard full agonist NECA. Istradefylline (1 μM) had minimum effect, but it slightly lowered both basal value and the maximum effect. This concentration of istradefylline (K_i = 2.2 nM) should be sufficient to saturate the orthosteric A_{2A} AR binding site. Curiously, crisaborole also increased cAMP accumulation in A_{2B} AR-expressing HEK293



cells, but it was weaker than at the A_{2A} AR. At the human A_3 AR, paroxetine did not show any agonist activity at 100 μM , although it displayed a binding K_i value of 14.5 μM , suggesting antagonist activity. A summary table of *in vitro* data for compounds tested against adenosine receptors is showed in Table 2.

A_1 AR- β -Arrestin Assay

We used A_1 AR-*bla* U2OS cells to test activation of A_1 AR receptor by crisaborole and paroxetine. This parental cell line stably expresses a beta-arrestin/TEV protease fusion protein and the beta-lactamase reporter gene under the control of a UAS response element. Paroxetine and crisaborole showed no activation in this system (Supplementary Figure S5). We also used a secondary assay PathHunter β -Arrestin assay, which monitors the activation of A_1 AR in a homogenous, non-imaging assay format using a technology developed by DiscoverX called Enzyme Fragment Complementation (EFC) with β -galactosidase (β -Gal) as the functional reporter. This data was normalized to the maximal and minimal response observed in the presence of control agonist CPA and vehicle (Supplementary Figure S6), and no activation of the A_1 AR receptor was observed in this assay at the maximum crisaborole concentration of 20 μM .

A_1 AR-Calcium Influx Assay

Crisaborole was tested using cellular and nuclear receptor functional Assays (Eurofins) for calcium influx assay and showed no activity of the A_1 AR receptor at the maximum concentration tested (20 μM) (Supplementary Figure S7).

DISCUSSION

While there have been several previous attempts to use machine learning for ARs (Saad et al., 2019; Wang et al., 2021), few have performed external validation. One recent study used deep learning combined with pharmacophore and docking approaches to identify novel A_1/A_{2A} antagonists (Wang et al., 2021). In contrast, we were keen to use machine learning alone to potentially repurpose existing drugs for ARs. Using our initial machine learning model, we have identified crisaborole as weakly binding to A_1 AR, but without activity on the cAMP, β -arrestin and calcium influx assays. However, crisaborole can activate A_{2A} AR and A_{2B} AR at the highest concentrations examined. Unexpectedly, the presence of an orthosteric A_{2A} AR antagonist istradefylline did not antagonize the effect of crisaborole, suggesting a mechanism of crisaborole-induced cAMP accumulation that is different from standard full agonist NECA. Paroxetine induced weak activation of A_{2A} AR, but

no activation of A₃AR, despite a binding K_d of 14.5 ± 9.7 μM. The lack of A₃AR activation suggested that paroxetine is an antagonist at this subtype. The structures of the three hit compounds do not resemble AR-targeting drugs that have been studied in clinical trials previously (Jacobson et al., 2019) (**Supplementary Figure S8**).

We evaluated the activity of crisaborole using several different *in vitro* assays. Crisaborole is an inhibitor of phosphodiesterase 4 (PDE4), which is responsible for the hydrolysis and subsequent inactivation of cyclic nucleotides such as cAMP. A₁AR activation promotes inhibition of adenylate cyclase and consequently inhibits cAMP production leading to the inhibition of presynaptic glutamate release (Wardas, 2002). Thus, since crisaborole is an inhibitor of PDE4 and A₁AR, it may have different effects on cAMP levels that are antagonistic. When crisaborole was tested in a second independent β-arrestin assay using the A₁AR-*bla* U2OS Cells and PathHunter technology, it showed no agonist activity at the A₁AR (**Supplementary Figures S5, S6**) and had no activity in the calcium influx assay (**Supplementary Figure S7**).

In the United States, crisaborole is indicated for topical treatment of mild to moderate atopic dermatitis in people 3 months of age and older (Schlessinger et al., 2020). Crisaborole enhances cellular control of inflammation by inhibiting PDE4 and its ability to degrade intracellular cAMP. Apparent A_{2A}AR agonist-like activity of crisaborole in combination with its PDE4 inhibitory activity may contribute when used topically in the clinic, regardless of the mechanism of A_{2A}AR activation.

The medicinal chemistry surrounding the development of novel adenosine receptor ligands has largely been driven by derivatization of the adenosine and other purine-like scaffolds to gain understanding of the structure-activity relationships especially in the early stages to distinguish between A₁AR and A_{2A}AR (Geldenhuys et al., 2017). From these studies, novel scaffolds were developed, such as the A_{2A}AR antagonist core 8-styrylxanthine. It was discovered that substitution of the styryl moiety with an 8-phenoxyethyl moiety leads to a dual A₁/A_{2A} receptor antagonist (Harmse et al., 2016). The current study provides additional scaffolds based on approved drugs that could be modified in the future to improve activities against these receptors.

The A_{2A}AR receptor is also expressed in the brain, where it has important roles in the regulation of glutamate and dopamine release, making it a potential therapeutic target for the treatment of conditions such as insomnia, pain, depression, and Parkinson's disease (Borea et al., 2018). A_{2A}AR is recognized as the main adenosine subtype located in the striatum, where it is colocalized with dopamine D₂ receptors (D₂R). This results in A_{2A}AR/D₂R heteromers that have a crucial role in the modulation of motor function (Borea et al., 2018). A_{2A}AR may be a therapeutic target in Alzheimer's disease, Huntington's disease, epilepsy, acute and chronic stress, and memory fear (Borea et al., 2018). Pharmacological agents that increase the activation of A₁AR in response to adenosine would be useful for the treatment of CNS, cardiovascular, and inflammatory pathologies (Borea et al., 2018). Coactivation of two AR subtypes might be therapeutically beneficial, such as both A₁AR and A₃AR in

cardioprotection (Jacobson et al., 2005). Understanding the mechanisms of drug actions at GPCRs and translating this understanding into more selective and effective medicines remains a challenge (May et al., 2007). The effects of an allosteric modulator on ligand efficacy and on affinity at the orthosteric site do not always correlate, such that a modulator can increase the affinity of an orthosteric ligand while decreasing the efficacy and vice versa (May et al., 2007).

CONCLUSION

The goal of this work was to use machine learning approaches to assist in identifying new molecules to modulate ARs. In the process we have identified several approved drugs with *in vitro* functional activity against the A_{2A}AR, A_{2B}AR and A₃AR subtypes, which could potentially be repurposed. The three molecules derived from machine learning each had a distinct pharmacological activity, which diverged in the different *in vitro* assays used and, in some cases, suggested non-canonical interaction with these receptors. Subsequent pharmacological characterization, including the use of AR-knockout mice (Xiao et al., 2019), will be needed to better understand their respective modes of action in future. The data generated in this study may also be used to improve our machine learning models and provide further structural diversity for starting points for medicinal chemistry efforts for AR modulators.

DATA AVAILABILITY STATEMENT

The original contributions presented in the study are included in the article/**Supplementary Material**, further inquiries can be directed to the corresponding authors.

AUTHOR CONTRIBUTIONS

AP performed data analysis, drafted the manuscript, assisted in providing funding for this project. SE drafted the manuscript and assisted in providing funding for this project. Z-GG and KJ performed pharmacological studies and data analysis. All authors contributed to conceptual design and editing of the manuscript.

FUNDING

We kindly acknowledge NIH funding: R44GM122196-02A1 from NIGMS, NIEHS for 1R43ES031038-01 and 3R43ES031038-01S1, NIDDK Intramural Res. for ZIADK031117. "Research reported in this publication was supported by the National Institute of Environmental Health Sciences of the National Institutes of Health under Award Number R43ES031038. The content is solely the responsibility of the authors and does not necessarily represent the official views of the National Institutes of Health."

ACKNOWLEDGMENTS

We kindly acknowledge assistance from Dr. Fabio Urbina and Ms. Kimberley Zorn. Dr. Alex M. Clark (Molecular Materials Informatics, Inc.) is thanked for support of the earlier version of Assay Central®.

REFERENCES

- Anantpadma, M., Lane, T., Zorn, K. M., Lingerfelt, M. A., Clark, A. M., Freundlich, J. S., et al. (2019). Ebola Virus Bayesian Machine Learning Models Enable New *In Vitro* Leads. *ACS Omega* 4 (1), 2353–2361. doi:10.1021/acsomega.8b02948
- Ballesteros-Yáñez, I., Castillo, C. A., Merighi, S., and Gessi, S. (2017). The Role of Adenosine Receptors in Psychostimulant Addiction. *Front. Pharmacol.* 8, 985. doi:10.3389/fphar.2017.00985
- Baraldi, P. G., Preti, D., Borea, P. A., and Varani, K. (2012). Medicinal Chemistry of A₃ Adenosine Receptor Modulators: Pharmacological Activities and Therapeutic Implications. *J. Med. Chem.* 55 (12), 5676–5703. doi:10.1021/jm300087j
- Borea, P. A., Gessi, S., Merighi, S., and Varani, K. (2016). Adenosine as a Multi-Signalling Guardian Angel in Human Diseases: When, Where and How Does it Exert its Protective Effects? *Trends Pharmacol. Sci.* 37 (6), 419–434. doi:10.1016/j.tips.2016.02.006
- Borea, P. A., Gessi, S., Merighi, S., Vincenzi, F., and Varani, K. (2018). Pharmacology of Adenosine Receptors: The State of the Art. *Physiol. Rev.* 98 (3), 1591–1625. doi:10.1152/physrev.00049.2017
- Cekic, C., and Linden, J. (2016). Purinergic Regulation of the Immune System. *Nat. Rev. Immunol.* 16 (3), 177–192. doi:10.1038/nri.2016.4
- Cheng, R. K. Y., Segala, E., Robertson, N., Defflorian, F., Doré, A. S., Errey, J. C., et al. (2017). Structures of Human A1 and A2A Adenosine Receptors with Xanthines Reveal Determinants of Selectivity. *Structure* 25 (8), 1275–1285. doi:10.1016/j.str.2017.06.012
- Ciruela, F., Casadó, V., Rodrigues, R. J., Luján, R., Burgueño, J., Canals, M., et al. (2006). Presynaptic Control of Striatal Glutamatergic Neurotransmission by Adenosine A1-A2A Receptor Heteromers. *J. Neurosci.* 26 (7), 2080–2087. doi:10.1523/JNEUROSCI.3574-05.2006
- Clark, A. M., Dole, K., Coulon-Spektor, A., McNutt, A., Grass, G., Freundlich, J. S., et al. (2015). Open Source Bayesian Models. 1. Application to ADME/Tox and Drug Discovery Datasets. *J. Chem. Inf. Model* 55 (6), 1231–1245. doi:10.1021/acs.jcim.5b00143
- Clark, A. M., and Ekins, S. (2015). Open Source Bayesian Models. 2. Mining a "Big Dataset" To Create and Validate Models with ChEMBL. *J. Chem. Inf. Model* 55 (6), 1246–1260. doi:10.1021/acs.jcim.5b00144
- Dalecki, A. G., Zorn, K. M., Clark, A. M., Ekins, S., Narmore, W. T., Tower, N., et al. (2019). High-Throughput Screening and Bayesian Machine Learning for Copper-Dependent Inhibitors of *Staphylococcus A. Metallomics* 11 (3), 696–706. doi:10.1039/c8mt00342d
- Effendi, W. I., Nagano, T., Kobayashi, K., and Nishimura, Y. (2020). Focusing on Adenosine Receptors as a Potential Targeted Therapy in Human Diseases. *Cells* 9 (3), 785. doi:10.3390/cells9030785
- Ekins, S., Gerlach, J., Zorn, K. M., Antonio, B. M., Lin, Z., and Gerlach, A. (2019). Repurposing Approved Drugs as Inhibitors of Kv7.1 and Nav1.8 to Treat Pitt Hopkins Syndrome. *Pharm. Res.* 36 (9), 137. doi:10.1007/s11095-019-2671-y
- Ekins, S., Puhl, A. C., Zorn, K. M., Lane, T. R., Russo, D. P., Klein, J. J., et al. (2019). Exploiting Machine Learning for End-To-End Drug Discovery and Development. *Nat. Mater* 18 (5), 435–441. doi:10.1038/s41563-019-0338-z
- Ekins, S., Mottin, M., Ramos, P. R. P. S., Sousa, B. K. P., Neves, B. J., Foil, D. H., et al. (2020). Déjà vu: Stimulating Open Drug Discovery for SARS-CoV-2. *Drug Discov. Today* 25 (5), 928–941. In press. doi:10.1016/j.drudis.2020.03.019
- Elmenhorst, D., Meyer, P. T., Winz, O. H., Matusch, A., Ermert, J., Coenen, H. H., et al. (2007). Sleep Deprivation Increases A1 Adenosine Receptor Binding in the Human Brain: A Positron Emission Tomography Study. *J. Neurosci.* 27 (9), 2410–2415. doi:10.1523/JNEUROSCI.5066-06.2007
- Fredholm, B. B., Ijzerman, A. P., Jacobson, K. A., Klotz, K. N., and Linden, J. (2001). International Union of Pharmacology. XXV. Nomenclature and Classification of Adenosine Receptors. *Pharmacol. Rev.* 53 (4), 527–552.
- Gao, Z. G., and Jacobson, K. A. (2017). Purinergic Signaling in Mast Cell Degranulation and Asthma. *Front. Pharmacol.* 8, 947. doi:10.3389/fphar.2017.00947
- Gao, Z. G., and Jacobson, K. A. (2019). A_{2B} Adenosine Receptor and Cancer. *Int. J. Mol. Sci.* 20 (20), 5139. doi:10.3390/ijms20205139
- Gaulton, A., Hersey, A., Nowotka, M., Bento, A. P., Chambers, J., Mendez, D., et al. (2017). The ChEMBL Database in 2017. *Nucleic Acids Res.* 45 (D1), D945–D954. doi:10.1093/nar/gkw1074
- Geldenhuis, W. J., Hanif, A., Yun, J., and Nayeem, M. A. (2017). Exploring Adenosine Receptor Ligands: Potential Role in the Treatment of Cardiovascular Diseases. *Molecules* 22 (6), 917. doi:10.3390/molecules22060917
- Harmse, R., van der Walt, M. M., Petzer, J. P., and Terre'Blanche, G. (2016). Discovery of 1,3-Diethyl-7-Methyl-8-(Phenoxymethyl)-Xanthine Derivatives as Novel Adenosine A1 and A2A Receptor Antagonists. *Bioorg Med. Chem. Lett.* 26 (24), 5951–5955. doi:10.1016/j.bmcl.2016.10.086
- Heider, F., Ansideri, F., Tesch, R., Pansar, T., Haun, U., Döring, E., et al. (2019). Pyridinylimidazoles as Dual Glycogen Synthase Kinase 3β/p38α Mitogen-Activated Protein Kinase Inhibitors. *Eur. J. Med. Chem.* 175, 309–329. doi:10.1016/j.ejmech.2019.04.035
- Hernandez, H. W., Soeung, M., Zorn, K. M., Ashoura, N., Mottin, M., Andrade, C. H., et al. (2018). High Throughput and Computational Repurposing for Neglected Diseases. *Pharm. Res.* 36 (2), 27. doi:10.1007/s11095-018-2558-3
- Jacobson, K. A., Gao, Z. G., Tchilibon, S., Duong, H. T., Joshi, B. V., Sonin, D., et al. (2005). Semi-Rational Design of (North)-Methanocarpa Nucleosides as Dual Acting A(1) and A(3) Adenosine Receptor Agonists: Novel Prototypes for Cardioprotection. *J. Med. Chem.* 48 (26), 8103–8107. doi:10.1021/jm050726b
- Jacobson, K. A., Tosh, D. K., Jain, S., and Gao, Z. G. (2019). Historical and Current Adenosine Receptor Agonists in Preclinical and Clinical Development. *Front. Cell Neurosci.* 13, 124. doi:10.3389/fncel.2019.00124
- Lane, T., Russo, D. P., Zorn, K. M., Clark, A. M., Korotcov, A., Tkachenko, V., et al. (2018). Comparing and Validating Machine Learning Models for *Mycobacterium T* Drug Discovery. *Mol. Pharm.* 15 (10), 4346–4360. doi:10.1021/acs.molpharmaceut.8b00083
- May, L. T., Leach, K., Sexton, P. M., and Christopoulos, A. (2007). Allosteric Modulation of G Protein-Coupled Receptors. *Annu. Rev. Pharmacol. Toxicol.* 47, 1–51. doi:10.1146/annurev.pharmtox.47.120505.105159
- Ohta, A., and Sitkovsky, M. (2001). Role of G-Protein-Coupled Adenosine Receptors in Downregulation of Inflammation and Protection from Tissue Damage. *Nature* 414 (6866), 916–920. doi:10.1038/414916a
- Okusa, M. D., Linden, J., Macdonald, T., and Huang, L. (1999). Selective A2A Adenosine Receptor Activation Reduces Ischemia-Reperfusion Injury in Rat Kidney. *Am. J. Physiol.* 277 (3), F404–F412. doi:10.1152/ajprenal.1999.277.3.F404
- Russo, D. P., Zorn, K. M., Clark, A. M., Zhu, H., and Ekins, S. (2018). Comparing Multiple Machine Learning Algorithms and Metrics for Estrogen Receptor Binding Prediction. *Mol. Pharm.* 15 (10), 4361–4370. doi:10.1021/acs.molpharmaceut.8b00546
- Saad, A. I., Omar, Y. M. K., and Maghraby, F. A. (2019). Predicting Drug Interaction with Adenosine Receptors Using Machine Learning and SMOTE Techniques. *IEEE Access* 7, 146953–146963. doi:10.1109/ACCESS.2019.2946314
- Sandoval, P. J., Zorn, K. M., Clark, A. M., Ekins, S., and Wright, S. H. (2018). Assessment of Substrate-Dependent Ligand Interactions at the Organic Cation Transporter OCT2 Using Six Model Substrates. *Mol. Pharmacol.* 94 (3), 1057–1068. doi:10.1124/mol.117.111443
- Schlessinger, J., Shepard, J. S., Gower, R., Su, J. C., Lynde, C., Cha, A., et al. (2020). Safety, Effectiveness, and Pharmacokinetics of Crisaborole in Infants Aged 3 to < 24 Months with Mild-To-Moderate Atopic Dermatitis: A Phase IV Open-Label Study (CrisAde CARE 1). *Am. J. Clin. Dermatol* 21 (2), 275–284. doi:10.1007/s40257-020-00510-6

SUPPLEMENTARY MATERIAL

The Supplementary Material for this article can be found online at: <https://www.frontiersin.org/articles/10.3389/fphar.2022.920643/full#supplementary-material>

- Siramshetty, V. B., Eckert, O. A., Gohlke, B. O., Goede, A., Chen, Q., Devarakonda, P., et al. (2018). SuperDRUG2: A One Stop Resource for Approved/Marketed Drugs. *Nucleic Acids Res.* 46 (D1), D1137–D1143. doi:10.1093/nar/gkx1088
- Stone, T. W., Ceruti, S., and Abbracchio, M. P. (2009). Adenosine Receptors and Neurological Disease: Neuroprotection and Neurodegeneration. *Handb. Exp. Pharmacol.* 193, 535–587. doi:10.1007/978-3-540-89615-9_17
- Tawfik, H. E., Schnermann, J., Oldenburg, P. J., and Mustafa, S. J. (2005). Role of A1 Adenosine Receptors in Regulation of Vascular Tone. *Am. J. Physiol. Heart Circ. Physiol.* 288 (3), H1411–H1416. doi:10.1152/ajpheart.00684.2004
- Wang, M., Hou, S., Wei, Y., Li, D., and Lin, J. (2021). Discovery of Novel Dual Adenosine A1/A2A Receptor Antagonists Using Deep Learning, Pharmacophore Modeling and Molecular Docking. *PLoS Comput. Biol.* 17 (3), e1008821. doi:10.1371/journal.pcbi.1008821
- Wang, P. F., Neiner, A., Lane, T. R., Zorn, K. M., Ekins, S., and Kharasch, E. D. (2019). Halogen Substitution Influences Ketamine Metabolism by Cytochrome P450 2B6: *In Vitro* and Computational Approaches. *Mol. Pharm.* 16 (2), 898–906. doi:10.1021/acs.molpharmaceut.8b01214
- Wardas, J. (2002). Neuroprotective Role of Adenosine in the CNS. *Pol. J. Pharmacol.* 54 (4), 313–326.
- Wu, L. G., and Saggau, P. (1997). Presynaptic Inhibition of Elicited Neurotransmitter Release. *Trends Neurosci.* 20 (5), 204–212. doi:10.1016/s0166-2236(96)01015-6
- Xiao, C., Liu, N., Jacobson, K. A., Gavrilo, O., and Reitman, M. L. (2019). Physiology and Effects of Nucleosides in Mice Lacking All Four Adenosine Receptors. *PLoS Biol.* 17 (3), e3000161. doi:10.1371/journal.pbio.3000161
- Ye, Q., Li, M., Zhou, Y., Pang, T., Xu, L., Cao, J., et al. (2013). Synthesis and Biological Evaluation of 3-Benzisoxazolyl-4-Indolylmaleimides as Potent, Selective Inhibitors of Glycogen Synthase Kinase-3 β . *Molecules* 18 (5), 5498–5516. doi:10.3390/molecules18055498
- Zhang, H. C., White, K. B., Ye, H., McComsey, D. F., Derian, C. K., Addo, M. F., et al. (2003). Macrocyclic Bisindolylmaleimides as Inhibitors of Protein Kinase C and Glycogen Synthase Kinase-3. *Bioorg. Med. Chem. Lett.* 13 (18), 3049–3053. doi:10.1016/s0960-894x(03)00644-9
- Zorn, K. M., Lane, T. R., Russo, D. P., Clark, A. M., Makarov, V., and Ekins, S. (2019). Multiple Machine Learning Comparisons of HIV Cell-Based and Reverse Transcriptase Data Sets. *Mol. Pharm.* 16 (4), 1620–1632. doi:10.1021/acs.molpharmaceut.8b01297

Conflict of Interest: SE is the owner and AP is an employee of Collaborations Pharmaceuticals, Inc.

The remaining authors declare that the research was conducted in the absence of any commercial or financial relationships that could be construed as a potential conflict of interest.

Publisher's Note: All claims expressed in this article are solely those of the authors and do not necessarily represent those of their affiliated organizations, or those of the publisher, the editors and the reviewers. Any product that may be evaluated in this article, or claim that may be made by its manufacturer, is not guaranteed or endorsed by the publisher.

Copyright © 2022 Puhl, Gao, Jacobson and Ekins. This is an open-access article distributed under the terms of the Creative Commons Attribution License (CC BY). The use, distribution or reproduction in other forums is permitted, provided the original author(s) and the copyright owner(s) are credited and that the original publication in this journal is cited, in accordance with accepted academic practice. No use, distribution or reproduction is permitted which does not comply with these terms.



OPEN ACCESS

EDITED BY

Kenneth A. Jacobson,
National Institutes of Health (NIH),
United States

REVIEWED BY

Eddy Sotelo,
Universidad de Santiago de
Compostela, Spain
Pier Andrea Borea,
University of Ferrara, Italy

*CORRESPONDENCE

Xiaoyi Yuan,
Xiaoyi.Yuan@uth.tmc.edu

SPECIALTY SECTION

This article was submitted to
Experimental Pharmacology and Drug
Discovery,
a section of the journal
Frontiers in Pharmacology

RECEIVED 16 May 2022

ACCEPTED 28 June 2022

PUBLISHED 15 July 2022

CITATION

Yuan X, Mills T, Doursout M-F, Evans SE,
Vidal Melo MF and Eltzschig HK (2022),
Alternative adenosine Receptor
activation: The netrin-Adora2b link.
Front. Pharmacol. 13:944994.
doi: 10.3389/fphar.2022.944994

COPYRIGHT

© 2022 Yuan, Mills, Doursout, Evans,
Vidal Melo and Eltzschig. This is an
open-access article distributed under
the terms of the [Creative Commons
Attribution License \(CC BY\)](#). The use,
distribution or reproduction in other
forums is permitted, provided the
original author(s) and the copyright
owner(s) are credited and that the
original publication in this journal is
cited, in accordance with accepted
academic practice. No use, distribution
or reproduction is permitted which does
not comply with these terms.

Alternative adenosine Receptor activation: The netrin-Adora2b link

Xiaoyi Yuan^{1*}, Tingting Mills², Marie-Francoise Doursout¹,
Scott E. Evans³, Marcos F. Vidal Melo⁴ and Holger K. Eltzschig¹

¹Department of Anesthesiology, McGovern Medical School, The University of Texas Health Science Center at Houston, Houston, TX, United States, ²Department of Biochemistry and Molecular Biology, The University of Texas Health Science Center at Houston, Houston, TX, United States, ³Department of Pulmonology, MD Anderson Cancer Center, Houston, TX, United States, ⁴Department of Anesthesiology, Columbia University, New York, NY, United States

During hypoxia or inflammation, extracellular adenosine levels are elevated. Studies using pharmacologic approaches or genetic animal models pertinent to extracellular adenosine signaling implicate this pathway in attenuating hypoxia-associated inflammation. There are four distinct adenosine receptors. Of these, it is not surprising that the Adora2b adenosine receptor functions as an endogenous feedback loop to control hypoxia-associated inflammation. First, Adora2b activation requires higher adenosine concentrations compared to other adenosine receptors, similar to those achieved during hypoxic inflammation. Second, Adora2b is transcriptionally induced during hypoxia or inflammation by hypoxia-inducible transcription factor HIF1A. Studies seeking an alternative adenosine receptor activation mechanism have linked netrin-1 with Adora2b. Netrin-1 was originally discovered as a neuronal guidance molecule but also functions as an immune-modulatory signaling molecule. Similar to Adora2b, netrin-1 is induced by HIF1A, and has been shown to enhance Adora2b signaling. Studies of acute respiratory distress syndrome (ARDS), intestinal inflammation, myocardial or hepatic ischemia and reperfusion implicate the netrin-Adora2b link in tissue protection. In this review, we will discuss the potential molecular linkage between netrin-1 and Adora2b, and explore studies demonstrating interactions between netrin-1 and Adora2b in attenuating tissue inflammation.

KEYWORDS

adenosine, netrin-1, Adora2b, hypoxia, inflammation

Introduction

Hypoxia and inflammation are highly interdependent (Taylor, 2008; Taylor and Colgan, 2017). Inflammatory lesions are characterized by an imbalance in metabolic supply and demand. The active inflammatory process consumes a large amount of oxygen. For example, polymorphonuclear neutrophils (PMNs) consume such vast amounts of oxygen when activated that they can cause hypoxic imprinting on neighboring stromal or epithelial cells (Campbell et al., 2014). Other inflammatory

cells such as natural killer cells (Victorino et al., 2015; Hoegl et al., 2016), eosinophils (Patel et al., 2014; Masterson et al., 2015; Wang et al., 2021a), macrophages (Gao et al., 2020), or T-cells (Sun et al., 2010; Clambey et al., 2012; Ehrentauf et al., 2012; Ehrentauf et al., 2013; Yuan et al., 2019) contribute to shaping the metabolic environment in inflammatory or infectious foci (Koeppen et al., 2011a; Gumbert et al., 2020). At the same time, the supply of metabolites from the bloodstream is often diminished due to microvascular occlusions, edema or shunting (Eltzschig and Collard, 2004). In addition, alterations of specific metabolites (e.g., accumulation of succinate) can further shape a hypoxic microenvironment and contribute to transcriptional reprogramming (Haerberle et al., 2008; Eckle et al., 2013a; Vohwinkel et al., 2021). Many studies have found that during hypoxia-induced inflammation (inflammatory hypoxia), extracellular levels of adenosine are elevated (Ohta and Sitkovsky, 2001; Sitkovsky et al., 2004; Sitkovsky and Lukashev, 2005; Thiel et al., 2005), and implicate extracellular adenosine signaling in an endogenous feedback loop to attenuate hypoxia-induced inflammation (Cronstein, 1994; Eltzschig and Carmeliet, 2011; Eltzschig et al., 2012).

Adenosine is part of a group of biomolecules termed purines, defined as heterocyclic aromatic molecules (Eltzschig, 2013). These molecules belong to the most ancient and conserved biochemical molecules during evolution (Miller and Urey, 1959). These relatively simple biochemical molecules are fitted together from adenine and guanine, resembling the most critical building block for mammalian genes (Fredholm and Verkhratsky, 2010). Therefore, the purine adenosine has earned its place as the biomolecular building block of the genetic code and as part of the universal biological energy currency, adenosine triphosphate (ATP) (Khakh and Burnstock, 2009; Eltzschig, 2013). However, adenosine plays diverse roles in physiological and pathophysiological conditions (Khakh and Burnstock, 2009). Beyond these functions, adenosine has been recognized as a signaling molecule through the activation of four receptors named A1, A2A, A2B, and A3 receptors (Adora1, Adora2a, Adora2b, Adora3). These G-protein coupled receptors have many biological functions. For example, activation of Adora1 slows the heart rate, allowing adenosine injection to be used for treating supraventricular tachycardia (Koeppen et al., 2009). Adora2a is expressed on immune cells, such as PMNs (Cronstein et al., 1990) and T-cells (Yang et al., 2006a), and has been shown to dampen harmful inflammation (Ohta and Sitkovsky, 2001; Hasko and Cronstein, 2004). Adora3 has been implicated in mast cell activation and the pathogenesis of asthmatic airway disease (Jin et al., 1997; Zhong et al., 2003).

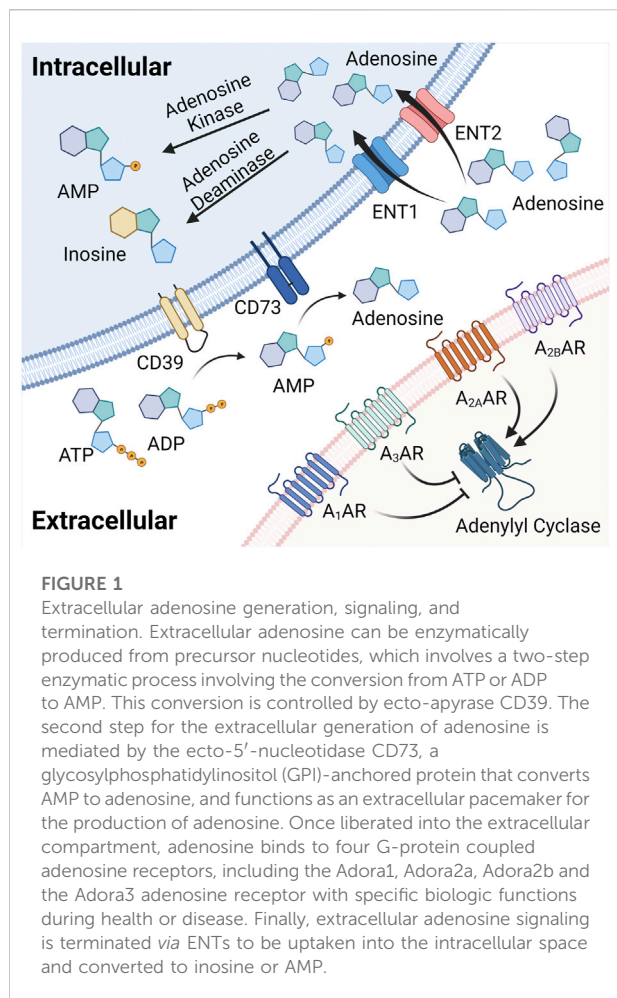
In contrast to the other three adenosine receptors, the Adora2b is somewhat unique in its role for hypoxia adaptation (Eltzschig et al., 2003; Kong et al., 2006) and has been considered a safety signal during inflammatory hypoxia (Grenz et al., 2011a; Koeppen et al., 2011b). Two features make

Adora2b well suited to hypoxia adaptation. First, Adora2b is transcriptionally induced by hypoxia-inducible transcription factor HIF1A (Kong et al., 2006; Poth et al., 2013), and therefore levels of Adora2b are highest during hypoxia or inflammatory states (Eckle et al., 2013b; Eckle et al., 2014; Hoegl et al., 2015; Wang et al., 2021b). Second, it is the most “insensitive” of the four adenosine receptors, requiring the highest adenosine concentrations to be activated (Feoktistov and Biaggioni, 1997; Aherne et al., 2011; Koeppen et al., 2011b). Such high concentrations of extracellular adenosine are present during hypoxia and inflammation and activate the Adora2b receptor (Feoktistov and Biaggioni, 1997; Feoktistov and Biaggioni, 2011).

Interestingly, several studies have suggested an alternative adenosine independent mechanism of Adora2b activation, particularly during hypoxia or inflammation. This process involves the neuronal guidance molecule netrin-1. Netrin-1 is one of neuronal guidance molecules that are critical for neuronal development by either attracting or repelling developing neurons (Serafini et al., 1994; Serafini et al., 1996; Corset et al., 2000; Mirakaj and Rosenberger, 2017; Keller et al., 2021). Several studies suggest that during inflammatory conditions, netrin-1-elicited organ protection during inflammatory hypoxia is dependent on Adora2b signaling (Rosenberger et al., 2009). Additionally, other studies indicate that netrin-1 is a direct ligand of Adora2b (Stein et al., 2001; Feoktistov and Biaggioni, 2011). In the present review, we will first discuss the role of Adora2b during hypoxia and inflammation. Subsequently, we will explore studies linking netrin-1 with Adora2b signaling during hypoxia, inflammation or ischemia and reperfusion. Finally, we will discuss potential molecular mechanisms connecting netrin-1 with Adora2b and the evidence that argues for and against a direct activation of the Adora2b by netrin-1.

Extracellular adenosine signaling during hypoxia and inflammation

That hypoxia is associated with increased extracellular adenosine levels has been known for many years. For example, studies from the early 1990s showed that plasma adenosine levels in rats rose from approximately 80 nM at baseline to approximately 190 nM following exposure to ambient hypoxia (8% oxygen) (Phillis et al., 1992). Hypoxia-driven increases of extracellular adenosine have been implicated as an endogenous feedback mechanism to promote hypoxia adaptation. For example, recent reports indicate that adenosine levels in plasma are induced in a rapid manner after high altitude exposure. Importantly, the induction is amplified upon re-ascent. This observation has been subsequently linked with faster adaptation to high altitudes



and more rapid acclimatization (Liu et al., 2016; Song et al., 2017; Sun et al., 2017).

Studies in genetic and pharmacologic models with altered adenosine production have provided insight into mechanisms controlling extracellular adenosine levels during hypoxia and inflammation. Extracellular adenosine can be enzymatically produced from precursor nucleotides, which involves a two-step enzymatic process (Figure 1). The first step involves the conversion of precursor nucleotides—such as ATP or ADP to AMP (Garcia-Morales et al., 2016a; Bowser et al., 2017a; Bowser et al., 2017b; Bowser et al., 2018). This conversion is controlled by ecto-apyrase CD39 (Kaczmarek et al., 1996; Enjyoji et al., 1999; Robson et al., 2001; Robson et al., 2005). During injurious conditions such as hypoxia or inflammation, many cells release precursor nucleotides (Eltzschig et al., 2006a; Faigle et al., 2008; Colgan and Eltzschig, 2012), and therefore the extracellular production of AMP is dramatically increased (Eltzschig et al., 2006b; Eckle et al., 2007a; Kohler et al., 2007; Eltzschig et al., 2009a; Friedman et al., 2009; Reutershan et al., 2009; Hart et al., 2010; Le et al., 2019). The second step for the

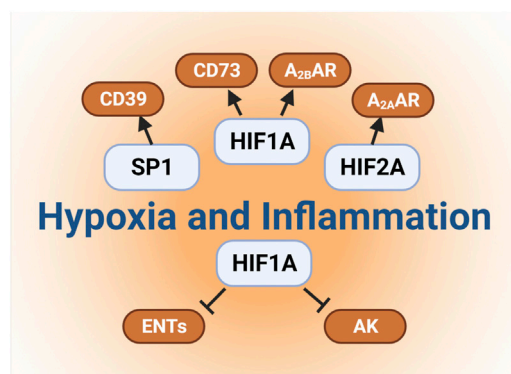


FIGURE 2

Links between hypoxia and extracellular adenosine. Several studies have elucidated the molecular mechanisms involved in hypoxia-dependent enhancement of extracellular adenosine signaling. Firstly, hypoxia and concomitant HIF1A stabilization directly induces the expressional levels of CD73. Secondly, hypoxia dependent CD39 induction is controlled by a transcriptional mechanism involving SP1. Furthermore, HIF1A and HIF2A stabilization results in the enhancement of adenosine receptors expression, such as Adora2b and Adora2a, respectively. Finally, previous studies also implicate HIF1A in the repression of both ENTs and adenosine kinases, which indirectly promotes the additional elevations of extracellular signaling events.

extracellular generation of adenosine is mediated by the ecto-5'-nucleotidase CD73, a glycosylphosphatidylinositol (GPI)-anchored protein that converts AMP to adenosine, and functions as extracellular pacemaker for the production of adenosine (Hansen et al., 1995; Weissmuller et al., 2005; Eltzschig et al., 2008; Zhang et al., 2013). Studies in mice with genetic deletion of *Cd39* or *Cd73* suggested that these animals have more severe vascular leakage and inflammatory responses during hypoxia exposure (Eltzschig et al., 2003; Eltzschig et al., 2004; Thompson et al., 2004). Similarly, they experience more profound tissue injury and inflammation when exposed to models of acute respiratory distress syndrome (ARDS) (Eckle et al., 2007a; Eckle et al., 2008a; Reutershan et al., 2009; Koeppen et al., 2011c), myocardial ischemia and reperfusion (Eckle et al., 2006; Eckle et al., 2007b; Kohler et al., 2007; Eckle et al., 2011), liver injury (Hart et al., 2008a; Hart et al., 2008b; Hart et al., 2010), or intestinal inflammation (Hart et al., 2008c; Hart et al., 2008d; Louis et al., 2008; Friedman et al., 2009; Hart et al., 2009). Taken together, these studies indicate that during inflammatory hypoxia, the production of extracellular adenosine is elevated and serves as an endogenous feedback signal to diminish excessive inflammation (Eltzschig et al., 2012).

Several studies have elucidated the molecular mechanisms involved in hypoxia-dependent enhancement of extracellular adenosine signaling (Figure 2). These studies identified a central regulatory role of HIF1A by regulating the expressional levels of CD73. Hypoxia signaling through HIFs

resembles an adaptive signaling pathway that has been selected from ancient atmospheres for survival benefit under fluctuating oxygen levels (Taylor and McElwain, 2010). During hypoxia or inflammation, HIF1A is stabilized and forms a transcriptionally active heterodimer with HIF1B. Subsequent translocation to the nucleus and binding to hypoxia response elements (HREs) in hypoxia-controlled target genes typically causes induction of the gene product (Eltzschig et al., 2014; Ju et al., 2016; Semenza, 2020). Notable HIF target genes include, for example, erythropoietin, the group of enzymes controlling the glycolytic flux of carbohydrate intermediates, and vascular endothelial growth factor (Wang and Semenza, 1993; Semenza et al., 1994; Wang et al., 1995; Forsythe et al., 1996; Semenza et al., 1996). The discovery of the HIF pathway was recognized by the 2019 Nobel Prize in medicine or physiology (Fandrey et al., 2019; Colgan et al., 2020). While most commonly HIF binding causes induction of target genes (Zheng et al., 2009), there are also many instances where HIF1A activity causes gene repression (Eltzschig et al., 2005; Loffler et al., 2007; Morote-Garcia et al., 2008; Morote-Garcia et al., 2009; Ju et al., 2021), such as by the induction of HIF-dependent microRNAs (Ferrari et al., 2016a; Ferrari et al., 2016b; Neudecker et al., 2016; Neudecker et al., 2017a; Lee et al., 2020a). Studies of hypoxia exposure of epithelial cells or vascular endothelia demonstrate that both CD39 and CD73 are induced by hypoxia (Synnestvedt et al., 2002; Eltzschig et al., 2003). While CD39 is controlled by SP1 (Eltzschig et al., 2009a; Hart et al., 2010), the promoter of CD73 contains an HRE, and studies with transcription factor binding and promoter constructs directly implicate HIF1A in the transcriptional induction of CD73 (Synnestvedt et al., 2002; Garcia-Morales et al., 2016b). Additional molecular mechanisms of HIF-dependent increases in extracellular adenosine during hypoxia and inflammation include transcriptional repression of adenosine uptake and metabolism (Eltzschig et al., 2005; Loffler et al., 2007; Morote-Garcia et al., 2008). Adenosine signaling is terminated by equilibrative nucleoside transporters, ENT1 or ENT2 mediated uptake of extracellular adenosine towards intracellular spaces (Rose et al., 2011; Eckle et al., 2013b; Morote-Garcia et al., 2013; Aherne et al., 2018; Wang et al., 2021b) (Figure 1). Previous studies implicate HIF1A in the repression of both ENT1 (Eltzschig et al., 2005) and ENT2 (Morote-Garcia et al., 2009) during hypoxia or inflammatory diseases, leading to additional elevations of extracellular signaling events (Loffler et al., 2007). Similarly, HIF1A causes transcriptional repression of the adenosine kinase (Morote-Garcia et al., 2008), a response that dampens intracellular adenosine metabolism from adenosine to AMP, thereby functioning to further enhance adenosine signaling events in the extracellular compartment (Decking et al., 1997; Ferrari et al., 2016a; Ferrari et al., 2016b; Ferrari et al., 2016c; Yuan et al., 2021). Taken together, these studies accentuate the functional role of HIF1A in the control of extracellular adenosine signaling during hypoxia and inflammation (Poth et al., 2013).

Adora2b during hypoxia and inflammation

Once liberated into the extracellular compartment, adenosine binds four G-protein coupled adenosine receptors: Adora1, Adora2a, Adora2b and Adora3 (Figure 1) (Hasko and Cronstein, 2004; Sitkovsky et al., 2004; Sitkovsky and Lukashev, 2005; Hasko et al., 2008; Eltzschig, 2009; Idzko et al., 2014a; Idzko et al., 2014b). Each of these receptors has been associated with specific biologic functions during health or disease states (Chen et al., 2013). For example, the Adora1 was suggested to mediate the heart-rate slowing effects of adenosine (Koeppen et al., 2009). As such, functional studies implicate this receptor in cardio-protection during ischemic pre- or post-conditioning (Matherne et al., 1997; Reichelt et al., 2005), an experimental strategy where short periods of non-lethal ischemia can be applied to increase myocardial resistance to ischemia (Eckle et al., 2006; Redel et al., 2008). The Adora2a is expressed on inflammatory cells and has been shown to dampen acute inflammatory responses in a variety of models (Cronstein et al., 1990; Ohta and Sitkovsky, 2001; Sitkovsky et al., 2004; Thiel et al., 2005; Hasko et al., 2008). The Adora3 has been shown to be expressed on mast-cells and has been implicated in asthmatic airway disease (Salvatore et al., 2000; Zhong et al., 2003), while studies in *Adora3*^{-/-} mice show elevated blood pressure, aggressiveness and hypoalgesia (Ledent et al., 1997). The Adora2b receptor has been identified as a “low-affinity” receptor (Feoktistov and Biaggioni, 1997; Feoktistov and Biaggioni, 2011), and since it appears to have many similar functions to the Adora2a (e.g., both receptors promote intracellular cAMP levels), it was initially thought to be redundant or lesser physiologic compared to the other adenosine receptors (Aherne et al., 2011). However, several factors have led to a rethinking of Adora2b, and have identified the Adora2b as a critical adenosine receptor during adaptation to hypoxia or inflammation. First, the fact that signaling events through the Adora2b require higher adenosine levels than other three adenosine receptors highlights that the Adora2b is particularly active during states of elevated adenosine levels, such as during hypoxia and inflammation (Van Linden and Eltzschig, 2007; Eltzschig et al., 2009b; Koeppen et al., 2011b; Wen et al., 2011; Zhang et al., 2011; Grenz et al., 2012; Karmouty-Quintana et al., 2012). Secondly, several studies provide evidence for selective induction of the Adora2b during hypoxia or inflammation. For example, a screen for transcriptional responses in human vascular endothelial cells exposed to hypoxia (2% oxygen) revealed that only the Adora2b transcript levels were induced (Eltzschig et al., 2003). Functional studies in *Adora2b*^{-/-} mice demonstrate that these mice experience more profound vascular inflammation, including significantly increased leukocyte adhesion to the vasculature and increased pro-inflammatory cytokine levels upon stimulation with LPS (Yang et al., 2006b). Similarly, *Adora2b*^{-/-} mice are more prone to obesity, delayed glucose

clearance and augmented insulin levels compared to controls (Johnston-Cox et al., 2012). Other studies highlight that *Adora2b*^{-/-} mice are susceptible to developing vascular lesions in vascular injury models (Yang et al., 2008). Together with other studies (Eltzschig et al., 2003; Eltzschig et al., 2004), these findings highlight functional roles for the Adora2b during tissue inflammation and hypoxia, as an endogenous feedback cue to control excessive inflammation.

Discovery and function of netrin-1 as a neuronal guidance molecule

Netrin-1 was initially discovered as a neuronal guidance molecule (Serafini et al., 1994; Serafini et al., 1996). The name netrin comes from the Sanskrit word “netr,” meaning “one who guides”. Netrin-1 belongs to the family of netrins, which are composed of secreted proteins that are critical to the developing brain, due to their function to attract or repel growing axons. Neuronal guidance is a critical aspect of brain development, where neurons send out axons to reach their correct targets (Colamarino and Tessier-Lavigne, 1995). Purification of proteins derived from embryonic chick brain has led to the identification of the protein netrin-1, which showed commissural axon outgrowth-promoting activity (Serafini et al., 1994). In addition, studies in gene-targeted mice for netrin-1 (*Ntn1*^{-/-} mice) revealed impaired spinal commissural axon projections, implicating functional roles of netrin-1 in axon guidance (Serafini et al., 1996). The neurologic defects in homozygous *Ntn1*^{-/-} mice are so severe that these mice are born and die withing a few days due to significant neurologic defects including the lacking of suckling, and inability to move their forelimbs (Serafini et al., 1996). Subsequent studies used transgenic mice with a “floxed” netrin-1 gene, so that studies in adult mice would be possible (Brunet et al., 2014; Varadarajan et al., 2017; Zhu et al., 2019; Li et al., 2021). Nevertheless, the above described early studies in mice gene-targeted for netrin-1 established netrin-1 as a guidance molecule that functions during vertebral brain development (Serafini et al., 1996).

Netrin-1 as a guidance cue during inflammation

The properties and functions on netrin-1 within the CNS as neuronal guidance molecule make it an ideal candidate for also guiding inflammatory cell trafficking events. In fact, several other neuronal guidance molecules (Konig et al., 2012; Mirakaj et al., 2012; Kohler et al., 2013; Kohler et al., 2020) have been implicated in immunomodulation and coordination of inflammatory events or resolution of inflammation (Mirakaj and Rosenberger, 2017; Keller et al., 2021). The unique characteristic of netrin-1 to repulse or abolish the attraction of developing neuronal cells

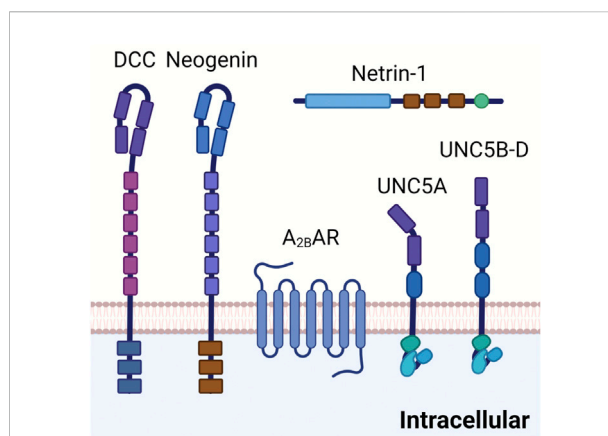


FIGURE 3

Netrin-1 receptors. DCC is a transmembrane protein composed of four immunoglobulin like repeats and six fibronectin type II like repeats on the extracellular site. It is involved in the netrin-1 mediated bi-functional guidance of neurons. Neogenin shares a similar structure to DCC and has been implicated in tissue morphogenesis, angiogenesis, as well as axon guidance. Adora2b has been identified as a netrin-1 coreceptor in netrin-1 signaling in certain tissues, although detailed mechanisms are still under investigation. UNC5 receptors (UNC5A-D) are composed of two immunoglobulin like repeats and two thrombospondin domains in the extracellular area. UNC5 receptors have been suggested in the long range and short range repulsion during axon guidance.

via signaling events through the UNC5b receptor makes it a perfect candidate gene for coordinating inflammatory cell migration (Figure 3). In line with this hypothesis, studies showed that netrin-1 is expressed on vascular endothelial cells, where its expression can be regulated by infection or inflammation. Similarly, UNC5b was found to be expressed on leukocytes and interacts with netrin-1 as migration inhibitor to different chemotaxis (Ly et al., 2005).

Subsequent studies suggest that netrin-1 can also function to promote atherosclerosis by entrapping macrophages in plaques (van Gils et al., 2012). In line with these findings, a recent study demonstrates that silencing of netrin-1 in the myeloid lineage promotes the resolution of inflammation and plaque regression (Schlegel et al., 2021). Netrin-1 signaling can also function as a macrophage retention signal for the promotion of chronic inflammation and insulin resistance in adipose tissue (Ramkhalawon et al., 2014) or in the pathogenesis of abdominal aortic aneurism in vascular smooth muscle cells (Hadi et al., 2018). Other studies suggest a functional role of netrin-1 signaling in osteoclast differentiation (Mediero et al., 2015), inflammatory arthritis (Mediero et al., 2016; Zhu et al., 2019), or pulmonary fibrosis (Gao et al., 2021). In line with the concept that netrin-1 can have highly diverse signaling functions, a very elegant study implicated netrin-1 signaling in the resolution process of inflammation, an intricate process involving pro-resolving mediators (Serhan and Levy, 2018;

Mirakaj, 2021). During zymosan-initiated peritoneal inflammation, the vagus nerve was found to regulate the local expression of netrin-1 (Mirakaj et al., 2014). A vagotomy results in delayed resolution through inhibition of pro-resolving mediators. Using genetic studies, the authors found that in mice with partial netrin-1 deficiency, pro-resolving mediator resolvin D1 failed to reduce neutrophil influx, thus dampening the resolution of peritonitis compared with controls. Similarly, when human monocytes were treated with recombinant netrin-1, their production of lipid proresolving mediators was increased. These findings suggest that the vagus nerve controls both netrin-1 and pro-resolving programs (Mirakaj et al., 2014). Beyond those studies, and pertinent to the present review, several studies over the past 2 decades have repeatedly shown that the anti-inflammatory and pro-resolution role of netrin-1 signaling can be mediated through the Adora2b adenosine receptor (Eltzschig, 2009; Aherne et al., 2013).

Linkages between Adora2b and netrin-1 signaling

Not long after its original discovery as a neuronal guidance molecule (Serafini et al., 1994; Colamarino and Tessier-Lavigne, 1995; Serafini et al., 1996), a study reported a previously unrecognized interaction between netrin-1 and the Adora2b adenosine receptor (Corset et al., 2000). This study was based on the notion that the interaction of netrin-1 with its receptor deleted in colorectal carcinoma (DCC) might involve an additional co-receptor, since netrin-1 protein only co-immunoprecipitate with DCC if cross-linked. Moreover, netrin-1 did not bind to a soluble fusion protein of the extracellular domain of DCC directly *in vitro* (Meyerhardt et al., 1999). To find such a co-receptor, a subsequent study utilized a two-hybrid screen of human brain complementary DNA and identified a fragment corresponding to the last 23 amino acids of the intracellular domain of the Adora2b with potential binding to intracellular domain of DCC. Using co-immunoprecipitation, they demonstrated a direct interaction of the Adora2b with DCC, but only in the presence of netrin-1. Additionally, they showed that the Adora2b can serve as a netrin-1 receptor, including the induction of cAMP elevations upon binding of netrin-1 to the Adora2b. Finally, they performed studies on netrin-1 mediated axon growth and described that netrin-1-mediated outgrowth of dorsal spinal cord axons requires Adora2b signaling (Corset et al., 2000). In contrast to those findings, a subsequent study found that netrin-1 directly regulates axon guidance, independent of the Adora2b (Stein et al., 2001). Moreover, another study demonstrated that netrin-1 does not bind to Adora2b. However, Adora2b activation by adenosine analogs facilitates neuron response to netrin-1 by reducing the levels of cell surface Unc-5 netrin receptor A (UNC5A) receptor, thereby supporting an indirect

interaction between Adora2b and netrin-1 in the developing brain (McKenna et al., 2008). Recently, the notion that netrin-1 and Adora2b signaling are linked was rejuvenated in a study of hypoxia-associated inflammation, where netrin-1 released from intestinal epithelial cells dampened inflammatory responses by activating Adora2b receptors expressed on polymorphonuclear granulocytes (PMNs) (Rosenberger et al., 2009), a finding that was subsequently confirmed in many other studies (He et al., 2014; Schlegel et al., 2016; Zhou et al., 2019; Chen et al., 2020).

Coordination of netrin-1 and Adora2b signaling by hypoxia

As discussed above, the interaction of netrin-1 with the Adora2b was first established in brain development (Corset et al., 2000), but did not find consistent support from subsequent studies (Stein et al., 2001; McKenna et al., 2008). However, studies on inflammatory responses explored the possibility of the Adora2b-netrin-1 link (Rosenberger et al., 2009). The first study linking Adora2b signaling with netrin-1 during inflammation was based on the hypothesis that hypoxia would elicit endogenous adaptive responses that could dampen hypoxia-associated inflammation. In line with this hypothesis, the authors found that netrin-1 is expressed in intestinal epithelial cells and is induced by hypoxia. Studies on the mechanism of hypoxia-dependent induction of netrin-1 identified an HRE within the promoter region of netrin-1 that interacts with HIF1A during conditions of hypoxia, as shown by studies of netrin-1 promoter constructs, chromatin immunoprecipitation, and *in vitro* and *in vivo* studies of HIF1A mutations (Rosenberger et al., 2009). For example, wild-type mice would have robust induction of netrin-1 in their intestinal epithelial cells upon exposure to ambient hypoxia (4 h in 8% oxygen), while mice with intestinal epithelial Hif1a deletion would fail to induce netrin-1 expression (Rosenberger et al., 2009; Grenz et al., 2012). Subsequent functional studies demonstrated that netrin-1 signaling dampens hypoxia-associated inflammation *via* signaling events through the Adora2b receptor expressed on PMNs. Several subsequent studies confirmed the role of HIF1A in inducing netrin-1, including studies in macrophages exposed to ambient hypoxia (Ramkhalawon et al., 2013) or during LPS induced inflammation (Berg et al., 2021). In this later study, an unbiased screen revealed that netrin-1 was the highest induced neuronal guidance molecule released from macrophages exposed to LPS. Similar to the above studies, the authors found an important role of HIF1A in inducing netrin-1 upon LPS stimulation, and demonstrated in functional *in vivo* studies, that mice with myeloid deletion of netrin-1 (*Ntn1*^{loxp/loxp} LysMCre + mice) experienced exaggerated mortality and lung inflammation. More detailed examination of the *Ntn1*^{loxp/loxp} LysMCre + mice demonstrated a functional role of netrin-1 in

repelling natural killer cells, a response which could potentially implicate Adora2b signaling (Berg et al., 2021). Other studies found upregulation of netrin-1 by hypoxia during cancer (Chen et al., 2016; Jin et al., 2019), or in promoting anti-apoptotic function in endothelial progenitor cells under hypoxia conditions (Jiang et al., 2022). In conjunction with previous studies demonstrated that the Adora2b is a classic HIF target gene (Kong et al., 2006), and is selectively induced during hypoxia (Eltzschig et al., 2003; Schingnitz et al., 2010), ischemia (Eckle et al., 2007b; Eckle et al., 2008b; Grenz et al., 2008) or inflammation (Frick et al., 2009; Hart et al., 2009; Csoka et al., 2010; Ehrentauf et al., 2012; Eckle et al., 2014; Aherne et al., 2015; Hoegl et al., 2015), the above findings introduce the possibility that conditions of hypoxia coordinate Adora2b and netrin-1 signaling. During inflammatory hypoxia, netrin-1 expression is increased, Adora2b is induced, leading to increased Adora2b-dependent signaling events. Therefore, it is not surprising that previous studies of hypoxia-associated inflammation have provided links between netrin-1 and Adora2b signaling (Aherne et al., 2013).

Netrin-1 in alternative adenosine receptor activation during inflammation or ischemia and reperfusion

As described above, inflammatory hypoxia is associated with heightened expression of netrin-1 and Adora2b receptors, setting the stage for interactions between netrin-1 and Adora2b signaling. Several studies have found a functional role of the netrin-1-Adora2b link during studies that examine inflammatory conditions in tissue compartments where hypoxia-associated inflammation and changes in metabolic supply and demand cause stabilization of HIFs. Examples include ARDS, inflammatory bowel disease, myocardial and hepatic ischemia and reperfusion injury.

Acute respiratory distress syndrome

ARDS is an inflammatory disease of the lungs characterized by acute onset, the presence of bilateral pulmonary edema in the absence of left heart failure, and profound hypoxia with PaO₂/FiO₂ less than 300 mmHg (Lee et al., 2019; Li et al., 2020). Patients frequently require mechanical ventilation (Williams et al., 2021), and ARDS carries a very high rate of morbidity and mortality (Eckle et al., 2009; Ranieri et al., 2012; Dengler et al., 2013; Bellani et al., 2016). Based on its effect on repelling leukocyte infiltration, one of the first studies to examine functional roles of netrin-1 during ARDS used injurious mechanical ventilation to induce ARDS, as neutrophilia is consistently observed in this model (Eckle et al., 2008a; Koeppen et al., 2011c). Studies of mice with partial netrin-1

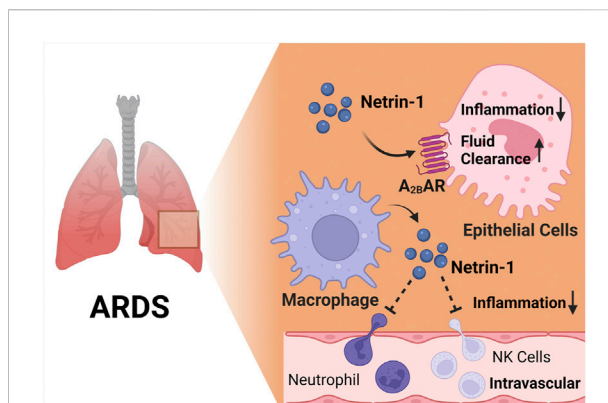


FIGURE 4

The netrin-1/Adora2b link in acute respiratory distress syndrome (ARDS). Several studies implicate that netrin-1 provide lung protection during ARDS. In alveolar epithelial cells, netrin-1 enhances alveolar fluid clearance and reduces alveolar inflammation, and this process is highly dependent on Adora2b signaling. Furthermore, macrophage derived netrin-1 inhibits neutrophil and natural killer cell recruitment, leading to reduced inflammation during endotoxin induced ARDS.

deficiency showed increased lung inflammation during injurious mechanical ventilation, and could be resuscitated by treatment with recombinant netrin-1 *via* inhalation or intravenous administration (Mirakaj et al., 2010). Another study confirmed the protective effects of netrin-1 treatment using a large animal model (Mutz et al., 2010). In this study, ARDS was induced by an intravenous infusion of LPS, and mice were subsequently treated with intravenous netrin-1 or inhaled netrin-1. Netrin-1 treatment provided lung protection by reducing inflammatory markers and histologic injury, and computed tomography corroborated attenuated pulmonary damage in both netrin-1 treatment arms (Mutz et al., 2010). Additional studies implicate HIF1A in the induction of netrin-1 and its protection during ARDS, and particularly implicate myeloid-derived netrin-1 in lung protection (Berg et al., 2021). Importantly, several previous studies demonstrate that HIF1A is stabilized during ARDS, and can function to dampen alveolar inflammation (Eckle et al., 2013a; Eckle et al., 2014; Vohwinkel et al., 2015; Garcia-Morales et al., 2016a; Vohwinkel et al., 2021). Studies on the signaling mechanism involved in netrin-1-elicited lung protection indicate that netrin-1 requires Adora2b signaling. For example, the lung protective effects during treatment with recombinant netrin-1 were completely abolished when applied in mice with global deletion of the Adora2b (*Adora2b*^{-/-} mice) (Mirakaj et al., 2010). Moreover, other studies implicate netrin-1 in promoting alveolar fluid clearance by enhancing Adora2b signaling during ARDS (He et al., 2014). These findings were based on previous studies that had demonstrated links between adenosine signaling and fluid clearance during ARDS (Factor et al., 2007; Kreindler and Shapiro, 2007). Indeed, measurements of alveolar fluid clearance directly implicate Adora2b signaling in the enhancement of

amiloride-sensitive fluid transport and elevations of pulmonary cAMP during ARDS induced by mechanical ventilation, suggesting that Adora2b agonist treatment (such as BAY 60-6583 or netrin-1) could provide protection during ARDS by “drying out” the lungs (Eckle et al., 2008c; Eckle et al., 2013b; Hoegl et al., 2015; Wang et al., 2021b). In summary, these studies provide evidence from genetic and pharmacologic studies that netrin-1 is protective during ARDS, and implicate Adora2b signaling in mediating the observed lung protection (Figure 4).

Inflammatory bowel disease

Inflammatory bowel disease (IBD) includes Crohn’s disease and ulcerative colitis, and is marked by persistent infiltration of the intestinal tissues with inflammatory cells. Due to its role orchestrating leukocyte trafficking, several studies have investigated the function of netrin-1 in IBD (Aherne et al., 2011; Aherne et al., 2013). Mice with partial netrin-1 deficiency (*Ntn1*^{+/-}) experience more profound weight-loss and intestinal inflammation when exposed to dextran sulfate sodium (DSS) (Aherne et al., 2012). Since previous studies had shown a protective role of Adora2b signaling during DSS colitis (Eltzschig et al., 2009b; Frick et al., 2009; Aherne et al., 2015; Aherne et al., 2018) or intestinal ischemia and reperfusion (Hart et al., 2009), subsequent studies addressed the functional role of the Adora2b in netrin-1-elicited gut protection. For this purpose, the authors used an osmotic pump system to treat mice with recombinant netrin-1 during DSS colitis (Aherne et al., 2012). These studies demonstrated that wild-type mice that were treated with exogenous mouse netrin-1 experienced dramatically reduced intestinal inflammation, disease severity and weight loss. When those studies were repeated using gene-targeted mice deficient of the Adora2b, the treatment effects of recombinant netrin-1 delivered by osmotic pump were completely abolished (Aherne et al., 2012). Importantly, previous studies had shown that the Adora2b is induced by HIF1A, and implicate Adora2b signaling in attenuating inflammation in a variety of models of intestinal inflammation (Eltzschig et al., 2009b; Frick et al., 2009; Hart et al., 2009; Aherne et al., 2015; Aherne et al., 2018). Together, these studies implicate the netrin-1-Adora2b link in attenuating intestinal inflammation, as shown during inflammatory bowel disease.

Myocardial infarction

Myocardial ischemia and reperfusion injury is a leading cause of morbidity and mortality world-wide. Therefore, the search for novel therapeutic approaches to enhance myocardial resistance to ischemia or dampen myocardial reperfusion injury are areas of intense research (Eltzschig and Eckle, 2011; Heusch, 2020). Several previous studies have implicated netrin-1 signaling in attenuating myocardial ischemia and reperfusion injury (Mao et al., 2014), and have also identified signaling events related to classic netrin-1

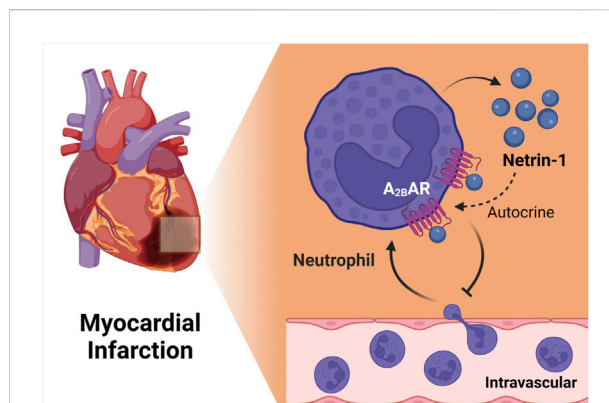


FIGURE 5

The netrin-1/Adora2b link in ischemia reperfusion injury of the heart. Myeloid cell derived netrin-1 has shown to be important for cardiac protection during ischemia reperfusion injury. Netrin-1 level increases during *in situ* myocardial infarction in mice and antibody mediated depletion of neutrophil abolished the induction, suggesting the importance of neutrophil as key sources of netrin-1. Furthermore, studies using treatment of recombinant netrin-1 implicated myeloid-dependent Adora2b signaling in cardioprotection, since the protection provided by netrin-1 treatment was completely abolished in *Ntn1*^{loxp/loxp} Myosin Cre + mice. Together, these findings implicate neutrophil-dependent netrin-1 release in mediating cardioprotection from ischemia and reperfusion by activating myeloid-dependent Adora2b adenosine receptors.

receptors, e.g., via DCC signaling (Zhang and Cai, 2010; Bouhidet et al., 2015; Li et al., 2015). A recent study examined tissue-specific functions as well as the role of the netrin-1-Adora2b link (Li et al., 2021). This study showed increased circulating netrin-1 levels in patients suffering from myocardial infarction or in mice exposed to *in situ* myocardial ischemia and reperfusion injury. Tissue-specific studies suggested a myeloid source of netrin, since mice with myeloid netrin-1 deletion (*Ntn1*^{loxp/loxp} LysMCre+) experienced larger myocardial infarct sizes, and showed attenuated netrin-1 blood levels (Li et al., 2021). Interestingly, mice with myocardial netrin-1 deletion (*Ntn1*^{loxp/loxp} Myosin Cre + mice) had no phenotype with regard to myocardial injury. Subsequent studies using antibody mediated depletion (Lys6G) of PMNs (Neudecker et al., 2017b) implicated neutrophils as a key source for the cellular release of netrin-1 into the blood during myocardial injury (Li et al., 2021). After establishing a pharmacologic protocol to use recombinant netrin-1 for the treatment of myocardial injury, the authors deleted *Adora2b* from different tissue compartments in the heart (Eckle et al., 2012; Eltzschig et al., 2013; Seo et al., 2015). These studies directly implicated myeloid-dependent Adora2b signaling in cardioprotection, since the protection provided by netrin-1 treatment was abolished in *Ntn1*^{loxp/loxp} Myosin Cre + mice. Together, these findings implicate neutrophil-dependent netrin-1 release in mediating cardioprotection from ischemia and reperfusion by activating myeloid-dependent Adora2b adenosine receptors

(Figure 5). These findings are also in line with previous studies showing a functional role of HIF in promoting Adora2b signaling during ischemia and reperfusion injury of the heart and cardioprotection (Eckle et al., 2008b; Eckle et al., 2012; Eltzschig et al., 2013; Koeppen et al., 2018; Lee et al., 2020b).

Hepatic ischemia and reperfusion

Hepatic ischemia and reperfusion injury occurs during major liver surgery, or during liver transplantation, and represents a major hurdle towards improving outcomes in these clinical scenarios (Ju et al., 2016; Lee et al., 2020a; Cata et al., 2020; Conrad and Eltzschig, 2020). Previous studies had implicated hypoxia-signaling in liver protection, and provided a strong rationale for exploring the netrin-Adora2b link during hepatic ischemia and reperfusion injury (Eltzschig et al., 2009b; Gao et al., 2020; Ibars et al., 2020; Wang et al., 2021a; Ju et al., 2021; Kim et al., 2021). In this context it is not surprising that studies in mice with partial netrin-1 deletion (*Ntn1*^{+/-}) experienced lower efficacy in reducing neutrophil infiltration, had lower levels of pro-inflammatory cytokines, and exhibited attenuated liver injury during hepatic ischemia/reperfusion injury compared to wildtype control animals (Schlegel et al., 2016). Similarly, treatment with recombinant netrin-1 promoted liver protection and repair, attenuated neutrophil influx, and dampened liver injury, and also stimulated the endogenous biosynthesis of pro-resolving mediators and growth factors. Since these liver-protective signaling effects were abolished in *Adora2b*^{-/-} mice, these studies directly implicate the netrin-Adora2b link in liver protection from ischemia and reperfusion injury (Schlegel et al., 2016).

Other examples for the netrin-Adora2b link during inflammatory diseases

Several other studies of disease that occur at the interface between inflammation and hypoxia have provided additional evidence for the netrin-Adora2b link in the resolution of injury. For example, a recent study implicates netrin-1 in diabetic corneal wound healing through Adora2b signaling events (Zhang et al., 2018). Other studies demonstrate resolution of inflammatory peritonitis by activation of the Adora2b (Mirakaj et al., 2011). Again, other studies suggest a functional role of netrin-1 signaling during acute or chronic kidney injury and implicate the netrin-Adora2b link in promoting the resolution of injury (Grenz et al., 2011b; Tak et al., 2013). Finally, some studies have implicated netrin-1 signaling via the Adora2b in the treatment of *Aspergillus fumigatus* infection of the cornea (Zhou et al., 2019). Taken together, these studies during inflammation or ischemia and reperfusion provide evidence for the netrin-Adora2b link in attenuating inflammation, promoting the resolution of inflammation and rescuing organ function (Aherne et al., 2013; Mirakaj and Rosenberger, 2017; Keller et al., 2021).

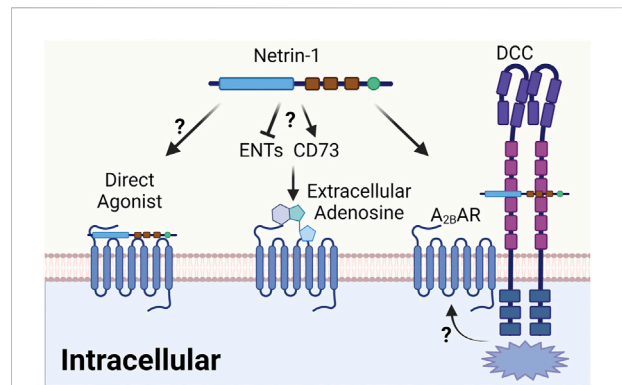


FIGURE 6

Proposed mechanism of the netrin-1/Adora2b linkage. The interaction between netrin-1 and Adora2b could have several different mechanisms. Firstly, the issue of a direct interaction between netrin-1 and the Adora2b is still controversial, although previous study has indicated netrin-1 as direct agonist. Alternatively, netrin-1 could function to enhance extracellular adenosine levels, and thereby promote anti-inflammatory signaling pathways that are under the control of the Adora2b. Such mechanisms could potentially involve increases in extracellular adenosine generation by activation of CD73 or inhibition of extracellular adenosine uptake via ENTs. An additional alternative of how netrin-1 signaling could enhance Adora2b signaling could involve an interaction of netrin-1 with a classic netrin-1 receptor, such as the DCC, which was indicated in previous studies. This could argue for a signaling pathway where netrin-1 binds to DCC and an interaction between DCC and the Adora2b promotes intracellular signaling cascades that are in line with Adora2b signaling.

Does netrin-1 function as a direct agonist of the Adora2b adenosine receptor?

The original report that identified the netrin-Adora2b link used a two-hybrid screen with the intracellular DCC domain as a bait, and identified binding of DCC and Adora2b intracellular domains (Corset et al., 2000). Subsequently, these studies indicated that netrin-1 signaling through the Adora2b promotes cAMP levels, and suggest the Adora2b as a direct netrin-1 receptor (Corset et al., 2000). Although intriguing, the issue of a direct interaction between netrin-1 and the Adora2b is controversial. For example, a subsequent study provides evidence that netrin-1-independent of Adora2b signaling-controls the responsiveness of neurons to netrin-1 by alternating cell surface UNC5A receptors (McKenna et al., 2008). As part of those studies, the authors demonstrate that COS cells with overexpression of the Adora2b did not show binding to this receptor, or responded with intracellular signal transduction when stimulated by netrin-1 (McKenna et al., 2008). On the other hand, *in vitro* studies of PMN transmigration following a chemotactic gradient was shown to be effectively attenuated in the presence of netrin-1, a signaling effect of netrin-1 on PMNs that could be effectively inhibited in the presence of a specific Adora2b agonist (PSB1115), or by using PMNs from *Adora2b*^{-/-} mice, implicating a direct functional role of Adora2b

signaling in netrin-1-mediated inhibition of inflammatory responses (Rosenberger et al., 2009).

In addition to conflicting findings regarding the potential activity of netrin-1 on the Adora2b, it also remains unclear how these signaling mechanisms occur from a molecular perspective. While the original description of the netrin-Adora2b link postulates a direct effect of netrin-1 as an endogenous Adora2b agonist (Corset et al., 2000), there are other models that could explain how netrin-1 would enhance Adora2b signaling without functioning as a direct Adora2b agonist (Figure 6). First, it is conceivable that netrin-1 functions to enhance extracellular adenosine levels, and thereby promote anti-inflammatory signaling pathways that are under the control of the Adora2b. Such mechanisms could potentially involve increases in extracellular adenosine generation by activation of CD73. Alternatively, netrin-1 could function to inhibit extracellular adenosine uptake *via* ENTs or intracellular adenosine metabolism by inhibiting adenosine kinase or adenosine deaminase (Eltzschig et al., 2006c; Van Linden and Eltzschig, 2007; Morote-Garcia et al., 2008). A recent study argues against this theory. In this study, the authors found that the presence of myeloid Adora2b receptors is necessary to mediate the cardioprotective effects of treatment with recombinant netrin-1 (Li et al., 2021). However, measurements of cardiac or circulating levels of adenosine were not altered by treatment doses of recombinant netrin-1 that were associated with attenuated myocardial infarct sizes (Li et al., 2021). An additional alternative explanation for how netrin-1 signaling could enhance Adora2b signaling involves a potential interaction of netrin-1 with a classic netrin-1 receptor, such as the DCC. In fact, the first description of Adora2b and netrin-1 signaling demonstrates an association of the Adora2b with DCC and netrin-1 by co-immunoprecipitation (Corset et al., 2000). This could argue for a signaling pathway where netrin-1 binds to DCC and an interaction between DCC and the Adora2b promotes intracellular signaling cascades that are in line with Adora2b signaling (Figure 6). Further molecular studies would be required to characterize the molecular events that govern netrin-1-elicited enhancements of Adora2b signaling.

Summary and discussion

Many studies support the notion that extracellular adenosine signaling is enhanced during limited oxygen availability, such as occur during ischemia or inflammatory diseases (Colgan et al., 2006; Eltzschig et al., 2008; Colgan and Eltzschig, 2012; Eltzschig et al., 2014). Signaling events through Adora2b have been shown to dampen inflammatory hypoxia during organ injury (Bowser et al., 2017b; Sun et al., 2017; Yuan et al., 2017; Bowser et al., 2018; Le et al., 2019; Li et al., 2020). Several studies have implicated netrin-1 in utilizing this pathway as a means of alternative activation of Adora2b signaling. While many of these studies

implicate netrin-1 in Adora2b signaling, the detailed molecular mechanisms of netrin-1-dependent Adora2b signaling have yet to be further characterized from a molecular perspective. In addition, clinical studies using this pathway would be desirable for the treatment of inflammatory or ischemic diseases. There could be several advantages of treatments with netrin-1 over other clinical strategies to enhance extracellular adenosine signaling through the Adora2b. First, netrin-1 has a much longer half-life than extracellular adenosine signaling, which has always been a concern about the use of direct adenosine treatment strategies (e.g. intravenous adenosine infusions). Secondly, unwanted side-effects of adenosine treatments (e.g. bradycardia or hypotension) may be less pronounced when using recombinant netrin. While it is unclear why direct Adora2b agonists have not been examined in clinical trials (e.g. BAY 60-6583) (Chen et al., 2009; Hart et al., 2009; Kosco et al., 2013), treatment with recombinant netrin-1 may be beneficial since netrin-1 represents an endogenous anti-inflammatory compound, and could therefore be safer and better tolerated as compared to an “engineered” pharmacologic Adora2b agonist.

Author contributions

HKE drafted the manuscript; TM, M-FD, SEE, and MFVM revised the manuscript; XY prepared the figures and finalized the manuscript.

Funding

National Institute of Health Grants R01HL154720, R01DK122796, R01HL133900 and Department of Defense Grant W81XWH2110032 to HKE; National Institute of Health Grants R01HL155950, Parker B. Francis Fellowship, and American Lung Association Catalyst Award CA-622265 to XY. National Institute of Health Grants R01 HL121228-08 to MFVM, and National Institute of Health Grants R01AR073284 to TM. National Institute of Health Grants R35HL144805 to SEE.

Conflict of interest

The authors declare that the research was conducted in the absence of any commercial or financial relationships that could be construed as a potential conflict of interest.

Publisher's note

All claims expressed in this article are solely those of the authors and do not necessarily represent those of their affiliated organizations,

or those of the publisher, the editors and the reviewers. Any product that may be evaluated in this article, or claim that may be made by its manufacturer, is not guaranteed or endorsed by the publisher.

References

- Aherne, C. M., Collins, C. B., and Eltzschig, H. K. (2013). Netrin-1 guides inflammatory cell migration to control mucosal immune responses during intestinal inflammation. *Tissue Barriers* 1, e24957. doi:10.4161/tisb.24957
- Aherne, C. M., Collins, C. B., Masterson, J. C., Tizzano, M., Boyle, T. A., Westrich, J. A., et al. (2012). Neuronal guidance molecule netrin-1 attenuates inflammatory cell trafficking during acute experimental colitis. *Gut* 61, 695–705. doi:10.1136/gutjnl-2011-300012
- Aherne, C. M., Collins, C. B., Rapp, C. R., Olli, K. E., Perrenoud, L., Jedlicka, P., et al. (2018). Coordination of ENT2-dependent adenosine transport and signaling dampens mucosal inflammation. *JCI Insight* 3, 121521. doi:10.1172/jci.insight.121521
- Aherne, C. M., Kewley, E. M., and Eltzschig, H. K. (2011). The resurgence of A2B adenosine receptor signaling. *Biochim. Biophys. Acta* 1808, 1329–1339. doi:10.1016/j.bbame.2010.05.016
- Aherne, C. M., Saeedi, B., Collins, C. B., Masterson, J. C., McNamee, E. N., Perrenoud, L., et al. (2015). Epithelial-specific A2B adenosine receptor signaling protects the colonic epithelial barrier during acute colitis. *Mucosal Immunol.* 8, 1324–1338. doi:10.1038/mi.2015.22
- Bellani, G., Laffey, J. G., Pham, T., Fan, E., Brochard, L., Esteban, A., et al. (2016). Epidemiology, patterns of care, and mortality for patients with acute respiratory distress syndrome in intensive care units in 50 countries. *JAMA* 315, 788–800. doi:10.1001/jama.2016.0291
- Berg, N. K., Li, J., Kim, B., Mills, T., Pei, G., Zhao, Z., et al. (2021). Hypoxia-inducible factor-dependent induction of myeloid-derived netrin-1 attenuates natural killer cell infiltration during endotoxin-induced lung injury. *FASEB J.* 35, e21334. doi:10.1096/fj.202002407R
- Bouhidel, J. O., Wang, P., Siu, K. L., Li, H., Youn, J. Y., Cai, H., et al. (2015). Netrin-1 improves post-injury cardiac function *in vivo* via DCC/NO-dependent preservation of mitochondrial integrity, while attenuating autophagy. *Biochim. Biophys. Acta* 1852, 277–289. doi:10.1016/j.bbdis.2014.06.005
- Bowser, J. L., Lee, J. W., Yuan, X., and Eltzschig, H. K. (2017). The hypoxia-adenosine link during inflammation. *J. Appl. Physiol.* (1985) 123, 1303–1320. doi:10.1152/japplphysiol.00101.2017
- Bowser, J. L., Lee, J. W., Yuan, X., and Eltzschig, H. K. (2017). The hypoxia-adenosine link during inflammation. *J. Appl. Physiol.* (1985) 123, 1303–1320. doi:10.1152/japplphysiol.00101.2017
- Bowser, J. L., Phan, L. H., and Eltzschig, H. K. (2018). The hypoxia-adenosine link during intestinal inflammation. *J. Immunol.* 200, 897–907. doi:10.4049/jimmunol.1701414
- Brunet, I., Gordon, E., Han, J., Cristofaro, B., Broqueres-You, D., Liu, C., et al. (2014). Netrin-1 controls sympathetic arterial innervation. *J. Clin. Invest.* 124, 3230–3240. doi:10.1172/JCI75181
- Campbell, E. L., Bruyninckx, W. J., Kelly, C. J., Glover, L. E., McNamee, E. N., Bowers, B. E., et al. (2014). Transmigrating neutrophils shape the mucosal microenvironment through localized oxygen depletion to influence resolution of inflammation. *Immunity* 40 (1), 66–77. doi:10.1016/j.immuni.2013.11.020
- Cata, J. P., Gorur, A., Yuan, X., Berg, N. K., Sood, A. K., Eltzschig, H. K., et al. (2020). Role of micro-RNA for pain after surgery: Narrative review of animal and human studies. *Anesth. Analg.* 130, 1638–1652. doi:10.1213/ANE.0000000000004767
- Chen, H., Chen, Q., and Luo, Q. (2016). Expression of netrin-1 by hypoxia contributes to the invasion and migration of prostate carcinoma cells by regulating YAP activity. *Exp. Cell Res.* 349, 302–309. doi:10.1016/j.yexcr.2016.10.023
- Chen, H., Yang, D., Carroll, S. H., Eltzschig, H. K., and Ravid, K. (2009). Activation of the macrophage A2b adenosine receptor regulates tumor necrosis factor- α levels following vascular injury. *Exp. Hematol.* 37, 533–538. doi:10.1016/j.exphem.2009.02.001
- Chen, J. F., Eltzschig, H. K., and Fredholm, B. B. (2013). Adenosine receptors as drug targets—what are the challenges? *Nat. Rev. Drug Discov.* 12, 265–286. doi:10.1038/nrd3955
- Chen, Z., Chen, Y., Zhou, J., Li, Y., Gong, C., Wang, X., et al. (2020). Netrin-1 reduces lung ischemia-reperfusion injury by increasing the proportion of regulatory T cells. *J. Int. Med. Res.* 48, 300060520926415. doi:10.1177/0300060520926415
- Clambey, E. T., McNamee, E. N., Westrich, J. A., Glover, L. E., Campbell, E. L., Jedlicka, P., et al. (2012). Hypoxia-inducible factor-1 α -dependent induction of FoxP3 drives regulatory T-cell abundance and function during inflammatory hypoxia of the mucosa. *Proc. Natl. Acad. Sci. U. S. A.* 109, E2784–E2793. doi:10.1073/pnas.1202366109
- Colamarino, S. A., and Tessier-Lavigne, M. (1995). The role of the floor plate in axon guidance. *Annu. Rev. Neurosci.* 18, 497–529. doi:10.1146/annurev.ne.18.030195.002433
- Colgan, S. P., and Eltzschig, H. K. (2012). Adenosine and hypoxia-inducible factor signaling in intestinal injury and recovery. *Annu. Rev. Physiol.* 74, 153–175. doi:10.1146/annurev-physiol-020911-153230
- Colgan, S. P., Eltzschig, H. K., Eckle, T., and Thompson, L. F. (2006). Physiological roles for ecto-5'-nucleotidase (CD73). *Purinergic Signal.* 2, 351–360. doi:10.1007/s11302-005-5302-5
- Colgan, S. P., Furuta, G. T., and Taylor, C. T. (2020). Hypoxia and innate immunity: Keeping up with the HIFsters. *Annu. Rev. Immunol.* 38, 341–363. doi:10.1146/annurev-immunol-100819-121537
- Conrad, C., and Eltzschig, H. K. (2020). Disease mechanisms of perioperative organ injury. *Anesth. Analg.* 131, 1730–1750. doi:10.1213/ANE.0000000000005191
- Corset, V., Nguyen-Ba-Charvet, K. T., Forcet, C., Moyse, E., Chedotal, A., and Mehlen, P. (2000). Netrin-1-mediated axon outgrowth and cAMP production requires interaction with adenosine A2b receptor. *Nature* 407, 747–750. doi:10.1038/35037600
- Cronstein, B. N. (1994). Adenosine, an endogenous anti-inflammatory agent. *J. Appl. Physiol.* 76, 5–13. doi:10.1152/jappl.1994.76.1.5
- Cronstein, B. N., Daguma, L., Nichols, D., Hutchison, A. J., and Williams, M. (1990). The adenosine/neutrophil paradox resolved: Human neutrophils possess both A1 and A2 receptors that promote chemotaxis and inhibit O₂ generation, respectively. *J. Clin. Invest.* 85, 1150–1157. doi:10.1172/JCI114547
- Csoka, B., Nemeth, Z. H., Rosenberger, P., Eltzschig, H. K., Spolarics, Z., Pacher, P., et al. (2010). A2B adenosine receptors protect against sepsis-induced mortality by dampening excessive inflammation. *J. Immunol.* 185, 542–550. doi:10.4049/jimmunol.0901295
- Decking, U. K. M., Schlieper, G., Kroll, K., and Schrader, J. (1997). Hypoxia-induced inhibition of adenosine kinase potentiates cardiac adenosine release. *Circ. Res.* 81, 154–164. doi:10.1161/01.res.81.2.154
- Dengler, V., Downey, G. P., Tuder, R. M., Eltzschig, H. K., and Schmidt, E. P. (2013). Neutrophil intercellular communication in acute lung injury. Emerging roles of microparticles and gap junctions. *Am. J. Respir. Cell Mol. Biol.* 49, 1–5. doi:10.1165/rcmb.2012-0472TR
- Eckle, T., Brodsky, K., Bonney, M., Packard, T., Han, J., Borchers, C. H., et al. (2013). HIF1A reduces acute lung injury by optimizing carbohydrate metabolism in the alveolar epithelium. *PLoS Biol.* 11, e1001665. doi:10.1371/journal.pbio.1001665
- Eckle, T., Fullbier, L., Grenz, A., and Eltzschig, H. K. (2008). Usefulness of pressure-controlled ventilation at high inspiratory pressures to induce acute lung injury in mice. *Am. J. Physiol. Lung Cell. Mol. Physiol.* 295, L718–L724. doi:10.1152/ajplung.90298.2008
- Eckle, T., Fullbier, L., Wehrmann, M., Khoury, J., Mittelbronn, M., Ibla, J., et al. (2007). Identification of ectonucleotidases CD39 and CD73 in innate protection during acute lung injury. *J. Immunol.* 178, 8127–8137. doi:10.4049/jimmunol.178.12.8127
- Eckle, T., Grenz, A., Kohler, D., Redel, A., Falk, M., Rolauffs, B., et al. (2006). Systematic evaluation of a novel model for cardiac ischemic preconditioning in mice. *Am. J. Physiol. Heart Circ. Physiol.* 291, H2533–H2540. doi:10.1152/ajpheart.00472.2006
- Eckle, T., Grenz, A., Laucher, S., and Eltzschig, H. K. (2008). A2B adenosine receptor signaling attenuates acute lung injury by enhancing alveolar fluid clearance in mice. *J. Clin. Invest.* 118, 3301–3315. doi:10.1172/JCI34203
- Eckle, T., Hartmann, K., Bonney, S., Reithel, S., Mittelbronn, M., Walker, L. A., et al. (2012). Adora2b-elicited Per2 stabilization promotes a HIF-dependent metabolic switch crucial for myocardial adaptation to ischemia. *Nat. Med.* 18, 774–782. doi:10.1038/nm.2728

Acknowledgments

All figures are created with [BioRender.com](https://www.biorender.com).

- Eckle, T., Hughes, K., Ehrentraut, H., Brodsky, K. S., Rosenberger, P., Choi, D. S., et al. (2013). Crosstalk between the equilibrative nucleoside transporter ENT2 and alveolar Adora2b adenosine receptors dampens acute lung injury. *FASEB J.* 27, 3078–3089. doi:10.1096/fj.13-228551
- Eckle, T., Kewley, E. M., Brodsky, K. S., Tak, E., Bonney, S., Gobel, M., et al. (2014). Identification of hypoxia-inducible factor HIF-1A as transcriptional regulator of the A2B adenosine receptor during acute lung injury. *J. Immunol.* 192, 1249–1256. doi:10.4049/jimmunol.1100593
- Eckle, T., Koeppen, M., and Eltzschig, H. K. (2009). Role of extracellular adenosine in acute lung injury. *Physiol. (Bethesda)* 24, 298–306. doi:10.1152/physiol.00022.2009
- Eckle, T., Koeppen, M., and Eltzschig, H. K. (2011). Use of a hanging weight system for coronary artery occlusion in mice. *J. Vis. Exp.* 50, 2526. doi:10.3791/2526
- Eckle, T., Kohler, D., Lehmann, R., El Kasmi, K. C., and Eltzschig, H. K. (2008). Hypoxia-inducible factor-1 is central to cardioprotection: A new paradigm for ischemic preconditioning. *Circulation* 118, 166–175. doi:10.1161/CIRCULATIONAHA.107.758516
- Eckle, T., Krahn, T., Grenz, A., Kohler, D., Mittelbronn, M., Ledent, C., et al. (2007). Cardioprotection by ecto-5'-nucleotidase (CD73) and A2B adenosine receptors. *Circulation* 115, 1581–1590. doi:10.1161/CIRCULATIONAHA.106.669697
- Ehrentraut, H., Clambey, E. T., McNamee, E. N., Brodsky, K. S., Ehrentraut, S. F., Poth, J. M., et al. (2013). CD73+ regulatory T cells contribute to adenosine-mediated resolution of acute lung injury. *FASEB J.* 27, 2207–2219. doi:10.1096/fj.12-225201
- Ehrentraut, H., Westrich, J. A., Eltzschig, H. K., and Clambey, E. T. (2012). Adora2b adenosine receptor engagement enhances regulatory T cell abundance during endotoxin-induced pulmonary inflammation. *PLoS One* 7, e32416. doi:10.1371/journal.pone.0032416
- Eltzschig, H. K., Abdulla, P., Hoffman, E., Hamilton, K. E., Daniels, D., Schonfeld, C., et al. (2005). HIF-1-dependent repression of equilibrative nucleoside transporter (ENT) in hypoxia. *J. Exp. Med.* 202, 1493–1505. doi:10.1084/jem.20050177
- Eltzschig, H. K. (2009). Adenosine: An old drug newly discovered. *Anesthesiology* 111, 904–915. doi:10.1097/ALN.0b013e3181b060f2
- Eltzschig, H. K., Bonney, S. K., and Eckle, T. (2013). Attenuating myocardial ischemia by targeting A2B adenosine receptors. *Trends Mol. Med.* 19, 345–354. doi:10.1016/j.molmed.2013.02.005
- Eltzschig, H. K., Bratton, D. L., and Colgan, S. P. (2014). Targeting hypoxia signalling for the treatment of ischaemic and inflammatory diseases. *Nat. Rev. Drug Discov.* 13, 852–869. doi:10.1038/nrd4422
- Eltzschig, H. K., and Carmeliet, P. (2011). Hypoxia and inflammation. *N. Engl. J. Med.* 364, 656–665. doi:10.1056/NEJMra0910283
- Eltzschig, H. K., and Collard, C. D. (2004). Vascular ischaemia and reperfusion injury. *Br. Med. Bull.* 70, 71–86. doi:10.1093/bmb/ldh025
- Eltzschig, H. K., and Eckle, T. (2011). Ischemia and reperfusion--from mechanism to translation. *Nat. Med.* 17, 1391–1401. doi:10.1038/nrm.2507
- Eltzschig, H. K., Eckle, T., Mager, A., Kuper, N., Karcher, C., Weissmuller, T., et al. (2006). ATP release from activated neutrophils occurs via connexin 43 and modulates adenosine-dependent endothelial cell function. *Circ. Res.* 99, 1100–1108. doi:10.1161/01.RES.0000250174.31269.70
- Eltzschig, H. K. (2013). Extracellular adenosine signaling in molecular medicine. *J. Mol. Med.* 91, 141–146. doi:10.1007/s00109-013-0999-z
- Eltzschig, H. K., Faigle, M., Knapp, S., Karhausen, J., Ibla, J., Rosenberger, P., et al. (2006). Endothelial catabolism of extracellular adenosine during hypoxia: The role of surface adenosine deaminase and CD26. *Blood* 108, 1602–1610. doi:10.1182/blood-2006-02-001016
- Eltzschig, H. K., Ibla, J. C., Furuta, G. T., Leonard, M. O., Jacobson, K. A., Enjoji, K., et al. (2003). Coordinated adenosine nucleotide phosphohydrolysis and nucleoside signaling in posthypoxic endothelium: Role of ectonucleotidases and adenosine A2B receptors. *J. Exp. Med.* 198, 783–796. doi:10.1084/jem.20030891
- Eltzschig, H. K., Kohler, D., Eckle, T., Kong, T., Robson, S. C., Colgan, S. P., et al. (2009). Central role of Sp1-regulated CD39 in hypoxia/ischemia protection. *Blood* 113, 224–232. doi:10.1182/blood-2008-06-165746
- Eltzschig, H. K., Macmanus, C. F., and Colgan, S. P. (2008). Neutrophils as sources of extracellular nucleotides: Functional consequences at the vascular interface. *Trends Cardiovasc. Med.* 18, 103–107. doi:10.1016/j.tcm.2008.01.006
- Eltzschig, H. K., Rivera-Nieves, J., and Colgan, S. P. (2009). Targeting the A2B adenosine receptor during gastrointestinal ischemia and inflammation. *Expert Opin. Ther. Targets* 13, 1267–1277. doi:10.1517/14728220903241666
- Eltzschig, H. K., Sitkovsky, M. V., and Robson, S. C. (2012). Purinergic signaling during inflammation. *N. Engl. J. Med.* 367, 2322–2333. doi:10.1056/NEJMra1205750
- Eltzschig, H. K., Thompson, L. F., Karhausen, J., Cotta, R. J., Ibla, J. C., Robson, S. C., et al. (2004). Endogenous adenosine produced during hypoxia attenuates neutrophil accumulation: Coordination by extracellular nucleotide metabolism. *Blood* 104, 3986–3992. doi:10.1182/blood-2004-06-2066
- Eltzschig, H. K., Weissmuller, T., Mager, A., and Eckle, T. (2006). Nucleotide metabolism and cell-cell interactions. *Methods Mol. Biol.* 341, 73–87. doi:10.1385/1-59745-113-4:73
- Enjoji, K., Sevigny, J., Lin, Y., Frenette, P. S., Christie, P. D., Esch, J. S., 2nd, et al. (1999). Targeted disruption of cd39/ATP diphosphohydrolase results in disordered hemostasis and thromboregulation. *Nat. Med.* 5, 1010–1017. doi:10.1038/12447
- Factor, P., Mutlu, G. M., Chen, L., Mohameed, J., Akhmedov, A. T., Meng, F. J., et al. (2007). Adenosine regulation of alveolar fluid clearance. *Proc. Natl. Acad. Sci. U. S. A.* 104, 4083–4088. doi:10.1073/pnas.0601117104
- Faigle, M., Seessle, J., Zug, S., El Kasmi, K. C., and Eltzschig, H. K. (2008). ATP release from vascular endothelia occurs across Cx43 hemichannels and is attenuated during hypoxia. *PLoS ONE* 3, e2801. doi:10.1371/journal.pone.0002801
- Fandrey, J., Schodel, J., Eckardt, K. U., Katschinski, D. M., and Wenger, R. H. (2019). Now a Nobel gas: Oxygen. *Pflugers Arch.* 471, 1343–1358. doi:10.1007/s00424-019-02334-8
- Feoktistov, I., and Biaggioni, I. (1997). Adenosine A2B receptors. *Pharmacol. Rev.* 49, 381–402.
- Feoktistov, I., and Biaggioni, I. (2011). Role of adenosine A(2B) receptors in inflammation. *Adv. Pharmacol.* 61, 115–144. doi:10.1016/B978-0-12-385526-8.00005-9
- Ferrari, D., Bianchi, N., Eltzschig, H. K., and Gambari, R. (2016). MicroRNAs modulate the purinergic signaling network. *Trends Mol. Med.* 22, 905–918. doi:10.1016/j.molmed.2016.08.006
- Ferrari, D., Bianchi, N., Eltzschig, H. K., and Gambari, R. (2016). MicroRNAs modulate the purinergic signaling network. *Trends Mol. Med.* 22, 905–918. doi:10.1016/j.molmed.2016.08.006
- Ferrari, D., McNamee, E. N., Idzko, M., Gambari, R., and Eltzschig, H. K. (2016). Purinergic signaling during immune cell trafficking. *Trends Immunol.* 37, 399–411. doi:10.1016/j.it.2016.04.004
- Forsythe, J., Jiang, B., Iyer, N., Agani, F., Leung, S., Koos, R., et al. (1996). Activation of vascular endothelial growth factor gene transcription by hypoxia-inducible factor 1. *Mol. Cell. Biol.* 16, 4604–4613. doi:10.1128/mcb.16.9.4604
- Fredholm, B., and Verkhratsky, A. (2010). Purines - 80 years and very much alive. *Acta Physiol.* 199, 91–92. doi:10.1111/j.1748-1716.2010.02113.x
- Frick, J. S., MacManus, C. F., Scully, M., Glover, L. E., Eltzschig, H. K., Colgan, S. P., et al. (2009). Contribution of adenosine A2B receptors to inflammatory parameters of experimental colitis. *J. Immunol.* 182, 4957–4964. doi:10.4049/jimmunol.0801324
- Friedman, D. J., Kunzli, B. M., Yi, A. R., Sevigny, J., Berberat, P. O., Enjoji, K., et al. (2009). From the cover: CD39 deletion exacerbates experimental murine colitis and human polymorphisms increase susceptibility to inflammatory bowel disease. *Proc. Natl. Acad. Sci. U. S. A.* 106, 16788–16793. doi:10.1073/pnas.0902869106
- Gao, R., Peng, X., Perry, C., Sun, H., Ntokou, A., Ryu, C., et al. (2021). Macrophage-derived netrin-1 drives adrenergic nerve-associated lung fibrosis. *J. Clin. Invest.* 131, 136542. doi:10.1172/JCI136542
- Gao, R. Y., Wang, M., Liu, Q., Feng, D., Wen, Y., Xia, Y., et al. (2020). Hypoxia-inducible factor-2a reprograms liver macrophages to protect against acute liver injury through the production of interleukin-6. *Hepatology* 71, 2105–2117. doi:10.1002/hep.30954
- García-Morales, L. J., Chen, N. Y., Weng, T., Luo, F., Davies, J., Philip, K., et al. (2016). Altered hypoxic-adenosine Axis and metabolism in group III pulmonary hypertension. *Am. J. Respir. Cell Mol. Biol.* 54, 574–583. doi:10.1165/rcmb.2015-0145OC
- García-Morales, L. J., Chen, N. Y., Weng, T., Luo, F., Davies, J., Philip, K., et al. (2016). Altered hypoxic-adenosine Axis and metabolism in group III pulmonary hypertension. *Am. J. Respir. Cell Mol. Biol.* 54 (4), 574–583. doi:10.1165/rcmb.2015-0145OC
- Grenz, A., Clambey, E., and Eltzschig, H. K. (2012). Hypoxia signaling during intestinal ischemia and inflammation. *Curr. Opin. Crit. Care* 18, 178–185. doi:10.1097/MCC.0b013e3283514bd0
- Grenz, A., Dalton, J. H., Bauerle, J. D., Badulak, A., Ridyard, D., Gandjeva, A., et al. (2011). Partial netrin-1 deficiency aggravates acute kidney injury. *PLoS One* 6, e14812. doi:10.1371/journal.pone.0014812

- Grenz, A., Homann, D., and Eltzschig, H. K. (2011). Extracellular adenosine: A safety signal that dampens hypoxia-induced inflammation during ischemia. *Antioxid. Redox Signal.* 15, 2221–2234. doi:10.1089/ars.2010.3665
- Grenz, A., Osswald, H., Eckle, T., Yang, D., Zhang, H., Tran, Z. V., et al. (2008). The reno-vascular A2B adenosine receptor protects the kidney from ischemia. *PLoS Med.* 5, e137. doi:10.1371/journal.pmed.0050137
- Gumbert, S. D., Kork, F., Jackson, M. L., Vanga, N., Ghebremichael, S. J., Wang, C. Y., et al. (2020). Perioperative acute kidney injury. *Anesthesiology* 132, 180–204. doi:10.1097/ALN.0000000000002968
- Hadi, T., Boytard, L., Silvestro, M., Alebrahim, D., Jacob, S., Feinstein, J., et al. (2018). Macrophage-derived netrin-1 promotes abdominal aortic aneurysm formation by activating MMP3 in vascular smooth muscle cells. *Nat. Commun.* 9, 5022. doi:10.1038/s41467-018-07495-1
- Haeberle, H. A., Durrstein, C., Rosenberger, P., Hosakote, Y. M., Kuhlicke, J., Kempf, V. A., et al. (2008). Oxygen-independent stabilization of hypoxia inducible factor (HIF)-1 during RSV infection. *PLoS ONE* 3, e3352. doi:10.1371/journal.pone.0003352
- Hansen, K. R., Resta, R., Webb, C. F., and Thompson, L. F. (1995). Isolation and characterization of the promoter of the human 5'-nucleotidase (CD73)-encoding gene. *Gene* 167, 307–312. doi:10.1016/0378-1119(95)00574-9
- Hart, M. L., Gorzolla, I. C., Schittenhelm, J., Robson, S. C., and Eltzschig, H. K. (2010). SP1-dependent induction of CD39 facilitates hepatic ischemic preconditioning. *J. Immunol.* 184, 4017–4024. doi:10.4049/jimmunol.0901851
- Hart, M. L., Henn, M., Kohler, D., Kloor, D., Mittelbronn, M., Gorzolla, I. C., et al. (2008). Role of extracellular nucleotide phosphohydrolysis in intestinal ischemia-reperfusion injury. *FASEB J.* 22, 2784–2797. doi:10.1096/fj.07-103911
- Hart, M. L., Jacobi, B., Schittenhelm, J., Henn, M., and Eltzschig, H. K. (2009). Cutting edge: A2B adenosine receptor signaling provides potent protection during intestinal ischemia/reperfusion injury. *J. Immunol.* 182, 3965–3968. doi:10.4049/jimmunol.0802193
- Hart, M. L., Kohler, D., Eckle, T., Kloor, D., Stahl, G. L., Eltzschig, H. K., et al. (2008). Direct treatment of mouse or human blood with soluble 5'-nucleotidase inhibits platelet aggregation. *Arterioscler. Thromb. Vasc. Biol.* 28, 1477–1483. doi:10.1161/ATVBAHA.108.169219
- Hart, M. L., Much, C., Gorzolla, I. C., Schittenhelm, J., Kloor, D., Stahl, G. L., et al. (2008). Extracellular adenosine production by ecto-5'-nucleotidase protects during murine hepatic ischemic preconditioning. *Gastroenterology* 135, 1739–1750. doi:10.1053/j.gastro.2008.07.064
- Hart, M. L., Much, C., Kohler, D., Schittenhelm, J., Gorzolla, I. C., Stahl, G. L., et al. (2008). Use of a hanging-weight system for liver ischemic preconditioning in mice. *Am. J. Physiol. Gastrointest. Liver Physiol.* 294, G1431–G1440. doi:10.1152/ajpgi.00083.2008
- Hasko, G., and Cronstein, B. N. (2004). Adenosine: An endogenous regulator of innate immunity. *Trends Immunol.* 25, 33–39. doi:10.1016/j.it.2003.11.003
- Hasko, G., Linden, J., Cronstein, B., and Pacher, P. (2008). Adenosine receptors: Therapeutic aspects for inflammatory and immune diseases. *Nat. Rev. Drug Discov.* 7, 759–770. doi:10.1038/nrd2638
- He, J., Zhao, Y., Deng, W., and Wang, D. X. (2014). Netrin-1 promotes epithelial sodium channel-mediated alveolar fluid clearance via activation of the adenosine 2B receptor in lipopolysaccharide-induced acute lung injury. *Respiration*. 87, 394–407. doi:10.1159/000358066
- Heusch, G. (2020). Myocardial ischaemia-reperfusion injury and cardioprotection in perspective. *Nat. Rev. Cardiol.* 17, 773–789. doi:10.1038/s41569-020-0403-y
- Hoegl, S., Brodsky, K. S., Blackburn, M. R., Karmouty-Quintana, H., Zwissler, B., Eltzschig, H. K., et al. (2015). Alveolar epithelial A2B adenosine receptors in pulmonary protection during acute lung injury. *J. Immunol.* 195, 1815–1824. doi:10.4049/jimmunol.1401957
- Hoegl, S., Ehrentauf, H., Brodsky, K. S., Victorino, F., Golden-Mason, L., Eltzschig, H. K., et al. (2016). NK cells regulate CXCR2+ neutrophil recruitment during acute lung injury. *J. Leukoc. Biol.* 101, 471–480. doi:10.1189/jlb.3A0516-227R
- Ibars, M., Maier, M. T., Yulianingsih, E., Perez, L., Cheang, R., Vilhelmsson, A., et al. (2020). Neuronal modulation of hepatic lipid accumulation induced by binge-like drinking. *Am. J. Physiol. Endocrinol. Metab.* 318, E655–E666. doi:10.1152/ajpendo.00218.2019
- Idzko, M., Ferrari, D., and Eltzschig, H. K. (2014). Nucleotide signalling during inflammation. *Nature* 509, 310–317. doi:10.1038/nature13085
- Idzko, M., Ferrari, D., Riegel, A. K., and Eltzschig, H. K. (2014). Extracellular nucleotide and nucleoside signaling in vascular and blood disease. *Blood* 124, 1029–1037. doi:10.1182/blood-2013-09-402560
- Jiang, R. C., Zheng, X. Y., Yang, S. L., Shi, H. J., Xi, J. H., Zou, Y. J., et al. (2022). CD146 mediates the anti-apoptotic role of Netrin-1 in endothelial progenitor cells under hypoxic conditions. *Mol. Med. Rep.* 25, 5. doi:10.3892/mmr.2021.12521
- Jin, X., Luan, H., Chai, H., Yan, L., Zhang, J., Wang, Q., et al. (2019). Netrin1 interference potentiates epithelial-to-mesenchymal transition through the PI3K/AKT pathway under the hypoxic microenvironment conditions of non-small cell lung cancer. *Int. J. Oncol.* 54, 1457–1465. doi:10.3892/ijo.2019.4716
- Jin, X., Shepherd, R. K., Duling, B. R., and Linden, J. (1997). Inosine binds to A3 adenosine receptors and stimulates mast cell degranulation. *J. Clin. Invest.* 100, 2849–2857. doi:10.1172/JCI119833
- Johnston-Cox, H., Koupenova, M., Yang, D., Corkey, B., Gokce, N., Farb, M. G., et al. (2012). The A2b adenosine receptor modulates glucose homeostasis and obesity. *PLoS One* 7, e40584. doi:10.1371/journal.pone.0040584
- Ju, C., Colgan, S. P., and Eltzschig, H. K. (2016). Hypoxia-inducible factors as molecular targets for liver diseases. *J. Mol. Med.* 94, 613–627. doi:10.1007/s00109-016-1408-1
- Ju, C., Wang, M., Tak, E., Kim, B., Emontzpohl, C., Yang, Y., et al. (2021). Hypoxia-inducible factor-1 α -dependent induction of miR122 enhances hepatic ischemic tolerance. *J. Clin. Invest.* 131, 140300. doi:10.1172/JCI140300
- Kaczmarek, E., Koziak, K., Sevigny, J., Siegel, J. B., Anrather, J., Beaudoin, A. R., et al. (1996). Identification and characterization of CD39/vascular ATP diphosphohydrolase. *J. Biol. Chem.* 271, 33116–33122. doi:10.1074/jbc.271.51.33116
- Karmouty-Quintana, H., Zhong, H., Acero, L., Weng, T., Melicoff, E., West, J. D., et al. (2012). The A2B adenosine receptor modulates pulmonary hypertension associated with interstitial lung disease. *FASEB J.* 26, 2546–2557. doi:10.1096/fj.11-200907
- Keller, M., Mirakaj, V., Koeppen, M., and Rosenberger, P. (2021). Neuronal guidance proteins in cardiovascular inflammation. *Basic Res. Cardiol.* 116, 6. doi:10.1007/s00395-021-00847-x
- Khakh, B. S., and Burnstock, G. (2009). The double life of ATP. *Sci. Am.* 301, 84–90. doi:10.1038/scientificamerican1209-84
- Kim, B., Guaregua, V., Chen, X., Zhao, C., Yeow, W., Berg, N. K., et al. (2021). Characterization of a murine model system to study MicroRNA-147 during inflammatory organ injury. *Inflammation* 44 (4), 1426–1440. doi:10.1007/s10753-021-01427-w
- Koeppen, M., Eckle, T., and Eltzschig, H. K. (2011). Interplay of hypoxia and A2B adenosine receptors in tissue protection. *Adv. Pharmacol.* 61, 145–186. doi:10.1016/B978-0-12-385526-8.00006-0
- Koeppen, M., Eckle, T., and Eltzschig, H. K. (2011). Pressure controlled ventilation to induce acute lung injury in mice. *J. Vis. Exp.* 51, 2525. doi:10.3791/2525
- Koeppen, M., Eckle, T., and Eltzschig, H. K. (2009). Selective deletion of the A1 adenosine receptor abolishes heart-rate slowing effects of intravascular adenosine in vivo. *PLoS One* 4, e6784. doi:10.1371/journal.pone.0006784
- Koeppen, M., Eckle, T., and Eltzschig, H. K. (2011). The hypoxia-inflammation link and potential drug targets. *Curr. Opin. Anaesthesiol.* 24, 363–369. doi:10.1097/ACO.0b013e328328473fd
- Koeppen, M., Lee, J. W., Seo, S. W., Brodsky, K. S., Kreth, S., Yang, I. V., et al. (2018). Hypoxia-inducible factor 2- α -dependent induction of amphiregulin dampens myocardial ischemia-reperfusion injury. *Nat. Commun.* 9, 816. doi:10.1038/s41467-018-03105-2
- Kohler, D., Eckle, T., Faigle, M., Grenz, A., Mittelbronn, M., Laucher, S., et al. (2007). CD39/ectonucleoside triphosphate diphosphohydrolase 1 provides myocardial protection during cardiac ischemia/reperfusion injury. *Circulation* 116, 1784–1794. doi:10.1161/CIRCULATIONAHA.107.690180
- Kohler, D., Granja, T., Volz, J., Koeppen, M., Langer, H. F., Hansmann, G., et al. (2020). Red blood cell-derived semaphorin 7A promotes thrombo-inflammation in myocardial ischemia-reperfusion injury through platelet GPIIb. *Nat. Commun.* 11, 1315. doi:10.1038/s41467-020-14958-x
- Kohler, D., Streissenberger, A., Konig, K., Granja, T., Roth, J. M., Lehmann, R., et al. (2013). The uncoordinated-5 homolog B (UNC5B) receptor increases myocardial ischemia-reperfusion injury. *PLoS One* 8, e69477. doi:10.1371/journal.pone.0069477
- Kong, T., Westerman, K. A., Faigle, M., Eltzschig, H. K., and Colgan, S. P. (2006). HIF-dependent induction of adenosine A2B receptor in hypoxia. *Faseb J.* 20, 2242–2250. doi:10.1096/fj.06-6419com
- Konig, K., Gatidou, D., Granja, T., Meier, J., Rosenberger, P., Mirakaj, V., et al. (2012). The axonal guidance receptor neogenin promotes acute inflammation. *PLoS One* 7, e32145. doi:10.1371/journal.pone.0032145
- Kosco, B., Trepakov, A., Csoka, B., Nemeth, Z. H., Pacher, P., Eltzschig, H. K., et al. (2013). Stimulation of A2B adenosine receptors protects against trauma-

hemorrhagic shock-induced lung injury. *Purinergic Signal*. 9, 427–432. doi:10.1007/s11302-013-9362-7

Kreindler, J. L., and Shapiro, S. D. (2007). Lung turns to AA (adenosine analogues) to dry out. *Nat. Med.* 13, 406–408. doi:10.1038/nm0407-406

Le, T. T., Berg, N. K., Harting, M. T., Li, X., Eltzschig, H. K., Yuan, X., et al. (2019). Purinergic signaling in pulmonary inflammation. *Front. Immunol.* 10, 1633. doi:10.3389/fimmu.2019.01633

Ledent, C., Vaugeois, J. M., Schiffmann, S. N., Pedrazzini, T., El Yacoubi, M., Vanderhaeghen, J. J., et al. (1997). Aggressiveness, hypoalgesia and high blood pressure in mice lacking the adenosine A2a receptor. *Nature* 388, 674–678. doi:10.1038/41771

Lee, J. W., Ko, J., Ju, C., and Eltzschig, H. K. (2019). Hypoxia signaling in human diseases and therapeutic targets. *Exp. Mol. Med.* 51, 1–13. doi:10.1038/s12276-019-0235-1

Lee, J. W., Koeppen, M., Seo, S. W., Bowser, J. L., Yuan, X., Li, J., et al. (2020). Transcription-independent induction of ERBB1 through hypoxia-inducible factor 2A provides cardioprotection during ischemia and reperfusion. *Anesthesiology* 132, 763–780. doi:10.1097/ALN.0000000000003037

Lee, T. J., Yuan, X., Kerr, K., Yoo, J. Y., Kim, D. H., Kaur, B., et al. (2020). Strategies to modulate MicroRNA functions for the treatment of cancer or organ injury. *Pharmacol. Rev.* 72, 639–667. doi:10.1124/pr.119.019026

Li, J., Conrad, C., Mills, T. W., Berg, N. K., Kim, B., Ruan, W., et al. (2021). PMN-derived netrin-1 attenuates cardiac ischemia-reperfusion injury via myeloid ADORA2B signaling. *J. Exp. Med.* 218, e20210008. doi:10.1084/jem.20210008

Li, Q., Wang, P., Ye, K., and Cai, H. (2015). Central role of SIAH inhibition in DCC-dependent cardioprotection provoked by netrin-1/NO. *Proc. Natl. Acad. Sci. U. S. A.* 112, 899–904. doi:10.1073/pnas.1420695112

Li, X., Berg, N. K., Mills, T., Zhang, K., Eltzschig, H. K., Yuan, X., et al. (2020). Adenosine at the interphase of hypoxia and inflammation in lung injury. *Front. Immunol.* 11, 604944. doi:10.3389/fimmu.2020.604944

Liu, H., Zhang, Y., Wu, H., D'Alessandro, A., Yegutkin, G. G., Song, A., et al. (2016). Beneficial role of erythrocyte adenosine A2B receptor-mediated AMP-activated protein kinase activation in high-altitude hypoxia. *Circulation* 134, 405–421. doi:10.1161/CIRCULATIONAHA.116.021311

Löffler, M., Morote-Garcia, J. C., Eltzschig, S. A., Coe, I. R., and Eltzschig, H. K. (2007). Physiological roles of vascular nucleoside transporters. *Arterioscler. Thromb. Vasc. Biol.* 27, 1004–1013. doi:10.1161/ATVBAHA.106.126714

Louis, N. A., Robinson, A. M., MacManus, C. F., Karhausen, J., Scully, M., Colgan, S. P., et al. (2008). Control of IFN- α by CD73: Implications for mucosal inflammation. *J. Immunol.* 180, 4246–4255. doi:10.4049/jimmunol.180.6.4246

Ly, N. P., Komatsuzaki, K., Fraser, I. P., Tseng, A. A., Prodhan, P., Moore, K. J., et al. (2005). Netrin-1 inhibits leukocyte migration *in vitro* and *in vivo*. *Proc. Natl. Acad. Sci. U. S. A.* 102, 14729–14734. doi:10.1073/pnas.0506233102

Mao, X., Xing, H., Mao, A., Jiang, H., Cheng, L., Liu, Y., et al. (2014). Netrin-1 attenuates cardiac ischemia reperfusion injury and generates alternatively activated macrophages. *Inflammation* 37, 573–580. doi:10.1007/s10753-013-9771-3

Masterson, J. C., McNamee, E. N., Fillon, S. A., Hosford, L., Harris, R., Fernando, S. D., et al. (2015). Eosinophil-mediated signalling attenuates inflammatory responses in experimental colitis. *Gut* 64, 1236–1247. doi:10.1136/gutjnl-2014-306998

Matherne, G. P., Linden, J., Byford, A. M., Gauthier, N. S., and Headrick, J. P. (1997). Transgenic A1 adenosine receptor overexpression increases myocardial resistance to ischemia. *Proc. Natl. Acad. Sci. U. S. A.* 94, 6541–6546. doi:10.1073/pnas.94.12.6541

McKenna, W. L., Wong-Staal, C., Kim, G. C., Macias, H., Hinck, L., Bartoe, J. L., et al. (2008). Netrin-1-independent adenosine A2b receptor activation regulates the response of axons to netrin-1 by controlling cell surface levels of UNC5A receptors. *J. Neurochem.* 104, 1081–1090. doi:10.1111/j.1471-4159.2007.05040.x

Mediero, A., Ramkhalawon, B., Perez-Aso, M., Moore, K. J., and Cronstein, B. N. (2015). Netrin-1 is a critical autocrine/paracrine factor for osteoclast differentiation. *J. Bone Min. Res.* 30, 837–854. doi:10.1002/jbmr.2421

Mediero, A., Wilder, T., Ramkhalawon, B., Moore, K. J., and Cronstein, B. N. (2016). Netrin-1 and its receptor Unc5b are novel targets for the treatment of inflammatory arthritis. *FASEB J.* 30, 3835–3844. doi:10.1096/fj.201600615R

Meyerhardt, J. A., Caca, K., Eckstrand, B. C., Hu, G., Lengauer, C., Banavali, S., et al. (1999). Netrin-1: Interaction with deleted in colorectal cancer (DCC) and alterations in brain tumors and neuroblastomas. *Cell Growth Differ.* 10, 35–42.

Miller, S. L., and Urey, H. C. (1959). Organic compound synthesis on the primitive Earth. *Science* 130, 245–251. doi:10.1126/science.130.3370.245

Mirakaj, V., Dalli, J., Granja, T., Rosenberger, P., and Serhan, C. N. (2014). Vagus nerve controls resolution and pro-resolving mediators of inflammation. *J. Exp. Med.* 211, 1037–1048. doi:10.1084/jem.20132103

Mirakaj, V., Gatidou, D., Potzsch, C., König, K., and Rosenberger, P. (2011). Netrin-1 signaling dampens inflammatory peritonitis. *J. Immunol.* 186, 549–555. doi:10.4049/jimmunol.1002671

Mirakaj, V. (2021). Immune cells-A curse and a blessing. *J. Exp. Med.* 218, e20210590. doi:10.1084/jem.20210590

Mirakaj, V., Jennewein, C., König, K., Granja, T., and Rosenberger, P. (2012). The guidance receptor neogenin promotes pulmonary inflammation during lung injury. *FASEB J.* 26, 1549–1558. doi:10.1096/fj.11-200063

Mirakaj, V., and Rosenberger, P. (2017). Immunomodulatory functions of neuronal guidance proteins. *Trends Immunol.* 38, 444–456. doi:10.1016/j.it.2017.03.007

Mirakaj, V., Thix, C. A., Laucher, S., Mielke, C., Morote-Garcia, J. C., Schmit, M. A., et al. (2010). Netrin-1 dampens pulmonary inflammation during acute lung injury. *Am. J. Respir. Crit. Care Med.* 181, 815–824. doi:10.1164/rccm.200905-0717OC

Morote-Garcia, J. C., Kohler, D., Roth, J. M., Mirakaj, V., Eldh, T., Eltzschig, H. K., et al. (2013). Repression of the equilibrative nucleoside transporters dampens inflammatory lung injury. *Am. J. Respir. Cell Mol. Biol.* 49, 296–305. doi:10.1165/rccm.2012-0457OC

Morote-Garcia, J. C., Rosenberger, P., Kuhlicke, J., and Eltzschig, H. K. (2008). HIF-1-dependent repression of adenosine kinase attenuates hypoxia-induced vascular leak. *Blood* 111, 5571–5580. doi:10.1182/blood-2007-11-126763

Morote-Garcia, J. C., Rosenberger, P., Nivillac, N. M., Coe, I. R., and Eltzschig, H. K. (2009). Hypoxia-inducible factor-dependent repression of equilibrative nucleoside transporter 2 attenuates mucosal inflammation during intestinal hypoxia. *Gastroenterology* 136, 607–618. doi:10.1053/j.gastro.2008.10.037

Mutz, C., Mirakaj, V., Vagts, D. A., Westermann, P., Waibler, K., König, K., et al. (2010). The neuronal guidance protein netrin-1 reduces alveolar inflammation in a porcine model of acute lung injury. *Crit. Care* 14, R189. doi:10.1186/cc9301

Neudecker, V., Brodsky, K. S., Clambey, E. T., Schmidt, E. P., Packard, T. A., Davenport, B., et al. (2017). Neutrophil transfer of miR-223 to lung epithelial cells dampens acute lung injury in mice. *Sci. Transl. Med.* 9, eaah5360. doi:10.1126/scitranslmed.aah5360

Neudecker, V., Brodsky, K. S., Kreth, S., Ginde, A. A., and Eltzschig, H. K. (2016). Emerging roles for MicroRNAs in perioperative medicine. *Anesthesiology* 124, 489–506. doi:10.1097/ALN.0000000000000969

Neudecker, V., Yuan, X., Bowser, J. L., and Eltzschig, H. K. (2017). MicroRNAs in mucosal inflammation. *J. Mol. Med.* 95, 935–949. doi:10.1007/s00109-017-1568-7

Ohta, A., and Sitkovsky, M. (2001). Role of G-protein-coupled adenosine receptors in downregulation of inflammation and protection from tissue damage. *Nature* 414, 916–920. doi:10.1038/414916a

Patel, N., Wu, W., Mishra, P. K., Chen, F., Millman, A., Csoka, B., et al. (2014). A2B adenosine receptor induces protective antihelminth type 2 immune responses. *Cell Host Microbe* 15, 339–350. doi:10.1016/j.chom.2014.02.001

Phillis, J. W., O'Regan, M. H., and Perkins, L. M. (1992). Measurement of rat plasma adenosine levels during normoxia and hypoxia. *Life Sci.* 51, PL149–52. doi:10.1016/0024-3205(92)90363-t

Poth, J. M., Brodsky, K., Ehrentauf, H., Grenz, A., and Eltzschig, H. K. (2013). Transcriptional control of adenosine signaling by hypoxia-inducible transcription factors during ischemic or inflammatory disease. *J. Mol. Med.* 91, 183–193. doi:10.1007/s00109-012-0988-7

Ramkhalawon, B., Hennessy, E. J., Menager, M., Ray, T. D., Sheedy, F. J., Hutchison, S., et al. (2014). Netrin-1 promotes adipose tissue macrophage retention and insulin resistance in obesity. *Nat. Med.* 20, 377–384. doi:10.1038/nm.3467

Ramkhalawon, B., Yang, Y., van Gils, J. M., Hewing, B., Rayner, K. J., Parathath, S., et al. (2013). Hypoxia induces netrin-1 and Unc5b in atherosclerotic plaques: Mechanism for macrophage retention and survival. *Arterioscler. Thromb. Vasc. Biol.* 33, 1180–1188. doi:10.1161/ATVBAHA.112.301008

Ranieri, V. M., Rubinfeld, G. D., Thompson, B. T., Ferguson, N. D., Caldwell, E., Fan, E., et al. (2012). Acute respiratory distress syndrome: The berlin definition. *JAMA* 307, 2526–2533. doi:10.1001/jama.2012.5669

Redel, A., Jazbutyte, V., Smul, T. M., Lange, M., Eckle, T., Eltzschig, H., et al. (2008). Impact of ischemia and reperfusion times on myocardial infarct size in mice *in vivo*. *Exp. Biol. Med.* 233, 84–93. doi:10.3181/0612-RM-308

Reichelt, M. E., Willems, L., Molina, J. G., Sun, C. X., Noble, J. C., Ashton, K. J., et al. (2005). Genetic deletion of the A1 adenosine receptor limits myocardial ischemic tolerance. *Circ. Res.* 96, 363–367. doi:10.1161/01.RES.0000156075.00127.C3

- Reutershan, J., Vollmer, I., Stark, S., Wagner, R., Ngamsri, K. C., Eltzschig, H. K., et al. (2009). Adenosine and inflammation: CD39 and CD73 are critical mediators in LPS-induced PMN trafficking into the lungs. *FASEB J.* 23, 473–482. doi:10.1096/fj.08-119701
- Robson, S. C., Enjyoji, K., Goepfert, C., Imai, M., Kaczmarek, E., Lin, Y., et al. (2001). Modulation of extracellular nucleotide-mediated signaling by CD39/nucleoside triphosphate diphosphohydrolase-1. *Drug Dev. Res.* 53, 193–207. doi:10.1002/ddr.1188
- Robson, S. C., Wu, Y., Sun, X., Knosalla, C., Dwyer, K., Enjyoji, K., et al. (2005). Ectonucleotidases of CD39 family modulate vascular inflammation and thrombosis in transplantation. *Semin. Thromb. Hemost.* 31, 217–233. doi:10.1055/s-2005-869527
- Rose, J. B., Naydenova, Z., Bang, A., Ramadan, A., Klawitter, J., Schram, K., et al. (2011). Absence of equilibrative nucleoside transporter 1 in ENT1 knockout mice leads to altered nucleoside levels following hypoxic challenge. *Life Sci.* 89, 621–630. doi:10.1016/j.lfs.2011.08.007
- Rosenberger, P., Schwab, J. M., Mirakaj, V., Masekowsky, E., Mager, A., Morote-Garcia, J. C., et al. (2009). Hypoxia-inducible factor-dependent induction of netrin-1 dampens inflammation caused by hypoxia. *Nat. Immunol.* 10, 195–202. doi:10.1038/ni.1683
- Salvatore, C. A., Tilley, S. L., Latour, A. M., Fletcher, D. S., Koller, B. H., Jacobson, M. A., et al. (2000). Disruption of the A(3) adenosine receptor gene in mice and its effect on stimulated inflammatory cells. *J. Biol. Chem.* 275, 4429–4434. doi:10.1074/jbc.275.6.4429
- Schingnitz, U., Hartmann, K., Macmanus, C. F., Eckle, T., Zug, S., Colgan, S. P., et al. (2010). Signaling through the A2B adenosine receptor dampens endotoxin-induced acute lung injury. *J. Immunol.* 184, 5271–5279. doi:10.4049/jimmunol.0903035
- Schlegel, M., Kohler, D., Korner, A., Granja, T., Straub, A., Giera, M., et al. (2016). The neuroimmune guidance cue netrin-1 controls resolution programs and promotes liver regeneration. *Hepatology* 63, 1689–1705. doi:10.1002/hep.28347
- Schlegel, M., Sharma, M., Brown, E. J., Newman, A. A. C., Cyr, Y., Afonso, M. S., et al. (2021). Silencing myeloid netrin-1 induces inflammation resolution and plaque regression. *Circ. Res.* 129, 530–546. doi:10.1161/CIRCRESAHA.121.319313
- Semenza, G. L., Jiang, B. H., Leung, S. W., Passantino, R., Concorde, J. P., Maire, P., et al. (1996). Hypoxia response elements in the aldolase A, enolase 1, and lactate dehydrogenase A gene promoters contain essential binding sites for hypoxia-inducible factor 1. *J. Biol. Chem.* 271, 32529–32537. doi:10.1074/jbc.271.51.32529
- Semenza, G. L., Roth, P. H., Fang, H. M., and Wang, G. L. (1994). Transcriptional regulation of genes encoding glycolytic enzymes by hypoxia-inducible factor 1. *J. Biol. Chem.* 269, 23757–23763. doi:10.1016/s0021-9258(17)31580-6
- Semenza, G. L. (2020). The genomics and genetics of oxygen homeostasis. *Annu. Rev. Genomics Hum. Genet.* 21, 183–204. doi:10.1146/annurev-genom-111119-073356
- Seo, S. W., Koeppen, M., Bonney, S., Gobel, M., Thayer, M., Harter, P. N., et al. (2015). Differential tissue-specific function of Adora2b in cardioprotection. *J. Immunol.* 195, 1732–1743. doi:10.4049/jimmunol.1402288
- Serafini, T., Colamarino, S. A., Leonardo, E. D., Wang, H., Beddington, R., Skarnes, W. C., et al. (1996). Netrin-1 is required for commissural axon guidance in the developing vertebrate nervous system. *Cell* 87, 1001–1014. doi:10.1016/s0092-8674(00)81795-x
- Serafini, T., Kennedy, T. E., Galko, M. J., Mirzayan, C., Jessell, T. M., Tessier-Lavigne, M., et al. (1994). The netrins define a family of axon outgrowth-promoting proteins homologous to *C. elegans* UNC-6. *Cell* 78, 409–424. doi:10.1016/0092-8674(94)90420-0
- Serhan, C. N., and Levy, B. D. (2018). Resolvins in inflammation: emergence of the pro-resolving superfamily of mediators. *J. Clin. Invest.* 128, 2657–2669. doi:10.1172/JCI97943
- Sitkovsky, M., and Lukashev, D. (2005). Regulation of immune cells by local-tissue oxygen tension: HIF1 alpha and adenosine receptors. *Nat. Rev. Immunol.* 5, 712–721. doi:10.1038/nri1685
- Sitkovsky, M. V., Lukashev, D., Apasov, S., Kojima, H., Koshiba, M., Caldwell, C., et al. (2004). Physiological control of immune response and inflammatory tissue damage by hypoxia-inducible factors and adenosine A2A receptors. *Annu. Rev. Immunol.* 22, 657–682. doi:10.1146/annurev.immunol.22.012703.104731
- Song, A., Zhang, Y., Han, L., Yegutkin, G. G., Liu, H., Sun, K., et al. (2017). Erythrocytes retain hypoxic adenosine response for faster acclimatization upon re-ascension. *Nat. Commun.* 8, 14108. doi:10.1038/ncomms14108
- Stein, E., Zou, Y., Poo, M., and Tessier-Lavigne, M. (2001). Binding of DCC by netrin-1 to mediate axon guidance independent of adenosine A2B receptor activation. *Science* 291, 1976–1982. doi:10.1126/science.1059391
- Sun, K., Liu, H., Song, A., Manalo, J. M., D'Alessandro, A., Hansen, K. C., et al. (2017). Erythrocyte purinergic signaling components underlie hypoxia adaptation. *J. Appl. Physiol.* (1985) 123, 951–956. doi:10.1152/japplphysiol.00155.2017
- Sun, X., Wu, Y., Gao, W., Enjyoji, K., Csizmadia, E., Muller, C. E., et al. (2010). CD39/ENTPD1 expression by CD4+Foxp3+ regulatory T cells promotes hepatic metastatic tumor growth in mice. *Gastroenterology* 139, 1030–1040. doi:10.1053/j.gastro.2010.05.007
- Synnestvedt, K., Furuta, G. T., Comerford, K. M., Louis, N., Karhausen, J., Eltzschig, H. K., et al. (2002). Ecto-5'-nucleotidase (CD73) regulation by hypoxia-inducible factor-1 mediates permeability changes in intestinal epithelia. *J. Clin. Invest.* 110, 993–1002. doi:10.1172/JCI15337
- Tak, E., Ridyard, D., Badulak, A., Giebler, A., Shabeka, U., Werner, T., et al. (2013). Protective role for netrin-1 during diabetic nephropathy. *J. Mol. Med.* 91, 1071–1080. doi:10.1007/s00109-013-1041-1
- Taylor, C. T., and Colgan, S. P. (2017). Regulation of immunity and inflammation by hypoxia in immunological niches. *Nat. Rev. Immunol.* 17, 774–785. doi:10.1038/nri.2017.103
- Taylor, C. T. (2008). Interdependent roles for hypoxia inducible factor and nuclear factor-kappaB in hypoxic inflammation. *J. Physiol.* 586, 4055–4059. doi:10.1113/jphysiol.2008.157669
- Taylor, C. T., and McElwain, J. C. (2010). Ancient atmospheres and the evolution of oxygen sensing via the hypoxia-inducible factor in metazoans. *Physiol. (Bethesda)* 25, 272–279. doi:10.1152/physiol.00029.2010
- Thiel, M., Chouker, A., Ohta, A., Jackson, E., Caldwell, C., Smith, P., et al. (2005). Oxygenation inhibits the physiological tissue-protecting mechanism and thereby exacerbates acute inflammatory lung injury. *PLoS Biol.* 3, e174. doi:10.1371/journal.pbio.0030174
- Thompson, L. F., Eltzschig, H. K., Ibla, J. C., Van De Wiele, C. J., Resta, R., Morote-Garcia, J. C., et al. (2004). Crucial role for ecto-5'-nucleotidase (CD73) in vascular leakage during hypoxia. *J. Exp. Med.* 200, 1395–1405. doi:10.1084/jem.20040915
- van Gils, J. M., Derby, M. C., Fernandes, L. R., Ramkhalawon, B., Ray, T. D., Rayner, K. J., et al. (2012). The neuroimmune guidance cue netrin-1 promotes atherosclerosis by inhibiting the emigration of macrophages from plaques. *Nat. Immunol.* 13, 136–143. doi:10.1038/ni.2205
- Van Linden, A., and Eltzschig, H. K. (2007). Role of pulmonary adenosine during hypoxia: extracellular generation, signaling and metabolism by surface adenosine deaminase/CD26. *Expert Opin. Biol. Ther.* 7, 1437–1447. doi:10.1517/14712598.7.9.1437
- Varadarajan, S. G., Kong, J. H., Phan, K. D., Kao, T. J., Panaitof, S. C., Cardin, J., et al. (2017). Netrin1 produced by neural progenitors, not floor plate cells, is required for axon guidance in the spinal cord. *Neuron* 94, 790–799. doi:10.1016/j.neuron.2017.03.007
- Victorino, F., Sojka, D. K., Brodsky, K. S., McNamee, E. N., Masterson, J. C., Homann, D., et al. (2015). Tissue-resident NK cells mediate ischemic kidney injury and are not depleted by anti-asialo-GM1 antibody. *J. Immunol.* 195, 4973–4985. doi:10.4049/jimmunol.1500651
- Vohwinkel, C. U., Coit, E. J., Burns, N., Elajaili, H., Hernandez-Saavedra, D., Yuan, X., et al. (2021). Targeting alveolar-specific succinate dehydrogenase A attenuates pulmonary inflammation during acute lung injury. *FASEB J.* 35, e21468. doi:10.1096/fj.202002778R
- Vohwinkel, C. U., Hoegl, S., and Eltzschig, H. K. (2015). Hypoxia signaling during acute lung injury. *J. Appl. Physiol.* (1985) 119, 1157–1163. doi:10.1152/japplphysiol.00226.2015
- Wang, G., Jiang, B., Rue, E., and Semenza, G. (1995). Hypoxia-inducible factor 1 is a basic-helix-loop-helix-PAS heterodimer regulated by cellular O2 tension. *Proc. Natl. Acad. Sci. U. S. A.* 92, 5510–5514. doi:10.1073/pnas.92.12.5510
- Wang, G. L., and Semenza, G. L. (1993). Characterization of hypoxia-inducible factor 1 and regulation of DNA binding activity by hypoxia. *J. Biol. Chem.* 268, 21513–21518. doi:10.1016/s0021-9258(20)80571-7
- Wang, W., Chen, N. Y., Ren, D., Davies, J., Philip, K., Eltzschig, H. K., et al. (2021). Enhancing extracellular adenosine levels restores barrier function in acute lung injury through expression of focal adhesion proteins. *Front. Mol. Biosci.* 8, 636678. doi:10.3389/fmolb.2021.636678
- Wang, Y., Yang, Y., Wang, M., Wang, S., Jeong, J. M., Xu, L., et al. (2021). Eosinophils attenuate hepatic ischemia-reperfusion injury in mice through ST2-dependent IL-13 production. *Sci. Transl. Med.* 13, eabb6576. doi:10.1126/scitranslmed.abb6576
- Weissmuller, T., Eltzschig, H. K., and Colgan, S. P. (2005). Dynamic purine signaling and metabolism during neutrophil-endothelial interactions. *Purinergic Signal.* 1, 229–239. doi:10.1007/s11302-005-6323-9

- Wen, J., Grenz, A., Zhang, Y., Dai, Y., Kellems, R. E., Blackburn, M. R., et al. (2011). A2B adenosine receptor contributes to penile erection via PI3K/AKT signaling cascade-mediated eNOS activation. *FASEB J.* 25, 2823–2830. doi:10.1096/fj.11-181057
- Williams, G. W., Berg, N. K., Reskallah, A., Yuan, X., and Eltzschig, H. K. (2021). Acute respiratory distress syndrome: Contemporary management and novel approaches during COVID-19. *Anesthesiology* 134, 270–282. doi:10.1097/aln.0000000000003571
- Yang, D., Koupenova, M., McCrann, D. J., Kopeikina, K. J., Kagan, H. M., Schreiber, B. M., et al. (2008). The A2b adenosine receptor protects against vascular injury. *Proc. Natl. Acad. Sci. U. S. A.* 105, 792–796. doi:10.1073/pnas.0705563105
- Yang, D., Zhang, Y., Nguyen, H. G., Koupenova, M., Chauhan, A. K., Makitalo, M., et al. (2006). The A2B adenosine receptor protects against inflammation and excessive vascular adhesion. *J. Clin. Invest.* 116, 1913–1923. doi:10.1172/JCI27933
- Yang, Z., Day, Y. J., Toufektsian, M. C., Xu, Y., Ramos, S. I., Marshall, M. A., et al. (2006). Myocardial infarct-sparing effect of adenosine A2A receptor activation is due to its action on CD4+ T lymphocytes. *Circulation* 114, 2056–2064. doi:10.1161/CIRCULATIONAHA.106.649244
- Yuan, X., Chang, C. Y., You, R., Shan, M., Gu, B. H., Madison, M. C., et al. (2019). Cigarette smoke-induced reduction of C1q promotes emphysema. *JCI Insight* 5, 124317. doi:10.1172/jci.insight.124317
- Yuan, X., Ferrari, D., Mills, T., Wang, Y., Czopik, A., Doursout, M. F., et al. (2021). Editorial: Purinergic signaling and inflammation. *Front. Immunol.* 12, 699069. doi:10.3389/fimmu.2021.699069
- Yuan, X., Lee, J. W., Bowser, J. L., Neudecker, V., Sridhar, S., and Eltzschig, H. K. (2017). Targeting hypoxia signaling for perioperative organ injury. *Anesth. Analg.* 126 (1), 308–321. doi:10.1213/ANE.0000000000002288
- Zhang, J., and Cai, H. (2010). Netrin-1 prevents ischemia/reperfusion-induced myocardial infarction via a DCC/ERK1/2/eNOS s1177/NO/DCC feed-forward mechanism. *J. Mol. Cell. Cardiol.* 48, 1060–1070. doi:10.1016/j.yjmcc.2009.11.020
- Zhang, W., Zhang, Y., Wang, W., Dai, Y., Ning, C., Luo, R., et al. (2013). Elevated ecto-5'-nucleotidase-mediated increased renal adenosine signaling via A2B adenosine receptor contributes to chronic hypertension. *Circ. Res.* 112, 1466–1478. doi:10.1161/CIRCRESAHA.111.300166
- Zhang, Y., Chen, P., Di, G., Qi, X., Zhou, Q., Gao, H., et al. (2018). Netrin-1 promotes diabetic corneal wound healing through molecular mechanisms mediated via the adenosine 2B receptor. *Sci. Rep.* 8, 5994. doi:10.1038/s41598-018-24506-9
- Zhang, Y., Dai, Y., Wen, J., Zhang, W., Grenz, A., Sun, H., et al. (2011). Detrimental effects of adenosine signaling in sickle cell disease. *Nat. Med.* 17, 79–86. doi:10.1038/nm.2280
- Zheng, W., Kuhlicke, J., Jackel, K., Eltzschig, H. K., Singh, A., Sjoblom, M., et al. (2009). Hypoxia inducible factor-1 (HIF-1)-mediated repression of cystic fibrosis transmembrane conductance regulator (CFTR) in the intestinal epithelium. *FASEB J.* 23, 204–213. doi:10.1096/fj.08-110221
- Zhong, H., Shlykov, S. G., Molina, J. G., Sanborn, B. M., Jacobson, M. A., Tilley, S. L., et al. (2003). Activation of murine lung mast cells by the adenosine A3 receptor. *J. Immunol.* 171, 338–345. doi:10.4049/jimmunol.171.1.338
- Zhou, Y., Lin, J., Peng, X., Li, C., Zhang, J., Wang, Q., et al. (2019). The role of netrin-1 in the mouse cornea during *Aspergillus fumigatus* infection. *Int. Immunopharmacol.* 71, 372–381. doi:10.1016/j.intimp.2019.03.047
- Zhu, S., Zhu, J., Zhen, G., Hu, Y., An, S., Li, Y., et al. (2019). Subchondral bone osteoclasts induce sensory innervation and osteoarthritis pain. *J. Clin. Invest.* 129, 1076–1093. doi:10.1172/JCI121561



OPEN ACCESS

EDITED BY

Kenneth A. Jacobson,
National Institutes of Health (NIH),
United States

REVIEWED BY

Yuriy Pankratov,
University of Warwick, United Kingdom
Ronald Sluyter,
University of Wollongong, Australia

*CORRESPONDENCE

Peter Illes,
peter.illes@medizin.uni-leipzig.de
Yong Tang,
tangyong@cdutcm.edu.cn

SPECIALTY SECTION

This article was submitted to
Experimental Pharmacology and Drug
Discovery,
a section of the journal
Frontiers in Pharmacology

RECEIVED 15 May 2022

ACCEPTED 29 June 2022

PUBLISHED 22 July 2022

CITATION

Zhang Y, Yin H-Y, Rubini P, Illes P and
Tang Y (2022), ATP indirectly stimulates
hippocampal CA1 and CA3 pyramidal
neurons via the activation of
neighboring P2X7 receptor-bearing
astrocytes and NG2 glial
cells, respectively.
Front. Pharmacol. 13:944541.
doi: 10.3389/fphar.2022.944541

COPYRIGHT

© 2022 Zhang, Yin, Rubini, Illes and
Tang. This is an open-access article
distributed under the terms of the
[Creative Commons Attribution License](#)
(CC BY). The use, distribution or
reproduction in other forums is
permitted, provided the original
author(s) and the copyright owner(s) are
credited and that the original
publication in this journal is cited, in
accordance with accepted academic
practice. No use, distribution or
reproduction is permitted which does
not comply with these terms.

ATP indirectly stimulates hippocampal CA1 and CA3 pyramidal neurons *via* the activation of neighboring P2X7 receptor-bearing astrocytes and NG2 glial cells, respectively

Ying Zhang¹, Hai-Yan Yin¹, Patrizia Rubini^{1,2}, Peter Illes^{1,2,3*} and
Yong Tang^{1,2,4*}

¹School of Acupuncture and Tuina, Chengdu University of Traditional Chinese Medicine, Chengdu, China, ²International Collaborative Center on Big Science Plan for Purinergic Signaling, Chengdu University of Traditional Chinese Medicine, Chengdu, China, ³Rudolf Boehm Institute for Pharmacology and Toxicology, University of Leipzig, Leipzig, Germany, ⁴Key Laboratory of Sichuan Province for Acupuncture and Chronobiology, Chengdu University of Traditional Chinese Medicine, Chengdu, China

There is ongoing dispute on the question whether CNS neurons possess ATP-sensitive P2X7 receptors (Rs) or whether only non-neuronal cells bear this receptor-type and indirectly signal to the neighboring neurons. We genetically deleted P2X7Rs specifically in astrocytes, oligodendrocytes and microglia, and then recorded current responses in neurons to the prototypic agonist of this receptor, dibenzoyl-ATP (Bz-ATP). These experiments were made in brain slice preparations taken from the indicated variants of the P2X7R KO animals. In hippocampal CA3, but not CA1 pyramidal neurons, the deletion of oligodendrocytic (NG2 glial) P2X7Rs abolished the Bz-ATP-induced current responses. In contrast to the Bz-ATP-induced currents in CA3 pyramidal neurons, current amplitudes evoked by the ionotropic glutamate/GABA_AR agonists AMPA/muscimol were not inhibited at all. Whereas in the CA3 area NG2 glia appeared to mediate the P2X7R-mediated stimulation of pyramidal neurons, in the CA1 area, astrocytic P2X7Rs had a somewhat similar effect. This was shown by recording the frequencies and amplitudes of spontaneous excitatory currents (sPSCs) in brain slice preparations. Bz-ATP increased the sPSC frequency in CA1, but not CA3 pyramidal neurons without altering the amplitude, indicating a P2X7R-mediated increase of the neuronal input. Micro-injection of the selective astrocytic toxin L- α -aminoadipate into both hippocampi, or the *in vitro* application of the GABA_AR antagonistic gabazine, completely blocked the frequency increases of sPSCs. Hence, CA1 and CA3 pyramidal neurons of the mouse did not possess P2X7Rs, but were indirectly modulated by astrocytic and oligodendrocytic P2X7Rs, respectively.

KEYWORDS

astrocytes, oligodendrocytes, microglia, pyramidal neurons, hippocampus, mouse

Introduction

P2X7 receptors (Rs) constitute a subtype of the ligand-gated P2XR superfamily and are activated by high concentrations of extracellular ATP released from the intracellular space in response to various injurious or inflammatory conditions (Surprenant et al., 1996; North, 2002). They are able to transit from the non-selective cationic-channel mode to a large membrane pore which allows the diffusion of molecules up to 900 Da [e.g., ATP, glutamate, GABA (Sperlágh et al., 2006), and fluorescent dyes (Bartlett et al., 2014)], according to their concentration gradient. While originally P2X7R-channels were thought to dilate on long-lasting or repetitive contact with ATP (Virginio et al., 1999), or alternatively to recruit the membrane channel pannexin-1 as a conduit (Pelegriin and Surprenant, 2006), more recently it was found that P2X7Rs permit the passage of large cationic molecules immediately from their initial activation, but at a much slower pace than that of the small cations Na⁺, K⁺, and Ca²⁺ (Harkat et al., 2017; Di Virgilio et al., 2018).

P2X7Rs are located at peripheral (lymphocytes, macrophages, dendritic cells) and central (microglia) immunocytes, where they initiate the synthesis and subsequent outflow of inflammatory mediators, such as cytokines, chemokines, proteases, reactive oxygen/nitrogen species, and the excitotoxic ATP and glutamate (Kigerl et al., 2009; Kettenmann et al., 2011; Zhao et al., 2022). In the CNS, P2X7Rs occur at the highest density at microglia, but there is also unequivocal evidence for their existence at astrocytes and oligodendrocytes (Zhao et al., 2021). With respect to their localization at neurons there has been a long-lasting controversy on the issue whether P2X7Rs directly or indirectly (*via* the release of astrocytic, oligodendrocytic or microglial signaling molecules) cause neuronal effects at the cellular and systemic levels (Illes et al., 2017; Miras-Portugal et al., 2017).

Molecular biology methods also failed to dissolve these controversies. On the one hand it was published that in different brain regions of a P2X7R conditional humanized mice, the respective mRNA was specifically expressed in glutamatergic pyramidal neurons of the CA3 hippocampal area (Metzger et al., 2017). In addition, P2X7Rs were identified in major non-neuronal lineages throughout the brain (i.e., astrocytes, oligodendrocytes, microglia). On the other hand, the generation of a P2X7 EGFP-tagged transgenic mouse and investigations on the expression of the respective protein in the brain, failed to indicate a neuronal localization of this receptor in the hippocampal CA1/CA3 pyramidal neurons, and dentate gyrus granule cells (Kaczmarek-Hajek et al., 2018). However, P2X7R-EGFP co-stained with microglial, oligodendrocytic and astrocytic

immunohistochemistry markers, whereas there was no co-staining with any of the standard neuronal markers. A handicap of these studies was that in both cases the functional identification of the P2X7R-mRNA or -protein was missing.

It has to be mentioned already at this stage, that besides astrocytes and oligodendrocytes, NG2 glial cells emerged during the last decades as a new type of neuroglial cells in the CNS (Seifert and Steinhäuser, 2018; Bedner et al., 2020; Zhao et al., 2021). They express in addition to the classic antigenic markers (e.g., oligodendrocyte transcription factor; Olig2) also the proteoglycan NG2. These cells are also referred to as oligodendrocyte precursor cells (OPCs) because in the white, but not grey matter they differentiate into myelinating oligodendrocytes (Nishiyama et al., 2016). In the hippocampus the number of NG2 cells amounts to about 20%–25% of that of astrocytes (Degen et al., 2012).

The aim of our present study was to fill this gap, by recording dibenzoyl ATP (Bz-ATP) currents from hippocampal CA1/CA3 neurons in brain slices of mice whose P2X7Rs were genetically deleted in astrocytes, oligodendrocytes (NG2 glia) or microglia. In addition, we searched for assumedly presynaptic P2X7Rs at the terminals of the Schaffer collaterals and mossy fibers ending at CA1 and CA3 pyramidal cells, respectively. There was no functional evidence for the existence of P2X7Rs at the investigated neuronal structures; by contrast, these receptors were associated with astrocytes or oligodendrocytes releasing signaling molecules onto the targeted pyramidal neurons upon the activation of their P2X7Rs.

Materials and methods

Animals

In most experiments, humanized P2X7R knockout (KO) mice (P2rx7^{tm1.2jdc}; MGI:6203042), generated on a mixed 129S2/SvxC57BL/6J background (Charles-River, Wilmington, MA, United States; Metzger et al., 2017) as well as their wild-type (WT) controls were used. The mice were kindly donated by Jan M. Deussing, Max Planck Institute of Psychiatry, Munich, Germany. In addition, C57BL/6J mice were used for the measurement of spontaneous postsynaptic current (sPSC) amplitude and frequency. Both strains of mice were housed under standard laboratory conditions and maintained on a 12 h light-dark cycle with food and water provided *ad libitum*. The animal study was reviewed and approved by the Institutional Review Board of the Chengdu University of Traditional Chinese

Medicine, Chengdu, China (protocol code, DC2472, 1 April 2019).

To generate astrocyte-specific deletion of P2X7Rs in mice (P2rX7flox/flox; GFAP-Cre/Esr1 mice), we crossed mice bearing P2rX7 floxed alleles to GFAP-Cre/Esr1 mice to obtain P2rX7flox/+; GFAP-Cre/Esr1 mice. In the next generation, we used P2rX7flox/+, GFAP-Cre/Esr1 mice to breed with P2rX7 flox/flox mice to generate P2rX7flox/flox; GFAP-Cre/Esr1 mice. The subsequent experiments were performed by using progenies of P2rX7 flox/flox mice crossed with P2rX7flox/flox; GFAP-Cre/Esr1 mice. A similar procedure was used to generate mice whose P2X7Rs were specifically deleted in their oligodendrocytes/NG2 glia (P2rX7flox/flox; Olig2-Cre/Esr1) or microglia (P2rX7flox/flox; CX3CR1-Cre/Esr1). We used P2rX7flox/flox mice as controls. The three types of Cre-mice were generous gifts from Yong-Jun Chen (Guangzhou University of Traditional Chinese Medicine, Guangzhou, China). It has to be noted that the yield of astrocyte-, oligodendrocyte-, and microglia-specific KO mice was quite low; they amounted only to 15%–30% of the final number of littermates.

Patch-clamp recordings in hippocampal slices and selection of neurons/astrocytes for experimentation

Coronal hippocampal slices were prepared from the brain of 10–15 days old mice and were used for patch-clamp recordings as described previously (Ficker et al., 2014; Khan et al., 2019). After decapitation, the brain was placed into ice-cold and oxygenated (95% O₂+5% CO₂) artificial cerebrospinal fluid (aCSF) of the following composition (in mM): KCl 2.5, NaCl 126, MgCl₂ 1.3, CaCl₂ 2.4, NaH₂PO₄ 1.2, NaHCO₃ 25 and glucose monohydrate 11. Hippocampal slices of mice were cut at the thickness of 200 μ m by using a vibratome (VT1200S; Leica Biosystem, Muttentz, Switzerland). To create low divalent cationic conditions (low X²⁺), MgCl₂ was omitted from the medium and the CaCl₂ concentration was decreased to 0.5 mM. The brain slices were superfused in an organ bath with 95% O₂+5% CO₂-saturated low X²⁺ aCSF at 37°C for 30 min, and then superfusion was continued at room temperature (20–24°C) throughout.

Neurons and astrocytes in the CA1 and CA3 region were visualized by using a 40 \times water immersion objective (Axio Examiner.A1, Carl Zeiss, Oberkochen, Germany). Patch pipettes were filled with intracellular solution of the following composition (in mM): K-gluconic acid 140, NaCl 10, MgCl₂ 1, HEPES 10, EGTA 11, Mg-ATP 1.5, Li-GTP 0.3; pH 7.3 adjusted with KOH. Pipettes (4–9 M Ω for neurons; 9–12 M Ω for astrocytes) were pulled by a horizontal micropipette puller (P-1000; Sutter Instruments, Novato, CA, United States) from borosilicate capillaries.

Whole-cell current-clamp and voltage-clamp recordings were made by a patch-clamp amplifier (MultiClamp 700B;

Molecular Devices, San Jose, CA, United States). In the current-clamp mode of recording, astrocytes were discriminated from neurons by their failure to fire action potentials in response to depolarizing current injection (–80 to –760 pA, in 60 pA increments). Most non-spiking cells belonged to the passive class (typical astrocytes) and only very few to the variably rectifying class; there were no in- or outwardly rectifying cells at all (Oliveira et al., 2011; Zhao et al., 2022). This is a clear distinction from microglia and oligodendrocytes, which both express under resting conditions an inwardly rectifying current pattern (Boucsein et al., 2000; Pérez-Samartín et al., 2017). Furthermore, earlier experiments showed that when Lucifer yellow diffused from the recording pipette into electrophysiologically-identified astrocytes, these cells also stained immunohistochemically for the astrocytic marker S100 β (Oliveira et al., 2011).

Recordings of agonist-induced currents and spontaneous postsynaptic current frequency/amplitude

In the voltage-clamp recording mode of the amplifier, the holding potential of astrocytes was set to –80 mV and that of neurons to –70 mV. Agonists were applied locally by means of a computer-controlled solenoid valve-driven pressurized superfusion system (VC38; ALA Scientific Instruments, Farmingdale, NY, United States). The drug application tip touched the surface of the brain slice and was placed 100–150 μ m from the patched cell. Agonists were diluted and applied in low X²⁺ solution for 10 s every 3 min, and each agonist was administered twice; the mean current response was calculated for statistical evaluation. pClamp 10.4 software (Molecular Devices) was used to store the recorded data, to perform online analysis/filtering, and to trigger the application system used.

Spontaneous postsynaptic currents (sPSCs) composing of both action potential-induced and spontaneous vesicular glutamate/GABA release were recorded from neurons at the holding potential of –70 mV. They were analyzed by means of the pClamp 10.4 software package, by detecting amplitudes exceeding the detection threshold set at three times the standard deviation above the baseline noise of the recordings. sPSCs were recorded for 5 min in the absence and for another 5 min in the presence of Bz-ATP. Then, the reversibility of the Bz-ATP effect was demonstrated by recording sPSCs for another 5 min after washing out Bz-ATP. Bz-ATP was investigated on preparations taken from L- α -amino adipate-treated mice (see below) or on preparations superfused with aCSF containing the GABA_AR antagonist gabazine (10 μ M) throughout. Superfusion with gabazine started at least 5 min before beginning the experiment.

In vivo drug-treatment protocols to selectively inactivate astrocytes or microglia

In order to selectively abrogate astrocytes, the astrocytic toxin L- α -amino adipate (20 $\mu\text{g}/\mu\text{l}$ stock, 2 μl at a constant rate of 0.4 $\mu\text{l}/\text{min}$) was infused into the bilateral hippocampus (Lima et al., 2014). The animals were anesthetized with isoflurane (5% induction, 2% maintenance) and fixed on a stereotactic platform (RWD Life Science, San Diego, CA, United States). The stereotactic coordinates for the positioning of the guide cannula into the bilateral hippocampus were -2 mm anterior-posterior, $\pm 1.5\text{ mm}$ lateral to bregma, and 1.5 mm below the surface of the skull. A micro-syringe (5 μl ; Hamilton Company, Reno, NV, United States) was used for injection, and constant rate infusion was delivered by a stereotactic injection syringe pump (RWD Life Science). At the end of the infusion, the dummy cannula was retained at the injection place to allow sufficient diffusion. To selectively inactivate microglia, mice were injected intraperitoneally (i.p.) with minocycline (40 mg/kg; Bassett et al., 2021). Animals were decapitated and their hippocampal slices were prepared the 3rd day after either pre-treatment.

Drugs and chemicals

The following drugs were used: L- α -amino adipic acid, 2'-(3')-O-(4-benzoylbenzoyl)adenosine-5'-triphosphate tri (triethylammonium) salt (Bz-ATP), gabazine, minocycline hydrochloride, muscimol, N-methyl-D-aspartic acid (NMDA) (S)- α -amino-3-hydroxy-5-methylisoxazole-4-propionic acid (S-AMPA) (Sigma-Aldrich, St. Louis, MO, United States). Chemicals for solutions were also from Sigma-Aldrich.

Statistical analysis

All data were expressed as means \pm SEM of n observations, where n stands for the number of cells recorded in hippocampal slices taken from at least four animals. There was no *a priori* sample size calculation, but instead we have set the number of measurements to 10 in all experimental groups. GraphPad Prism9 was used for the construction of Figures and for statistical evaluations. We tested for and found that, when using parametric tests, all sampled distributions satisfied the normality and equal variance criteria. Multiple comparisons between data were performed in case of their normal distribution by either one-way or two-way ANOVA, as appropriate, followed by the Tukey's or Dunnett's multiple comparison's tests, as appropriate. Two data sets were compared using the parametric Student's *t*-test or the non-parametric Mann-Whitney rank sum test, as appropriate. A

probability level of 0.05 or less was considered to be statistically significant.

Results

Effects of general and cell-specific deletion of P2X7Rs on responses to the Bz-ATP-induced stimulation of hippocampal astrocytes and neurons

In a first series of experiments, we recorded by means of the whole-cell patch-clamp technique agonist-induced membrane currents of hippocampal CA1 astrocytes in brain slices (Figures 1A–F). We applied selective agonists for the AMPA-type excitatory glutamate receptor (AMPA, 100 μM), the inhibitory amino acid receptor GABA_A (muscimol, 100 μM) and the non-selective agonist for excitatory P2X7Rs (Bz-ATP, 1,000 μM).

In this type of experiments, the same concentrations of the agonists were used throughout (Figures 1–4). AMPA, Bz-ATP and muscimol were applied twice in succession, and the mean of the two current responses was used for statistical evaluation. In order to potentiate the effect of Bz-ATP in WT astrocytes, a low X^{2+} -containing superfusion medium was used, which is known to largely increase P2X7R currents (Jiang, 2009). It is also noteworthy that Bz-ATP activates P2X1/P2X3Rs with an even higher efficiency than its supposed target site, the P2X7R; however, Bz-ATP is 10–30 times more potent at P2X7Rs than ATP itself and is considered therefore to be a prototypic agonist for this latter receptor-type (Anderson and Nedergaard, 2006; Illes et al., 2021). In spite of using Bz-ATP and a low cation-containing superfusion medium, a high agonistic concentration had to be applied, a finding, which agrees with the well-known low sensitivity of P2X7Rs to ATP when compared with that of the residual subtypes of the P2XR superfamily (Surprenant et al., 1996; Sperlágh et al., 2006). A further reason for the need to use high agonist concentrations was that mouse, in comparison with rat P2X7Rs, only weakly respond to ATP/Bz-ATP, due to differences in the amino acid composition of the ectodomains of the two receptor orthologs (Young et al., 2007). In fact, when concentration-response curves for Bz-ATP were constructed on astrocytes in brain slices of the pre-frontal cortex (Oliveira et al., 2011) or hippocampus (Zhao et al., 2022), a much lower agonist-sensitivity was found in the mouse than in the rat preparation. Actually, Bz-ATP at 1,000 μM elicited reproducible, submaximal current responses well suitable for further work.

Notwithstanding the necessity to utilize Bz-ATP concentrations in the millimolar range, a selective activation of P2X7Rs occurred, because in CA1 astrocytes of the general P2X7R KO mouse, no current response to this agonist was observed at all (compare Figures 1A,E with Figures 1B,E). In addition to the general deletion of P2X7Rs in all cells of the

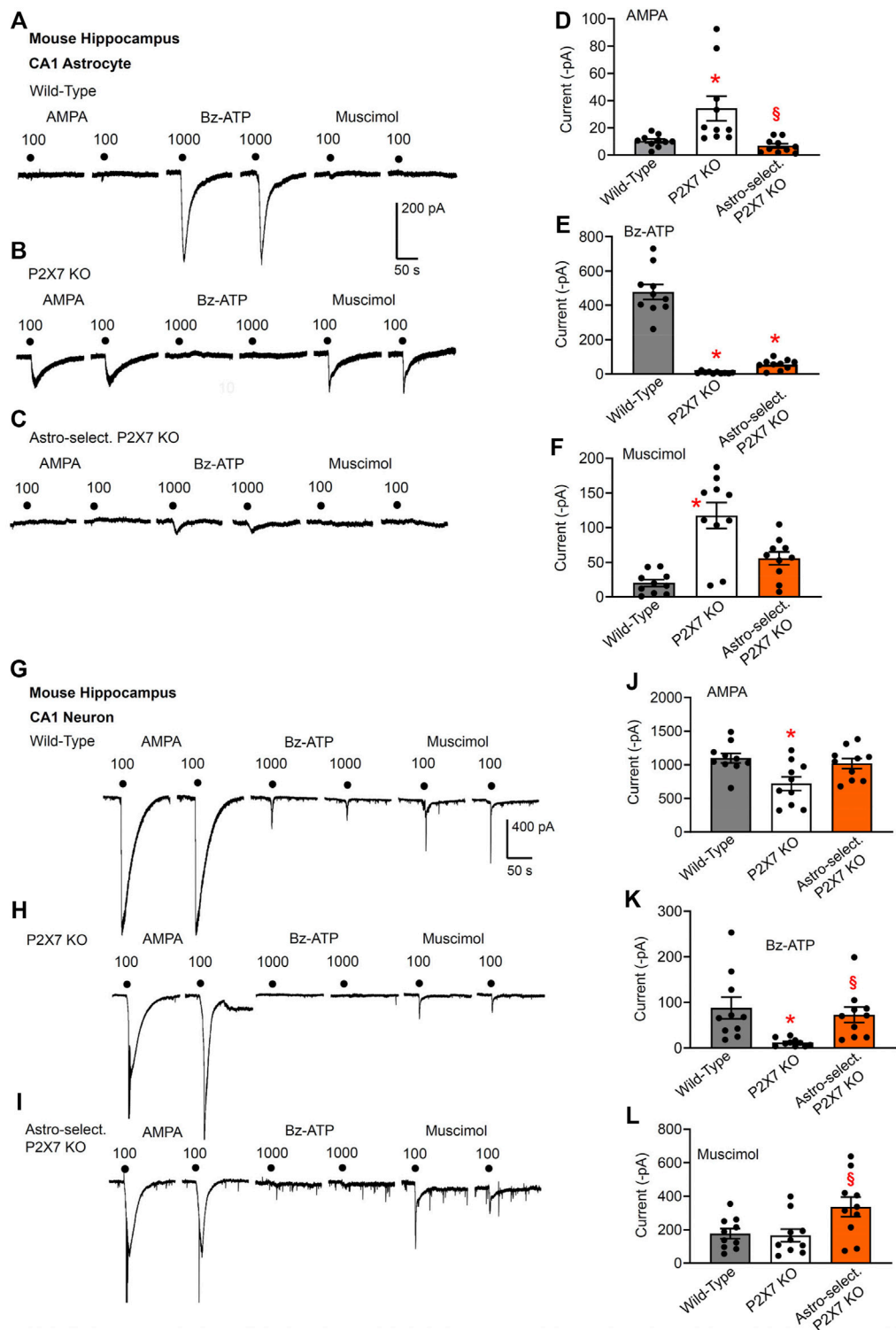


FIGURE 1
Current responses to ionotropic receptor agonists in the CA1 area of the mouse hippocampus. Hippocampal brain slices of 10–15 day-old wild-type (WT) mice, as well as mice whose P2X7Rs were genetically deleted either in all cells, or selectively in astrocytes. AMPA (100 μ M), Bz-ATP (1,000 μ M) and muscimol (100 μ M) were locally applied every 3 min, each agonist twice. (A–F) The membrane currents were recorded in astrocytes by means of the whole-cell patch-clamp method at a holding potential of -80 mV. The superfusion medium was in this and all further experiments a low X^{2+} -containing aCSF solution (see Methods). Representative tracings in (A–C). Effects of AMPA (D), Bz-ATP (E), and muscimol (F) in (Continued)

FIGURE 1 | the three types of animals. Each column indicates the mean \pm SEM of current amplitudes of 10 cells from at least four mice both in this Fig. as well as in all subsequent Figs. of the study. * $p < 0.05$; statistically significant difference from results in wild-type animals (AMPA, $F_{2,18} = 8.875$, $p = 0.0092$; Bz-ATP, $F_{2,18} = 92.93$, $p < 0.0001$; muscimol, $F_{2,18} = 19.74$, $p < 0.0001$; two-way ANOVA followed by the Tukey's test). [§] $p < 0.05$; statistically significant difference from general P2X7R KO animals (AMPA, $p = 0.0030$; Bz-ATP, $p < 0.0001$; muscimol, $p = 0.0026$; two-way ANOVA followed by the Tukey's test). (G–L) Similar experiments as in (A–F), but instead of astrocytes, pyramidal neurons were used for the investigations. The holding potential was -70 mV. Representative tracings in (G–I). Effects of AMPA (J), Bz-ATP (K), and muscimol (L) in the three types of animals. Mean \pm SEM current amplitudes. * $p < 0.05$; statistically significant difference from results in wild-type mice (AMPA, $F_{2,18} = 5.253$, $p = 0.0170$; Bz-ATP, $F_{2,18} = 6.852$, $p = 0.0069$; two-way ANOVA followed by the Tukey's test). [§] $p < 0.05$; statistically significant difference from general P2X7R KO animals (AMPA, $p = 0.0170$; Bz-ATP, $p = 0.0303$; muscimol, $F_{2,18} = 3.801$, $p = 0.0420$; two-way ANOVA followed by the Tukey's test).

mouse, also astrocyte-selective P2X7R KO mice were generated; in this case, the very small Bz-ATP current response confirmed the success of this manipulation (Figures 1C,E). The residual response to Bz-ATP may be due to the activation of a non-P2X7 receptor-type. The absence of P2X7Rs was accompanied by a compensatory increase in AMPA- and muscimol-sensitivities in the general knockouts (Figures 1B,D,F). For such an increase in the mentioned receptor-sensitivities apparently a complete absence of P2X7Rs is needed; a partial absence of this latter receptor-type is not sufficient.

In spite of the poor effect of AMPA and muscimol in WT astrocytes, both muscimol and especially AMPA caused large currents in CA1 neurons (Figures 1G,J,L). According to our expectations, the general deletion of P2X7Rs abolished the Bz-ATP (1,000 μ M)-induced current in CA1 neurons (Figures 1H,K). Similarly, the astrocyte-selective deletion of this receptor failed to cause any change of the Bz-ATP-induced current amplitudes, excluding the possibility that an astrocytic signaling molecule mediates neuronal activation (Figures 1I,K). There was no dramatic reduction of the responses to AMPA or muscimol either in the general knockouts or in the astrocyte-specific ones although the AMPA-induced current responses did decrease in the general knockouts (Figures 1G–J).

As discussed above, in CA1 astrocytes, the effects of AMPA and muscimol were increased in the general P2X7 KO mice relative to the responses to these agonists in WT and astrocyte-specific KO preparations; no similar changes occurred in neurons of the CA1 area. We have to confess that we do not know why the astrocytic and neuronal effects differed from each other. It is quite possible that there was no immediate and corresponding modulation of the excitatory and inhibitory amino acid-induced neuronal effects, but the astrocytic alterations would cause long-term changes due to a modified homeostatic function of this cell type (e.g., Illes et al., 2019; Verkhatsky et al., 2021).

Results in CA3 astrocytes and neurons roughly confirmed the data obtained in the analogous cells of the CA1 area (Figures 2A–L). The astrocyte-selective deletion of P2X7Rs once again failed to alter the effect of Bz-ATP in neurons, whereas this manipulation strongly inhibited the effect of Bz-ATP in astrocytes (compare Figure 2E with Figure 2K). However, the original recording in Figure 2I

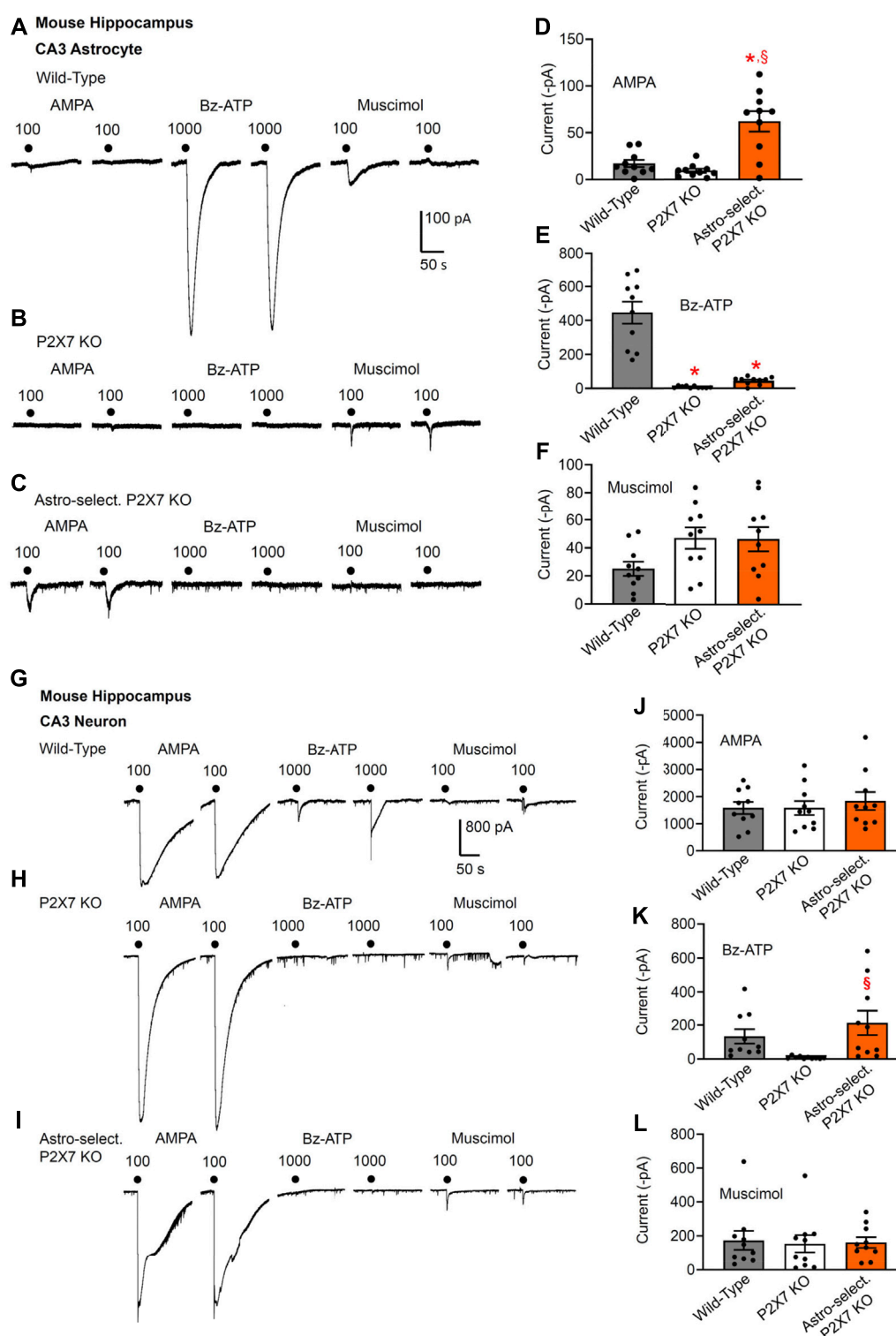
shows one of the neurons which after the astrocyte-selective genetic deletion of P2X7Rs did not respond to Bz-ATP at all (see Figure 2K). The larger current responses to AMPA in astrocytes of astrocyte-selective KO animals in comparison with their WT counterparts can be again explained with some compensatory mechanism, in that AMPA takes over the function of P2X7Rs under these conditions (Figure 2A).

Then, we checked the change of Bz-ATP-sensitivity in CA1/CA3 neurons after oligodendrocyte (NG2 glia)-selective deletion of P2X7Rs (Figures 3A,C–E). We did not find a statistically significant change in the CA1 pyramidal cell-sensitivity (although in the half of the total number of investigated cells there was no response to Bz-ATP at all Figures 3A,D); while in the analogous cells of the CA3 area the effect of Bz-ATP was almost abolished. This finding clearly indicates that in contrast to astrocytes, CA3 oligodendrocyte-like NG2 glia appear to secrete a signaling molecule onto the neighboring neurons upon stimulation of their P2X7Rs.

We also confirmed that the oligodendrocyte-selective deletion of P2X7Rs has no effect on the Bz-ATP-induced currents of CA1 astrocytes (Figure 3C), in contrast to the strong blockade of these responses in the CA1 astrocytes after the astrocyte-selective deletion of P2X7Rs (Figures 1C,E). In agreement with the compensatory increase of AMPA- and muscimol-induced currents in astrocytes of general P2X7R KO mice (Figures 1B,D,F), similar changes occurred also after the selective deletion of oligodendrocytic P2X7Rs (Figure 3C).

Eventually, a microglia-selective deletion of P2X7Rs did not alter AMPA-, Bz-ATP, or muscimol-evoked current responses in CA1/CA3 neurons of the hippocampus (Figures 3B,D,E). The original tracings in Figures 3A,B, show in addition that another ionotropic glutamate receptor agonist, NMDA also causes prominent effects in these neurons in a low X^{2+} -containing superfusion medium. This is possibly in concord with the well-known blockade of NMDA receptors by extracellular Mg^{2+} and their apparent disinhibition in the nominal absence of external Mg^{2+} .

It is interesting to note that the Bz-ATP-evoked currents in CA1 astrocytes appeared to decrease after a microglia-selective deletion of P2X7Rs (Figure 3C), although, as already mentioned, the neuronal current responses to Bz-ATP were not changed at

**FIGURE 2**

Current responses to ionotropic receptor agonists in the CA3 area of the mouse hippocampus. Hippocampal brain slices of 10–15 day-old wild-type mice, as well as mice whose P2X7Rs were genetically deleted either in all cells, or selectively in astrocytes. AMPA (100 μ M), Bz-ATP (1,000 μ M) and muscimol (100 μ M) were locally applied every 3 min, each agonist twice. (A–F) The membrane currents were recorded in astrocytes by means of the whole-cell patch-clamp method at a holding potential of -80 mV. Representative tracings in (A–C). Effects of AMPA (D), Bz-ATP (E), and muscimol (F) in the three types of animals. Mean \pm SEM current amplitudes. * $p < 0.05$; statistically significant difference from results in wild-type animals (AMPA, $F_{2,18} = 21.61$, $p = 0.0002$; Bz-ATP, $F_{2,18} = 42.03$, $p < 0.0001$; two-way ANOVA followed by the Tukey's test). § $p < 0.05$; (Continued)

FIGURE 2 | statistically significant difference from general P2X7R KO animals (AMPA, $p = 0.0030$; Bz-ATP, $p < 0.0001$; two-way ANOVA followed by the Tukey's test). (G–L) Similar experiments as in (A–F), but instead of astrocytes, pyramidal neurons were used for the investigations. The holding potential was -70 mV. Representative tracings in (G–I). Effects of AMPA (J), Bz-ATP (K), and muscimol (L) in the three types of animals. Mean \pm SEM current amplitudes. $^{\#}p < 0.05$; statistically significant difference from general P2X7R KO animals (Bz-ATP, $F_{2,18} = 3.748$, $p = 0.0360$; two-way ANOVA followed by the Tukey's test).

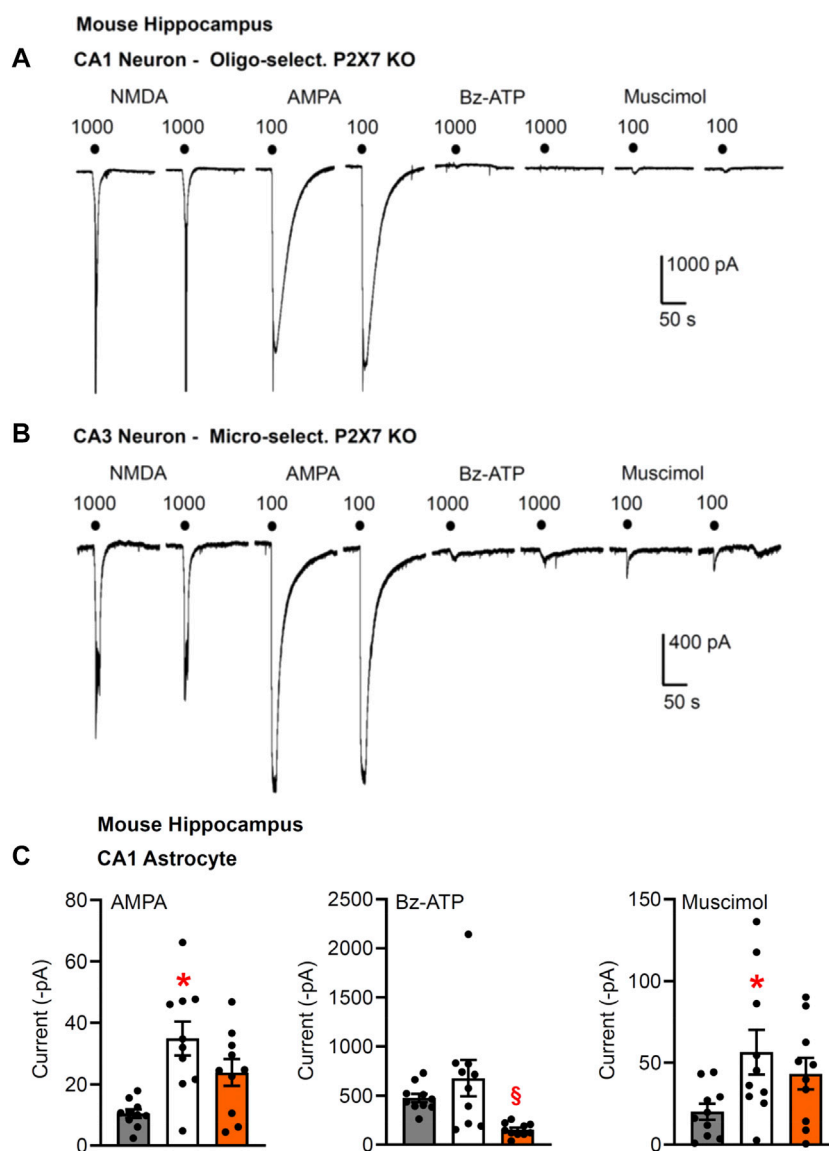


FIGURE 3

Current responses to ionotropic receptor agonists in the CA1 and CA3 areas of the mouse hippocampus. Hippocampal brain slices of 10–15 day-old wild-type mice, as well as mice whose P2X7Rs were genetically deleted in all cells, or selectively in oligodendrocytes or microglia. NMDA (100 μ M), AMPA (100 μ M), Bz-ATP (1,000 μ M) and muscimol (100 μ M) were locally superfused every 3 min, each agonist twice. The membrane currents were recorded in astrocytes by means of the whole-cell patch-clamp method at a holding potential of -80 mV, and in neurons at a holding potential of -70 mV. Representative tracings in neurons (A,B). (C–E) Mean \pm SEM current amplitudes. (C) Effects of AMPA, Bz-ATP, and muscimol in CA1 astrocytes of the three types of animals. * $p < 0.05$; statistically significant difference from results in wild-type animals (AMPA, $F_{2,18} = 7.565$, $p = 0.0030$; muscimol, $F_{2,18} = 3.553$, $p < 0.0427$; two-way ANOVA followed by the Tukey's test). (D,E) Similar experiments as in C, but instead of astrocytes, CA1 or CA3 pyramidal neurons were used for the investigations. Mean \pm SEM current amplitudes. * $p < 0.05$; statistically significant difference from results in wild-type mice (Bz-ATP, $F_{2,18} = 3.632$, $p = 0.0432$; two-way ANOVA followed by the Tukey's test).

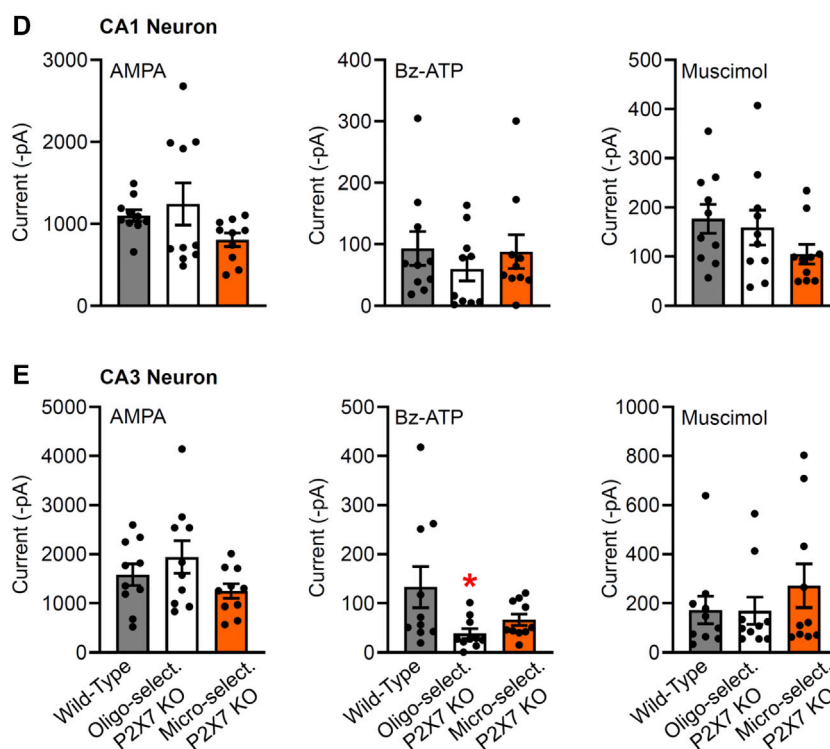


FIGURE 3
(Continued).

all. A similar decrease of the CA1 astrocytic currents was also observed after treatment with minocycline, known to block microglial activation (see below).

Effects of interference by minocycline with microglial activation on Bz-ATP-induced currents in hippocampal astrocytes and neurons

Minocycline is commonly used to inhibit microglial activation (Bassett et al., 2021). However, microglia exert dual functions, that is pro-inflammatory and anti-inflammatory ones (Illes et al., 2020). In addition, to the classically activated M1 microglial phenotype, releasing the previously mentioned pro-inflammatory mediators and causing neurodegeneration, the alternatively activated M2-phenotype clears cellular debris through phagocytosis and releases numerous protective factors [IL-4, IL-13, nerve growth factor (NGF), fibroblast growth factor (FGF)], thereby contributing to neuroregeneration (Kettenmann et al., 2013). It was reported that minocycline selectively inhibits the microglial polarization to a pro-inflammatory state, and leaves the pro-regenerative functions undisturbed (Kobayashi et al., 2013).

In the light of these results we investigated the modulation by i.p. minocycline of the astrocytic and neuronal effects of Bz-ATP in the hippocampal CA1 and CA3 area of the mouse. A somewhat unexpected finding of these series of experiments was that Bz-ATP-induced current responses in CA3 neurons increased, rather than decreased in minocycline-treated brain slices (Figures 4B,F). In addition, the same responses in CA1 responses also showed some tendency to increase although this change was not statistically significant (Figures 4A,D). In both cell-types, we also tested the application of the solvent aCSF to confirm that the mechanical strain of the superfusion did not cause any current response (Figures 4A,B). The rises of the AMPA and muscimol currents in the CA1 astrocytes, assumedly compensating the reduced P2X7R activity, could be again observed (Figures 1, 4C,E).

Our explanation for the potentiation of the Bz-ATP responses in the CA3 neurons is based on the selective blockade of the pro-inflammatory M1 phenotype of microglia, under the assumption that certain cytokines and growth factors amplify the outflow of ATP from its astrocytic pools or alternatively promote the sensitivity of various P2Rs to the ATP released (Heine et al., 2006; Heine et al., 2007; Oliveira et al., 2016). In consequence, an unexpected facilitation of P2X7R functions may develop on the CA3 pyramidal neurons.

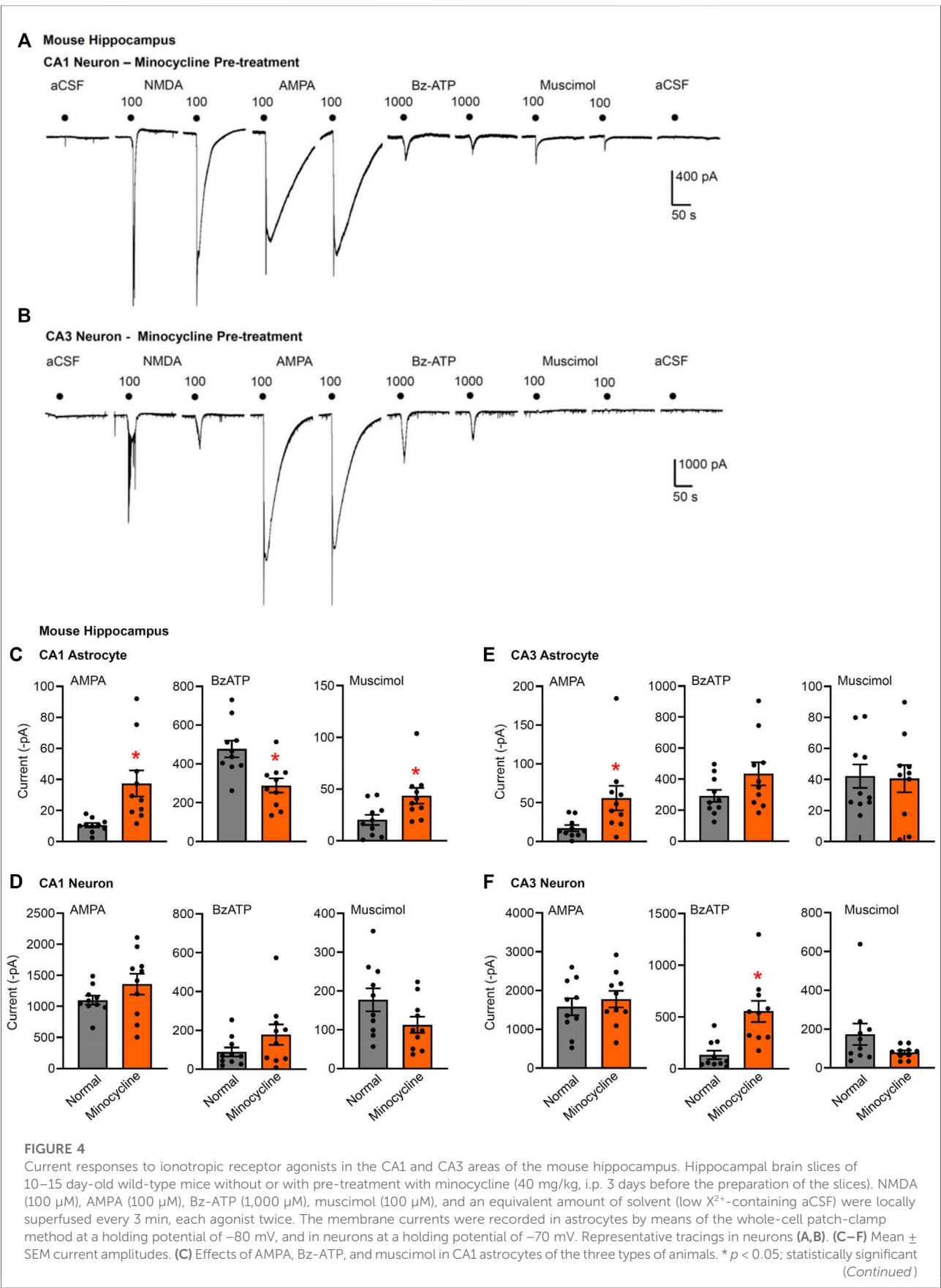


FIGURE 4 | difference from results in wild-type animals (AMPA, $p < 0.0001$, Mann-Whitney test; Bz-ATP, $p = 0.0036$, unpaired t -test; muscimol, $p = 0.0205$, unpaired t -test). (D) Effects of AMPA, Bz-ATP, and muscimol in CA1 neurons of the three types of animals. (E) Effects of AMPA, Bz-ATP, and muscimol in CA3 astrocytes of the three types of animals. * $p < 0.05$; statistically significant difference from results in wild-type mice (AMPA, $p = 0.0279$, unpaired t -test). (F) Effects of AMPA, Bz-ATP, and muscimol in CA3 neurons of the three types of animals * $p < 0.05$; statistically significant difference from results in wild-type mice (Bz-ATP, $p = 0.0013$, unpaired t -test).

Increase by Bz-ATP of the frequency but not amplitude of spontaneous postsynaptic currents in CA1 hippocampal neurons

After having dealt with the possibly postsynaptic neuronal P2X7Rs, we turned our attention to their assumedly presynaptic counterparts. In fact, we discriminated by the usual technique CA1 pyramidal neurons from neighboring astrocytes by injecting depolarizing current pulses into the cells and deciding that action potential firing is a neuronal property (Figure 5A). Then, we have set the holding potential to -70 mV and recorded sPSCs before, during, and after the application of Bz-ATP ($300 \mu\text{M}$) for 5 min each (Figure 5B). Bz-ATP increased the mean sPSC frequency, without altering the mean sPSC amplitude (Figures 5C,D). This effect may be considered to be an indication for the boosting of the spontaneous release of glutamate/GABA from the glutamatergic mossy fiber nerve terminals and GABAergic interneurons (Khan et al., 2019). However, a third possibility also exists, namely that the source of these transmitters are P2X7R possessing astrocytes sending their processes to the CA1 pyramidal neurons.

This latter assumption was supported by the abolishment of the Bz-ATP effect in brain slices of mice previously treated by intrahippocampal injection of the astrocytic toxin L- α -aminoadipate (Figure 5E). L- α -aminoadipate is a glutamate homologue which selectively ablates astrocytes without influencing neuronal density and function (Khurgel et al., 1996; Gochenauer and Robinson, 2001). In addition, the GABA_AR antagonist gabazine ($10 \mu\text{M}$) also inhibited the effect of Bz-ATP on the frequency of sPSCs (Figure 5F). In contrast to the observed effects of Bz-ATP on the sPSC frequency of CA1 pyramidal cells, there was no comparable influence on CA3 pyramidal cells and in consequence L- α -aminoadipate pre-treatment did not cause a further effect in the latter area of the brain (Figures 5G,H). In consequence, it is suggested that Bz-ATP increases the exocytotic release of astrocytic signaling molecules rather than that of their neuronal counterparts (see Discussion).

Discussion

The main finding of this study is that the oligodendrocyte-selective genetic deletion of P2X7Rs in the hippocampal CA3 area resulted in an indirect reduction of the P2X7R-mediated current responses at the neighboring pyramidal neurons. Hence, these data exclude the assumption that

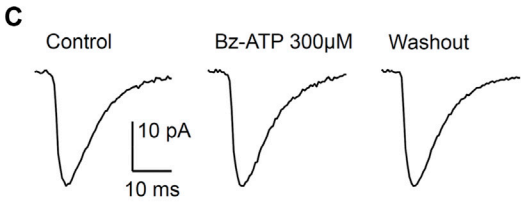
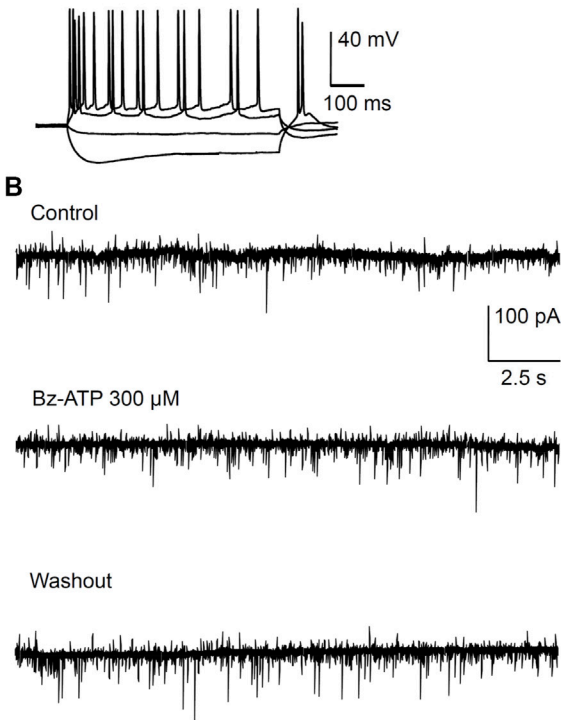
P2X7R-mRNA in CA3 pyramidal neurons of mice indicates the presence of the respective receptor protein (Metzger et al., 2017). The validity of our findings is strengthened by the fact that we used the mouse line generated by Metzger et al. (2017), in which the humanized P2rX7 allele being accessible to spatially and temporally controlled Cre recombinase-mediated inactivation allowed a cell-type specific deletion of P2X7Rs. Thus, we caution against drawing conclusions from the presence of mRNA for any type of functional protein in a given cell-type.

In previously available and broadly used P2rX7^{-/-} mouse models the knockout strategy did not result in complete inactivation of the P2rX7 gene (Kaczmarek-Hájek et al., 2012; Bartlett et al., 2014). In the mouse line established by Glaxo, the P2rX7 gene was disrupted by targeted insertion of a lacZ/Neo reporter cassette into exon 1, which manipulation, however, left the translation of the highly functional P2rX7k splice variant unaltered (Nicke et al., 2009). In the mouse line produced by Pfizer, a portion of exon 13 has been deleted and replaced by a neomycin resistance cassette (Solle et al., 2001). In this case several C-terminally truncated variants escaped deletion (Masin et al., 2012). In contrast to these conventional KO mice, none of the described P2rX7 splice variants evaded the null allele in the humanized P2rX7 KO mouse of Metzger et al. (2017).

However, our data are only in partial accordance with another study concluding that P2X7Rs are probably absent in any neuron of the CNS (Kaczmarek-Hajek et al., 2018). As mentioned earlier, this study reported the generation of a P2rX7 BAC transgenic mice which allowed the visualization of EGFP-tagged P2X7Rs in the brain. The authors criticized previous results obtained with a transgenic reporter mouse [Tg (p2rX7 EGFP)FY174Gsat] which showed a wide neuronal P2X7R expression in the brain (Engel et al., 2012; Jimenez-Pacheco et al., 2013). Kaczmarek-Hajek et al. (2018) believe that alterations in gene structure introduced into the GenSat P2rX7 BAC EGFP mouse influenced post-transcriptional and translational regulatory mechanisms. In fact, they ascribed all neuronal effects to indirect stimulation mediated by oligodendrocytic signaling molecules. Our data perfectly agree with this suggestion, but only in case of the CA3 hippocampal region; in CA1 pyramidal neurons, astrocytes, rather than oligodendrocytes released GABA in response to stimulation of their P2X7Rs.

A whole plethora of findings strongly support the notion that astrocytes are able to secrete signaling molecules and thereby are

A Mouse Hippocampus
CA1 Neuron



G CA3 Neuron

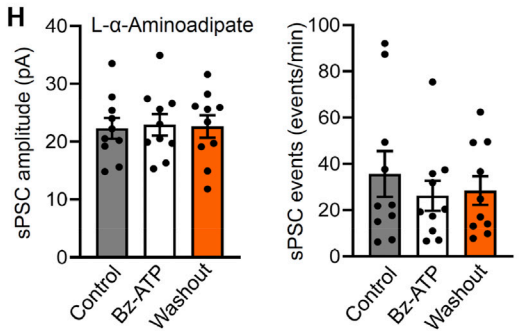
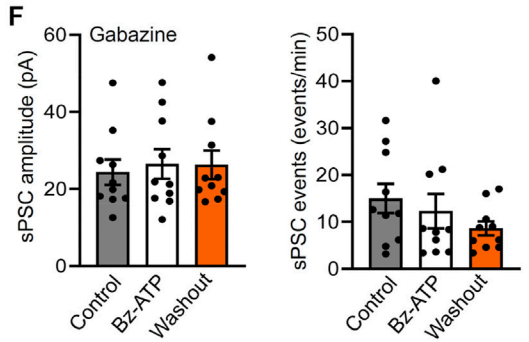
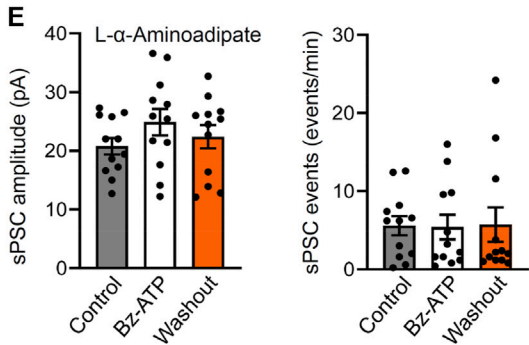
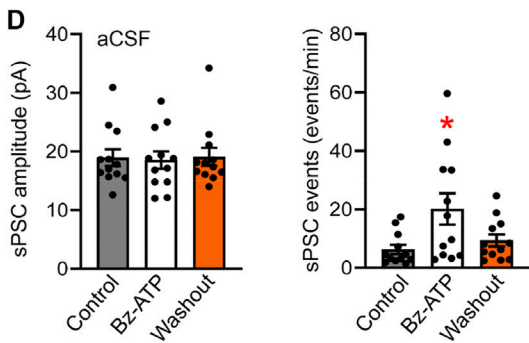
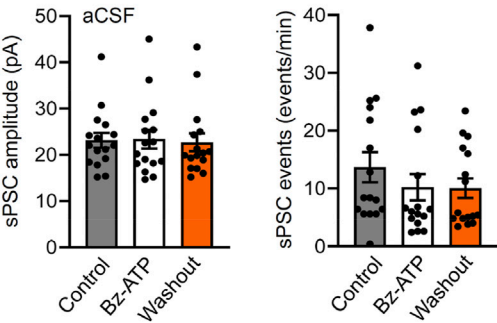


FIGURE 5
Spontaneous postsynaptic currents (sPSCs) in CA1 and CA3 neurons in brain slices of mice; effects of Bz-ATP after or without L- α -aminoadipate pre-treatment. **(A)** Identification of CA1 neurons by current injection into whole-cell patch-clamped cells. **(B–D)** Effect of Bz-ATP (300 μ M) on the amplitude and frequency of sPSCs in a low X^{2+} -containing aCSF. Representative recordings of sPSCs before, during and after superfusion with Bz-ATP for 5 min **(B)**. Representative, averaged sPSC amplitudes before, during and after a 5-min superfusion with Bz-ATP **(C)**. **(D)** Mean \pm SEM sPSC amplitudes and frequencies in brain slices prepared from untreated mice. * $p < 0.05$; statistically significant difference from control sPSCs (Continued)

FIGURE 5 | ($F_{2,33} = 4.477$, $p = 0.0142$; one-way ANOVA followed by the Dunnett's test). (E) Mean \pm SEM sPSC amplitudes and frequencies in brain slices prepared from mice pre-treated with L- α -aminoadipate (intrahippocampal application, 20 μ g; see Methods). (F) Mean \pm SEM sPSC amplitudes and frequencies in brain slices prepared from untreated mice continuously superfused with aCSF containing gabazine (10 μ M). Pre-treatment schedule with the selective astrocytic toxin L- α -aminoadipate, or blockade of GABA_ARs by gabazine, both abolished the effect of Bz-ATP. Experiments were made also in CA3 neurons of hippocampal brain slices prepared from untreated (G) and L- α -aminoadipate pre-treated (H) mice.

capable of regulating neuronal circuit functions and animal behavior (Illes et al., 2019; Hirrlinger and Nimmerjahn, 2022). The tripartite synapse hypothesis suggests that presynaptic neuronal elements, postsynaptic dendritic specializations and astrocytic processes that contact or even enwrap the synapse, together form a mutually interacting unit (Araque et al., 1999; Pascual et al., 2005). Neurotransmitters originating from presynaptic axon terminals may induce the release of gliotransmitters (glutamate, GABA, ATP, D-serine, taurine), which act at the postsynaptic specializations of neurons. The release mechanisms of ATP from astrocytes is through Ca^{2+} -dependent exocytosis (Lalo et al., 2014; Pankratov and Lalo, 2014), most likely from lysosomes (Zhang et al., 2007). However, a non-exocytotic release by means of channel molecules, including connexin hemichannels, pannexin-1 channels, maxi-anion channels, volume-regulated ion channels, Bestrophin1 channels, and the calcium homeostasis modulator 1 (CALHM1) is also possible (Dahl, 2015; Illes et al., 2020).

Specifically, in CA1 pyramidal cell-containing brain slices, Bz-ATP caused inward currents both in neurons and in neighboring astrocytes (Ficker et al., 2014). The effect of Bz-ATP was depressed by the selective P2X7R antagonist A-438079, and neuronal, but not astrocytic Bz-ATP currents were strongly inhibited by a combination of the ionotropic glutamate receptor antagonists AP-5 and CNQX, as well as the GABA_AR antagonist gabazine. This finding has borne out the conclusion that P2X7Rs are possibly situated at astrocytes which release glutamate/GABA to stimulate pyramidal neurons. In fact, astrocytic P2X7Rs have been shown to mediate the release glutamate (Duan et al., 2003; Fellin et al., 2006), GABA (Wirkner et al., 2005), and ATP itself (Suadicani et al., 2006; Illes et al., 2017).

Bz-ATP potentiated the frequency of sPSCs (consisting of glutamatergic, GABAergic and ATPergic synaptic potentials) in CA1 pyramidal cells in a hippocampal slice preparation of rats, without altering the amplitude of these spontaneous events (Khan et al., 2019). The selective P2X7R antagonist A-438079 abolished the potentiation by Bz-ATP, assigning this effect to the stimulation of the respective receptors. However, the question still remained to be answered, whether the P2X7Rs are localized at glutamatergic or GABAergic neurons or alternatively at neighboring astrocytes. The GABA_AR antagonist gabazine and the selective astrocytic toxin fluorocitrate (Clarke, 1991), both abolished the effect of Bz-ATP when applied under *in vitro* conditions. Further, a series of electrophysiological experiments excluded the participation of GABAergic interneurons in the

stratum radiatum as possible sources of external GABA and left the astrocytic release as an undisputable opportunity (Khan et al., 2019). Hence, it was concluded that the release of GABA is potentiated by P2X7R activation and astrocytes rather than GABAergic interneurons are involved in this effect.

Our present experiments fully agree with this conclusion, by confirming the blockade of a previously observed Bz-ATP-induced increase of sPSC frequency both by locally applied gabazine and by pre-treatment of mice with another selective astrocytic toxin, L- α -aminoadipate (Khurgel et al., 1996; Gochenauer and Robinson, 2001). Hence, CA1 pyramidal cells of both rats and mice appear to be innervated by Schaffer collaterals subjected to GABAergic modulation by gliotransmitter release from local astrocytic processes.

Oligodendrocytes just as astrocytes, also possess P2X7Rs (Matute, 2008; Zhao et al., 2021). P2X7Rs in oligodendrocytes are highly permeable to Ca^{2+} and prolonged activation of these receptors is lethal to differentiated oligodendrocytes in culture and to mature oligodendrocytes in isolated optic nerves *in vitro* and *in vivo*. *In vitro* ischemia achieved by replacing O_2 by N_2 , external glucose by sucrose, and by adding iodoacetate to the incubation medium to block glycolysis, induced inward currents in cultured oligodendrocytes, which could be reversed by the P2X7R antagonist Brilliant Blue, the ATP degrading enzyme apyrase, and by blockers of pannexin hemichannels (Domercq et al., 2010). Because oligodendrocytes constitute the myelin sheath of central fiber tracts, they are localized in the white matter insulating individual axons in order to permit spatially separated and rapid conduction of actions potentials.

In the hippocampus, oligodendrocyte precursor cells (OPCs) occur, giving rise to mature oligodendrocytes in the white matter, but functioning as a separate type of glial cells, the so called NG2 glia, in grey matter (Seifert and Steinhäuser, 2018; Bedner et al., 2020; see also Introduction). Bz-ATP was reported to increase intracellular Ca^{2+} in cultured NG2 glia in a manner fully dependent on extracellular Ca^{2+} and blocked by the P2X7R antagonistic oxidized ATP (Agresti et al., 2005a; Agresti et al., 2005b). Our findings implicate that in the CA3 area of the hippocampus P2X7R-bearing NG2 glia mediate the purportedly neuronal effects of Bz-ATP.

As a fourth type of non-neuronal cells capable of releasing a whole range of signaling molecules in response to P2X7R stimulation, microglia have to be taken into consideration (Kigerl et al., 2009; Kettenmann et al., 2011). Microglia are secreting ATP both by exocytosis (Imura et al., 2013) and by the shedding of extracellular vesicles (Graner, 2018). In addition, microglia were reported to release glutamate within a range of further neurotoxic molecules (Illes et al.,

2020; Lindhout et al., 2021). While especially the upregulation of A2ARs occupied by adenosine, an enzymatic degradation product of ATP, drives the transition of resting/surveillance microglia to its amoeboid phenotype, P2X7Rs are involved in the secretory functions of these phagocytic microglial cells. Many studies have focused on the interactions between the cellular processes of surveillance microglia and synaptic elements, including axonal boutons and dendritic spines (Wu et al., 2015; Weinhard et al., 2018). Recently, it was reported that microglia senses ATP via P2Y12Rs, thereafter a microglia-dependent production of adenosine ensues, and adenosine suppresses neuronal responses via its A2AR-type (Badimon et al., 2020). However, under the present conditions we did not find evidence for the involvement of microglial P2X7Rs in neuronal responses to Bz-ATP.

In conclusion, we supply evidence for the participation of astrocytic and oligodendrocytic P2X7Rs in the indirect stimulation of certain neuronal structures in the hippocampus of mice, but cannot exclude the presence of P2X7Rs at the residual CNS neurons. We have to point out as well that our conclusions are based on the finding that 1,000 μ M of Bz-ATP causes near-maximum current amplitudes in pyramidal neurons of the mouse hippocampus (Zhao et al., 2022) (also reported for organotypic spinal cord slices of the mouse substantia gelatinosa; Gao et al., 2017), and a further increase of the Bz-ATP concentration would not unmask a previously absent P2X7R-sensitivity.

Another caveat is due to the age of the animals. It was reported that in the mouse neocortex, stimulation of neuronal afferents triggers complex glial synaptic currents (GSCs mediated by NMDA, P2X and AMPA-Rs as well as glutamate transporters) (Lalo et al., 2011; Boué-Grabot and Pankratov, 2017). The P2X component of GSCs is the smallest in young, maximal in adult, and once more decreases in old mice. Somewhat similar, the exocytotic release of ATP from astrocytes exhibits an age-dependent decrease (Lalo et al., 2014). In view of these complexities it has to be concluded, that our findings relate to P10-15 mice and any extrapolation to older mice is only hypothetical, especially because ATP is considered to be an ontogenetically and phylogenetically primitive signaling molecule (Gao et al., 2017; Verkhratsky, 2021).

Data availability statement

The original contributions presented in the study are included in the article, further inquiries can be directed to the corresponding authors.

Ethics statement

The animal study was reviewed and approved by the Institutional Review Board of the Chengdu University of TCM.

Author contributions

YZ carried out the experiments; PR, PI, and YT designed the study and supervised the experiments; PI and YT wrote the first version of the manuscript; H-YY and PR, reviewed the manuscript, and critically revised it, including the re-interpretation of some results; all authors have read and agreed with the published version of the paper.

Funding

Our work was made possible by a grant (“The Project First-Class Disciplines Development”; CZYHW1901) of the Chengdu University of Traditional Chinese Medicine to YT and PI in order to build up “The International Collaborative Center for Purinergic Signaling,” and grants of the Sichuan State Administration of Foreign Affairs to support the stays of PI and PR in Chengdu (G20190236012). Financial support from the Innovation Team and Talents Cultivation Program of National Administration of Traditional Chinese Medicine (ZYYCXTD-D-202003) and Sichuan Science and Technology Program (2019YFH0108, 2022YFH0006) are also gratefully acknowledged.

Conflict of interest

The authors declare that the research was conducted in the absence of any commercial or financial relationships that could be construed as a potential conflict of interest.

Publisher’s note

All claims expressed in this article are solely those of the authors and do not necessarily represent those of their affiliated organizations, or those of the publisher, the editors and the reviewers. Any product that may be evaluated in this article, or claim that may be made by its manufacturer, is not guaranteed or endorsed by the publisher.

Acknowledgments

We are grateful to Jan M. Deussing (Max Planck Institute of Psychiatry, Munich, Germany) for the generous gift of P2X7R knockout mice. We also thank Yong-Jun Chen (Guangzhou University of Traditional Chinese Medicine, Guangzhou, China) for supplying us with the Cre-mice used.

References

- Agresti, C., Meomartini, M. E., Amadio, S., Ambrosini, E., Serafini, B., Franchini, L., et al. (2005a). Metabotropic P2 receptor activation regulates oligodendrocyte progenitor migration and development. *Glia* 50, 132–144. doi:10.1002/glia.20160
- Agresti, C., Meomartini, M. E., Amadio, S., Ambrosini, E., Volonté, C., Aloisi, F., et al. (2005b). ATP regulates oligodendrocyte progenitor migration, proliferation, and differentiation: Involvement of metabotropic P2 receptors. *Brain Res. Brain Res. Rev.* 48, 157–165. doi:10.1016/j.brainresrev.2004.12.005
- Anderson, C. M., and Nedergaard, M. (2006). Emerging challenges of assigning P2X7 receptor function and immunoreactivity in neurons. *Trends Neurosci.* 29, 257–262. doi:10.1016/j.tins.2006.03.003
- Araque, A., Parpura, V., Sanzgiri, R. P., and Haydon, P. G. (1999). Tripartite synapses: Glia, the unacknowledged partner. *Trends Neurosci.* 22, 208–215. doi:10.1016/s0166-2236(98)001349-6
- Badimon, A., Strasburger, H. J., Ayata, P., Chen, X., Nair, A., Ikegami, A., et al. (2020). Negative feedback control of neuronal activity by microglia. *Nature* 586, 417–423. doi:10.1038/s41586-020-2777-8
- Bartlett, R., Stokes, L., and Sluyter, R. (2014). The P2X7 receptor channel: Recent developments and the use of P2X7 antagonists in models of disease. *Pharmacol. Rev.* 66, 638–675. doi:10.1124/pr.113.008003
- Bassett, B., Subramaniam, S., Fan, Y., Varney, S., Pan, H., Carneiro, A. M. D., et al. (2021). Minocycline alleviates depression-like symptoms by rescuing decrease in neurogenesis in dorsal hippocampus via blocking microglia activation/phagocytosis. *Brain Behav. Immun.* 91, 519–530. doi:10.1016/j.bbi.2020.11.009
- Bedner, P., Jabs, R., and Steinhäuser, C. (2020). Properties of human astrocytes and NG2 glia. *Glia* 68, 756–767. doi:10.1002/glia.23725
- Boucsein, C., Kettenmann, H., and Nolte, C. (2000). Electrophysiological properties of microglial cells in normal and pathologic rat brain slices. *Eur. J. Neurosci.* 12, 2049–2058. doi:10.1046/j.1460-9568.2000.00100.x
- Boué-Grabot, E., and Pankratov, Y. (2017). Modulation of central synapses by astrocyte-released ATP and postsynaptic P2X receptors. *Neural Plast.* 2017, 9454275. doi:10.1155/2017/9454275
- Clarke, D. D. (1991). Fluoroacetate and fluorocitrate: Mechanism of action. *Neurochem. Res.* 16, 1055–1058. doi:10.1007/BF00965850
- Dahl, G. (2015). ATP release through pannexon channels. *Philos. Trans. R. Soc. Lond. B Biol. Sci.* 370, 20140191. doi:10.1098/rstb.2014.0191
- Degen, J., Dublin, P., Zhang, J., Dobrowolski, R., Jokwitz, M., Karraam, K., et al. (2012). Dual reporter approach for identification of Cre efficacy and astrocyte heterogeneity. *FASEB J.* 26, 4576–4583. doi:10.1096/fj.12-207183
- Di Virgilio, F., Schmalzing, G., and Markwardt, F. (2018). The elusive P2X7 macropore. *Trends Cell. Biol.* 28, 392–404. doi:10.1016/j.tcb.2018.01.005
- Domercq, M., Perez-Samartin, A., Aparicio, D., Alberdi, E., Pampliega, O., Matute, C., et al. (2010). P2X7 receptors mediate ischemic damage to oligodendrocytes. *Glia* 58, 730–740. doi:10.1002/glia.20958
- Duan, S., Anderson, C. M., Keung, E. C., Chen, Y., Chen, Y., Swanson, R. A., et al. (2003). P2X7 receptor-mediated release of excitatory amino acids from astrocytes. *J. Neurosci.* 23, 1320–1328. doi:10.1523/JNEUROSCI.23-04-01320.2003
- Engel, T., Jimenez-Pacheco, A., Miras-Portugal, M. T., Diaz-Hernandez, M., and Henshall, D. C. (2012). P2X7 receptor in epilepsy; role in pathophysiology and potential targeting for seizure control. *Int. J. Physiol. Pathophysiol. Pharmacol.* 4, 174–187.
- Fellin, T., Sul, J.-Y., D'Ascenzo, M., Takano, H., Pascual, O., Haydon, P. G., et al. (2006). Bidirectional astrocyte-neuron communication: The many roles of glutamate and ATP. *Novartis Found. Symp.* 276, 208–217. doi:10.1002/9780470032244.ch16
- Ficker, C., Rozmer, K., Kató, E., Andó, R. D., Schumann, L., Krügel, U., et al. (2014). Astrocyte-neuron interaction in the substantia gelatinosa of the spinal cord dorsal horn via P2X7 receptor-mediated release of glutamate and reactive oxygen species. *Glia* 62, 1671–1686. doi:10.1002/glia.22707
- Gao, P., Ding, X., Khan, T. M., Rong, W., Franke, H., Illes, P., et al. (2017). P2X7 receptor-sensitivity of astrocytes and neurons in the substantia gelatinosa of organotypic spinal cord slices of the mouse depends on the length of the culture period. *Neuroscience* 349, 195–207. doi:10.1016/j.neuroscience.2017.02.030
- Gochenauer, G. E., and Robinson, M. B. (2001). Dibutyl-*l*-cAMP (dbcAMP) up-regulates astrocytic chloride-dependent L-[³H]glutamate transport and expression of both system xc(-) subunits. *J. Neurochem.* 78, 276–286. doi:10.1046/j.1471-4159.2001.00385.x
- Graner, M. W. (2018). Extracellular vesicles in cancer immune responses: Roles of purinergic receptors. *Semin. Immunopathol.* 40, 465–475. doi:10.1007/s00281-018-0706-9
- Harkat, M., Peverini, L., Cerdan, A. H., Dunning, K., Beudez, J., Martz, A., et al. (2017). On the permeation of large organic cations through the pore of ATP-gated P2X receptors. *Proc. Natl. Acad. Sci. U. S. A.* 114, E3786–E3795. doi:10.1073/pnas.1701379114
- Heine, C., Heimrich, B., Vogt, J., Wegner, A., Illes, P., and Franke, H. (2006). P2 receptor-stimulation influences axonal outgrowth in the developing hippocampus *in vitro*. *Neuroscience* 138, 303–311. doi:10.1016/j.neuroscience.2005.11.056
- Heine, C., Wegner, A., Grosche, J., Allgaier, C., Illes, P., and Franke, H. (2007). P2 receptor expression in the dopaminergic system of the rat brain during development. *Neuroscience* 149, 165–181. doi:10.1016/j.neuroscience.2007.07.015
- Hirrlinger, J., and Nimmerjahn, A. (2022). A perspective on astrocyte regulation of neural circuit function and animal behavior. *Glia* 70, 1554–1580. doi:10.1002/glia.24168
- Illes, P., Burnstock, G., and Tang, Y. (2019). Astroglia-derived ATP modulates CNS neuronal circuits. *Trends Neurosci.* 42, 885–898. doi:10.1016/j.tins.2019.09.006
- Illes, P., Khan, T. M., and Rubini, P. (2017). Neuronal P2X7 receptors revisited: Do they really exist? *J. Neurosci.* 37, 7049–7062. doi:10.1523/JNEUROSCI.3103-16.2017
- Illes, P., Müller, C. E., Jacobson, K. A., Grutter, T., Nicke, A., Fountain, S. J., et al. (2021). Update of P2X receptor properties and their pharmacology: IUPHAR Review 30. *Br. J. Pharmacol.* 178, 489–514. doi:10.1111/bph.15299
- Illes, P., Rubini, P., Ulrich, H., Zhao, Y., and Tang, Y. (2020). Regulation of microglial functions by purinergic mechanisms in the healthy and diseased CNS. *Cells* 9, 1108. doi:10.3390/cells9051108
- Imura, Y., Morizawa, Y., Komatsu, R., Shibata, K., Shinozaki, Y., Kasai, H., et al. (2013). Microglia release ATP by exocytosis. *Glia* 61, 1320–1330. doi:10.1002/glia.22517
- Jiang, L.-H. (2009). Inhibition of P2X7 receptors by divalent cations: Old action and new insight. *Eur. Biophys. J.* 38, 339–346. doi:10.1007/s00249-008-0315-y
- Jimenez-Pacheco, A., Mesuret, G., Sanz-Rodriguez, A., Tanaka, K., Mooney, C., Conroy, R., et al. (2013). Increased neocortical expression of the P2X7 receptor after status epilepticus and anticonvulsant effect of P2X7 receptor antagonist A-438079. *Epilepsia* 54, 1551–1561. doi:10.1111/epi.12257
- Kaczmarek-Hájek, K., Lörinczi, E., Hausmann, R., and Nicke, A. (2012). Molecular and functional properties of P2X receptors—recent progress and persisting challenges. *Purinergic Signal.* 8, 375–417. doi:10.1007/s11302-012-9314-7
- Kaczmarek-Hájek, K., Zhang, J., Kopp, R., Grosche, A., Rissiek, B., Saul, A., et al. (2018). Re-evaluation of neuronal P2X7 expression using novel mouse models and a P2X7-specific nanobody. *Elife* 7, e36217. doi:10.7554/eLife.36217
- Kettenmann, H., Hanisch, U.-K., Noda, M., and Verkhratsky, A. (2011). Physiology of microglia. *Physiol. Rev.* 91, 461–553. doi:10.1152/physrev.00011.2010
- Kettenmann, H., Kirchhoff, F., and Verkhratsky, A. (2013). Microglia: New roles for the synaptic stripper. *Neuron* 77, 10–18. doi:10.1016/j.neuron.2012.12.023
- Khan, M. T., Deussing, J., Tang, Y., and Illes, P. (2019). Astrocytic rather than neuronal P2X7 receptors modulate the function of the tri-synaptic network in the rodent hippocampus. *Brain Res. Bull.* 151, 164–173. doi:10.1016/j.brainresbull.2018.07.016
- Khurgel, M., Koo, A. C., and Ivy, G. O. (1996). Selective ablation of astrocytes by intracerebral injections of alpha-aminoadipate. *Glia* 16, 351–358. doi:10.1002/(SICI)1098-1136(199604)16:4<351::AID-GLIA7>3.0.CO;2-2
- Kigerl, K. A., Gensel, J. C., Ankeny, D. P., Alexander, J. K., Donnelly, D. J., Popovich, P. G., et al. (2009). Identification of two distinct macrophage subsets with divergent effects causing either neurotoxicity or regeneration in the injured mouse spinal cord. *J. Neurosci.* 29, 13435–13444. doi:10.1523/JNEUROSCI.3257-09.2009
- Kobayashi, K., Imagama, S., Ohgomori, T., Hirano, K., Uchimura, K., Sakamoto, K., et al. (2013). Minocycline selectively inhibits M1 polarization of microglia. *Cell. Death Dis.* 4, e525. doi:10.1038/cddis.2013.54
- Lalo, U., Palygin, O., North, R. A., Verkhratsky, A., and Pankratov, Y. (2011). Age-dependent remodelling of ionotropic signalling in cortical astroglia. *Aging Cell.* 10, 392–402. doi:10.1111/j.1474-9726.2011.00682.x

- Lalo, U., Palygin, O., Rasooli-Nejad, S., Andrew, J., Haydon, P. G., Pankratov, Y., et al. (2014). Exocytosis of ATP from astrocytes modulates phasic and tonic inhibition in the neocortex. *PLoS Biol.* 12, e1001747. doi:10.1371/journal.pbio.1001747
- Lima, A., Sardinha, V. M., Oliveira, A. F., Reis, M., Mota, C., Silva, M. A., et al. (2014). Astrocyte pathology in the prefrontal cortex impairs the cognitive function of rats. *Mol. Psychiatry* 19, 834–841. doi:10.1038/mp.2013.182
- Lindhout, I. A., Murray, T. E., Richards, C. M., and Klegeris, A. (2021). Potential neurotoxic activity of diverse molecules released by microglia. *Neurochem. Int.* 148, 105117. doi:10.1016/j.neuint.2021.105117
- Masin, M., Young, C., Lim, K., Barnes, S. J., Xu, X. J., Marschall, V., et al. (2012). Expression, assembly and function of novel C-terminal truncated variants of the mouse P2X7 receptor: Re-evaluation of P2X7 knockouts. *Br. J. Pharmacol.* 165, 978–993. doi:10.1111/j.1476-5381.2011.01624.x
- Matute, C. (2008). P2X7 receptors in oligodendrocytes: A novel target for neuroprotection. *Mol. Neurobiol.* 38, 123–128. doi:10.1007/s12035-008-8028-x
- Metzger, M. W., Walser, S. M., Aprile-Garcia, F., Dedic, N., Chen, A., Holsboer, F., et al. (2017). Genetically dissecting P2rx7 expression within the central nervous system using conditional humanized mice. *Purinergic Signal.* 13, 153–170. doi:10.1007/s11302-016-9546-z
- Miras-Portugal, M. T., Sebastián-Serrano, Á., Diego García, L. D., and Díaz-Hernández, M. (2017). Neuronal P2X7 receptor: Involvement in neuronal physiology and pathology. *J. Neurosci.* 37, 7063–7072. doi:10.1523/JNEUROSCI.3104-16.2017
- Nicke, A., Kuan, Y.-H., Masin, M., Rettinger, J., Marquez-Klaka, B., Bender, O., et al. (2009). A functional P2X7 splice variant with an alternative transmembrane domain 1 escapes gene inactivation in P2X7 knock-out mice. *J. Biol. Chem.* 284, 25813–25822. doi:10.1074/jbc.M109.033134
- Nishiyama, A., Boshans, L., Goncalves, C. M., Wegrzyn, J., and Patel, K. D. (2016). Lineage, fate, and fate potential of NG2-glia. *Brain Res.* 1638, 116–128. doi:10.1016/j.brainres.2015.08.013
- North, R. A. (2002). Molecular physiology of P2X receptors. *Physiol. Rev.* 82, 1013–1067. doi:10.1152/physrev.00015.2002
- Oliveira, J. F., Riedel, T., Leichsenring, A., Heine, C., Franke, H., Krügel, U., et al. (2011). Rodent cortical astroglia express *in situ* functional P2X7 receptors sensing pathologically high ATP concentrations. *Cereb. Cortex* 21, 806–820. doi:10.1093/cercor/bhq154
- Oliveira, Á., Illes, P., and Ulrich, H. (2016). Purinergic receptors in embryonic and adult neurogenesis. *Neuropharmacology* 104, 272–281. doi:10.1016/j.neuropharm.2015.10.008
- Pankratov, Y., and Lalo, U. (2014). Calcium permeability of ligand-gated Ca²⁺ channels. *Eur. J. Pharmacol.* 739, 60–73. doi:10.1016/j.ejphar.2013.11.017
- Pascual, O., Casper, K. B., Kubera, C., Zhang, J., Revilla-Sanchez, R., Sul, J.-Y., et al. (2005). Astrocytic purinergic signaling coordinates synaptic networks. *Science* 310, 113–116. doi:10.1126/science.1116916
- Pelegrin, P., and Surprenant, A. (2006). Pannexin-1 mediates large pore formation and interleukin-1 β release by the ATP-gated P2X7 receptor. *EMBO J.* 25, 5071–5082. doi:10.1038/sj.emboj.7601378
- Pérez-Samartín, A., Garay, E., Moctezuma, J. P. H., Cisneros-Mejorado, A., Sánchez-Gómez, M. V., Martel-Gallegos, G., et al. (2017). Inwardly rectifying K⁺ currents in cultured oligodendrocytes from rat optic nerve are insensitive to pH. *Neurochem. Res.* 42, 2443–2455. doi:10.1007/s11064-017-2242-8
- Seifert, G., and Steinhäuser, C. (2018). Heterogeneity and function of hippocampal macroglia. *Cell. Tissue Res.* 373, 653–670. doi:10.1007/s00441-017-2746-1
- Solle, M., Labasi, J., Perregaux, D. G., Stam, E., Petrushova, N., Koller, B. H., et al. (2001). Altered cytokine production in mice lacking P2X7 receptors. *J. Biol. Chem.* 276, 125–132. doi:10.1074/jbc.M006781200
- Sperlágh, B., Vizi, E. S., Wirkner, K., and Illes, P. (2006). P2X7 receptors in the nervous system. *Prog. Neurobiol.* 78, 327–346. doi:10.1016/j.pneurobio.2006.03.007
- Suadcani, S. O., Brosnan, C. F., and Scemes, E. (2006). P2X7 receptors mediate ATP release and amplification of astrocytic intercellular Ca²⁺ signaling. *J. Neurosci.* 26, 1378–1385. doi:10.1523/JNEUROSCI.3902-05.2006
- Surprenant, A., Rassendren, F., Kawashima, E., North, R. A., and Buell, G. (1996). The cytolytic P2Z receptor for extracellular ATP identified as a P2X receptor (P2X7). *Science* 272, 735–738. doi:10.1126/science.272.5262.735
- Verkhatsky, A. (2021). Early evolutionary history (from bacteria to hemichordata) of the omnipresent purinergic signalling: A tribute to Geoff Burnstock inquisitive mind. *Biochem. Pharmacol.* 187, 114261. doi:10.1016/j.bcp.2020.114261
- Verkhatsky, A., Parpura, V., Li, B., and Scuderi, C. (2021). Astrocytes: The housekeepers and guardians of the CNS. *Adv. Neurobiol.* 26, 21–53. doi:10.1007/978-3-030-77375-5_2
- Virginio, C., MacKenzie, A., Rassendren, F. A., North, R. A., and Surprenant, A. (1999). Pore dilation of neuronal P2X receptor channels. *Nat. Neurosci.* 2, 315–321. doi:10.1038/7225
- Weinhard, L., Di Bartolomei, G., Bolasco, G., Machado, P., Schieber, N. L., Neniskyte, U., et al. (2018). Microglia remodel synapses by presynaptic trogocytosis and spine head filopodia induction. *Nat. Commun.* 9, 1228. doi:10.1038/s41467-018-03566-5
- Wirkner, K., Köfalvi, A., Fischer, W., Günther, A., Franke, H., Gröger-Arndt, H., et al. (2005). Supersensitivity of P2X receptors in cerebrocortical cell cultures after *in vitro* ischemia. *J. Neurochem.* 95, 1421–1437. doi:10.1111/j.1471-4159.2005.03465.x
- Wu, Y., Dissing-Olesen, L., MacVicar, B. A., and Stevens, B. (2015). Microglia: Dynamic mediators of synapse development and plasticity. *Trends Immunol.* 36, 605–613. doi:10.1016/j.it.2015.08.008
- Young, M. T., Pelegrin, P., and Surprenant, A. (2007). Amino acid residues in the P2X7 receptor that mediate differential sensitivity to ATP and BzATP. *Mol. Pharmacol.* 71, 92–100. doi:10.1124/mol.106.030163
- Zhang, Z., Chen, G., Zhou, W., Song, A., Xu, T., Luo, Q., et al. (2007). Regulated ATP release from astrocytes through lysosome exocytosis. *Nat. Cell. Biol.* 9, 945–953. doi:10.1038/ncb1620
- Zhao, Y.-F., Ren, W.-J., Zhang, Y., He, J.-R., Yin, H.-Y., Liao, Y., et al. (2022). High, in contrast to low levels of acute stress induce depressive-like behavior by involving astrocytic, in addition to microglial P2X7 receptors in the rodent Hippocampus. *Int. J. Mol. Sci.* 23, 1904. doi:10.3390/ijms23031904
- Zhao, Y. F., Tang, Y., and Illes, P. (2021). Astrocytic and oligodendrocytic P2X7 receptors determine neuronal functions in the CNS. *Front. Mol. Neurosci.* 14, 641570. doi:10.3389/fnmol.2021.641570



OPEN ACCESS

EDITED BY

Hugo Gutiérrez De Teran,
Uppsala University, Sweden

REVIEWED BY

Stefania Ceruti,
University of Milan, Italy
Hai-Ying Shen,
Legacy Research Institute, United States

*CORRESPONDENCE

Patrizia Di Iorio,
patrizia.diiorio@unich.it

SPECIALTY SECTION

This article was submitted to
Experimental Pharmacology and Drug
Discovery,
a section of the journal
Frontiers in Pharmacology

RECEIVED 16 June 2022

ACCEPTED 23 August 2022

PUBLISHED 19 September 2022

CITATION

Garozzo R, Zuccarini M, Giuliani P,
Di Liberto V, Mudò G, Caciagli F,
Ciccarelli R, Ciruela F, Di Iorio P and
Condorelli DF (2022), Guanine inhibits
the growth of human glioma and
melanoma cell lines by interacting
with GPR23.
Front. Pharmacol. 13:970891.
doi: 10.3389/fphar.2022.970891

COPYRIGHT

© 2022 Garozzo, Zuccarini, Giuliani, Di
Liberto, Mudò, Caciagli, Ciccarelli,
Ciruela, Di Iorio and Condorelli. This is
an open-access article distributed
under the terms of the [Creative
Commons Attribution License \(CC BY\)](#).
The use, distribution or reproduction in
other forums is permitted, provided the
original author(s) and the copyright
owner(s) are credited and that the
original publication in this journal is
cited, in accordance with accepted
academic practice. No use, distribution
or reproduction is permitted which does
not comply with these terms.

Guanine inhibits the growth of human glioma and melanoma cell lines by interacting with GPR23

Roberta Garozzo¹, Mariachiara Zuccarini^{2,3}, Patricia Giuliani^{2,3},
Valentina Di Liberto⁴, Giuseppa Mudò⁴, Francesco Caciagli³,
Renata Ciccarelli³, Francisco Ciruela^{5,6}, Patrizia Di Iorio^{2,3*} and
Daniele F. Condorelli¹

¹Department of Biomedical and Biotechnological, Section of Medical Biochemistry, University of Catania, Catania, Italy, ²Department of Medical, Oral and Biotechnological Sciences, Section of Pharmacology and Toxicology, School of Medicine, University of Chieti-Pescara, Chieti, Italy, ³Center for Advanced Studies and Technologies (CAST), University of Chieti-Pescara, Chieti, Italy, ⁴Department of Biomedicine, Neuroscience and Advanced Diagnostic, University of Palermo, Palermo, Italy, ⁵Pharmacology Unit, Department of Pathology and Experimental Therapeutics, Faculty of Medicine and Health Sciences, Institute of Neurosciences, University of Barcelona, Barcelona, Spain, ⁶Neuropharmacology and Pain Group, Neuroscience Program, Institut d'Investigació Biomèdica de Bellvitge, IDIBELL, Barcelona, Spain

Guanine-based purines (GBPs) exert numerous biological effects at the central nervous system through putative membrane receptors, the existence of which is still elusive. To shed light on this question, we screened orphan and poorly characterized G protein-coupled receptors (GPRs), selecting those that showed a high purinoreceptor similarity and were expressed in glioma cells, where GBPs exerted a powerful antiproliferative effect. Of the GPRs chosen, only the silencing of GPR23, also known as lysophosphatidic acid (LPA) 4 receptor, counteracted GBP-induced growth inhibition in U87 cells. Guanine (GUA) was the most potent compound behind the GPR23-mediated effect, acting as the endpoint effector of GBP antiproliferative effects. Accordingly, cells stably expressing GPR23 showed increased sensitivity to GUA. Furthermore, while GPR23 expression was low in a hypoxanthine-guanine phosphoribosyl-transferase (HGPRT)-mutated melanoma cell line showing poor sensitivity to GBPs, and in HGPRT-silenced glioma cells, GPR23-induced expression in both cell types rescued GUA-mediated cell growth inhibition. Finally, binding experiments using [³H]-GUA and U87 cell membranes revealed the existence of a selective GUA binding ($K_D = 29.44 \pm 4.07$ nM; $B_{max} 1.007 \pm 0.035$ pmol/mg prot) likely to GPR23. Overall, these data suggest GPR23 involvement in modulating responses to GUA in tumor cell lines, although further research needs to verify whether this receptor mediates other GUA effects.

KEYWORDS

guanine-based purines (GBPs), guanine (GUA), purine nucleoside phosphorylase (PNP), antiproliferative effects, G protein-coupled receptor 23 (GPR23), glioma cell lines, melanoma cell lines, lysophosphatidic acid (LPA)

Introduction

While adenine-based purines (ABPs), including adenosine triphosphate, diphosphate, and monophosphate (ATP, ADP, and AMP, respectively), and adenosine (ADO), have been extensively studied as extracellular signalling molecules in the central nervous system (CNS) (Burnstock, 2018; Jacobson et al., 2020; Illes et al., 2021), the guanine-based purines (GBPs), comprising guanosine triphosphate and monophosphate (GTP and GMP, respectively), guanosine (GUO), and guanine (GUA) has attracted less interest, although they also display CNS effects. Indeed, numerous studies have shown that GBPs are effective neuroprotective agents as they contribute to nervous tissue repair upon brain injury mostly by preventing glutamate excitotoxicity (reviewed in Di Liberto et al., 2016; Mancinelli et al., 2020; Massari et al., 2021; Di Iorio et al., 2021). Furthermore, they exert antiparkinsonian, anticonvulsant, antidepressant, and anxiolytic/amnestic effects (Di Iorio et al., 2021), which have mostly been attributed to GUO. Interestingly, GUA, the nucleobase resulting from purine nucleoside phosphorylase (PNP)-mediated GUO metabolism, exhibited activity in the CNS different from that of GUO, as GUA improved learning and memory formation in behaving animals (Giuliani et al., 2012; Zuccarini et al., 2018). In addition, GBPs stimulate the proliferation of neural stem cells and astrocytes (Ciccarelli et al., 2000; Su et al., 2013) as well as promote the differentiation of neuroblastoma cells or C2C12 skeletal muscle cells (Mancinelli et al., 2012; Belluardo et al., 2021). However, in some tumoral cell lines GBPs, in particular GUA, showed anti-proliferative effects mainly linked to an S-phase cell cycle arrest (Garozzo et al., 2010).

The lack of reliable plasma membrane receptors to account for the multiple though sometimes conflicting effects induced by GBPs in the CNS has historically reduced the interest of the scientific community, thus substantially diminishing the study of the guanergic signalling. So far, a high affinity binding site for [^3H]-GUO on rat brain has been described (Traversa et al., 2002). In addition, several G-protein-coupled GUO-mediated effects involving cyclic nucleotides and mitogen activated protein kinase (MAPK) and/or phosphoinositol-3-kinase (PI3K)/Akt pathways have been reported (Gysbers and Rathbone, 1992; Di Iorio et al., 2004; Molz et al., 2011; Giuliani et al., 2015). Interestingly, it has been postulated that adenosine A_1 and A_{2A} receptors (i.e., $A_1\text{R}$ and $A_{2A}\text{R}$, respectively) might be somehow involved in GUO-mediated neuroprotection by the stimulation of $A_1\text{R}/A_{2A}\text{R}$ heteromers (Lanznaster et al., 2019). GTP also seems to harbour specific binding sites, likely $G_{\alpha i/o}$ protein-coupled receptors, in mouse skeletal muscle cells (Pietrangelo et al., 2002). Finally, although the antiproliferative effect of GUA cited above has been referred to an intracellular metabolism of GUA (Garozzo et al., 2010), following the discovery of receptors sensing nucleobases such as adenine (Bender et al., 2002; Gorzalka et al., 2005) it has been reported that isolated

basolateral membranes of renal proximal tubule express a $G_{\alpha i/o}$ protein-coupled receptor for GUA, whose stimulation inhibits the activity of Na^+ -ATPase (Wengert et al., 2011).

Altogether, these findings point towards the possible existence of plasma membrane GBP receptors mediating the physiological effects associated to this important group of purines. Accordingly, we aimed to conduct a purinoreceptor homology-based screening within the group of orphan and poorly characterized G protein-coupled receptors (GPCRs) to pinpoint those responding to GBPs. Our bioinformatic approach revealed some potential candidates within these GPCRs, which were subsequently studied in some cancer cell lines previously used for assessing GBP functionality (Garozzo et al., 2010).

Materials and methods

Chemical compounds

GUA, GUO, GMP, GTP and ADO were purchased from Sigma-Aldrich (Steinheim, Germany). In all the experiments, nucleobases and nucleosides were dissolved in 1 N NaOH and added to the culture medium at the final concentration of 0.001 N NaOH whereas nucleotides were dissolved in aqueous solution. Geneticin was from Gibco (Invitrogen, Thermo Fisher Scientific, Milan, Italy); Deoxyribonuclease I amplification Grade (DNase, 1U/ul) was from Invitrogen (Thermo Fisher Scientific, Milan, Italy). Forodesine was purchased from D.B.A (Segrate, Italy). Tritiated GUA, [$8\text{-}^3\text{H}$]-GUA (100 $\mu\text{Ci}/\text{ml}$; specific activity $>5\text{ Ci}/\text{mmol}$), was purchased from Moravex Inc. (Brea, CA, United States).

Cell cultures

The human tumoral cell lines were obtained from the American Type Culture Collection (ATCC, Teddington, UK). Human glioma cell lines, (U87-MG ATCC number: HTB-14 and U373-MG ATCC number: HBT-17) were cultured in RPMI 1640 (Cat. No. 61870-010, Gibco, Invitrogen); human amelanotic melanoma (C32, ATCC number: CRL 1585 and C32TG ATCC number: CRL 1579) in MEM (Cat. No. 41090-028, Gibco, Invitrogen) supplemented with non-essential amino acids (0.1 mM) (Cat. No. 11140-035, Gibco, Invitrogen) and sodium pyruvate (1 mM); C32TG cells were grown in medium supplemented with thioguanine (30 μM). Each growing medium was integrated with 10% (vol/vol) heat-inactivated foetal bovine serum (FBS, Cat. No. 10270-106, Gibco, Invitrogen) and penicillin-streptomycin (50 units-50 $\mu\text{g}/\text{ml}$). Due to serum supplementation, a final concentration of 0.5 μM GUA and 0.1 μM GUO was present in each growing media, evaluated by HPLC method as previously described (Giuliani et al., 2016); however, these concentrations can be considered

negligible for experiments herein reported. The cell cultures were incubated at 37°C in a humidified 5% CO₂ incubator and the culture medium was changed twice a week.

BLAST search for purinoreceptor homology

Analysis of the GenBank™ database containing the human genome sequence was performed by BLAST (Basic Local Alignment Search Tool, NCBI) program to search for orphan GPCRs sharing protein sequence similarity to human A₁R, A_{2A}R, A₃R and P2Y₁R were used as queries. Only orphan GPCRs (i.e., included in the IUPHAR list of class A orphan receptors at 2022) or de-orphanized GPCRs with evidence of possible multiple unknown endogenous ligands, showing protein sequence similarity to one or more purinoreceptors with an Expected (E) value <0.05 were selected from the BLAST list search. The list was further refined excluding those receptors not showing an expression in normal brain tissue and glioblastoma samples by analysis of RNA-sequencing data provided by The Cancer Genome Atlas (TCGA) (<https://www.cancer.gov/about-nci/organization/ccg/research/structural-genomics/tcga>). The mRNA expression of the selected receptors was further analyzed in glioma cell lines (i.e., U87 and U373) by qualitative RT-PCR.

Tumor cell line RNAs and cDNA synthesis

Total RNA from U87 and U373 cell lines was extracted as previously described (Chomczynski and Sacchi, 1987). Total RNA from C32TG was extracted with the RNeasy plus mini kit (Qiagen, Hilden, Germany). Total RNA was treated with Deoxyribonuclease I amplification Grade to remove genomic contamination. Reverse transcription was performed using total RNA, RNase H-reverse transcriptase (Superscript II, Gibco BRL, Life Technologies, Gaithersburg, MD, United States) and random primer hexamers.

Identification of GPCR mRNA expression by polymerase chain reaction (qualitative PCR)

First strand cDNA was subjected to PCR amplification using a set of specific primers corresponding to the nucleotide sequences of the GPCRs reported in the [Supplementary Table S1](#).

The PCR program used was the following: a first denaturation step at 95°C for 5 min, followed by 35 cycles at 95°C for 1 min, 54–60°C (depending on annealing temperature of the primer set) for 2 min and 72°C for 3 min. Then, a final elongation step at 72°C for 10 min was performed. PCR products

were examined by electrophoresis in 1.8% agarose 1x TAE gels and ethidium bromide or sybr-safe staining (Invitrogen).

Quantitative real-time RT-PCR

Quantitative Real-time PCR (qRT-PCR) experiments were performed in the ABI Prism 7700 Sequence Detection System from Applied Biosystems. For each GPCR mRNA expression, three sequence-specific oligonucleotides were designed using the Primer Express oligo design software (Applied Biosystem, Carlsbad, CA, United States). Two of them were forward (Fw) and Reverse (Rv) primers used for PCR amplification. The third sequence (TaqMan Probe, Applied Biosystem) was a fluorogenic probe labelled with a fluorescent reporter dye (6-FAM) and a quencher dye (TAMRA) attached at the 5' and 3' end, respectively. The probe was designed to hybridize the portion of PCR amplicon between Fw and Rv primers. The primers and probe used are reported in [Supplementary Table S2](#).

The difference in the initial amount of total RNA between the samples was normalized in every assay using glyceraldehydes-3-phosphate dehydrogenase housekeeping gene expression as an internal standard (TaqMan Human GAPDH Control Reagent, Applied Biosystem). Each PCR reaction was carried out in 50 µl final volume using TaqMan Universal PCR Master Mix (Applied Biosystems), 900 nM of primers and 200 nM of probe. Finally, 2.5 µl of diluted cDNA (1/10 vol/vol) was added for each reaction. Each sample was loaded in triplicate. Then, standard conditions were used for PCR amplification (50°C for 2 min, 95°C for 10 min, followed by 50 cycles at 95°C for 15 s, 60°C for 1 min). Reactions without cDNA were performed as negative control (No Template Control, NTC). Glyceraldehyde-3-phosphate dehydrogenase (GAPDH) PCR amplification was carried out under the same conditions, except that for concentrations of primers and probe, in which 100 and 200 nM were used, respectively. Relative quantification of RNA expression was calculated using comparative C_T method based on the threshold cycles (Ct values) of the gene of interest and of the internal reference gene (GAPDH).

siRNAs design and synthesis

siRNAs corresponding to GPR3, GPR21, GPR22, GPR23 and LPAR6/P2Y₅ mRNAs as well as those corresponding to hypoxanthine-guanine phosphoribosyl transferase (HGPRT) (GenBank accession number NG_012329.1) gene were designed according to the report of Elbashir et al. (2001). The siRNAs used for GPCRs and HGPRT are listed in [Supplementary Table S3](#). RNA not complementary to any cellular transcript (ctrl RNA) was used as control (see [Supplementary Table S3](#)). The sequences were subjected to BLAST search to confirm the absence of homology to other additional known coding

sequences in the genome human project. siRNAs were chemically synthesized by MWG Biotech AG (Ebersberg, Germany) and resuspended according to the manufacturer's instructions.

siRNA transfection, treatments and MTT colorimetric assay

Glioma cells were transfected with siRNAs at 50% confluency using Oligofectamine (Invitrogen). The day before transfection, the cells were trypsinized, counted, plated at 4×10^3 cells/well in 96 well plates "Nunclo TM Microwell TM" (Nunc, Roskilde, Denmark) in the medium containing 10% FBS, and were incubated at 37°C. After 24 h, cells were transfected according to the manufacturer's procedure in the absence (mock transfected), in the presence of the ctrl RNA, or in the presence of specific siRNAs (final concentration 50 nM). After 24 h, the transfected cells were exposed to GBPs at the concentrations indicated in the related figures. Microplates were incubated at 37°C in a humidified 5% CO₂ incubator for 24, 48 and 72 h and then the growth inhibition was measured with a colorimetric assay based on the use of tetrazolium salt MTT (3-(4,5-dimethylthiazol-2-yl)-2,5-diphenyl tetrazolium bromide) (Mosman, 1983), currently used also to measure drug-induced cytotoxicity. The results were read on a multiwell scanning spectrophotometer ((Spectracount™, PerkinElmer, Waltham, MS, United States), using a wavelength of 570 nm. Each value was the average of 4–10 wells (standard deviations were less than 20%). The % of cell growth was calculated according to NCI (National Cancer Institute, Bethesda, Maryland): $100 \times (T - T_0) / (C - T_0)$ (T is the optical density of the test well after an established period of exposure to test compound; T₀ is the optical density at the beginning of the treatment with GUA, GUO, GMP; C is the optical density of the controls). IC₅₀ was calculated using GraphPad Prism version 6.0 for Windows, after fitting the dose-response data to a sigmoidal curve (nonlinear regression).

Human GPR23: Subcloning in expression vectors and generation of stably transfected cell lines

The PCR product containing the entire coding sequence of the human GPR23 mRNA was cloned into the expression vector pcDNA™ 3.1D/V5-His-TOPO (Invitrogen, Scotland, UK). The GPR23 ORF fragment was amplified with the following primers: Fw 5'-CACCATGGGTGACAGAAGAT-3' and Rv 5'-TGCTAGAATC CACCTTTTAG-3'. To confirm the orientation of the GPR23 insert, the construct, pcDNA 3.1 D/V5-His-TOPO/GPR23 was subjected to restriction enzyme digestion in the appropriate analysis buffer with BamH I

(Promega, Madison, WI, United States) and, to double digestion with XbaI/HindIII (Promega). The digestion products were analyzed by electrophoresis in 0.8% agarose 1 x TAE gel and ethidium bromide staining. Moreover, to confirm the identity of the GPR23 entire open reading frame, DNA sequencing was performed by standard fluorescent dideoxy chain-termination procedure with the Abi Prism 377 automatic sequencer (Thermo Fisher). MACAW alignment allowed us to compare the sequence of the insert with the GPR23 gene. U87 and U373 cell lines were stably transfected with the pcDNA 3.1D/V5-His-TOPO/GPR23, or with the control vector, pcDNA 3.1D/V5-His-TOPO/lacZ, using lipofectamine reagent (Invitrogen) according to the manufacturer's procedure. C32TG cell lines were stably transfected with the pcDNA 3.1 D/V5-His-TOPO/GPR23 or with the control vector, pcDNA 3.1D/V5-His-TOPO/lacZ, using oligofectamine reagent (Invitrogen). 48 h after transfection, cells were cultured in the growth medium supplemented with geneticin (G418, 600 µg/ml). After 1–2 weeks, individual clones were isolated to select clones with the highest expression of receptors. The different clones were maintained in their medium containing 500 µg/ml G418. GPR23 mRNA expression was evaluated by qualitative PCR and qRT-PCR, as previously described (Yin et al., 2009; Garozzo et al., 2010). For GUA dose-response experiments, two different overexpressing stable clones were used for U87 (U87cl12, U87cl8), U373 (U373cl6, U373cl18), and C32TG cells (C32TGcl10, C32TGcl19). The parental cell lines (wtU87-wtU373-wtC32TG) and clones derived by stable transfection of the lacZ gene (U87-, U373-, C32TG-lacZ) were used as controls.

Detecting of GPR23-tagged V5 protein by immunofluorescence

To allow the expression of native protein in GPR23-expressing stable U87 cell line (U87-GPR23), we used the Tag-On-Demand System (Invitrogen). One day before transduction, 10⁴ U87-GPR23 cells were plated in chamber slides (Nunc, Roskilde, Denmark) in 100 µl of complete growth medium and incubated at 37°C overnight. On the day of transduction, the growth medium was removed from each well of cells and replaced with 50 µl of fresh growth medium. Then the adenovirus was added to each well using a Multiplicity of Infection (MOI) of 50 and cells were incubated for 5–6 h at 37°C. Afterwards, the medium containing virus was removed from the cells and fresh complete growth medium was added to the cells.

Assay for C-terminally-tagged recombinant protein expression was performed 24 h post-transduction, with immunofluorescence, using Anti-V5-FITC conjugated antibodies (Invitrogen) prepared by crosslinking the

appropriate primary antibody with the FITC fluorophore. Briefly, cells were washed twice with PBS and fixed by adding 200 μ l of room temperature 100% methanol. After incubation, cells were washed 5 \times 2 min with PBS and, to reduce non-specific binding of antibody, were incubated for 20 min at room temperature with 200 μ l of blocking solution (PBS containing 10% FBS). Then, 100 μ l of blocking solution containing the 1:2000 dilution of antibody were added and the mixture was incubated for 1 h at room temperature in the dark. Cells were washed again 2 \times 5 min with PBS and observed cells with a fluorescence microscope (Zeiss Axio Scope A1, White Plains, NY, United States) equipped with a FITC filter.

[³H] guanine binding assay

We started with the preparation of membranes from U87 cell lines, according to the previously published procedure (Traversa et al., 2002; Frinchi et al., 2020). Cultured cells (1 \times 10⁶ cells) were collected and homogenized in ice-cold buffer (0.25 M sucrose, 5 mM HEPES pH 7.4) by teflon-glass homogenizer (350 rpm, 7 up and down strokes). The homogenate was centrifuged at 1000 \times g (10 min, 4°C). The pellet, resuspended in 2 ml buffer, was centrifuged as aforementioned and the supernatants were pooled and centrifuged at 11,000 \times g (20 min, 4°C). The pellet was resuspended in cold HEPES (20 mM, pH 7.4) and centrifuged at 100,000 \times g (30 min, 4°C). The final pellet, resuspended in the same buffer to a final protein concentration of 100 μ g per 1 ml, was aliquoted (100 μ l per vial) and stored at –80°C. Before using in binding experiments, the membranes were washed twice with PBS buffer (8.8 mM, pH 7.4). The protein concentration was determined by the Bradford method (Bradford, 1976). Subsequently, the measurement of [³H]-GUA binding was carried out. Membranes (50 μ g) were preincubated (10 min, 25°C) in binding buffer (20 mM Tris-HCl, 1 mM EGTA, 5 mM MgCl₂, 100 mM NaCl, pH 7.4) and then incubated (30 min, 25°C) with [³H]GUA in a total volume of 0.5 ml binding buffer. For saturation experiments, a concentration range of 6.25–300 nM [³H]-GUA was used. Nonspecific binding was determined by adding 500 μ M unlabeled GUA and specific binding was calculated by subtracting nonspecific from total binding. In competition experiments, displacing agents at different concentrations and 50 nM [³H]-GUA were added, and the reaction started by adding the membranes. After 30 min, the reaction was stopped by adding 3 ml of cold binding buffer. The samples were rapidly filtered by vacuum filtration using Whatman GF/B glass fiber filters. These filters were then washed four times (2.5 ml cold binding buffer each time), dried for 1 h at 30°C, transferred in scintillation vials filled with 5 ml of Filter count scintillation cocktail (Beckman Coulter, Inc.; Fullerton, CA, United States). Bound radioactivity was measured in a Beckman Coulter LS6500 Multipurpose Scintillation Counter (Beckman Coulter, Inc.). For saturation

and displacement curves, the pooled data were fitted by a computerized nonlinear regression analysis and resolved for the presence of a single high-affinity binding site.

Enzyme assay to determine PNP activity in the extracellular medium of U87 glioma cells

Samples containing PNP were obtained as previously described by Giuliani et al. (2016). Briefly, U87 glioma cells were incubated in serum-free medium. After 1, 6 and 12 h, an aliquot of medium was taken and the enzyme present was concentrated using Amicon Ultra 2 ml filters (cutoff 10 K, Merck Life Science, Milan, Italy), while cells were scraped in lysis buffer (5 mM HEPES pH 8.5, 2 mM EDTA, and protease inhibitor cocktail) and sonicated to obtain cytosolic extracts. Protein content was quantified using a colorimetric protein assay kit (Bio-Rad, Segrate, Italy). PNP activity was evaluated by measuring the transformation of GUO, the enzyme's substrate, into GUA by HPLC analysis. The enzymatic reaction was performed in HEPES (50 mM; pH 7.0) containing 50 mM inorganic phosphate plus an aliquot of the concentrated medium as a source of PNP. 100 μ M GUO was then added and the mixture was incubated by shaking at 37°C for 15 min. The reaction was stopped by heating the mixture at 70°C for 5 min. After centrifugation, the supernatant was filtrated before HPLC analysis. The HPLC (Agilent 1100 Series, Waldbronn, Germany) was equipped with a thermostated column compartment, a diode array detector, and a fluorescence detector. The separation was achieved by a Phenomenex Kinetex pentafluorophenyl analytical column (Phenomenex INC.; Bologna, Italy) kept at 35°C and applying a 15-min nonlinear gradient with a flow rate of 1 ml/min (for further details see Giuliani et al., 2017). The excitation and emission wavelengths for monitoring fluorescent GUO and GUA were 260 and 375 nm, respectively. PNP activity is usually defined as international units (IU), 1 IU corresponding to the amount of the enzyme that catalyzes the conversion of 1 μ mol of substrate per minute under the specified conditions of the assay method. Accordingly, given the small amount of cells and thereby of PNP activity, we expressed it as micro-international units (μ IU), 1 μ IU corresponding to the amount of PNP that catalyzes the conversion of 1 pmol of substrate per min (pmol/min).

Statistical analysis

All experiments were usually performed from three to four times, unless differently specified. The quantitative data are expressed as mean \pm SD. Time-response curves were calculated by using nonlinear regression (GraphPad Prism

6.0 software, San Diego, CA, United States). Statistical analyses were performed by Prism 6.0 software, using Student's *t* test coupled to the Holm-Sidak method or two-way analysis of variance (ANOVA). Group differences with $p < 0.05$ were considered statistically significant.

Results

BLAST search for human class A orphan GPCRs with purinoreceptor similarity

Since GBP signalling has been somewhat related to certain purinergic receptors, we aimed to identify human class A GPCRs with only preliminary evidence of the existence of an endogenous ligand or as-yet unidentified, showing sequence similarity to purinoreceptors. To this end, a bioinformatic search was performed by BLAST, using as a query the protein sequences of human A₁R, A_{2A}R and A₃R responsive to ADO and P2Y₁R responsive mainly to ADP (Supplementary Data S1). Thirty-three GPCRs showing similarity to one or more ADO or P2Y₁ receptors, with an *E* value < 0.05 (matrix BLOSUM 45), were selected from the BLAST search list (Supplementary Data S2) according to multiple criteria: 1) they belonged to the class A orphan receptors according to IUPHAR/BPS Guide to PHARMACOLOGY (<http://www.guidetopharmacology.org/GRAC/FamilyDisplayForward?familyId=694>), or 2) they belonged to a group of de-orphanized GPCRs (LPAR4,5,6) for which experimental evidence of additional unknown endogenous ligands was available (Noguchi et al., 2003; Lee et al., 2007; Yanagida et al., 2007) and 3) they were expressed in normal brain tissues and in glioblastoma samples (averaged transcript per kilobase million (TPM) > 0.1 in glioblastoma samples and normal brain tissues of the TCGA consortium). Subsequently, the mRNA expression of the selected orphan GPCRs was analysed by qRT-PCR in human glioma cell lines (U87, U373), which were previously reported to be responsive to GUO (Garozzo et al., 2010). Four receptors, namely GPR21, GPR22, GPR23 and LPAR6/P2Y₅R, expressed at relatively high levels in both cell lines, were then selected for further experiments. In addition, a GPCR expressed only in U87 cells, namely GPR3, was also included.

Silencing selected GPCRs in U87 cell line

Subsequently, the mRNA expression of the selected receptors, namely GPR3, GPR21, GPR22, GPR23 and LPAR6/P2Y₅, was silenced in U87 cell line by short interference RNA (siRNA) methodology (25). To this end, a pair of specific siRNAs targeting the coding region of each receptor was designed and synthesized (Supplementary Table S3). Thus, as shown in Supplementary Figure S1, GPR3, GPR21, GPR22, GPR23 and LPAR6/P2Y₅ mRNA levels, measured 48 h after siRNA lipo-

transfection into the U87 cell line, were persistently decreased by about 75%, 72%, 90%, 75% and 90%, respectively. Importantly, the downregulation of the selected receptors did not affect cell survival, except for a significant cell growth inhibition (38%) observed with GPR21 silencing (data not shown). Overall, these results validated our experimental strategy for silencing orphan GPCRs in the U87 cell line.

Effect of silencing orphan GPCRs in GBP-mediated growth inhibition of U87 cells

A functional signature of GBPs, as compared to other purines, is the profound antiproliferative effect on human tumoral cell lines, including U87 cells (Garozzo et al., 2010). Accordingly, we questioned if silencing the selected orphan GPCRs would have any impact on the GBP-mediated growth inhibition of U87 cells. Thus, twenty-four hours after siRNA transfection, U87 cells were exposed to GUO and GMP (300 μ M) for 24, 48, or 72 h and, at the end of the treatment, cell proliferation was assessed through the MTT assay. Indeed, GUO and GMP treatment triggered a maximal antiproliferative effect of $\sim 80\%$ after 24 h which lasted until 72 h upon incubation (Figure 1), in agreement with previous data (Garozzo et al., 2010). The inhibition of cell proliferation in non-transfected cells was similar to that observed in mock and ctrl-RNA transfected cells, ranging from 70 to 80%. Importantly, the antiproliferative effect of GUO and GMP after 72 h of treatment was significantly reduced ($\sim 50\%$; $p < 0.01$) in cells silenced for GPR23 (Figures 1A,B). In contrast, silencing of GPR21 or GPR22 receptors did not preclude GUO or GMP antiproliferative effects, while that of GPR3 and LPAR6/P2Y₅ receptors, although significant ($p < 0.05$), had a limited effect on GUO- and GMP-mediated cell growth inhibition (5%–15% reduction). Collectively, these results suggested that GPR23 might play a potential role in GBP-mediated antiproliferative effects of U87 cells, thus we subsequently focus on this receptor.

Pharmacological characterization of GPR23-dependent antiproliferative effect in U87 cells

As shown previously, silencing of the GPR23 had an impact in the GBP-mediated growth inhibition of U87 cells. Now, we aimed at pharmacologically characterizing this GPR23-dependent antiproliferative effect by constructing concentration-response curves for GUO, GMP and GUA. To this end, U87 cells were GPR23 silenced or mock transfected before being exposed to increasing concentrations of GUO, GMP and GUA for 72 h and the cell proliferation assayed. Interestingly, we also included GUA as this compound, which usually derives from the metabolism of GUO, has been shown to be an active GBP in other cell lines (Wengert et al., 2011; Giuliani et al., 2012).

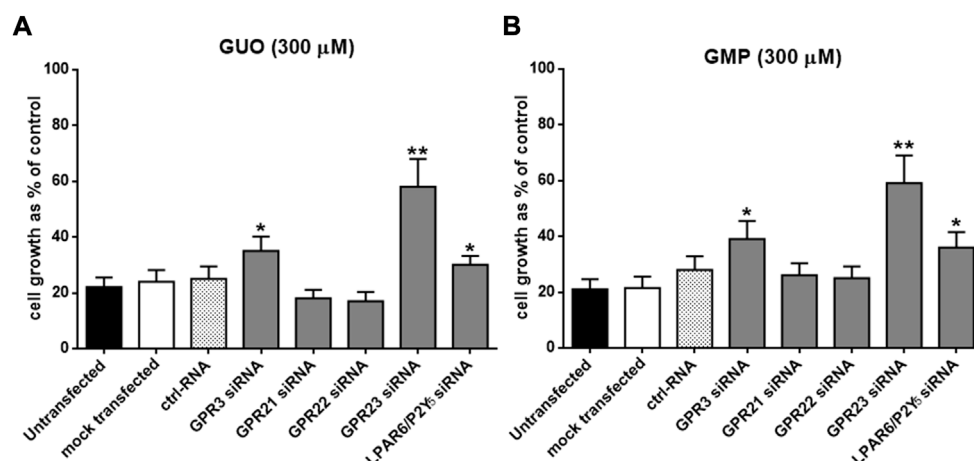


FIGURE 1

Effects of lipotransfection with different GPCR-siRNAs on sensitivity to GUO (A) and GMP (B). U87 cells, grown up to 50% confluency into 96 multiwell plates, were lipotransfected in the absence of siRNAs (mock transfected), in the presence of 50 nM ctrlRNA or in the presence of 50 nM GPR3-siRNA, GPR21-siRNA, GPR22-siRNA, LPAR6/P2Y₅-siRNA and GPR23-siRNA and then incubated in growth medium. After 24 h cells were treated with GUO or GMP (300 μ M) for 72 h. Cell growth was evaluated by the MTT assay. Results are expressed as the percentage of cell growth evaluated in untreated cells (control). Each point represents the mean \pm SD of 3 independent experiments. Statistical significance: * p < 0.05 ** p < 0.01 vs. mock transfected cells (Student's t test).

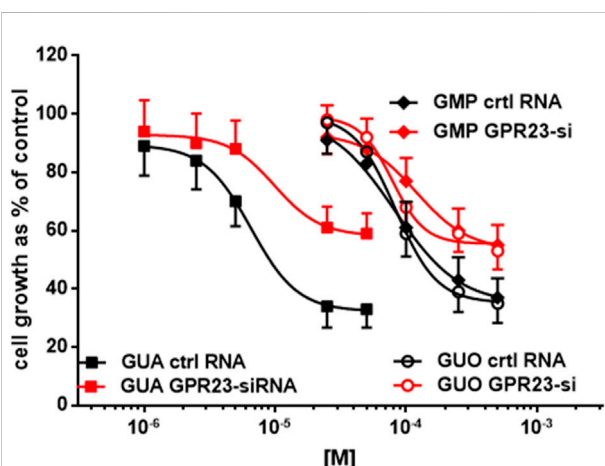


FIGURE 2

Effect of lipotransfection with GPR23-siRNA on sensitivity to GUA, GUO and GMP. Twenty-four hours after lipotransfection with GPR23-siRNA, U87 cells were treated with GUO or GMP (50–500 μ M) or GUA (1–50 μ M) for 72 h. Results are expressed as the percentage of cell growth evaluated in untreated cells (control) by the MTT assay. Each value is the mean \pm SD of 10 different samples. Statistical significance of data obtained in GPR23-siRNA cells vs. control (ctrl) RNA transfected cells: p < 0.001 for data relating to GUA effect and p < 0.01 for those relating to GUO and GMP effects (two-way ANOVA test).

All three GBPs caused a concentration-dependent inhibition of proliferation in mock transfected U87 cells and with similar efficacy (i.e., maximal growth inhibition of 80%) (Figure 2). Indeed, the antiproliferative effect induced by

GUA, GUO, or GMP was concentration-dependent also in GPR23-silenced cells, but significantly lower than that observed in the respective controls, as expected. Remarkably, GUA showed to be the most potent GBP inducing growth inhibition both in control (i.e., transfected with RNA not complementary to any cellular transcript, ctrlRNA) and GPR23 silenced U87 cells. Accordingly, IC₅₀ values for GUA, GUO, or GMP were 40 μ M, ~ 190 and ~170 μ M, respectively. Overall, these results indicated that GPR23 silencing modified the antiproliferative efficacy of GBPs but not their potency (Figure 2), thus pointing to GUA as the most reliable ligand for GPR23.

Evaluation of GBPs-mediated antiproliferative effects upon heterologous expression of GPR23 in U87 and U373 cells

Conversely, to support the dependence of the GUA-induced inhibition of cell growth on GPR23 activation we assessed GUA effects in U87 and U373 cells overexpressing this receptor. To this end, U87 or U373 wild type (wt) cells were transfected with lacZ control vector or with the cDNA encoding the GPR23 receptor (U87 clones 12 and 8; U373 clones 6 and 18). GPR23 protein density was monitored upon receptor transduction in U87 and U373 cells by immunofluorescence detection. This assay showed, for instance, a superior expression of V5-tagged GPR23 receptor in U87 cells clone 12 (U87cl12)

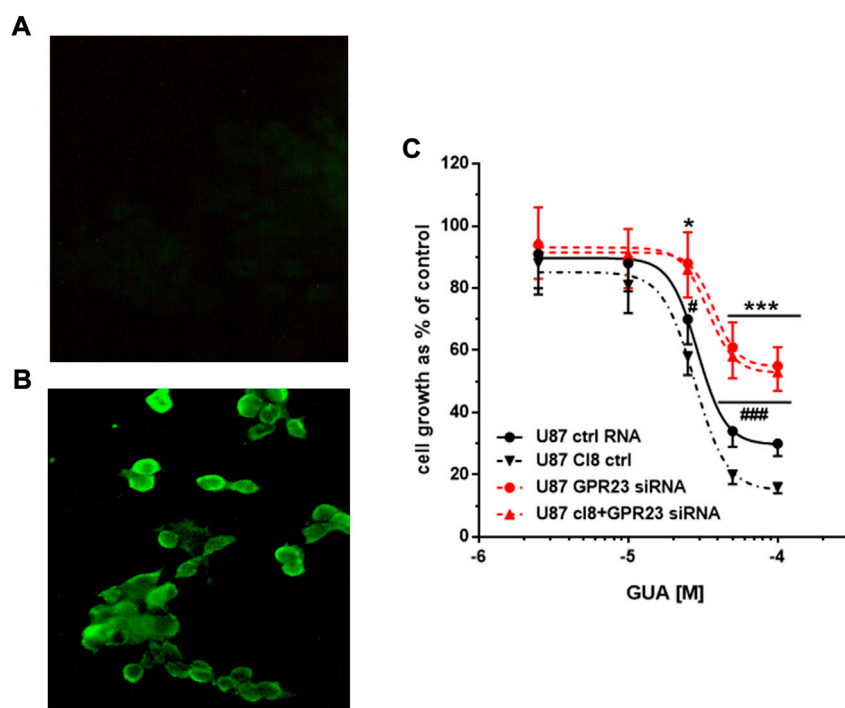


FIGURE 3

Effect of GPR23 overexpression on sensitivity to GUA. (A,B) Immunofluorescence microphotographs of a GPR23-overexpressing U87 cell clone (U87cl12). Expression of V5-tagged recombinant GPR23 was induced in U87cl12 cells by TAG on Demand adenoviral transduction and detected by the anti-V5-FITC conjugated antibody. (A) not-transduced U87cl12 cells stained with anti-V5-FITC antibody; (B) transduced U87cl12 cells stained with anti-V5-FITC antibody. The images are representative of six independent experiments performed with different clones overexpressing GPR23, which gave similar results. (C) Following stable overexpression of GPR23, some of these cells (U87cl8) were lipotransfected in the presence of 50 nM ctrlRNA (ctrl RNA) or GPR3-siRNA (GPR23siRNA). Twenty-four hours after this procedure, all cells were exposed to GUA (1–100 μ M) for 72 h. Results, expressed as the percentage of cell growth evaluated in untreated cells (control) by the MTT assay, are the mean \pm SD of 4 different experiments for each cell type. * p < 0.05 ** p < 0.001 and # p < 0.05 ### p < 0.001: statistical significance vs. U87 ctrl RNA and U87 cl8, respectively (Student's *t* test).

TABLE 1 Inhibitory growth effect caused by GUA in U87 or U373 cell lines, wild type (WT) or overexpressing GPR23 receptor (U87 clones 12 and 8; U373 clones 6 and 18) or lacZ control vector.

Drug under evaluation	U87 cells				U373 cells			
	WT	LacZ	cl12	cl8	WT	lacZ	cl6	cl18
IC ₅₀ (μ M)	37.1 \pm 2.25	39.4 \pm 9.11	32.7 \pm 4.48	30.3 \pm 3.73	49.5 \pm 7.42	56.9 \pm 5.55	49.5 \pm 3.46	43.5 \pm 4.43
Efficacy at the IC ₅₀ concentration	61.2 \pm 4.02	57.4 \pm 6.21 (NS)	75.1 \pm 3.13 (p < 0.05)	82.5 \pm 4.47 (p < 0.01)	57.5 \pm 4.34	56.3 \pm 7.71 (NS)	60.6 \pm 5.33 (NS)	77.4 \pm 8.12 (p < 0.05)

Cells were treated with increasing concentrations of GUA (1–500 μ M) for 72 h before the proliferation inhibition was determined by MTT assay. Accordingly, IC₅₀ values were calculated for each cell type and reported in the Table. Subsequently, the effect of GUA administered at its IC₅₀ for 72 h on the growth of each cell type was determined by MTT assay and expressed as the percentage of cell growth in untreated cells (used as control). All values are the mean \pm SD of n. 3 independent experiments. Statistical significance evaluated by Student's *t* test (p values are indicated between brackets; NS, not significant difference).

(Figure 3B). Similar results were obtained with other clones such as U87cl8, U373cl6 and U373cl18 cells. Thus, these clones showing the highest GPR23 mRNA expression were used for the next experiments. As controls, the parental cell lines

(wtU87 and wtU373) and clones derived by stable transfection of the lacZ gene (U87lacZ and U373lacZ) were used (Figure 3A).

Subsequently, the GUA-mediated antiproliferative effect in GPR23 overexpressing U87 and U373 cells was determined by

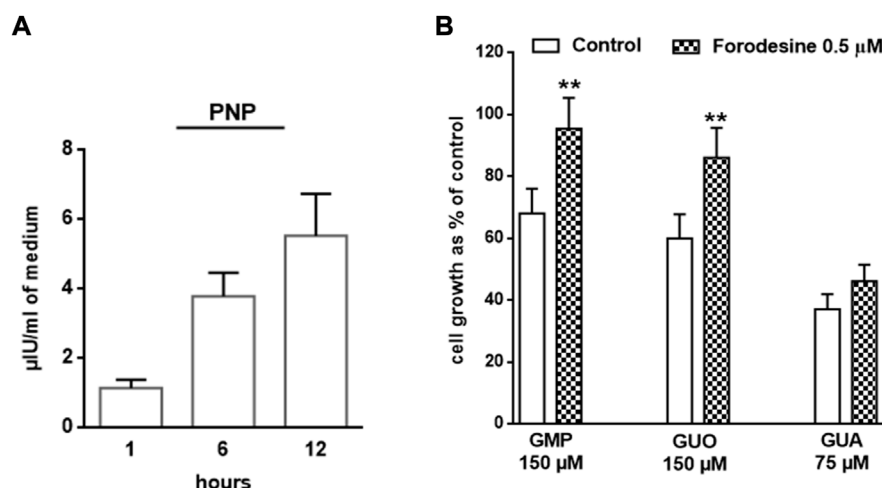


FIGURE 4

Involvement of PNP activity in GBPs-mediated U87 cell growth inhibition. (A) Activity of PNP present in the U87 cell culture medium. The growth medium of cells was collected at different times (i.e., 1, 6 and 12 h) and the PNP activity determined (see Materials and Methods). (B) Impact of PNP inhibition on GBPs-dependent antiproliferative effect. U87 cells were exposed to GMP, GUO or GUA for 72 h, in the presence or absence (w/t) of forodesine, a PNP inhibitor. Results are expressed as the percentage of cell growth evaluated by the MTT assay in untreated cells (control). All values are the mean \pm SD of 4 independent experiments. Statistical significance: ** $p < 0.01$ vs. cells not treated with forodesine (Student's t test).

the MTT assay (Table 1). As expected, while no significant difference was found among the IC_{50} values related to the GUA effect in any cell line assayed, a significant increment in the GUA-induced growth inhibition was observed in U87cl12, U87cl8 and U373cl18 cells (Table 1).

Importantly, in U87cl8 cells transfected with GPR23-siRNA the GUA antiproliferative efficacy was dramatically decreased as compared to the effect obtained in U87 transfected with control RNA and the obtained concentration-response curve was very similar to that of wt-U87 cells transfected with GPR23 siRNA (Figure 3C). Similar results were obtained for U373cl18 cells. Overall, these findings provided complementary evidence indicating the involvement of GPR23 in GBPs-mediated antiproliferative effects.

Outlining the role of GUA in GPR23-mediated effects

To further define the prevalent GPR23-dependent GUA role on U87 cell growth, we questioned whether the effects of GUO and GMP were intertwined with those of GUA. It is well-known that GMP and GUO catabolism ends into GUA production by the activity of the PNP. This enzyme is secreted to the extracellular milieu by different neural cells (10, 26), thus we assessed whether U87 cells also secrete PNP. Indeed, extracellular PNP activity increases in a time dependent fashion in the culture medium of U87 cells (Figure 4A).

Importantly, when U87 cells were pre-treated with forodesine, a selective PNP inhibitor, the antiproliferative effects of GMP and

GUO, but not that caused by GUA, were abolished (Figure 4B). These results suggested that GUA behaves as an endpoint effector of GBPs-mediated antiproliferative effects.

Since nucleobases are recovered by cells to be reused intracellularly, we evaluated the involvement of HGPRT, a key enzyme in the purine salvage pathway, in the GUA-mediated antiproliferative effect. Interestingly, HGPRT, by converting GUA and hypoxanthine into GMP and inosine monophosphate, respectively, regulates GUA levels. To this end, C32 melanoma cells bearing an active or inactive (C32TG cells) form of this enzyme were used to assess the impact of HGPRT activity on GUA-mediated inhibition of cell growth. Interestingly, while GUA inhibited concentration-dependently the proliferation of C32 cells, it was ineffective in C32TG cells (Figure 5A). Conversely, silencing HGPRT in U87 cells significantly reduced the antiproliferative efficacy of GUA (Figure 5B). Overall, these results suggested an involvement of this purine salvage enzyme in GUA signaling, in agreement with previous findings reported by Garozzo et al. (2010).

Next, to ascertain the relationship of HGPRT with GUA signaling we determined GPR23 mRNA expression in cells lacking HGPRT activity. Importantly, C32TG cells showed very low expression of GPR23 as compared to C32 cells (Figure 5C). In addition, silencing HGPRT in U87 cells significantly reduced the mRNA expression of GPR23 (Figure 5D). Conversely, GPR23 transfection of C32TG and U87 cells silenced for HGPRT expression rescued the GUA-mediated antiproliferative effect (Figures 5E,F). These results may suggest that HGPRT regulation of GUA levels will define GPR23 content and signaling. Collectively, these findings reinforce the idea that GUA

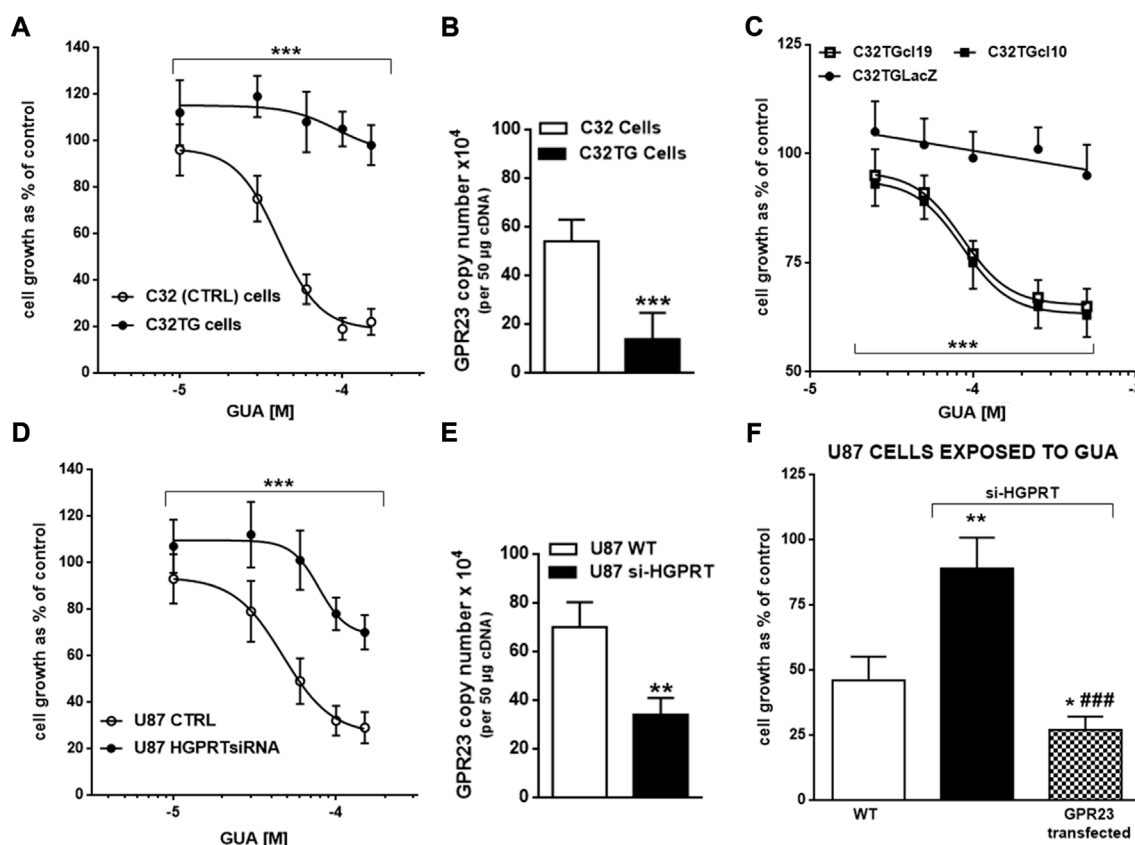


FIGURE 5

Involvement of HGPRT enzyme in GUA-mediated cell growth inhibition. Concentration-response curves of GUA-mediated antiproliferative effect in (A) C32 melanoma cells expressing normal (WT, wild type) or inactive HGPRT form (C32TG cells) or (B) U87 wild type cells (WT) or silenced for HGPRT (U87 HGPRTsiRNA). Furthermore, the mRNA expression of GPR23 was evaluated in C32 (C) and U87 (D) cells by qRT-PCR. Finally, (E) C32TG cells with mutated HGPRT were transfected to overexpress GPR23 (C32TGcl19 and C32TGcl10) or LacZ construct (C32TGLacZ). Likewise, (F) U87 WT or HGPRT silenced cells were transfected to overexpress GPR23. Afterwards, cells were exposed to GUA as described above. For the entire duration of experiments, C32TG, -LacZ cells and GPR23 overexpressing clones were cultured in the medium without thioguanine. Results are expressed as the percentage of cell growth evaluated by the MTT assay in untreated cells (control) in (A,B,E,F) Panels. In all panels, values represent the mean \pm SD of 3 independent experiments. Statistical significance: *** p < 0.001 vs. C32 or U87 WT cells (as for Panels (A,B)) or vs. C32TGLacZ cells (only as for Panel (E) (ANOVA two-way test); ** p < 0.01 and *** p < 0.001 vs. C32 cells with normal HGPRT form or U87 WT cells; ### p < 0.001 vs. U87 si-HGPRT cells (Student's t test as for panels (C,D,F)).

effect on cell growth would mediate by GUA interaction with GPR23.

GUA binding to U87 cell membranes

To unequivocally demonstrate that GUA interacts with GPR23 we performed radioligand binding experiments using [3 H]-GUA and membrane extracts from control and GPR23 silenced U87 cells. Competition binding experiments showed that GUA concentration-dependently reduced [3 H]-GUA binding within 2 min (K_i = 0.028 ± 0.0048 μ M) (Figure 6A). GUO also reduced [3 H]-GUA binding in a concentration-dependent manner, but with much lower potency (K_i = 277.2 ± 48.4 μ M). Other GBPs (GMP, GTP)

tested or adenosine (ADO), even administered at concentrations up to 10 mM, showed a low percentage of [3 H]-GUA binding with a $K_i \geq 1,000$ μ M (data not shown).

Additionally, we performed saturation isotherm experiments in which we observed that the binding became saturable at [3 H]-GUA concentrations higher than 100 nM (Figure 6B). The obtained results were fitted by a computerized non-linear regression analysis and resolved for the presence of a single high affinity binding site with a K_D = 29.44 ± 4.07 nM and B_{max} 1.007 ± 0.035 pmol/mg prot. (Figure 6C). Importantly, when GPR23 silenced U87 cells membrane extracts were used the calculated K_D value was of 29.59 ± 7.57 nM, whereas B_{max} was significantly lower (0.434 ± 0.038 pmol/mg prot) (Figures 6B,C). Collectively, these results demonstrate the existence of a specific GUA binding site in membrane extracts from U87, likely being the GPR23.

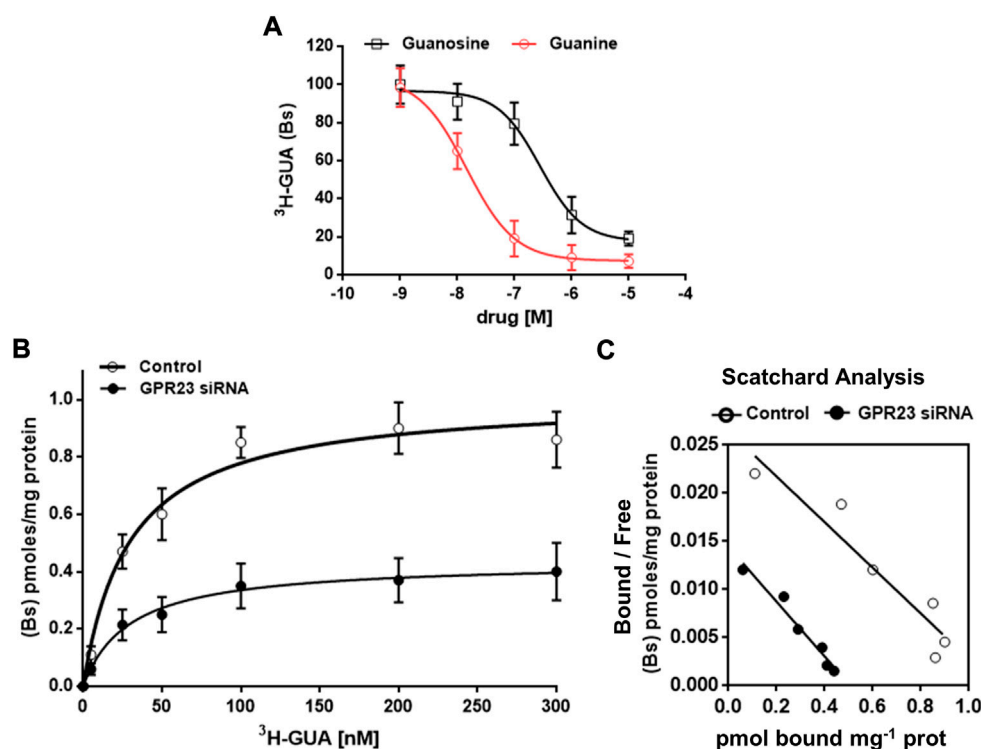


FIGURE 6

Characterization of [3 H]-GUA radioligand binding to U87 cells membrane extracts. In all experiments membrane extracts were incubated with the indicated drugs under standard assay conditions, i.e., 30 min incubation time, 25°C temperature, pH 7.4). (A) Displacement of 50 nM [3 H]-GUA binding from U87 cell membrane (50 μ g protein) by unlabeled GUA or guanosine (GUO) (both at concentrations in the range from 0.001 to 10 μ M). The values are the mean \pm SD of three independent experiments, each point in triplicate. Statistical significance (two-way ANOVA test): *** p < 0.001 GUO vs. GUA displacement curve. (B) Saturation binding of [3 H]-GUA at 25°C using control and GPR23 silenced U87 cell membranes (50 μ g protein), which were incubated with increasing concentrations (6.25–300 nM) of [3 H]-GUA under standard assay conditions. Non-specific binding was defined in the presence of 500 μ M GUA. Values are the means \pm SD of four experiments, each point performed in triplicate. Data in the Panel (A,B) were fitted by a computerized nonlinear regression analysis and resolved with a one site model. (C) Scatchard analysis of the data shown in (B). For the panels B and C, Bs, bound specific; statistical significance (two-way ANOVA test): *** p < 0.001 vs. control.

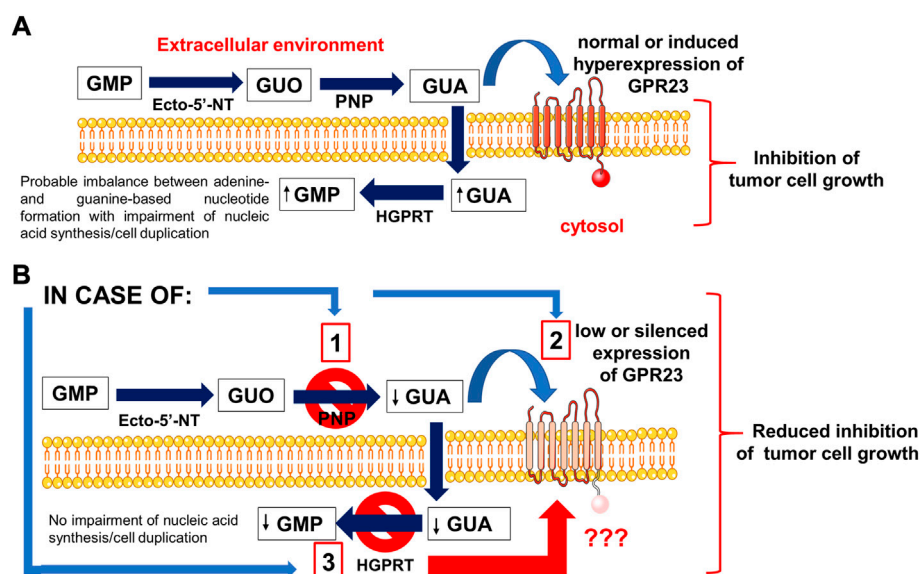
Discussion

In the present study, we identified GPR23 as a potential GPCR mediating some of the GBP-induced biological effects reported so far (Di Liberto et al., 2016; Mancinelli et al., 2020; Di Iorio et al., 2021; Massari et al., 2021). In particular, we found that GUA can interact with this receptor causing antiproliferative effects in tumoral cell lines of glioma and melanoma.

As the first step in our research, we investigated which GPCRs, whose ligands are still unknown or poorly characterized, showed sequence similarity to P1-P2 receptors. Once selected some of them as possible candidates, i.e.; GPR3, GPR21, GPR22, GPR23, LPAR6/P2Y₅ receptors, and after checking for their expression in cell lines, such as U87 and U873 glioma cell lines responsive to GBPs (Garozzo et al., 2010), we tested the effect of GBPs, namely GMP, GUO, and GUA, on the growth of U87 cells. We found that all GBPs decreased cell proliferation but with different efficacy and potency in their effects, GUA being the most potent compound. Furthermore, by specific siRNA silencing of the receptors aforementioned we

observed that only GPR23-silencing reduced the GBP antiproliferative effects in two different glioma cell lines, mainly that induced by GUA. Additionally, GPR23-overexpressing clones, stably transfected with recombinant expression vectors, displayed an enhanced sensitivity to GUA that was reverted by siRNA-mediated silencing, thus confirming the role of GPR23 in GUA responses (see the Scheme 1).

The GPR23 gene (Accession Number NM_005296) (also called P2Y₉ and LPAR4/P2Y₅-like) is located on chromosome Xq13-q21.1, and contains an intronless open reading frame of 1113 bp encoding 370 amino acids (O'Dowd et al., 1997). The protein sequence shows 33% identities and 56% conserved amino acid residues vs. P2Y₁ ADP receptor. Moreover, specific sites, involved in ligand interaction and conserved in P2Y protein family, are present in GPR23 protein. The consensus sequence SILFLTCIS, found in almost all functionally defined P2Y receptors (von Kügelgen and Wetter, 2000), is conserved in GPR23-protein sequence with a single substitution (SMLFLTCIS). The P2Y₁ residue



SCHEME 1

An outline of the effects promoted by GBPs, mainly GUA, in tumor cell lines. **(A)** GMP and guanosine (GUO), which are converted to guanine (GUA) by the sequential activity of the enzymes ecto-5'-nucleotidase and purine nucleoside phosphorylase (PNP), reduced the proliferation of cancer cell lines used in this study. Indeed, GUA was the actual effector of the effects induced by GMP and GUO, as the inhibition of PNP activity hindered the effects of these compounds but not that of GUA. GUA inhibited cell growth by interacting with GPR23 receptor, which was selected by a bioinformatic approach among potential candidates within a list of orphan and/or poorly characterized G-protein coupled receptors with high purinoceptor similarity. In fact, the enhanced expression of GPR23 in glioma cells or hypoxanthine-guanine phosphoribosyl-transferase (HGPRT)-mutated melanoma cell lines increased the sensitivity of these cells to GUA. **(B)** Conversely, silencing of the GPR23 receptor, as induced in glioma cells, or its low expression, as observed in melanoma cell lines with HGPRT-mutated form, reduced GUA antiproliferative effects. These findings, together with the results from binding experiments, confirmed the involvement of GPR23 in modulating responses to GUA in cancer cell lines, although further research is needed to better investigate the relationship between the activity of HGPRT and GPR23 receptor expression as well as to verify whether this orphan receptor mediates other effects of GUA.

Ser314, that, by mutagenesis studies, has been shown to be involved in H bond formation with N1 of purine (Jiang et al., 1997; Moro et al., 1998) is also conserved (+T301), while no residues involved in interaction with 5'-diphosphate groups are conserved (Abbracchio et al., 2003; Costanzi et al., 2004).

Further results herein reported convinced us that GPR23 could be a receptor site for GUA. In particular, we found that U87 cells released in the extracellular medium the enzyme PNP that converts GUO (also that deriving from guanine-based nucleotide metabolism) into GUA. Accordingly, cell exposure to the enzyme inhibitor, forodesine, curtailed the inhibitory effect of GMP or GUO on U87 cell growth, but not that of GUA (see the Scheme 1).

It has also to be mentioned that we previously reported (Garozzo et al., 2010) that the loss of GUA-induced antiproliferative effects in a melanoma cell line (C32TG) is related to expression of a mutated inactive form of HGPRT by these cells. Likewise, we observed a decreased potency of GUA in causing antiproliferative effects in U87 cells silenced for HGPRT transcripts. Noteworthy, the enzyme HGPRT, which catalyzes the conversion of hypoxanthine or guanine and 5-phospho- α -D-ribose 1-diphosphate (PRPP) to, respectively, inosine 5'-monophosphate

(IMP) or GMP and pyrophosphate (PPi), has recently been demonstrated to be crucial in other tumoral cells such as those involved in acute myeloid leukemia (Wang et al., 2022). We have previously suggested that the excessive intracellular conversion of GUA in GMP mediated by HGPRT produced an imbalance of purine nucleotides resulting in a S-phase block of cell cycle (Garozzo et al., 2010). Accordingly, GBP recycling determined by HGPRT activity primes differentiation of these cells, reducing their growth and aggressiveness. Thus, here we wanted to ascertain if HGPRT were the only determinant factor in accounting for GUA inhibitory effects on cell growth. Our results showed that both mutated HGPRT-negative melanoma cell line as well as U87 cells, in which HGPRT has previously been silenced, expressed very low levels of GPR23. Clearly, this finding shows a close relationship between the lack of HGPRT activity and the low GPR23 expression, which has no obvious explanation and, therefore, needs to be further investigated. Anyway, the antiproliferative effects of GUA were re-established by stable transfection of a GPR23 expression construct in both cell types. Thus, as outlined in the Scheme 1, these results indicate that the metabolic mechanism linked to the purine salvage pathway could not be the only one responsible for the growth inhibitory action of GUA.

Finally, the last experiments showing the existence of a specific binding site for tritiated GUA in membrane of U87 cells add consistency to the other results so far discussed, demonstrating that GUA exerts its inhibitory effects on different tumoral cells lines, at least, by interacting with GPR23. Noteworthy, [^3H]-GUA binding was displaced by unlabelled GUO, but at concentrations higher than those of unlabelled GUA, suggesting that GUO could also bind GPR23 but with lower affinity. Clearly, this aspect deserves further investigation. In contrast, guanine-based nucleotides or ADO displaced tritiated GUA at so high concentrations which are usually considered as not consistent with a selective binding of these compounds to a receptor, GPR23 in our case.

Regarding specific ligands and biological functions of GPR23, previous functional studies reported that is activated by LPA (Noguchi et al., 2003; Lee et al., 2007; Yanagida et al., 2007). For this compound different receptor isoforms (LPA₁₋₆) have been recognized, which are distinguished into isoforms belonging to the endothelial differentiating gene (Edg) family of GPCR and non-Edg family of purinergic receptors. Among GPCRs, three receptors for LPA have been identified, termed LPA1, LPA2, and LPA3 (previously Edg2, Edg4 and Edg7, respectively), with LPA1/Edg2 being the first identified and most widely expressed subtype. LPA1, LPA2 and LPA3 receptors are found in many cell types, exhibit relatively close homology with each other and show a high affinity for LPA (in the nanomolar range). In contrast, LPA₄ (GPR23/P2Y₉), LPA₅ (GPR92), and LPA₆ (P2RY₅) belong to a non-Edg subfamily of purinergic GPCR clusters (reviewed in Meduri et al., 2021). Since GPR23 has been suggested to be a fourth receptor for LPA, structurally different from EDG receptors, it could not be excluded that the decrease of the GUA-induced antiproliferative effects observed following GPR23 silencing were a consequence of a decreased LPA-induced activity of this receptor. However, the basal LPA concentration in the culture medium, due to the serum supplementation, is probably too low (0.1 μM) to induce receptor activation. Clearly, future investigation will address whether and how LPA, besides GUA, might modify tumor cell growth interacting with the same receptor, maybe on different sites. About this possibility, Wetter et al. (2009) have reported that unknown serum-born compounds can activate GPR23 or potentiate the response of this receptor to LPA. On the other hand, the notion that LPA represents the main agonist of GPR23 has been challenged by Yin et al. (2009) that, using a GPCR assay that measures beta-arrestin binding to GPCRs, did not observe any response of GPR23 to LPA up to 100 μM .

In conclusion, findings herein reported indicate that GPR23 protein can represent a membrane receptor responsive to extracellular GUA, although the existence of intracellular mechanisms, even HGPRT-independent and potentiated by GPR23 expression could be an alternative explanation that cannot be ruled out. On the other hand, it has been reported that isolated basolateral membranes of renal proximal tubule express a Gi

protein-coupled receptor for GUA, whose stimulation inhibits the activity of Na⁺/K⁺-ATPase (Wengert et al., 2011). To clarify these aspects, further experiments are necessary, which will allow to better characterize the modality through which GUA acts as well as to define the role played by GPR23 as the membrane receptor mediating the extracellular activity of GUA.

Data availability statement

The gene expression datasets used in this study can be found in [Supplementary Material](#) and online repositories, whose link are reported in the article.

Author contributions

Conceptualization, DC, FCa, and FCi; Data curation, RG, MZ, PG, VL, GM, and PI; Writing—original draft preparation, DC, FCa, FCi, and RC; Writing—review and editing, all authors; Supervision, DC, FCi, RC, and PI. All authors have read and agreed to the published version of the manuscript.

Acknowledgments

We thank Centres de Recerca de Catalunya (CERCA) Programme/Generalitat de Catalunya for IDIBELL institutional support.

Conflict of interest

The authors declare that the research was conducted in the absence of any commercial or financial relationships that could be construed as a potential conflict of interest.

Publisher's note

All claims expressed in this article are solely those of the authors and do not necessarily represent those of their affiliated organizations, or those of the publisher, the editors and the reviewers. Any product that may be evaluated in this article, or claim that may be made by its manufacturer, is not guaranteed or endorsed by the publisher.

Supplementary material

The Supplementary Material for this article can be found online at: <https://www.frontiersin.org/articles/10.3389/fphar.2022.970891/full#supplementary-material>

References

- Abbracchio, M. P., Boeynaems, J. M., Barnard, E. A., Boyer, J. L., Kennedy, C., Portugal, M. T., et al. (2003). Characterization of the UDP-glucose receptor (re-named here the P2Y₁₄ receptor) adds diversity to the P2Y receptor family. *Trends Pharmacol. Sci.* 24, 52–55. doi:10.1016/S0165-6147(02)00038-X
- Belluardo, N., Mudò, G., Di Liberto, V., Frinchi, M., Condorelli, D. F., Traversa, U., et al. (2021). Investigating the role of guanosine on human neuroblastoma cell differentiation and the underlying molecular mechanisms. *Front. Pharmacol.* 12, 658806. doi:10.3389/fphar.2021.658806
- Bender, E., Buist, A., Jurzak, M., Langlois, X., Baggerman, G., Verhasselt, P., et al. (2002). Characterization of an orphan G protein-coupled receptor localized in the dorsal root ganglia reveals adenine as a signaling molecule. *Proc. Natl. Acad. Sci. U. S. A.* 99, 8573–8578. doi:10.1073/pnas.122016499
- Bradford, M. M. (1976). A rapid and sensitive method for the quantitation of microgram quantities of protein utilizing the principle of protein-dye binding. *Anal. Biochem.* 72, 248–254. doi:10.1006/abio.1976.9999
- Burnstock, G. (2018). Purine and purinergic receptors. *Brain Neurosci. Adv.* 2, 2398212818817494. doi:10.1177/2398212818817494
- Chomczynski, P., and Sacchi, N. (1987). Single-step method of RNA isolation by acid guanidinium thiocyanate-phenol-chloroform extraction. *Anal. Biochem.* 162 (1), 156–159. doi:10.1006/abio.1987.9999
- Ciccarelli, R., Di Iorio, P., D'Alimonte, I., Giuliani, P., Florio, T., Caciagli, F., et al. (2000). Cultured astrocyte proliferation induced by extracellular guanosine involves endogenous adenosine and is raised by the co-presence of microglia. *Glia* 29, 202–211. doi:10.1002/(sici)1098-1136(20000201)29:3<202::aid-glia2>3.0.co;2-c
- Costanzi, S., Mamedova, L., Gao, Z. G., and Jacobson, K. A. (2004). Architecture of P2Y nucleotide receptors: Structural comparison based on sequence analysis, mutagenesis, and homology modeling. *J. Med. Chem.* 47 (22), 5393–5404. doi:10.1021/jm049914c
- Di Iorio, P., Ballerini, P., Traversa, U., Nicoletti, F., D'Alimonte, I., Kleywegt, S., et al. (2004). The antiapoptotic effect of guanosine is mediated by the activation of the PI 3-kinase/AKT/PKB pathway in cultured rat astrocytes. *Glia* 46, 356–368. doi:10.1002/glia.20002
- Di Iorio, P., Beggiato, S., Ronci, M., Nedel, C. B., Tasca, C. I., and Zuccarini, M. (2021). Unfolding new roles for guanine-based purines and their metabolizing enzymes in cancer and aging disorders. *Front. Pharmacol.* 12, 653549. doi:10.3389/fphar.2021.653549
- Di Liberto, V., Mudò, G., Garozzo, R., Frinchi, M., Fernandez-Dueñas, V., Di Iorio, P., et al. (2016). The guanine-based purinergic system: The tale of an orphan neuromodulation. *Front. Pharmacol.* 7, 158. doi:10.3389/fphar.2016.00158
- Elbashir, S. M., Harborth, J., Lendeckel, W., Yalcin, A., Weber, K., and Tuschl, T. (2001). Duplexes of 21-nucleotide RNAs mediate RNA interference in cultured mammalian cells. *Nature* 411 (6836), 494–498. doi:10.1038/35078107
- Frinchi, M., Verdi, V., Plescia, F., Ciruela, F., Grillo, M., Garozzo, R., et al. (2020). Guanosine-mediated anxiolytic-like effect: Interplay with adenosine A₁ and A_{2A} receptors. *Int. J. Mol. Sci.* 21 (23), 9281. doi:10.3390/ijms21239281
- Garozzo, R., Sortino, M. A., Vancheri, C., and Condorelli, D. F. (2010). Antiproliferative effects induced by guanine-based purines require hypoxanthine-guanine phosphoribosyltransferase activity. *Biol. Chem.* 391 (9), 1079–1089. doi:10.1515/BC.2010.106
- Giuliani, P., Ballerini, P., Buccella, S., Ciccarelli, R., Rathbone, M. P., Romano, S., et al. (2015). Guanosine protects glial cells against 6-hydroxydopamine toxicity. *Adv. Exp. Med. Biol.* 837, 23–33. doi:10.1007/5584_2014_73
- Giuliani, P., Buccella, S., Ballerini, P., Ciccarelli, R., D'Alimonte, I., Cicchitti, S., et al. (2012). Guanine-based purines modulate the effect of L-NAME on learning and memory in rats. *Panminerva Med.* 54, 53–58. doi:10.1006/nlme.1998.3866
- Giuliani, P., Zuccarini, M., Buccella, S., Peña-Altamira, L. E., Polazzi, E., Virgili, M., et al. (2017). Evidence for purine nucleoside phosphorylase (PNP) release from rat C6 glioma cells. *J. Neurochem.* 141 (2), 208–221. doi:10.1111/jnc.14004
- Giuliani, P., Zuccarini, M., Buccella, S., Rossini, M., D'Alimonte, I., Ciccarelli, R., et al. (2016). Development of a new HPLC method using fluorescence detection without derivatization for determining purine nucleoside phosphorylase activity in human plasma. *J. Chromatogr. B Anal. Technol. Biomed. Life Sci.* 1009–1010, 114–121. doi:10.1016/j.jchromb.2015.12.012
- Gorzalka, S., Vittori, S., Volpini, R., Cristalli, G., von Kügelgen, I., and Müller, E. C. (2005). Evidence for the functional expression and pharmacological characterization of adenine receptors in native cells and tissues. *Mol. Pharmacol.* 67 (3), 955–964. doi:10.1124/mol.104.006601
- Gysbers, J. W., and Rathbone, M. P. (1992). Guanosine enhances NGF-stimulated neurite outgrowth in PC12 cells. *Neuroreport* 3, 997–1000. doi:10.1097/00001756-199211000-00013
- Illes, P., Müller, C. E., Jacobson, K. A., Grutter, T., Nicke, A., Fountain, S. J., et al. (2021). Update of P2X receptor properties and their pharmacology: IUPHAR review 30. *Br. J. Pharmacol.* 178 (3), 489–514. doi:10.1111/bph.15299
- Jacobson, K. A., Delicado, E. G., Gachet, C., Kennedy, C., von Kügelgen, I., Li, B., et al. (2020). Update of P2Y receptor pharmacology: IUPHAR review 27. *Br. J. Pharmacol.* 177 (11), 2413–2433. doi:10.1111/bph.15005
- Jiang, Q., Guo, D., Lee, B. X., Van Rhee, A. M., Kim, Y. C., Nicholas, R. A., et al. (1997). A mutational analysis of residues essential for ligand recognition at the human P2Y₁ receptor. *Mol. Pharmacol.* 52, 499–507. doi:10.1124/mol.52.3.499
- Lanzaster, D., Massari, C. M., Marková, V., Šimková, T., Duroux, R., Jacobson, K. A., et al. (2019). Adenosine A₁-a_{2a} receptor-receptor interaction: Contribution to guanosine-mediated effects. *Cells* 8 (12), 1630. doi:10.3390/cells8121630
- Lee, C. W., Rivera, R., Dubin, A. E., and Chun, J. (2007). LPA(4)/GPR23 is a lysophosphatidic acid (LPA) receptor utilizing G(s)-G(q)/G(i)-mediated calcium signaling and G(12/13)-mediated Rho activation. *J. Biol. Chem.* 282 (7), 4310–4317. doi:10.1074/jbc.M610826200
- Mancinelli, R., Fanò-Illic, G., Pietrangelo, T., and Fulle, S. (2020). Guanosine-based nucleotides, the sons of a lesser god in the purinergic signal scenario of excitable tissues. *Int. J. Mol. Sci.* 21 (5), 1591. doi:10.3390/ijms21051591
- Mancinelli, R., Pietrangelo, T., Burnstock, G., Fanò, G., and Fulle, S. (2012). Transcriptional profile of GTP-mediated differentiation of C2C12 skeletal muscle cells. *Purinergic Signal.* 8 (2), 207–221. doi:10.1007/s11302-011-9266-3
- Massari, C. M., Zuccarini, M., Di Iorio, P., and Tasca, C. I. (2021). Guanosine mechanisms of action: Toward molecular targets. *Front. Pharmacol.* 12, 653146. doi:10.3389/fphar.2021.653146
- Meduri, B., Pujar, G. V., Durai Ananda Kumar, T., Akshatha, H. S., Sethu, A. K., Singh, M., et al. (2021). Lysophosphatidic acid (LPA) receptor modulators: Structural features and recent development. *Eur. J. Med. Chem.* 222, 113574. doi:10.1016/j.ejmech.2021.113574
- Molz, S., Dal-Cim, T., Budni, J., Martín-de-Saavedra, M. D., Egea, J., Romero, A., et al. (2011). Neuroprotective effect of guanosine against glutamate-induced cell death in rat hippocampal slices is mediated by the phosphatidylinositol-3 kinase/Akt/glycogen synthase kinase 3 β pathway activation and inducible nitric oxide synthase inhibition. *J. Neurosci. Res.* 89 (9), 1400–1408. doi:10.1002/jnr.22681
- Moro, S., Guo, D., Camaioni, E., Boyer, J. L., Harden, T. K., and Jacobson, K. A. (1998). Human P2Y₁ receptor: Molecular modeling and site-directed mutagenesis as tools to identify agonist and antagonist recognition sites. *J. Med. Chem.* 41, 1456–1466. doi:10.1021/jm970684u
- Mosman, T. (1983). Rapid colorimetric assay for cellular growth and survival: Application to proliferation and cytotoxicity assays. *J. Immunol. Methods* 65, 55–63. doi:10.1016/0022-1759(83)90303-4
- Noguchi, K., Ishii, S., and Shimizu, T. (2003). Identification of p2y₉/GPR23 as a novel G protein-coupled receptor for lysophosphatidic acid, structurally distant from the Edg family. *J. Biol. Chem.* 278, 25600–25606. doi:10.1074/jbc.M302648200
- O'Dowd, B. F., Nguyen, T., Jung, B. P., Marchese, A., Cheng, R., Heng, H. H., et al. (1997). Cloning and chromosomal mapping of four putative novel human G-protein-coupled receptor genes. *Gene* 187, 75–81. doi:10.1016/s0378-1119(96)00722-6
- Pietrangelo, T., Mariggiò, M. A., Lorenzon, P., Fulle, S., Protasi, F., Rathbone, M. P., et al. (2002). Characterization of specific GTP binding sites in C2C12 mouse skeletal muscle cells. *J. Muscle Res. Cell Motil.* 23 (2), 107–118. doi:10.1023/a:1020288117082
- Su, C., Wang, P., Jiang, C., Ballerini, P., Caciagli, F., Rathbone, M. P., et al. (2013). Guanosine promotes proliferation of neural stem cells through cAMP-CREB pathway. *J. Biol. Regul. Homeost. Agents* 27, 673–680.
- Traversa, U., Bombi, G., Di Iorio, P., Ciccarelli, R., Werstiuk, E. S., and Rathbone, M. P. (2002). Specific (3H)-guanosine binding sites in rat brain membranes. *Br. J. Pharmacol.* 135, 969–976. doi:10.1038/sj.bjp.0704542
- von Kügelgen, I., and Wetter, A. (2000). Molecular pharmacology of P2Y₁ receptors. *Naunyn. Schmiedeberg. Arch. Pharmacol.* 362, 310–323. doi:10.1007/s002100000310

Wang, H., He, X., Li, Z., Jin, H., Wang, X., and Li, L. (2022). Guanosine primes acute myeloid leukemia for differentiation via guanine nucleotide salvage synthesis. *Am. J. Cancer Res.* 12 (1), 427–444.

Wengert, M., Adão-Novaes, J., Leão-Ferreira, L. R., and Caruso-Neves, C. (2011). Guanine-induced inhibition of renal Na(+)-ATPase activity: Evidence for the involvement of the G_i protein-coupled receptor. *Arch. Biochem. Biophys.* 513 (2), 126–130. doi:10.1016/j.abb.2011.07.007

Wetter, J. A., Revankar, C., and Hanson, B. J. (2009). Utilization of the Tango beta-arrestin recruitment technology for cell-based EDG receptor assay development and interrogation. *J. Biomol. Screen.* 14 (9), 1134–1141. doi:10.1177/1087057109343809

Yanagida, K., Ishii, S., Hamano, F., Noguchi, K., and Shimizu, T. (2007). LPA4/p2y9/GPR23 mediates rho-dependent morphological changes in a rat neuronal cell line. *J. Biol. Chem.* 282 (8), 5814–5824. doi:10.1074/jbc.M610767200

Yin, H., Chu, A., Li, W., Wang, B., Shelton, F., Otero, F., et al. (2009). Lipid G protein-coupled receptor ligand identification using beta-arrestin PathHunter assay. *J. Biol. Chem.* 284 (18), 12328–12338. doi:10.1074/jbc.M806516200

Zuccarini, M., Giuliani, P., Frinchi, M., Mudò, G., Serio, R. M., Belluardo, N., et al. (2018). Uncovering the signaling pathway behind extracellular guanine- induced activation of NO system: New perspectives in memory-related disorders. *Front. Pharmacol.* 9, 110. doi:10.3389/fphar.2018.00110



OPEN ACCESS

EDITED BY

Kenneth A. Jacobson,
National Institutes of Health (NIH),
United States

REVIEWED BY

Celine Valant,
Monash University, Australia

*CORRESPONDENCE

Katia Varani,
vrk@unife.it

SPECIALTY SECTION

This article was submitted to
Experimental Pharmacology and Drug
Discovery,
a section of the journal
Frontiers in Pharmacology

RECEIVED 29 August 2022

ACCEPTED 20 September 2022

PUBLISHED 05 October 2022

CITATION

Pasquini S, Contri C, Cappello M,
Borea PA, Varani K and Vincenzi F
(2022), Update on the recent
development of allosteric modulators
for adenosine receptors and their
therapeutic applications.
Front. Pharmacol. 13:1030895.
doi: 10.3389/fphar.2022.1030895

COPYRIGHT

© 2022 Pasquini, Contri, Cappello,
Borea, Varani and Vincenzi. This is an
open-access article distributed under
the terms of the [Creative Commons
Attribution License \(CC BY\)](#). The use,
distribution or reproduction in other
forums is permitted, provided the
original author(s) and the copyright
owner(s) are credited and that the
original publication in this journal is
cited, in accordance with accepted
academic practice. No use, distribution
or reproduction is permitted which does
not comply with these terms.

Update on the recent development of allosteric modulators for adenosine receptors and their therapeutic applications

Silvia Pasquini¹, Chiara Contri², Martina Cappello²,
Pier Andrea Borea³, Katia Varani^{2*} and Fabrizio Vincenzi²

¹Department of Chemical, Pharmaceutical and Agricultural Sciences, University of Ferrara, Ferrara, Italy, ²Department of Translational Medicine, University of Ferrara, Ferrara, Italy, ³University of Ferrara, Ferrara, Italy

Adenosine receptors (ARs) have been identified as promising therapeutic targets for countless pathological conditions, spanning from inflammatory diseases to central nervous system disorders, from cancer to metabolic diseases, from cardiovascular pathologies to respiratory diseases, and beyond. This extraordinary therapeutic potential is mainly due to the plurality of pathophysiological actions of adenosine and the ubiquitous expression of its receptors. This is, however, a double-edged sword that makes the clinical development of effective ligands with tolerable side effects difficult. Evidence of this is the low number of AR agonists or antagonists that have reached the market. An alternative approach is to target allosteric sites *via* allosteric modulators, compounds endowed with several advantages over orthosteric ligands. In addition to the typical advantages of allosteric modulators, those acting on ARs could benefit from the fact that adenosine levels are elevated in pathological tissues, thus potentially having negligible effects on normal tissues where adenosine levels are maintained low. Several A₁ and various A₃AR allosteric modulators have been identified so far, and some of them have been validated in different preclinical settings, achieving promising results. Less fruitful, instead, has been the discovery of A_{2A} and A_{2B}AR allosteric modulators, although the results obtained up to now are encouraging. Collectively, data in the literature suggests that allosteric modulators of ARs could represent valuable pharmacological tools, potentially able to overcome the limitations of orthosteric ligands.

KEYWORDS

adenosine, allosteric modulators, GPCRs, adenosine receptors, drug development

Introduction

Adenosine is a fundamental component of human physiology. It is a major constituent of nucleic acids, of life's "energy currency" and signaling molecule adenosine triphosphate (ATP), as well as a ubiquitous cell function modulator itself. Adenosine acts as an autocrine/paracrine mediator with a short half-life whose low extracellular levels in healthy tissues are maintained mostly by rapid cellular uptake and cytosolic metabolism by adenosine deaminase or adenosine kinase (Haskó et al., 2008). However, following tissue injury, cells release large amounts of ATP, which is then converted to adenosine by ecto-nucleotidases. Generally, the resulting increased concentration of adenosine has largely beneficial effects in acute pathological conditions by restoring tissue homeostasis (Borea et al., 2016), while its chronic overproduction can be detrimental and cause inflammation, fibrosis, and organ damage (Borea et al., 2017). Adenosine triggers its effects through the interaction with four G-protein coupled receptors (GPCRs), named A₁, A_{2A}, A_{2B}, and A₃ adenosine receptors (ARs). Some of the biological functions of adenosine include, but are not limited to, regulation of neurotransmitter release, neuronal excitability, heart rate and contractility, blood flow, platelet aggregation, inflammation and immune system responses, wound healing, and metabolic processes (Borea et al., 2018). In addition to the several physiological effects of adenosine, its receptor-mediated signaling has many documented effects on the progression of countless pathological states (Karmouty-Quintana et al., 2013). Among the main ones, modulation of adenosine receptors has been indicated as a promising therapeutic strategy in pathological states such as cancer (Vijayan et al., 2017; Allard et al., 2020), cardiovascular diseases (Reiss et al., 2019), pain (Vincenzi et al., 2020a), neurological/neurodegenerative diseases (Blum et al., 2018; Sebastião et al., 2018; Jenner et al., 2021; Merighi et al., 2021), neuropsychiatric disorders (Pasquini et al., 2022), inflammatory diseases (Pasquini et al., 2021; Antonioli et al., 2022), respiratory diseases (Caruso et al., 2013), ocular diseases (Spinozzi et al., 2021), diabetes, and other metabolic disorders (Antonioli et al., 2015; Sanni and Terre'Blanche, 2021). Despite this encouraging profusion of experimental evidence, relatively few adenosinergic system-based drugs have so far achieved clinical approval. When looking for accountability for this lack of finalization, this cannot be attributed to the lack of highly affine and selective ligands, as the search for new ligands has been quite productive (Jacobson et al., 2021; IJzerman et al., 2022), but rather the redundancy of adenosine signaling, the agonist-dependent receptor desensitization, and the broad expression of ARs provide the biggest challenges (Peleli et al., 2017). As a result of these drawbacks, most attempts to test orthosteric AR ligands in clinical trials have failed due to inefficiency or serious and unfavorable side effects. Different strategies were explored to overcome the above-mentioned

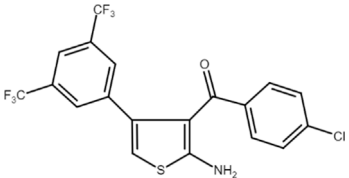
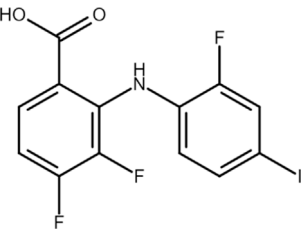
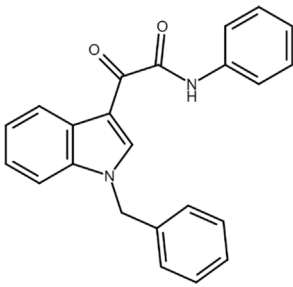
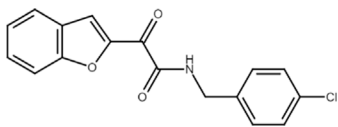
obstacles, including partial agonists (Greene et al., 2016; Voors et al., 2019), indirect receptor targeting (Kutryb-Zajac et al., 2020; Wang et al., 2021), prodrugs (Suresh et al., 2020), multi-target drugs (Huang et al., 2011), but one of the most promising seems to be allosteric modulation. By affecting endogenous agonist affinity and/or efficacy, a positive allosteric modulator (PAM) is an allosteric ligand that enhances an agonist-mediated receptor response, while a negative allosteric modulator (NAM) attenuates activity (Gentry et al., 2015). Other classes include neutral allosteric ligands (NAL) that bind at the allosteric site without affecting receptor or orthosteric ligand activity and allosteric agonists, ligands that directly activate the receptors from the allosteric site even in the absence of an orthosteric agonist. Traditionally, GPCRs have been targeted using compounds that bind to the orthosteric site. Allosteric ligands, binding at sites that are topologically distinct from the orthosteric sites, have expanded the ways to manipulate GPCR functionality, providing several pharmacological advantages and potential therapeutic benefits (Wootton et al., 2013). Due to the reduced evolutionary pressure that would ordinarily be necessary to maintain an orthosteric binding pocket capable of accepting the endogenous ligand, allosteric sites are less conserved among related receptor subtypes (Wild et al., 2014). Furthermore, since allosteric modulators may cause a variety of conformational changes in GPCR structures, they can be rationally tailored to create a strong biased signaling response from a GPCR triggered by an otherwise non-biased orthosteric ligand (Wold and Zhou, 2018). By imparting biased modulation upon orthosteric agonists, these allosteric modulators have the ability to only enhance therapeutically relevant signaling while preventing on-target side effects (Gao et al., 2011; Slosky et al., 2021). Apart from allosteric agonists, allosteric modulators such as PAMs and NAMs only have an effect in the presence of orthosteric ligands and can enhance or decrease receptor activation induced by endogenous agonists. Therefore, they act more physiologically and are predicted to have fewer adverse effects and tolerance-inducing consequences than orthosteric ligands. A particularly crucial element in the case of the short-lived molecule adenosine is the ability of PAMs and NAMs to finely tune its activity by following the spatiotemporal distribution of its extracellular concentration. Another important advantage is the reciprocal communication with the orthosteric domain: the allosteric modulator exerts an effect on the binding of the endogenous ligand, but the latter can also affect the binding of the modulator. This mechanism supports the selectivity of allosteric ligands, especially under conditions where there is a pathology-dependent alteration in the concentration of the endogenous agonist at a particular site (Draper-Joyce et al., 2021). This review summarizes the advances in the development of ARs allosteric modulators (Table 1) that may provide support for their use as new therapeutic options.

TABLE 1 Selected *in vitro* and *in vivo* studies on AR allosteric modulators.

Compound	Type	<i>In vivo</i> models	Main results	References
PD 81,723 ((2-amino-4,5-dimethylthiophen-3-yl)-[3-(trifluoromethyl)phenyl]methanone)	A ₁ AR PAM	Hyperglycemic cerebral ischemia and reperfusion in rats	Hippocampal injury reduction and Morris water maze performance improvement	Meno et al. (2003)
		Renal ischemia-reperfusion injury in mice	Renal tubular necrosis and inflammation reduction	Park et al. (2012)
T62 ((2-amino-4,5,6,7-tetrahydro-1-benzothiophen-3-yl)-(4-chlorophenyl) methanone)	A ₁ AR PAM	Spinal nerve ligation-induced mechanical hypersensitivity in rats	Mechanical hypersensitivity decrease	Pan et al. (2001)
		Carrageenin-induced thermal hypersensitivity in rats	Thermal hypersensitivity decrease	Li et al. (2003)
		Plantar incision-induced hypersensitivity in rats	Mechanical hypersensitivity reduction	Obata et al. (2004)
TRR469 ((2-Amino-4-[(4-(phenyl)piperazin-1-yl)methyl]-5-(4-fluorophenyl)thiophen-3-yl)-(4-chlorophenyl)methanone)	A ₁ AR PAM	Formalin and writhing tests, and streptozotocin-induced diabetic neuropathic pain in mice	Acute and chronic pain reduction	Vincenzi et al. (2014)
		Anxiety behavioral paradigms in mice	Anxiolytic-like effects	Vincenzi et al. (2016)
		Glutamate-induced injury in PC12 cells	Cell death, caspase activation, ROS production, and mitochondrial membrane potential loss abrogation	Vincenzi et al. (2020b)
VCP333 (<i>tert</i> -butyl 2-amino-3-(4-chlorobenzoyl)-7,8-dihydro-4H-thieno [2,3-d]azepine-6(5H)-carboxylate)	A ₁ AR PAM	Ischemia-reperfusion in murine isolated hearts	Cardiac function improvement and myocardial cell death reduction	Butcher et al. (2013)
VCP171 ((2-amino-4-[3-(trifluoromethyl)phenyl]thiophen-3-yl)-phenylmethanone)	A ₁ AR PAM	Partial nerve-injury neuropathic pain in rats	eEPSC amplitude of nerve-injury inhibition	Imlach et al. (2015)

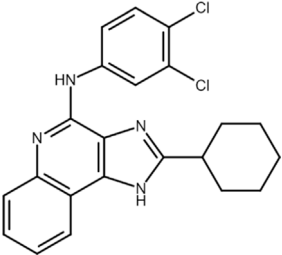
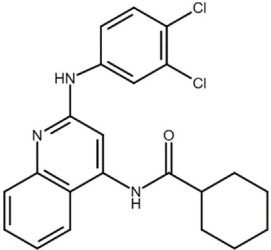
(Continued on following page)

TABLE 1 (Continued) Selected *in vitro* and *in vivo* studies on AR allosteric modulators.

Compound	Type	<i>In vivo</i> models	Main results	References
MIPS521 (2-amino-4-(3,5-bis(trifluoromethyl)phenyl)thiophen-3-yl) (4-chlorophenyl) methanone) <div>  </div>	A ₁ AR PAM	Partial nerve ligation-induced neuropathic pain in rats	Spinal nociceptive signaling and mechanical allodynia reduction	Draper-Joyce et al. (2021)
AEA061 (Chemical structure not disclosed)	A _{2A} AR PAM	LPS-induced endotoxemia in mice	Plasma TNF-α and MCP-1 level reduction, and IL-10 increase	Welihinda and Amento (2014)
		LPS-stimulated splenic monocytes/macrophages	Cytokine/chemokine reduction	Welihinda and Amento (2014; Welihinda et al. (2018))
		Imiquimod- or IL-23-induced psoriasis-like dermatitis in mice	Clinical score and cytokine expression reduction	Welihinda et al. (2022)
A2AR PAM-1 (3,4-difluoro-2-((2-fluoro-4-iodophenyl)amino) benzoic acid) <div>  </div>	A _{2A} AR PAM	EEG/EMG electrodes implanted in mice	Slow-wave sleep induction	Korkutata et al. (2017, 2019)
KI-7 (2-(1-benzyl-1H-indol-3-yl)-2-oxo-N-phenylacetamide) <div>  </div>	A _{2B} AR PAM	Mesenchymal stem cells	Osteoblast differentiation and survival increase	Trincavelli et al. (2014a)
Compound 9 (N-(4-chlorobenzyl)-2-(benzofuran-2-yl)glyoxylamide) <div>  </div>	A _{2B} AR PAM	Mesenchymal stem cells	Matrix mineralization stimulation	Barresi et al. (2021a)

(Continued on following page)

TABLE 1 (Continued) Selected *in vitro* and *in vivo* studies on AR allosteric modulators.

Compound	Type	<i>In vivo</i> models	Main results	References
LUF6000 (CF602) 	A ₃ AR PAM	Adjuvant-induced arthritis in rats Monoiodoacetate-induced osteoarthritis in rats Concanavalin A-induced liver inflammation in mice Diabetic erectile dysfunction in rats	Arthritis clinical score reduction Knee swelling and edema decrease Serum glutamic pyruvate transaminase and serum glutamic oxaloacetic transaminase decrease Intracavernosal pressure increase	Cohen et al. (2014) Itzhak et al. (2022)
LUF6096 (N-[2-(3,4-dichloroanilino) quinolin-4-yl]cyclohexane carboxamide) 	A ₃ AR PAM	Myocardial ischemia/reperfusion injury in dogs	Infarct size reduction	Du et al. (2012)

Allosteric modulation of ARs

A₁AR allosteric modulators

A₁ARs are widespread and implicated in many physiological mechanisms, therefore they are regarded as a prominent drug target for different diseases. Adenosine through A₁ARs exerts sedative, anticonvulsant, anxiolytic, and locomotor depressant effects (Varani et al., 2017). Furthermore, the heart rate and rhythm, the conduction speed in the atrioventricular node, and cardiac muscle contraction are negatively controlled by A₁ARs (Deb et al., 2019; Jacobson et al., 2019). In particular, A₁AR agonists mediate cardioprotection through the inhibition of norepinephrine release (Dinh et al., 2017). An important role of A₁ARs is in nociception, due to their location in peripheral sensory nerve terminals in the spinal cord dorsal horn and in supraspinal pain-processing structures (Sawynok, 2016; Vincenzi et al., 2020a). Many studies have been conducted to exploit the therapeutic potential of these receptors, but the development of orthosteric agonists has been hampered by several drawbacks, the main ones being cardiac side effects and receptor desensitization. An alternative strategy to exploit the positive effects of A₁AR stimulation is allosteric modulation. Much research effort in recent decades has been devoted to the synthesis and *in vitro* and *in vivo* evaluation of A₁AR PAMs (Romagnoli et al., 2015b; Jacobson and Gao, 2016). The first and most extensively studied class of compounds synthesized are the benzoylthiophene derivatives, the prototype of which is PD 81,723 (Bruns et al., 1990). Different studies revealed a potential application of PD 81,723 in ischemic injury (Meno et al., 2003; Park et al., 2012). Another extensively studied compound belonging to this class of modulators is T62 (Baraldi et al., 2000). It was effective in reducing nociception and hypersensitivity in animal models of neuropathic pain (Pan et al., 2001; Li et al., 2002, 2003; Obata et al., 2004). It was also used in a phase II clinical trial for postherpetic neuropathic pain. However, the study was abandoned due to a lack of efficacy and the presence of transient high levels of liver transaminase in some patients (Giorgi and Nieri, 2013). Subsequently, numerous other derivatives were discovered, endowed with greater allosteric activity (Romagnoli et al., 2008, 2012, 2013, 2014; 2015a). Of these, TRR469 was selected for *in vivo* studies. TRR469 has been reported to have an analgesic effect comparable to that of morphine in animal models of both acute and neuropathic pain without showing the side effects typical of orthosteric A₁AR agonists such as locomotor disturbances or sedation (Vincenzi et al., 2014). This compound also proved effective as an anxiolytic in several mouse models of anxiety with an effect comparable to that of diazepam but without the locomotor side effects typical of benzodiazepines (Vincenzi et al., 2016). Also noteworthy is the

protective effect of TRR469 found in an *in vitro* model of glutamate-induced cytotoxicity in neuronal cells (Vincenzi et al., 2020b). Another series of 2-amino-3-benzoylthiophene A₁AR PAMs were synthesized (Aurelio et al., 2009), including VCP171, whose *in vivo* analgesic effect in a model of neuropathic pain proved weaker than that of the orthosteric A₁AR agonist, but which nevertheless has greater therapeutic potential due to fewer side effects, particularly in tissues with higher adenosine concentrations or A₁AR tone (Imlach et al., 2015). Instead, VCP333 has been shown to improve cardiac function and reduce cardiomyocyte death following cardiac ischemia (Butcher et al., 2013). The most recently synthesized is MIPS521, an A₁AR PAM that has shown analgesic effects in models of neuropathic pain by being able to modulate the high concentrations of adenosine present. Interestingly, a new binding pocket was identified by studying the structure of the A₁AR bound to adenosine, MIPS521, and the Gi protein. This led to hypothesize that the modulator also exerts its effects by stabilizing the adenosine-receptor-G protein complex (Draper-Joyce et al., 2021). Recently, a multisite binding model for A₁AR allosteric modulation has been proposed. It predicts that there are several extracellular sites capable of binding the modulator, not just a distinct pocket generally located on the second extracellular loop (Deganutti et al., 2021).

A_{2A}AR allosteric modulators

Adenosine, mainly through the activation of A_{2A}ARs expressed in peripheral immune cells, represents a potent inflammatory self-limiting factor (Antonioli et al., 2022). Depending on the pathology, this can have both positive and negative impacts. On the positive side, A_{2A}AR activation is potentially useful for the treatment of autoimmune and inflammatory diseases (Vincenzi et al., 2013), as evidenced by the fact that the anti-inflammatory and immunosuppressive effects of methotrexate, a gold standard for the treatment of rheumatoid arthritis, as well as some of the anti-inflammatory effects of sulfasalazine, are mediated by adenosine (Cronstein and Sitkovsky, 2017). Although A_{2A}AR agonists may be effective in the treatment of inflammatory illnesses, they are likely to have too many adverse effects to be tolerated, mainly owing to their significant hypotensive effect. One alternative approach that could potentially circumvent the agonist-related side effects while enhancing the potent anti-inflammatory action of adenosine is represented by A_{2A}AR PAMs. On the negative side of adenosine-mediated inflammation suppression, many solid tumors escape immune response by increasing the concentration of adenosine in the tumor microenvironment. Both animal studies and clinical trials have shown that blocking A_{2A}AR can induce tumor regression (Sun et al., 2022). Although not yet tested, one can speculate that A_{2A}AR

NAM could potentially counteract in a spatial-selective manner the tumor-increased adenosine immunosuppressive action. In the CNS, blockade of A_{2A} ARs is indicated, with varying degrees of preclinical and clinical evidence, as a promising therapeutic strategy for Parkinson's disease, supported by the recent approval of the antagonist istradefylline as add-on therapy (Chen and Cunha, 2020), but also for Alzheimer's disease (Merighi et al., 2022), acute brain dysfunction (Cunha, 2016), and some neuropsychiatric disorders such as fragile X syndrome, depression, and anxiety (Domenici et al., 2019).

Unfortunately, only a small number of A_{2A} AR allosteric modulators have been reported so far. Some N^6 -1,3-diphenylurea derivatives of 2-phenyl-9-benzyladenines and 8-azaadenines have been suggested to act as allosteric modulators at the A_{2A} ARs (Giorgi et al., 2008). Later, using a fragment screening technique, some PAMs and NAMs of ARs were identified. In particular, ZB1854 potentiated the action of the A_{2A} AR agonist CGS 21680, thereby behaving as a PAM (Chen et al., 2012). A compound denoted as AEA061 increased adenosine's anti-inflammatory properties by allosterically enhancing its activity at A_{2A} ARs in the lipopolysaccharide (LPS)-induced mouse model of inflammation (Welihinda and Amento, 2014). In a subsequent work, AEA061 was also shown to enhance inosine-mediated A_{2A} AR activation and consequent inhibition of pro-inflammatory cytokine and chemokine production in splenic monocytes (Welihinda et al., 2018). Very recently, AEA061 also reduced clinical scores and cytokine expression in two different models of psoriasis-like dermatitis induced by imiquimod or IL-23 (Welihinda et al., 2022). Another A_{2A} AR PAM, named A_{2A} AR PAM-1, increased the total amount of slow wave sleep, from which individuals with insomnia might benefit, without affecting blood pressure, heart rhythm, and body temperature as the agonist CGS21680 did (Korkutata et al., 2017, 2019).

A_{2B} AR allosteric modulators

The A_{2B} AR is widely expressed in organs such as the bladder, intestine, and lung, as well as in various cell types such as fibroblasts, smooth muscle, endothelial, immune, and alveolar epithelial cells (Borea et al., 2018). Of all the ARs, the A_{2B} subtype is the least characterized from a pharmacological point of view. It has been proposed as a potential target in acute lung injury, as its activation with the agonist BAY 60-6583 led to a reduction in inflammation and pulmonary edema, and an increase in alveolar fluid clearance (Eckle et al., 2013; Hoegl et al., 2015; Wang et al., 2020). Recently, Gnad and others found that activation of A_{2B} ARs restores muscle and brown fat function in elderly and obese mice to that of young, lean animals, establishing its anti-aging and anti-obesity potential (Gnad et al., 2022). In addition, it has been suggested that A_{2B} ARs have therapeutic potential in bone diseases, as their activation appears to promote osteoblast

differentiation and bone formation (Carroll et al., 2012; Corciulo et al., 2016).

The first class of allosteric modulators for the A_{2B} AR, a series of 1-benzyl-3-ketoindoles, was serendipitously discovered (starting from a scaffold previously used to develop benzodiazepine receptor ligands) and consisted of three PAM and four NAM (Taliani et al., 2013; Trincavelli et al., 2014b). Subsequently, one of these A_{2B} AR PAMs, denoted as KI-7, was shown to enhance the effects of adenosine and synthetic A_{2B} AR agonists in the differentiation of mesenchymal stem cells (MSC) to osteoblasts while also increasing differentiated osteoblast viability (Trincavelli et al., 2014a). More recently, a series of novel derivatives chemically related to those previously synthesized has been reported. One of these compounds, a benzofurane derivative that was confirmed to behave as A_{2B} AR PAM, stimulated matrix mineralization in MSC, making it a lead structure for the synthesis of new compounds with anti-osteoporosis properties (Barresi et al., 2021a; 2021b).

Since A_{2B} AR blockade may represent a promising approach for the treatment of some diseases, such as in cancer immunotherapy (Gao and Jacobson, 2019), A_{2B} AR NAM could also result in a valuable pharmacological resource. Interestingly, the well-known selective A_{2B} AR antagonist PSB 603 was recently suggested to act as a NAM, at least in A_{2B} -mediated cAMP accumulation in HEK 293 cells (Goulding et al., 2018).

A_3 AR allosteric modulators

A_3 AR is expressed in the brain, heart, testis, lung, placenta, uterus, kidneys, spleen, liver, bladder, and proximal colon, but, while low expression is found in normal cells, this receptor subtype is overexpressed in immune and cancer cells (Gessi et al., 2008). The activation of A_3 AR mediates anti-inflammatory, antitumor, and anti-ischemic beneficial effects, showing a therapeutic potential for the treatment of inflammatory diseases, such as rheumatoid arthritis and psoriasis, hepatitis, cancer, glaucoma, cardiovascular diseases, and cerebral ischemia (Borea et al., 2015).

In addition to some selective A_3 AR agonists, several series of allosteric modulators, mainly PAMs, have also been developed, representing an alternative approach for the treatment of those aforementioned diseases in which A_3 AR activation appears to be a promising therapeutic strategy (Gao et al., 2001, 2002; Göblyös et al., 2006; Heitman et al., 2009; Kim et al., 2009). However, as opposed to orthosteric agonists, A_3 AR PAMs have the benefit of being able to target regions where adenosine levels are elevated, such as tumor and inflammatory sites, with low or no effects on normal tissues where adenosine levels are low.

Among the most well-known A_3 AR PAMS are the LUF6000 and LUF6096. LUF6000 is an imidazoquinolinamine

PAM at the A₃AR that showed anti-inflammatory effects in a rat adjuvant-induced arthritis model, inhibited monoiodoacetate-induced osteoarthritis development, and exhibited protective effects in a liver inflammation model of acute hepatitis in mice. At the molecular level, LUF6000 administration resulted in a marked deregulation of the NF- κ B signaling pathway (Cohen et al., 2014). Itzhak and co-workers evaluated the effect of LUF6000 (also known as CF602) on resolving erectile dysfunction (ED) in a diabetic ED rat model. CF602 increased intracavernosal pressure, endothelial nitric oxide synthase (eNOS), and vascular endothelial growth factor (VEGF) levels, improving erectile function (Itzhak et al., 2022). This compound may thus provide an alternative treatment for phosphodiesterase 5 (PDE5) inhibitors, which are usually employed in ED therapy, considering that half of the patients with diabetes do not respond to PDE5 inhibitors.

In addition, LUF6096, which is structurally similar to LUF6000, reduced infarct size in a barbitol-anesthetized dog model of myocardial ischemia/reperfusion injury. The infarct size reduction was equally evident when LUF6096 was administered in two doses before coronary artery occlusion and immediately before reperfusion or a single dose immediately before reperfusion (Du et al., 2012).

Studies conducted by Lane and others suggest that the endocannabinoid two- arachidonylglycerol (2-AG) acts as a NAM at the A₃AR. This evidence may be especially important in certain pathological conditions like cerebral ischemia when levels of 2-AG are elevated and could interact with A₃AR expressed in astrocytes and microglia (Lane et al., 2010).

Conclusion

GPCR allosteric modulators are promising therapeutic agents. By altering the receptor conformation, they potentiate or attenuate the effect of the endogenous agonist, acting more physiologically than orthosteric ligands and offering spatiotemporal selectivity. The adenosinergic system, making use of a short-lived autocrine/paracrine mediator, represents an ideal situation to take advantage of the benefits of allosteric modulation. The available preclinical results are encouraging, and there is hope for an acceleration that may

lead to the clinical use of allosteric modulators of ARs. Nevertheless, no allosteric modulator has entered clinical trials to date, underlining the challenges in the discovery and development of this class of compounds. Allosteric sites generally have a shallow structure-activity relationship and are often unknown or difficult to discover as they are only accessible in specific protein conformations. The fact that allosteric sites are less evolutionarily conserved than orthosteric ones can lead to species differences that can hamper their validation. Furthermore, allosteric modulators have a high propensity for molecular switching and can show complex *in vivo* pharmacology. Despite these challenges to identifying, validating, and developing allosteric modulators for GPCRs, they have the potential to become one of the most highly effective and minimally toxic pharmacological agents.

Author contributions

SP, PB, KV, and FV conceived the work and wrote the manuscript. CC and MC contributed to writing and editing. All authors contributed to the article and approved the submitted version.

Conflict of interest

The authors declare that the research was conducted in the absence of any commercial or financial relationships that could be construed as a potential conflict of interest.

Publisher's note

All claims expressed in this article are solely those of the authors and do not necessarily represent those of their affiliated organizations, or those of the publisher, the editors and the reviewers. Any product that may be evaluated in this article, or claim that may be made by its manufacturer, is not guaranteed or endorsed by the publisher.

References

- Allard, B., Allard, D., Buisseret, L., and Stagg, J. (2020). The adenosine pathway in immuno-oncology. *Nat. Rev. Clin. Oncol.* 17, 611–629. doi:10.1038/s41571-020-0382-2
- Antonioli, L., Blandizzi, C., Csóka, B., Pacher, P., and Haskó, G. (2015). Adenosine signalling in diabetes mellitus--pathophysiology and therapeutic considerations. *Nat. Rev. Endocrinol.* 11, 228–241. doi:10.1038/nrendo.2015.10
- Antonioli, L., Pacher, P., and Haskó, G. (2022). Adenosine and inflammation: it's time to (re)solve the problem. *Trends Pharmacol. Sci.* 43, 43–55. doi:10.1016/j.tips.2021.10.010
- Aurelio, L., Valant, C., Flynn, B. L., Sexton, P. M., Christopoulos, A., and Scammells, P. J. (2009). Allosteric modulators of the adenosine A1 receptor: Synthesis and pharmacological evaluation of 4-substituted 2-Amino-3-benzoylthiophenes. *J. Med. Chem.* 52, 4543–4547. doi:10.1021/jm9002582
- Baraldi, P. G., Zaid, A. N., Lampronti, I., Fruttarolo, F., Pavani, M. G., Tabrizi, M. A., et al. (2000). Synthesis and biological effects of a new series of 2-amino-3-benzoylthiophenes as allosteric enhancers of A1-adenosine receptor. *Bioorg. Med. Chem. Lett.* 10, 1953–1957. doi:10.1016/S0960-894X(00)00379-6
- Barresi, E., Giacomelli, C., Marchetti, L., Baglini, E., Salerno, S., Greco, G., et al. (2021a). Novel positive allosteric modulators of A2B adenosine receptor acting as

- bone mineralisation promoters. *J. Enzyme Inhib. Med. Chem.* 36, 286–294. doi:10.1080/14756366.2020.1862103
- Barresi, E., Martini, C., Da Settimo, F., Greco, G., Taliani, S., Giacomelli, C., et al. (2021b). Allosterism vs. Orthosterism: Recent findings and future perspectives on A2B AR physio-pathological implications. *Front. Pharmacol.* 12, 652121. doi:10.3389/fphar.2021.652121
- Blum, D., Chern, Y., Domenici, M. R., Buée, L., Lin, C.-Y., Rea, W., et al. (2018). The role of adenosine tone and adenosine receptors in huntington's disease. *J. Caffeine Adenosine Res.* 8, 43–58. doi:10.1089/caff.2018.0006
- Borea, P. A., Gessi, S., Merighi, S., and Varani, K. (2016). Adenosine as a multi-signalling guardian angel in human diseases: When, where and how does it exert its protective effects? *Trends Pharmacol. Sci.* 37, 419–434. doi:10.1016/j.tips.2016.02.006
- Borea, P. A., Gessi, S., Merighi, S., Vincenzi, F., and Varani, K. (2017). Pathological overproduction: The bad side of adenosine. *Br. J. Pharmacol.* 174, 1945–1960. doi:10.1111/bph.13763
- Borea, P. A., Gessi, S., Merighi, S., Vincenzi, F., and Varani, K. (2018). Pharmacology of adenosine receptors: The state of the art. *Physiol. Rev.* 98, 1591–1625. doi:10.1152/physrev.00049.2017
- Borea, P. A., Varani, K., Vincenzi, F., Baraldi, P. G., Tabrizi, M. A., Merighi, S., et al. (2015). The A3 adenosine receptor: History and perspectives. *Pharmacol. Rev.* 67, 74–102. doi:10.1124/pr.113.008540
- Bruns, R. F., Fergus, J. H., Coughenour, L. L., Courtland, G. G., Pugsley, T. A., Dodd, J. H., et al. (1990). Structure-activity relationships for enhancement of adenosine A1 receptor binding by 2-amino-3-benzoylthiophenes. *Mol. Pharmacol.* 38, 950–958.
- Butcher, A., Scammells, P. J., White, P. J., Devine, S. M., and Rose'meyer, R. B. (2013). An allosteric modulator of the adenosine A1 receptor improves cardiac function following ischaemia in murine isolated hearts. *Pharm. (Basel)* 6, 546–556. doi:10.3390/ph6040546
- Carroll, S. H., Wigner, N. A., Kulkarni, N., Johnston-Cox, H., Gerstenfeld, L. C., and Ravid, K. (2012). A2B adenosine receptor promotes mesenchymal stem cell differentiation to osteoblasts and bone formation *in vivo*. *J. Biol. Chem.* 287, 15718–15727. doi:10.1074/jbc.M112.344994
- Caruso, M., Alamo, A., Crisafulli, E., Raciti, C., Fisichella, A., and Polosa, R. (2013). Adenosine signaling pathways as potential therapeutic targets in respiratory disease. *Expert Opin. Ther. Targets* 17, 761–772. doi:10.1517/14728222.2013.795220
- Chen, D., Errey, J. C., Heitman, L. H., Marshall, F. H., Ijzerman, A. P., and Siegal, G. (2012). Fragment screening of GPCRs using biophysical methods: Identification of ligands of the adenosine A2A receptor with novel biological activity. *ACS Chem. Biol.* 7, 2064–2073. doi:10.1021/cb300436c
- Chen, J.-F., and Cunha, R. A. (2020). The belated US FDA approval of the adenosine A2A receptor antagonist istradefylline for treatment of Parkinson's disease. *Purinergic Signal.* 16, 167–174. doi:10.1007/s11302-020-09694-2
- Cohen, S., Barer, F., Bar-Yehuda, S., Ijzerman, A. P., Jacobson, K. A., and Fishman, P. (2014). A3 adenosine receptor allosteric modulator induces an anti-inflammatory effect: *In vivo* studies and molecular mechanism of action. *Mediat. Inflamm.* 2014, 708746. doi:10.1155/2014/708746
- Corciulo, C., Wilder, T., and Cronstein, B. N. (2016). Adenosine A2B receptors play an important role in bone homeostasis. *Purinergic Signal.* 12, 537–547. doi:10.1007/s11302-016-9519-2
- Cronstein, B. N., and Sitkovsky, M. (2017). Adenosine and adenosine receptors in the pathogenesis and treatment of rheumatic diseases. *Nat. Rev. Rheumatol.* 13, 41–51. doi:10.1038/nrrheum.2016.178
- Cunha, R. A. (2016). How does adenosine control neuronal dysfunction and neurodegeneration? *J. Neurochem.* 139, 1019–1055. doi:10.1111/jnc.13724
- Deb, P. K., Deka, S., Borah, P., Abed, S. N., and Klotz, K.-N. (2019). Medicinal chemistry and therapeutic potential of agonists, antagonists and allosteric modulators of A1 adenosine receptor: Current status and perspectives. *Curr. Pharm. Des.* 25, 2697–2715. doi:10.2174/1381612825666190716100509
- Deganutti, G., Barkan, K., Ladds, G., and Reynolds, C. A. (2021). Multisite model of allosterism for the adenosine A1 receptor. *J. Chem. Inf. Model.* 61, 2001–2015. doi:10.1021/acs.jcim.0c01331
- Dinh, W., Albrecht-Küpper, B., Gheorghiadu, M., Voors, A. A., van der Laan, M., and Sabbah, H. N. (2017). Partial adenosine A1 agonist in heart failure. *Handb. Exp. Pharmacol.* 243, 177–203. doi:10.1007/164_2016_83
- Domenici, M. R., Ferrante, A., Martire, A., Chiodi, V., Pepponi, R., Tebano, M. T., et al. (2019). Adenosine A2A receptor as potential therapeutic target in neuropsychiatric disorders. *Pharmacol. Res.* 147, 104338. doi:10.1016/j.phrs.2019.104338
- Draper-Joyce, C. J., Bhola, R., Wang, J., Bhattarai, A., Nguyen, A. T. N., Cowie-Kent, I., et al. (2021). Positive allosteric mechanisms of adenosine A1 receptor-mediated analgesia. *Nature* 597, 571–576. doi:10.1038/s41586-021-03897-2
- Du, L., Gao, Z.-G., Nithipatikom, K., Ijzerman, A. P., Veldhoven, J. P. D. van, Jacobson, K. A., et al. (2012). Protection from myocardial ischemia/reperfusion injury by a positive allosteric modulator of the A3 adenosine receptor. *J. Pharmacol. Exp. Ther.* 340, 210–217. doi:10.1124/jpet.111.187559
- Eckle, T., Hughes, K., Ehrentauf, H., Brodsky, K. S., Rosenberger, P., Choi, D.-S., et al. (2013). Crosstalk between the equilibrative nucleoside transporter ENT2 and alveolar Adora2b adenosine receptors dampens acute lung injury. *FASEB J.* 27, 3078–3089. doi:10.1096/fj.13-228551
- Gao, Z.-G., and Jacobson, K. A. (2019). A2B adenosine receptor and cancer. *Int. J. Mol. Sci.* 20, 5139. doi:10.3390/ijms20205139
- Gao, Z.-G., Kim, S. G., Soltysiak, K. A., Melman, N., Ijzerman, A. P., and Jacobson, K. A. (2002). Selective allosteric enhancement of agonist binding and function at human A3 adenosine receptors by a series of imidazoquinoline derivatives. *Mol. Pharmacol.* 62, 81–89. doi:10.1124/mol.62.1.81
- Gao, Z.-G., Verzijl, D., Zweemer, A., Ye, K., Göblyös, A., Ijzerman, A. P., et al. (2011). Functionally biased modulation of A(3) adenosine receptor agonist efficacy and potency by imidazoquinolinamine allosteric enhancers. *Biochem. Pharmacol.* 82, 658–668. doi:10.1016/j.bcp.2011.06.017
- Gao, Z. G., Van Muijlwijk-Koezen, J. E., Chen, A., Müller, C. E., Ijzerman, A. P., and Jacobson, K. A. (2001). Allosteric modulation of A(3) adenosine receptors by a series of 3-(2-pyridinyl)isoquinoline derivatives. *Mol. Pharmacol.* 60, 1057–1063. doi:10.1124/mol.60.5.1057
- Gentry, P. R., Sexton, P. M., and Christopoulos, A. (2015). Novel allosteric modulators of G protein-coupled receptors. *J. Biol. Chem.* 290, 19478–19488. doi:10.1074/jbc.R115.662759
- Gessi, S., Merighi, S., Varani, K., Leung, E., Mac Lennan, S., and Borea, P. A. (2008). The A3 adenosine receptor: An enigmatic player in cell biology. *Pharmacol. Ther.* 117, 123–140. doi:10.1016/j.pharmthera.2007.09.002
- Giorgi, I., Biagi, G., Bianucci, A. M., Borghini, A., Livi, O., Leonardi, M., et al. (2008). N6-1, 3-diphenylurea derivatives of 2-phenyl-9-benzyladenines and 8-azaadenines: Synthesis and biological evaluation as allosteric modulators of A2A adenosine receptors. *Eur. J. Med. Chem.* 43, 1639–1647. doi:10.1016/j.ejmech.2007.10.021
- Giorgi, I., and Nieri, P. (2013). Adenosine A1 modulators: A patent update (2008 to present). *Expert Opin. Ther. Pat.* 23, 1109–1121. doi:10.1517/13543776.2013.799142
- Gnad, T., Navarro, G., Lahesmaa, M., Reverte-Salisa, L., Copperi, F., Cordomi, A., et al. (2022). Adenosine/A2B receptor signaling ameliorates the effects of aging and counteracts obesity. *Cell Metab.* 34, 56–70. doi:10.1016/j.cmet.2020.06.006
- Göblyös, A., Gao, Z.-G., Brussee, J., Connestari, R., Santiago, S. N., Ye, K., et al. (2006). Structure-activity relationships of new 1H-imidazo[4, 5-c]quinolin-4-amine derivatives as allosteric enhancers of the A3 adenosine receptor. *J. Med. Chem.* 49, 3354–3361. doi:10.1021/jm060086s
- Goulding, J., May, L. T., and Hill, S. J. (2018). Characterisation of endogenous A2A and A2B receptor-mediated cyclic AMP responses in HEK 293 cells using the GloSensor™ biosensor: Evidence for an allosteric mechanism of action for the A2B-selective antagonist PSB 603. *Biochem. Pharmacol.* 147, 55–66. doi:10.1016/j.bcp.2017.10.013
- Greene, S. J., Sabbah, H. N., Butler, J., Voors, A. A., Albrecht-Küpper, B. E., Dungen, H.-D., et al. (2016). Partial adenosine A1 receptor agonism: A potential new therapeutic strategy for heart failure. *Heart fail. Rev.* 21, 95–102. doi:10.1007/s10741-015-9522-7
- Haskó, G., Linden, J., Cronstein, B., and Pacher, P. (2008). Adenosine receptors: Therapeutic aspects for inflammatory and immune diseases. *Nat. Rev. Drug Discov.* 7, 759–770. doi:10.1038/nrd2638
- Heitman, L. H., Göblyös, A., Zweemer, A. M., Bakker, R., Mulder-Krieger, T., van Veldhoven, J. P. D., et al. (2009). A series of 2, 4-disubstituted quinolines as a new class of allosteric enhancers of the adenosine A3 receptor. *J. Med. Chem.* 52, 926–931. doi:10.1021/jm8014052
- Hoegl, S., Brodsky, K. S., Blackburn, M. R., Karmouty-Quintana, H., Zwissler, B., and Eltzschig, H. K. (2015). Alveolar epithelial A2B adenosine receptors in pulmonary protection during acute lung injury. *J. Immunol.* 195, 1815–1824. doi:10.4049/jimmunol.1401957
- Huang, N.-K., Lin, J.-H., Lin, J.-T., Lin, C.-I., Liu, E. M., Lin, C.-J., et al. (2011). A new drug design targeting the adenosinergic system for huntington's disease. *PLOS ONE* 6, e20934. doi:10.1371/journal.pone.0020934
- Ijzerman, A. P., Jacobson, K. A., Müller, C. E., Cronstein, B. N., and Cunha, R. A. (2022). International union of basic and clinical Pharmacology. CXII: Adenosine receptors: A further update. *Pharmacol. Rev.* 74, 340–372. doi:10.1124/pharmrev.121.000445

- Imlach, W. L., Bhola, R. F., May, L. T., Christopoulos, A., and Christie, M. J. (2015). A positive allosteric modulator of the adenosine A1 receptor selectively inhibits primary afferent synaptic transmission in a neuropathic pain model. *Mol. Pharmacol.* 88, 460–468. doi:10.1124/mol.115.099499
- Itzhak, I., Cohen, S., Fishman, S., and Fishman, P. (2022). A3 adenosine receptor allosteric modulator CF602 reverses erectile dysfunction in a diabetic rat model. *Andrologia* 54, e14498. doi:10.1111/and.14498
- Jacobson, K. A., and Gao, Z.-G. (2016). CHAPTER 11:allosteric modulators of adenosine, P2Y and P2X receptors. *Allostereism in Drug Discovery*, 247–270. doi:10.1039/9781782629276-00247
- Jacobson, K. A., Ijzerman, A. P., and Müller, C. E. (2021). Medicinal chemistry of P2 and adenosine receptors: Common scaffolds adapted for multiple targets. *Biochem. Pharmacol.* 187, 114311. doi:10.1016/j.bcp.2020.114311
- Jacobson, K. A., Tosh, D. K., Jain, S., and Gao, Z.-G. (2019). Historical and current adenosine receptor agonists in preclinical and clinical development. *Front. Cell. Neurosci.* 13, 124. doi:10.3389/fncel.2019.00124
- Jenner, P., Mori, A., Aradi, S. D., and Hauser, R. A. (2021). Istradefylline - a first generation adenosine A2A antagonist for the treatment of Parkinson's disease. *Expert Rev. Neurother.* 21, 317–333. doi:10.1080/14737175.2021.1880896
- Karmouty-Quintana, H., Xia, Y., and Blackburn, M. R. (2013). Adenosine signaling during acute and chronic disease states. *J. Mol. Med.* 91, 173–181. doi:10.1007/s00109-013-0997-1
- Kim, Y., de Castro, S., Gao, Z.-G., Ijzerman, A. P., and Jacobson, K. A. (2009). Novel 2- and 4-substituted 1H-imidazo[4, 5-c]quinolin-4-amine derivatives as allosteric modulators of the A3 adenosine receptor. *J. Med. Chem.* 52, 2098–2108. doi:10.1021/jm801659w
- Korkutata, M., Saitoh, T., Cherasse, Y., Ioka, S., Duo, F., Qin, R., et al. (2019). Enhancing endogenous adenosine A2A receptor signaling induces slow-wave sleep without affecting body temperature and cardiovascular function. *Neuropharmacology* 144, 122–132. doi:10.1016/j.neuropharm.2018.10.022
- Korkutata, M., Saitoh, T., Feng, D., Murakoshi, N., Sugiyama, F., Cherasse, Y., et al. (2017). Allosteric modulation of adenosine A2A receptors in mice induces slow-wave sleep without cardiovascular effects. *Sleep. Med.* 40, e181. doi:10.1016/j.sleep.2017.11.530
- Kutryb-Zajac, B., Mierzejewska, P., Slominska, E. M., and Smolenski, R. T. (2020). Therapeutic perspectives of adenosine deaminase inhibition in cardiovascular diseases. *Molecules* 25, E4652. doi:10.3390/molecules25204652
- Lane, J. R., Beukers, M. W., Mulder-Krieger, T., and Ijzerman, A. P. (2010). The endocannabinoid 2-arachidonylglycerol is a negative allosteric modulator of the human A3 adenosine receptor. *Biochem. Pharmacol.* 79, 48–56. doi:10.1016/j.bcp.2009.07.024
- Li, X., Conklin, D., Ma, W., Zhu, X., and Eisenach, J. C. (2002). Spinal noradrenergic activation mediates allodynia reduction from an allosteric adenosine modulator in a rat model of neuropathic pain. *Pain* 97, 117–125. doi:10.1016/s0304-3959(02)00011-8
- Li, X., Conklin, D., Pan, H.-L., and Eisenach, J. C. (2003). Allosteric adenosine receptor modulation reduces hypersensitivity following peripheral inflammation by a central mechanism. *J. Pharmacol. Exp. Ther.* 305, 950–955. doi:10.1124/jpet.102.047951
- Meno, J. R., Higashi, H., Cambray, A. J., Zhou, J., D'Ambrosio, R., and Winn, H. R. (2003). Hippocampal injury and neurobehavioral deficits are improved by PD 81, 723 following hyperglycemic cerebral ischemia. *Exp. Neurol.* 183, 188–196. doi:10.1016/s0014-4886(03)00162-6
- Merighi, S., Borea, P. A., Varani, K., Vincenzi, F., Travagli, A., Nigro, M., et al. (2022). Pathophysiological role and medicinal chemistry of A2A adenosine receptor antagonists in Alzheimer's disease. *Molecules* 27, 2680. doi:10.3390/molecules27092680
- Merighi, S., Poloni, T. E., Pelloni, L., Pasquini, S., Varani, K., Vincenzi, F., et al. (2021). An open question: Is the A2A adenosine receptor a novel target for Alzheimer's disease treatment? *Front. Pharmacol.* 12, 652455. doi:10.3389/fphar.2021.652455
- Obata, H., Li, X., and Eisenach, J. C. (2004). Spinal adenosine receptor activation reduces hypersensitivity after surgery by a different mechanism than after nerve injury. *Anesthesiology* 100, 1258–1262. doi:10.1097/00000542-200405000-00030
- Pan, H. L., Xu, Z., Leung, E., and Eisenach, J. C. (2001). Allosteric adenosine modulation to reduce allodynia. *Anesthesiology* 95, 416–420. doi:10.1097/00000542-200108000-00025
- Park, S. W., Kim, J. Y., Ham, A., Brown, K. M., Kim, M., D'Agati, V. D., et al. (2012). A1 adenosine receptor allosteric enhancer PD-81723 protects against renal ischemia-reperfusion injury. *Am. J. Physiol. Ren. Physiol.* 303, F721–F732. doi:10.1152/ajprenal.00157.2012
- Pasquini, S., Contri, C., Borea, P. A., Vincenzi, F., and Varani, K. (2021). Adenosine and inflammation: Here, there and everywhere. *Int. J. Mol. Sci.* 22, 7685. doi:10.3390/ijms22147685
- Pasquini, S., Contri, C., Merighi, S., Gessi, S., Borea, P. A., Varani, K., et al. (2022). Adenosine receptors in neuropsychiatric disorders: Fine regulators of neurotransmission and potential therapeutic targets. *Int. J. Mol. Sci.* 23, 1219. doi:10.3390/ijms23031219
- Peleti, M., Fredholm, B. B., Sobrevia, L., and Carlström, M. (2017). Pharmacological targeting of adenosine receptor signaling. *Mol. Asp. Med.* 55, 4–8. doi:10.1016/j.mam.2016.12.002
- Reiss, A. B., Grossfeld, D., Kasselman, L. J., Renna, H. A., Vernice, N. A., Drewes, W., et al. (2019). Adenosine and the cardiovascular system. *Am. J. Cardiovasc. Drugs* 19, 449–464. doi:10.1007/s40256-019-00345-5
- Romagnoli, R., Baraldi, P. G., Carrion, M. D., Cara, C. L., Cruz-Lopez, O., Iaconinoto, M. A., et al. (2008). Synthesis and biological evaluation of 2-amino-3-(4-chlorobenzoyl)-4-[N-(Substituted) piperazin-1-yl]Thiophenes as potent allosteric enhancers of the A1 adenosine receptor. *J. Med. Chem.* 51, 5875–5879. doi:10.1021/jm800586p
- Romagnoli, R., Baraldi, P. G., Carrion, M. D., Cara, C. L., Cruz-Lopez, O., Salvador, M. K., et al. (2012). Synthesis and biological evaluation of 2-amino-3-(4-chlorobenzoyl)-4-[(4-arylpiperazin-1-yl)methyl]-5-substituted-thiophenes. effect of the 5-modification on allosteric enhancer activity at the A1 adenosine receptor. *J. Med. Chem.* 55, 7719–7735. doi:10.1021/jm3007504
- Romagnoli, R., Baraldi, P. G., Carrion, M. D., Lopez Cara, C., Kimatrai Salvador, M., Preti, D., et al. (2013). Synthesis and biological effects of novel 2-amino-3-(4-chlorobenzoyl)-4-substituted thiophenes as allosteric enhancers of the A1 adenosine receptor. *Eur. J. Med. Chem.* 67, 409–427. doi:10.1016/j.ejmech.2013.07.002
- Romagnoli, R., Baraldi, P. G., Ijzerman, A. P., Massink, A., Cruz-Lopez, O., Lopez-Cara, L. C., et al. (2014). Synthesis and biological evaluation of novel allosteric enhancers of the A1 adenosine receptor based on 2-amino-3-(4'-chlorobenzoyl)-4-substituted-5-arylethynyl thiophene. *J. Med. Chem.* 57, 7673–7686. doi:10.1021/jm5008853
- Romagnoli, R., Baraldi, P. G., Lopez-Cara, C., Cruz-Lopez, O., Moorman, A. R., Massink, A., et al. (2015a). Synthesis and biological evaluation of a new series of 2-amino-3-aryl thiophene derivatives as agonist allosteric modulators of the A1 adenosine receptor. A position-dependent effect study. *Eur. J. Med. Chem.* 101, 185–204. doi:10.1016/j.ejmech.2015.06.041
- Romagnoli, R., Baraldi, P. G., Moorman, A. R., Borea, P. A., and Varani, K. (2015b). Current status of A1 adenosine receptor allosteric enhancers. *Future Med. Chem.* 7, 1247–1259. doi:10.4155/fmc.15.65
- Sanni, O., and Terre'Blanche, G. (2021). Therapeutic potentials of agonist and antagonist of adenosine receptors in type 2 diabetes. *Rev. Endocr. Metab. Disord.* 22, 1073–1090. doi:10.1007/s11154-021-09668-8
- Sawynok, J. (2016). Adenosine receptor targets for pain. *Neuroscience* 338, 1–18. doi:10.1016/j.neuroscience.2015.10.031
- Sebastião, A. M., Rei, N., and Ribeiro, J. A. (2018). Amyotrophic lateral sclerosis (ALS) and adenosine receptors. *Front. Pharmacol.* 9, 267. doi:10.3389/fphar.2018.00267
- Slosky, L. M., Caron, M. G., and Barak, L. S. (2021). Biased allosteric modulators: New Frontiers in GPCR drug discovery. *Trends Pharmacol. Sci.* 42, 283–299. doi:10.1016/j.tips.2020.12.005
- Spinozzi, E., Baldassarri, C., Acquaticci, L., Del Bello, F., Grifantini, M., Cappellacci, L., et al. (2021). Adenosine receptors as promising targets for the management of ocular diseases. *Med. Chem. Res.* 30, 353–370. doi:10.1007/s00044-021-02704-x
- Sun, C., Wang, B., and Hao, S. (2022). Adenosine-A2A receptor pathway in cancer immunotherapy. *Front. Immunol.* 13. Available at: <https://www.frontiersin.org/articles/10.3389/fimmu.2022.837230> (Accessed August 11, 2022).
- Suresh, R. R., Jain, S., Chen, Z., Tosh, D. K., Ma, Y., Podszun, M. C., et al. (2020). Design and in vivo activity of A3 adenosine receptor agonist prodrugs. *Purinergic Signal.* 16, 367–377. doi:10.1007/s11302-020-09715-0
- Taliani, S., Trincavelli, M. L., Cosimelli, B., Laneri, S., Severi, E., Barresi, E., et al. (2013). Modulation of A2B adenosine receptor by 1-Benzyl-3-ketoindole derivatives. *Eur. J. Med. Chem.* 69, 331–337. doi:10.1016/j.ejmech.2013.09.001
- Trincavelli, M. L., Daniele, S., Giacomelli, C., Taliani, S., Da Settimo, F., Cosimelli, B., et al. (2014a). Osteoblast differentiation and survival: A role for A2B adenosine receptor allosteric modulators. *Biochim. Biophys. Acta* 1843, 2957–2966. doi:10.1016/j.bbamcr.2014.09.013
- Trincavelli, M. L., Giacomelli, C., Daniele, S., Taliani, S., Cosimelli, B., Laneri, S., et al. (2014b). Allosteric modulators of human A2B adenosine receptor. *Biochim. Biophys. Acta* 1840, 1194–1203. doi:10.1016/j.bbagen.2013.12.021

- Varani, K., Vincenzi, F., Merighi, S., Gessi, S., and Borea, P. A. (2017). Biochemical and pharmacological role of A1 adenosine receptors and their modulation as novel therapeutic strategy. *Adv. Exp. Med. Biol.* 1051, 193–232. doi:10.1007/5584_2017_61
- Vijayan, D., Young, A., Teng, M. W. L., and Smyth, M. J. (2017). Targeting immunosuppressive adenosine in cancer. *Nat. Rev. Cancer* 17, 709–724. doi:10.1038/nrc.2017.86
- Vincenzi, F., Padovan, M., Targa, M., Corciulo, C., Giacuzzo, S., Merighi, S., et al. (2013). A(2A) adenosine receptors are differentially modulated by pharmacological treatments in rheumatoid arthritis patients and their stimulation ameliorates adjuvant-induced arthritis in rats. *PLoS One* 8, e54195. doi:10.1371/journal.pone.0054195
- Vincenzi, F., Pasquini, S., Borea, P. A., and Varani, K. (2020a). Targeting adenosine receptors: A potential pharmacological avenue for acute and chronic pain. *Int. J. Mol. Sci.* 21, E8710. doi:10.3390/ijms21228710
- Vincenzi, F., Pasquini, S., Gessi, S., Merighi, S., Romagnoli, R., Borea, P. A., et al. (2020b). The detrimental action of adenosine on glutamate-induced cytotoxicity in PC12 cells can be shifted towards a neuroprotective role through A1AR positive allosteric modulation. *Cells* 9. doi:10.3390/cells9051242
- Vincenzi, F., Ravani, A., Pasquini, S., Merighi, S., Gessi, S., Romagnoli, R., et al. (2016). Positive allosteric modulation of A1 adenosine receptors as a novel and promising therapeutic strategy for anxiety. *Neuropharmacology* 111, 283–292. doi:10.1016/j.neuropharm.2016.09.015
- Vincenzi, F., Targa, M., Romagnoli, R., Merighi, S., Gessi, S., Baraldi, P. G., et al. (2014). TRR469, a potent A1 adenosine receptor allosteric modulator, exhibits antinociceptive properties in acute and neuropathic pain models in mice. *Neuropharmacology* 81, 6–14. doi:10.1016/j.neuropharm.2014.01.028
- Voors, A. A., Bax, J. J., Hernandez, A. F., Wirtz, A. B., Pap, A. F., Ferreira, A. C., et al. (2019). Safety and efficacy of the partial adenosine A1 receptor agonist neladenoson bialanate in patients with chronic heart failure with reduced ejection fraction: A phase IIb, randomized, double-blind, placebo-controlled trial. *Eur. J. Heart Fail.* 21, 1426–1433. doi:10.1002/ehf.1591
- Wang, L., Londono, L. M., Cowell, J., Saatci, O., Aras, M., Ersan, P. G., et al. (2021). Targeting adenosine with adenosine deaminase 2 to inhibit growth of solid tumors. *Cancer Res.* 81, 3319–3332. doi:10.1158/0008-5472.CAN-21-0340
- Wang, M., Guo, X., Zhao, H., Lv, J., Wang, H., and An, Y. (2020). Adenosine A2B receptor activation stimulates alveolar fluid clearance through alveolar epithelial sodium channel via cAMP pathway in endotoxin-induced lung injury. *Am. J. Physiol. Lung Cell. Mol. Physiol.* 318, L787–L800. doi:10.1152/ajplung.00195.2019
- Welihinda, A. A., and Amento, E. P. (2014). Positive allosteric modulation of the adenosine A2a receptor attenuates inflammation. *J. Inflamm.* 11, 37. doi:10.1186/s12950-014-0037-0
- Welihinda, A. A., Kaur, M., Raveendran, K. S., and Amento, E. P. (2018). Enhancement of inosine-mediated A2AR signaling through positive allosteric modulation. *Cell. Signal.* 42, 227–235. doi:10.1016/j.cellsig.2017.11.002
- Welihinda, A., Ravikumar, P., Kaur, M., Mechanic, J., Yadav, S., Kang, G. J., et al. (2022). Positive allosteric modulation of A2AR alters immune cell responses and ameliorates psoriasis-like dermatitis in mice. *J. Invest. Dermatol.* 142, 624–632. e6. doi:10.1016/j.jid.2021.07.174
- Wild, C., Cunningham, K. A., and Zhou, J. (2014). Allosteric modulation of G protein-coupled receptors: An emerging approach of drug discovery. *Austin J. Pharmacol. Ther.* 2, 1101.
- Wold, E. A., and Zhou, J. (2018). GPCR allosteric modulators: Mechanistic advantages and therapeutic applications. *Curr. Top. Med. Chem.* 18, 2002–2006. doi:10.2174/1568026619999190101151837
- Wootten, D., Christopoulos, A., and Sexton, P. M. (2013). Emerging paradigms in GPCR allostery: Implications for drug discovery. *Nat. Rev. Drug Discov.* 12, 630–644. doi:10.1038/nrd4052



OPEN ACCESS

EDITED BY

Kenneth A. Jacobson,
National Institutes of Health (NIH),
United States

REVIEWED BY

Yong Tang,
Chengdu University of Traditional
Chinese Medicine, China
Heike Wulff,
University of California, Davis,
United States

*CORRESPONDENCE

Friedrich Koch-Nolte,
nolte@uke.de

†PRESENT ADDRESS

Catelijne Stortelers,
VIB Discovery Sciences, Ghent, Belgium

SPECIALTY SECTION

This article was submitted to
Experimental Pharmacology and Drug
Discovery,
a section of the journal
Frontiers in Pharmacology

RECEIVED 27 August 2022

ACCEPTED 23 September 2022

PUBLISHED 10 October 2022

CITATION

Pinto-Espinoza C, Guillou C, Rissiek B,
Wilmes M, Javidi E, Schwarz N, Junge M,
Haag F, Liaukouskaya N, Wanner N,
Nicke A, Stortelers C, Tan Y-V,
Adriouch S, Magnus T and Koch-Nolte F
(2022), Effective targeting of microglial
P2X7 following intracerebroventricular
delivery of nanobodies and nanobody-
encoding AAVs.
Front. Pharmacol. 13:1029236.
doi: 10.3389/fphar.2022.1029236

COPYRIGHT

© 2022 Pinto-Espinoza, Guillou, Rissiek,
Wilmes, Javidi, Schwarz, Junge, Haag,
Liaukouskaya, Wanner, Nicke,
Stortelers, Tan, Adriouch, Magnus and
Koch-Nolte. This is an open-access
article distributed under the terms of the
[Creative Commons Attribution License](https://creativecommons.org/licenses/by/4.0/)
(CC BY). The use, distribution or
reproduction in other forums is
permitted, provided the original
author(s) and the copyright owner(s) are
credited and that the original
publication in this journal is cited, in
accordance with accepted academic
practice. No use, distribution or
reproduction is permitted which does
not comply with these terms.

Effective targeting of microglial P2X7 following intracerebroventricular delivery of nanobodies and nanobody-encoding AAVs

Carolina Pinto-Espinoza^{1,2}, Charlotte Guillou³, Björn Rissiek², Maximilian Wilmes², Ehsan Javidi², Nicole Schwarz^{1,4}, Marten Junge¹, Friedrich Haag¹, Nastassia Liaukouskaya⁵, Nicola Wanner⁵, Annette Nicke⁶, Catelijne Stortelers^{7†}, Yossan-Var Tan³, Sahil Adriouch³, Tim Magnus² and Friedrich Koch-Nolte^{1*}

¹Institute of Immunology, University Medical Center Hamburg-Eppendorf, Hamburg, Germany,

²Department of Neurology, University Medical Center Hamburg-Eppendorf, Hamburg, Germany,

³Normandie Univ, UNIROUEN, INSERM U1234, Pathophysiology, Autoimmunity and Immunotherapy (PanTHER), Rouen, France, ⁴MSH- Medical School Hamburg- Dep. Anatomy, Hamburg, Germany,

⁵Department of Nephrology, University Medical Centre Hamburg-Eppendorf, Hamburg, Germany,

⁶Walther Straub Institute of Pharmacology and Toxicology, Faculty of Medicine, LMU Munich, Munich, Germany, ⁷Ablynx-Sanofi, Ghent, Belgium

The P2X7 ion channel is a key sensor for extracellular ATP and a key trigger of sterile inflammation. Intravenous injection of nanobodies that block P2X7 has shown to be beneficial in mouse models of systemic inflammation. P2X7 has also emerged as an attractive therapeutic target for inflammatory brain diseases. However, little is known about the ability of nanobodies to cross the BBB. Here we evaluated the ability of P2X7-specific nanobodies to reach and to block P2X7 on microglia following intravenous or intracerebral administration. For this study, we reformatted and sequence-optimized P2X7 nanobodies for higher stability and elevated isoelectric point. Following injection of nanobodies or nanobody-encoding adeno-associated viral vectors (AAV), we monitored the occupancy and blockade of microglial P2X7 *in vivo* using *ex vivo* flow cytometry. Our results show that P2X7 on microglia was within minutes completely occupied and blocked by intracerebroventricularly injected nanobodies, even at low doses. In contrast, very high doses were required to achieve similar effects when injected intravenously. The endogenous production of P2X7-antagonistic nanobodies following intracerebral or intramuscular injection of nanobody-encoding AAVs resulted in a long-term occupancy and blockade of P2X7 on microglia. Our results provide new insights into the conditions for the delivery of nanobodies to

Abbreviations: AAV, adeno-associated viral vector; i.v., intravenous; i.c.v., intracerebroventricular; i.c.m., intracisterna magna; i.m., intramuscular; Nb, nanobody; VHH, variable heavy-chain antibody fragment.

microglial P2X7 and point to AAV-mediated delivery of P2X7 nanobodies as a promising strategy for the treatment of sterile brain inflammation.

KEYWORDS

P2X7 nanobodies, receptor occupancy, functional blockade, intracerebroventricular delivery, AAV-mediated delivery

1 Introduction

P2X7 is a ligand-gated non-selective cation channel that structurally assembles as a homomeric trimer (Nicke, 2008). P2X7 is expressed on the cell surface of various leukocytes, particularly at high levels on macrophages, microglia (Ferrari et al., 1996; He et al., 2017; Metzger et al., 2017) and resident T cells of the kidney (Stark et al., 2018; Borges da Silva et al., 2020). The physiological ligand of P2X7 is extracellular ATP. During inflammation, stressed and injured cells release large amounts of ATP that act as a danger associated molecular pattern (DAMP) (Choi et al., 2007; Falzoni et al., 2013). In LPS-primed microglia and monocytes, gating of P2X7 by ATP leads to the influx of Na⁺ and Ca²⁺ and the efflux of K⁺ (Choi and Kim, 1996; Egan and Khakh, 2004). Intracellular K⁺ depletion triggers the assembly of the NLRP3 inflammasome, a multiprotein complex that drives caspase-1-mediated maturation and release of leaderless IL-1 β , a key cytokine of the inflammatory response (Perregaux and Gabel, 1994; Ferrari et al., 1997; Sanz and Di Virgilio, 2000). Caspase-1 also cleaves Gasdermin D to generate free N-terminal domains which oligomerize at the plasma membrane to form pores through which mature IL-1 β is released (Shi et al., 2015; Ding et al., 2016; Evavold et al., 2018; Heilig et al., 2018). *In vitro*, ATP-induced pore formation has also been used to monitor P2X7 activation based on the increased membrane permeability to fluorescent molecules as for instance DNA-staining dyes such as DAPI (Yan et al., 2008).

In the CNS, inflammation and ischemia result in the local release of ATP at the site of tissue injury (Melani et al., 2005; Sanz et al., 2009; Grygorowicz et al., 2016). In addition, P2X7 activation on microglia has been implicated in the pathogenesis of experimental autoimmune encephalomyelitis (EAE) (Matute et al., 2007; Grygorowicz and Struzynska, 2019), Alzheimer disease (AD) (McLarnon et al., 2006), and stroke (Franke et al., 2004; Melani et al., 2006; Skaper et al., 2006), which are often associated with an increased release of IL-1 β (Boutin et al., 2001; Rampe et al., 2004; Jin et al., 2008; Sanz et al., 2009; Maysami et al., 2016; Grygorowicz and Struzynska, 2019).

Pharmacological antagonists of P2X7 have been proposed as potential therapeutic tools to control inflammation in the brain. Because most of them have shown lack of specificity, low potency, diverse pharmacodynamics, and conversion into ineffective or toxic metabolites (Bartlett et al., 2014; Bhattacharya and Biber, 2016; Andrejew et al., 2020), only the BBB-penetrant JNJ-54175446 has entered into phase II clinical trials for inflammation (Recourt et al., 2020). Antibodies are highly desirable therapeutic molecules as they offer high specificity, safety, uniform pharmacodynamics, and low

toxicity. Nanobodies are antibody fragments consisting of a single variable domain (VHH) of a heavy chain antibody. Nanobodies are highly soluble and with a small size (~12 kDa), they bind to their target with high specificity, similar to conventional antibodies (Hamers-Casterman et al., 1993; Nguyen et al., 2000; Conrath et al., 2005; Wesolowski et al., 2009). We have previously generated highly specific P2X7-antagonistic nanobodies that dampened inflammation in mouse models of allergic contact dermatitis and experimental glomerulonephritis (Danquah et al., 2016). However, similar to other biologics, the therapeutic application of P2X7-antagonistic nanobodies in CNS inflammation encounters the BBB as physical obstacle which restricts the passage of molecules with a MW > 500 Da (Fischer et al., 1998; Pardridge, 2005).

Our goal was to evaluate the CNS delivery of two potent P2X7-blocking nanobodies, that differ in their isoelectric point (pI), using different routes of administration. Nanobody 13A7 (pI 5.9) specifically blocks ATP-induced activation of mouse P2X7 while nanobody 1c81^s (pI 9.7) blocks both mouse and human P2X7, making it of interest for translational studies. We developed a sensitive cell-based assay to determine the level of P2X7 occupancy on brain cells (microglia) in contrast to cells in peripheral tissue (resident T cells of the kidney, T_{RMS}). We chose these cell types because of their known high levels of P2X7 on the cell surface (Metzger et al., 2017; Stark et al., 2018). We used this assay to evaluate the pharmacodynamics of P2X7 nanobodies after intravenous or intracerebral injections, as well as after intramuscular delivery of nanobody-encoding AAV1. The results demonstrate that an effective targeting of P2X7 on microglia *in vivo* can be readily achieved by intracerebroventricular injection of P2X7 antagonistic nanobodies, even at low doses, but very high doses are required when injected intravenously. Furthermore, the endogenous production of P2X7-antagonistic nanobodies 120 days after transduction of muscle cells with nanobody-encoding AAVs resulted in a high, albeit not complete, occupancy and blockade of P2X7 on microglia, whereas transduction of brain cells with nanobody-encoding AAVs resulted, 28 days later, in a complete blockade of P2X7 on microglia.

2 Materials and methods

2.1 Antibodies and reagents

The following fluorochrome conjugated monoclonal antibodies (mAbs) were used for flow cytometry: anti-CD45

(30-F11), anti-CD4 (GK1.5), anti-CD8 (53-6.7), anti-CD69 (H1.2F3), anti-CD11b (M1/70), anti-mouse IgG1 (RMG1-1), and purified anti-CD16/CD32, all purchased from Biolegend. Purified anti-VHH mouse IgG1 antibodies mAbH0077 and mAbH0074 were received from Ablynx and mAbs specific for mouse P2X1, P2X4, P2X7 were produced in house (Moller et al., 2007). Dead-cell staining was performed using DAPI and/or the AlexaFluor700 LIVE/DEAD Fixable Read Dead Stain Kit (Biolegend). For immunofluorescence microscopy the following fluorochrome conjugated reagents were used: isolectin purchased from Thermofisher, anti-GFP B-2 mAb (sc-9996) from Santa Cruz, anti-ALFA tag nanobody (1G5) from Nano-tag technologies and purified anti-ALFA tag nanobody fused to a rabbit IgG produced in house. DNA staining was performed with Hoechst 33342 (Thermofisher). ATP disodium salt was purchased from Sigma.

2.2 Construction and production of dimeric half-life extended nanobodies

P2X7-specific nanobodies 13A7, 14D5 and a sequence optimized variant of 1c81 with higher stability and elevated isoelectric point were engineered into bivalent half-life extended nanobodies, or bivalent Fc-fused format, as previously described (Danquah et al., 2016). Nanobody-constructs were subcloned into the pCSE2.5 expression vector either carrying at the C-terminus a tandem SNB tag (Schaffer et al., 2010) or carrying at the N-terminus an ALFA-tag (Gotzke et al., 2019). All nanobody constructs were produced as secretory proteins in transiently transfected HEK-6E cells cultivated in serum-free medium (cells provided by Ives Durocher, Montreal, Canada). After 6 days, cell-supernatants were harvested and clarified by centrifugation. Nanobodies were purified from the supernatants by affinity chromatography using protein A columns (GE Healthcare) and formulated at high concentrations (15–50 mg/ml) in an in-house low aggregation buffer (5.8 mg/ml sodium phosphate monobasic, monohydrate; 1.2 mg/ml sodium phosphate dibasic, anhydrous; 60 mg/ml trehalose; 0.4 mg/ml Tween®; pH 6.5). Integrity and purity were confirmed by SDS-PAGE and Coomassie brilliant blue staining.

2.3 Cell-based P2X7 binding assay

HEK 293 cells were transiently transfected with expression plasmids encoding the indicated proteins (eGFP, P2X1, P2X4, P2X7) using Lipofectamine 2000 (Life Technologies) according to the manufacturer's recommendations. Cells were then sequentially incubated with the indicated nanobodies, mAbH0077 and BV421-conjugated anti-mouse IgG1 antibody. For the expression controls, cells were stained with the indicated

AF647-conjugated specific mAbs (anti-mouse P2X1, P2X4, P2X7, in house). Cells were analyzed by flow cytometry (BD-FACS-Celesta).

2.4 Real-time and endpoint calcium influx and DAPI uptake assays

For the real time experiments, primary mixed glial co-cultures were loaded with 2 μ M Fluo-4 (Invitrogen) for 15 min at 37°C, washed and resuspended in PBS supplemented with Ca^{2+} and Mg^{2+} . Cells were incubated with 1 μ g of the indicated nanobodies for 20 min and after addition of DAPI, cells were analyzed by flow cytometry (BD-FACS-Canto). An infrared lamp was used to maintain a constant temperature during sample measurement. After equilibration, 0.5 mM ATP (Sigma) was added at the indicated time point (Veltkamp et al., 2022). Alternatively, Fluo-4 loaded HEK cells stably expressing mouse P2X7 were incubated with the indicated serially diluted nanobodies and stimulated with 1.5 mM ATP for 15 min. Intracellular Ca^{2+} was measured by fluorimetry on a plate reader heated at 37°C (Victor3, Perkin Elmer). For endpoint DAPI uptake assay, brain cells from nanobody-injected mice were stimulated with 0.5 mM ATP in RPMI containing DAPI, in presence or absence of 0.5 μ g of the same nanobody. Cells were washed in ice cold FACS buffer and CD11b⁺ CD45⁺ microglia were analyzed by flow cytometry.

2.5 IL-1 β release assays

Mixed glial primary co-cultures were incubated at 37°C sequentially with LPS (1 μ g/ml) for 4 h and with serial dilutions of the respective nanobodies for an additional 30 min. ATP (0.5 mM) was then added to the cells and, after 30 min of stimulation, the cells were centrifuged. IL-1 β levels were determined in the supernatants by ELISA (Biolegend).

2.6 Animals

Wild-type, P2X7^{-/-} (Labasi et al., 2002) and BAC transgenic P2X7-eGFP (line 17) (Kaczmarek-Hajek et al., 2018) mice in C57BL/6 background (8–12 weeks old) were bred in the animal facility of the University Medical Center Hamburg-Eppendorf. Animals had free access to water and standard animal chow. All animal experiments and experiments involving tissue derived from animals were performed with approval of the responsible regulatory committee (Hamburger Behörde für Justiz und Verbraucherschutz, G12/130, N006/2018, 021/18, and French Ministry of Higher Education, Research, and Innovation, APAFIS #27816). All methods were performed in accordance with the relevant guidelines and regulations.

2.7 Systemic injections of nanobodies and fluorochrome-conjugated CD45-specific mAb

Purified nanobodies were adjusted to the indicated concentrations in a sodium-phosphate buffer containing trehalose (60 mg/ml) and Tween® (0.4 mg/ml) and injected at the indicated doses either i.v. (100 µl) into the tail vein or i.c.v. (2 µl). PerCP-conjugated anti-CD45 mAb was adjusted to a concentration of 10 µg/ml, and 100 µl (1 µg) were injected into the tail vein 2–3 min before sacrifice. Mice were deeply anesthetized by isoflurane inhalation and then perfused transcardially with PBS-heparin (10 U/ml) for 4 min using a peristaltic pump at a rate of 8 ml/min. Shortly before perfusion, blood was drawn by terminal cardiac puncture. Nanobody encoding-AAV1 viral vectors were produced by Virovek, Hayward, United States (Gonde et al., 2021). For muscle transduction, mice were anesthetized and 10¹¹ viral genomes in 50 µl of PBS were injected per mouse in the gastrocnemius muscle located in the hindlimb. For CNS cell transduction, as above, 10¹¹ viral genomes of nanobody-encoding AAV1 viral vectors were administered either i.c.v. (4 µl) or intracisterna magna (i.c.m.) (20 µl) per mouse.

2.8 Preparation of microglia-astrocyte co-cultures

Neonatal C57BL6 mice were sacrificed by decapitation. Brains were dissected and the olfactory bulb, cerebellum and meninges were removed under the microscope. A cell suspension was prepared by mincing brain tissue in Hank's balanced salt solution. Cell pellets were collected and treated with 0.5 mg/ml papain (Sigma) and 0.01 mg/ml deoxyribonuclease type I (Sigma) in Hank's balanced salt solution, for 30 min at 37°C. Cells were then resuspended with BME medium supplemented with 10% FCS and filtered through a 70 µm cell strainer (EASY strainer, GBO). Cell pellets were collected, resuspended in 10% FCS BME medium and cultured in T-75 flasks (Sigma) for 21 days at 37°C with 5% CO₂.

2.9 Preparation of primary brain microglia, kidney leukocytes and splenocytes

After removal of the olfactory bulb and cerebellum, brains were cut into small 1–5 mm pieces in DMEM containing 1 mg/ml collagenase A (Roche) and 0.01 mg/ml deoxyribonuclease type I (Sigma) and incubated for 30 min at 37°C. Tissue fragments were dissociated using a 40 µm cell strainer (EASY strainer, GBO). Kidneys were cut into small 1–5 mm fragments in DMEM containing 10% fetal calf serum, 0.4 mg/ml collagenase D (Roche) and 0.02 mg/ml deoxyribonuclease

type I (Sigma) and dissociated at 37°C for 30 min using a GentleMACS apparatus (Miltenyi Biotec). Cell pellets were gently resuspended and layered onto a 30% (brain cells) or 40% (kidney cells) Percoll gradient (GE healthcare) and bands corresponding to leucocytes were collected. Spleens were minced in DMEM, 10% FCS using a 70 µm cell strainer (EASY strainer, GBO). Cells were washed and red-blood-cells were lysed using ACK erythrocyte lysis buffer (155 mM NH₄Cl, 10 mM KHCO₃, 0.1 mM EDTA, pH 7.2). After washing, cells were resuspended in FACS Buffer.

2.10 Immunofluorescence microscopy

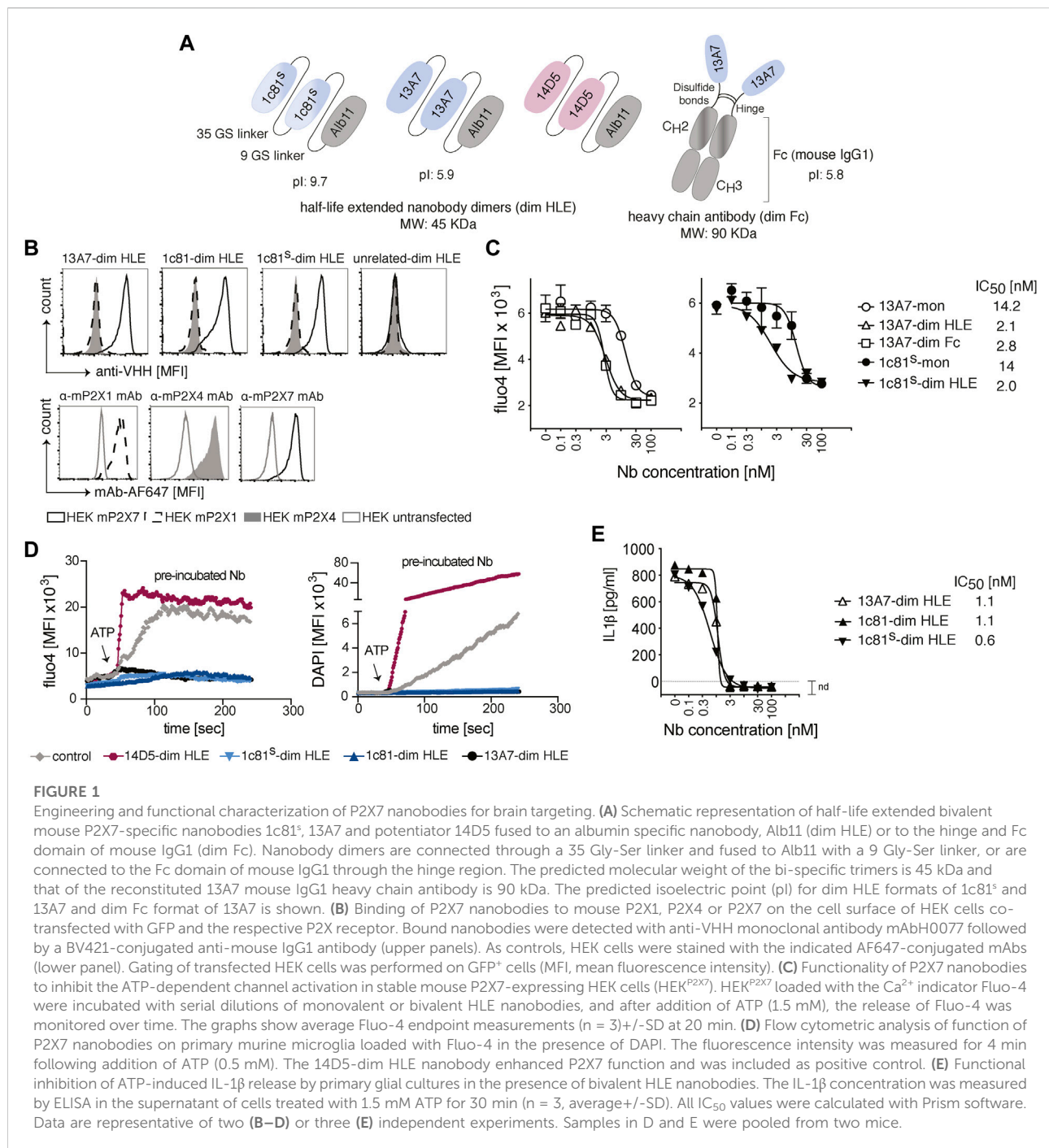
Frozen brain sections from i.c.v. injected mice (5 µm thick) were air-dried, fixed with methanol for 10 min at –20°C and washed with PBS. Autofluorescence was quenched with 50 mM NH₄Cl for 7 min at room temperature. After washing, unspecific binding was blocked with 5% BSA in PBS for 45 min at room temperature. For immunostaining, sections were rinsed with PBS and incubated with an anti-ALFA-tag nanobody-rabbit IgG in blocking solution overnight at 4°C. After washing with PBS supplement with Ca²⁺ and Mg²⁺, sections were stained with AF488-conjugated isolectin (1:100) and either a AF555-conjugated anti-rabbit IgG antibody or an AF647-conjugated anti-ALFA-tag nanobody (1:500). Sections were counterstained with Hoechst 33342 in PBS supplement with Ca²⁺ and Mg²⁺ for 45 min at room temperature and mounted with ProLongTM Gold antifade mountant (Invitrogen) on glass slides. Staining was evaluated with a THUNDER Imager 3D microscope (Leica Microsystems, Mannheim, Germany) fitted with a LED8 filter setup and a 4.2 MP sCMOS camera. Images were acquired using 40x (NA: 1.1) and 63x (NA: 1.1) objectives.

2.11 Flow cytometry

All incubations with antibodies were carried out at 4°C for 20 min, washing steps and cell-resuspension with FACS Buffer (2% BSA, 1 mM EDTA in PBS). Data was collected with a (BD-FACS-Celesta) system using Diva software, and data was analyzed using the Flowjo software (Tree Star).

2.12 Statistical analyses

All statistical analyses were performed with the SPSS package and Graph Pad Prism 5.1 software. All data are expressed as means ± SE. The student t test was used for comparison between two groups. In case of three or more groups, one-way ANOVA was used, followed by a post hoc analysis with Bonferroni's test for multiple comparisons.



3 Results

3.1 Engineering and functional characterization of nanobodies

The P2X7-specific nanobodies (Nb) used in this study were engineered as half-life extended bivalent formats of 13A7 (antagonist) (Danquah et al., 2016), a sequence optimized variant of 1c81 (antagonist) and 14D5 (allosteric enhancer)

(Danquah et al., 2016). Dimerization was conceived to increase the binding avidity and thus enhance functional potencies. The half-life extension was achieved either by C-terminal fusion to an albumin-specific nanobody Alb11 (Tijink et al., 2008) (dim HLE), or by fusion to the Fc domain of mouse IgG1 (dim Fc) (Figure 1A). Alb11 binds to the serum albumin, thereby increasing the half-life of the construct, and the Fc-region mediates a longer half-life by binding to the neonatal Fc receptor (FcRn). The molecular weight of the dim HLE format is 45 kDa and that of the dim Fc format is

90 kDa. The increase in size also contributes to half-life extension by reducing renal filtration.

Previous studies reported that anti-GFP nanobodies with an isoelectric point (pI) > 8 show enhanced passage across the BBB, likely following the adsorptive mediated transcytosis mechanism (Li et al., 2012; Li et al., 2016). Therefore, we increased the pI of 1c81 by introducing two basic amino acids in framework regions 1 and 4 (Q3K, Q122K), and fusing to the C-terminus a tandem of the highly basic SNB tag (Schaffer et al., 2010) (Figure 1A).

To verify that the sequence modification did not affect the target binding of 1c81, we analyzed by flow cytometry the binding of 1c81-dim HLE, 1c81^s-dim HLE and 13A7-dim to HEK cells co-transfected with GFP and expression constructs for either mouse P2X1, P2X4 or P2X7. All engineered nanobodies bound specifically to P2X7 but not to P2X1 and P2X4 (Figure 1B). We also confirmed that the dimerization of these nanobodies increased their blocking potency. For this we monitored the ATP-induced gating of P2X7 revealed by the influx of Ca²⁺ into HEK cells stably expressing mouse P2X7 (HEKP2X7). Fluorometric analyses of Fluo-4 loaded HEKP2X7 showed that bivalent nanobodies blocked the ATP-induced Ca²⁺ influx with 7-fold higher potencies than their monovalent counterparts (Figure 1C). Since extracellular ATP also induces large pore formation in P2X7-expressing cells, we simultaneously monitored DAPI uptake and Ca²⁺ influx in adult primary microglia by real-time flow cytometry. The results showed that 13A7-dim HLE, 1c81-dim HLE and 1c81^s-dim HLE effectively blocked, during the entire time of measurement, both ATP-induced DAPI uptake and Ca²⁺ influx in microglia. In contrast, 14D5-dim HLE enhanced both ATP-induced induced effects in microglia (Figure 1D).

ATP binding to P2X7 also triggers a K⁺ influx that activates the inflammasome to process caspase-1 (Perregaux and Gabel, 1994). In turn, active caspase-1 cleaves Gasdermin D (GSDMD) and pro-IL-1 β into mature IL-1 β . Next, the N-terminal GSDMD forms pores in the plasma membrane that mediate the release of IL-1 β (Heilig et al., 2018). To assess whether P2X7-antagonistic bivalent HLE nanobodies block IL-1 β release by microglia, we measured by ELISA the levels of IL-1 β in the supernatant of mixed primary glial cultures primed with LPS and treated with ATP. All evaluated P2X7-antagonistic bivalent HLE nanobodies (13A7-dim HLE, 1c81-dim HLE and 1c81^s-dim HLE) inhibited the release of IL-1 β from microglia in a dose dependent fashion and with high potency (Figure 1E). Taken together, these data demonstrate that ATP-induced Ca²⁺ influx, DAPI uptake and IL-1 β release by primary mouse microglia is mediated by P2X7 and that the engineered P2X7-specific nanobodies block with high potency all these effects.

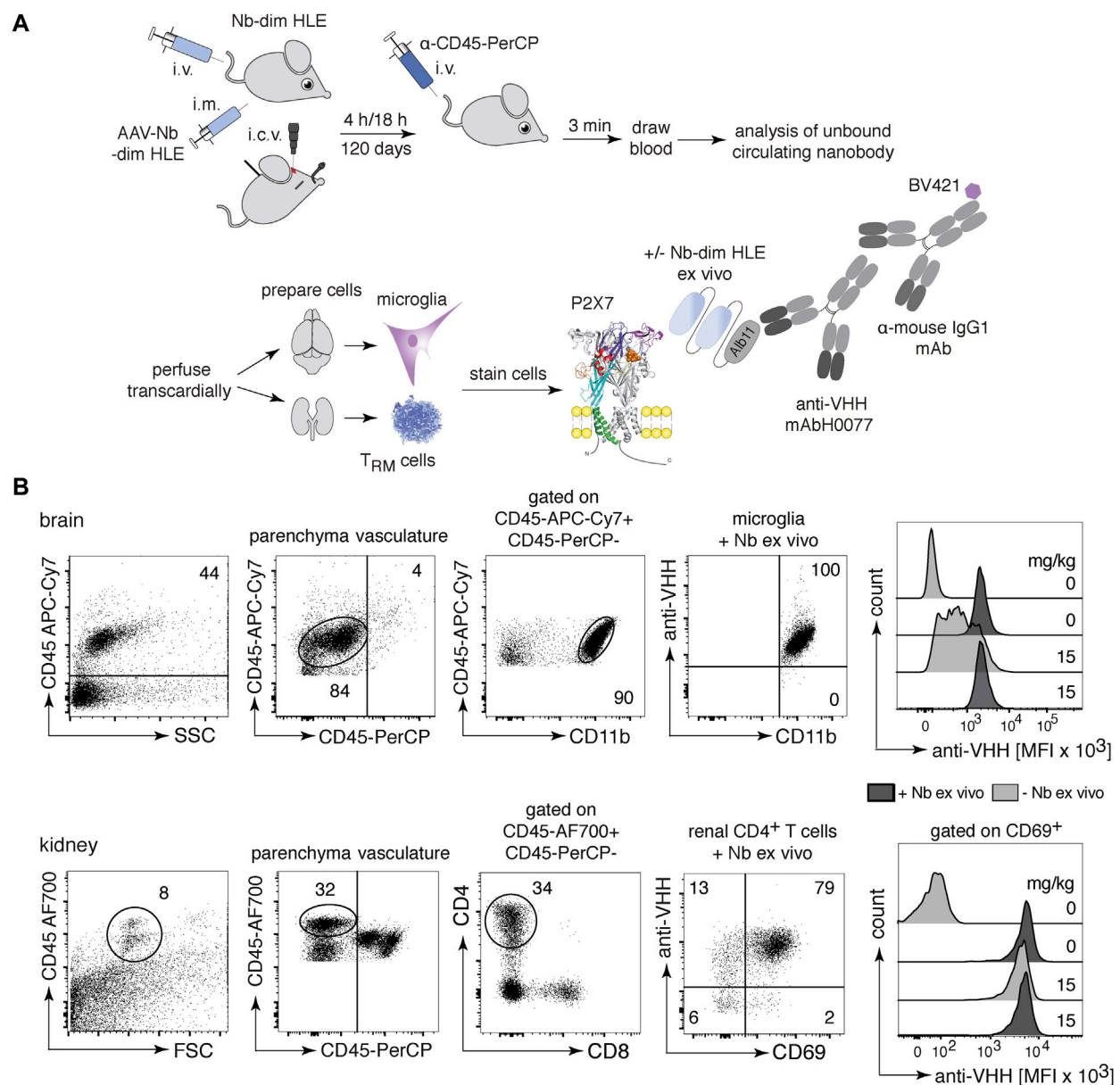
3.2 *In vivo* binding of P2X7 bivalent HLE nanobodies to immune cells in the brain and in the kidney

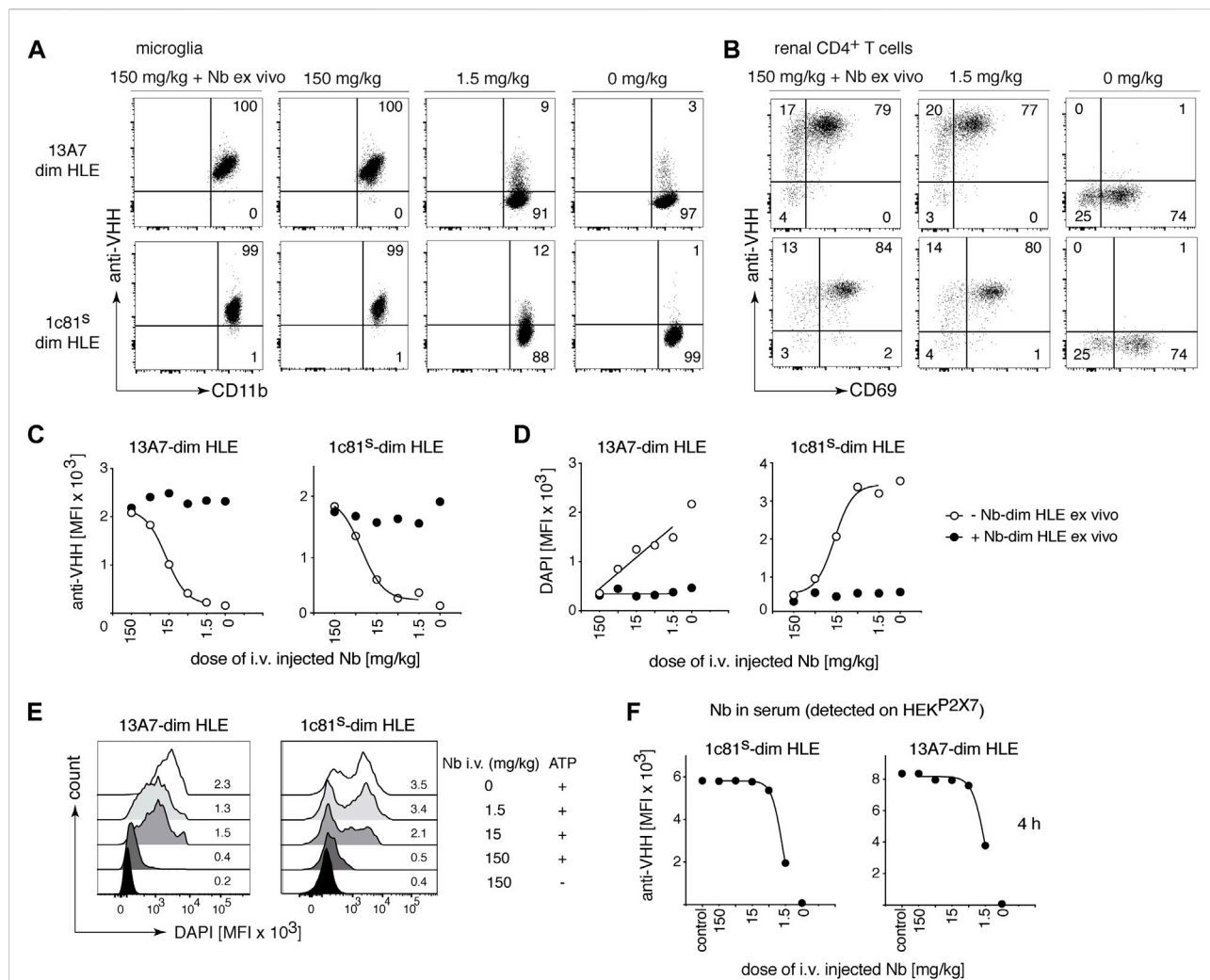
To assess the ability of P2X7-specific nanobodies to reach immune cells in various tissues following different routes of

administration, we designed a flow cytometric assay that allows detection of the injected nanobody on the cell surface of P2X7-expressing cells (Figure 2A). Briefly, purified nanobodies were injected into mice either i.v. or i.c.v. or produced endogenously after intramuscular injection of nanobody-encoding AAV. Respectively after 4 h, 18 h or 120 days of injection, we evaluated the binding of P2X7-specific nanobodies on target cells. Three minutes before sacrifice, mice were injected with a PerCP-conjugated CD45-specific mAb to label vascular immune cells and thereby distinguish them from resident cells in the parenchyma (Anderson et al., 2014). Blood samples were collected to determine the concentration of unbound soluble nanobodies in serum. Residual vascular nanobodies were removed by perfusion with PBS-heparin (Figure 2A). Cell suspensions from brain and kidney were prepared and counterstained *ex vivo* with two panels of antibodies, including a second, fluorochrome-conjugated CD45-specific mAb (Figure 2B). The degree of P2X7 occupancy achieved by the injected nanobody was analyzed on brain microglia and resident memory T cells (T_{RM}) from the kidney, two cell types known to express high levels of P2X7 (Stark et al., 2018; Borges da Silva et al., 2020) (Figure 2B). To validate this assay, we first injected i.v. 15 mg/kg of 1c81-dim HLE and analyzed the samples 4 h later. Bivalent HLE nanobodies bound to P2X7 on microglia and T_{RM}s were detected with anti-VHH mAbH0077, that binds to Alb11, followed by a BV421-conjugated mouse IgG1-specific mAb. For comparison, we determined the maximal occupancy of P2X7 by bivalent HLE nanobodies on both cell-types by incubating a separate aliquot with a saturating dose of the same nanobody construct (Figures 2A,B). The data validated the assay and demonstrated the presence of bivalent HLE nanobodies at the surface of both cell types, fully occupying P2X7 on kidney T_{RM}s and, as expected, at a lower level of occupancy on microglia (Figures 2A,B). We analyzed brain levels of bivalent HLE nanobodies for up to 7 days after i.v. injection and 28 days after i.c.v. injection. The time points shown in the following three figures correspond to those at which plateau levels of maximal P2X7 occupancy were reached in the brain.

3.3 Intravenous injection of a high dose of bivalent HLE nanobodies results in full occupancy and full blockade of P2X7 on microglia

Conventional antibodies (150 kDa), hardly penetrate the brain. In fact, only between 0.1 and 0.7% of the injected antibody dose was detected in the brain (Rubenstein et al., 2003; Abuqayyas and Balthasar, 2013; Bousquet and Janin, 2014; Bousquet et al., 2016). In case of nanobodies, it has been reported that a high pI increases brain penetration (Li et al., 2012; Li et al., 2016). To test whether the pI effect also

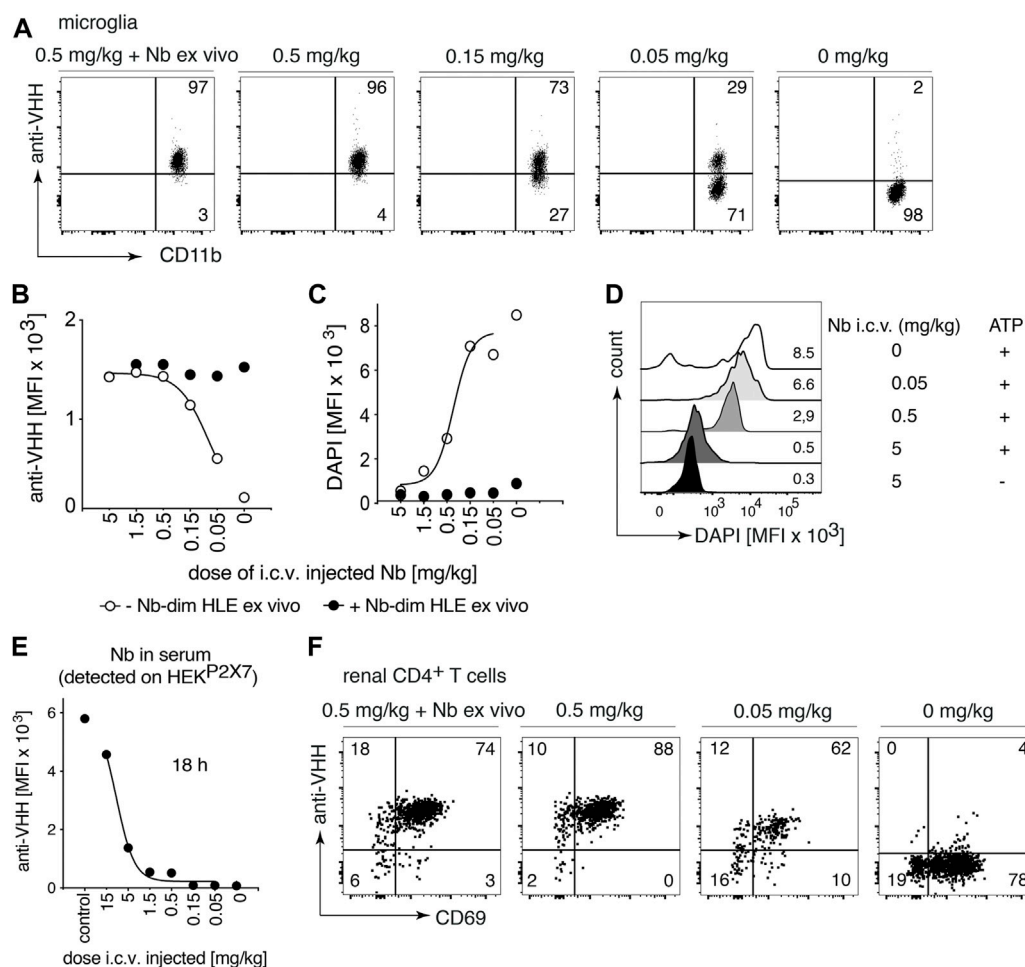


**FIGURE 3**

Full occupancy and full blockade of P2X7 on microglia is achieved by a high dose of intravenously injected P2X7 nanobodies. Titrated amounts of the indicated bivalent HLE nanobodies were injected i. v. and 4 h later the occupancy of P2X7 by the nanobody was analyzed on microglia and kidney-resident helper T cells (T_{RM} s), as described in Figure 2. Flow cytometry dot plots of microglia (A) or renal CD4⁺ T cells (B) illustrate the relative occupancy of P2X7 achieved by the indicated concentrations of i. v. injected nanobodies. The maximal target occupancy is depicted after *ex vivo* addition of a saturating dose of nanobodies (+ Nb *ex vivo*). (C) Graphs display the dose-dependent MFI of P2X7 staining on microglia obtained by i. v. injection of nanobodies (open circles); closed circles = maximal staining obtained after *ex vivo* addition of saturating nanobodies. (D) P2X7 function, as determined by the ATP-induced DAPI uptake by microglia, was assessed by flow cytometry in the absence (open circles) or presence (closed circles) of saturating nanobodies added *ex vivo*. Cells were treated with 0.5 mM ATP at 37°C for 5 min (E) MFI of DAPI is displayed here as overlaid histograms. (F) Circulating nanobodies were analyzed in the serum of injected mice. Serum (1:100) was incubated with HEK^{P2X7} and bound bivalent HLE-nanobodies were detected by anti-VHH mAb. Graphs illustrate the MFI of HEK^{P2X7} cells versus the dose of i. v. injected Nb-dim HLE. Data are representative of three (13A7-dim HLE) and five (1c81^S-dim HLE) (A–C), or three (13A7-dim HLE) and six (1c81^S-dim HLE) (D–F) independent experiments. Dot plots shown are from a single mouse. An independent experiment refers to an experiment with a single mouse per condition, in which all mice were analyzed on the same day.

modulates the BBB crossing of bivalent HLE nanobodies, mice were administered i.v. with P2X7 nanobodies with a high pI (1c81^S-dim HLE) or a low pI (13A7-dim HLE) in serially titrated doses from 150 mg/kg to 1.5 mg/kg. Four hours later, nanobody binding to P2X7 on microglia in the brain (Figure 3A) and T_{RM} s in the kidney (Figure 3B) was analyzed. Both nanobodies bound to cell-surface P2X7 on microglia in a dose dependent manner (Figures 3A,C), reaching full occupancy of P2X7 on microglia

only with the highest dose (150 mg/kg) (Figures 3A,C). Following injection of the lowest dose of 1.5 mg/kg, bivalent HLE nanobodies were barely detectable on microglia. In contrast, this low dose was sufficient to fully occupy P2X7 on T_{RM} cells within 4 h after injection (Figure 3B). These results show that the pI of a bivalent HLE nanobody does not appear to be a critical determinant for brain penetration, and that penetration into the brain parenchyma requires >100-fold higher doses of i.v. injected

**FIGURE 4**

Full occupancy of P2X7 on microglia is achieved after an i.c.v. injection of a low dose of P2X7 nanobody. Titrated amounts of bivalent HLE nanobody 1c81⁺-dim HLE were injected i. c.v. and 18 h later the occupancy of P2X7 by the nanobody was analyzed on microglia and kidney-resident helper T cells (T_{RM}), as described in Figure 2. Flow cytometry dot plots of microglia (**A**) or renal CD4⁺ T cells (**F**) illustrate the relative occupancy of P2X7 achieved by the indicated concentrations of i. c.v. injected nanobodies versus the maximal occupancy achieved after *ex vivo* addition of saturating nanobodies (+ Nb *ex vivo*). (**B**) Graph displays the dose-dependent MFI of P2X7 staining on microglia obtained by i.c.v. injection of nanobodies (open circles); closed circles = maximal staining obtained after *ex vivo* addition of saturating nanobodies added *ex vivo*. (**C**) P2X7 function, as determined by the ATP-induced uptake of DAPI by microglia, was assessed by flow cytometry in the absence (open circles) or presence (closed circles) of saturating nanobodies added *ex vivo*. (**D**) MFI of DAPI displayed as overlaid histograms. (**E**) The presence of circulating nanobodies was evaluated in the serum of injected mice. Bivalent HLE-nanobodies in serum (1:100) bound to HEK^{P2X7} cells were detected by anti-VHH mAb. Graphs illustrate the MFI of HEK^{P2X7} cells versus the dose of i.c.v. injected Nb-dim HLE. Data are representative of four (**A,B** and **F**) or five independent experiments (**C–E**). Dot plots shown are from a single mouse. An independent experiment refers to an experiment with a single mouse per condition, in which all mice were analyzed on the same day.

nanobodies than those required to penetrate into the kidney parenchyma.

To evaluate the capacity of the *in vivo*-bound bivalent HLE nanobodies to block gating of P2X7 on microglia, brain cells were incubated with ATP in the presence of DAPI and the ATP-induced uptake of DAPI by microglia was measured by flow cytometry (Figure 3D). The results show a dose dependent inhibition of ATP-induced DAPI uptake by microglia (Figures 3D,E). Only the highest injected dose (150 mg/kg) achieved almost complete blockade of P2X7-mediated DAPI uptake (Figures 3D,E).

The serum levels of bivalent HLE nanobodies 4 h after i.v. administration was determined by flow cytometry assay on stable HEK-mouse P2X7 cells (HEK^{P2X7}) (Figure 3F). The results revealed that the level of unbound nanobodies in the serum of mice that had received doses higher than 5 mg/kg saturated all available P2X7 on HEK^{P2X7} cells, whereas the serum of mice that had received 1.5 mg/kg showed ~2-fold lower levels of unbound nanobodies (Figure 3F). ELISA analyses (Supplementary Figure S1A) indicate that the concentration of unbound bivalent HLE nanobodies circulating in serum at 4 h correlate with the injected

dose (Supplementary Figure S1B), revealing that approximately 60% of the injected dose was still circulating in serum 4 h after injection.

3.4 Intracerebroventricular injection of a low dose of bivalent HLE nanobodies results in full occupancy and full blockade of P2X7 on microglia

The BBB restricts the access of i.v. administered nanobodies to cells within the CNS. It has been shown that the i.c.v. route of administration was efficient to deliver nanobodies to their target throughout the brain (Gomes et al., 2018). To evaluate whether P2X7 nanobodies bind to their target on microglia following i.c.v. injection, we carried out a dose response analysis with 1c81^s-dim HLE (Figure 4). Doses from 5 mg/kg to 0.05 mg/kg were injected in a small volume (2 µl) into a cerebral ventricle and 18 h later, binding of nanobodies to P2X7 on microglia was analyzed. The results show that a dose of 0.5 mg/kg of bivalent HLE nanobodies achieved full occupancy of P2X7 on the surface of microglia, and even the low dose of 0.15 mg/kg results in almost complete P2X7 occupancy on microglia (Figures 4A,B). A dose of 5 mg/kg sufficed to fully block ATP-induced DAPI uptake by microglia (Figures 4C,D).

To determine whether i.c.v. injected bivalent HLE nanobodies had leaked into peripheral circulation, the level of nanobodies in serum was determined indirectly by staining HEK^{P2X7} cells with these sera. The results show detectable nanobody levels in circulation which, however, do not suffice to fully occupy P2X7 on HEK^{P2X7} cells (Figure 4E). The determination of the concentration of circulating bivalent HLE nanobodies by ELISA (Supplementary Figure S1A) showed that approximately 10–30% of the injected dose was detected in serum 18 h after i.c.v. injection (Supplementary Figure S1C).

To determine whether nanobodies that had leaked into peripheral circulation also reached P2X7 on the cell surface of parenchymal T cells of the kidney, renal T_{RM} cells were analyzed for occupancy of P2X7 18 h after i.c.v. administration of 1c81^s-dim HLE (Figure 4F). The results show full occupancy of P2X7 on T_{RM} cells of the kidney after injection of doses starting at 0.5 mg/kg and higher, and a substantial occupancy already after an injection of 0.05 mg/kg (Figure 4F).

3.5 P2X7 nanobodies are detected on the cell surface of microglia on brain sections 24 h after i.c.v. administration

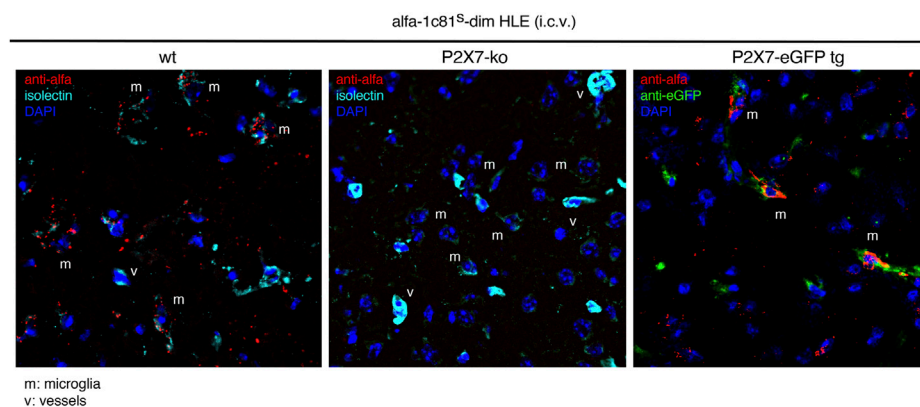
We next set out to directly visualize on brain sections the occupancy of P2X7 on the cell surface of microglia after i.c.v. injection of bivalent HLE nanobodies. Since the mAbH0077-based detection system did not yield signals in fluorescence microscopy, we

constructed a bivalent HLE nanobody bearing at the N-terminus the ALFA-tag (Gotzke et al., 2019). The ALFA-tagged 1c81^s-dim HLE nanobody was injected i.c.v. to mice (1.5 mg/kg), and 24 h later P2X7-bound nanobodies were detected *via* their ALFA-tag with an ALFA-specific nanobody. As controls we injected N-ter tagged 1c81^s-dim^s HLE into P2X7-deficient mice (Labasi et al., 2002) and P2X7-transgenic mice that overexpress a P2X7-eGFP fusion protein under the control of the endogenous P2X7 promotor (Kaczmarek-Hajek et al., 2018) (Figure 5). Our findings show that 1c81^s-dim HLE bound to the cell surface of microglia on brain cryosections of wt mice but not that of P2X7^{-/-} mice (Figure 5). Moreover, sections of P2X7-eGFP transgenic mice showed colocalization of P2X7-eGFP with the injected nanobody on microglia (Figure 5). These results confirm that the i.c.v. injection route efficiently delivers P2X7-targeting nanobodies to microglia.

3.6 A low dose of i.c.v. injected bivalent HLE nanobodies suffices to rapidly and durably occupy and block P2X7 on microglia

To study the kinetics of P2X7 occupancy on microglia by 1c81^s-dim HLE after i.c.v. administration, we injected i.c.v. into mice 1.5 mg/kg of this nanobody in 2 µl, and analyzed P2X7 occupancy by flow cytometry at different time points from 10 min to 28 days (Figure 6). The results show, that 1c81^s-dim HLE already completely occupied all available P2X7 on microglia within 10 min after injection (Figures 6A,C). P2X7 on microglia remained fully occupied by 1c81^s-dim HLE until day 3. A steady decrease in the occupancy of microglial P2X7 by 1c81^s-dim^s HLE was observed in the following 2 weeks until it reached a plateau at day 21 (Figures 6A,C). Because we had previously observed that i.c.v. injected 1c81^s-dim HLE leaked into systemic circulation and reached P2X7 on the cell surface of T_{RM} cells in the kidney (Figure 4F), we analyzed P2X7 occupancy by the injected nanobody on these cells at the indicated time points. The results show that little if any 1c81^s-dim HLE had reached P2X7 on the cell surface of kidney T_{RM}s within 10 min after i.c.v. injection (Figures 6B,D). However, within the next hour, 1c81^s-dim HLE leaked into peripheral circulation, reaching full occupancy of P2X7 on T_{RM} cells at 80 min after i.c.v. injection (Figures 6B,D). Subsequently, occupancy of P2X7 on T_{RM}s declined much faster than that of P2X7 on microglia (Figures 6C,D). By day 14, P2X7 occupancy on T_{RM}s had already diminished to a low level suggesting that most of the nanobody had been cleared from the circulation (Figures 6B,D). Controls showing the *ex vivo* staining with saturating amounts of nanobodies, indicate that the levels of cell surface P2X7 remained high during the entire duration of the experiment (Figures 6C,D).

Our findings demonstrated that a single i.c.v. injection of 30 µg 1c81^s-dim HLE leads to rapid and long-term occupancy of P2X7 on microglia (Figures 6A,C). Consistently, a long-term

**FIGURE 5**

Detection of P2X7 nanobodies bound to the cell surface of microglia on brain sections. Target binding of 1c81^s-dim HLE nanobody on brain cryosections was determined 24 h following i. c.v. injection of a low dose of 0.5 mg/kg in wildtype mice. P2X7-deficient mouse and a P2X7-eGFP transgenic mouse expressing high levels of P2X7-eGFP fusion protein were used as controls. For this experiment an ALFA-tagged version of 1c81^s-dim HLE nanobody has been used, allowing detection on brain sections with an ALFA-specific nanobody (red). Microglia are stained with isolectin (cyan) and P2X7-eGFP with an eGFP-specific mouse monoclonal antibody (mAb) (green). (v) point to blood vessels brightly stained with isolectin and (m) shows microglial cells weakly stained with isolectin. Data are representative of two independent experiments. Dot plots shown are from a single mouse. An independent experiment refers to an experiment with a single mouse per condition, in which all mice were analyzed on the same day.

blockade of ATP-induced DAPI-uptake by microglia was observed up to 17 days after i.c.v. injection (Figure 6E).

In addition, the level of 1c81^s-dim HLE in serum was determined by staining of HEK^{P2X7} with sera of the injected mice (Figure 6F). The results confirmed that nanobodies were barely detectable in serum at 10 min after i.c.v. injection, but subsequently the nanobodies leaked into systemic circulation reaching maximum levels in serum at 40 min after i.c.v. injection. After this time point, the amount of 1c81^s-dim HLE in serum progressively decreased until it was no longer detectable after day 10 (Figure 6F). Notably, the levels of 1c81^s-dim HLE detected in serum show a similar time course of appearance and clearance as the levels of P2X7 occupancy on renal T_{RM} cells, with nanobody levels in serum peaking a few minutes earlier than on T_{RM}s (Figures 6D,F).

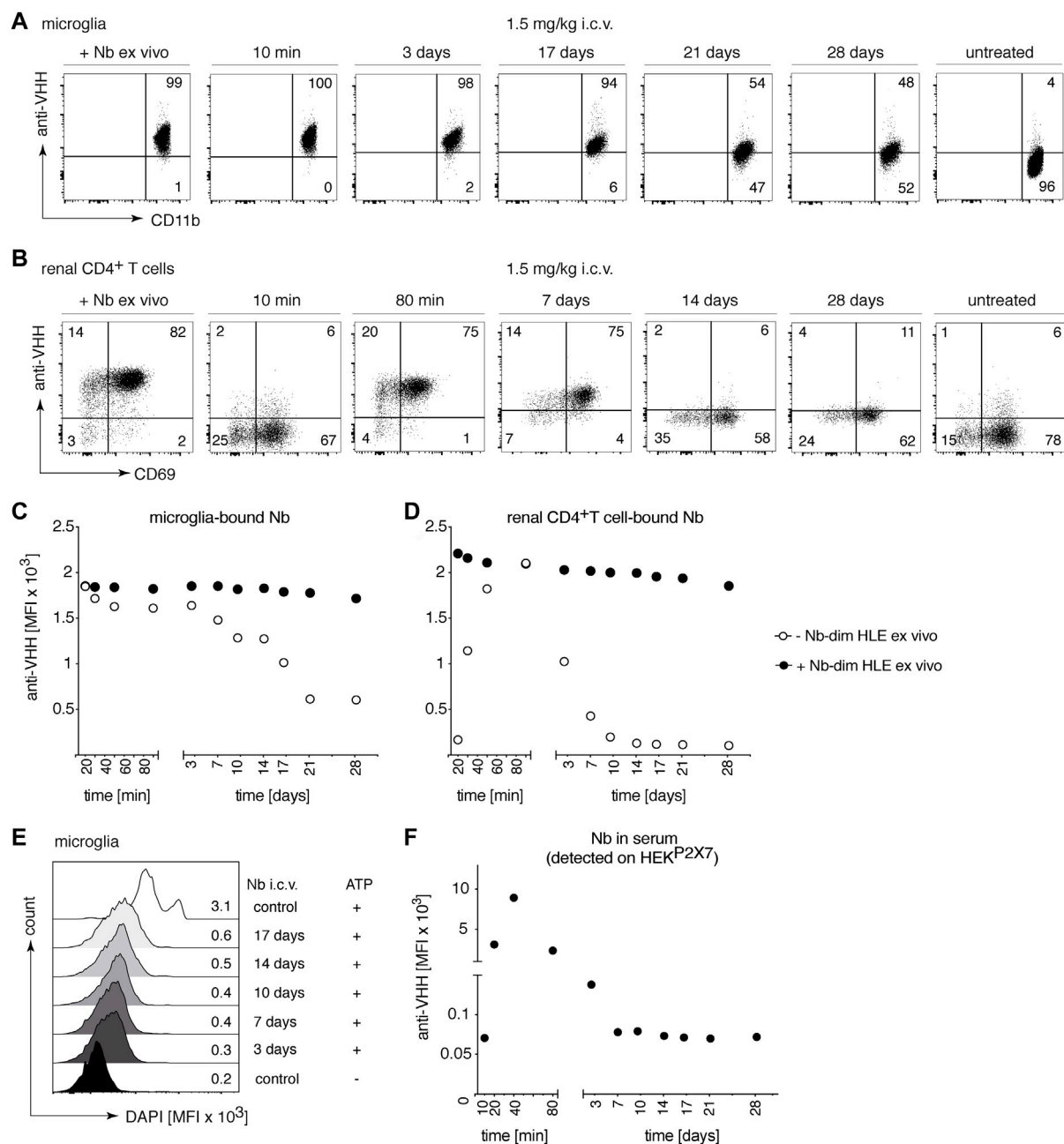
3.7 Intracerebral injection of an AAV1 encoding 13A7-dim Fc results, 28 days later, in a complete functional blockade of P2X7 on microglia and splenic T cells

We have recently shown that AAV-mediated *in vivo* delivery of nanobody-encoding genes is an effective alternative route for nanobody administration, i.e., by endogenous production of nanobodies by AAV transduced muscle cells (Gonde et al., 2021). To determine whether nanobodies endogenously produced in the brain can reach P2X7 on the surface of microglia, we injected i.c.v or intracisterna magna (i.c.m.) an

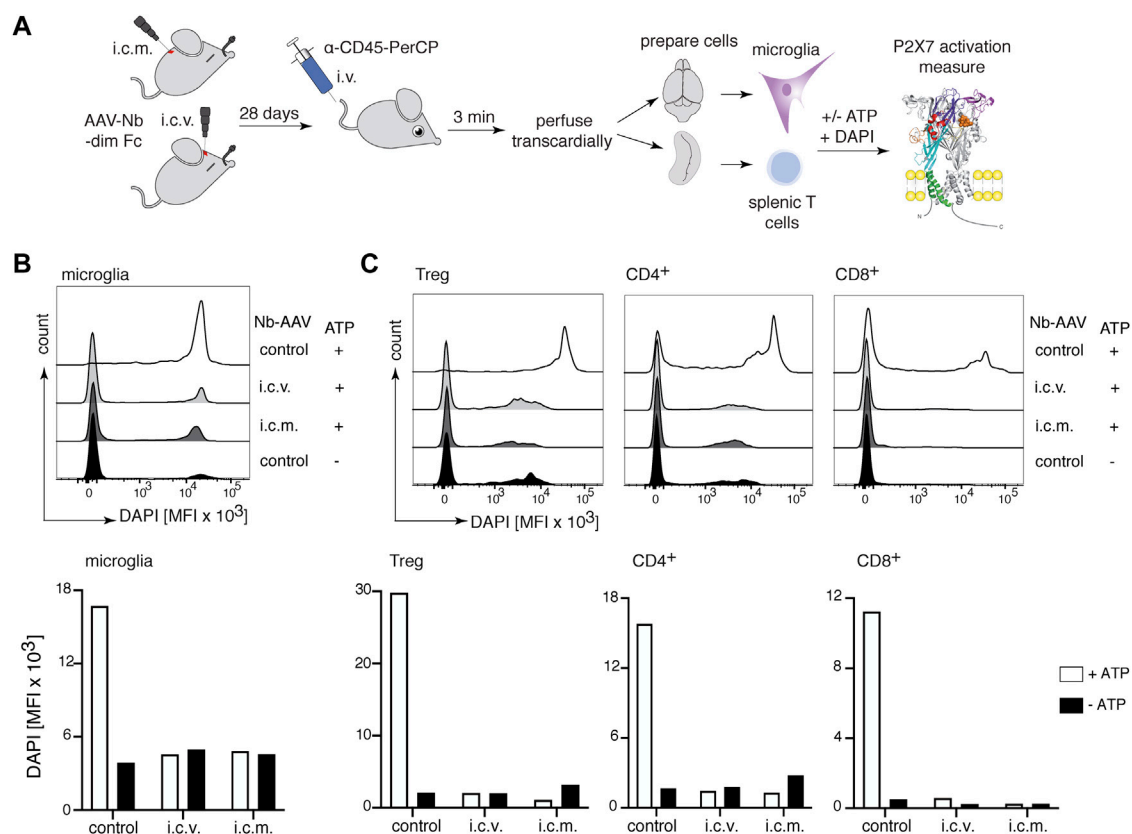
AAV1 vector coding for the P2X7-blocking 13A7-dim Fc (Figure 1A) (Gonde et al., 2021). P2X7 blockade of DAPI-uptake was evaluated on microglia 28 days after injection of AAV1 coding for 13A7-dim Fc (Figure 7A). The results show a marked ATP-induced uptake of DAPI by microglia of control animals but not of mice injected with AAV1 coding for 13A7-dim Fc (Figure 7B). Similar effects were observed for splenic T cells (Figure 7C), indicating that nanobodies that were produced in the brain had also entered the circulation and reached the spleen. These results reveal the ability of the AAV1 to transduce cells within the CNS, which mediated the *in vivo* production and delivery of nanobodies both locally to microglia in the CNS and systemically to T cells in the spleen.

3.8 Complete P2X7 inhibition on microglia was achieved 120 days after i.m. injection of AAV1-encoding 13A7-dim Fc, and almost full P2X7 occupancy after injection of AAV1-encoding 13A7-dim HLE

Since our results indicate that a very high systemic dose of nanobodies (150 mg/kg) is required to detect effective brain uptake, we next sought to determine the effect of long-term endogenous production of nanobodies by AAV-transduced muscle cells. We injected into the gastrocnemius muscle AAV1 coding for P2X7 nanobodies in two bivalent formats, 13A7-dim HLE and 13A7-dim Fc (Figure 1A). The level of P2X7 occupancy by the endogenously produced nanobody-construction was analyzed on microglia and T_{RM} cells of the

**FIGURE 6**

Long-term occupancy and blocking of P2X7 on microglia are achieved after a single i.c.v. injection of a low dose of P2X7 nanobody. Mice were injected i.c.v. with 1.5 mg/kg 1c81st-dim HLE in 2 μ l volume. At the indicated time points, the occupancy of P2X7 by the nanobody was analyzed on microglia and kidney-resident helper T cells (T_{RM}), as described in Figure 2. Flow cytometry dot plots of microglia (A) or renal CD4⁺ T cells (B) illustrate the relative occupancy of P2X7 achieved at the indicated time points after i.c.v. injection of nanobodies versus the maximal occupancy achieved after *ex vivo* addition of saturating nanobodies (+ Nb *ex vivo*). Graphs display the time-dependent MFI of P2X7 staining on microglia (C) and renal CD4⁺ T cells (D) obtained by i.c.v. injection of nanobodies (open circles); closed circles = maximal staining obtained after *ex vivo* addition of saturating nanobodies. (E) P2X7 function, as determined by the ATP-induced DAPI uptake by microglia, was assessed by flow cytometry. Histograms display the MFI of DAPI uptake by microglia. (F) The presence of circulating nanobodies was evaluated in the serum of injected mice. Bivalent HLE nanobodies in serum (1:100) bound to HEK^{P2X7} cells were detected by anti-VHH mAb. Graph illustrates the MFI of HEK^{P2X7} cells versus the time after i.c.v. injection of Nb-dim HLE. Data are representative of five (A–D and F) or four independent experiments (E). Dot plots shown are from a single mouse. An independent experiment refers to an experiment with a single mouse per condition, in which all mice were analyzed on the same day.

**FIGURE 7**

Complete inhibition of P2X7 on microglia and splenic T cells 28 days after intracerebral injection of P2X7 nanobody-encoding AAV1. **(A)** Mice were injected into the brain either i.c.v. or intracisterna magna (i.c.m.) with 10^{11} viral genomes of an AAV1 vector coding for 13A7-dim Fc (Figure 1). After 28 days, P2X7 function, as determined by the ATP-induced DAPI uptake by microglia and splenic T cells, was analyzed by flow cytometry. Histograms show the MFI of DAPI uptake by microglia **(B)** or splenic Tregs and conventional CD4⁺ and CD8⁺ T cells **(C)**. Below, bar diagrams illustrate the ATP-induced DAPI uptake by the indicated cell population of AAV1-injected mice or control mice. Data are representative of two independent experiments. Dot plots shown are from a single mouse. An independent experiment refers to an experiment with a single mouse per condition, in which all mice were analyzed on the same day.

kidney 120 days after AAV-transduction (Figure 8). The results show that 13A7-dim HLE had achieved a substantial coverage of P2X7 on microglia (Figure 8A) and complete P2X7 occupancy on kidney T_{RM} cells (Figure 8B). Consistently, the sustained *in vivo* expression of 13A7-dim HLE led to a significant, albeit only partial blockade of ATP-induced DAPI-uptake by microglia. Interestingly, endogenously produced 13A7-dim Fc completely blocked P2X7 function on microglia (Figure 8C). In addition, levels of 13A7 dim-HLE in serum were analyzed indirectly by staining of HEK^{P2X7} cells with sera from AAV-transduced mice (Figure 8D) and by ELISA (Supplementary Figure S1A,D). The results indicate that the serum contained saturating amounts of antibodies even after 120 days of i.m. injection of nanobody encoding AAV. Together, AAV1-nanobody delivery in the muscle provides sufficient high systemic levels of nanobodies to reach P2X7 on the cell surface of microglia in the brain.

4 Discussion

In the present study we show that P2X7 expressed on the cell surface of microglia can be effectively targeted by intracerebroventricular injection of P2X7 antagonistic nanobodies, as well as by the AAV-mediated endogenous production of such nanobodies after intracerebral or intramuscular injection of nanobody-encoding AAV1.

We evaluated the brain delivery of P2X7-antagonistic nanobodies to target microglia in the brain using different routes of administration: i.v., i.c.v. and the AAV-mediated endogenous production of nanobodies after transduction of brain or muscle cells with nanobody-encoding AAVs. Two antagonistic and well characterized anti-P2X7 nanobodies were used in this study, 13A7 and 1c81, which have similar blocking potencies (Danquah et al., 2016). Bivalent formats with extended serum half-life were used, generated either by

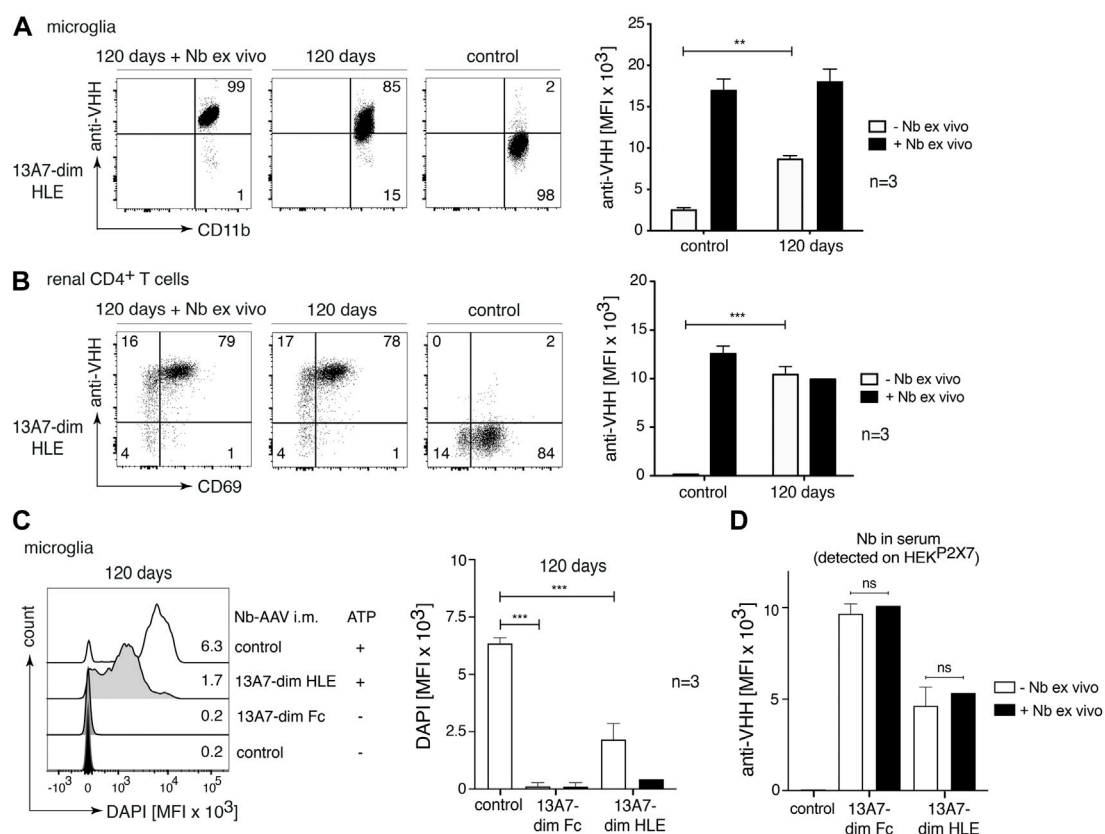


FIGURE 8

Near complete target occupancy and complete P2X7 inhibition on microglia 120 days after i.m. injection of AAV1 vectors coding for P2X7 nanobodies. Mice were injected i.m. with 10¹¹ viral genomes of AAV1 coding for 13A7-dim HLE and 13A7-dim Fc. After 120 days, the occupancy of P2X7 by the nanobodies was analysed on microglia and kidney-resident helper T cells (T_{RM}s), as described in Figure 2. Flow cytometry dot plots of microglia (A) or renal CD4⁺ T cells (B) illustrate the relative occupancy of P2X7 at 120 days after i.m. injection of AAV1-Nb versus the maximal occupancy achieved after *ex vivo* addition of saturating nanobodies (+ Nb *ex vivo*). Bar diagrams illustrate the occupancy of P2X7 on microglia (A) and renal CD4⁺ T cells (B) obtained from AAV1-Nb injected and control mice (n = 3/group). (C) P2X7 function, as determined by the ATP-induced uptake of DAPI by microglia, was assessed by flow cytometry. Bar diagrams illustrate DAPI uptake by microglia from three AAV1-Nb injected and three control mice in the absence (- Nb *ex vivo*) or presence (+ Nb *ex vivo*) of saturating nanobodies added *ex vivo*. (D) Circulating nanobodies were measured in the serum of transduced mice. Serum (1:100) was incubated with HEK^{P2X7} cells. Bound 13A7-dim HLE nanobodies were detected by anti-VHH mAb and BV421-conjugated IgG1-specific mAb, and bound 13A7-dim Fc nanobodies by BV421-conjugated IgG1-specific mAb. Bar diagrams illustrate the MFI of HEK^{P2X7} cells from AAV1-Nb injected and control mice (n = 3/group). Dot plots shown are from a single mouse. An independent experiment refers to an experiment with a single mouse per condition, in which all mice were analyzed on the same day.

fusion to the hinge and Fc domain of mouse IgG1, or by fusion to an albumin-specific nanobody. The intravenous route is the easiest to translate to the clinic but also proved to be the least effective. Very high amounts of nanobodies were necessary to achieve coverage of P2X7 on microglia. The i.c.v. route was most effective, achieving rapid and long-term coverage of P2X7 on microglia after injection of very low doses. However, as a highly invasive procedure, this would be restricted to exceptional cases in the clinic. A single injection of nanobody encoding AAV1 into either the skeletal muscle or the cerebrospinal fluid also provided effective and long-term delivery of P2X7-blocking nanobodies to microglia in the brain. A major problem of this mode of application is the difficulty to control the levels

and duration of antibody production *in vivo*. Moreover, due to the induction of a host antibody response directed against the AAV capsid, this mode of application is limited, at best, to a single injection per AAV serotype.

It is well known that the BBB restricts the passage of intravenously injected therapeutic proteins from the circulation into the brain. Preclinical studies in mice showed that only a small fraction of antibodies reaches the brain after intravenous injection (e.g., 0.7% of the injected dose of 8 mg/kg) (Abuqayyas and Balthasar, 2013). In humans treated intravenously with therapeutic antibodies trastuzumab or rituximab, the concentrations in the cerebrospinal fluid reached around 0.1–0.2% of the serum concentration (Rubenstein et al., 2003; Bousquet and Janin, 2014). In

addition, it has been shown that the access to the brain of systemically administered anti-rabies nanobodies is dependent on the dose and the half-life of the nanobody construct. Thus, a high dose (75 mg/kg) of intraperitoneally injected half-life extended rabies nanobodies rescued mice from disease (Terry et al., 2014). Our results are consistent with these studies. We showed that intravenously injected nanobodies required a very high dose (150 mg/kg) in order to effectively cover P2X7 on microglia within the brain parenchyma. Previous studies reported that nanobodies with a high pI show better translocation into the brain than the corresponding variants with a lower pI (Li et al., 2012; Li et al., 2016). However, in the case of the high pI nanobody 1c81^s, intravenous injections did not result in an improved access to microglial cells in the brain parenchyma. A possible explanation for the discrepancy between our and previous findings could be the different sizes of the nanobody constructs that were used, i.e., monomeric nanobodies (15 kDa) (Li et al., 2012; Li et al., 2016), three times smaller than those used in our study (bivalent half-life extended nanobodies, 45 kDa). Fusion of the P2X7-blocking nanobodies to a ligand for a receptor or molecule that induce transcytosis across the BBB would be a conceivable option for improving brain uptake of systemically injected proteins, e.g., fusion to a transferrin receptor binding agent (Niewoehner et al., 2014; Haqqani et al., 2018; Wouters et al., 2020; Stocki et al., 2021).

As expected, using the intracerebroventricularly route, a 100-fold lower dose of 1c81^s-dim HLE (0.5 mg/kg) was sufficient to achieve complete occupancy and blockade of P2X7, which lasted up to 3 weeks after injection. Notably, 10 min after i.c.v. injection, P2X7 was already completely occupied on microglial cells in the brain. Interestingly, we found that i.c.v. injected nanobodies also bound to P2X7 on peripheral parenchymal CD4⁺ T cells of the kidney, indicating that the i.c.v. injected nanobody rapidly reached the blood circulation. Renal parenchymal CD4⁺ T cells revealed complete occupancy of P2X7 by the i.c.v. injected nanobody within 80 min, which lasted up to 7 days.

Furthermore, and consistent with the observed relatively low levels of circulating nanobodies in serum, the occupancy of P2X7 by the injected nanobody faded more rapidly on parenchymal renal CD4⁺ T cells than on microglia. These findings are consistent with the notion that proteins are cleared from the CSF to blood circulation *via* arachnoid projections and lymphatic vessels (Ma et al., 2017; Hladky and Barrand, 2018).

Finally, our study evaluated the capacity of endogenously produced nanobodies to reach P2X7 on microglia. In a previous study we had shown that AAV-mediated delivery of nanobody-encoding genes into the skeletal muscle results in long term endogenous production of nanobodies by the AAV-transduced muscle cells (Gonde et al., 2021). Here we show that a single injection of a heavy chain antibody-encoding AAV1 into the intracerebral ventricle or the cisterna magna results in an efficient production of the antibodies in the brain, leading to a full functional blockade of P2X7 within at least 28 days. Moreover, even a single

intramuscular injection of AAV1 coding for 2 different formats of P2X7 nanobodies (dim-Fc or dim-HLE) achieved a strong functional blockade of P2X7 on microglia 120 days after transduction. The slightly more effective blockade achieved by the heavy chain antibody (dim-Fc) in comparison to the bivalent-HLE (dim-HLE) could reflect differences in endogenous production or longer serum half-life in mice.

In conclusion, our data provide new and deeper insights into the conditions (route, dose, and time of administration) for nanobody-mediated targeting of P2X7 on microglia. Our results suggest that, in particular, the nanobody-encoded AAV delivery, either intracerebral or intramuscular, could be a promising new therapeutic strategy for the treatment of sterile brain inflammation.

Data availability statement

The original contributions presented in the study are included in the article/Supplementary Material, further inquiries can be directed to the corresponding author.

Ethics statement

The animal study was reviewed and approved by Hamburger Behörde für Justiz und Verbraucherschutz: G12/130, N006/2018, 021/18 and French Ministry of Higher Education, Research, and Innovation: APAFIS #27816.

Author contributions

FK-N, CP-E designed the study. CP-E, CG, BR, MW, EJ, NS, MJ, NL, NW, CS, Y-VT, and SA conducted the experiments. All authors contributed to the planning and the analysis of the study. CP-E and FK-N wrote the manuscript.

Funding

This study was supported by grants from the Deutsche Forschungsgemeinschaft as parts of the Forschergruppe 2879 (A1 to TM and FK-N), the Sonderforschungsbereich 1192 (B5 to FK-N and NW), the Sonderforschungsbereich 1328 (Project-ID: 335447717, Z02 to FH, BR and FK-N, A15 to AN) and a tandem DFG/ANR grant (No310-13 to FKN and ANR-18-CE92-0046 to SA).

Acknowledgments

The authors thank Gudrun Dubberke, Fabienne Seyfried and Natalie Tode, Institute of Immunology, and Jasmin

Pabla, Karolyn Gustmann and Oliver Schnapauff, Department of Neurology for their excellent technical assistance with production and purification of recombinant nanobodies, and in the handling of mice. The authors thank Prof. Victor Puelles and his group, UKE III. Medical Department, for access and technical assistance with the Thunder Imager 3D microscope, and the UKE Microscopy Imaging Facility, for assistance with image editing. The authors thank Prof. Eva Tolosa, Institute of Immunology, and Prof. Victor Puelles for critical review of the manuscript.

Conflict of interest

FK-N and CS are co-inventors of a patent covering P2X7-antagonistic nanobodies.

The remaining authors declare(s) that the research was conducted in the absence of any commercial or financial

relationships that could be construed as a potential conflict of interest.

Publisher's note

All claims expressed in this article are solely those of the authors and do not necessarily represent those of their affiliated organizations, or those of the publisher, the editors and the reviewers. Any product that may be evaluated in this article, or claim that may be made by its manufacturer, is not guaranteed or endorsed by the publisher.

Supplementary material

The Supplementary Material for this article can be found online at: <https://www.frontiersin.org/articles/10.3389/fphar.2022.1029236/full#supplementary-material>

References

- Abuqayyas, L., and Balthasar, J. P. (2013). Investigation of the role of FcγR and FcRn in mAb distribution to the brain. *Mol. Pharm.* 10, 1505–1513. doi:10.1021/mp300214k
- Anderson, K. G., Mayer-Barber, K., Sung, H., Beura, L., James, B. R., Taylor, J. J., et al. (2014). Intravascular staining for discrimination of vascular and tissue leukocytes. *Nat. Protoc.* 9, 209–222. doi:10.1038/nprot.2014.005
- Andrejew, R., Oliveira-Giacomelli, A., Ribeiro, D. E., Glaser, T., Arnaud-Sampaio, V. F., Lameu, C., et al. (2020). The P2X7 receptor: central hub of brain diseases. *Front. Mol. Neurosci.* 13, 124. doi:10.3389/fnmol.2020.00124
- Bartlett, R., Stokes, L., and Sluyter, R. (2014). The P2X7 receptor channel: recent developments and the use of P2X7 antagonists in models of disease. *Pharmacol. Rev.* 66, 638–675. doi:10.1124/pr.113.008003
- Bhattacharya, A., and Biber, K. (2016). The microglial ATP-gated ion channel P2X7 as a CNS drug target. *Glia* 64, 1772–1787. doi:10.1002/glia.23001
- Borges da Silva, H., Peng, C., Wang, H., Wanhainen, K. M., Ma, C., Lopez, S., et al. (2020). Sensing of ATP via the purinergic receptor P2RX7 promotes CD8+ trm cell generation by enhancing their sensitivity to the cytokine TGF-β. *Immunity* 53, 158–171. doi:10.1016/j.immuni.2020.06.010
- Bousquet, G., Darrouzain, F., de Bazelaire, C., Ternant, D., Barranger, E., Winterman, S., et al. (2016). Intrathecal trastuzumab halts progression of CNS metastases in breast cancer. *J. Clin. Oncol.* 34, e151–e155. doi:10.1200/JCO.2012.44.8894
- Bousquet, G., and Janin, A. (2014). Passage of humanized monoclonal antibodies across the blood-brain barrier: relevance in the treatment of cancer brain metastases? *J. Appl. Biopharm. Pharmacokinet.* 2, 50–58. doi:10.14205/2309-4435.2014.02.02
- Boutin, H., LeFeuvre, R. A., Horai, R., Asano, M., Iwakura, Y., and Rothwell, N. J. (2001). Role of IL-1α and IL-1β in ischemic brain damage. *J. Neurosci.* 21, 5528–5534. doi:10.1523/jneurosci.21-15-05528.2001
- Choi, H. B., Ryu, J. K., Kim, S. U., and McLarnon, J. G. (2007). Modulation of the purinergic P2X7 receptor attenuates lipopolysaccharide-mediated microglial activation and neuronal damage in inflamed brain. *J. Neurosci.* 27, 4957–4968. doi:10.1523/JNEUROSCI.5417-06.2007
- Choi, S. Y., and Kim, K. T. (1996). Characterization of Na⁺ influx mediated by ATP(4⁻)-activated P2 purinoceptors in PC12 cells. *Br. J. Pharmacol.* 118, 935–940. doi:10.1111/j.1476-5381.1996.tb15489.x
- Conrath, K., Vincke, C., Stijlemans, B., Schymkowitz, J., Decanniere, K., Wyns, L., et al. (2005). Antigen binding and solubility effects upon the veneering of a camel VHH in framework-2 to mimic a VH. *J. Mol. Biol.* 350, 112–125. doi:10.1016/j.jmb.2005.04.050
- Danquah, W., Meyer-Schwesinger, C., Rissiek, B., Pinto, C., Serracant-Prat, A., Amadi, M., et al. (2016). Nanobodies that block gating of the P2X7 ion channel ameliorate inflammation. *Sci. Transl. Med.* 8, 366ra162. doi:10.1126/scitranslmed.aaf8463
- Ding, J., Wang, K., Liu, W., She, Y., Sun, Q., Shi, J., et al. (2016). Pore-forming activity and structural autoinhibition of the gasdermin family. *Nature* 535, 111–116. doi:10.1038/nature18590
- Egan, T. M., and Khakh, B. S. (2004). Contribution of calcium ions to P2X channel responses. *J. Neurosci.* 24, 3413–3420. doi:10.1523/JNEUROSCI.5429-03.2004
- Evavold, C. L., Ruan, J., Tan, Y., Xia, S., Wu, H., and Kagan, J. C. (2018). The pore-forming protein gasdermin D regulates interleukin-1 secretion from living macrophages. *Immunity* 48, 35–44. doi:10.1016/j.immuni.2017.11.013
- Falzone, S., Donvito, G., and Di Virgilio, F. (2013). Detecting adenosine triphosphate in the pericellular space. *Interface Focus* 3, 20120101. doi:10.1098/rsfs.2012.0101
- Ferrari, D., Chiozzi, P., Falzone, S., Hanau, S., and Di Virgilio, F. (1997). Purinergic modulation of interleukin-1 beta release from microglial cells stimulated with bacterial endotoxin. *J. Exp. Med.* 185, 579–582. doi:10.1084/jem.185.3.579
- Ferrari, D., Villalba, M., Chiozzi, P., Falzone, S., Ricciardi-Castagnoli, P., and Di Virgilio, F. (1996). Mouse microglial cells express a plasma membrane pore gated by extracellular ATP. *J. Immunol.* 156, 1531–1539.
- Fischer, H., Gottschlich, R., and Seelig, A. (1998). Blood-brain barrier permeation: molecular parameters governing passive diffusion. *J. Membr. Biol.* 165, 201–211. doi:10.1007/s002329900434
- Franke, H., Gunther, A., Grosche, J., Schmidt, R., Rossner, S., Reinhardt, R., et al. (2004). P2X7 receptor expression after ischemia in the cerebral cortex of rats. *J. Neuropathol. Exp. Neurol.* 63, 686–699. doi:10.1093/jnen/63.7.686
- Gomes, J. R., Cabrito, I., Soares, H. R., Costelha, S., Teixeira, A., Wittelsberger, A., et al. (2018). Delivery of an anti-transthyretin Nanobody to the brain through intranasal administration reveals transthyretin expression and secretion by motor neurons. *J. Neurochem.* 145, 393–408. doi:10.1111/jnc.14332
- Gonde, H., Demeules, M., Hardet, R., Scarpitta, A., Junge, M., Pinto-Espinoza, C., et al. (2021). A methodological approach using rAAV vectors encoding nanobody-based biologics to evaluate ARTC2.2 and P2X7 *in vivo*. *Front. Immunol.* 12, 704408. doi:10.3389/fimmu.2021.704408
- Gotzke, H., Kilisch, M., Martinez-Carranza, M., Sograte-Idrissi, S., Rajavel, A., Schlichthaerle, T., et al. (2019). The ALFA-tag is a highly versatile tool for nanobody-based bioscience applications. *Nat. Commun.* 10, 4403. doi:10.1038/s41467-019-12301-7

- Grygorowicz, T., and Struzynska, L. (2019). Early P2X7R-dependent activation of microglia during the asymptomatic phase of autoimmune encephalomyelitis. *Inflammopharmacology* 27, 129–137. doi:10.1007/s10787-018-0528-3
- Grygorowicz, T., Welniak-Kaminska, M., and Struzynska, L. (2016). Early P2X7R-related astrogliosis in autoimmune encephalomyelitis. *Mol. Cell. Neurosci.* 74, 1–9. doi:10.1016/j.mcn.2016.02.003
- Hamers-Casterman, C., Atarhouch, T., Muyldermans, S., Robinson, G., Hamers, C., Songa, E. B., et al. (1993). Naturally occurring antibodies devoid of light chains. *Nature* 363, 446–448. doi:10.1038/363446a0
- Haqqani, A. S., Delaney, C. E., Brunette, E., Baumann, E., Farrington, G. K., Sisk, W., et al. (2018). Endosomal trafficking regulates receptor-mediated transcytosis of antibodies across the blood brain barrier. *J. Cereb. Blood Flow. Metab.* 38, 727–740. doi:10.1177/0271678X17740031
- He, Y., Taylor, N., Fourgeaud, L., and Bhattacharya, A. (2017). The role of microglial P2X7: modulation of cell death and cytokine release. *J. Neuroinflammation* 14, 135. doi:10.1186/s12974-017-0904-8
- Heilig, R., Dick, M. S., Sborgi, L., Meunier, E., Hiller, S., and Broz, P. (2018). The Gasdermin-D pore acts as a conduit for IL-1 β secretion in mice. *Eur. J. Immunol.* 48, 584–592. doi:10.1002/eji.201747404
- Hladky, S. B., and Barrand, M. A. (2018). Elimination of substances from the brain parenchyma: efflux via perivascular pathways and via the blood-brain barrier. *Fluids Barriers CNS* 15, 30. doi:10.1186/s12987-018-0113-6
- Jin, J. J., Kim, H. D., Maxwell, J. A., Li, L., and Fukuchi, K. (2008). Toll-like receptor 4-dependent upregulation of cytokines in a transgenic mouse model of Alzheimer's disease. *J. Neuroinflammation* 5, 23. doi:10.1186/1742-2094-5-23
- Kaczmarek-Hajek, K., Zhang, J., Kopp, R., Grosche, A., Rissiek, B., Saul, A., et al. (2018). Re-evaluation of neuronal P2X7 expression using novel mouse models and a P2X7-specific nanobody. *Elife* 7, e36217. doi:10.7554/eLife.36217
- Labasi, J. M., Petrushova, N., Donovan, C., McCurdy, S., Lira, P., Payette, M. M., et al. (2002). Absence of the P2X7 receptor alters leukocyte function and attenuates an inflammatory response. *J. Immunol.* 168, 6436–6445. doi:10.4049/jimmunol.168.12.6436
- Li, T., Bourgeois, J. P., Celli, S., Glacial, F., Le Sourd, A. M., Mecheri, S., et al. (2012). Cell-penetrating anti-GFAP VHH and corresponding fluorescent fusion protein VHH-GFP spontaneously cross the blood-brain barrier and specifically recognize astrocytes: application to brain imaging. *FASEB J.* 26, 3969–3979. doi:10.1096/fj.11-201384
- Li, T., Vandesquille, M., Koukoulis, F., Duffeant, C., Youssef, I., Lenormand, P., et al. (2016). Camelid single-domain antibodies: A versatile tool for *in vivo* imaging of extracellular and intracellular brain targets. *J. Control. Release* 243, 1–10. doi:10.1016/j.jconrel.2016.09.019
- Ma, Q., Ineichen, B. V., Detmar, M., and Proulx, S. T. (2017). Outflow of cerebrospinal fluid is predominantly through lymphatic vessels and is reduced in aged mice. *Nat. Commun.* 8, 1434. doi:10.1038/s41467-017-01484-6
- Matute, C., Torre, I., Perez-Cerdá, F., Perez-Samartin, A., Alberdi, E., Etxebarria, E., et al. (2007). P2X7(7) receptor blockade prevents ATP excitotoxicity in oligodendrocytes and ameliorates experimental autoimmune encephalomyelitis. *J. Neurosci.* 27, 9525–9533. doi:10.1523/JNEUROSCI.0579-07.2007
- Maysami, S., Wong, R., Pradillo, J. M., Denes, A., Dhungana, H., Malm, T., et al. (2016). A cross-laboratory preclinical study on the effectiveness of interleukin-1 receptor antagonist in stroke. *J. Cereb. Blood Flow. Metab.* 36, 596–605. doi:10.1177/0271678X15606714
- McLarnon, J. G., Ryu, J. K., Walker, D. G., and Choi, H. B. (2006). Upregulated expression of purinergic P2X(7) receptor in Alzheimer disease and amyloid-beta peptide-treated microglia and in peptide-injected rat hippocampus. *J. Neuropathol. Exp. Neurol.* 65, 1090–1097. doi:10.1097/01.jnen.0000240470.97295.d3
- Melani, A., Amadio, S., Gianfriddo, M., Vannucchi, M. G., Volonte, C., Bernardi, G., et al. (2006). P2X7 receptor modulation on microglial cells and reduction of brain infarct caused by middle cerebral artery occlusion in rat. *J. Cereb. Blood Flow. Metab.* 26, 974–982. doi:10.1038/sj.jcbfm.9600250
- Melani, A., Turchi, D., Vannucchi, M. G., Cipriani, S., Gianfriddo, M., and Pedata, F. (2005). ATP extracellular concentrations are increased in the rat striatum during *in vivo* ischemia. *Neurochem. Int.* 47, 442–448. doi:10.1016/j.neuint.2005.05.014
- Metzger, M. W., Walser, S. M., Aprile-Garcia, F., Dedic, N., Chen, A., Holsboer, F., et al. (2017). Genetically dissecting P2rx7 expression within the central nervous system using conditional humanized mice. *Purinergic Signal.* 13, 153–170. doi:10.1007/s11302-016-9546-z
- Moller, S., Jung, C., Adriouch, S., Dubberke, G., Seyfried, F., Seman, M., et al. (2007). Monitoring the expression of purinoceptors and nucleotide-metabolizing ecto-enzymes with antibodies directed against proteins in native conformation. *Purinergic Signal.* 3, 359–366. doi:10.1007/s11302-007-9084-9
- Nguyen, V. K., Hamers, R., Wyns, L., and Muyldermans, S. (2000). Camel heavy-chain antibodies: diverse germline V(H)H and specific mechanisms enlarge the antigen-binding repertoire. *EMBO J.* 19, 921–930. doi:10.1093/emboj/19.5.921
- Nicke, A. (2008). Homotrimeric complexes are the dominant assembly state of native P2X7 subunits. *Biochem. Biophys. Res. Commun.* 377, 803–808. doi:10.1016/j.bbrc.2008.10.042
- Niewoehner, J., Bohrmann, B., Collin, L., Ulrich, E., Sade, H., Maier, P., et al. (2014). Increased brain penetration and potency of a therapeutic antibody using a monovalent molecular shuttle. *Neuron* 81, 49–60. doi:10.1016/j.neuron.2013.10.061
- Pardridge, W. M. (2005). The blood-brain barrier: bottleneck in brain drug development. *NeuroRx* 2, 3–14. doi:10.1602/neurorx.2.1.3
- Perregaux, D., and Gabel, C. A. (1994). Interleukin-1 beta maturation and release in response to ATP and nigericin. Evidence that potassium depletion mediated by these agents is a necessary and common feature of their activity. *J. Biol. Chem.* 269, 15195–15203. doi:10.1016/s0021-9258(17)36591-2
- Rampe, D., Wang, L., and Ringheim, G. E. (2004). P2X7 receptor modulation of beta-amyloid- and LPS-induced cytokine secretion from human macrophages and microglia. *J. Neuroimmunol.* 147, 56–61. doi:10.1016/j.jneuroim.2003.10.014
- Recourt, K., van der Aart, J., Jacobs, G., de Kam, M., Drevets, W., van Nueten, L., et al. (2020). Characterisation of the pharmacodynamic effects of the P2X7 receptor antagonist JNJ-54175446 using an oral dexamphetamine challenge model in healthy males in a randomised, double-blind, placebo-controlled, multiple ascending dose trial. *J. Psychopharmacol.* 34, 1030–1042. doi:10.1177/0269881120914206
- Rubenstein, J. L., Combs, D., Rosenberg, J., Levy, A., McDermott, M., Damon, L., et al. (2003). Rituximab therapy for CNS lymphomas: targeting the leptomeningeal compartment. *Blood* 101, 466–468. doi:10.1182/blood-2002-06-1636
- Sanz, J. M., Chiozzi, P., Ferrari, D., Colaiana, M., Idzko, M., Falzoni, S., et al. (2009). Activation of microglia by amyloid β requires P2X7 receptor expression. *J. Immunol.* 182, 4378–4385. doi:10.4049/jimmunol.0803612
- Sanz, J. M., and Di Virgilio, F. (2000). Kinetics and mechanism of ATP-dependent IL-1 beta release from microglial cells. *J. Immunol.* 164, 4893–4898. doi:10.4049/jimmunol.164.9.4893
- Schaffer, U., Schlosser, A., Muller, K. M., Schafer, A., Katava, N., Baumeister, R., et al. (2010). SnAvi—a new tandem tag for high-affinity protein-complex purification. *Nucleic Acids Res.* 38, e91. doi:10.1093/nar/gkp1178
- Shi, J., Zhao, Y., Wang, K., Shi, X., Wang, Y., Huang, H., et al. (2015). Cleavage of GSDMD by inflammatory caspases determines pyroptotic cell death. *Nature* 526, 660–665. doi:10.1038/nature15514
- Skaper, S. D., Facci, L., Culbert, A. A., Evans, N. A., Chessell, I., Davis, J. B., et al. (2006). P2X(7) receptors on microglial cells mediate injury to cortical neurons *in vitro*. *Glia* 54, 234–242. doi:10.1002/glia.20379
- Stark, R., Wesselink, T. H., Behr, F. M., Kragten, N. A. M., Arens, R., Koch-Nolte, F., et al. (2018). T_{RM} maintenance is regulated by tissue damage via P2RX7. *Sci. Immunol.* 3, eaau1022. doi:10.1126/sciimmunol.aau1022
- Stocki, P., Szary, J., Rasmussen, C. L. M., Demychuk, M., Northall, L., Logan, D. B., et al. (2021). Blood-brain barrier transport using a high affinity, brain-selective VNAR antibody targeting transferrin receptor 1. *FASEB J.* 35, e21172. doi:10.1096/fj.202001787R
- Terryn, S., Francart, A., Lamoral, S., Hultberg, A., Rommelaere, H., Wittelsberger, A., et al. (2014). Protective effect of different anti-rabies virus VHH constructs against rabies disease in mice. *PLoS One* 9, e109367. doi:10.1371/journal.pone.0109367
- Tijink, B. M., Laeremans, T., Budde, M., Stigter-van Walsum, M., Dreier, T., de Haard, H. J., et al. (2008). Improved tumor targeting of anti-epidermal growth factor receptor nanobodies through albumin binding: taking advantage of modular nanobody technology. *Mol. Cancer Ther.* 7, 2288–2297. doi:10.1158/1535-7163.MCT-07-2384
- Veltkamp, A. W., Magnus, T., and Rissiek, B. (2022). Real-time flow cytometry as a tool to monitor cellular consequences of P2X7 activation in multiple cell populations mixed in a single FACS tube. *Methods Mol. Biol.* 2510, 291–302. doi:10.1007/978-1-0716-2384-8_16
- Wesolowski, J., Alzogaray, V., Reyelt, J., Unger, M., Juarez, K., Urrutia, M., et al. (2009). Single domain antibodies: promising experimental and therapeutic tools in infection and immunity. *Med. Microbiol. Immunol.* 198, 157–174. doi:10.1007/s00430-009-0116-7
- Wouters, Y., Jaspers, T., De Strooper, B., and Dewilde, M. (2020). Identification and *in vivo* characterization of a brain-penetrating nanobody. *Fluids Barriers CNS* 17, 62. doi:10.1186/s12987-020-00226-z
- Yan, Z., Li, S., Liang, Z., Tomic, M., and Stojiljkovic, S. S. (2008). The P2X7 receptor channel pore dilates under physiological ion conditions. *J. Gen. Physiol.* 132, 563–573. doi:10.1085/jgp.200810059



OPEN ACCESS

EDITED BY

Kenneth A. Jacobson,
National Institutes of Health (NIH),
United States

REVIEWED BY

Anindya Bhattacharya,
Janssen R&D, United States
James Saville Wiley,
University of Melbourne, Australia

*CORRESPONDENCE

Friedrich Koch-Nolte,
nolte@uke.de

[†]These authors share first authorship

SPECIALTY SECTION

This article was submitted to
Experimental Pharmacology
and Drug Discovery,
a section of the journal
Frontiers in Pharmacology

RECEIVED 31 August 2022

ACCEPTED 28 October 2022

PUBLISHED 18 November 2022

CITATION

Schäfer W, Stähler T, Pinto Espinoza C,
Danquah W, Knop JH, Rissiek B, Haag F
and Koch-Nolte F (2022), Origin,
distribution, and function of three
frequent coding polymorphisms in the
gene for the human P2X7 ion channel.
Front. Pharmacol. 13:1033135.
doi: 10.3389/fphar.2022.1033135

COPYRIGHT

© 2022 Schäfer, Stähler, Pinto Espinoza,
Danquah, Knop, Rissiek, Haag and
Koch-Nolte. This is an open-access
article distributed under the terms of the
[Creative Commons Attribution License](#)
(CC BY). The use, distribution or
reproduction in other forums is
permitted, provided the original
author(s) and the copyright owner(s) are
credited and that the original
publication in this journal is cited, in
accordance with accepted academic
practice. No use, distribution or
reproduction is permitted which does
not comply with these terms.

Origin, distribution, and function of three frequent coding polymorphisms in the gene for the human P2X7 ion channel

Waldemar Schäfer^{1†}, Tobias Stähler^{1†}, Carolina Pinto Espinoza^{1,2},
Welbeck Danquah¹, Jan Hendrik Knop¹, Björn Rissiek^{1,2},
Friedrich Haag¹ and Friedrich Koch-Nolte^{1*}

¹Institute of Immunology, University Medical Center Hamburg-Eppendorf, Hamburg, Germany,

²Department of Neurology, University Medical Center Hamburg-Eppendorf, Hamburg, Germany

P2X7, an ion channel gated by extracellular ATP, is widely expressed on the plasma membrane of immune cells and plays important roles in inflammation and apoptosis. Several single nucleotide polymorphisms have been identified in the human *P2RX7* gene. In contrast to other members of the P2X family, non-synonymous polymorphisms in P2X7 are common. Three of these occur at overall frequencies of more than 25% and affect residues in the extracellular “head”-domain of P2X7 (155 Y/H), its “lower body” (270 R/H), and its “tail” in the second transmembrane domain (348 T/A). Comparison of the P2X7 orthologues of human and other great apes indicates that the ancestral allele is Y–R–T (at 155–270–348). Interestingly, each single amino acid variant displays lower ATP-sensitivity than the ancestral allele. The originally published reference sequence of human P2X7, often referred to as “wildtype,” differs from the ancestral allele at all three positions, i.e. H–H–A. The 1,000 Genome Project determined the sequences of both alleles of 2,500 human individuals, including roughly 500 persons from each of the five major continental regions. This rich resource shows that the ancestral alleles Y155, R270, and T348 occur in all analyzed human populations, albeit at strikingly different frequencies in various subpopulations (e.g., 25%–59% for Y155, 59%–77% for R270, and 13%–47% for T348). BLAST analyses of ancient human genome sequences uncovered several homozygous carriers of variant P2X7 alleles, possibly reflecting a high degree of inbreeding, e.g., H–R–T for a 50,000 year old Neanderthal, H–R–A for a 24,000 year old Siberian, and Y–R–A for a 7,000 year old mesolithic European. In contrast, most present-day individuals co-express two copies of P2X7 that differ in one or more amino acids at positions 155, 270, and 348. Our results improve the understanding of how P2X7 structure affects its function and suggest the importance of considering P2X7 variants of participants when designing clinical trials targeting P2X7.

Abbreviations: ATP, adenosine triphosphate; maf, minor allele frequency; P2X7 ATP-gated P2X ion channel, ionotropic purinergic receptor; *P2RX7*, gene encoding P2X7; SNP, single nucleotide polymorphism.

KEYWORDS

ATP, adenosine triphosphate, P2X7, ATP-gated P2X ion channel, ion channel, purinergic receptor, single nucleotide polymorphism, loss of function

Introduction

Extracellular ATP is an important signaling molecule that can regulate numerous biological processes (Zimmermann 2000; la Sala et al., 2003; Lazarowski et al., 2003; Burnstock 2006; Khakh and North, 2006). The human genome encodes seven ionotropic P2X purinoceptors, i.e., ATP-gated ion channels designated P2X1-P2X7 (with corresponding genes designated *P2RX1-P2RX7*) (Di Virgilio et al., 2001; North 2002; Vial et al., 2004). Among these, P2X7 is widely expressed on the plasma membrane of immune cells and plays important roles in inflammation and apoptosis (Di Virgilio 1995; Surprenant et al., 1996; Ferrari et al., 2006). P2X7 differs from other P2X receptors by its relatively low sensitivity to ATP and by its relatively long cytoplasmic C-terminus (North and Surprenant, 2000; North, 2002). P2X7 has been proposed to function as a key regulator of inflammation and plays a crucial role in the ATP-dependent processing and release of the leader-less proinflammatory cytokines IL-1 β and IL-18 (Ferrari et al., 1997; Perregaux et al., 2000; MacKenzie et al., 2001; Solle et al., 2001; Gudipaty et al., 2003; Mariathasan et al., 2006). P2X7 has been implicated in the killing of mycobacteria and chlamydia residing inside macrophages (Lammas et al., 1997; Fairbairn et al., 2001; Coutinho-Silva et al., 2003), fusion of monocyte-derived cells into multinucleated epithelioid cells (Chiozzi et al., 1997; Di Virgilio et al., 1999), the apoptosis of regulatory T cells (Seman et al., 2003; Aswad et al., 2005; Auger et al., 2005; Hubert et al., 2010), and the shedding of the CD62L homing receptor from circulating T cells (Jamieson et al., 1996; Gu et al., 1998; Seman et al., 2003).

The crystal structure of truncated panda (*Ailuropoda melanoleuca*) P2X7 encompassing the extracellular ATP-binding domain and two transmembrane segments (Karasawa and Kawate, 2016; Karasawa et al., 2017) as well as the cryo-EM structure of native rat P2X7 (McCarthy et al., 2019) have provided insights into the modes of ATP binding and gating.

In the human population, single amino acid polymorphic substitutions (R307Q, T357S, E496A, and I568N) and a 5'-intronic splice site polymorphism have been shown to result in a reduced or absent P2X7 functions (Gu et al., 2001; Wiley et al., 2003; Gu et al., 2004; Sluyter et al., 2004; Skarratt et al., 2005; Shemon et al., 2006). Moreover, splice variants leading to receptors lacking the cytoplasmic tail have been detected, which may account for reduced P2X7 functions in some normal tissues as well as in tumor cells overexpressing

those variants by antagonizing the function of the normal variant (Feng et al., 2006). Two polymorphisms in the sequence of the human P2X7, H155Y, and A348T were reported as gain-of-function mutants (Cabrini et al., 2005).

The 1,000 Genomes Project provides the reconstructed genomes of a global sample of 2,504 individuals from 26 populations with about 500 samples from each of five continent ancestry groups in Africa (AFR), East Asia (EAS), Europe (EUR), South Asia (SAS), and the Americas (AMR) (Clarke et al., 2012; Delaneau et al., 2014; Auton et al., 2015; Clarke et al., 2017). This resource provides a rich data set on the distribution of common and rare genetic variations in humans. A typical human genome contains an estimated 4.1–5 million single nucleotide polymorphisms (SNPs) and short indels and 2,100 to 2,500 structural variants that affect more bases, e.g., large deletions, copy number variants, inversions (Auton et al., 2015). The majority of SNPs are rare (64 Mio with a frequency of <0.5%), a smaller proportion (12 Mio) has a frequency between 0.5% and 5% and even fewer SNPs (8 Mio) have a frequency of >5%. A typical human genome contains 10,000 to 12,000 sites with peptide-altering sequence variants, i.e., on the average one such variant in every other protein-coding gene.

The goal of this study was to compare the distribution of coding SNPs in human P2X7 to those in its paralogues, its orthologues in today's great apes and DNA samples from ancient humans. We established protocols to determine the alleles of P2X7 and measure their sensitivity to ATP in human blood samples. Our results indicate that most humans co-express two alleles of P2X7 that differ in one or more amino acids. This correlates with high interindividual variation in the sensitivity of lymphocytes to extracellular ATP.

Methods

Database searches and sequence analyses

Data on coding SNPs in the *P2RX* gene family was retrieved from the 1,000 Genome Project via the Ensemble genome browser (Cunningham et al., 2022). Blastp and Tblastn (Madden et al., 1996; Ye et al., 2006) searches of the NCBI nucleotide database were performed using the “wildtype” human P2X7 sequence (Rassendren et al., 1997) as query. P2X7 amino acid sequences were aligned using T-Coffee (Notredame et al., 2000).

TABLE 1 Frequencies of 20 coding SNPs in the human *P2X7* gene. SNPs are sorted according to the minor allele frequency (maf) in the sample of the 1,000 Genomes Project; maf (Stokes) refers to a sample of 3,430 Caucasians genotyped by Stokes et al., 2010.

SNP	maf	maf (Stokes)	residue	exon	mutation
rs208294	0.461	0.439	155	5	Y/H
rs1718119	0.308	0.400	348	11	A/T
rs7958311	0.289	0.255	270	8	R/H
rs3751143	0.192	0.175	496	13	E/A
rs2230911	0.144	0.083	357	8	T/S
rs2230912	0.068	0.170	460	13	Q/R
rs17525809	0.054	0.062	76	2	V/A
rs2230913	0.037		521	13	H/Q
rs10160951	0.036		430	12	P/R
rs28360459	0.029		433	13	A/V
rs74357548	0.011		423	12	D/N
rs28360447	0.010	0.018	150	5	G/R
rs7958316	0.010	0.020	276	8	R/H
rs1653624	0.009	0.029	568	13	N/I
rs34219304	0.010		522	13	V/I
rs16950860	0.008		270	8	R/C
rs28360457	0.004	0.013	307		R/Q
rs28360460	0.003		578		R/Q
rs28360445	0.002		117		R/W
rs200840067	0.002		582		P/S

Sequencing of human *P2RX7* gene fragments and structural modelling of *P2X7* variants

Genomic DNA was isolated from peripheral blood mononuclear cells (PBMC) using a commercial DNA isolation kit (StemCell Technologies). Appropriate primer pairs were used to PCR amplify exons 5, 8, and 11. PCR amplification products were analyzed by agarose gel electrophoresis. Bands of the expected size were extracted from gel slices using a commercial DNA fragment purification kit (Qiagen). Fragments were sequenced using appropriate primers. DNA sequences were analyzed using Genescript (Hudek et al., 2003). *P2X7* variants were modelled using AlphaFold 2 (Jumper et al., 2021; Jumper and Hassabis, 2022).

Evaluation of the functionality of *P2X7* variants by flow cytometry

PBMC were pre-incubated with *P2X7*-specific mAb L4 (Buell et al., 1998) or Nb Dano1 (Danquah et al., 2016) for 15 min at 4°C and then further incubated for 20 min at 37°C in RPMI medium in the absence or presence of ATP (Seman et al., 2003; Adriouch et al., 2008). Cells were then stained with fluorochrome-conjugated Annexin V and antibodies

against CD62L (DREG-56), CD4 (RPA-T4), and CD8 (SK1) for 20 min before analysis by flow cytometry on a FACS-Canto (BD).

Results

The human *P2RX7* gene contains sixteen coding SNPs with a minor allele frequency of >0.5%

We used the resource of the 1,000 Genome Project (Clarke et al., 2012; Delaneau et al., 2014; Auton et al., 2015; Clarke et al., 2017) to determine the distribution of common coding mutations in *P2RX7*. The results reveal three frequent variants (minor allele frequency >25%) (Table 1). Two of these affect amino acid residues in the extracellular ATP-binding domain (Y155H, R270H) while the third affects an amino acid in the transmembrane domain (T348A). The *P2RX7* gene contains four further common non-synonymous variants with a minor allele frequency of >5% (E496A, T357S, Q460R, and V76A) and nine coding SNPs with a frequency of 0.5%–5%. Table 1 also shows the minor allele frequencies of eleven coding SNPs determined previously by the Wiley lab by genotyping *P2RX7* of 3,430 Caucasians (Stokes et al., 2010). Three of these coding SNPs occur at more than two-fold higher frequency in the Caucasian population.

The six paralogues of the *P2RX7* gene together contain seven SNPs with a minor allele frequency of >0.5%

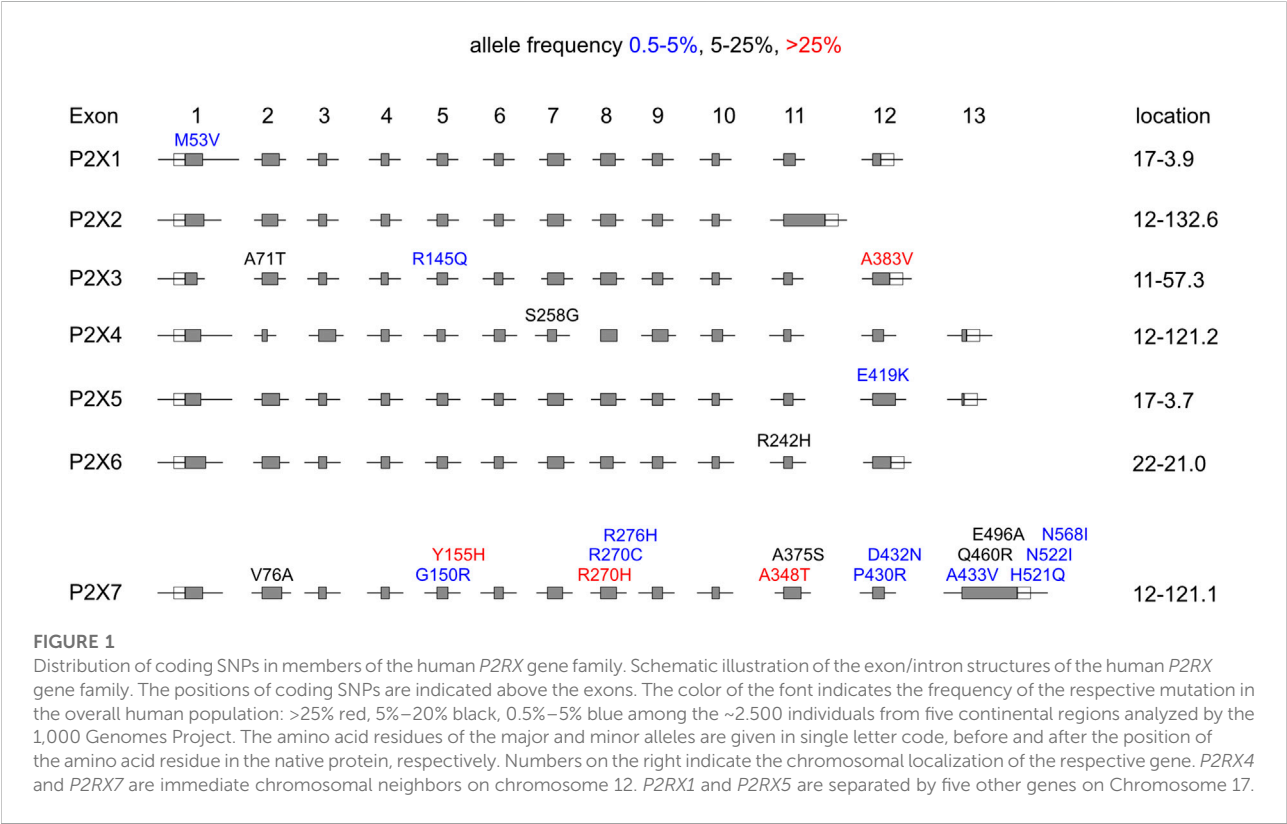
We performed similar analyses for the other six members of the *P2RX* gene family. The results reveal that the six paralogues of *P2RX7* contain much fewer coding SNPs than *P2RX7* (Table 2). *P2RX3* contains a single coding SNP with a frequency of >25% (A383E). *P2RX4* and *P2RX6* each contain a single coding SNP with a frequency of 5%–25% (S258G, R242H, respectively). And the six genes together contain only four further non-synonymous variants with a frequency of 0.5%–5%. Figure 1 schematically illustrates the location of the coding SNPs with frequencies >0.5% in the human *P2RX* gene family.

The three high frequency polymorphisms of human *P2X7* (H155Y, R270H, and A348T) occur in all major human subpopulations

We next compared the allele frequencies of the three most frequent coding SNPs in human *P2RX7* in different human

TABLE 2 Coding SNPs in other members of the P2RX gene family with a frequency >0.5%. nd = none detected.

SNP	Gene	exons	Length (aa)	maf	exon	mutation
rs34617528	<i>P2RX1</i>	12	399	0.008	1	M53V
Nd	<i>P2RX2</i>	11	471	nd	nd	nd
rs34572680	<i>P2RX3</i>	12	397	0.019	2	A71T
rs115850675	<i>P2RX3</i>	12	397	0.005	5	R145Q
rs2276038	<i>P2RX3</i>	12	397	0.432	12	A383V
rs25644	<i>P2RX4</i>	12	404	0.176	7	S258G
rs61748727	<i>P2RX5</i>	12	444	0.018	12	E419K
rs2277838	<i>P2RX6</i>	12	441	0.078	7	R242H



populations. The results show that both alleles are found in all analyzed human populations, albeit with strikingly different allele frequencies in some subpopulations (Figure 2). For example, 86% of alleles of Peruvians in Lima (PEL) carry the SNP coding for Histidine at position 155, whereas 78% of alleles of Luhya in Webuye, Kenya (LWK) encode Tyrosine at this position. For the 270 R/H SNP, the majority of alleles in all human populations encode R270 (from as low as 56% of Chinese in Beijing (CHB) to as high as 94% of Indian Telugu in the UK (ITU). And for the SNP encoding residue 348, the vast majority of alleles (94%) in Peruvians in Lima (PEL)

encode A348, while a small majority of alleles of Esan in Nigeria (ESN) (53%) encode T at this position.

Y155, R270, and T348 represent the ancestral haplotype of P2X7

The cDNA for human P2X7 that was originally cloned by Rassendren et al. (1997) from a commercially available cDNA library (Clontech, San Diego, United States) contained H155, H270 and A348, i.e., it contained the major allele of the AMR

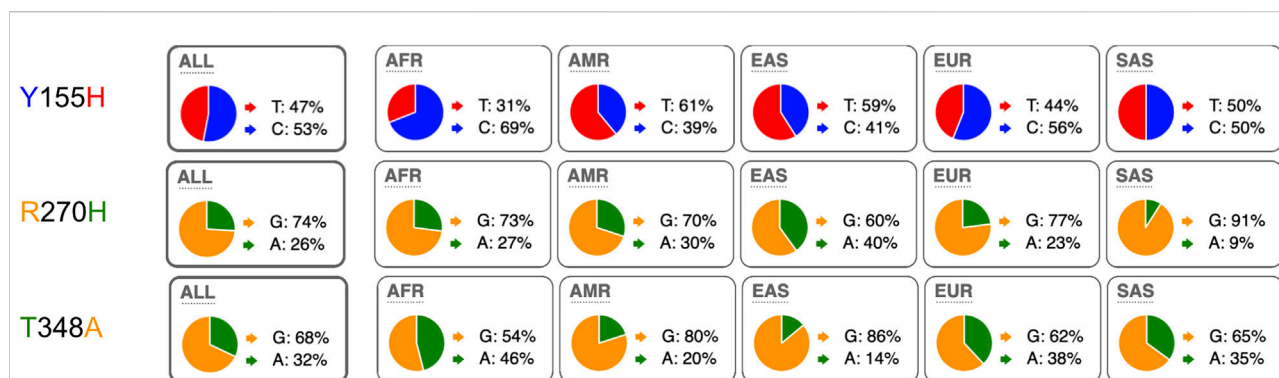


FIGURE 2

Distribution of minor and major alleles of the three most frequent coding SNPs in the human P2X7 gene (coding for amino acids 155, 270, and 348). The pie charts illustrate the allele frequencies of the major and minor alleles of P2RX7 encoding amino acid positions 155, 270, and 348 of human P2X7 in humans from the five major continental regions. The data were retrieved from the 1,000 Genomes Project. ALL: ($n = 2,504$ individuals) with about 500 from each region: AFR: African ($n = 247$), AMR: American ($n = 181$), EAS: East-Asian ($n = 286$), EUR: European ($n = 379$). ALL: ($n = 1,092$ humans).

population at positions 155 and 348, but the minor allele at position 270. In this paper, Rassendren et al. (1997) compared the predicted amino acid sequence of human P2X7 with that of its previously cloned orthologue from rat (Surprenant et al., 1996). Interestingly, at each of these positions rat P2X7 carries the respective other allele (Y155, R270, and T348) (Surprenant et al., 1996).

Using the “wildtype” sequence cloned by Rassendren et al. (1997) as query for BLAST analyses of the NCBI gene database, we obtained the deduced amino acid sequences of the P2X7 orthologues from chimpanzee, bonobo, and gorilla. Figure 3 shows the amino acid sequence alignment of the P2X7 orthologues of the great apes. The results show that all sequenced great apes carry Y155, R270, and T348, indicating that these represent the ancestral haplotype of P2X7. The “wildtype” human P2X7 deviates from the chimpanzee sequence only at these positions (H155, A270, and A348). The bonobo P2X7 sequence differs from human and the other great apes only at position F483L. Gorilla P2X7 differs from that of the other great apes at three other positions (N158K, R518Q, and A528T).

Mutations from the ancestral allele were present already in ancient humans

With BLAST analyses we also retrieved P2X7 variants from several ancient human DNA samples (Table 3). Interestingly, a 7,000 year old Spanish human carried the ancestral Y155 allele, while the older Siberian (24 ka) and Neanderthal (60 ka) carried the variant H155 allele. At position 348, the Neanderthal carried the ancestral

T348 allele, whereas the younger Siberian and Spanish humans carried the variant A348 allele. The results indicate that both, the ancestral and variant alleles, were present in ancient human DNAs.

Most present-day humans carry two different alleles of P2RX7

The allele frequencies illustrated by the pie charts in Figure 2 suggest that most human beings carry two different alleles of P2X7. Native P2X7 is expressed as a homotrimer on the cell surface. If both alleles were co-expressed, P2X7 receptors on the cell surface would be composed of a mixture of four different combinations of two polypeptide chains. In order to identify the variants of P2X7 at these positions in different human samples, we established a protocol to PCR amplify and sequence the three exons (5, 8, and 11) carrying these mutations. The results show that this strategy allows the rapid genotyping of the P2XR7 gene in different individuals (Figure 4).

To determine whether the different genotypes affect the function of P2X7, we used an established, simple flow-cytometry assay (Danquah et al., 2016). For this, we treated BMCs for 30 min with ATP and monitored ATP-induced shedding of CD62L and externalization of phosphatidylserine by T cells (Figure 5). As a specificity control, we used P2X7-blocking antibodies, i.e., the nanobody Dano1 and the monoclonal antibody L4. The results show that individuals carrying the Y155 and/or T348 variants respond more sensitively to ATP than individuals carrying the H155 or A348 variants.

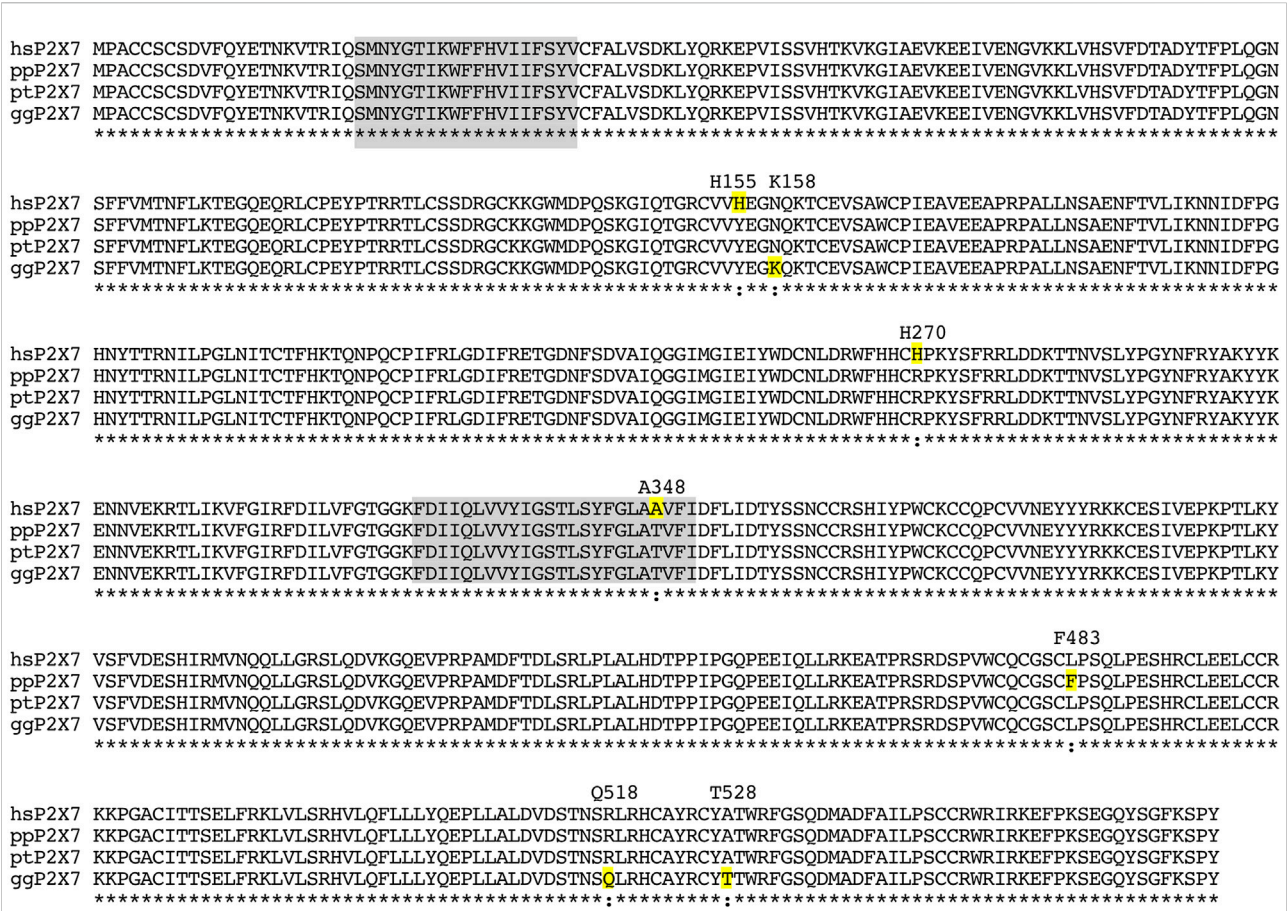


FIGURE 3
Amino acid sequence alignment of the P2X7 orthologues of the great apes. Residues highlighted in grey correspond to the two transmembrane domains. Residues highlighted in yellow indicate substitutions relative to the presumed ancestral version. The sequence of chimpanzee P2X7 corresponds completely to the presumed ancestral allele. Amino acid residues that deviate from the ancestral allele are indicated with their respective positions in the native protein above the alignment. hs: *homo sapiens*; pp: *pan paniscus* (bonobo); pt: *pan troglodytes* (chimpanzee); gg: gorilla gorilla.

TABLE 3 Distribution of three most common human P2X7 coding SNPs in ancient humans.

residue	Ancestral	“wt”	60 ka Neanderthal	24 ka Siberian	7 ka Spanish
155	Y	H	H	H	Y
348	R	H	R	R	R
270	T	A	T	A	A

The three high frequency SNPs code for amino acids in the head, body and tail domains of P2X7

We used AlphaFold 2 to predict the 3D-structures of ancestral human P2X7 (Y155, R270, and T348) and “wildtype” P2X7 (H155, H270, and A348) (Figure 6). The cartoon model in Figure 6A illustrates the localization of these

variants in the so-called dolphin model of P2X7. H155 is located in the extracellular head domain, H270R in the extracellular right flipper, and A348T in the second transmembrane domain, i.e. in the tail of the dolphin. Figure 6B shows the 3D models of the variant and wildtype P2X7 variants predicted by AlphaFold 2. The three variant residues are indicated in the color coding used also in Figure 2. The results indicate that the conformational changes induced by these substitutions are rather subtle.

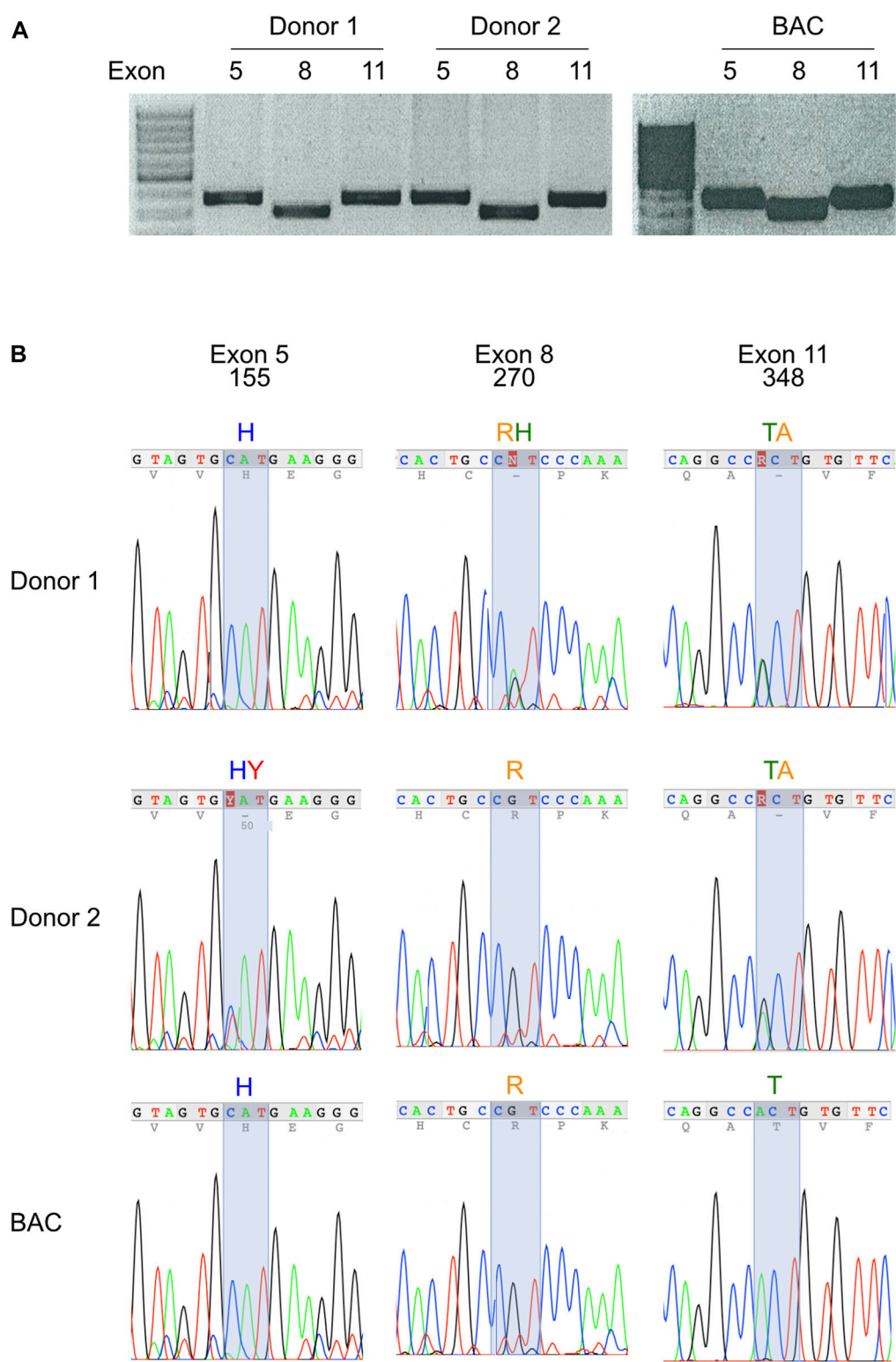


FIGURE 4
Most modern-day humans carry two variants of the P2X7 gene. **(A)** Exons 5, 8, and 11 of the human P2X7 gene were PCR-amplified from genomic DNA of peripheral blood leukocytes. Amplification products were size fractionated by agarose gel electrophoresis and stained with ethidium bromide. **(B)** PCR amplification products were purified from gel fragments and sequenced with internal primers. Fluorograms illustrate homozygosity or heterozygosity of PCR amplification products at the positions of the three most frequent SNPs of human P2RX7. The deduced amino acids are indicated above the fluorographs.

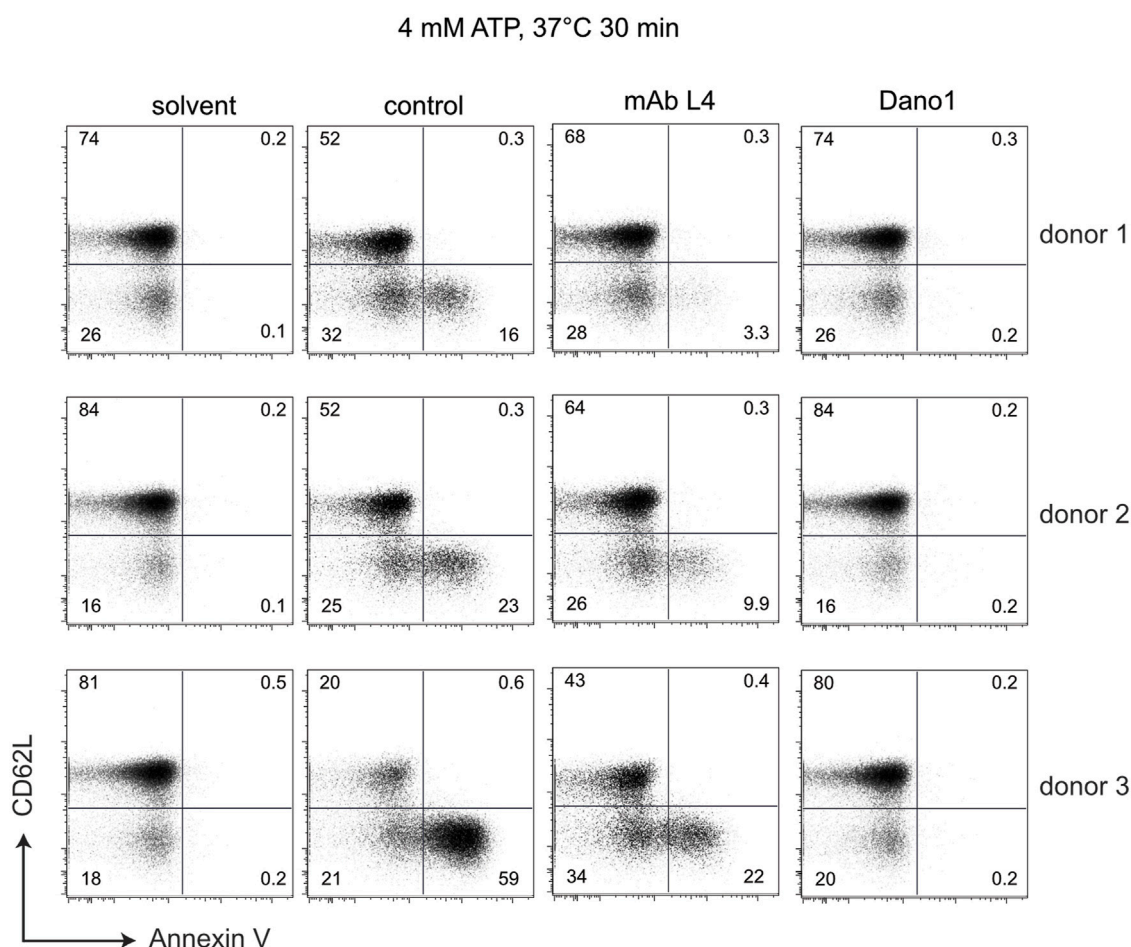


FIGURE 5

Sensitivity of peripheral blood T cells to ATP-induced shedding of CD62L varies with the genotype at positions 155, 270, and 348 of P2X7. Human blood samples were incubated for 30 min at 37°C in the absence (solvent) or presence of 4 mM ATP and the additional absence (control) or presence of the P2X7-antagonizing monoclonal antibody L4 or the nanobody Dano1. Cells were then washed and co-stained with antibodies directed against CD4 and CD62L as well as with Annexin V to visualize externalization of phosphatidylserine.

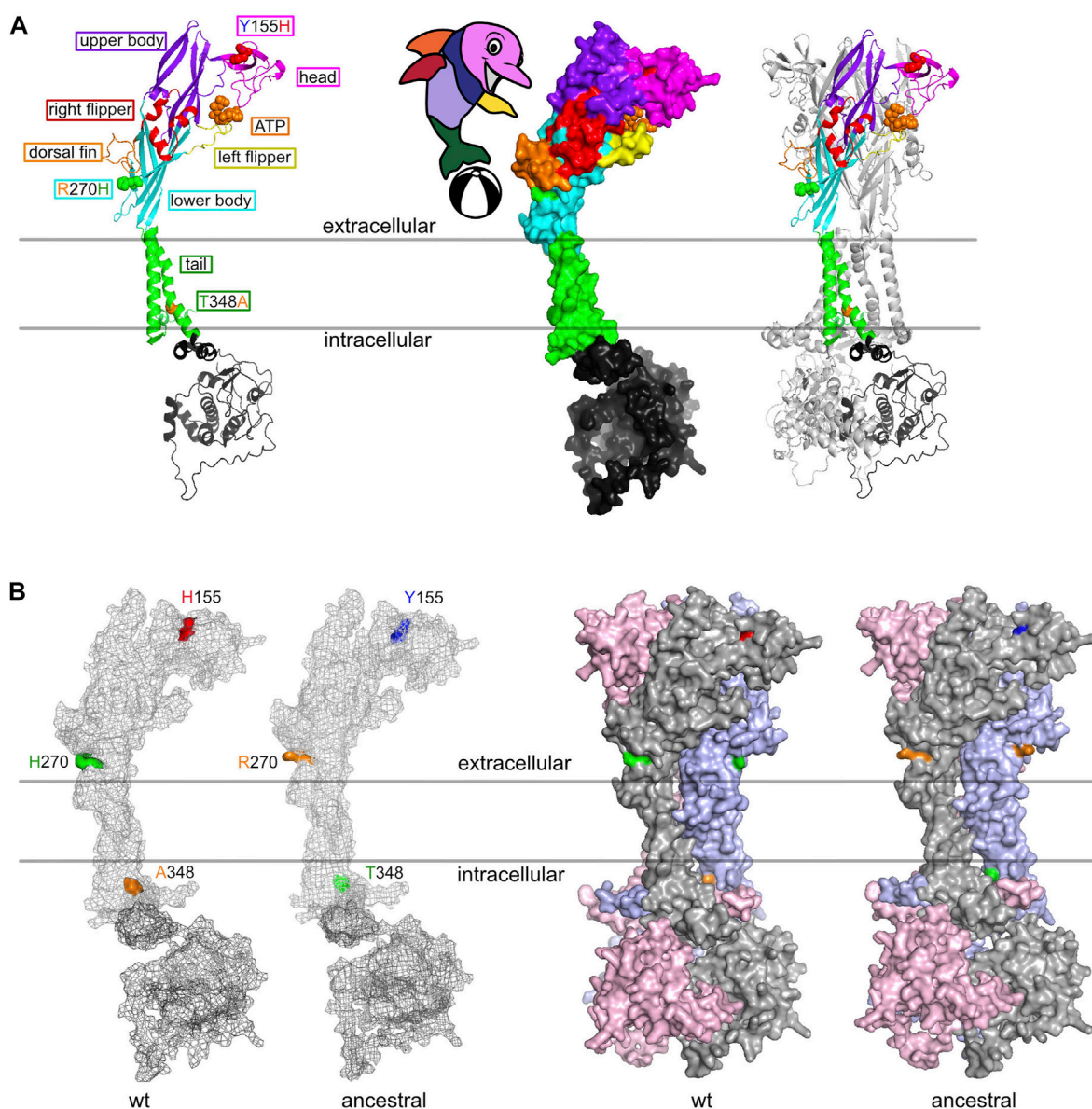
Discussion

Our results show that three coding SNPs of P2X7 occur at allele frequencies of more than 25%: 155 Y/H, 270 R/H, and 348 T/A. Furthermore, *P2RX7* contains 13 additional SNPs with a frequency of >0.5% (Table 1). This is in striking contrast to other members of the P2X gene family (Table 2): Only *P2RX3* contains a coding SNP with a frequency of >25% (A383E). *P2RX4*, the immediate chromosomal neighbour of *P2RX7* contains a SNP with a frequency of 18% (S258G) but no other SNPs with a frequency of >0.5%.

The three high frequency variant residues of *P2RX7* are located in the head, lower body, and tail domains of P2X7 (Figure 6). Comparison of the P2X7 orthologues of human and other great apes indicates that the ancestral allele is Y - R - T at these positions (Figure 4). The originally published

reference sequence of human P2X7 is often referred to as “wildtype” (Rassendren et al., 1997). This variant H - H - A differs from the ancestral allele at all three positions. Analysis of the data of the 1,000 Genome Project reveals a broad range of frequencies of the ancestral P2X7 alleles at these positions in different human populations (e.g., 39%–69% for Y155, 60%–91% for R270, and 14%–46% for T348) (Figure 2).

In a seminal study, Stokes et al. (2010) genotyped the *P2RX7* gene of 3,430 Caucasian subjects and determined the minor allele frequencies for eleven coding SNPs (Table 1). As in previous studies (Rassendren et al., 1997), Stokes et al. (2010) refer to the common haplotype of Caucasians H155-H270-A348 as “wildtype” (P2X7-1). The authors performed detailed comparative analyses of P2X7-1 with a variant, designated P2X7-4, that corresponds to the ancestral Y155-R270-T348. Remarkably, however, the variant analyzed by Stokes et al. (2010) also

**FIGURE 6**

3D structure models of “wildtype” (HHA) and ancestral (YRT) human P2X7. **(A)** The ribbon diagram highlights the positions of the three frequent coding SNPs in the different “body-parts” of the dolphin model of P2X7 (Karasawa and Kawate, 2016). Y155H is located in the head domain, R270H in the right flipper, and A348T in the tail of the dolphin. **(B)** 3D-structure models were generated using AlphaFold 2 and color-coded in pymol. The three divergent amino acid residues are color-coded as in Figures 2, 4.

carries the minor allele of the Q460R SNP (R460 instead of the ancestral Q460). Starting from “wildtype” P2X7-1, i.e., H155-H270-A348, Stokes et al. (2010) individually mutated residues 155 to Y and 270 to R, as well as 460 to R. Starting from P2X7-4, i.e., ancestral Y155-R270-T348 with the minor R460 allele, Stokes et al. (2010) individually mutated the “gain of function” residues back to wild type, i.e., Y155 to H, R270 to H, and T348 to A. By expressing these P2X7 variants in transiently transfected HEK cells, the authors verified gain of function effects of Y155, R270,

and A348, as well as slight loss of function effect of R460. For the Q460R SNP, Stokes et al. (2010) noted a strong pairwise linkage disequilibrium with the three “gain of function” SNPs (Y155, R270, and T348), suggesting that the Q460R SNP was acquired by an individual carrying the ancestral P2X7 haplotype.

BLAST analyses of ancient human genome sequences uncovered several homozygous carriers of variant P2X7 alleles, possibly reflecting a high degree of inbreeding, e.g., H—R—T for a 50,000-year-old Neanderthal, H—R—A for a 24,000 year old

Siberian, and Y—R—A for a 7,000 year old mesolithic European (Table 3). In contrast, most present-day human individuals co-express two copies of P2X7 that differ in one or more amino acids at positions 155, 270, and 348 (Figure 4). These results indicated an ancient origin of these alleles and the maintenance of a balanced polymorphism in most present-day human populations.

Peripheral blood T cells from individuals carrying the variant amino acid His at position 155 or Ala at position 348 show a reduced sensitivity to ATP-induced shedding of CD62L and externalization of phosphatidylserine compared to individuals that are homozygous for the ancestral variants Tyr and Thr at these positions (Figure 5). The fact that these ATP-induced effects are completely blocked by the highly specific P2X7-antagonizing Nanobody Dano1 (Figure 5) confirms that these are mediated through P2X7.

The major finding of our results is the strikingly high degree of allelic polymorphism in the P2XR7 gene in the human population. In fact, the data indicate that most human beings today are heterozygous at this locus and express two variants of the P2X7 protein that differ at one or more amino acid residues. It is difficult to determine whether the reduced function of the H155, H270, and A348 variants confer any benefit against inflammatory disease and/or enhanced susceptibility to infection, e.g., by *Mycobacterium tuberculosis*. The extremely high polymorphism at the MHC locus is thought to confer disease resistance on the population level, as a large number of variants in a population could provide a kind of group protection that checks the spread of infection (Trowsdale, 2011). By analogy, it is tempting to speculate that different sensitivities of human leucocytes in the population might be beneficial, e.g., by providing flexible response strategies to pandemic infectious agents on a population level. As P2X7 plays a key role in the activation of the inflammasome and in the release of IL-1 β (Ferrari et al., 1997; Gudipaty et al., 2003; Ferrari et al., 2006; Mariathasans et al., 2006; Pelegrin and Surprenant, 2006), its sensitivity to ATP may have been moulded during evolution to prevent its excessive activation. Fine-tuning the sensitivity of P2X7-expressing inflammatory cells to very high levels of ATP released from cells at sites of tissue damage may have reduced the risk of exaggerated inflammatory responses. Conceivably, such evolutionary pressures may also be responsible for the numerous natural loss of function mutations found for human P2X7 and the remarkably high frequency of these mutations in human populations (Smart et al., 2003; Gu et al., 2004; Shemon et al., 2006).

P2X7 has been proposed as a therapeutic target for a variety of infectious (Di Virgilio et al., 2017), inflammatory (Arulkumaran et al., 2011; Adinolfi et al., 2018; Burnstock and Knight, 2018; Magalhaes and Castelucci, 2021; Verma et al., 2022), autoimmune (Cao et al., 2019), bone (Zeng et al., 2019; Dong et al., 2020), muscular (Gorecki, 2019), cardiovascular (Chen et al., 2018; Cisneros-Mejorado et al., 2020; Shokoples et al., 2021), oncological (Burnstock and Knight, 2018; Li et al., 2020; Drill et al., 2021; Pegoraro and Adinolfi, 2021; Zhu et al.,

2021) and neurologic diseases (Rech et al., 2016; Bhattacharya, 2018; Domercq and Matute, 2019; Engel et al., 2021), including COVID-19 (Pacheco and Faria, 2021), rheumatoid arthritis (Baroja-Mazo and Pelegrin, 2012; McInnes et al., 2014), diabetic retinopathy (Tassetto et al., 2021), alcoholic liver disease (Le Dare et al., 2021), Alzheimer (Illes et al., 2019) and depression (Deussing and Arzt, 2018; Wei et al., 2018; Huang and Tan, 2021), multiple sclerosis (Domercq and Matute, 2019), amyotrophic lateral sclerosis (Sluyter et al., 2017; McKenzie et al., 2022). Our results indicate that it may be wise to monitor the genotype of P2RX7 and the ATP-sensitivity of its gene product P2X7 in clinical studies designed to evaluate the therapeutic benefit of P2X7-targeting drugs and antibodies (Bartlett et al., 2014; De Marchi et al., 2016; Park and Kim, 2017; Young and Gorecki, 2018; Koch-Nolte et al., 2019; Recourt et al., 2020; Mishra et al., 2021; Genetzakis et al., 2022). The assays shown in Figures 4, 5 provide a straightforward protocol to do so.

Considering that P2X7 is a key player in inflammation, selection in the human population of numerous variants displaying reduced function may confer some benefit against the deleterious effects of excessive inflammation. The very low sensitivity of P2X7 to extracellular ATP, as compared to the other P2X receptor, may in itself also reflect the action of selective pressures acting to lower the level of inflammation. Our results may aid in understanding the relation between P2X7 structure and function as well as the evolutionary pressures that maintain its low sensitivity to ATP.

Data availability statement

The original contributions presented in the study are included in the article, further inquiries can be directed to the corresponding author.

Author contributions

FK-N and FH designed the study. CPE, JK, WD, and BR performed and analyzed PCR, and flow cytometry assays. WS, TS, and FK-N performed the modelling studies, database analyses, and wrote the first draft of the manuscript. BR, FH, and FK-N were responsible for the funding acquisition. All authors contributed to manuscript revision, read, and approved the submitted version.

Funding

This work was supported by grants from the Deutsche Forschungsgemeinschaft to FK-N (No310/11, No310/13, and No310/14) and to BR, FH, and FK-N (SFB1328, Z02).

Acknowledgments

The authors thank Fabienne Seyfried and Gudrun Dubberke for excellent technical assistance.

Conflict of interest

WD and FK-N are coinventors on patent applications for P2X7-specific nanobodies. FK-N and FH obtain a share of the sales of antibody generated in their lab *via* MediGate GmbH, the technology transfer office and 100% subsidy of the University Hospital Hamburg-Eppendorf.

References

- Adinolfi, E., Giuliani, A. L., De Marchi, E., Pegoraro, A., Orioli, E., and Di Virgilio, F. (2018). The P2X7 receptor: A main player in inflammation. *Biochem. Pharmacol.* 151, 234–244. doi:10.1016/j.bcp.2017.12.021
- Adriouch, S., Bannas, P., Schwarz, N., Fliegert, R., Guse, A. H., Seman, M., et al. (2008). ADP-ribosylation at R125 gates the P2X7 ion channel by presenting a covalent ligand to its nucleotide binding site. *FASEB J.* 22 (3), 861–869. doi:10.1096/fj.07-9294com
- Arulkumaran, N., Unwin, R. J., and Tam, F. W. (2011). A potential therapeutic role for P2X7 receptor (P2X7R) antagonists in the treatment of inflammatory diseases. *Expert Opin. Investig. Drugs* 20 (7), 897–915. doi:10.1517/13543784.2011.578068
- Aswad, F., Kawamura, H., and Dennert, G. (2005). High sensitivity of CD4+CD25+ regulatory T cells to extracellular metabolites nicotinamide adenine dinucleotide and ATP: A role for P2X7 receptors. *J. Immunol.* 175 (5), 3075–3083. doi:10.4049/jimmunol.175.5.3075
- Auger, R., Motta, I., Benihoud, K., Ojcius, D. M., and Kanellopoulos, J. M. (2005). A role for mitogen-activated protein kinase (Erk1/2) activation and non-selective pore formation in P2X7 receptor-mediated thymocyte death. *J. Biol. Chem.* 280 (30), 28142–28151. doi:10.1074/jbc.M501290200
- AutonBrooks, L. D., Durbin, R. M., Garrison, E. P., Kang, H. M., Korbel, J. O., Marchini, J. L., et al. (2015). A global reference for human genetic variation. *Nature* 526 (7571), 68–74. doi:10.1038/nature15393
- Baroja-Mazo, A., and Pelegrin, P. (2012). Modulating P2X7 receptor signaling during rheumatoid arthritis: New therapeutic approaches for bisphosphonates. *J. Osteoporos.* 2012, 408242. doi:10.1155/2012/408242
- Bartlett, R., Stokes, L., and Sluyter, R. (2014). The P2X7 receptor channel: Recent developments and the use of P2X7 antagonists in models of disease. *Pharmacol. Rev.* 66 (3), 638–675. doi:10.1124/pr.113.008003
- Bhattacharya, A. (2018). Recent advances in CNS P2X7 physiology and Pharmacology: Focus on neuropsychiatric disorders. *Front. Pharmacol.* 9, 30. doi:10.3389/fphar.2018.00030
- Buell, G., Chessell, I. P., Michel, A. D., Collo, G., Salazzo, M., Herren, S., et al. (1998). Blockade of human P2X7 receptor function with a monoclonal antibody. *Blood* 92 (10), 3521–3528. doi:10.1182/blood.v92.10.3521.422k50_3521_3528
- Burnstock, G., and Knight, G. E. (2018). The potential of P2X7 receptors as a therapeutic target, including inflammation and tumour progression. *Purinergic Signal.* 14 (1), 1–18. doi:10.1007/s11302-017-9593-0
- Burnstock, G. (2006). Pathophysiology and therapeutic potential of purinergic signaling. *Pharmacol. Rev.* 58 (1), 58–86. doi:10.1124/pr.58.1.5
- Cabrini, G., Falzoni, S., Forchap, S. L., Pellegatti, P., Balboni, A., Agostini, P., et al. (2005). A His-155 to Tyr polymorphism confers gain-of-function to the human P2X7 receptor of human leukemic lymphocytes. *J. Immunol.* 175 (1), 82–89. doi:10.4049/jimmunol.175.1.82
- Cao, F., Hu, L. Q., Yao, S. R., Hu, Y., Wang, D. G., Fan, Y. G., et al. (2019). P2X7 receptor: A potential therapeutic target for autoimmune diseases. *Autoimmun. Rev.* 18 (8), 767–777. doi:10.1016/j.autrev.2019.06.009
- Chen, Z., He, L., Li, L., and Chen, L. (2018). The P2X7 purinergic receptor: An emerging therapeutic target in cardiovascular diseases. *Clin. Chim. Acta.* 479, 196–207. doi:10.1016/j.cca.2018.01.032
- Chiozzi, P., Sanz, J. M., Ferrari, D., Falzoni, S., Aleotti, A., Buell, G. N., et al. (1997). Spontaneous cell fusion in macrophage cultures expressing high levels of the P2Z/P2X7 receptor. *J. Cell Biol.* 138 (3), 697–706. doi:10.1083/jcb.138.3.697
- Cisneros-Mejorado, A. J., Perez-Samartin, A., Domercq, M., Arellano, R. O., Gottlieb, M., Koch-Nolte, F., et al. (2020). P2X7 receptors as a therapeutic target in cerebrovascular diseases. *Front. Mol. Neurosci.* 13, 92. doi:10.3389/fnmol.2020.00092
- Clarke, L., Fairley, S., Zheng-Bradley, X., Streeter, I., Perry, E., Lowy, E., et al. (2017). The international genome sample resource (igsr): A worldwide collection of genome variation incorporating the 1000 genomes Project data. *Nucleic Acids Res.* 45 (1), D854–D859. doi:10.1093/nar/gkw829
- Clarke, L., Zheng-Bradley, X., Smith, R., Kulesha, E., Xiao, C., Toneva, I., et al. (2012). The 1000 genomes Project: Data management and community access. *Nat. Methods* 9 (5), 459–462. doi:10.1038/nmeth.1974
- Coutinho-Silva, R., Stahl, L., Raymond, M. N., Jungas, T., Verbeke, P., Burnstock, G., et al. (2003). Inhibition of chlamydial infectious activity due to P2X7R-dependent phospholipase D activation. *Immunity* 19 (3), 403–412. doi:10.1016/s1074-7613(03)00235-8
- Cunningham, F., Allen, J. E., Allen, J., Alvarez-Jarreta, J., Amode, M. R., Armean, I. M., et al. (2022). Ensembl 2022. *Nucleic Acids Res.* 50 (D1), D988–D995. doi:10.1093/nar/gkab1049
- Danquah, W., Meyer-Schwesinger, C., Rissiek, B., Pinto, C., Serracant-Prat, A., Amadi, M., et al. (2016). Nanobodies that block gating of the P2X7 ion channel ameliorate inflammation. *Sci. Transl. Med.* 8 (366), 366ra162. doi:10.1126/scitranslmed.aaf8463
- De Marchi, E., Orioli, E., Dal Ben, D., and Adinolfi, E. (2016). P2X7 receptor as a therapeutic target. *Adv. Protein Chem. Struct. Biol.* 104, 39–79. doi:10.1016/bs.apectsb.2015.11.004
- Delaneau, O., Marchini, J., and Genomes, P. C. (2014). Integrating sequence and array data to create an improved 1000 Genomes Project haplotype reference panel. *Nat. Commun.* 5, 3934. doi:10.1038/ncomms4934
- Deussing, J. M., and Arzt, E. (2018). P2X7 receptor: A potential therapeutic target for depression? *Trends Mol. Med.* 24 (9), 736–747. doi:10.1016/j.molmed.2018.07.005
- Di Virgilio, F., Chiozzi, P., Ferrari, D., Falzoni, S., Sanz, J. M., Morelli, A., et al. (2001). Nucleotide receptors: An emerging family of regulatory molecules in blood cells. *Blood* 97, 587–600. doi:10.1182/blood.v97.3.587
- Di Virgilio, F., Dal Ben, D., Sarti, A. C., Giuliani, A. L., and Falzoni, S. (2017). The P2X7 receptor in infection and inflammation. *Immunity* 47 (1), 15–31. doi:10.1016/j.immuni.2017.06.020
- Di Virgilio, F., Falzoni, S., Chiozzi, P., Sanz, J. M., Ferrari, D., and Buell, G. N. (1999). ATP receptors and giant cell formation. *J. Leukoc. Biol.* 66 (5), 723–726. doi:10.1002/jlb.66.5.723
- Di Virgilio, F. (1995). The P2Z purinoceptor: An intriguing role in immunity, inflammation and cell death. *Immunol. Today* 16 (11), 524–528. doi:10.1016/0167-5699(95)80045-X
- Domercq, M., and Matute, C. (2019). Targeting P2X4 and P2X7 receptors in multiple sclerosis. *Curr. Opin. Pharmacol.* 47, 119–125. doi:10.1016/j.coph.2019.03.010

The remaining authors declare that the research was conducted in the absence of any commercial or financial relationships that could be construed as a potential conflict of interest.

Publisher's note

All claims expressed in this article are solely those of the authors and do not necessarily represent those of their affiliated organizations, or those of the publisher, the editors and the reviewers. Any product that may be evaluated in this article, or claim that may be made by its manufacturer, is not guaranteed or endorsed by the publisher.

- Dong, Y., Chen, Y., Zhang, L., Tian, Z., and Dong, S. (2020). P2X7 receptor acts as an efficient drug target in regulating bone metabolism system. *Biomed. Pharmacother.* 125, 110010. doi:10.1016/j.biopha.2020.110010
- Drill, M., Jones, N. C., Hunn, M., O'Brien, T. J., and Monif, M. (2021). Antagonism of the ATP-gated P2X7 receptor: A potential therapeutic strategy for cancer. *Purinergic Signal.* 17 (2), 215–227. doi:10.1007/s11302-021-09776-9
- Engel, T., Nicke, A., Deussing, J. M., Sperlagh, B., and Diaz-Hernandez, M. (2021). Editorial: P2X7 as common therapeutic target in Brain diseases. *Front. Mol. Neurosci.* 14, 656011. doi:10.3389/fnmol.2021.656011
- Fairbairn, I. P., Stober, C. B., Kumararatne, D. S., and Lammass, D. A. (2001). ATP-mediated killing of intracellular mycobacteria by macrophages is a P2X(7)-dependent process inducing bacterial death by phagosome-lysosome fusion. *J. Immunol.* 167 (6), 3300–3307. doi:10.4049/jimmunol.167.6.3300
- Feng, Y. H., Li, X., Wang, L., Zhou, L., and Gorodeski, G. I. (2006). A truncated P2X7 receptor variant (P2X7-j) endogenously expressed in cervical cancer cells antagonizes the full-length P2X7 receptor through hetero-oligomerization. *J. Biol. Chem.* 281 (25), 17228–17237. doi:10.1074/jbc.M602999200
- Ferrari, D., Chiozzi, P., Falzoni, S., Dal Susino, M., Melchiorri, L., Baricordi, O. R., et al. (1997). Extracellular ATP triggers IL-1 beta release by activating the purinergic P2Z receptor of human macrophages. *J. Immunol.* 159 (3), 1451–1458.
- Ferrari, D., Pizzirani, C., Adinolfi, E., Lemoli, R. M., Curti, A., Idzko, M., et al. (2006). The P2X7 receptor: A key player in IL-1 processing and release. *J. Immunol.* 176 (7), 3877–3883. doi:10.4049/jimmunol.176.7.3877
- Genetzakis, E., Gilchrist, J., Kassiou, M., and Figtree, G. A. (2022). Development and clinical translation of P2X7 receptor antagonists: A potential therapeutic target in coronary artery disease? *Pharmacol. Ther.* 237, 108228. doi:10.1016/j.pharmthera.2022.108228
- Gorecki, D. C. (2019). P2X7 purinoceptor as a therapeutic target in muscular dystrophies. *Curr. Opin. Pharmacol.* 47, 40–45. doi:10.1016/j.coph.2019.02.003
- Gu, B., Bendall, L. J., and Wiley, J. S. (1998). Adenosine triphosphate-induced shedding of CD23 and L-selectin (CD62L) from lymphocytes is mediated by the same receptor but different metalloproteases. *Blood* 92 (3), 946–951. doi:10.1182/blood.v92.3.946
- Gu, B. J., Sluyter, R., Skarratt, K. K., Shemon, A. N., Dao-Ung, L. P., Fuller, S. J., et al. (2004). An Arg307 to Gln polymorphism within the ATP-binding site causes loss of function of the human P2X7 receptor. *J. Biol. Chem.* 279 (30), 31287–31295. doi:10.1074/jbc.M313902200
- Gu, B. J., Zhang, W., Worthington, R. A., Sluyter, R., Dao-Ung, P., Petrou, S., et al. (2001). A Glu-496 to Ala polymorphism leads to loss of function of the human P2X7 receptor. *J. Biol. Chem.* 276 (14), 11135–11142. doi:10.1074/jbc.M010353200
- Gudipaty, L., Munetz, J., Verhoef, P. A., and Dubyak, G. R. (2003). Essential role for Ca²⁺ in regulation of IL-1beta secretion by P2X7 nucleotide receptor in monocytes, macrophages, and HEK-293 cells. *Am. J. Physiol. Cell Physiol.* 285 (2), C286–C299. doi:10.1152/ajpcell.00070.2003
- Huang, Z., and Tan, S. (2021). P2X7 receptor as a potential target for major depressive disorder. *Curr. Drug Targets* 22 (10), 1108–1120. doi:10.2174/1389450122666210120141908
- Hubert, S., Rissiek, B., Klages, K., Huehn, J., Sparwasser, T., Haag, F., et al. (2010). Extracellular NAD⁺ shapes the Foxp3+ regulatory T cell compartment through the ART2-P2X7 pathway. *J. Exp. Med.* 207 (12), 2561–2568. doi:10.1084/jem.20091154
- Hudek, A. K., Cheung, J., Boright, A. P., and Scherer, S. W. (2003). Genescript: DNA sequence annotation pipeline. *Bioinformatics* 19 (9), 1177–1178. doi:10.1093/bioinformatics/btg134
- Illes, P., Rubini, P., Huang, L., and Tang, Y. (2019). The P2X7 receptor: A new therapeutic target in alzheimer's disease. *Expert Opin. Ther. Targets* 23 (3), 165–176. doi:10.1080/14728222.2019.1575811
- Jamieson, G. P., Snook, M. B., Thurlow, P. J., and Wiley, J. S. (1996). Extracellular ATP causes loss of L-selectin from human lymphocytes via occupancy of P2Z purinoceptors. *J. Cell. Physiol.* 166 (3), 637–642. doi:10.1002/(SICI)1097-4652(199603)166:3<637::AID-JCP19>3.0.CO;2-3
- Jumper, J., Evans, R., Pritzel, A., Green, T., Figurnov, M., Ronneberger, O., et al. (2021). Highly accurate protein structure prediction with AlphaFold. *Nature* 596 (7873), 583–589. doi:10.1038/s41586-021-03819-2
- Jumper, J., and Hassabis, D. (2022). Protein structure predictions to atomic accuracy with AlphaFold. *Nat. Methods* 19 (1), 11–12. doi:10.1038/s41592-021-01362-6
- Karasawa, A., and Kawate, T. (2016). Structural basis for subtype-specific inhibition of the P2X7 receptor. *Elife* 5, e22153. doi:10.7554/eLife.22153
- Karasawa, A., Michalski, K., Mikhelzon, P., and Kawate, T. (2017). The P2X7 receptor forms a dye-permeable pore independent of its intracellular domain but dependent on membrane lipid composition. *Elife* 6, e31186. doi:10.7554/eLife.31186
- Khakh, B. S., and North, R. A. (2006). P2X receptors as cell-surface ATP sensors in health and disease. *Nature* 442 (7102), 527–532. doi:10.1038/nature04886
- Koch-Nolte, F., Eichhoff, A., Pinto-Espinoza, C., Schwarz, N., Schafer, T., Menzel, S., et al. (2019). "Novel biologics targeting the P2X7 ion channel Curr Opin Pharmacol: Curr. Opin. Pharmacol.", 47, 110–118. doi:10.1016/j.coph.2019.03.001
- la Sala, A., Ferrari, D., Di Virgilio, F., Idzko, M., Norgauer, J., and Girolomoni, G. (2003). Alerting and tuning the immune response by extracellular nucleotides. *J. Leukoc. Biol.* 73 (3), 339–343. doi:10.1189/jlb.0802418
- Lammass, D. A., Stober, C., Harvey, C. J., Kendrick, N., Panchalingam, S., and Kumararatne, D. S. (1997). ATP-induced killing of mycobacteria by human macrophages is mediated by purinergic P2Z(P2X7) receptors. *Immunity* 7, 433–444. doi:10.1016/s1074-7613(00)80364-7
- Lazarowski, E. R., Boucher, R. C., and Harden, T. K. (2003). Mechanisms of release of nucleotides and integration of their action as P2X- and P2Y-receptor activating molecules. *Mol. Pharmacol.* 64 (4), 785–795. doi:10.1124/mol.64.4.785
- Le Dare, B., Ferron, P. J., and Gicquel, T. (2021). The purinergic P2X7 receptor-NLRP3 inflammasome pathway: A new target in alcoholic liver disease? *Int. J. Mol. Sci.* 22 (4), 2139. doi:10.3390/ijms22042139
- Li, Q., Zhu, X., Song, W., Peng, X., and Zhao, R. (2020). The P2X7 purinergic receptor: A potential therapeutic target for lung cancer. *J. Cancer Res. Clin. Oncol.* 146 (11), 2731–2741. doi:10.1007/s00432-020-03379-4
- MacKenzie, A., Wilson, H. L., Kiss-Toth, E., Dower, S. K., North, R. A., and Surprenant, A. (2001). Rapid secretion of interleukin-1beta by microvesicle shedding. *Immunity* 15, 825–835. doi:10.1016/s1074-7613(01)00229-1
- Madden, T. L., Tatusov, R. L., and Zhang, J. (1996). Applications of network BLAST server. *Methods Enzymol.* 266, 131–141. doi:10.1016/s0076-6879(96)66011-x
- Magalhaes, H. I. R., and Castelucci, P. (2021). Enteric nervous system and inflammatory bowel diseases: Correlated impacts and therapeutic approaches through the P2X7 receptor. *World J. Gastroenterol.* 27 (46), 7909–7924. doi:10.3748/wjg.v27.i46.7909
- Mariathasan, S., Weiss, D. S., Newton, K., McBride, J., O'Rourke, K., Roose-Girma, M., et al. (2006). Cryopyrin activates the inflammasome in response to toxins and ATP. *Nature* 440 (7081), 228–232. doi:10.1038/nature04515
- McCarthy, A. E., Yoshioka, C., and Mansoor, S. E. (2019). Full-Length P2X7 structures reveal how palmitoylation prevents channel desensitization. *Cell* 179 (3), 659–670. e613. doi:10.1016/j.cell.2019.09.017
- McInnes, I. B., Cruwys, S., Bowers, K., and Braddock, M. (2014). Targeting the P2X7 receptor in rheumatoid arthritis: Biological rationale for P2X7 antagonism. *Clin. Exp. Rheumatol.* 32 (6), 878–882.
- McKenzie, A. D. J., Garrett, T. R., Werry, E. L., and Kassiou, M. (2022). Purinergic P2X7 receptor: A therapeutic target in amyotrophic lateral sclerosis. *ACS Chem. Neurosci.* 13 (10), 1479–1490. doi:10.1021/acscchemneuro.2c00133
- Mishra, A., Behura, A., Kumar, A., Naik, L., Swain, A., Das, M., et al. (2021). P2X7 receptor in multifaceted cellular signalling and its relevance as a potential therapeutic target in different diseases. *Eur. J. Pharmacol.* 906, 174235. doi:10.1016/j.ejphar.2021.174235
- North, R. A. (2002). Molecular physiology of P2X receptors. *Physiol. Rev.* 82 (4), 1013–1067. doi:10.1152/physrev.00015.2002
- R. A. North and A. Surprenant (2000). "Pharmacology of cloned P2X receptors," *Annu. Rev. Pharmacol. Toxicol.*, 40, 563, doi:10.1146/annurev.pharmtox.40.1.563
- Notredame, C., Higgins, D. G., and Heringa, J. (2000). T-coffee: A novel method for fast and accurate multiple sequence alignment. *J. Mol. Biol.* 302 (1), 205–217. doi:10.1006/jmbi.2000.4042
- Pacheco, P. A. F., and Faria, R. X. (2021). The potential involvement of P2X7 receptor in COVID-19 pathogenesis: A new therapeutic target? *Scand. J. Immunol.* 93 (2), e12960. doi:10.1111/sji.12960
- Park, J. H., and Kim, Y. C. (2017). P2X7 receptor antagonists: A patent review (2010–2015). *Expert Opin. Ther. Pat.* 27 (3), 257–267. doi:10.1080/13543776.2017.1246538
- Pegoraro, A., and Adinolfi, E. (2021). The ATP/P2X7 axis is a crucial regulator of leukemic initiating cells proliferation and homing and an emerging therapeutic target in acute myeloid leukemia. *Purinergic Signal.* 17 (3), 319–321. doi:10.1007/s11302-021-09789-4
- Pelegrin, P., and Surprenant, A. (2006). Pannexin-1 mediates large pore formation and interleukin-1beta release by the ATP-gated P2X7 receptor. *EMBO J.* 25 (21), 5071–5082. doi:10.1038/sj.emboj.7601378
- Perregaux, D. G., McNiff, P., Laliberte, R., Conklyn, M., and Gabel, C. A. (2000). ATP acts as an agonist to promote stimulus-induced secretion of IL-1 beta and IL-18 in human blood. *J. Immunol.* 165 (8), 4615–4623. doi:10.4049/jimmunol.165.8.4615

- Rassendren, F., Buell, G. N., Virginio, C., Collo, G., North, R. A., and Surprenant, A. (1997). The permeabilizing ATP receptor, P2X7. Cloning and expression of a human cDNA. *J. Biol. Chem.* 272 (9), 5482–5486. doi:10.1074/jbc.272.9.5482
- Rech, J. C., Bhattacharya, A., Letavic, M. A., and Savall, B. M. (2016). The evolution of P2X7 antagonists with a focus on CNS indications. *Bioorg. Med. Chem. Lett.* 26 (16), 3838–3845. doi:10.1016/j.bmcl.2016.06.048
- Recourt, K., van der Aart, J., Jacobs, G., de Kam, M., Drevets, W., van Nueten, L., et al. (2020). Characterisation of the pharmacodynamic effects of the P2X7 receptor antagonist JNJ-54175446 using an oral dexamphetamine challenge model in healthy males in a randomised, double-blind, placebo-controlled, multiple ascending dose trial. *J. Psychopharmacol.* 34 (9), 1030–1042. doi:10.1177/0269881120914206
- Seman, M., Adriouch, S., Scheuplein, F., Krebs, C., Freese, D., Glowacki, G., et al. (2003). NAD-Induced T cell death: ADP-ribosylation of cell surface proteins by ART2 activates the cytolytic P2X7 purinoceptor. *Immunity* 19 (4), 571–582. doi:10.1016/s1074-7613(03)00266-8
- Shemon, A. N., Sluyter, R., Fernando, S. L., Clarke, A. L., Dao-Ung, L. P., Skarratt, K. K., et al. (2006). A Thr357 to Ser polymorphism in homozygous and compound heterozygous subjects causes absent or reduced P2X7 function and impairs ATP-induced mycobacterial killing by macrophages. *J. Biol. Chem.* 281 (4), 2079–2086. doi:10.1074/jbc.M507816200
- Shokoples, B. G., Paradis, P., and Schiffrin, E. L. (2021). P2X7 receptors: An untapped target for the management of cardiovascular disease. *Arterioscler. Thromb. Vasc. Biol.* 41 (1), 186–199. doi:10.1161/ATVBAHA.120.315116
- Skarratt, K. K., Fuller, S. J., Sluyter, R., Dao-Ung, L. P., Gu, B. J., and Wiley, J. S. (2005). A 5' intronic splice site polymorphism leads to a null allele of the P2X7 gene in 1–2% of the Caucasian population. *FEBS Lett.* 579 (12), 2675–2678. doi:10.1016/j.febslet.2005.03.091
- Sluyter, R., Bartlett, R., Ly, D., and Yerbury, J. J. (2017). P2X7 receptor antagonism in amyotrophic lateral sclerosis. *Neural Regen. Res.* 12 (5), 749–750. doi:10.4103/1673-5374.206643
- Sluyter, R., Shemon, A. N., and Wiley, J. S. (2004). Glu496 to Ala polymorphism in the P2X7 receptor impairs ATP-induced IL-1 beta release from human monocytes. *J. Immunol.* 172 (6), 3399–3405. doi:10.4049/jimmunol.172.6.3399
- Smart, M. L., Gu, B., Panchal, R. G., Wiley, J., Cromer, B., Williams, D. A., et al. (2003). P2X7 receptor cell surface expression and cytolytic pore formation are regulated by a distal C-terminal region. *J. Biol. Chem.* 278 (10), 8853–8860. doi:10.1074/jbc.M211094200
- Solle, M., Labasi, J., Perregaux, D. G., Stam, E., Petrushova, N., Koller, B. H., et al. (2001). Altered cytokine production in mice lacking P2X(7) receptors. *J. Biol. Chem.* 276 (1), 125–132. doi:10.1074/jbc.M006781200
- Stokes, L., Fuller, S. J., Sluyter, R., Skarratt, K. K., Gu, B. J., and Wiley, J. S. (2010). Two haplotypes of the P2X(7) receptor containing the Ala-348 to Thr polymorphism exhibit a gain-of-function effect and enhanced interleukin-1beta secretion. *FASEB J.* 24 (8), 2916–2927. doi:10.1096/fj.09-150862
- Surprenant, A., Rassendren, F., Kawashima, E., North, R. A., and Buell, G. (1996). The cytolytic P2Z receptor for extracellular ATP identified as a P2X receptor (P2X7). *Science* 272, 735–738. doi:10.1126/science.272.5262.735
- Tassetto, M., Scialdone, A., Solini, A., and Di Virgilio, F. (2021). The P2X7 receptor: A promising pharmacological target in diabetic retinopathy. *Int. J. Mol. Sci.* 22 (13), 7110. doi:10.3390/ijms22137110
- Trowsdale, J. (2011). The MHC, disease and selection. *Immunol. Lett.* 137 (1–2), 1–8. doi:10.1016/j.imlet.2011.01.002
- Verma, A., Pittala, S., Alhozeel, B., Shteinifer-Kuzmine, A., Ohana, E., Gupta, R., et al. (2022). The role of the mitochondrial protein VDAC1 in inflammatory bowel disease: A potential therapeutic target. *Mol. Ther.* 30 (2), 726–744. doi:10.1016/j.ymthe.2021.06.024
- Vial, C., Roberts, J. A., and Evans, R. J. (2004). Molecular properties of ATP-gated P2X receptor ion channels. *Trends Pharmacol. Sci.* 25 (9), 487–493. doi:10.1016/j.tips.2004.07.008
- Wei, L., Syed Mortadza, S. A., Yan, J., Zhang, L., Wang, L., Yin, Y., et al. (2018). ATP-activated P2X7 receptor in the pathophysiology of mood disorders and as an emerging target for the development of novel antidepressant therapeutics. *Neurosci. Biobehav. Rev.* 87, 192–205. doi:10.1016/j.neubiorev.2018.02.005
- Wiley, J. S., Dao-Ung, L. P., Li, C., Shemon, A. N., Gu, B. J., Smart, M. L., et al. (2003). An Ile-568 to Asn polymorphism prevents normal trafficking and function of the human P2X7 receptor. *J. Biol. Chem.* 278 (19), 17108–17113. doi:10.1074/jbc.M212759200
- Ye, J., McGinnis, S., and Madden, T. L. (2006). Blast: Improvements for better sequence analysis. *Nucleic Acids Res.* 34, W6–W9. (Web Server issue): W6–9. doi:10.1093/nar/gkl164
- Young, C. N. J., and Gorecki, D. C. (2018). P2RX7 purinoceptor as a therapeutic target-the second coming? *Front. Chem.* 6, 248. doi:10.3389/fchem.2018.00248
- Zeng, D., Yao, P., and Zhao, H. (2019). P2X7, a critical regulator and potential target for bone and joint diseases. *J. Cell. Physiol.* 234 (3), 2095–2103. doi:10.1002/jcp.27544
- Zhu, X., Li, Q., Song, W., Peng, X., and Zhao, R. (2021). P2X7 receptor: A critical regulator and potential target for breast cancer. *J. Mol. Med.* 99 (3), 349–358. doi:10.1007/s00109-021-02041-x
- Zimmermann, H. (2000). Extracellular metabolism of ATP and other nucleotides. *Naunyn. Schmiedeberg. Arch. Pharmacol.* 362 (4–5), 299–309. doi:10.1007/s002100000309



OPEN ACCESS

EDITED BY

Francisco Ciruela,
University of Barcelona, Spain

REVIEWED BY

Peter Illes,
Leipzig University, Germany
Kristian Agmund Haanes,
University of Copenhagen, Denmark

*CORRESPONDENCE

Didier Communi,
Didier.Communi@ulb.be

[†]These authors have contributed equally
to this work and share last authorship

SPECIALTY SECTION

This article was submitted to
Experimental Pharmacology
and Drug Discovery,
a section of the journal
Frontiers in Pharmacology

RECEIVED 20 September 2022

ACCEPTED 22 November 2022

PUBLISHED 02 December 2022

CITATION

Horckmans M, Diaz Villamil E, Verdier C,
Laurell H, Ruidavets J-B, De Roeck L,
Combes G, Martinez LO and
Communi D (2022), Loss-of-function
N178T variant of the human P2Y₄
receptor is associated with decreased
severity of coronary artery disease and
improved glucose homeostasis.
Front. Pharmacol. 13:1049696.
doi: 10.3389/fphar.2022.1049696

COPYRIGHT

© 2022 Horckmans, Diaz Villamil,
Verdier, Laurell, Ruidavets, De Roeck,
Combes, Martinez and Communi. This is
an open-access article distributed
under the terms of the [Creative
Commons Attribution License \(CC BY\)](#).
The use, distribution or reproduction in
other forums is permitted, provided the
original author(s) and the copyright
owner(s) are credited and that the
original publication in this journal is
cited, in accordance with accepted
academic practice. No use, distribution
or reproduction is permitted which does
not comply with these terms.

Loss-of-function N178T variant of the human P2Y₄ receptor is associated with decreased severity of coronary artery disease and improved glucose homeostasis

Michael Horckmans¹, Esteban Diaz Villamil¹, Céline Verdier^{2,3},
Henrik Laurell², Jean-Bernard Ruidavets^{3,4}, Lucas De Roeck¹,
Guillaume Combes², Laurent O. Martinez^{2†} and
Didier Communi¹ ^{1†*}

¹Institute of Interdisciplinary Research, IRIBHM, Free University of Brussels, Brussels, Belgium, ²Institut des Maladies Métaboliques et Cardiovasculaires, I2MC, Inserm, Université de Toulouse, Université Toulouse III—Paul Sabatier (UPS), UMR1297, Toulouse, France, ³CHU de Toulouse, Toulouse University Hospital, Toulouse, France, ⁴CERPOP UMR, Inserm, University of Toulouse III, UPS, Toulouse, France

Human P2Y₄ is a UTP receptor, while in mice it is activated by both ATP and UTP. P2Y₄ knockout (KO) in mice protects against myocardial infarction and is characterized by increased adiponectin secretion by adipocytes, and decreased cardiac inflammation and permeability under ischemic conditions. The relevance of these data has, however, not been explored to date in humans. In a population study comprising 50 patients with coronary artery disease (CAD) and 50 age-matched control individuals, we analyzed P2RY4 mutations and their potential association with CAD severity and fasting plasma parameters. Among the mutations identified, we focused our attention on a coding region polymorphism (rs3745601) that results in replacement of the asparagine at residue 178 with threonine (N178T) located in the second extracellular loop of the P2Y₄ receptor. The N178T variant is a loss-of-function mutation of the human P2Y₄ receptor and is encountered less frequently in coronary patients than in control individuals. In coronary patients, carriers of the N178T variant had significantly reduced jeopardy and Gensini cardiac severity scores, as well as lower resting heart rates and plasma levels of N-terminal pro-brain natriuretic peptide (NT-proBNP). Regarding fasting plasma parameters, the N178T variant was associated with a lower concentration of glucose. Accordingly, P2Y₄ KO mice had significantly improved glucose tolerance and insulin sensitivity compared with their WT littermate controls. The improvement of insulin sensitivity resulting from lack of the P2Y₄ receptor was no longer observed in the absence of adiponectin. The present study identifies a frequent loss-of-function P2Y₄ variant associated with less severe coronary artery atherosclerosis and lower fasting plasma glucose in coronary patients. The role of the P2Y₄ receptor in glucose homeostasis was confirmed in mouse. P2Y₄

antagonists could thus have therapeutic applications in the treatment of myocardial infarction and type 2 diabetes.

KEYWORDS

P2Y receptor, cardioprotection, extracellular nucleotides, glucose homeostasis, cardiac ischemia

Introduction

Patients suffering from coronary artery disease represent a heterogeneous group, with major differences in comorbidities and other metabolic factors such as insulin resistance. The risks of individual patients and the potential benefit they will experience from specific treatments depend on these various factors. The characterization of specific gene mutations in patients with adverse outcomes could improve the identification of patients at higher risk, as well as the follow-up after myocardial infarction (MI).

The human P2Y₄ subtype is a UTP receptor, originally cloned in our laboratory (Communi et al., 1995), and is activated by both ATP and UTP in mouse (Suarez-Huerta et al., 2001). We previously observed that the heart of mice deficient for the P2Y₄ subtype receptor had a significantly reduced size at adult age due to an angiogenic defect in the early days of postnatal development (Horckmans et al., 2012a). We also showed that P2Y₄ KO mice have decreased resistance in forced exercise tests with cardiac monitoring (Horckmans et al., 2012b). In another study, we observed that P2Y₄ KO mice are protected against myocardial infarction: they display smaller infarcts in the left anterior descending coronary artery ligation model (LAD ligation model), as well as a significant decrease in cardiac inflammation and permeability (Horckmans et al., 2015). Interestingly a higher level of adiponectin, which is a cardioprotective adipokine, correlated with an increased mass of cardiac adipose tissue in P2Y₄ KO mice (Horckmans et al., 2015; Lemaire et al., 2017).

Several studies have been undertaken to assess the genetic risk for MI in individuals independently of conventional risk factors (Nishihama et al., 2007). Different polymorphisms related to MI risk have been identified in genes such as glycoprotein Ib alpha, insulin promoter factor 1, and methylenetetrahydrofolate reductase, as well as in many other genes (Nishihama et al., 2007; Sakowicz et al., 2013). Other studies have focused on the association of polymorphisms in a particular gene, such as angiotensinogen or angiotensin-converting enzyme, and MI risk (Hamelin et al., 2011; Li et al., 2021). More specifically, AGT p.Thr174Met may increase the risk for MI, especially in the Asian population (Li et al., 2021), and the ACE-I/D polymorphism appears to be a genetic risk factor for MI at a young age (Hamelin et al., 2011). Several mutations have already been identified in P2Y receptor subtypes such as the P2Y₁₂ and P2Y₁ receptors (Lev et al., 2007), the P2Y₁₁ receptor (Amisten et al., 2007), and the P2Y₁₃ receptor (Amisten et al., 2008; Verdier et al., 2019). Only the Ala-87-Thr variant (rs3732757) of the human ATP receptor

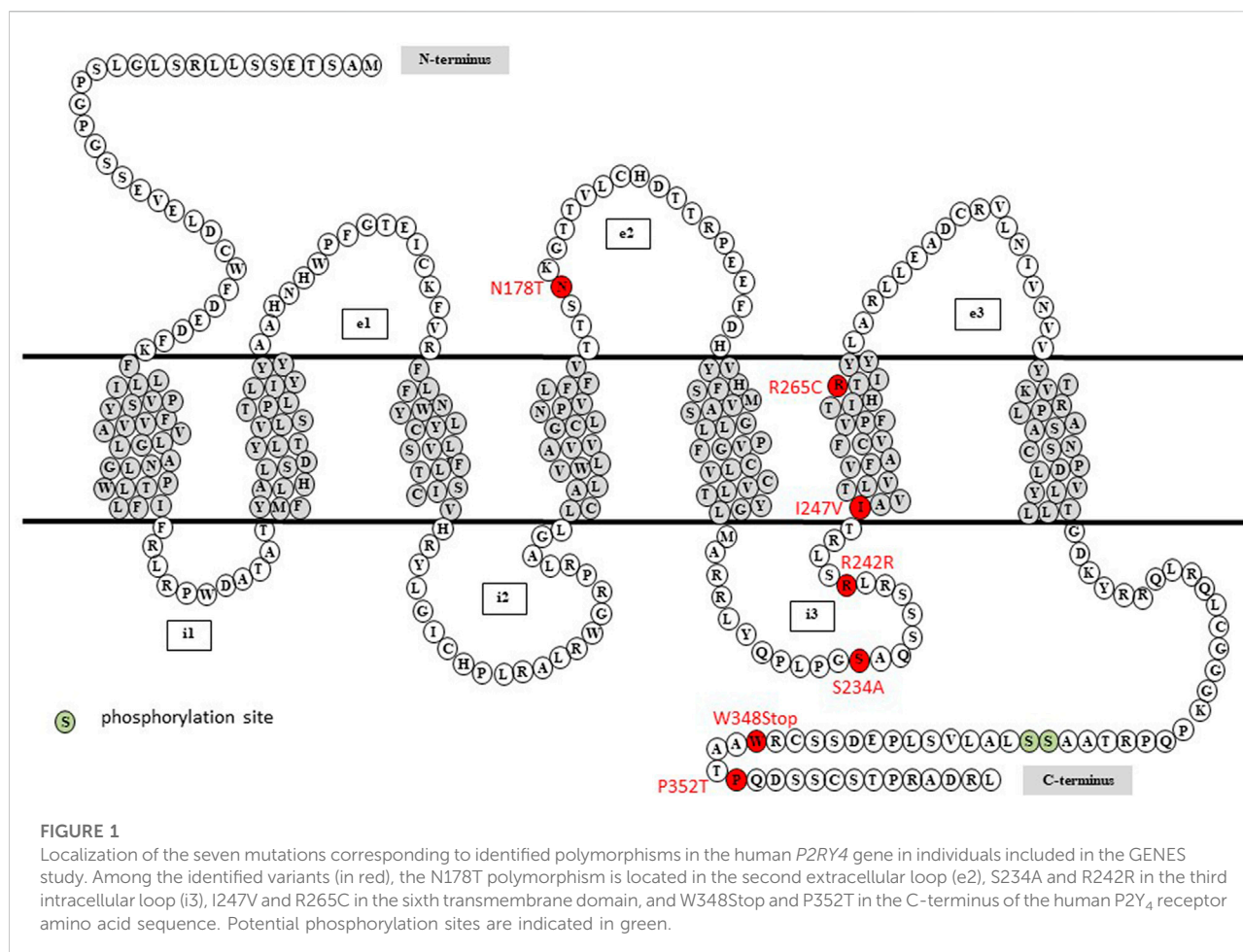
P2Y₁₁ has been associated with an increased risk of acute MI (Amisten et al., 2007), while the synonymous variant Ile-80-Ile (rs3732757) of the human ADP receptor P2Y₁₃ is associated with increased fat mass and a lower heart rate (Verdier et al., 2019).

Besides well-established leading risk factors for heart disease such as diabetes, obesity, high blood pressure and high level of low-density lipoprotein cholesterol (LDL-C), N-terminal pro-brain natriuretic peptide (NT-proBNP), a cardiac marker indicative of myocardial damages, has been related to heart failure severity and insulin resistance (Palazzuoli et al., 2010; Baldassarre et al., 2017). The present study aimed to analyze association of a common P2Y₄ receptor missense mutation with markers of cardiometabolic health and with the severity of CAD.

Materials and methods

Study sample

The GENES (Génétique et ENvironnement en Europe du Sud) study is a case-control study designed to assess the role of genetic, biological, and environmental determinants in the occurrence of CAD. As previously described (Genoux et al., 2016), all participants were men, recruited from 2001 to 2004, aged 45–74 years and living in the Toulouse area (south-western France). Stable CAD patients (cases) were recruited after admission to the Department of Cardiology of Toulouse University Hospital and control subjects were selected from the general population using electoral rolls. Stratification into decadal age groups was used to match the age distribution of the people with and without stable CAD. Stable CAD was defined as a history of acute coronary syndrome, a history of coronary artery revascularization, documented myocardial ischemia, stable angina, or the presence upon coronary angiography of coronary stenosis of 50% or more. Diffusion of coronary heart disease lesions was assessed by calculation of the Gensini score and the Duke jeopardy score based on data from coronary angiography (Califf et al., 1985). All participants underwent a medical examination at the same health center during the same period, including clinical and anthropometric measurements. Resting heart rate was measured after ≥5 min of rest, using an automatic sphygmomanometer and systolic blood pressure was detected with a hand-held Doppler probe. Information on cardiovascular risk factors were collected through standardized face-to-face interviews, performed by a single physician. Presence of dyslipidemia, diabetes mellitus or hypertension was assessed from the subjects' current treatments. Past medical history was collected and, for cases,



was also checked in the patients' medical files. Patients' medications at discharge were also considered. Blood was collected after an overnight fast, and a blood sample collection was constituted. Fasting plasma lipids, glucose, N-terminal pro-brain natriuretic peptide (NT-proBNP) and high-sensitivity cardiac troponin T (hs-TnT) were assayed with enzymatic reagents on automated analyzers (Hitachi 912 and Cobas 8000[®]; Roche Diagnostics, Meylan, France) (Genoux et al., 2016).

In the present study, the *P2RY4* gene was sequenced in 50 randomly selected CAD patients from the initial sample, age-matched to 50 control subjects (mean age 61.17 ± 7.26 and 60.55 ± 8.14 years, respectively).

P2RY4 sequencing and mutation analyses

Genomic deoxyribonucleic acid (gDNA) was isolated from ethylenediaminetetraacetic acid (EDTA)-treated blood samples using silica columns (NucleoSpin[®] Extract II; Macherey-Nagel, Duren, Germany). *P2RY4* is a 2.04 kb gene located in the q13 region of the X chromosome and is composed of one exon

encoding a 365-amino acid protein (Supplementary Material; Figure 1). The *P2RY4* gene was amplified from 100 ng gDNA using specific primers A and B flanking the open reading frame and 60°C as annealing temperature (Table 1), and sequencing was then carried out on 20 ng of DNA with six primers (A to F) specific for the *P2RY4* gene (Table 1) (3.2 pmol each), 1.5 µl of BigDye[™] 5x buffer, 0.8 µl of Ready Reaction Premix, and 10 µl of water. Reactions and readings were performed using an Applied Biosystems 3130 analyzer (Thermo Fisher Scientific). The obtained sequences were compared to the wild-type *P2RY4* gene sequence using SeqScape v2.5 software (Thermo Fisher Scientific) or Ape (A plasmid editor). Minor allele frequency (MAF) values were retrieved from the NCBI dbSNP database.

Functional analysis of the human P2Y₄ N178T variant

To compare the nucleotide response of N178T variant and wild-type (WT) *P2Y₄* receptors, the *P2RY4* gene sequence was inserted in a pcDNA3 expression vector and transfected in

TABLE 1 Sets of specific primers for the human *P2RY4* gene.

Primer name	Sequence (5' to 3')	PCR	qRT-PCR	Sequencing
A (forward)	CAGCTCTCCCTAGTGCTTCAA	X		X
B (reverse)	TCTCCAGAGCCTGGAAAAGA	X		X
C (forward)	CAAGTTCGTCCGCTTTCTTT		X	X
D (reverse)	GGCTACGACCAACCAAACTG		X	X
E (forward)	TGAACATTGTCAACGTGGTCT			X
F (reverse)	CGTCGATATTGTCCCCAGT			X

Primers A and B were used to amplify the entire *P2RY4* coding sequence from all individuals. All primers were used to determine the presence or absence of SNPs in *P2RY4* gene in all individuals. Primers C and D were used to determine the level of *P2Y₄* mRNA in quantitative reverse transcription-PCR experiments in stably transfected 1321N1 cells.

1321N1 cells, in parallel with WT *P2Y₄* receptor transfection. The transfected 1321N1 cells were harvested in PBS-EDTA (5 mM) at 37°C and then resuspended at 2×10^6 cells/ml in DMEM supplemented with 10% FBS (fetal bovine serum). Two days after transfection, the 1321N1 transfected cells were selected with 400 µg/ml G418 (Life Technologies, Inc., Merelbeke, Belgium) and maintained in the same medium. From the pool of transfected 1321N1 cells, individual clones were isolated by limiting dilution and tested for their *P2Y₄* mRNA expression by quantitative reverse transcription PCR (qRT-PCR). The transfected 1321N1 cells were then loaded with Calcium Sensor Dye 514 (2 µl/ml) and incubated for 30 min at 37°C. UTP 100 µM and ATP 100 µM calcium responses were quantified in N178T *P2Y₄*-transfected and WT *P2Y₄*-transfected cells and expressed as a percentage of the ionomycin response (5 µg/ml). UTP, ATP, and ionomycin calcium responses were recorded by flow cytometry with a high-speed acquisition during 60 s and quantified for different clonal 1321N1 cell cultures with various expression levels of N178T and WT *P2Y₄* mRNA.

P2Y₄-GFP constructs were then generated by insertion of the GFP coding sequence in frame with the N178T *P2Y₄* and WT *P2Y₄* coding sequences in a pEGFPN1 vector. To generate these constructs, WT and c.533T>G (p.N178T) mutated *P2Y₄* sequences were produced with a Hind III restriction site inserted directly upstream of the stop codon of the *P2RY4* gene. The obtained constructs were transiently transfected into HEK-293 cells to analyze the expression of GFP-tagged N178T *P2Y₄* and GFP-WT *P2Y₄* receptors, and to compare the GFP signal using ZoeTM Fluorescent Cell Imager (Bio-Rad Laboratories, Temse, Belgium).

Quantitative reverse transcription PCR

Total mRNAs were extracted from different clonal transfected 1321N1 cell cultures in TRIzol reagent followed by purification with RNeasy kit column (Qiagen, Antwerp, Belgium). mRNA was reverse transcribed using random hexamers and Superscript II Reverse Transcriptase

(Invitrogen, Thermo Fisher Scientific, Carlsbad, CA, United States). qRT-PCR amplification mixtures contained 10 ng template cDNA and the specific *P2Y₄* primers C and D (Table 1). Reactions were run on a 7500 Fast Real Time PCR System (Applied Biosystems, Foster City, CA, United States) with an annealing temperature of 60°C for primers C and D. qRT-PCR data were expressed as Ct obtained for *P2Y₄* mRNA in clonal transfected 1321 cells.

Glucose and insulin tolerance tests

Adiponectin knockout (KO) mice named B6; 129-Adipo^{tm1Chan/J} were purchased at JAX, The Jackson Laboratory (Bar Harbor, ME, United States). C57BL/6J *P2Y₄* KO and *P2Y₄*/adiponectin double-KO mice were generated in our laboratory. Glucose and insulin tolerance tests were performed with a comparable amount of male and female 9- to 11-week-old *P2Y₄* KO, adiponectin KO, and *P2Y₄*/adiponectin double-KO mice. Briefly, 6-h fasted mice were weighed and then injected intraperitoneally with either glucose (2 g/kg body weight) or insulin (0.5 U/kg body weight). Blood samples were collected from the tail vein, and glucose concentrations were measured before and at 10, 20, 30, 60, and 120 min after intraperitoneal injection. Plasma glucose readings were taken from the tail blood using teststrips for OneTouch Ultra2 blood glucose meter (LifeScan, Inc.). The area under the curve was calculated using GraphPad software.

Statistics

Quantitative parameters are expressed as means ± standard error of the mean (SEM). Between-group differences for quantitative variables were tested using Student's *t*-test for unpaired series (Welch's test in case of heteroscedasticity), and the statistical analyses were performed with Prism Software (version 6; GraphPad, CA, United States). All the data obtained from the mouse strain analyses are expressed as means ± SEM. For parallel repeated-measures studies, ANOVA

was used with Bonferroni *post hoc* evaluation to determine the significance of individual time points. A two-tailed $p < 0.05$ was considered significant.

Study approval

The study protocol was approved by the local ethics committee (CCPPRB, Toulouse/Sud-Ouest, file #1-99-48, Feb 2000), with all patients having provided written informed consent prior to participation. The biological sample collection was declared as DC-2008-463 #1 to the French Ministry of Research and to the Regional Health authority. Information and biological samples were collected from individuals according to the principles expressed in the Declaration of Helsinki.

All animal work and *in vivo* models were conducted in accordance with the European Community guidelines for the care and use of laboratory animals and approved by the ethics committee of the Free University of Brussels (current approved protocols 659N and 714N).

Results

P2RY4 gene mutations in individuals from the GENES study

We sequenced the *P2RY4* gene in 50 male patients with CAD and 50 age-matched male control subjects taken from the Génétique et Environnement en Europe du Sud (GENES) study for which different clinical, biological and cardiac parameters at baseline are shown in Table 3. Briefly, CAD patients had a higher systolic blood pressure than controls subjects and were more treated for diabetes, dyslipidemia and hypertension. Among metabolic markers, total cholesterol and LDL-cholesterol were lower in CAD patients, reflecting the effect of the larger proportion of patients treated for dyslipidemia compared to control subjects. However, CAD patients displayed higher levels of triglycerides and lower HDL-C.

Sequencing chromatograms for *P2RY4* are available as Supplementary Material. We identified seven single-nucleotide variants in the *P2RY4* coding sequence (Supplementary Table S1) located in different parts of the corresponding P2Y₄ amino acid sequence: the N178T substitution is located in the second extracellular loop (e2), S234A and R242R in the third intracellular loop (i3), I247V and R265C in the sixth transmembrane domain (TM6), and W348Stop and P352T in the C-terminus (Figure 1; Table 2).

Among these variants, we decided to focus our analysis on the most common c.533T>G (p.N178T) variant (further referred to as the N178T variant) that was found with a higher frequency in control individuals than in CAD patients (Table 3). The

N178T variant frequency was searched for in the dbSNP database to determine its prevalence in certain geographic populations (Figure 2A). The worldwide distribution of the N178T variant revealed that it is very frequent (33.12% in total, 87674/264690, TOPMED) and predominant in Africa and East Asia (Figure 2A). Effectively, the frequency of N178T variant was 65% in Africa and 52.5% in East Asia in the dbSNP database. In our study population, representative of the south-west France, we observed a reduction of N178T variant frequency in CAD patients compared with control individuals. The frequency was 32% in the 50 control individuals versus 18% in the 50 CAD patients ($p = 0.11$; Figure 2B; Table 3).

Cardiometabolic health in coronary patients carrying the N178T variant of P2Y₄ receptor

In the CAD patients of our study population, carriers of the N178T variant had less severe coronary artery atherosclerosis compared to WT patients, as estimated by the jeopardy score documenting the diffusion of coronary heart disease lesions, and the Gensini score documenting the number, location, and degree of stenosis of coronary artery lesions (Figure 2C). Regarding markers of cardiac function, the resting heart rates were lower in CAD patients carrying the N178T variant (Table 4, 55.5 ± 3.4 versus 64.6 ± 1.5 bpm in WT; mean \pm SEM, $p = 0.015$) as well as the plasma level of NT-proBNP (Figure 2D; Table 4, 177.6 ± 56.3 versus 493.3 ± 89.1 pg/ml in WT; mean \pm SEM, $p = 0.004$). Regarding plasma biological parameters, the presence of the N178T variant was associated with a significant lower concentration of fasting plasma glucose (Figure 2E; Table 4). No differences were seen between N178T and WT patients regarding plasma lipids levels or anthropometric parameters such as age, waist circumference, and body mass index (Table 4).

N178T polymorphism is a loss-of-function mutation of the P2Y₄ receptor

We have previously demonstrated that knockout of the P2Y₄ receptor in mice induced cardioprotection in the LAD ligation model (Horckmans et al., 2015). A possible link could exist between reduced cardiac severity scores associated with the N178T P2Y₄ human receptor and the cardioprotective effect of P2Y₄ receptor loss in mouse. We hence compared the nucleotide response of the N178T and WT P2Y₄ human receptors. The N178T P2Y₄ coding sequence was inserted in a pcDNA3 expression vector and transfected into 1321N1 astrocytoma cells, in parallel with WT P2Y₄ receptor-pcDNA3 transfection of 1321N1 cells. 1321N1 astrocytoma cells are commonly used for nucleotide receptor transfection due to their unique lack of endogenous nucleotide receptors. We

TABLE 2 Identification of *P2RY4* gene variants in control individuals and CAD patients.

Reference	Nucleotide position in CDS and substitution (transcript allele change)	MAF (ToPMed)	Protein: Amino acid change and position	Protein: Position	Control individuals (<i>n</i> = 50): Number of carriers	CAD patients (<i>n</i> = 50): Number of carriers
rs1152187	c.533 T>G (AAC → ACC)	0.331	N178T	e2	16	9
rs3829709	c.700 A>C (TCT → GCT)	0.133	S234A	i3	6	5
rs3829708	c.726 G>T (CGC → CGA)	0.100	R242R	i3	6	5
rs56217451	c.739 T>C (ATA → GTA)	0.040	I247V	TM6	4	2
rs147302991	c.793 G>A (CGC → TGC)	<0.001	R265C	TM6	1	0
rs41310667	c.1043 C>T (TGG → TAG)	0.014	W348(Stop)	C-term	5	3
rs72628860	c.1054 G>T (CCC → ACC)	0.040	P352T	C-term	4	2

Mutations identified after sequencing the human *P2RY4* gene in 50 control individuals and 50 individuals with coronary artery disease (CAD). Identification numbers, minor allele frequencies, and the positions in the human P2Y₄ receptor (e2, extracellular loop 2; i3, intracellular loop 3; TM6, transmembrane domain 6; C-term, C-terminal region) are indicated for each identified P2Y₄ variant. CDS (c.), coding DNA sequence; MAF, minor allele frequency.

TABLE 3 Baseline characteristics of the population from the GENES case-control study, according to status for CAD.

	Control (No CAD) <i>n</i> = 50	Case (CAD) <i>n</i> = 50	<i>p</i> -value ^a
Clinical			
Age, years	60.6 (1.2)	61.0 (1.0)	0.78
Body mass index, kg/m ²	26.8 (0.66)	27.9 (0.59)	0.24
Waist circumference, cm	96.0 (1.6)	99.7 (1.5)	0.11
Biological (fasting)			
Glucose, mmol/L	5.37 (0.11)	5.70 (0.25)	0.24 ^b
Triglycerides, g/L	1.34 (0.20)	1.70 (0.12)	0.0015 ^{c**}
Total cholesterol, g/L	2.23 (0.06)	2.01 (0.06)	0.016*
LDL-C, g/L	1.43 (0.05)	1.25 (0.06)	0.018*
HDL-C, g/L	0.55 (0.02)	0.43 (0.01)	0.001**
Cardiac parameters			
Resting heart rate, bpm	63.0 (1.2)	63.0 (1.5)	0.99
Systolic blood pressure, mmHg	134 (2.5)	144 (3.4)	0.016*
NT-proBNP, pg/mL	n.a	436.5 (75.5)	—
hs-TnT, pg/mL	n.a	81.1 (30.1)	—
Treatments			
Diabetes, <i>n</i> (%)	2 (4%)	13 (26%)	0.0021**
Dyslipidemia, <i>n</i> (%)	9 (18%)	34 (68%)	0.001**
Hypertension, <i>n</i> (%)	16 (32%)	35 (70%)	0.001**
N178T, <i>n</i> (%)	16 (32%)	9 (18%)	0.11

Variables were measured at baseline (i.e., when individuals were first included in the GENES cohort). For continuous variables, values are expressed as mean ± SEM. For categorical variables, values are expressed as number with frequency (%) in parentheses.

^aPaired Student's *t*-test, unless.

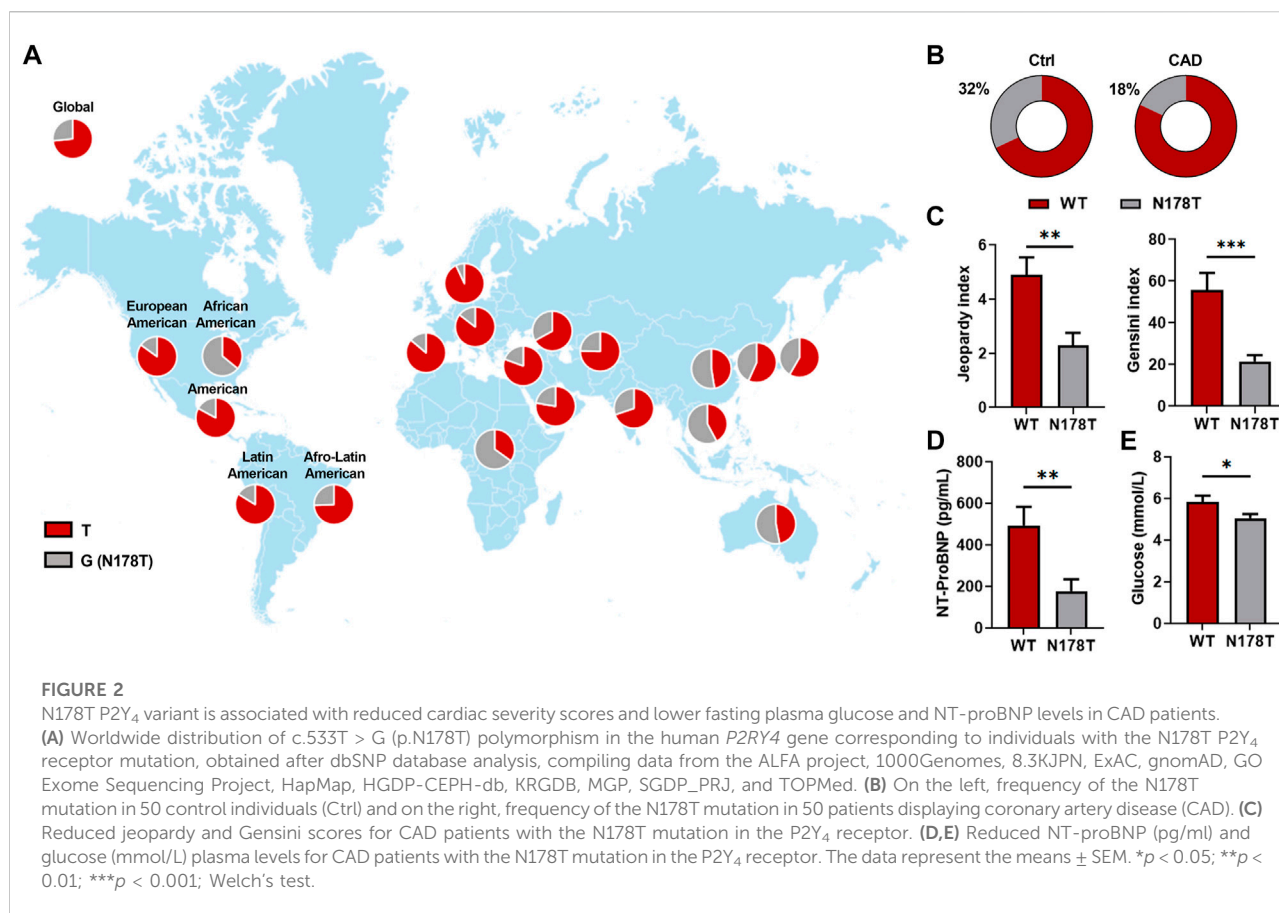
^bWelch's test in case of heteroscedasticity.

^cAnalyses performed on log transformed data. **p* < 0.05; ***p* < 0.01.

Bpm, beats per minute; CAD, coronary artery disease; HDL-C, high-density lipoprotein cholesterol; hs-TnT, high-sensitivity cardiac troponin T; LDL-C, low-density lipoprotein cholesterol; n.a., not available; NT-proBNP, N-terminal pro-brain natriuretic peptide.

observed a strong reduction of UTP and ATP calcium responses in a pool of pcDNA3-N178T P2Y₄ compared to pcDNA3-WT P2Y₄ G418-resistant transfected cells (Figure 3A). These reduced

calcium responses to UTP and ATP were observed in individual G418-resistant clones of transfected 1321N1 cells that had various expression levels (expressed as the Ct obtained in



qPCR experiments) (Figure 3A, right panels). We also analyzed the expression of green fluorescent protein (GFP)-N178T P2Y₄ and GFP-WT P2Y₄ receptors after construction and transient transfection of their respective pEGFPN1 expression vectors in HEK-293 cells. Microscopy analysis using ZoeTM Fluorescent Cell Imager revealed a loss of fluorescent signal for the N178T P2Y₄ receptor compared to the WT P2Y₄ receptor (Figure 3B).

Lack of P2Y₄ correlates with improved glucose tolerance and insulin sensitivity in mice

A possible association between cardioprotection and glucose homeostasis was further investigated in P2Y₄ KO mice using glucose and insulin tolerance tests (Figures 4A,B). P2Y₄ KO mice, characterized by adiponectin overexpression (Lemaire et al., 2017), had a significantly increased glucose tolerance and insulin sensitivity compared to their WT littermate controls (Figures 4A,B). Conversely, adiponectin KO and adiponectin/P2Y₄ double-KO (DKO) mice exhibited similar impaired glucose tolerance and insulin sensitivity, compared with P2Y₄ KO mice (Figures 4A,B). In glucose tolerance tests, the difference between

WT and P2Y₄ KO mice is only significant 15 min after glucose injection (Figure 4A, left panel), and on the area under the curve (Figure 4A, right panel). Significant interindividual variability was observed in insulin tolerance tests, especially for WT and adiponectin KO mice (Figure 4B). We observed a higher insulin sensitivity in P2Y₄ KO mice, significant 60 and 120 min after insulin injection, and impaired insulin sensitivity in adiponectin KO and DKO mice, compared to WT mice (Figure 4B).

Discussion

Whereas nucleotide receptors such as the P2Y₁ and P2Y₂ receptors are ubiquitously expressed, the P2Y₄ subtype has a more confined tissue distribution restricted mainly to the intestine, lung, heart, cardiac adipose tissue, pancreas and placenta (Communi et al., 1995; Suarez-Huerta et al., 2001; Horckmans et al., 2012a; Lemaire et al., 2017). The human P2Y₄ receptor is a UTP receptor, while the mouse P2Y₄ receptor is activated by both ATP and UTP (Suarez-Huerta et al., 2001). We have extensively studied the cardiac phenotype of P2Y₄ KO mice, which are characterized by reduced post-natal heart development (Horckmans et al.,

TABLE 4 Baseline characteristics of CAD patients, according to N178T status.

	CAD WT <i>n</i> = 41	CAD N178T <i>n</i> = 9	<i>p</i> -value ^a
Clinical			
Age, years	61.7 (1.0)	57.7 (3.4)	0.12
Body mass index, kg/m ²	27.7 (0.7)	28.7 (1.3)	0.51
Waist circumference, cm	99.6 (1.7)	100.0 (4.0)	0.93
Biological (fasting)			
Glucose, mmol/L	5.84 (0.30)	5.05 (0.20)	0.034 ^{b*}
Triglycerides, g/L	1.68 (0.13)	1.74 (0.29)	0.79 ^c
Total cholesterol, g/L	1.99 (0.07)	2.13 (0.13)	0.41
LDL-C, g/L	1.22 (0.07)	1.34 (0.11)	0.45
HDL-C, g/L	0.43 (0.02)	0.44 (0.02)	0.79
Cardiac parameters			
Resting heart rate, bpm	64.6 (1.5)	55.5 (3.4)	0.015 [*]
Systolic blood pressure, mmHg	145 (3.6)	138 (9.3)	0.41
NT-proBNP, pg/mL	493.3 (89.1)	177.6 (56.3)	0.004 ^{b**}
hs-TnT, pg/mL	92.6 (36.5)	28.9 (10.2)	0.10 ^b
Treatments			
Diabetes, <i>n</i> (%)	12 (29%)	1 (11%)	0.26
Dyslipidemia, <i>n</i> (%)	27 (66%)	7 (78%)	0.48
Hypertension, <i>n</i> (%)	30 (73%)	5 (56%)	0.29

Variables were measured at baseline (i.e., when individuals were first included in the GENES cohort). For continuous variables, values are expressed as mean \pm SEM. For categorical variables, values are expressed as number with frequency (%) in parentheses.

^aPaired Student's *t*-test, unless.

^bWelch's test in case of heteroscedasticity.

^cAnalyses performed on log transformed data. **p* < 0.05; ***p* < 0.01.

Bpm, beats per minute; CAD, coronary artery disease; HDL-C, high-density lipoprotein cholesterol; hs-TnT, high-sensitivity cardiac troponin T; LDL-C, low-density lipoprotein cholesterol; NT-proBNP, N-terminal pro-brain natriuretic peptide.

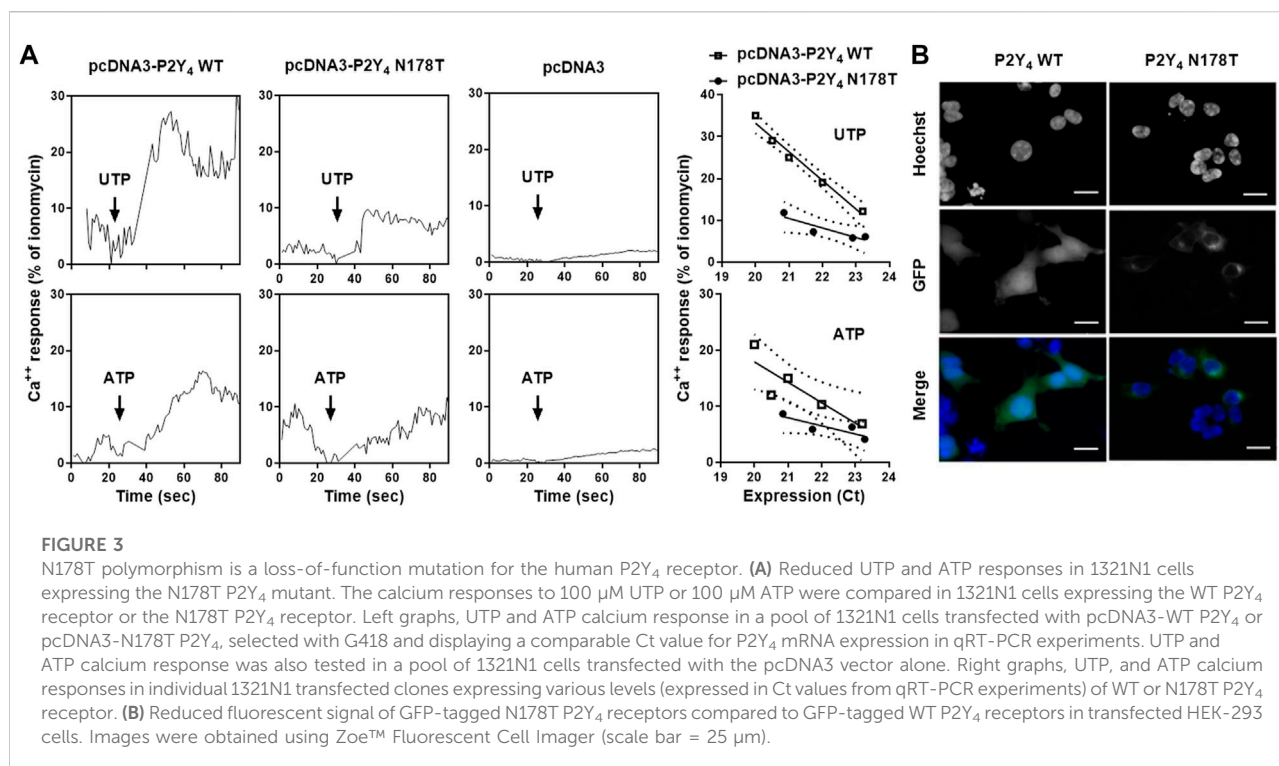
2012a), decreased resistance to exercise (Horckmans et al., 2012b), and protection against myocardial infarction (Horckmans et al., 2015). More specifically, P2Y₄ KO mice exhibit smaller infarcts in the LAD ligation model, as well as a significant decrease in cardiac inflammation and adiponectin overexpression (Horckmans et al., 2015).

Among the mutations identified in the human *P2RY4* gene in the present study, we focused our attention on the single nucleotide polymorphism c.533T>G (p.N178T) (rs1152187), corresponding to N178T substitution in the second extracellular loop of the human P2Y₄ receptor. This particular polymorphism was detected significantly less in CAD patients than in control individuals, albeit in a limited sequencing of the human *P2RY4* gene in 50 normal individuals and 50 patients. This missense P2Y₄ variant is widely present worldwide in the general population, and it is predominant in Africa and East Asia.

The frequency of N178T polymorphism in control individuals reported in the present study population, representative of the south-west France, is comparable to its mean worldwide distribution, with a frequency of 33%. Although ischemic heart disease remains relatively uncommon in sub-Saharan Africa, its incidence is rising due to the increasing prevalence of risk factors (Onen, 2013; Yao et al., 2022). The

epidemiology of ischemic heart disease in Africa remains largely enigmatic due to a lack of cardiologists and reliable health statistics (Keates et al., 2017). Higher stroke rates but lower coronary heart disease have been observed in Asian countries compared to Western countries (Ueshima et al., 2018). Analysis of outcomes after acute myocardial infarction (AMI) between South Asian, Chinese, and white patients has revealed significantly lower long-term mortality in South Asian patients (Khan et al., 2010). Naturally, the genetics of CAD is very complex, and heart disease statistics depend on multiple risk factors. No direct link can thus be made between these AMI incidence data and the worldwide distribution of the highly common N178T P2Y₄ receptor polymorphism.

Most interestingly, the presence of the N178T P2Y₄ variant in CAD patients is correlated with reduced jeopardy and Gensini scores of CAD severity. We investigated whether the N178T substitution could affect human P2Y₄ receptor activity, given that mice deficient in the P2Y₄ receptor are protected from myocardial infarction (Horckmans et al., 2015). We performed functional experiments on 1321N1 cell lines stably expressing both the wild-type and the N178T human P2Y₄ receptor. A loss of function of the N178T P2Y₄ receptor was observed in response to both UTP and ATP. ATP binds both



human and rat P2Y₄ receptor homologs, but whereas ATP activates the rat and mouse receptors, it antagonizes the human receptor (Herold et al., 2004). Interestingly, the N178T polymorphism is located in the second extracellular loop of the human P2Y₄ receptor, which has been reported to be a major determinant of agonist versus antagonist activity of ATP in rat and human P2Y₄ homologs (Herold et al., 2004). When a chimeric receptor is generated in which the second extracellular loop of the human P2Y₄ receptor is replaced with the corresponding region of the rat P2Y₄ receptor, ATP is fully agonistic toward the generated chimera (Herold et al., 2004). ATP is described as a partial agonist and even an antagonist of the human wild-type P2Y₄ receptor depending on its membrane expression level (Communi et al., 1995; Herold et al., 2004). The loss-of-function N178T polymorphism of the human P2Y₄ receptor identified in the present study led to its decreased membrane expression, but this mutation could also affect the structure of the second extracellular loop, which is important for nucleotide affinity.

Although reduced jeopardy and Gensini scores were observed in CAD patients with the N178T P2Y₄ variant, comparison with protection against myocardial infarction in P2Y₄ KO ischemic mice must be undertaken with caution. Among the other cardiac and metabolic parameters analyzed in CAD patients, we observed slower heart rates and reduced glucose plasma levels in patients with the N178T P2Y₄ receptor. Interestingly, glucose and insulin tolerance tests demonstrated

that P2Y₄ KO mice, characterized by adiponectin overexpression, had lower glycemia and a higher sensitivity to insulin than WT mice. As expected, insulin resistance was identified in adiponectin KO mice and higher sensitivity to insulin resulting from P2Y₄ loss was no longer observed in the absence of adiponectin in adiponectin/P2Y₄ double-KO mice.

The present study shows that the P2Y₄ receptor could be considered as a member of the P2Y receptor family involved in the regulation of glucose metabolism. The P2Y₄ receptor is able to couple to G_{q/11} proteins, but also to G_i proteins (Communi et al., 1996), which are known to have an antilipolytic effect. Another study has demonstrated that mice lacking adipocyte P2Y₆ receptor were protected from diet-induced obesity and were characterized by improved glucose tolerance and insulin sensitivity (Jain et al., 2020). It has been also shown that P2Y₂ and P2Y₄ receptors can regulate Cl⁻ and K⁺ channels and intracellular Ca²⁺ signalling in pancreatic ducts (Hede et al., 2005; Novak, 2008). More generally, the activation of nucleotide receptors by ATP participates in the potentiation of glucose-stimulated insulin secretion by increasing the exocytosis of insulin granules in pancreatic β-Cells (Mesto et al., 2022).

Among the measured parameters that were significantly different between wild-type and N178T CAD patients, NT-proBNP was particularly reduced in N178T CAD patients. The level of NT-proBNP is considered to be a cardiovascular risk factor and of prognostic value in patients with previous myocardial infarction (Reinstadler et al., 2016; Cao et al., 2022).

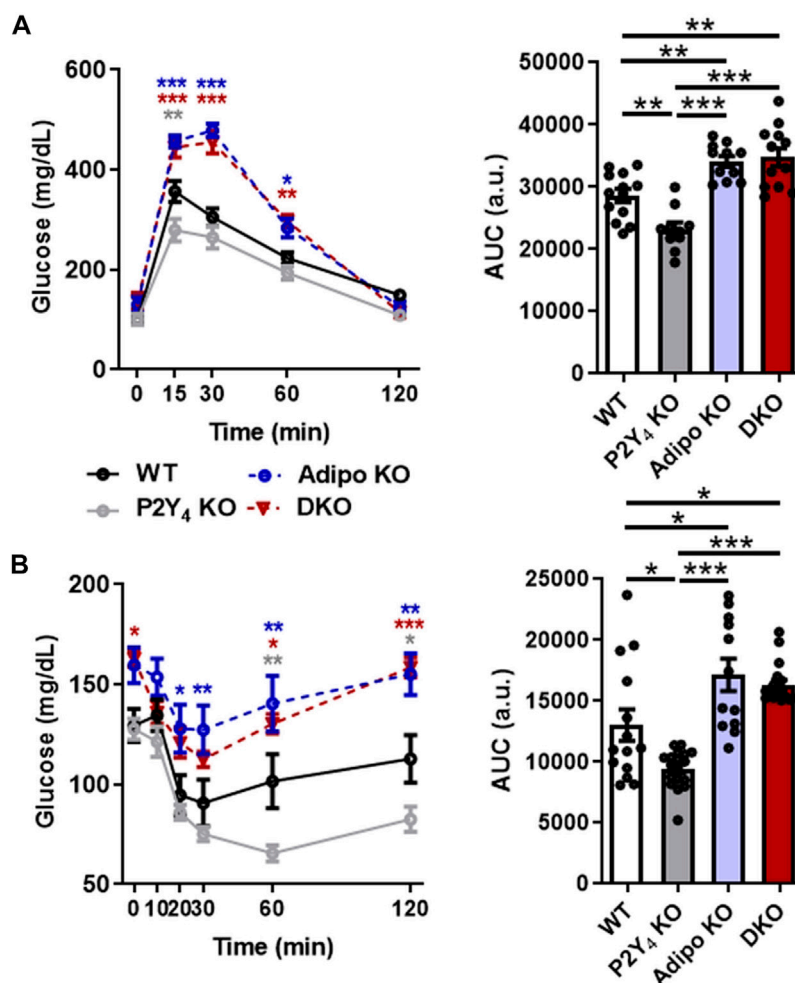


FIGURE 4

Loss of mouse P2Y₄ receptor improves glucose metabolism. **(A)** Glucose tolerance test in P2Y₄ KO mice. After 6 h-fasting, glucose (2 g/kg) was intraperitoneally injected, and blood glucose levels were monitored in WT, P2Y₄ KO, adiponectin KO (AdipoKO) and P2Y₄/adiponectin double-KO (DKO) mice ($n = 12-14$). Statistical differences from the control values (WT mice) are shown. **(B)** Insulin tolerance test in P2Y₄ KO mice. After 6 h-fasting, insulin (0.5 U/kg) was intraperitoneally injected, and blood glucose levels were monitored ($n = 8-14$). The area under the curve was quantified both in panels **(A,B)** with GraphPad Prism software (a.u., arbitrary unit). The data represent the means \pm SEM. * $p < 0.05$; ** $p < 0.01$; *** $p < 0.001$. Values for individual time points (left graph) and area under the curve (right graph) were analyzed using respectively one-way ANOVA test and two-way ANOVA test with Bonferroni *post hoc* evaluation.

The identification of biomarkers related to a high-risk population and prognosis prediction is a major factor in CAD preventive measures. NT-proBNP is a neurohormone synthesized and released by the heart in response to increased wall tension (Rorth et al., 2020). NT-proBNP is thus a key marker for heart failure but also a risk marker for the prediction of major adverse cardiovascular events (Redfors et al., 2018; Liu et al., 2021). Ischemic myocardium secretes elevated levels of NT-proBNP, even in the absence of left ventricular dysfunction (Goetze et al., 2003). The risk of a recurrent cardiac event is significantly higher in patients with elevated NT-proBNP levels (Cao et al., 2022). The level of specific biomarkers during a chronic or later phase is a better predictor of prognosis of cardiac

function than their level during the acute phase. Our study could contribute to the NT-proBNP level being taken into account in the risk assessment of patients with previous MI, in association with the detection of *P2RY4* gene polymorphisms.

The identification of this specific N178T P2Y₄ variant could be useful and contributive when combined with other known cardiac gene polymorphisms to predict the severity of infarction in humans. A personal approach based on individual genetic factors and metabolic parameters is important in the treatment of myocardial infarction. Nucleotide receptors can be considered to be key players in the regulation of cardioprotection and glucose homeostasis. Nucleotide receptors such as the P2Y₄ subtype, expressed in adipose tissues and regulating the production of

adipokines, can facilitate the onset of insulin resistance. Antagonists of P2Y receptors could thus have therapeutic applications in the treatment of type 2 diabetes. The present identification of a cardioprotective loss-of-function polymorphism of the human *P2RY4* gene correlated with reduced plasma levels of fasting glucose and NT-proBNP in CAD patients, as well as the insulin sensitivity in P2Y₄-deficient mice, support the notion that this nucleotide receptor constitutes another candidate for the development of such antagonists.

Data availability statement

The original contributions presented in the study are included in the article/**Supplementary Materials**, further inquiries can be directed to the corresponding author.

Ethics statement

The studies involving human participants were reviewed and approved by the Comité consultatif de protection des personnes dans la recherche biomédicale (CCPPRB), Toulouse/Sud-Ouest. The patients/participants provided their written informed consent to participate in this study. The animal study was reviewed and approved by the Comité d'Ethique du Bien-Etre Animal (CEBEA), Free University of Brussels.

Author contributions

MH, LOM, and DC designed the research study; MH, EDV, CV, HL, and J-BR analyzed the data; MH, EDV, CV, LDR, and GC conducted the experiments and acquired the data, MH, LOM, and DC wrote the manuscript.

Funding

This work was supported by Research Project and Research Credit of the Fonds National de la Recherche Scientifique (F.N.R.S.) of Belgium (J.0060.18 CDR grant), by an ATIMI (Attract Brains for Brussels, Belgium) grant of Innoviris Brussels (2019-BFB-106 ATIMI grants), by the Fonds pour la Chirurgie Cardiaque (FCC489698), by the Fund Lokumo, King Baudouin Foundation, Belgium (2017-B7131100-207336 grant), by Action de Recherche Concertée of the Communauté Française

de Belgique, by the Fonds d'Encouragement à la Recherche (F.E.R., U.L.B.) and by the Fédération Française de Cardiologie (FFC—MARTINEZ—Dotation Recherche 2022). MH was supported by ATIMI (Attract Brains for Brussels, Belgium) grants of Innoviris Brussels. EDV was supported by the F.R.I.A., Fonds National de la Recherche Scientifique, Communauté Française de Belgique, Belgium. LDR is supported by ULB, Belgium. DC is a Senior Research Associate of the Fonds National de la Recherche Scientifique, Communauté Française de Belgique, Belgium.

Acknowledgments

The authors thank Ingrid Langer for technical advice and help related to the realization of the P2Y₄ receptor expression vectors. The authors thank all the participants in the GENES Study and the Biological Resource Center for Biobanking [CHU Toulouse, Centre de Ressource Biologique (CRB Toulouse BioRessources), place Baylac—TSA 40031—Toulouse F-31059]. The authors thank Jean Ferrières and Bertrand Perret (Toulouse University Hospital) for their contributions to the GENES study design.

Conflict of interest

The authors declare that the research was conducted in the absence of any commercial or financial relationships that could be construed as a potential conflict of interest.

Publisher's note

All claims expressed in this article are solely those of the authors and do not necessarily represent those of their affiliated organizations, or those of the publisher, the editors and the reviewers. Any product that may be evaluated in this article, or claim that may be made by its manufacturer, is not guaranteed or endorsed by the publisher.

Supplementary material

The Supplementary Material for this article can be found online at: <https://www.frontiersin.org/articles/10.3389/fphar.2022.1049696/full#supplementary-material>

References

- Amisten, S., Braun, O., Johansson, L., Ridderstrale, M., Melander, O., and Erlinge, D. (2008). The P2Y₁₃ Met-158-Thr polymorphism, which is in linkage disequilibrium with P2Y₁₂ locus, is not associated with acute myocardial infarction. *Plos One* 3 (1), e1462. doi:10.1371/journal.pone.0001462

- Amisten, S., Melander, O., Wihlborg, A.-K., Berglund, G., and Erlinge, D. (2007). Increased risk of acute myocardial infarction and elevated levels of C-reactive protein in carriers of the Thr-87 variant of the ATP receptor P2Y₁₁. *Eur. Heart J.* 28, 13–18. doi:10.1093/eurheartj/ehl410
- Baldassarre, S., Fragapani, S., Panero, A., Fedele, D., Pinach, S., Lucchiari, M., et al. (2017). NTproBNP in insulin-resistance mediated conditions : Overweight/obesity, metabolic syndrome and diabetes. The population-based casale monferrato study. *Cardiovasc. Diabetol.* 16, 119. doi:10.1186/s12933-017-0601-z
- Califf, R. M., Phillips, H. R., 3rd, Hindman, M. C., Mark, D. B., Lee, K. L., Behar, V. S., et al. (1985). Prognostic value of a coronary artery jeopardy score. *J. Am. Coll. Cardiol.* 5 (5), 1055–1063. doi:10.1016/s0735-1097(85)80005-x
- Cao, Y.-X., Li, S., Liu, H.-H., Zhang, M., Guo, Y.-L., Wu, N.-Q., et al. (2022). Prognostic value of N-terminal pro-B-type natriuretic peptide and high-sensitivity C-reactive protein in patients with previous myocardial infarction. *Front. Cardiovasc. Med.* 9, 797297. doi:10.3389/fcvm.2022.797297
- Communi, D., Motte, S., Boeynaems, J.-M., and Piroton, S. (1996). Pharmacological characterization of the human P2Y₄ receptor. *Eur. J. Pharmacol.* 317, 383–389. doi:10.1016/s0014-2999(96)00740-6
- Communi, D., Piroton, S., Parmentier, M., and Boeynaems, J.-M. (1995). Cloning and functional expression of a human uridine nucleotide receptor. *J. Biol. Chem.* 270, 30849–30852. doi:10.1074/jbc.270.52.30849
- Genoux, A., Lichtenstein, L., Ferrières, J., Duparc, T., Bongard, V., Vervueren, P.-L., et al. (2016). Serum levels of mitochondrial inhibitory factor 1 are independently associated with long-term prognosis in coronary artery disease: The GENES study. *BMC Med.* 14 (1), 125. doi:10.1186/s12916-016-0672-9
- Goetze, J. P., Christoffersen, C., Perko, M., Arendrup, H., Rehfeld, J. F., Kastrup, J., et al. (2003). Increased cardiac BNP expression associated with myocardial ischemia. *FASEB J.* 17, 1105–1107. doi:10.1096/fj.02-0796fje
- Hamelin, B. A., Zakrzewski-Jakubiak, M., Robitaille, N. M., Bogaty, P., Labbé, L., and Turgeon, J. (2011). Increased risk of myocardial infarction associated with angiotensin-converting enzyme gene polymorphism is age dependent. *J. Clin. Pharmacol.* 51, 1286–1292. doi:10.1177/0091270010382420
- Hede, S. E., Amstrup, J., Klaerke, D. A., and Novak, I. (2005). P2Y₂ and P2Y₄ receptors regulate pancreatic Ca(2+)-activated K⁺ channels differently. *Pflugers Arch.* 450 (6), 429–436. doi:10.1007/s00424-005-1433-3
- Herold, C. L., Qi, A.-D., Harden, T. K., and Nicholas, R. A. (2004). Agonist versus antagonist action of ATP at the P2Y₄ receptor is determined by the second extracellular loop. *J. Biol. Chem.* 279 (12), 11456–11464. doi:10.1074/jbc.M301734200
- Horckmans, M., Esfahani, H., Beauloye, C., Clouet, S., di Pietrantonio, L., Robaye, B., et al. (2015). Loss of mouse P2Y₄ nucleotide receptor protects against myocardial infarction through endothelin-1 downregulation. *J. Immunol.* 194 (4), 1874–1881. doi:10.4049/jimmunol.1401364
- Horckmans, M., Robaye, B., León-Gómez, E., Lantz, N., Unger, P., Dol-Gleizes, F., et al. (2012). P2Y₄ nucleotide receptor: A novel actor in post-natal cardiac development and function. *Angiogenesis* 15 (3), 349–360. doi:10.1007/s10456-012-9265-1
- Horckmans, M., León-Gómez, E., Robaye, B., Balligand, J. L., Boeynaems, J. M., Dessy, C., et al. (2012). Gene deletion of P2Y₄ receptor lowers exercise capacity and reduces myocardial hypertrophy with swimming exercise. *Am. J. Physiol. Heart Circ. Physiol.* 303 (7), H835–H843. doi:10.1152/ajpheart.00256.2012
- Jain, S., Pydi, S., Toti, K. S., Robaye, B., Idzko, M., Gavrilova, O., et al. (2020). Lack of adipocyte purinergic P2Y₆ receptor greatly improves whole body glucose homeostasis. *Proc. Natl. Acad. Sci. U. S. A.* 117 (48), 30763–30774. doi:10.1073/pnas.2006578117
- Keates, A. K., Mocumbi, A. O., Ntsekhe, M., Sliwa, K., and Steward, S. (2017). Cardiovascular disease in Africa: Epidemiological profile and challenges. *Nat. Rev. Cardiol.* 14, 273–293. doi:10.1038/nrcardio.2017.19
- Khan, N. A., Grubisic, M., Hemmelgarn, B., Humphries, K., King, K. M., and Quan, H. (2010). Outcomes after acute myocardial infarction in South Asian, Chinese, and white patients. *Circulation* 122, 1570–1577. doi:10.1161/CIRCULATIONAHA.109.850297
- Lemaire, A., Vanorlé, M., Horckmans, M., di Pietrantonio, L., Clouet, S., Robaye, B., et al. (2017). Mouse P2Y₄ nucleotide receptor is a negative regulator of cardiac adipose-derived stem cell differentiation and cardiac fat formation. *Stem Cells Dev.* 26 (5), 363–373. doi:10.1089/scd.2016.0166
- Lev, E. I., Patel, R. T., Guthikonda, S., Lopez, D., Bray, P. F., and Kleiman, N. S. (2007). Genetic polymorphisms of the platelet receptors P2Y₁₂, P2Y₁ and GPIIb/IIIa and response to aspirin and clopidogrel. *Thromb. Res.* 119, 355–360. doi:10.1016/j.thromres.2006.02.006
- Li, Y.-Y., Wang, H., Wang, H., and Zhang, Y.-Y. (2021). Myocardial infarction and AGT p.Thr174Met polymorphism: A meta-analysis of 7657 subjects. *Cardiovasc. Ther.* 2021, 6667934. doi:10.1155/2021/6667934
- Liu, H. H., Cao, Y. X., Jin, J. L., Guo, Y. L., Zhu, C. G., Wu, N. Q., et al. (2021). Prognostic value of NT-proBNP in patients with chronic coronary syndrome and normal left ventricular systolic function according to glucose status: A prospective cohort study. *Cardiovasc. Diabetol.* 20, 84. doi:10.1186/s12933-021-01271-0
- Mesto, N., Bailbe, D., Eskandar, M., Pommier, G., Gil, S., Stefania, T., et al. (2022). Involvement of P2Y signaling in the restoration of glucose-induced insulin exocytosis in pancreatic β cells exposed to glucotoxicity. *J. Cell. Physiol.* 237, 881–896. doi:10.1002/jcp.30564
- Nishihama, K., Yamada, Y., Matsuo, H., Segawa, T., Watanabe, S., Kato, K., et al. (2007). Association of gene polymorphisms with myocardial infarction in individuals with or without conventional coronary risk factors. *Int. J. Mol. Med.* 19, 129–141. doi:10.3892/ijmm.19.1.129
- Novak, I. (2008). Purinergic receptors in the endocrine and exocrine pancreas. *Purinergic Signal.* 4 (3), 237–253. doi:10.1007/s11302-007-9087-6
- Onen, C. L. (2013). Epidemiology of ischaemic heart disease in sub-Saharan Africa. *Cardiovasc. J. Afr.* 24, 34–42. doi:10.5830/CVJA-2012-071
- Palazzuoli, A., Gallotta, M., Quatrini, I., and Nuti, R. (2010). Natriuretic peptides (BNP and NT-proBNP) : Measurement and relevance in heart failure. *Vasc. Health Risk Manag.* 6, 411–418. doi:10.2147/vhrm.s5789
- Redfors, B., Chen, S., Crowley, A., Ben-Yehuda, O., Gersh, B. J., Lembo, N. J., et al. (2018). B-Type natriuretic peptide assessment in patients undergoing revascularization for left main coronary artery disease: Analysis from the EXCEL trial. *Circulation* 138, 469–478. doi:10.1161/CIRCULATIONAHA.118.033631
- Reinstadler, S. J., Feistritzer, H.-J., Reindl, M., Klug, G., and Metzler, B. (2016). Utility of NT-proBNP in predicting infarct scar and left ventricular dysfunction at a chronic stage after myocardial infarction. *Eur. J. Intern. Med.* 29, e16–e18. doi:10.1016/j.ejim.2015.12.018
- Rorth, R., Jhund, P. S., Yilmaz, M. B., Kristensen, S. L., Welsh, P., Desai, A. S., et al. (2020). Comparison of BNP and NT-proBNP in patients with heart failure and reduced ejection fraction. *Circ. Heart Fail.* 13, e006541. doi:10.1161/CIRCHEARTFAILURE.119.006541
- Sakowicz, A., Fendler, W., Lelonek, M., Sakowicz, B., and Pietrucha, T. (2013). Genetic polymorphisms and the risk of myocardial infarction in patients under 45 years of age. *Biochem. Genet.* 51, 230–242. doi:10.1007/s10528-012-9558-5
- Suarez-Huerta, N., Pouillon, V., Boeynaems, J.-M., and Robaye, B. (2001). Molecular cloning and characterization of the mouse P2Y₄ nucleotide receptor. *Eur. J. Pharmacol.* 416, 197–202. doi:10.1016/s0014-2999(01)00875-5
- Ueshima, H., Sekikawa, A., Miura, K., Chowdhury Turin, T., Takashima, N., Kita, Y., et al. (2018). Cardiovascular disease and risk factors in Asia: A selected review. *Circulation* 118 (25), 2702–2709. doi:10.1161/CIRCULATIONAHA.108.790048
- Verdier, C., Ruidavets, J. B., Genoux, A., Combes, G., Bongard, V., Taraszkiewicz, D., et al. (2019). Common p2y13 polymorphisms are associated with plasma inhibitory factor 1 and lipoprotein(a) concentrations, heart rate and body fat mass: The GENES study. *Arch. Cardiovasc. Dis.* 112 (2), 124–134. doi:10.1016/j.acvd.2018.09.003
- Yao, H., Ekou, A., Niamkey, T., Hounhoui Gan, S., Kouamé, I., Afassinou, Y., et al. (2022). Acute coronary syndromes in sub-saharan Africa: A 10-year systematic review. *J. Am. Heart Assoc.* 11, e021107. doi:10.1161/JAHA.120.021107



OPEN ACCESS

EDITED BY

Kenneth A. Jacobson,
National Institutes of Health (NIH),
United States

REVIEWED BY

Joanna Lecka,
INRS Eau Terre Environnement, Canada
Thomas Grutter,
Université de Strasbourg, France

*CORRESPONDENCE

Mark T. Young,
✉ youngmt@cardiff.ac.uk

SPECIALTY SECTION

This article was submitted to
Experimental Pharmacology and Drug
Discovery,
a section of the journal
Frontiers in Pharmacology

RECEIVED 10 November 2022

ACCEPTED 12 December 2022

PUBLISHED 12 January 2023

CITATION

Pasqualetto G, Zuanon M, Brancale A
and Young MT (2023), Identification of a
novel P2X7 antagonist using structure-
based virtual screening.
Front. Pharmacol. 13:1094607.
doi: 10.3389/fphar.2022.1094607

COPYRIGHT

© 2023 Pasqualetto, Zuanon, Brancale
and Young. This is an open-access
article distributed under the terms of the
[Creative Commons Attribution License](https://creativecommons.org/licenses/by/4.0/)
(CC BY). The use, distribution or
reproduction in other forums is
permitted, provided the original
author(s) and the copyright owner(s) are
credited and that the original
publication in this journal is cited, in
accordance with accepted academic
practice. No use, distribution or
reproduction is permitted which does
not comply with these terms.

Identification of a novel P2X7 antagonist using structure-based virtual screening

Gaia Pasqualetto¹, Marika Zuanon¹, Andrea Brancale^{2,3} and
Mark T. Young^{1*}

¹School of Biosciences, Cardiff University, Cardiff, United Kingdom, ²School of Pharmacy and
Pharmaceutical Sciences, Cardiff University, Cardiff, United Kingdom, ³Department of Organic
Chemistry, University of Chemistry and Technology, Prague, Czechia

P2X4 and P2X7 receptors are ATP-gated ion channels, which play important roles in neuropathic and inflammatory pain, and as such they are important drug targets in diseases of inflammatory origin. While several compounds targeting P2X4 and P2X7 receptors have been developed using traditional high-throughput screening approaches, relatively few compounds have been developed using structure-based design. We initially set out to develop compounds targeting human P2X4, by performing virtual screening on the orthosteric (ATP-binding) pocket of a molecular model of human P2X4 based on the crystal structure of the *Danio rerio* receptor. The screening of a library of approximately 300,000 commercially available drug-like compounds led to the initial selection of 17 compounds; however, none of these compounds displayed a significant antagonist effect at P2X4 in a Fluo-4 ATP-induced calcium influx assay. When the same set of compounds was tested against human P2X7 in an ATP-stimulated Yo-Pro1 dye uptake assay, one compound (an indeno(1,2-b)pyridine derivative; GP-25) reduced the response by greater than 50% when applied at a concentration of 30 μ M. GP-25 displayed an IC₅₀ value of 8.7 μ M at human P2X7 and 24.4 μ M at rat P2X7, and was confirmed to be active using whole-cell patch clamp electrophysiology and not cytotoxic. Schild analysis suggested that mode of action of GP-25 was orthosteric. Screening of a further 16 commercially available analogues of GP-25 led to the discovery of five additional compounds with antagonist activity at human P2X7, enabling us to investigate the structure-activity relationship. Finally, docking of the R- and S-enantiomers of GP-25 into the orthosteric pocket of molecular models of human P2X4 and human P2X7 revealed that, while both enantiomers were able to make multiple interactions between their carboxyl moieties and conserved positively charged amino-acids in human P2X7, only the S-enantiomer of GP-25 was able to do this in human P2X4, potentially explaining the lack of activity of GP-25 at this receptor.

KEYWORDS

P2X7, P2X4, virtual screen, structure-based drug design, antagonist

1 Introduction

P2X receptors are a family of seven ATP-gated ion channels, which have important functions in neurotransmission, pain and inflammation (Sheng and Hattori, 2022). The P2X4 and P2X7 subtypes in particular are involved in modulation of inflammation and chronic inflammatory pain. P2X4 receptors are involved in tactile allodynia following nerve damage (Tsuda et al., 2003), and P2X7 receptors are thought to modulate inflammatory responses in conditions including arthritis, Crohn's disease and age-related macular degeneration, as well as being involved in cancer progression and mood disorders (Ren and Illes, 2022). Due to their involvement in inflammatory disease, P2X receptors are important drug targets (Dane et al., 2022) and many P2X4 and P2X7 antagonists have been discovered and developed, largely using high throughput screening approaches (Hernandez-Olmos et al., 2012; Ase et al., 2015; Müller and Namasivayam, 2022), but also by structure-based screening (Caseley et al., 2016; Zhao et al., 2021). The discovery of novel P2X4 receptor antagonists has been more of a challenge than for P2X7, and this may be because many antagonists (including BX430 and 5-BDBD for P2X4 (Fischer et al., 2004; Ase et al., 2015), and A740003, A804598, AZ10606120, GW791343, JNJ47965567, A438079 and AZ11645373 for P2X7 (Honore et al., 2006; Karasawa and Kawate, 2016; Allsopp et al., 2018; Bin Dayel et al., 2019)) bind to an allosteric pocket in the extracellular domain, which is smaller in P2X4 than P2X7 (Karasawa and Kawate, 2016).

Structure-based virtual screening is an efficient approach for the discovery of novel "hit" compounds with activity against a target protein. In this process, compounds are docked *in silico* into a crystal structure or molecular model. The quality of the docking is scored and then the top-scoring "hits" are selected for biological assay. If a library of commercially available drug-like molecules is used for the screen, the compounds can be purchased for assay without requiring any chemical synthesis. Crystal structures are now available for *Danio rerio* (zebrafish) P2X4 in complex with ATP (Hattori and Gouaux, 2012), human P2X3 in complex with ATP and the competitive antagonists A-317491 and TNP-ATP (Mansoor et al., 2016), and giant panda P2X7 in complex with allosteric antagonists (Karasawa and Kawate, 2016), as well as the cryoEM structure of full-length rat P2X7 in complex with ATP (McCarthy et al., 2019), giving a series of good starting points to develop molecular models of P2X receptors. Structure-based screening on the ATP-binding (orthosteric) pocket of P2X7 has also been used successfully, leading to the identification of hit compounds with selectivity for P2X7 over P2X4 (Caseley et al., 2016). A similar approach has also been used to discover P2X4 and P2X1 antagonists, although their potency was in the high micromolar range (Beswick et al., 2019).

In this work we used structure-based virtual screening on the orthosteric pocket of a molecular model of human P2X4 based upon the zebrafish P2X4 crystal structure (Hattori and Gouaux,

2012). We first validated our docking algorithms by docking ATP into the orthosteric pocket, then performed a virtual screen of the Specs library of commercially available drug-like compounds (Specs.net), selecting a total of 17 compounds for biological assay. None of the compound candidates displayed antagonist activity at human P2X4 in an ATP-induced calcium influx assay at 10 μ M. However we identified one compound (GP-25; an indeno(1,2-b)pyridine derivative) with antagonist activity at both human and rat P2X7 in an ATP-induced dye uptake (YoPro-1) assay, with IC_{50} values of 8.7 μ M at human P2X7 and 24.4 μ M at rat P2X7. We confirmed the antagonist activity of GP-25 in whole-cell patch clamp experiments, and Schild analysis suggested orthosteric antagonism [although there was a reduction in peak response at the highest antagonist concentration tested (100 μ M)]. Sixteen compound analogues to GP-25 were then purchased and tested on human and rat P2X7, leading to the identification of a further five molecules with antagonist activity and permitting the analysis of the structure-activity relationship. *In silico* docking simulations performed on the orthosteric pocket suggested that both the R- and S-enantiomers of GP-25 (as well as GP-47, one of the other analogues with antagonist activity) could bind to human P2X7, as opposed to only the S-enantiomer of GP-25 in human P2X4. Both the R- and S-enantiomers of GP-25 and GP-47 were able to occupy the P2X7 orthosteric pocket in a way that preserved key interactions between carboxyl groups and conserved positively charged amino-acids in the orthosteric pocket, but only the S-enantiomer of GP-25 was able to do this in human P2X4. This gave a potential molecular explanation for the lack of activity of GP-25 that we observed at human P2X4. In summary, our work describes both the structure-based discovery of a novel orthosteric human P2X7 antagonist, and an analysis of the molecular basis for the differential potencies observed at different receptor subtypes.

2 Materials and methods

2.1 Development of 1321N1 cells stably expressing human P2X4, human and rat P2X7 receptors

1321N1 astrocytoma cells and HEK-293 cells were cultured (at 37°C, 5% CO₂) in Dulbecco's modified Eagle's medium (DMEM/F-12 with Glutamax) supplemented with 10% foetal bovine serum (FBS) and 200 unit/ml of penicillin and streptomycin antibiotics (Fisher Scientific). For stable cell line generation, cells were transfected using FuGene HD Transfection Reagent (Promega) according to the manufacturer's protocol with plasmids encoding either human P2X4 with a C-terminal (His)₁₀ tag (Young et al., 2008), human P2X7 with a C-terminal EYMPME tag (kindly provided by R.A. North) or rat P2X7 C-terminally tagged with a GFP-(His)₈ tag, generated by PCR amplification of the coding

sequence for rat P2X7 from a pcDNA-based expression vector (Young et al., 2007), adding XhoI and EcoRI sites at the 5'- and 3'- ends respectively, followed by restriction digestion and ligation into a zebrafish P2X4-GFP expression vector based on pEGFP-C1 (kindly provided by Eric Gouaux; Kawate and Gouaux, 2006) to replace the zebrafish P2X4 coding region with rP2X7. Transfected clones were grown in DMEM/F-12 with Glutamax medium supplemented with G-418 (Geneticin®, Fisher Scientific), 600 µg/ml and 150 µg/ml during selection and maintenance respectively. Each clone was tested for P2X4 or P2X7 receptor expression by Western blot and clones, which displayed receptor expression were assessed for functionality using the Ca²⁺ influx assay (P2X4) or the Yopro-1 uptake assay (P2X7). HEK-293 cells stably expressing human P2X7 (Adinolfi et al., 2010) were a kind gift from Elena Adinolfi.

2.2 Homology modelling and ligand docking

In silico simulations were performed on a MAC pro 2.80 GHz Quad-Core Intel Xeon running Ubuntu 12.04 LTS. Graphical representations were generated with MOE (Molecular Operating Environment, 2014.09; Chemical Computing Group ULC, Canada). Structure files retrieved from the RCSB Protein Data Bank (<http://www.rcsb.org>) as PDB file format were used as template to build P2X4 [PDB ID 4DW1 (Hattori and Gouaux, 2012)] and P2X7 [PDB ID 6U9W (McCarthy et al., 2019)] receptor homology models using MOE 2014.09, single template mode and default settings with AMBER12:EHT force field, including the crystallized ATP molecules for the induced-fit mode. Each model was checked visually and *via* the Rampage Server, Molprobit (Lovell et al., 2003) and PROCHECK (Laskowski et al., 1993) to exclude gross errors in protein geometry. For validation, ATP coordinates in the crystal structure were used to set the centroid coordinated for a box of 10 Å³ grid used in the docking. FlexX 2.1.3 with default parameters (Rarey et al., 1996), PLANTS (Korb et al., 2006) and Glide Standard Precision (<https://www.schrodinger.com/products/ glide>) simulations were used for the docking. 20 auto ants (for the explorative docking algorithm) and standard parameters were set for simulations with PLANTS. 10 or more poses generated in each simulation were visually inspected.

2.3 Structure-based virtual screening and docking

Preparation of compound structure was performed with the LigPrep module (<https://www.schrodinger.com/>

[products/ligprep](#)), using the Specs library of commercially available compounds (~300,000 entries; [Specs.net](#)). Briefly, hydrogens were added and possible ionization states were generated for pH 7.0 ± 2.0 using the OPLS_2005 forcefield; possible tautomers were generated for each molecule as well as all possible enantiomers for structures with non-specified chiralities. The center of the binding region was defined by either manual selection of the pocket residues or by selecting the superposed ligand. Ligands were initially docked using the Glide High throughput Screening (HTVS) protocol, the top 15% best scored poses were re-docked with the Glide Standard Precision protocol, and then rescored (without performing ulterior docking) using the Glide Extra Precision (XP) protocol, FlexX and PLANTS (in parallel). A consensus score from all 3 re-scorings was calculated (Bassetto et al., 2013), and poses that ranked best according to Glide XP, FlexX and PLANTS—were selected for visual inspection. Docking of GP-25 and analogues were performed on the human P2X7 and human P2X4 models using Glide XP protocol using a grid appropriate for 14 Å³ ligand length, with crystallized ATP coordinates as grid centroid. Poses were visually inspected before final selection of compounds for assay. Criteria in the choice of ligands included i) ability to entertain multiple H-bond or ionic interactions with key residues in the ATP binding pocket and ii) at least a partial overlap between the docked ligand conformation and the superposed adenine of the ATP. Additional interactions were also a favorable criteria.

2.4 Fluo4 calcium influx assay

Cells were plated the day before assay into poly-lysine-coated 96-well plates at 40–65,000 cells/ml. To load cells with calcium-sensitive fluorescent dye, culture medium was replaced with modified Ringer's buffer (140 mM NaCl, 10 mM HEPES, 10 mM Glucose, 1 mM MgCl₂, 1 mM CaCl₂, 2.5 mM KCl, .5% BSA, pH = 7.4) containing 2.6 µM FLUO4-AM (Fisher Scientific) and 250 µM Probenecid (Sigma), and cells were incubated for 20–30 min. Immediately prior to assay, buffer was replaced with fresh modified Ringer's buffer containing 500 µM Probenecid. Compounds were dissolved in DMSO at 1,000× the required assay concentration prior to diluting in assay buffer and the final DMSO concentration did not exceed .1%. A Fluoroskan Ascent FL plate reader (Fisher Scientific) equipped with a solution dispenser and an appropriate filter pair (excitation: 485 nm, emission: 538 nm) was used to record 5 s baseline followed by P2X4-mediated calcium influx measurements for 20–25 s after ATP stimulation (20 µL injection of solutions dissolved in modified Ringer's buffer). The amplitude of ATP responses was calculated as ΔF/

F_0 , where $\Delta F = F_1 - F_0$, subtracting the fluorescent background as suggested by Bootman et al. (2013).

2.5 Yopro-1 uptake assay

Cells were plated as for the calcium influx assay (Section 2.4). Culture medium was replaced with low divalent cation containing extracellular solution (ECS-LD; 147 mM NaCl, 10 mM HEPES, 13 mM Glucose, .2 mM CaCl_2 , 2 mM KCl. pH = 7.4 in MilliQ water) and 5 μM Yopro-1. Compounds were dissolved in DMSO at 1,000 \times the required assay concentration prior to diluting in assay buffer and the final DMSO concentration did not exceeded .1%. The baseline was measured with a BMG Clariostar instrument for 5–10 cycles, followed by addition of ATP (or BzATP) and recording for at least 30 further cycles (approx. 1 min per data point). The collected responses were normalized to the first data-point recorded after ATP addition. The initial gradient of the dye uptake curve was used to calculate the response to ATP.

2.6 Patch-clamp electrophysiology

Whole-cell patch-clamp traces were recorded at room temperature using patch pipettes pulled from borosilicate glass (World Precision Instruments, Sarasota, FL, United States). Pipettes were filled with internal solution (IS) containing (in mM): 145 NaCl, 10 EGTA and 10 HEPES, with the pH adjusted to 7.3 with NaOH and had resistances of 3–5 M Ω . Cells were constantly perfused in a bath with ECS-LD. Currents were recorded at a holding membrane potential of -60 mV using an Axon Instruments Axopatch Multiclamp 700A amplifier and Digidata 1322A A/D interface (Molecular Devices, Sunnyvale, CA, United States). ATP working solutions were prepared fresh and solutions with compounds had a final concentration of DMSO equal or lower than .1% (.1% DMSO was included as vehicle control). ATP applications were made at 90-s intervals. Solutions were applied to patch-clamped cells with the help of a rapid perfusion system (RSC-160, Biologic, Claix, France), allowing solution exchange times in the range 20–100 ms.

2.7 Cell viability assay

To assess hit compound toxicity, CellTiter-Blue Cell Viability Assay (Promega, Southampton, United Kingdom) was used as recommended by the manufacturer on not transfected HEK-293. Cells were seeded in 96-well plates (100 μL at a concentration of 30–35,000 cells/ml) in culture media and a day later media was replaced with 100 μL fresh

media containing 30 μM of tested compounds (10 μM of A740003). After 24 h incubation at 37 $^{\circ}\text{C}$, 5% CO_2 , 20 μL of CellTiter Blue reagent was added to each well and incubated for 3 h at 37 $^{\circ}\text{C}$. Fluorescence was then measured with a BMG Clariostar using excitation/emission wavelengths of 560/590 nm. Data were normalized to vehicle control-treated cells (.1% DMSO).

2.8 Data analysis and statistics

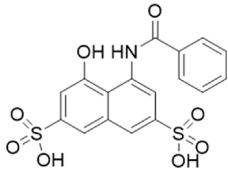
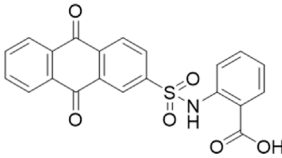
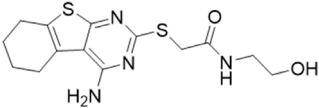
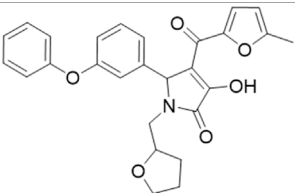
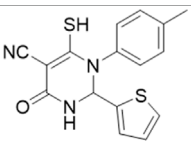
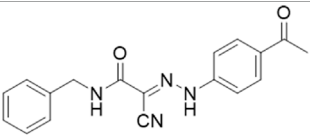
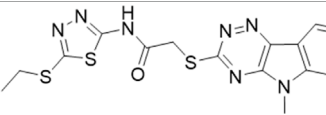
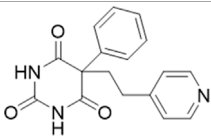
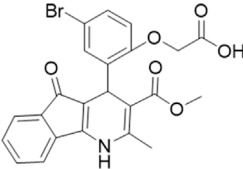
Data processing and data analysis were carried out using Graphpad Prism version 6 for Mac. Figures are presented as mean \pm SEM. Statistical significance of any difference observed between samples was calculated through one-way ANOVA followed by Dunnett's multiple comparisons test with a single pooled variance (control, unless otherwise specified) or, when comparing only two sets of data, using an unpaired t-test with Welch's correction. When comparing data obtained from multiple independent experiments (N), each dataset was normalized to the mean value obtained for the vehicle control before pooling data. A non-linear regression (curve fit) with four parameters was applied to determine any dose-response correlation and the presence of any inhibition trend during the compound testing (curve-fit constraints were applied to normalized data). $Y = \text{Bottom} + (\text{Top} - \text{Bottom}) / (1 + 10^{((\text{LogEC}_{50} - X) * \text{Hill Slope}))}$ Where: X: agonist (or antagonist) concentrations expressed as logarithmic scale. Y: response measurements (raw or normalized value) This formula was also used for inhibition curve fitting by substituting the value of EC_{50} with IC_{50} .

3 Results

3.1 Virtual screening and compound selection

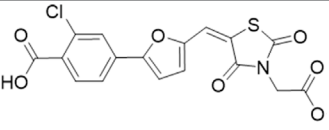
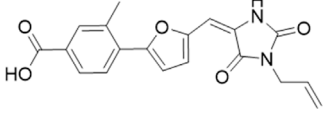
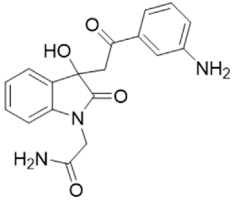
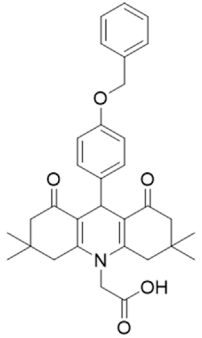
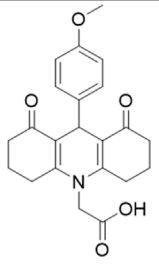
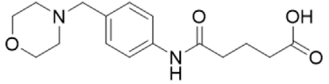
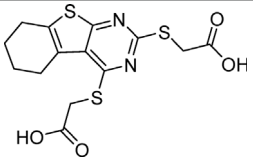
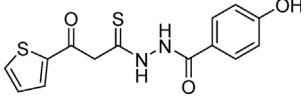
We generated a molecular model of human P2X4 based on the crystal structure of zebrafish P2X4 bound to ATP (Hattori and Gouaux, 2012). Three docking algorithms were validated—later employed in the virtual screening (PLANTS, FlexX and Glide SP)—by docking ATP in the model. In each simulation the docked pose of ATP was similar to that observed for ATP in the crystal structure (superposed, shown in grey lines in Supplementary Figure S1); in the dock obtained using PLANTS (Supplementary Figure S1A) the adenine ring was translated (positioned less deep in the pocket), with FlexX (Supplementary Figure S1B) the phosphate chain conformation was different (the β and gamma phosphates in the docking occupied the α and β positions in the model derived from the crystal structure), and with Glide SP (Supplementary Figure S1C) there was the greatest similarity. A protein-ligand interaction fingerprint (PLIF) showed comparable interactions in

TABLE 1 List of compounds identified by virtual screening in the P2X4 ATP-binding pocket (numbered 1–17) and GP-25 analogues (numbered 18–33).

ID	Structure	Specs ID	MW	% Inhibition at hP2X7	% Inhibition at rP2X7
1		AE-641/00786016	423.42	41	n.d
2		AE-641/42133418	407.40	38	n.d
3		AF-399/40634562	338.45	—	n.d
4		AF-399/41900709	459.50	<10	n.d
5		AF-399/42810490	327.43	—	n.d
6		AF-407/33312043	320.35	<10	n.d
7		AG-205/36698032	417.54	n.d	n.d.
8		AG-670/36765017	309.32	—	n.d
9 (GP-25)		AH-487/14758206	484.30	~75	47

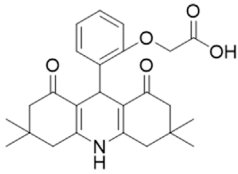
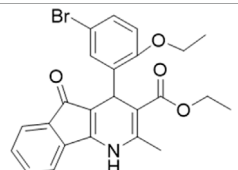
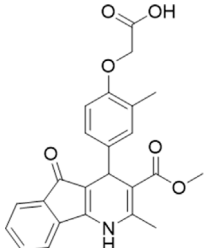
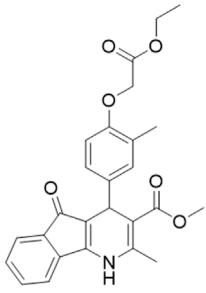
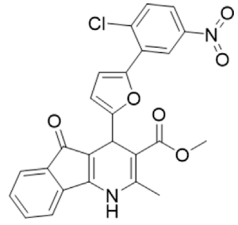
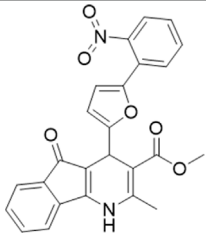
(Continued on following page)

TABLE 1 (Continued) List of compounds identified by virtual screening in the P2X4 ATP-binding pocket (numbered 1–17) and GP-25 analogues (numbered 18–33).

ID	Structure	Specs ID	MW	% Inhibition at hP2X7	% Inhibition at rP2X7
10		AH-487/40935627	435.84	—	n.d.
11		AH-487/41955121	352.34	25	n.d.
12		AK-778/41182449	339.35	12	n.d.
13		AN-988/40787450	513.63	29	n.d.
14		AN-988/40787687	381.43	—	n.d.
15		AO-080/43441580	306.36	11	n.d.
16		AO-476/41610193	370.47	<10	n.d.
17		AO-990/15068055	321.38	<10	n.d.

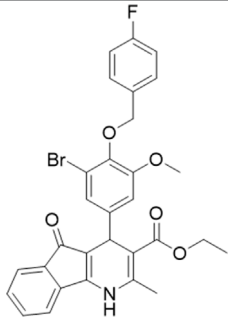
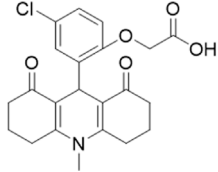
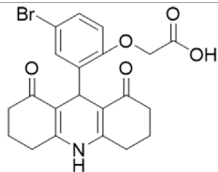
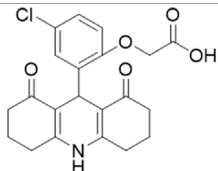
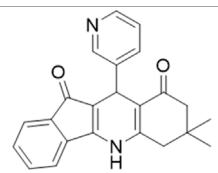
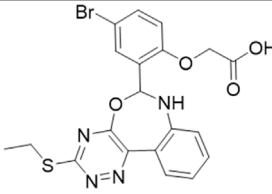
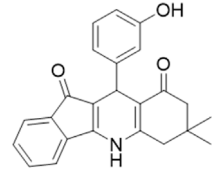
(Continued on following page)

TABLE 1 (Continued) List of compounds identified by virtual screening in the P2X₄ ATP-binding pocket (numbered 1–17) and GP-25 analogues (numbered 18–33).

ID	Structure	Specs ID	MW	% Inhibition at hP2X ₇	% Inhibition at rP2X ₇
18		AK-968/15604330	423.51	—	—
19		AH-487/15150556	468.35	—	13
20 (GP-47)		AH-487/14757970	439.85	77	—
21		AH-487/14758229	433.46	<10	—
22 (GP-50)		AG-690/40638872	476.87	69	—
23		AG-690/40638873	442.43	30	—

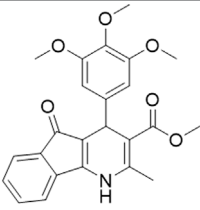
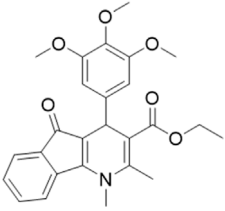
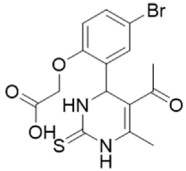
(Continued on following page)

TABLE 1 (Continued) List of compounds identified by virtual screening in the P2X4 ATP-binding pocket (numbered 1–17) and GP-25 analogues (numbered 18–33).

ID	Structure	Specs ID	MW	% Inhibition at hP2X7	% Inhibition at rP2X7
24		AN-988/40667255	578.43	12	16
25		AM-879/42012121	415.87	20	—
26		AM-879/42012369	446.3	22	—
27		AM-879/42012458	401.84	16	—
28		AJ-292/42032071	356.42	32	—
29		AK-968/11109126	489.35	20	—
30		AJ-292/14827035	371.43	27	—

(Continued on following page)

TABLE 1 (Continued) List of compounds identified by virtual screening in the P2X4 ATP-binding pocket (numbered 1–17) and GP-25 analogues (numbered 18–33).

ID	Structure	Specs ID	MW	% Inhibition at hP2X7	% Inhibition at rP2X7
31		AH-487/14758041	421.45	29	<10
32 (GP-66)		AK-454/40961396	449.5	55	19
33		AN-655/41064474	399.27	18	16

Specs IDs, identification number according to the supplier ([specs.net](https://www.specs.net)). MW, molecular weight (g/mol). Approx. % inhibition at 30 μ M at human P2X7 and rat P2X7. —for compound displaying increased responses vs. control. n.d., not determined.

the zebrafish P2X4 crystal structure (4DW1) and our three docking simulations (Supplementary Figure S1D). In our docking simulations we observed some additional interactions with Leu-188 (surface contact), Lys-190 (sidechain hydrogen bond acceptor and ionic attraction), Leu-214 (sidechain hydrogen bond donor and surface contact) and Ser-289 (sidechain and backbone hydrogen bond acceptor). Our results suggested that each algorithm was capable of replicating the binding pose of ATP in the orthosteric pocket, but as Glide performed the best, this was used as the main algorithm for subsequent virtual screening.

A library of commercially available drug-like compounds (Specs, 2022) with approximately 300,000 molecules was docked *in silico* into the orthosteric pocket of our human P2X4 model, selecting a total of 17 compounds for biological assay (Table 1).

3.2 Identification of a P2X7 antagonist among the screened compounds

The antagonist activity of the 17 compounds (applied at 10 μ M) was assayed initially on 1321N1 astrocytoma cells stably expressing human P2X4 receptors by measuring the ATP-induced (applied at 1.2 μ M) increase in Fluo-4 fluorescence due to calcium influx *via*

P2X4, using 2 μ M BX430 as a positive control (Figure 1A). Compound 7 was excluded from biological assay due to very low solubility. None of the compounds showed a statistically significant reduction in response, suggesting no antagonist activity at human P2X4. The same compounds were then assayed at a single concentration of 30 μ M (we initially expected that, having designed the compounds to bind to P2X4, they would likely be less potent at P2X7, and need to be applied at a higher concentration to observe an effect) on 1321N1 astrocytoma cells stably expressing human P2X7. The ATP-induced rate of uptake of YoPro-1 dye was measured upon application of at 300 μ M ATP, using .1 μ M A740003 as a positive control (Figure 1B). Several compounds showed at least 25% reduction in response (Table 1) and, strikingly, one compound (GP-25; (4-bromo-2-(3-(methoxycarbonyl)-2-methyl-5-oxo-4,5-dihydro-1H-indeno(1,2-b)pyridine-4-yl)phenoxy)acetic acid) inhibited the response by approximately 74.6%, and was taken forward for further analysis.

3.3 Characterization of GP-25 antagonism at P2X7

Concentration-response curves for both human and rat P2X7 receptors were constructed using the ATP-induced

YoPro-1 uptake assay, and EC_{50} values of 183.5 and 138.3 μ M were determined for human and rat P2X7, respectively (Figure 2A). Concentration-inhibition curves were constructed for GP-25 at both human and rat P2X7 using the YoPro-1 uptake assay (Figure 2B; 300 μ M ATP), and IC_{50} values of 8.7 μ M at human P2X7 and 24.4 μ M at rat P2X7 were determined, demonstrating moderate selectivity of GP-25 for human P2X7 over the rat orthologue. To confirm antagonist action in an independent assay, whole-cell patch clamp experiments were performed on human embryonic kidney (HEK-293) cells stably expressing rat P2X7-GFP (Figure 2C), and a concentration-dependent inhibition was observed when GP-25 was pre-applied for 2 min (300 μ M ATP application). A statistically significant reduction in P2X7 activity was observed upon application of 25 μ M GP-25 in both the YoPro-1 and patch clamp assays confirming GP-25 activity in the low micromolar range (Figure 2D). In order to confirm GP-25 as a competitive (orthosteric) antagonist, BzATP concentration-response curves (ranging between

300 μ M and .03 μ M) were constructed for rat P2X7-GFP in the YoPro-1 uptake assay in the presence of increasing concentrations of GP-25 (Figure 3A). Maximal responses were observed in all except the highest GP-25 concentration (100 μ M). Schild analysis, plotting the logarithm of the ratio of apparent EC_{50} values ((antagonist/control) – 1) against the logarithm of GP25 concentration (Figure 3B) gave a straight line with a slope not significantly different than 1 (at $p = .05$ as determined by one-sample t-test against the theoretical value 1; 3 biological replicates), indicative of competitive (orthosteric) antagonism.

3.4 Activities of GP-25 analogues at human and rat P2X7

A small library of 16 commercially available compounds was selected according to the presence of the same scaffold as GP-25, (70% similarity, Tanimoto index) and/or presence of

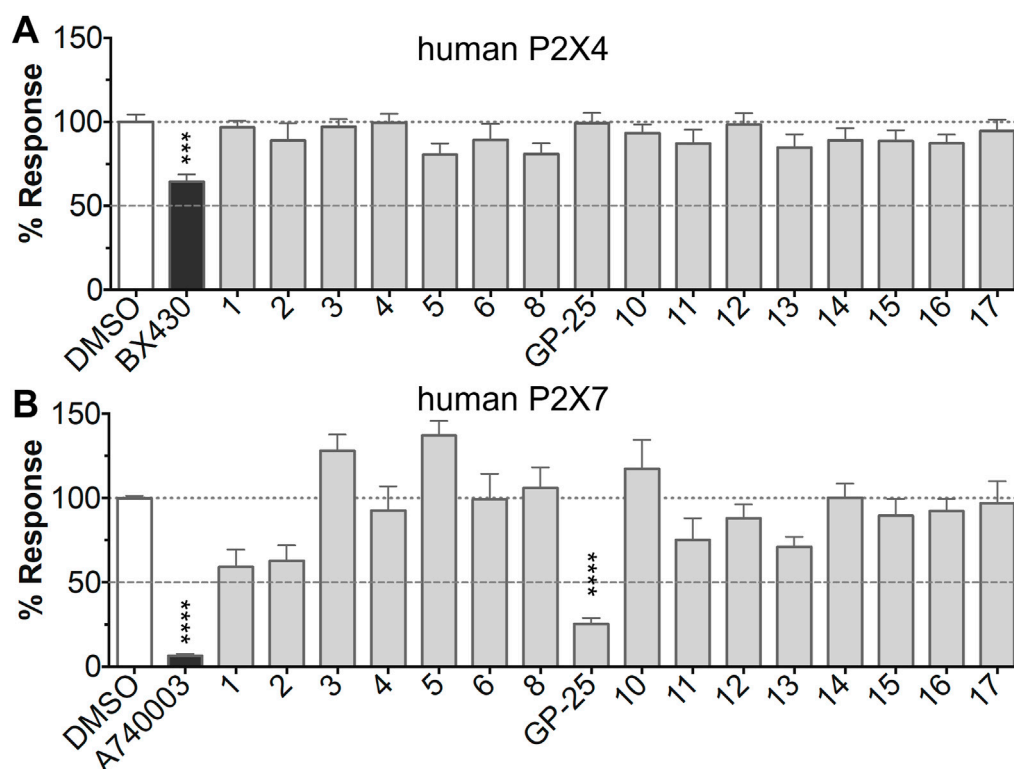


FIGURE 1

Initial screening of compounds at human P2X4 and human P2X7. **(A)** Normalized % response of 1321N1 astrocytoma cells stably transfected with human P2X4 to 1.2 μ M ATP (Fluo-4 calcium uptake assay) incubated in the absence (DMSO) or presence of either 2 μ M BX-430 or 10 μ M Specs compound (1–16; GP-25 is compound 9). **(B)** Normalized % response of 1321N1 astrocytoma cells stably transfected with human P2X7 to 300 μ M ATP (YoPro-1 dye uptake assay) incubated in the absence (DMSO) or presence of either .1 μ M A740003 or 30 μ M Specs compound. The final concentration of DMSO did not exceed .1%. Asterisks represent significant differences from control (DMSO) as measured by one-way ANOVA and Dunnett's test (***, $p \leq .001$; ****, $p \leq .0001$). Data represents two or more independent experiments ($n = 3$ –4 each).

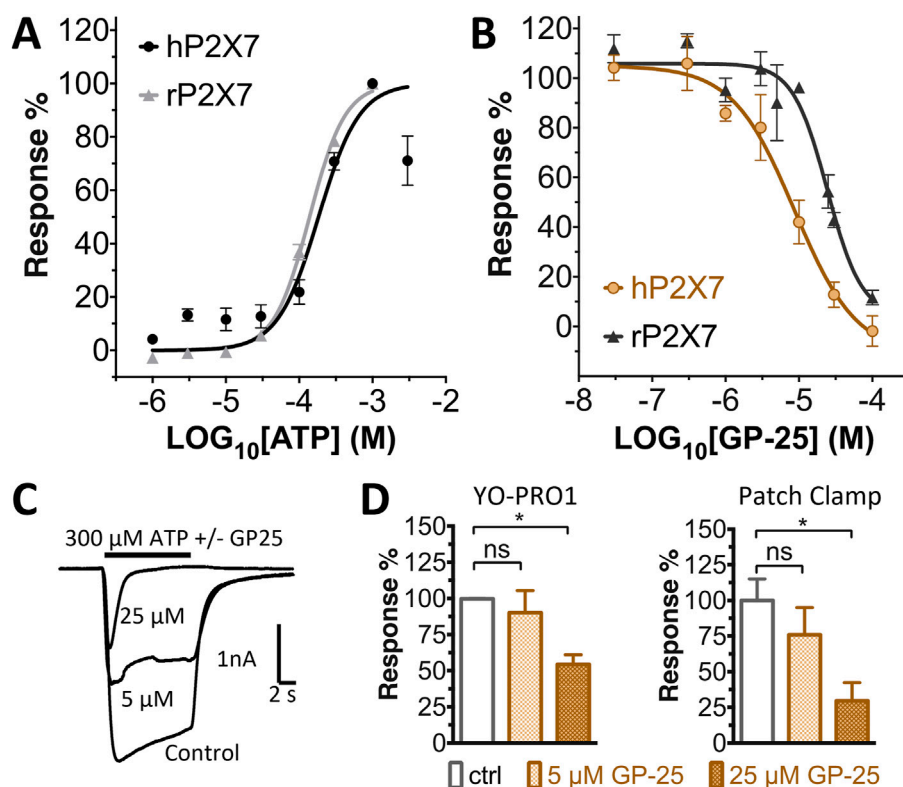


FIGURE 2

Functional characterization of GP-25. **(A)** ATP concentration-response curves (YoPro-1 assay) for human P2X7 (black line, circles) and rat P2X7 (grey line, triangles). Estimated EC_{50} values were 183.5 and 138.3 μ M for human and rat P2X7, respectively. **(B)** GP-25 concentration-inhibition curves (YoPro-1 assay) for human P2X7 (brown line, circles) and rat P2X7 (black line, triangles) (300 μ M ATP). Estimated IC_{50} values were 8.7 μ M at human P2X7 and 24.4 μ M at rat P2X7. **(C)** Representative traces for human P2X7 showing inhibition of ATP-evoked currents by GP-25 (concentrations indicated) in whole-cell patch clamp. **(D)** Summary of GP-25 inhibition data from YoPro-1 (left) and patch clamp (right) experiments. *: $p \leq .05$ (One-way ANOVA). ns; non-significant. YoPro-1 assay data represents two independent experiments ($n = 3-5$ each); electrophysiology $n = 5-7$ for each GP-25 concentration.

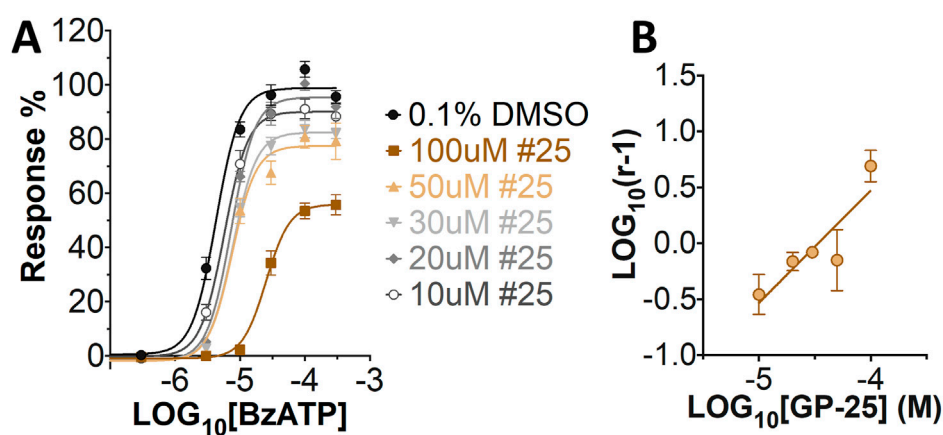


FIGURE 3

GP-25 is an orthosteric P2X7 antagonist. **(A)** BzATP concentration-response curves in increasing concentrations of GP-25 (compared to control; .1% DMSO). Curves are fitted without constraints (simple 4-parameter fitting). **(B)** Schild plot of the relationship between GP-25 concentration and the dose ratio. The equation for the line of best fit was $Y = 1.004 \cdot X + 4.489$; $R^2 = .5785$. Slope was $1.004 \pm .2584$; not significantly different from the theoretical value of 1 at $p = .05$. Data represents three independent experiments ($n = 3$ each).

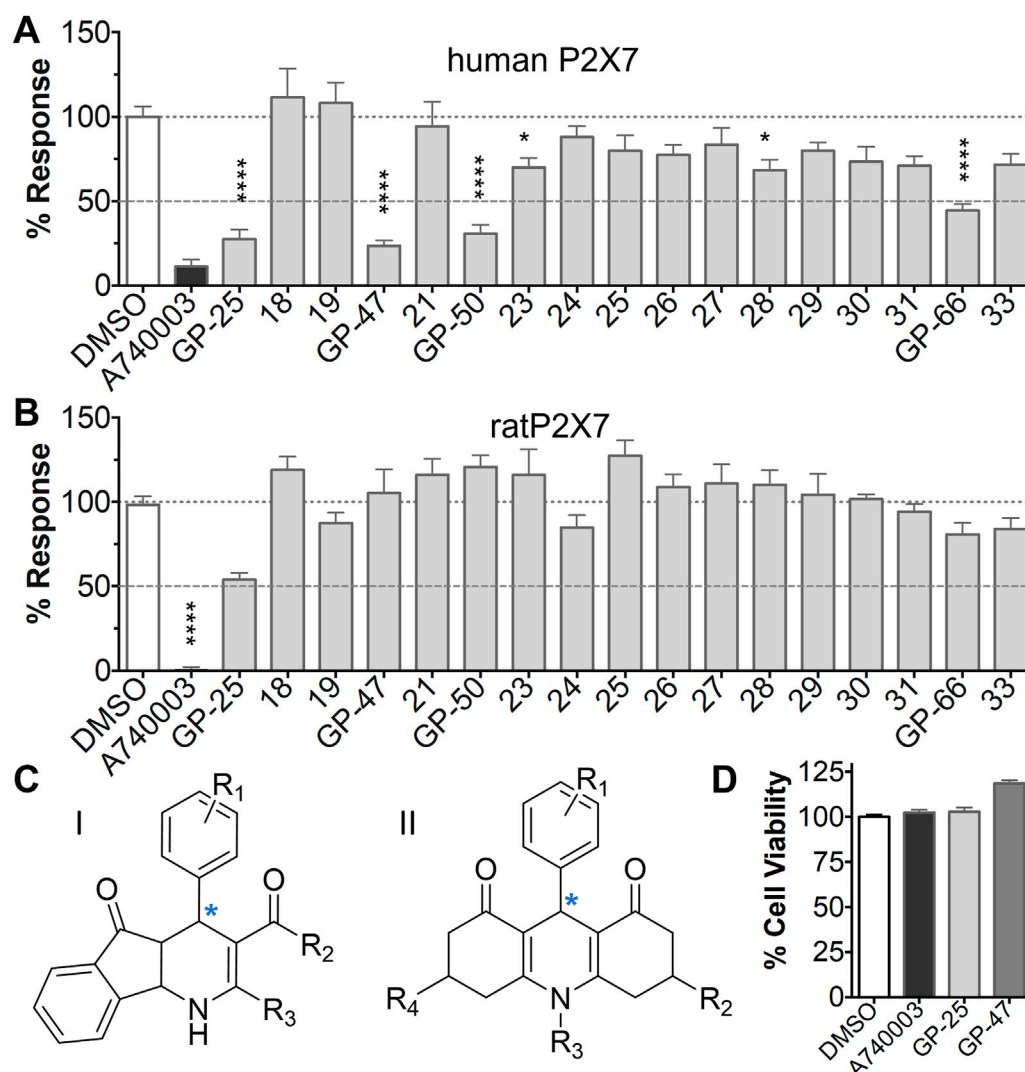


FIGURE 4

Activity of GP-25 analogues at human and rat P2X7. (A,B) Normalized % response of HEK cells transfected with either human P2X7 (A) or rat P2X7-GFP (B) to 300 μ M ATP (YoPro-1 dye uptake assay) incubated in the absence (DMSO) or presence of either .1 μ M A740003 or 30 μ M Specs compound (18–33; GP-25 is compound 9, GP-47 is compound 20, GP-50 is compound 22 and GP-66 is compound 32). (*, $p \leq .05$; ****, $p \leq .0001$). Data represents two or more independent experiments ($n = 3$ –4 each). (C) GP-25 analogue common chemical scaffolds. Scaffold I: R1, halogen, methoxyl-, methoxycarbonyl- and/or hydroxyl-. Compound 28 presents a pyridinyl- instead of the phenyl-. R2, methoxyl-, ethoxyl-, or cyclized ketone. R3, methyl-. Compound 28 presents a pyridinyl- instead of the phenyl-. GP-66 has an N-methyl substitution on the indeno(1,2-b) pyridine moiety. Scaffold II: R1, halogen, methoxyl-, methoxycarbonyl- and/or hydroxyl-. R2 and R4, -H, dimethyl-. R3, -H, methyl-. Chiral center marked with a blue star. (D). HEK cell viability (CellTiter Blue assay) following a 24 h incubation with either .1% DMSO (vehicle control) or 10 μ M A740003, or 30 μ M GP-25 or GP-47.

at least one functional group we hypothesized could contribute to GP-25 activity (e.g. carboxylic acid, halogen substituent to the aromatic ring, ester, etc.) (Compounds 18–33; Table 1). When human P2X7-expressing cells were incubated with 30 μ M of compounds (Figure 4A), several GP-25 analogues caused a statistically significant reduction in ATP-induced dye uptake (300 μ M ATP, approx. EC₇₀ measured in our experiments), including GP-47, GP-50,

Compound 23, Compound 28 and GP-66. None of these compounds displayed antagonist activity at rat P2X7 (Figure 4B and summarized in Table 1). Although the number of compounds tested was limited by their availability via a commercial source, the numerous ‘hits’ allowed for a basic structure-relationship (SAR) analysis. 13 out of 16 compounds presented either scaffold I or scaffold II—Scaffold I being the one shared among most of

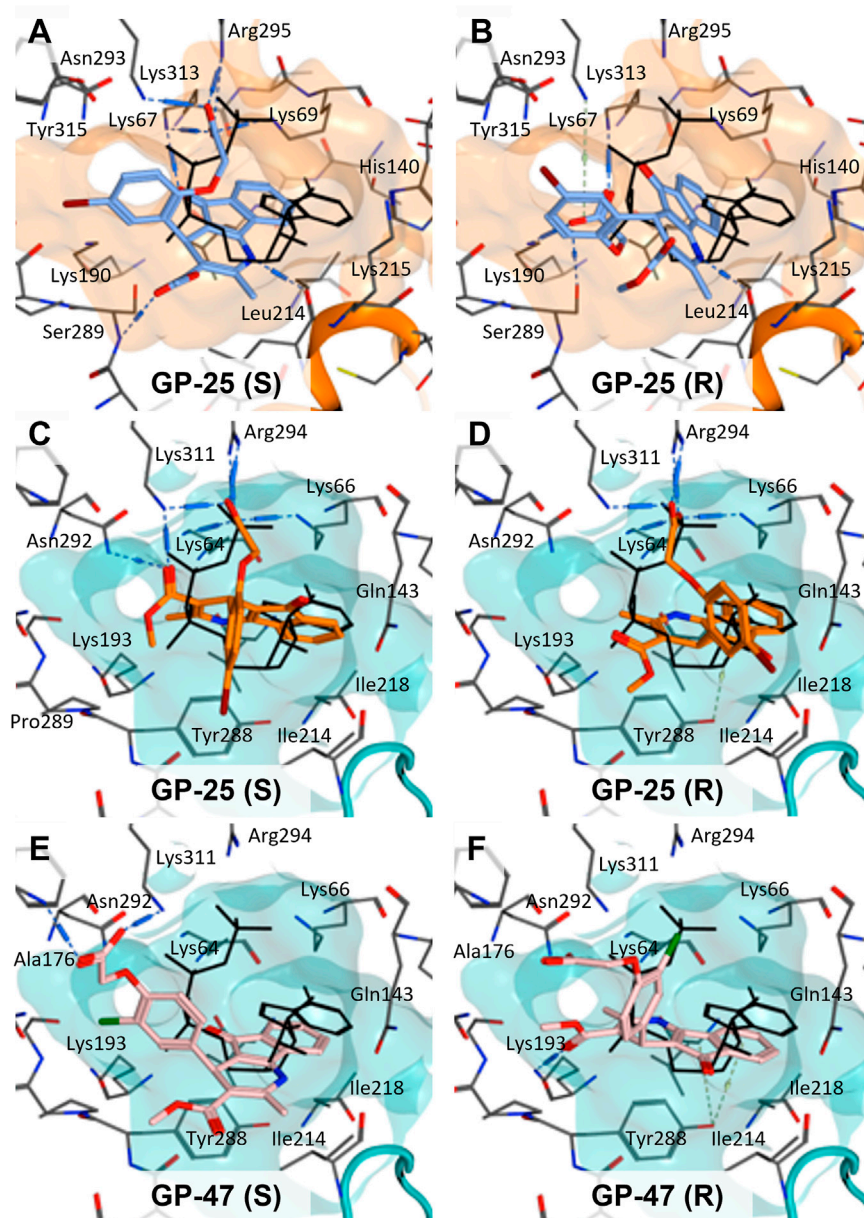


FIGURE 5

Docking of GP-25 and GP-47 into the orthosteric pockets of molecular models of human P2X4 and rat P2X7. (A,B) Docking of GP-25 (lilac) into human P2X4 (wheat). (C,D) Docking of GP-25 (orange) into human P2X7 (pale blue). (E,F) Docking of GP-47 (pale pink) into human P2X7 (pale blue). (A,C,E) represents the S-enantiomer and (B,D,F) represents the R-enantiomer. The ATP pose derived from the original crystal or cryoEM structure is shown in black lines for reference. Interactions are shown as dashed lines.

the compounds that showed moderate or good activity (Figure 4C). A methoxyl acetate as substituent (R1) on the phenyl ring (Scaffold I) appears to be important for compound activity, as substitution with a methoxyl group completely abolished the activity (as for Compound 19; Figure 4A and Table 1). Methoxyl acetate as either an ortho- or para-substituent (R1) was tolerated, as were halogens in the meta-position in the phenyl ring (R1), both

moieties improving activity in Scaffold I. The introduction of a furan linker between the dihydro-1H-indeno(1,2-b)pyridine-3-carboxylate and the phenyl moiety (scaffold very similar to that of Scaffold I; Figure 4C) was permitted without loss of activity provided that there was of a halogen in the ortho- and a nitro-group in the para-position of the phenyl moiety (GP-50). However, we observed that GP-50 was less soluble than GP-47 or GP-25. Compounds bearing Scaffold II (Compound

13, 14, 18, 25, 26, 27) did not show activity over 25% at 30 μ M, indicating that the substitution of the carboxylate to a cyclic ketone is not favored.

Finally, GP-25 and GP-47 were tested in a cytotoxicity assay showing that a 24-h incubation did not significantly reduce cell viability in HEK-293 wild-type (Figure 4D). As GP-50 showed low solubility, it was excluded from the cell viability assay.

3.5 Docking of GP-25 and GP-47 in the orthosteric pocket

To investigate potential binding modes of GP-25 to P2X4 and P2X7, docking of the ligands was performed in the orthosteric pockets of our human P2X4 model (GP-25 was re-docked), and of a model of human P2X7 built from the cryoEM structure of rat P2X7 bound to ATP (PDB ID: 6U9W; McCarthy et al., 2019). Both GP-25 and GP-47 contain a chiral center and were purchased as mixture of enantiomers (no info on % composition provided by the supplier). Our docking investigated the binding mode of both enantiomers (S and R, Figure 5) in the orthosteric pocket using Glide Extra Precision (XP).

The carboxyl groups of the S-enantiomer of GP-25 form extensive interactions with many of the polar residues in a similar fashion to that of the gamma phosphate of ATP (Lys-67, Lys-69, Arg-295 and Lys-313 (human P2X4 numbering); upper part of Figure 5A). However, docking the R-enantiomer of GP-25 showed a flipped pose with the carboxyl moiety pointing toward the bottom of the pocket (lower part of Figure 5B), lacking the interactions with residues that coordinate the gamma phosphate in ATP. Conversely, for human P2X7, we were able to obtain (for both GP-25 enantiomers), poses where the carboxylic group made strong multiple interactions with polar residues known to interact with ATP in the crystal structure, specifically coordinating the gamma phosphate (Figure 5C, D), including Lys-311, Lys-64, Lys-66 and Arg-294 (human P2X7 numbering). Additionally, the hetero-tricyclic scaffold of GP-25 tightly occupies the cavity where the adenine ring of ATP is found in the cryoEM structure, unlike in human P2X4 (compare Figure 5C, D with Figure 5A, B). Docking of GP-47 into the orthosteric pocket of human P2X7 (Figure 5E, F) gave rise to poses where some interactions between the carboxylic acid moieties and key positively charged amino-acids (e.g. Lys-311 in the S-enantiomer; Figure 5E) were present, and the adenine pocket at least partially occupied by the tricyclic ring. The combination of lack of key interactions with conserved phosphate-coordinating amino-acids and lack of occupation of the adenine pocket for one of the two enantiomers may explain why GP-25 displays little antagonist activity at human P2X4 compared to human P2X7.

4 Discussion

In this work we have discovered a novel orthosteric P2X7 receptor antagonist using structure-based virtual screening, and screened analogues to analyze the molecular determinants of subtype-specific potency. Using a molecular model of human P2X4 based upon the ATP-bound *Danio rerio* crystal structure, we validated 3 separate docking algorithms by comparing the poses of docked ATP with the pose analogous to the crystal structure. We then performed a virtual screen, selecting the top 17 best-scoring compounds (according to a combination of the three algorithms) for functional assay. While none of the compounds in our initial screen displayed antagonist activity at human P2X4, several compounds were active at human P2X7, including GP-25, and we were able to confirm its antagonist activity in two separate assays (ATP-induced dye uptake and patch-clamp electrophysiology). Schild analysis suggested an orthosteric mode of action, with the caveat that the maximum response was reduced at the highest antagonist concentration tested. Screening a series of commercially available GP-25 analogues enabled the identification of several additional antagonists, and the development of a structure-activity relationship. Finally, docking of the two enantiomers of GP-25 and its close analogue GP-47 into models of human P2X4 and P2X7 enabled us to determine why GP-25 lacks activity at human P2X4, and why GP-25 and its analogues are more active at human P2X7 than rat P2X7.

The inter-subunit ATP-binding site of P2X receptors is highly conserved, and the overall shape and size of the ATP binding pocket is very similar between receptor subtypes (Kawate, 2017; Pasqualetto et al., 2018). Indeed, the binding pose of ATP in the pocket is strikingly similar in *Danio rerio* P2X4, human P2X3, gulf coast tick P2X and rat P2X7, adopting a U-shaped conformation where conserved lysine and arginine residues coordinate the phosphates. The presence of the gamma phosphate is crucial for agonist activity, as well as the conformation of the ribose moiety and the localization of the adenine moiety into a relatively hydrophobic pocket (Dal Ben et al., 2019; Gasparri et al., 2019; Grimes et al., 2020). We chose a model of human P2X4 based on the ATP-bound structure of *Danio rerio* P2X4 for virtual screening and validated our docking algorithms using ATP (in a model where the bound ATP was removed prior to docking). Overall, our algorithms replicated the pose of bound ATP quite well, giving us confidence that our virtual screening would yield molecules capable of docking to the orthosteric pocket.

Structure-based virtual screening has been used previously to discover novel P2X7 antagonists, using both the orthosteric (Caseley et al., 2016) and allosteric (Zhao et al., 2021) pocket. In both cases molecular models of human P2X7 based on homologous P2X receptor crystal structures were used and hit

compounds with micromolar potency were obtained. This previous success with P2X7 models indicates that our strategy is valid, and a similar approach to ours has recently been carried out on a molecular model of human P2X4 (Beswick et al., 2019), discovering hit compounds, but with very low (high micromolar) potency. There has been a lower success with a similar approach for human P2X4 and the discovery of antagonists using the hP2X4 orthosteric pocket in virtual screenings has been more challenging. Indeed, in our study, multiple compounds initially selected as candidates from a P2X4 virtual screening displayed no activity at human P2X4, but instead displayed activity at human P2X7, including GP-25, which to our knowledge represents a novel P2X7 antagonist with no activity at human P2X4 receptors. A GP-25 analogue ((4-bromo-2-[3-(ethoxycarbonyl)-2-methyl-5-oxo-4,5-dihydro-1H-indeno[1,2-b]pyridin-4-yl]phenoxy) acetic acid; Chembridge ID 6422575) has previously been shown to bind to the tyrosine kinase Syk with a K_d of 6.2 μ M, and inhibition of antibody binding of 81% in an antibody displacement assay, but its IC_{50} for inhibiting mast cell degranulation (a key functional consequence of Syk activation) was ≥ 20 μ M, suggesting a lack of biological effect, and no further studies were undertaken with this molecule (Villoutreix et al., 2011).

The fact that our virtual screen was performed on P2X4, yet we discovered compounds with activity at P2X7, seems surprising, and may appear to cast doubt on the value or validity of the virtual screening process. However, we suggest that the process was successful in part because of the high degree of similarity between the orthosteric pockets of P2X4 and P2X7, and in part because of the favorable binding of both enantiomers of GP-25 to the orthosteric pocket of P2X7 (see below). Screening GP-25 analogues, we found three (GP-47, GP-50, and GP-66) with similar activity to GP-25 at human P2X7 (but displaying no activity at the rat isoform), and confirmed a lack of cytotoxicity in both GP-25 and GP-47. Future studies could focus on chemical modification to these compounds to improve their potency, and experiments with other P2X7 subtypes to confirm selectivity.

The characterization of GP-25 included Schild analysis, which suggested a competitive (orthosteric) mode of action. However, the maximum concentration of GP25 that we could apply was 100 μ M (due to solubility issues), and at this concentration we did observe a small reduction in maximum response. It is difficult to address this directly by making mutations in the orthosteric pocket, as these impair P2X receptor function (Chataigneau et al., 2013). Binding to the allosteric pocket could be confirmed or refuted in future experiments by assessing the ability of GP25 to antagonise receptors with mutations in the allosteric pocket, as demonstrated for the P2X7 antagonist AZ10606120 (Allsopp et al., 2017). This would not, however, rule out the possibility of binding at a distinct allosteric site.

In future, direct structural study may be the only way to confirm the orthosteric binding of GP-25.

Given that GP-25 was initially selected in a screen against human P2X4, we considered potential reasons for its lack of activity at human P2X4 compared to human P2X7. GP-25 and its analogues have two possible enantiomers (R- and S-) due to the presence of a chiral center (Figure 4C, marked with a blue star) linking the heterotricyclic ring to the phenyl moiety, and we used molecular docking of both enantiomers of GP-25 into human P2X4 and P2X7, and both enantiomers of its analogue GP-47 into human P2X7, to try to address this. We found that, in human P2X4, only the S-enantiomer of GP-25 was able to make extensive interactions between its carboxylic acid moieties and the amino-acids known to coordinate the gamma phosphate of ATP, whereas in human P2X7, both enantiomers were capable of this. Furthermore, in human P2X4, the S-enantiomer of GP-25 made an additional stabilizing H-bond interaction with the backbone of Ser-289 and Leu-214 (the reason why it was chosen after visual inspection to be included in the initial screening). In the dock of the R-enantiomer of GP-25 into human P2X4, the carboxylic acid moieties were flipped towards the “bottom” of the orthosteric pocket, and while multiple interactions were observed, (a π -cation interaction with the phenyl moiety and Lys-313, and multiple H-bond interactions with Leu-214, Ser-289, Lys-67), the network of interactions was less complex than that of the S-enantiomer, and did not include Lys-69 or Arg-295. The lack of ability of the R-enantiomer of GP-25 to make interactions with the amino-acids that coordinate the gamma phosphate may explain the lack of activity at human P2X4. It is important to state that we do not know the proportions of R- and S-enantiomers present in the supplied compound; if it were a 50:50 mixture, according to our hypothesis above, we might have expected to observe some inhibition of P2X4 when 10 μ M compound was applied, or inhibition at higher concentrations (e.g., 30–100 μ M, which we did not test). However, if the R-enantiomer predominates, we would not necessarily expect to observe inhibition even at high concentrations. A possible reason why docking of the R-enantiomer of GP-25 resulted in a flipped conformation in P2X4 but not P2X7 is the reduced and more enclosed pocket in P2X4 compared to P2X7, due to the presence of a 4-amino-acid longer loop lining the side of the pocket (Pasqualetto et al., 2018).

In our docking of the S-enantiomer of GP-25 into human P2X7, the methoxycarbonyl moiety made further stabilizing interactions with Asn-292 and Lys-311. The necessity for there to be a non-planar dihedral angle between the ester and the Asn-292 and Lys-64 (to ensure optimal geometry for hydrogen bond formation) may at least partially explain that replacement of the freely rotating bond of the ester with a constrained cyclized carbonyl (e.g., in compound 18, 25, 26, 27, 28 or 30) always resulted in loss of activity. The hydroxyl group of Tyr-288 in human P2X7 also appears to be important for stabilizing the heterotricyclic ring of either GP-25 or GP-47. One of the very few differences between

human P2X7 and rat P2X7 is the presence of a phenylalanine at position 288 (Phe-288), and weaker additional stabilization of GP-25 and its analogues in the orthosteric pocket may explain the moderate difference in potency of GP-25 at human over rat P2X7 and the loss of potency of GP-47 in rat P2X7.

In summary, we have discovered a novel P2X7 antagonist with an IC_{50} value of 8.7 μ M at human P2X7, which displays no activity at human P2X4. Pharmacological and molecular docking analysis suggests that it may bind in the orthosteric pocket of the receptor, and that interactions between carboxylic acid moieties and positively charged amino-acids in the orthosteric pocket are potentially important for its activity and selectivity.

Data availability statement

The raw data supporting the conclusion of this article will be made available by the authors, without undue reservation.

Author contributions

GP, MY and AB participated in research design. GP and MZ conducted experiments. GP, MZ, and MY performed data analysis. GP and MY wrote the manuscript. All authors contributed to the article and approved the submitted version.

References

- Adinolfi, E., Cirillo, M., Woltersdorf, R., Falzoni, S., Chiozzi, P., Pellegatti, P., et al. (2010). Trophic activity of a naturally occurring truncated isoform of the P2X7 receptor. *FASEB J.* 24, 3393–3404. doi:10.1096/FJ.09-153601
- Allsopp, R. C., Dayl, S., Bin Dayel, A., Schmid, R., and Evans, R. J. (2018). Mapping the allosteric action of antagonists A740003 and A438079 reveals a role for the left flipper in ligand sensitivity at P2X7 receptors. *Mol. Pharmacol.* 93, 553–562. doi:10.1124/mol.117.111021
- Allsopp, R. C., Dayl, S., Schmid, R., and Evans, R. J. (2017). Unique residues in the ATP gated human P2X7 receptor define a novel allosteric binding pocket for the selective antagonist AZ10606120. *Sci. Rep.* 7, 725. doi:10.1038/S41598-017-00732-5
- Ase, A. R., Honson, N. S., Zaghdane, H., Pfeifer, T. A., and Séguéla, P. (2015). Identification and characterization of a selective allosteric antagonist of human P2X4 receptor channels. *Mol. Pharmacol.* 87, 606–616. doi:10.1124/mol.114.096222
- Bassetto, M., De Burghgraeve, T., Delang, L., Massarotti, A., Coluccia, A., Zonta, N., et al. (2013). Computer-aided identification, design and synthesis of a novel series of compounds with selective antiviral activity against chikungunya virus. *Antiviral Res.* 98, 12–18. doi:10.1016/j.antiviral.2013.01.002
- Beswick, P., Wahab, B., Honey, M. A., Paradowski, M., Jiang, K., Lochner, M., et al. (2019). A challenge finding P2X1 and P2X4 ligands. *Neuropharmacology* 157, 107674. doi:10.1016/j.neuropharm.2019.107674
- Bin Dayel, A., Evans, R. J., and Schmid, R. (2019). Mapping the site of action of human P2X7 receptor antagonists AZ11645373, brilliant blue G, KN-62, calmidazolium, and ZINC58368839 to the intersubunit allosteric pocket. *Mol. Pharmacol.* 96, 355–363. doi:10.1124/mol.119.116715
- Bootman, M. D., Rietdorf, K., Collins, T., Walker, S., and Sanderson, M. (2013). Ca²⁺-sensitive fluorescent dyes and intracellular Ca²⁺ imaging. *Cold Spring Harb. Protoc.* 8, 83–99. doi:10.1101/pdb.top066050
- Caseley, E. A., Muench, S. P., Fishwick, C. W., and Jiang, L. H. (2016). Structure-based identification and characterisation of structurally novel human P2X7 receptor antagonists. *Biochem. Pharmacol.* 116, 130–139. doi:10.1016/j.bcp.2016.07.020
- Chataigneau, T., Lemoine, D., and Grutter, T. (2013). Exploring the ATP-binding site of P2X receptors. *Front. Cell Neurosci.* 7, 273. doi:10.3389/FNCEL.2013.00273
- Dal Ben, D., Buccioni, M., Lambertucci, C., Marucci, G., Spinaci, A., Marchenkova, A., et al. (2019). Investigation on 2', 3'-O-substituted ATP derivatives and analogs as novel P2X3 receptor antagonists. *ACS Med. Chem. Lett.* 10, 493–498. doi:10.1021/acsmedchemlett.8b00524
- Dane, C., Stokes, L., and Jorgensen, W. T. (2022). P2X receptor antagonists and their potential as therapeutics: A patent review (2010–2021). *Expert Opin. Ther. Pat.* 32, 769–790. doi:10.1080/13543776.2022.2069010
- Fischer, R., Kalthof, B., Grützmann, R., Woltering, E., Stelte-Ludwig, B., and Wuttke, M. (2004). Benzofuro-1,4-diazepin-2-one derivatives. *Patent No WO2004085440A1*. Switzerland: World Intellectual Property Organisation.
- Gasparri, F., Wengel, J., Grutter, T., and Pless, S. A. (2019). Molecular determinants for agonist recognition and discrimination in P2X2 receptors. *J. General Physiology* 151, 898–911. doi:10.1085/jgp.201912347
- Grimes, L., Griffiths, J., Pasqualetto, G., Brancale, A., Kemp, P. J., Young, M. T., et al. (2020). Drosophila taste neurons as an agonist-screening platform for P2X receptors. *Sci. Rep.* 10, 8292. doi:10.1038/s41598-020-65169-9
- Hattori, M., and Gouaux, E. (2012). Molecular mechanism of ATP binding and ion channel activation in P2X receptors. *Nature* 485, 207–212. doi:10.1038/NATURE11010
- Hernandez-Olmos, V., Abdelrahman, A., El-Tayeb, A., Freudendahl, D., Weinhausen, S., and Müller, C. E. (2012). N-substituted phenoxazine and

Funding

GP was supported by a Life Sciences Research Network Wales PhD studentship. MZ was supported by a Sight Research UK PhD studentship (RES013).

Conflict of interest

The authors declare that the research was conducted in the absence of any commercial or financial relationships that could be construed as a potential conflict of interest.

Publisher's note

All claims expressed in this article are solely those of the authors and do not necessarily represent those of their affiliated organizations, or those of the publisher, the editors and the reviewers. Any product that may be evaluated in this article, or claim that may be made by its manufacturer, is not guaranteed or endorsed by the publisher.

Supplementary material

The Supplementary Material for this article can be found online at: <https://www.frontiersin.org/articles/10.3389/fphar.2022.1094607/full#supplementary-material>

acridone derivatives: Structure-activity relationships of potent P2X4 receptor antagonists. *J. Med. Chem.* 55, 9576–9588. doi:10.1021/jm300845v

Honore, P., Donnelly-Roberts, D., Namovic, M. T., Hsieh, G., Zhu, C. Z., Mikusa, J. P., et al. (2006). A-740003 [N-(1-((cyanoimino)(5-quinolinylamino) methyl) amino)-2, 2- dimethylpropyl)-2-(3, 4-dimethoxyphenyl)acetamide], a novel and selective P2X7 receptor antagonist, dose-dependently reduces neuropathic pain in the rat. *J. Pharmacol. Exp. Ther.* 319, 1376–1385. doi:10.1124/jpet.106.111559

Karasawa, A., and Kawate, T. (2016). Structural basis for subtype-specific inhibition of the P2X7 receptor. *Elife* 5, e22153. doi:10.7554/eLife.22153

Kawate, T., and Gouaux, E. (2006). Fluorescence-detection size-exclusion chromatography for precrystallization screening of integral membrane proteins. *Structure* 14, 673–681. doi:10.1016/j.str.2006.01.013

Kawate, T. (2017). P2X receptor activation. *Adv. Exp. Med. Biol.* 1051, 55–69. doi:10.1007/5584_2017_55

Korb, O., Stützel, T., and Exner, T. E. (2006). Plants: Application of ant colony optimization to structure-based drug design. *Lect. Notes Comput. Sci. Incl. Subser. Lect. Notes Artif. Intell. Lect. Notes Bioinforma.* 4150, 247–258. doi:10.1007/11839088_22/COVER

Laskowski, R. A., MacArthur, M. W., Moss, D. S., and Thornton, J. M. (1993). Procheck: A program to check the stereochemical quality of protein structures. *J. Appl. Crystallogr.* 26, 283–291. doi:10.1107/S0021889892009944

Lovell, S. C., Davis, I. W., Arendall, W. B., de Bakker, P. I. W., Word, J. M., Prisant, M. G., et al. (2003). Structure validation by calpha geometry: Phi, psi and cbeta deviation. *Proteins Struct. Funct. Genet.* 50, 437–450. doi:10.1002/prot.10286

Mansoor, S. E., Lü, W., Oosterheert, W., Shekhar, M., Tajkhorshid, E., and Gouaux, E. (2016). X-ray structures define human P2X 3 receptor gating cycle and antagonist action. *Nature* 538, 66–71. doi:10.1038/nature19367

McCarthy, A. E., Yoshioka, C., and Mansoor, S. E. (2019). Full-length P2X7 structures reveal how palmitoylation prevents channel desensitization. *Cell* 179, 659–670. e13. doi:10.1016/j.cell.2019.09.017

Müller, C. E., and Namasivayam, V. (2022). Agonists, antagonists, and modulators of P2X7 receptors. *Methods Mol. Biol.* 2510, 31–52. doi:10.1007/978-1-0716-2384-8_2

Pasqualetto, G., Brancale, A., and Young, M. T. (2018). The molecular determinants of small-molecule ligand binding at P2X receptors. *Front. Pharmacol.* 9, 58. doi:10.3389/fphar.2018.00058

Rarey, M., Kramer, B., Lengauer, T., and Klebe, G. (1996). A fast flexible docking method using an incremental construction algorithm. *J. Mol. Biol.* 261, 470–489. doi:10.1006/jmbi.1996.0477

Ren, W. J., and Illes, P. (2022). Involvement of P2X7 receptors in chronic pain disorders. *Purinergic Signal* 18, 83–92. doi:10.1007/s11302-021-09796-5

Sheng, D., and Hattori, M. (2022). Recent progress in the structural biology of P2X receptors. *Proteins Struct. Funct. Bioinforma.* 90, 1779–1785. doi:10.1002/prot.26302

Specs (2022). Specs - compound management services and research compounds for the Life science industry. Available at: <https://www.specs.net/index.php> [Accessed August 1, 2022].

Tsuda, M., Shigemoto-Mogami, Y., Koizumi, S., Mizokoshi, A., Kohsaka, S., Salter, M. W., et al. (2003). P2X4 receptors induced in spinal microglia gate tactile allodynia after nerve injury. *Nature* 424, 778–783. doi:10.1038/nature01786

Villoutreix, B. O., Laconde, G., Lagorce, D., Martineau, P., Miteva, M. A., and Dariavach, P. (2011). Tyrosine kinase syk non-enzymatic inhibitors and potential anti-allergic drug-like compounds discovered by virtual and *in vitro* screening. *PLoS One* 6, e21117. doi:10.1371/journal.pone.0021117

Young, M. T., Fisher, J. A., Fountain, S. J., Ford, R. C., North, R. A., and Khakh, B. S. (2008). Molecular shape, architecture, and size of P2X4 receptors determined using fluorescence resonance energy transfer and electron microscopy. *J. Biol. Chem.* 283, 26241–26251. doi:10.1074/jbc.M804458200

Young, M. T., Pelegrin, P., and Surprenant, A. (2007). Amino acid residues in the P2X₇ receptor that mediate differential sensitivity to ATP and BzATP. *Mol. Pharmacol.* 71, 92–100. doi:10.1124/mol.106.030163

Zhao, Y., Chen, X., Lyu, S., Ding, Z., Wu, Y., Gao, Y., et al. (2021). Identification of novel P2X7R antagonists by using structure-based virtual screening and cell-based assays. *Chem. Biol. Drug Des.* 98, 192–205. doi:10.1111/cbdd.13867



OPEN ACCESS

EDITED BY

Kenneth A. Jacobson,
National Institutes of Health (NIH),
United States

REVIEWED BY

Nao Hasuzawa,
Kurume University, Japan
Talita Glaser,
University of São Paulo, Brazil

*CORRESPONDENCE

J. Pablo Huidobro-Toro,
✉ juan.garcia-huidobro@usach.cl

SPECIALTY SECTION

This article was submitted to Experimental Pharmacology and Drug Discovery, a section of the journal Frontiers in Pharmacology

RECEIVED 29 August 2022

ACCEPTED 22 December 2022

PUBLISHED 20 January 2023

CITATION

Donoso MV, Hernández F, Barra R and Huidobro-Toro JP (2023), Nanomolar clodronate induces adenosine accumulation in the perfused rat mesenteric bed and mesentery-derived endothelial cells.
Front. Pharmacol. 13:1031223.
doi: 10.3389/fphar.2022.1031223

COPYRIGHT

© 2023 Donoso, Hernández, Barra and Huidobro-Toro. This is an open-access article distributed under the terms of the [Creative Commons Attribution License \(CC BY\)](https://creativecommons.org/licenses/by/4.0/). The use, distribution or reproduction in other forums is permitted, provided the original author(s) and the copyright owner(s) are credited and that the original publication in this journal is cited, in accordance with accepted academic practice. No use, distribution or reproduction is permitted which does not comply with these terms.

Nanomolar clodronate induces adenosine accumulation in the perfused rat mesenteric bed and mesentery-derived endothelial cells

M. Verónica Donoso¹, Felipe Hernández¹, Rafael Barra² and J. Pablo Huidobro-Toro ^{1,3*}

¹Laboratorio de Farmacología, Departamento de Biología, Facultad de Química y Biología, Universidad de Santiago de Chile, Santiago, Chile, ²Centro de Investigación Biomédica y Aplicada (CIBAP), Escuela de Medicina, Facultad de Ciencias Médicas, Universidad de Santiago de Chile, Santiago, Chile, ³Centro de Nanociencia y Nanotecnología, Universidad de Santiago de Chile, Santiago, Chile

The vesicular nucleotide transporter (VNUT) is critical for sympathetic co-transmission and purinergic transmission maintenance. To examine this proposal, we assessed whether the bisphosphonate clodronate, claimed as a potent *in vitro* VNUT blocker, modified spontaneous and/or the electrically evoked overflow of ATP/metabolites and NA from mesentery sympathetic perivascular nerve terminals. Additionally, in primary endothelial cell cultures derived from this tissue, we also evaluated whether clodronate interfered with ATP/metabolite cell outflow and metabolism of N⁶-etheno adenosine 5'-triphosphate (eATP), N⁶-etheno adenosine (eADO), and adenosine deaminase enzyme activity. Rat mesenteries were perfused in the absence or presence of .01–1,000 nM clodronate, 1–1,000 nM Evans blue (EB), and 1–10 μM DIDS; tissue perfusates were collected to determine ATP/metabolites and NA before, during, and after perivascular electrical nerve terminal depolarization. An amount of 1–1,000 nM clodronate did not modify the time course of ATP or NA overflow elicited by nerve terminal depolarization, and only 10 nM clodronate significantly augmented perfusate adenosine. Electrical nerve terminal stimulation increased tissue perfusion pressure that was significantly reduced only by 10 nM clodronate [90.0 ± 18.6 ($n = 8$) to 35.0 ± 10.4 ($n = 7$), $p = .0277$]. As controls, EB, DIDS, or reserpine treatment reduced the overflow of ATP/metabolites and NA in a concentration-dependent manner elicited by nerve terminal depolarization. Moreover, mechanical stimulation of primary endothelial cell cultures from the rat mesentery added with 10 or 100 nM clodronate increased adenosine in the cell media. eATP was metabolized by endothelial cells to the same extent with and without 1–1,000 nM clodronate, suggesting the bisphosphonate did not interfere with nucleotide ectoenzyme metabolism. In contrast, extracellular eADO remained intact, indicating that this nucleoside is neither metabolized nor transported intracellularly. Furthermore, only 10 nM clodronate inhibited (15.5%) adenosine metabolism to inosine in endothelial cells as well as in a commercial crude adenosine deaminase enzyme preparation (12.7%), and both effects proved the significance ($p < .05$). Altogether, present data allow inferring that clodronate inhibits adenosine deaminase activity in isolated endothelial cells as in a crude extract preparation, a finding that may account for adenosine accumulation following clodronate mesentery perfusion.

KEYWORDS

clodronate, VNUT inhibitors, purinergic signaling, rat mesenteric bed, ATP/metabolite's, adenosine deaminase

Introduction

The role of adenosine 5'-triphosphate (ATP) as an extracellular signaling molecule is firmly rooted. ATP metabolites such as adenosine 5'-diphosphate (ADP) or adenosine (ADO) are also extracellular messengers, the former mimicking ATP activity mainly through P2Y receptor activation, while the latter through its four ADO receptors. Some authors claim ADO is released as such to the synaptic cleft or is a consequence of ATP ectoATPase hydrolysis (Burnstock, 2018). In addition, purines also play a role as modulators of sympathetic transmission both in the brain and periphery *via* presynaptic mechanisms. From an evolutionary viewpoint, Estevez-Herrera et al. (2016) proposed that ATP is an ancient signaling molecule, functioning in cellular communications since early life stages. This thesis gets ample support from the Burnstock (2018) proposal recognizing the universal and primitive messenger role of ATP, as early as amino acids, and substantially earlier than amino acid-derived transmitters such as catechol, imidazole, or indol ethyl amines.

In support of the transmitter role of ATP, extracellular nucleotides have a short half-life in the synaptic space due to rapid hydrolysis to ADP, adenosine 5'-monophosphate (AMP), or ADO by several ectoATPases (Navarrete et al., 2014). Critical to the extracellular messenger ATP role, Moriyama and others described a vesicular nucleotide transporter (VNUT) as a key player in purinergic signaling (Sawada et al., 2008), a feature common to the recycling processes of most transmitters. The transporter ensures the maintenance of the purinergic synaptic transmission component including effects at peripheral neuroeffector junction sympathetic co-transmission. The VNUT is highly expressed in the brain and peripheral tissues such as the pancreas, liver, skeletal muscles, adrenals, and lungs (Moriyama et al., 2017). Although the crystal structure of the VNUT is lacking, it was early recognized to have a strong primary sequence homology to the brain glutamate transporter (VGLUT) as reported by Sawada et al. (2008). Based on indirect evidence, the first pharmacological characterization of the VNUT was based on VGLUT inhibitors such as Evans blue (EB) or 4,4'-diisothiocyantostilbene-2,2'-disulfonate (DIDS).

The former is a symmetric azo dye with nanomolar potency, while the latter is a stilbene markedly less potent than EB requiring 100–300 times larger concentrations to block VNUT activity (Sawada et al., 2008). More recently, dichloromethylene diphosphonic acid (clodronate), a first-generation bisphosphonate, a drug clinically used for over 60 years to treat bone diseases, was alleged by Moriyama and Nomura (2018) to act as a selective and potent VNUT inhibitor. It was initially proposed that clodronate, based on its two negative phosphates, competes with chloride ions at an allosteric VNUT binding pocket with an affinity similar to acetoacetate, a prototype ketone body ligand (Moriyama and Nomura, 2018). Within few years, studies were extended to a series of novel bisphosphonates, including N-containing compounds, which also proved VNUT inhibitors in the Moriyama *in vitro* assay. Moreover, Kato et al. (2017) observed that clodronate impaired ATP vesicular release from neurons, astrocytes, or brain immune cells. Out of the several bisphosphonates investigated, clodronate proved the most potent with nanomolar potency as a VNUT blocker. Furthermore, Kato et al. (2017) highlighted clodronate's analgesic potential with a unique analgesic profile against neuropathic pain, a pharmacologic effect tentatively related to its

alleged VNUT-blocking property. This finding allows relating purinergic signaling to chronic or neuropathic pain. Based on its pharmacological profile, clodronate may be considered a valuable research tool to explore ATP exocytosis in purinergic transmission, mimicking other drugs that block transmitter transport which turned critical to establish nerve endings recycling dynamics.

Therefore, whether clodronate interferes with the recycling of ATP in sympathetic nerve endings of the rat mesentery vascular bed was examined, where ATP is known to be co-released together with noradrenaline (NA) and constitutes an example of sympathetic co-transmission, Donoso et al. (2006) used this tissue to characterize sympathetic transmission in a peripheral neuroeffector junction and described its purinergic component. We proposed as a working hypothesis that clodronate, as a VNUT inhibitor, should decrease vesicular ATP storage in sympathetic nerve endings, reducing ATP overflow following electrical nerve terminal depolarization, impairing sympathetic co-transmitter overflow. Two aims guided the present investigation: 1) Assessing whether nanomolar clodronate rat mesentery perfusion reduced purine outflow induced by electrical depolarization of the perivascular nerve endings, decreasing ATP overflow to the mesentery perfusate. As a positive control EB, DIDS, and reserpine were used; the latter blocks the vesicular catecholamine transporter reducing monoamine storage in sympathetic neuroeffector junctions (Hillarp, 1960; Huidobro-Toro 1985; Mandela et al., 2010), 2) Examining whether clodronate increases ATP metabolism, an alternative explanation for the anticipated reduction in transmitter overflow to the mesentery perfusate. To this aim, we examined N⁶-etheno adenosine 5'-triphosphate (eATP) or N⁶-etheno adenosine (eADO) metabolism by primary cultures of endothelial cells derived from the rat mesentery since these etheno derivatives were previously characterized as exclusive endothelial cell ectoATPase substrates (Jackson et al., 2020). We extended the current study to assay adenosine deaminase (ADA) activity in cultured endothelial cells as in a calf intestinal mucosa type II crude powder.

The present results show that contrary to expectations, clodronate, even after a 3-h tissue incubation, did not reduce ATP or NA perfusate overflow elicited by electrical nerve terminal depolarization. Notwithstanding, the ADO output in mesentery perfusates was significantly increased. The increase in extracellular ADO might account for the reduction of the perfusion pressure elicited by the electrically evoked mesentery nerve terminal depolarization in preparations perfused with 10 nM clodronate. In contrast, EB, DIDS, and reserpine evidenced concentration-dependent reductions in the ATP/metabolites and NA outflow elicited by nerve terminal depolarization. Moreover, in primary cultures of endothelial cells or an ADA calf intestinal mucosa type II crude powder bioassay, 10 nM clodronate reduced ADA activity consonant with the significant ADO increase observed in mesentery perfusates.

Experimental procedures

Animals

Adult male Sprague–Dawley rats (250–350 g) bred at the Animal Reproduction Facility of the Faculty of Biological Sciences of the P. Catholic University were used, and the different protocols added 122 rats, distributed in the different group series. Animal handling

conformed to animal care and NIH (United States) guidelines and procedures for laboratory animals' use. The Faculty and the University ethical committees for use of animals for biological research approved the specific protocols designed and supervised our strict adherence to the subscribed guidelines, as certified by consent protocol number 121/2017-USACH. All efforts were enforced to minimize the number of rats used and their suffering. The animals were anesthetized with a mixture of ketamine: xylazine (25: 2.5 mg/kg) i.p.

Drugs and chemicals

ATP and its metabolic degradation products as sodium salts as well as clodronate disodium, Evans blue (EB), 4,4'-diisothiocyanatostilbene-2,2'-disulfonate (DIDS), noradrenaline hydrochloride (NA), 3,4-dihydroxybenzylamine hydrobromide, reserpine chlorhydrate, quercetin, cyclodextrin adenine, and adenosine deaminase (ADA) from calf intestinal mucosa type II crude powder were purchased from Sigma-Aldrich Chemicals (Saint Louis, MO, United States). N⁶-etheno-purine standards for chromatographic column calibration or the development of specific experimental protocols (eATP and eADO) were previously synthesized in our laboratory. Chemicals used to prepare buffers and mobile chromatography phases were of analytical grade and purchased from Merck Chemicals (Darmstadt, Germany).

Perfusion of the rat arterial mesenteric bed and collection of the mesenteric perfusate aliquots upon electrical depolarization of the perivascular nerve endings to quantify outflow of ATP/metabolites and NA

Upon animal anesthesia, the abdominal cavity was excised at the midline; the superior mesenteric artery was isolated and cannulated with plastic tubing to initiate Tyrode buffer perfusion at a 2 mL/min flow (37°C) bubbled with a mixture of 95% O₂/5% CO₂. The Tyrode solution composition was (mM): 118 NaCl, 5.4 KCl, 2.5 CaCl₂, 1.2 KH₂PO₄, 1.2 MgSO₄, 23.8 NaHCO₃, and 11.1 D-glucose. With surgical scissors, the vascular mesenteric bed was disconnected from the intestines (McGregor, 1965) and transferred to a warmed tissue chamber to maintain Tyrode buffer perfusion; a pressure transducer was connected to the perfusion cannula. Continuous changes in perfusion pressure were monitored *via* a multichannel Grass polygraph (Donoso et al., 2006; Donoso et al., 2018b). In the meantime, the rats were killed under deep anesthesia by pneumothorax plus aortic bleeding (Donoso et al., 2006). The equilibration period consisted of a 40-min Tyrode buffer perfusion in the absence or presence of either clodronate, EB, or DIDS. Immediately thereafter, electrical stimulation of the perivascular nerve terminals, surrounding the superior mesenteric artery, commenced (20 Hz, 1 ms trains of 60 V) for 1 min; nerve depolarization was delivered *via* platinum electrodes connected to a Grass S44 stimulator. In all these protocols, the mesentery perfusate effluent was collected at 2-min intervals in pre-chilled 5-mL plastic tubes, 8 min before, during, and 22 min after the electrical depolarization. Sample collection commenced after the end of the equilibrium period. This protocol optimized perfusate collection to determine ATP/purines and NA overflow, before, during, and after the

electrical nerve terminal stimulation. The co-transmitter overflow was quantified in the same perfusate aliquot.

For the clodronate protocol series, 30 separate mesenteries were perfused with .01–1,000 nM clodronate and eight separate tissues that were perfused without this drug. Likewise, for the EB series, 21 mesenteries were perfused in the presence of EB and eight mesenteries were perfused in its absence; likewise, for 1–10 μM DIDS perfusion series, 12 separate tissues were perfused with DIDS, while 10 were perfused without this chemical. For animals' distribution to the different drug concentration group series, see Table 1; Supplementary Table S1. Additional experiments were conducted to extend the clodronate perfusion period for 180 min, four tissues were perfused with Tyrode buffer in the absence of clodronate, and four preparations were perfused in the presence of 10 nM clodronate. Fresh clodronate stock dilutions were prepared prior to each protocol. Non-drug-perfused mesenteries that served as controls were spaced along the course of the study period to rule out seasonal variations or other non-controlled variables that may cause data inconsistencies.

Reserpine treatment

To compare the effect of putative VNUT inhibitors, with an inhibitor of the vesicular NA transporter on the outflow of ATP/metabolites or NA, a series of protocols were performed using mesenteries from rats pretreated with either .2 or 2 mg/kg reserpine or vehicle. Matched groups of rats were treated with either vehicle (five rats) or a single sub-cutaneous dose of .2 mg/kg (three rats) or 2 mg/kg (five rats) reserpine; mesenteries from these rats were dissected 48 h after reserpine–vehicle treatment. Protocols were conducted as usual to examine spontaneous ATP/metabolites and NA outflow as well as electrically evoked co-transmitter outflow. The vehicle composition was as follows: acetic acid, propylene glycol, ethanol, and water, 2%, 4%, 4%, and 90% respectively.

Quantification of the increase in tissue perfusion pressure elicited by perivascular nerve depolarization

In all series of mesenteries electrically depolarized, the increment in the mesentery pressure elicited by electrical depolarization was obtained by subtracting basal values, which normally were between 25 and 30 mm Hg; the values were expressed as the Δ increase in the mesentery perfusion pressure in mm Hg. This applied to tissues perfused with either drugs or only perfused with vehicle or Tyrode buffer.

Isolation and harvesting of primary endothelial cell cultures and protocol description

Additional five rats were used to harvest endothelial cells seeded in the 24 multi-well plates (Donoso et al., 2018a), and the protocol used to determine the spontaneous extracellular ATP/metabolites as well as following mechanical stimulation by cell medium displacement of the cell culture medium was described previously (Donoso et al., 2018a). To examine the effect of clodronate on extracellular ATP/metabolites, cell medium purines were analytically assessed in cell wells not exposed to clodronate, incubated with 400 μL Tyrode buffer

TABLE 1 Clodronate concentration-dependent effects on spontaneous and electrically evoked ATP/metabolites and NA overflow from the mesentery neuroeffector junction.

Spontaneous overflow (pmol), X ± S.E.M.							
Clodronate nM							
	0 (n=8)	0.01 (n=5)	0.1 (n=5)	1 (n=5)	10 (n=7)	100 (n=4)	1000 (n=4)
ATP	8.05 ± 2.49	16.64 ± 8.55	52.97 ± 20.45	4.31 ± 1.69	38.98 ± 18.41	10.67 ± 3.69	20.23 ± 10.81
ADP	15.53 ± 3.55	17.80 ± 5.19	55.75 ± 17.75	15.69 ± 7.52	33.92 ± 12.31	15.07 ± 1.88	27.31 ± 6.57
AMP	13.38 ± 4.74	3.54 ± 1.16	21.50 ± 4.77	5.53 ± 1.65	13.29 ± 3.23	14.54 ± 3.84	13.25 ± 3.62
ADO	7.12 ± 1.35	4.41 ± 0.82	15.82 ± 4.58	5.86 ± 0.89	8.84 ± 1.31	6.08 ± 1.45	13.40 ± 0.58 *
NA	0.65 ± 0.12	0.23 ± 0.13	0.58 ± 0.41	0.42 ± 0.37	0.55 ± 0.29	1.48 ± 0.60	1.51 ± 0.05 **
Total overflow elicited by nerve terminal depolarization (pmol), X ± S.E.M							
Clodronate nM							
	0 (n=8)	0.01 (n=5)	0.1 (n=5)	1 (n=5)	10 (n=7)	100 (n=4)	1000 (n=4)
ATP	91.59 ± 15.86	159.11 ± 71.72	244.70 ± 159.30	133.30 ± 40.33	141.89 ± 52.83	143.72 ± 21.22	778.38 ± 260.37
ADP	141.90 ± 35.58	148.20 ± 43.31	234.80 ± 152.10	232.83 ± 64.36	221.36 ± 39.74	326.06 ± 104.20	494.54 ± 168.78
AMP	197.20 ± 52.36	136.50 ± 36.08	170.20 ± 114.40	239.96 ± 38.57	280.01 ± 74.45	399.11 ± 51.35 *	278.95 ± 52.89
ADO	152.03 ± 26.86	98.73 ± 47.20	227.08 ± 94.46	186.45 ± 47.83	304.04 ± 35.88 **	481.12 ± 123.42	181.97 ± 35.64
NA	28.00 ± 5.68	24.06 ± 4.78	24.05 ± 2.28	23.46 ± 5.93	25.90 ± 3.86	19.98 ± 1.84	22.61 ± 4.32

In parenthesis, the number of preparations assessed. * $p < .05$; ** $p < .01$ unpaired t-test as compared to tissues perfused without clodronate.

10 mM HEPES, or matched parallel wells incubated with Tyrode buffer 10 mM HEPES added with .01–1,000 nM clodronate for 40 min. This bisphosphonate concentration and its exposure time were chosen since in the mesentery perfusion protocols, it reduced the vasomotor response elicited by electrical nerve terminal depolarization. Some wells were not mechanically stimulated and represent spontaneous basal ATP/metabolite secretion, while other wells were mechanically stimulated by gently pipetting the cell media, a stimulus standardized previously that augments extracellular ATP in the cell media (Donoso et al., 2018a).

An aliquot (200 μ L) of the cell media was retrieved for purine analysis from non-stimulated cell wells or 1 min after mechanical stimulation, a procedure we had used in the past to elicit ATP release to the cell media (Donoso et al., 2018a). At the end of the protocol, the wells were rinsed with Tyrode buffer 10 mM HEPES, and supernatants were discarded. The plate was placed at -20°C until Bradford's protein determination was performed in each well. The extracellular ATP/metabolites in the cell media of each separate well were divided by the protein values of each well (pmol purines/mg protein), and expressed as percentage of the control (obtained in the absence of clodronate).

Nucleotide metabolism by ectoATPases; protocols using etheno derivatives

To further examine endothelial cells' nucleotide metabolism, we used eATP or eADO, which are exclusively metabolized by ectoATPases since these compounds do not freely cross cell membranes (Jackson et al., 2020). Four rats were used to harvest 24 multi-well plates with endothelial cell cultures, and the cells were

added with 480 μ L Tyrode buffer supplemented with 10 mM HEPES, in the absence or presence of 1–1,000 nM clodronate for 40 min. Two protocols were followed: in the first, endothelial cell wells were applied with 20 μ L of 50 nM eATP, while in a second set of duplicate protocols, 20 μ L of 25 nM eADO was applied. Stock solutions of both etheno derivatives were dissolved in HPLC water. The time course of the eATP/eADO cell nucleotide hydrolysis was within 30 min. The samples were retrieved at 1, 15, and 30 min, and the remaining eATP or eADO in the cell media were determined analytically by HPLC separation techniques followed by fluorescent detection as will be described. At the end of the protocol, the wells were rinsed with Tyrode buffer 10 mM HEPES, and the supernatants were discarded. The plate was kept at -20°C until Bradford's protein determination assays were conducted. The eATP or eADO in the cell media of each separate well was expressed as pmol/mg protein. As control for these experiments, the samples of eATP or eADO were added to a parallel set of test tubes containing 480 μ L of Tyrode buffer supplemented with 10 mM HEPES without cells; in this case, the results were expressed as pmol/mg protein, which corresponded to the average protein of the 24 multi-well plates with cell results that are expressed as the percentage of the respective eATP or the eADO concentrations.

ADA activity

The colorimetric ADA enzyme assay described by Giusti and Galanti (1984) was followed. The procedure titrates the ammonia generated which can be determined by the indophenol reaction, synthesizing a blue-colored compound monitored

spectrophotometrically. Two separate protocols assessed ADO metabolism: 1) ADO incubation with mesentery cells. Cell incubation was performed in sodium phosphate buffer 50 mM, pH 6.5, 37°C, in the absence or presence of 1–1,000 nM clodronate, adding exogenous ADO as a substrate. Three separate rats were used to harvest the 24-well plate cultured cells to achieve these protocols. The cells were incubated for 60 min with 10 mM ADO to start the enzyme reaction in excess substrate, and the chemical reaction was stopped in due time by retrieving a 400 μ L aliquot of the cell media which was added to a test tube containing 1.4 mL phenol–sodium nitroprusside (106 mM phenol; .17 mM sodium nitroprusside). The samples were vortexed and 1.4 mL hypochlorite solution was added (11 mM of NaOCl, 125 mM NaOH). The samples are vortexed again and incubated for 30 min at 37°C prior to 620-nm spectrophotometric monitoring. A standard calibration curve was built with 3–300 μ M ammonium sulfate in sodium phosphate buffer. At the end of the protocol, the wells were rinsed with sodium phosphate buffer, and the supernatants were discarded. The plate was stored at –20°C until Bradford's protein determinations ensued, and the resulting cell medium ammonia of each separate well was divided by its protein content. The results of these studies are expressed as percentage of the ammonia produced by the reaction in the absence of clodronate, as compared to samples incubated with varying clodronate concentrations. As internal enzyme inhibition, 10 or 30 μ M quercetin was used (Melzig, 1996). The vehicle for quercetin was β -cyclodextrin (18.5 mg/1 mL H₂O). 2) crude enzyme assay. Reactions were performed in 96-well plates with the 6.25 mU/mL enzyme incubated in sodium phosphate buffer 50 mM, pH 6.5, 37°C, with reagents added in the following order: first, 10 μ L of the several inhibitors used, second, 10 μ L of the enzyme dilution (.78–50 mU/mL), and last, 10 μ L of ADO (.01–20 mM). The reaction was incubated for 60 min at 37°C. The reaction was stopped by adding 93 μ L phenol–sodium nitroprusside (106 mM phenol; .17 mM sodium nitroprusside), vortexed, and 93 μ L hypochlorite solution was added (11 mM of NaOCl in 125 mM NaOH). The samples are vortexed again and incubated for additional 30 min at 37°C prior to 620-nm spectrophotometric readings. A standard calibration curve was built with 3–300 μ M ammonium sulfate in sodium phosphate buffer. Test inhibitors used were 1–1,000 nM clodronate, 1 mM quercetin (El-Said et al., 2022), vehicle for quercetin β -cyclodextrin (18.5 mg/1 mL H₂O), and .7 mM adenine (Alunni et al., 2008).

Analytical procedures for ATP/metabolites and NA quantifications

Purine analytical determinations

Purines were quantified following a chemical reaction with chloro-acetaldehyde to generate the corresponding fluorescent N⁶-etheno purines. To this aim, a 200- μ L aliquot of the 4-mL sample perfusate retrieved or the cell media from cell wells were used to react with 100 μ L buffer phosphate–citrate, pH 4, and 10 μ L of chloro-acetaldehyde. The samples were heated in a dry bath for 40 min at 80°C, a procedure that synthesized fluorescent derivatives which allowed picomolar detection of eATP, eADP, eAMP, and eADO. The chemical reaction was stopped by ice chilling for 5 min. The samples were stored at 4°C and analyzed within 24 h. HPLC procedures were used to separate and identify purines using the appropriate standards as previously detailed (Buvinic et al., 2007).

The Merck-Hitachi HPLC instrument was used, equipped with a fluorescence detector at excitation and emission wavelengths of 233 nm and 415 nm, respectively. A 20 μ L aliquot of each sample was injected into a Chromolith HPLC column equilibrated with the mobile phase at a flow of 1.5 mL/min (.2 M Na₂HPO₄, .2 M NaH₂PO₄, and 5 mM tetrabutylammonium; pH 6). A calibration curve was performed daily, and linearity was routinely attained between .0012 and 10 pmol/20 μ L purines. The ATP/metabolite overflow to the mesentery perfusate was expressed as pmol collected per 4 mL fraction or was expressed as the total overflow accessible to the perfusate after electrical depolarization (fraction addition during and after perivascular nerve depolarization subtracting the spontaneous efflux); values were expressed as pmol.

NA determinations

Of the 4 mL of the mesentery perfusate collected, a 200- μ L aliquot sample was separated on ice for the purine assay; the residual 3.8 mL was supplemented with 1.75 pmol 3,4-dihydroxybenzylamine, used as an internal standard. The lumenally accessible NA was concentrated by Sep-Pak C-18 reverse-phase cartridges (Waters, Milford, MA, United States) eluted with the HPLC mobile phase used to assay NA by electrochemical detection. The eluates were evaporated to dryness and stored at –20°C. The samples were reconstituted in 200 μ L water and quantified by HPLC, using the Merck L6200 A, Intelligent Pump, the Eicom electrochemical detector ECD-700S. A 100 μ L aliquot of each sample was injected into a LiChroCART 125-4 HPLC column equilibrated with the mobile phase at a flow of 1.0 mL/min (.1 M NaH₂PO₄–H₂O, .9 mM Triplex III, .66 mM 1-octanesulfonic acid, and acetonitrile 15 mL per liter; pH 2.8). A calibration curve was performed, and linearity was routinely attained between .35 and 5 pmol/100 μ L NA and .5–7.0 pmol/100 μ L 3,4-dihydroxybenzylamine. The released NA overflow was expressed as pmol collected per fraction (4 mL). The total overflow accessible to the perfusate following electrical nerve endings depolarization (amount obtained by adding all the fractions, after normalizing by subtracting the spontaneous NA efflux, values attained prior to the electrical depolarization), is expressed in pmol, as shown in Donoso et al. (2006).

Statistical analysis

The results are expressed as the mean average values \pm standard error of the mean. For statistical analysis, GraphPad Prism version 8.0.0 for Windows, GraphPad Software, San Diego, California United States, was routinely used. Normal data distribution was determined by the Shapiro–Wilk test. To compare two sets of data with normal distribution, the unpaired t-test or unpaired t-test with Welch's correction was used in cases of variance differences. The Mann–Whitney test was used to compare two sets of data with non-parametric distributions. In the case of normal distribution, time course protocols used the one-way ANOVA, and in non-parametric distributions, the Kruskal–Wallis test was followed. The two-way ANOVA compared time course protocols of non-drug treated versus those treated with drug applications. In all cases, the significance level was set with an α value of less than .05.

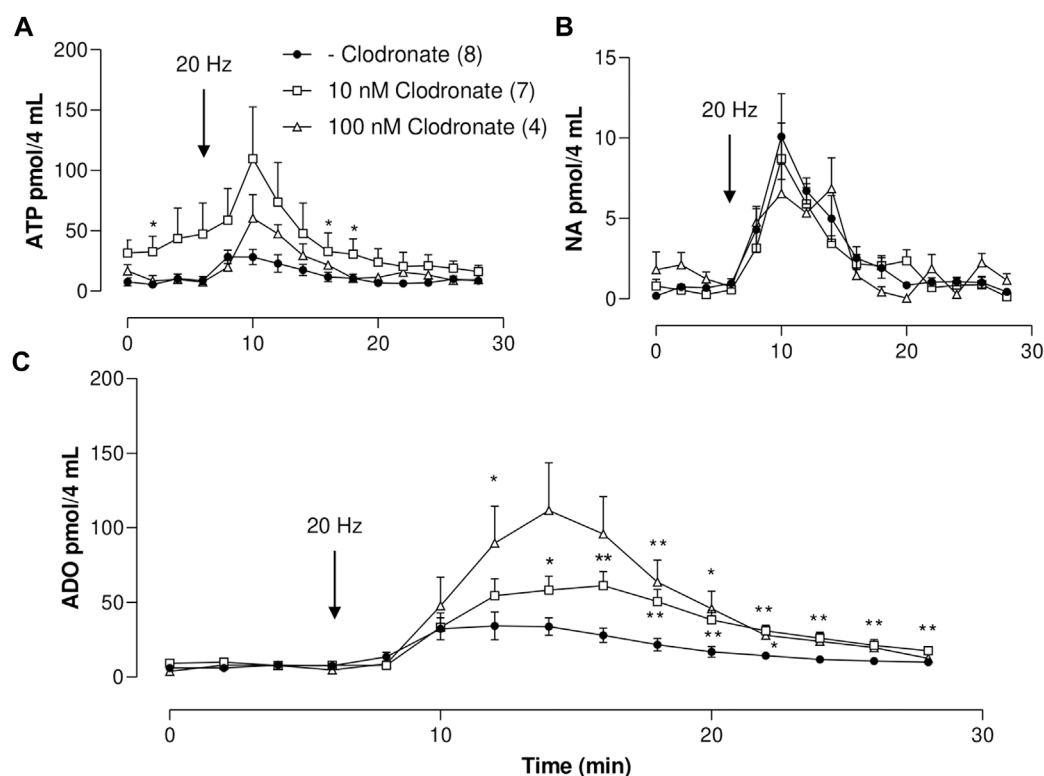


FIGURE 1

ATP, ADO, and NA outflow to the mesenteric perfusate elicited by electrical nerve endings stimulation in mesenteries perfused in the absence or presence of either 10 or 100 nM clodronate; a time course study. (A) Overflow of ATP, (B) NA overflow, and (C) ADO overflow. Mesenteries were perfused prior to, during, and after nerve endings depolarization, in the absence (closed circles, $n = 8$) or presence of either 10 nM clodronate ($n = 7$, open squares) or 100 nM clodronate ($n = 4$, open triangles). The arrows indicate the initiation of the 1-min nerve endings depolarization (20 Hz, 1 ms trains of 60 V) to elicit co-transmitter release from the nerve terminals. Symbols indicate mean values; bars the S.E.M. *, $p < .05$; **, $p < .01$ unpaired t-test compared to perfusions without clodronate.

Results

Changes in spontaneous or electrically evoked purines or NA overflow elicited in the presence of .01–1,000 nM clodronate: Time course studies

ATP

Mesentery perivascular nerve endings electrical stimulation elicited an increase in ATP outflow [Figure 1A, one-way ANOVA $F(14,105) = 3.723$, $p < .0001$]. Notwithstanding, mesentery perfusion with .01–1,000 nM clodronate did not modify the spontaneous overflow nor the total outflow induced by electrical stimulation as compared to perfusions in the absence of bisphosphonate (Table 1). Perfusion with either 10 nM or 100 nM clodronate time responses are shown in Figure 1A, and no ATP outflow reduction induced by clodronate was observed. Values of two-way ANOVA analysis for .01–100 nM clodronate were $F(14,165) = 2.004$, $p = .0203$; $F(14,165) = 1.909$, $p = .0286$; $F(14,165) = 0$, $p = .1297$; $F(14,195) = .8745$, $p = .5875$; $F(14,150) = 1.952$, $p = .0253$.

ADP

As with ATP, a significant increase in the mesentery perfusate was attained following nerve terminal electrical stimulation [one-way ANOVA $F(14,105) = 3.398$, $p = .002$]. Mesentery perfusion with

.01–1,000 nM clodronate did not modify the spontaneous overflow nor the total outflow induced by electrical stimulation as compared to perfusions in the absence of bisphosphonate (Table 1). These findings are supported by two-way ANOVA for .01–100 nM: $F(14,165) = .2800$, $p = .9954$; $F(14,165) = 1.079$, $p = .3800$; $F(14,165) = .3450$, $p = .9867$ and $F(14,195) = 1.032$, $p = .4234$; $F(14,150) = 1.852$, $p = .0361$. We never observed that clodronate reduced purine overflow.

AMP

Following perivascular electrical nerve stimulation, we consistently observed an increase in AMP outflow [one-way ANOVA $F(14,105) = 2.485$, $p = .0044$]. The purine spontaneous outflow was not modified by perfusion with .01–1,000 nM clodronate as compared to those perfused without clodronate (Table 1). Only 100 nM clodronate increases the total overflow elicited by nerve terminal depolarization (Table 1). Values of the two-way ANOVA analysis for .01–1,000 nM clodronate were $F(14,165) = .4059$, $p = .9716$; $F(14,165) = .2444$, $p = .9978$; $F(14,165) = .7514$, $p = .7199$; $F(14,195) = .5997$, $p = .8634$; $F(14,150) = .9479$, $p = .5095$; $F(14,150) = 1.670$, $p = .0674$. These results support the lack of clodronate-induced AMP overflow inhibition.

ADO

As with the previous results, perivascular electrical nerve stimulation of mesentery preparations elicited a significant increase

in ADO outflow [Figure 1C, one-way ANOVA $F(14,105) = 5.958$, $p < .0001$]. This ADO increase was delayed as compared to the ATP increase (compare time courses in Figures 1A–C), supporting the notion that the ADO overflow may derive mainly from tissue ectoATPase metabolism. The nucleoside outflow elicited by nerve terminal depolarization did not change following perfusion with .01–1 nM clodronate as compared to those in the absence of clodronate (Table 1). Two-way ANOVA revealed that time courses of ADO outflow for .01–1 nM clodronate values were $F(14,165) = .8247$, $p = .6415$; $F(14,165) = .3784$, $p = .9794$; and $F(14,165) = .2334$, $p = .9983$, indicating no change as compared with tissues perfused in the absence of clodronate. Notwithstanding, only 10 nM clodronate increased ADO outflow (Table 1); the two-way ANOVA value was $F(14,195) = 2.693$, $p = .0012$. Further increasing clodronate concentration to 100–1,000 nM did not alter the ADO outflow (Table 1).

NA

Perivascular electrical nerve stimulation elicited a clear increase in the NA outflow (Figure 1B), the value of one-way ANOVA was $F(14,105) = 9.065$, $p < .0001$. Moreover, the bioamine outflow was not altered by .01–1,000 nM clodronate as compared to parallel experiments perfused in the absence of bisphosphonate, the results of the two-way ANOVA analysis for .1–1,000 nM clodronate were $F(14,165) = .2095$, $p = .9991$; $F(14,165) = .3042$, $p = .9929$; $F(14,165) = .6355$, $p = .8325$; $F(14,195) = .3588$, $p = .9842$; $F(14,150) = .9465$, $p = .5110$, or $F(14,150) = .4829$, $p = .939$. These values are detailed in Table 1 and support the lack of clodronate-induced inhibition of NA overflow.

Perfusion with 10 nM clodronate was lengthened to 180 min

Due to the lack of significant clodronate effects on the total overflow of ATP/metabolites or NA elicited by electrical depolarization, we argued that perhaps it was necessary to extend the duration of the perfusion with 10 nM clodronate. In the case of the spontaneous ATP outflow, the value was $1.26 \pm .81$ pmol ($n = 4$) vs. 2.99 ± 1.04 pmol ($n = 4$), $p = .239$ by the unpaired t-test, following prolonged 10 nM clodronate treatment. The total ATP outflow was increased after nerve depolarization, from 106.73 ± 25.16 pmol ($n = 4$) to 458.82 ± 137.65 pmol ($n = 4$), $p = .0455$ by the unpaired t-test by prolonged 10 nM clodronate perfusion. Neither the spontaneous overflow nor the total ADP, AMP, or NA outflow elicited by transmural perivascular electrical nerve stimulation was modified by clodronate. The spontaneous ADP overflow was from 4.23 ± 2.36 pmol ($n = 4$) to 9.62 ± 1.18 pmol ($n = 4$), $p = .0873$ by the unpaired t-test, while after nerve stimulation, the total ADP values were 300.90 ± 59.27 pmol ($n = 4$) vs. 438.30 ± 125.70 pmol ($n = 4$), $p = .3513$ by the unpaired t-test. Spontaneous AMP overflow values were 2.64 ± 1.34 pmol ($n = 4$) vs. $2.89 \pm .82$ pmol ($n = 4$), $p = .8783$ by the unpaired t-test. After nerve depolarization, the total AMP control was 363.08 ± 60.52 pmol ($n = 4$), and following 10 nM clodronate treatment, the total AMP was 227.20 ± 33.44 pmol ($n = 4$), $p = .0970$ by the unpaired t-test. In contrast, spontaneous ADO outcome increased 3.9-fold from 1.81 ± 1.19 pmol ($n = 4$) to 7.19 ± 1.63 pmol ($n = 4$), $p = .0378$ by the unpaired t-test; however, the total ADO

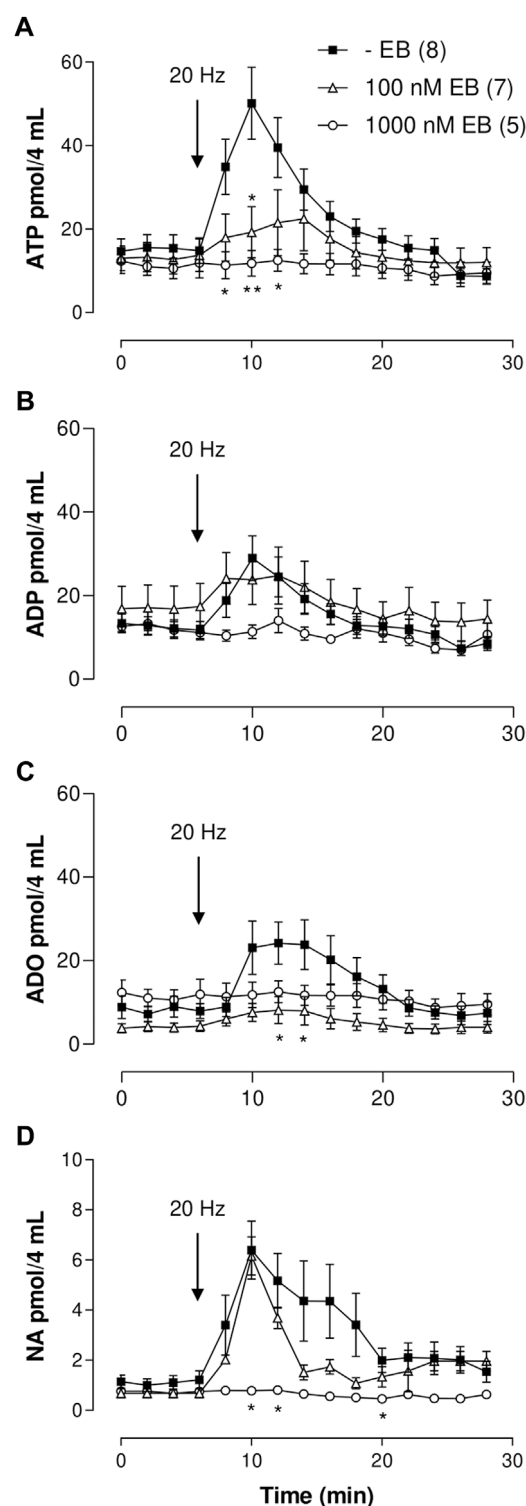


FIGURE 2

ATP/metabolites or NA mesenteric perfusate outflow time course elicited by sympathetic nerve terminal depolarization in preparations perfused with either 100 or 1,000 nM Evans blue (EB). (A–D) show the overflow of ATP, ADP, ADO, and NA, respectively. Tissues were perfused prior to, during, and after nerve depolarization in the absence (closed squares, $n = 8$); or presence of either 100 nM EB (open triangles, $n = 7$) or 1,000 nM EB (open circles, $n = 5$). Arrows indicate perivascular electrical nerve endings stimulation (20 Hz, 1 ms trains of 60 V during 1 min). *, $p < .05$, **, $p < .01$, unpaired t-test as compared to values in the absence of EB.

overflow following electrical nerve depolarization halved from 333.75 ± 40.01 pmol ($n = 4$) to 157.16 ± 48.62 pmol ($n = 4$), $p = .0310$ by the unpaired t-test. Moreover, neither the spontaneous NA outflow ($.72 \pm .28$ pmol, $n = 4$) nor the total evoked by electrical stimulation (32.90 ± 5.35 pmol, $n = 4$) was modified by 10 nM clodronate ($.30 \pm .21$ pmol, $n = 4$), versus 28.66 ± 3.85 pmol, $n = 4$), for the spontaneous outflow and total elicited by electrical stimulation, respectively (unpaired t-test analysis was $p = .5439$ and $p = .2822$, respectively).

Evans blue reduced the concentration-dependent overflow of ATP/metabolites and NA time course studies

ATP outflow

In sharp contrast with clodronate, mesentery perfusions with 100 or 1,000 nM EB reduced the nucleotide overflow as compared to matched experiments perfused without EB (Figure 2A; Supplementary Table S1). Perivascular electrical nerve endings stimulation of mesenteries elicited an increase in the outflow of ATP [one-way ANOVA $F(14,195) = 6.101$, $p < .0001$], which was not modified in mesenteries perfused with 1–10 nM EB as compared to those perfused without this dye; two-way ANOVA values for 1 nM or 10 nM EB were $F(14,240) = .8986$, $p = .5610$ and $F(14,255) = 1.220$, $p = .2605$, respectively. However, perfusion with 100 or 1,000 nM EB significantly reduced and flattened the ATP overflow elicited by electrical stimulation up to the point that no significance was observed in the nucleotide overflow (one-way ANOVA values for 100 or 1,000 nM EB were $F(14,90) = .5647$, $p = .8836$ and $F(14,60) = .1741$, $p = .9996$), respectively, evidencing that 100–1,000 nM EB diminished ATP overflow.

ADP outflow

Perivascular nerve terminal stimulation of mesenteries evidenced an increased overflow of this purine [one-way ANOVA $F(14,195) = 3.526$, $p < .0001$]. As with ATP, perfusion with 1–100 nM EB did not modify the ADP outflow as compared to results with perfusions in EB absence (Supplementary Table S1); two-way ANOVA values for 1, 10, or 100 nM EB were $F(14,240) = .7333$, $p = .7398$; $F(14,255) = .3130$, $p = .9921$; and $F(14,285) = .3952$, $p = .9757$, respectively. Increasing EB to 1,000 nM showed a flattened overflow curve, and an indication of ADP outflow was annulled [one-way ANOVA $F(14,60) = .9582$, $p = .5052$, Figure 2B; Supplementary Table S1].

AMP outflow

Likewise, nerve endings depolarization augmented AMP outflow [one-way ANOVA $F(14,195) = 3.585$, $p < .0001$]. An amount of 1 nM EB increased the spontaneous and electrically evoked AMP overflow compared to perfusions without EB; the value of two-way ANOVA was $F(14,240) = 3.26$, $p < .0001$ (Supplementary Table S1). However, mesenteries perfused with 10, 100 or 1,000 nM EB did not show a significant change in the electrically evoked overflow as compared with tissues perfused without EB, as shown in Supplementary Table S1; two-way ANOVA values for 10, 100, or 1,000 nM EB were $F(14,255) = .8945$, $p = .5654$; $F(14,285) = .5306$, $p = .9143$; and $F(14,255) = .4424$, $p = .9594$, respectively.

ADO outflow

Electrical nerve terminal depolarization evidenced a delayed but significant ADO overflow increase with respect to ATP overflow [Figure 2C, Kruskal–Wallis test $\chi^2(14) = 28.73$, $p = .0114$]. Mesenteries perfused with 1–1,000 nM EB did not show a significant change in the spontaneous overflow as compared with tissues perfused without EB (Supplementary Table S1); 1 nM EB increased the electrically evoked overflow as compared with tissues perfused without EB, and 10–1,000 nM EB reduced the ADO overflow (Supplementary Table S1). Two-way ANOVA values for 1 and 10 nM EB were $F(14,240) = .5968$, $p = .8665$ and $F(14,255) = .4903$, $p = .9373$, respectively. Increasing EB to 100 or 1,000 nM flattened the ADO increase; one-way ANOVA values for 100 and 1,000 nM EB were $F(14,90) = .7925$, $p = .7396$ and $F(14,60) = .1741$, $p = .9996$, respectively, showing ADO overflow annulment.

NA outflow

Electrical stimulation of the perivascular nerve terminals induced a significant increase in NA overflow [Kruskal–Wallis test $\chi^2(14) = 38.04$, $p < .0005$]. Perfusion with 1–100 nM EB did not alter the NA output. Two-way ANOVA values for 1–100 nM clodronate as compared to perfusions without EB were $F(14,240) = .2259$, $p = .9986$; $F(14,255) = .6492$, $p = .8221$; and $F(14,285) = .3740$, $p = .9812$, respectively. Increasing EB to 1,000 nM flattened the time course curve [one-way ANOVA $F(14,60) = 1.703$, $p = .0789$, Figure 2D], indicating complete blockade of the bioamine overflow. Supplementary Table S1 summarizes the results of the spontaneous and electrically evoked overflow.

As a further analysis, when the outflow of ATP or NA elicited by electrical nerve stimulation was compared between the two independent series of protocols performed without clodronate or EB, no statistical differences were observed in the nucleotide outflow in the two-way ANOVA $F(14,280) = .8135$, $p = .6543$ nor the catecholamine outflow [two-way ANOVA $F(14,280) = 1.511$, $p = .1061$ for NA], indicating only minor experimental variability between assays occurred.

DIDS was less potent than EB to reduce ATP/metabolite perfusate overflow

ATP outflow

Electrical stimulation of the nerve terminals induced a significant ATP overflow [one-way ANOVA $F(14,135) = 3.890$, $p < .0001$]. DIDS proved less potent than EB to reduce the output of electrically evoked ATP output since while 1 μ M DIDS perfusion did not modify its output as compared to tissues perfused without DIDS [two-way ANOVA $F(14,210) = .8138$, $p = .6537$]; however, 10 μ M DIDS flattened the nucleotide output [one-way ANOVA $F(14,75) = .1907$, $p = .9993$], highlighting a substantial reduction in the nucleotide outflow induced by electrical stimulation (Supplementary Table S1).

ADP outflow

Likewise, electrical stimulation of the nerve terminals induced a significant ADP overflow [one-way ANOVA $F(14,135) = 2.128$, $p = .0138$]. Perfusion with 1–10 μ M DIDS did not modify the ADP overflow compared with tissues perfused without DIDS [two-way ANOVA $F(14,210) = .2722$, $p = .9961$; $F(14,210) = 1.665$, $p = .0649$], as shown in Supplementary Table S1.

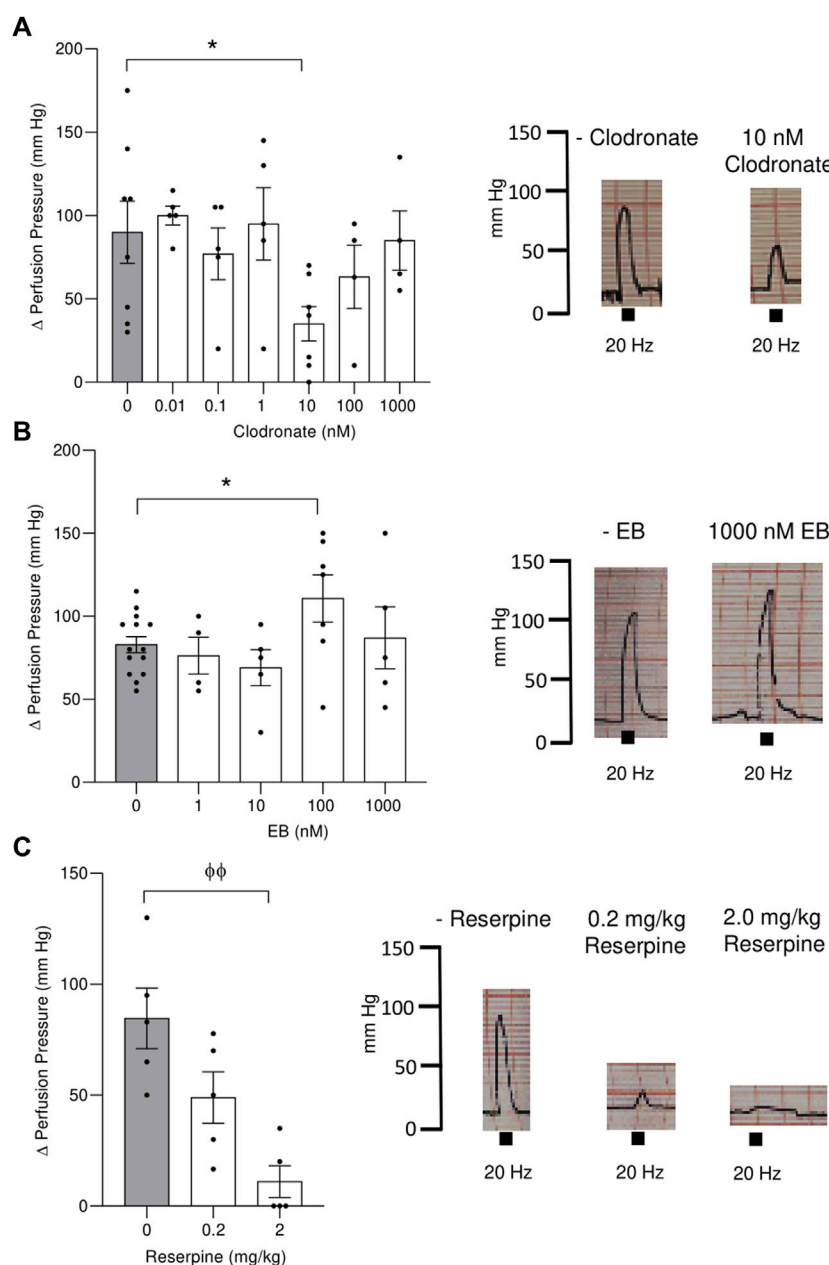


FIGURE 3

Electrical stimulation evoked an increase in the perfusion pressure of the mesenteric bed vascular territory and its modification following perfusion with either clodronate or Evans blue (EB) or mesenteries from rats pretreated with reserpine for 48 h. Left panel show columns depicting the increase in the mesentery perfusion pressure elicited by electrical nerve endings stimulation (20 Hz train of electrical pulses) expressed as the Δ increase in the mesentery perfusion pressure in preparations perfused with several clodronate concentrations, upper (A); Evans blue middle (B) or rats pretreated with .2 or 2 mg/kg reserpine for 48 h lower (C). Right panel shows representative polygraphic traces of the changes in perfusion pressure recordings, with the respective calibrations (mm Hg). Columns represent mean values; bars the S.E.M. Gray columns represent matched tissues without drugs. Each closed circle in the columns represents experimental values obtained from separate rats. * $p < .05$, unpaired t-test; $\Phi \Phi$, $p < .01$, Mann–Whitney test, as compared to tissues without drugs.

AMP outflow

Nerve endings electrical stimulation induced a significant AMP increase in its overflow [one-way ANOVA $F(14,135) = 2.682$, $p = .0017$]. However, neither perfusion with 1 nor 10 μM DIDS modified the AMP overflow induced by electrical nerve depolarization as compared to the tissues perfused without DIDS. Two-way ANOVA analysis values for 1 or 10 μM DIDS were [$F(14,210) = .7700$, $p =$

.7009 and $F(14,210) = .1262$, $p = .9999$], respectively, as shown in [Supplementary Table S1](#).

ADO outflow

Electrical stimulation of the nerve endings increased ADO overflow [Kruskal–Wallis test $\chi^2(14) = 27.36$, $p = .0173$]. An amount of 1 μM DIDS shifts the outflow curve up, and the two-

TABLE 2 Clodronate concentration-dependent effects on the spontaneous and mechanically evoked ATP/metabolites from primary cultures of endothelial cells from the rat mesentery.

Spontaneous extracellular purines expressed as % of purines in the absence of clodronate; X ± S.E.M.								
Clodronate nM								
	0 (n=28)	0.01 (n=6)	0.1 (n=8)	1 (n=8)	10 (n=12)	100 (n=10)	300 (n=10)	1000 (n=15)
ATP	93.37 ± 8.58	45.12 ± 9.19*	75.08 ± 13.23	91.87 ± 11.87	91.48 ± 10.51	94.33 ± 18.13	100.40 ± 31.21	165.00 ± 28.67**
ADP	100.00 ± 7.94	108.28 ± 27.25	144.34 ± 18.11*	129.84 ± 18.73	113.38 ± 9.80	206.05 ± 57.53 **	106.52 ± 33.60	205.56 ± 26.59****
AMP	100.00 ± 7.12	87.94 ± 13.93	92.16 ± 7.8	80.32 ± 17.14	94.08 ± 6.78	109.26 ± 25.81	114.59 ± 22.31	88.04 ± 12.76
ADO	100.00 ± 7.04	150.27 ± 16.53*	144.21 ± 17.78*	156.55 ± 23.79**	137.14 ± 7.78**	190.54 ± 44.14**	155.31 ± 31.79	131.57 ± 15.95
Mechanical stimulation-induced ATP/metabolite release, expressed as % purines in the absence of clodronate; X ± S.E.M.								
Clodronate nM								
	0 (n=28)	0.01 (n=6)	0.1 (n=8)	1 (n=8)	10 (n=9)	100 (n=9)	300 (n=12)	1000 (n=14)
ATP	98.46 ± 9.24	106.30 ± 22.02	107.58 ± 27.67	126.86 ± 21.00	136.44 ± 10.29*	127.61 ± 26.59	94.41 ± 13.09	98.12 ± 11.47
ADP	100.00 ± 7.36	87.87 ± 9.81	85.14 ± 8.00	103.52 ± 11.83	141.89 ± 9.87**	144.27 ± 27.14*	101.62 ± 10.43	108.11 ± 6.54
AMP	100.00 ± 6.82	90.59 ± 16.08	80.18 ± 5.10	111.31 ± 12.95	154.92 ± 15.67***	117.73 ± 22.12	91.07 ± 12.69	83.37 ± 8.83
ADO	100.00 ± 3.74	73.42 ± 8.28**	116.32 ± 33.94	102.94 ± 15.07	122.46 ± 9.71 Φ	177.33 ± 34.09***	105.00 ± 8.98	134.60 ± 10.94ΦΦ

Numbers in parenthesis indicate the cell wells analyzed from five separate rats. *, $p < .05$; **, $p < .01$; ***, $p < .001$; ****, $p < .0001$; unpaired t-test as compared to cells without clodronate. Φ, $p < .05$; ΦΦ, $p < .01$, Mann-Whitney test as compared to cells incubated without clodronate addition.

way ANOVA value is $[F(14,210) = 1.980, p = .0203]$. However, 10 μM DIDS did not change the nucleoside outflow $[F(14,210) = .6313, p = .8380]$ as compared to the perfusions performed in the absence of DIDS. [Supplementary Table S1](#) summarizes the results of the spontaneous and electrically evoked overflow.

NA outflow

Electrical stimulation of the nerve endings induced a significant NA overflow [Kruskal–Wallis test $\chi^2(14) = 37.68, p = .0006$]. However, 1 or 10 μM DIDS showed a tendency toward a reduction in the catecholamine outflow, and the values did not reach statistical significance as compared with tissues perfused without DIDS ([Supplementary Table S1](#)). The two-way ANOVA values for 1 μM or 10 μM DIDS were $F(14,210) = .3745, p = .9728$; $F(14,210) = .6468, p = .8235$, respectively.

Effect of reserpine treatment on spontaneous and electrically evoked ATP/metabolites and NA outflow

Pretreatment with .2 mg/kg reserpine did not modify the spontaneous nor the electrically evoked overflow of ATP/metabolites or NA as compared to the vehicle ([Supplementary Table S2](#)). However, 2 mg/kg reserpine which did not modify the spontaneous outflow of ATP/metabolites or NA decreased by 60% the total perfusate ATP overflow or 84% the NA outflow elicited by nerve endings depolarization ([Supplementary Table S2](#)), without modifying ADP, AMP, or ADO. The 2 mg/kg reserpine pretreatment flattened the increase in ATP overflow induced by nerve terminal stimulation [one-way ANOVA $F(14,60) = 1.681, p = .0840$]; likewise, it obliterated the NA overflow as evidenced by the one-way ANOVA $[F(14,60) = 1.082, p = .3920]$, supporting the ATP and NA overflow annulment.

Changes in perfusion pressure elicited by electrical depolarization of perivascular mesenteric nerve endings in tissues perfused with clodronate, EB, and DIDS or the perfused mesenteries of reserpine-treated rats

Electrical nerve depolarization was associated with an abrupt increase in the mesentery perfusion pressure. This increase ensued within the first seconds of electrical depolarization, returning to baseline few seconds after stopping the 1-min nerve terminal stimulation. Representative vasomotor tracings are shown in [Figure 3](#).

- 1) Clodronate: The increase in perfusion pressure elicited by nerve terminal electrical stimulation in preparation perfused without this drug was 90.00 ± 18.61 mm Hg ($n = 8$), a value that was reduced to 35.00 ± 10.35 mm Hg ($n = 7, p = .028$, unpaired t-test) in preparations perfused with 10 nM clodronate ([Figure 3A](#)). Neither smaller nor larger clodronate perfusate concentrations modified the increase in perfusion pressure evoked by nerve terminal stimulation ([Figure 3A](#)). Parallel experiments which prolonged the 10 nM clodronate perfusion for 180 min did not modify the increase in perfusion pressure elicited by nerve depolarization ($83.33 \pm 21.2, n = 4$) vs. perfusions without clodronate (95.00 ± 5.40 mm Hg, $n = 4$), unpaired t-test $p = .6135$.
- 2) EB: Although perfusions with 1,000 nM markedly reduced the overflow of ATP/metabolites and NA, it did not modify the increase in perfusion pressure elicited by nerve terminal stimulation. However, perfusion with 100 nM showed a minor but significant increase in the vasomotor response ([Figure 3B](#)) compared to tissues perfused without this dye. We infer that despite the reduced outflow of ATP/metabolites and NA, the co-transmitter concentration that reaches the neuroeffector junction causes the full vasomotor response.

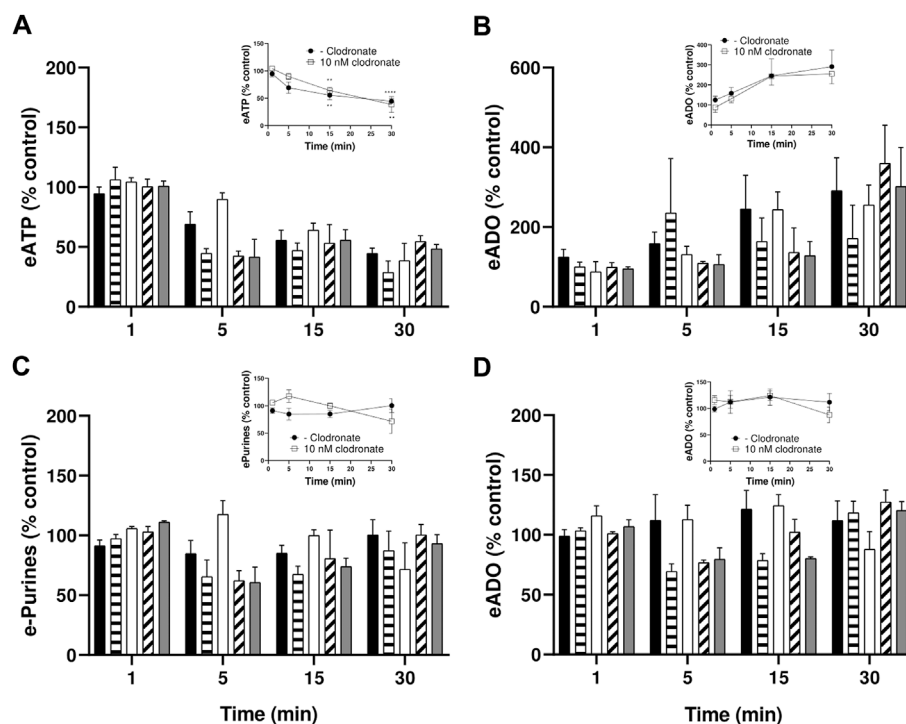


FIGURE 4

Endothelial cells metabolize eATP but not eADO, lack of inhibition by 1–1,000 nM clodronate. To ascertain whether clodronate interferes with ectoATPase cell metabolism, cultures of mesentery cells were incubated with eATP, and its metabolism was followed over 30 min. (A) Decay of 50 mM eATP added to the extracellular media. (B) shows the corresponding eADO accumulation in cells treated with eATP, while (C) depicts the total etheno purines from the same cells depicted, evidencing that the extracellular etheno purines were maintained over time. In contrast, (D) shows the application of 25 nM eADO to a separate, but parallel, set of endothelial mesentery cells. Closed columns represent controls in the absence of clodronate ($n = 8$), dashed columns depict 1 nM clodronate ($n = 4$), open columns 10 nM clodronate ($n = 6$), oblique dashed columns 100 nM clodronate ($n = 4$), and gray columns 1,000 nM clodronate ($n = 4$). Bars in the columns show the S.E.M. No significant difference was observed when comparing controls versus the clodronate effect at each incubation time. Insets of these Figures show the effect of 10 nM clodronate (open squares, $n = 6$) compared to a parallel set of cells incubated in the absence of the bisphosphonate (closed circles, controls, $n = 8$). Symbols indicate the mean S.E.M. **, $p < .01$, and ****, $p < .0001$ unpaired t-test compared to the corresponding 1-min controls.

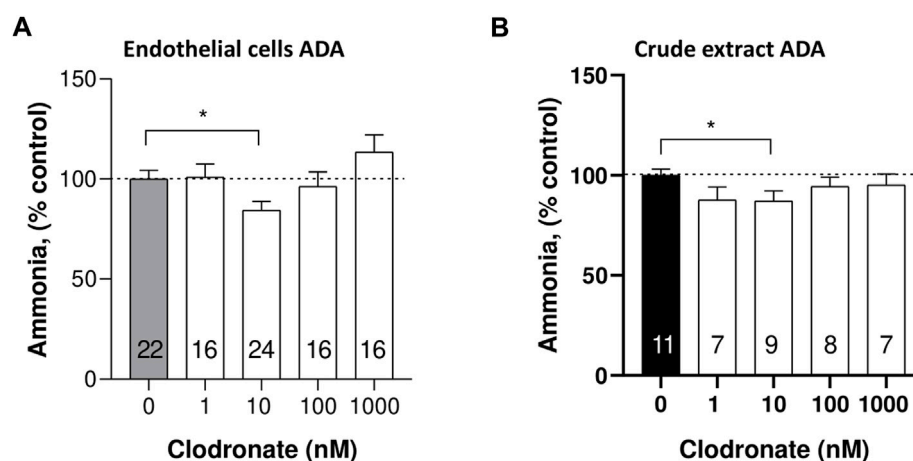


FIGURE 5

Comparison of ADA activity inhibition by 10 nM clodronate in mesentery endothelial cells or a crude calf intestinal enzyme preparation. To assess whether clodronate interferes with ADA activity, mesentery cells (A) or a crude calf intestine extract (B) was used to examine putative enzyme inhibition elicited by clodronate. ADA activity was determined via a colorimetric titration of the ammonia generated as a byproduct of enzyme reaction. Columns indicate the mean values and bars the S.E.M. of multiple enzyme assays performed in the absence or presence of 1–1,000 nM clodronate. Numbers inside the columns refer to the separate mesentery cell wells assays or crude enzyme activity assay. Results are expressed as % ammonia formed compared to parallel controls without clodronate. *, $p < .05$ unpaired t-test, compared with control, without clodronate.

- 3) DIDS: Perfusions with 1 or 10 μM did not change significantly the motor responses elicited by electrical nerve endings stimulation. The Δ perfusion pressure (mm Hg) in tissues without the drug was 110.6 ± 11.98 ($n = 10$), while the increase in perfusion pressure averaged 100.29 ± 28.28 ($n = 6$) in tissues perfused with 1 μM DIDS or 73.26 ± 18.97 ($n = 6$) following 10 μM DIDS.
- 4) Reserpine: A gradual dose-dependent decrease in the increase of the perfusion pressure elicited by nerve endings depolarization was observed in mesenteries of animals pre-treated with either .2 or 2 mg/kg reserpine, compared to the respective vehicles (Figure 3C). While the .2 mg/kg reserpine pretreatment only attenuated the elicited increase in perfusion pressure, a 10-fold higher dose caused a consistent and profound reduction of the vasomotor responses from 84.60 ± 13.70 ($n = 5$) to 11.00 ± 7.14 mm Hg ($n = 5$), Mann-Whitney test, $p = .0079$.

Extracellular ATP/metabolites in primary cultures of endothelial cells incubated with .01–1,000 nM clodronate

To assess and confirm whether clodronate increases ADO in isolated endothelial cells, primary cultures of the rat mesentery endothelium were prepared to assess clodronate effects in non-neuronal mesentery components. Endothelial cell incubation with .01–100 nM clodronate increased the spontaneous extracellular ADO, while 300 or 1,000 nM clodronate did not. Moreover, only 1,000 nM clodronate augmented the spontaneously released extracellular ATP and ADP. These results are summarized in Table 2. Moreover, following mechanical stimulation, a procedure used to elicit purine release to the cell media release, 10 nM clodronate significantly increased extracellular ATP, ADP, AMP, and ADO (Table 2). Increasing the bisphosphonate to 100 nM or 1,000 nM only modified extracellular ADO (Table 2). As with the perfusion studies, 10 nM clodronate or higher augmented extracellular ADO. No clear clodronate concentration dependence was observed for ADO, except that perhaps clodronate elicited a bell-shaped curve.

eATP hydrolysis time course protocols confirm lack of clodronate-induced inhibition of ATP metabolism and of eADO metabolism

To examine whether clodronate (1–1,000 nM) modified endothelial cell extracellular ATP metabolism, eATP time course studies were followed, and eATP hydrolysis and metabolic by-products were determined in parallel. Parallel protocols examined whether eADO is enzymatically degraded or transported intracellularly by isolated endothelial cell cultures.

eATP is a substrate of ectoATPases; therefore, it is metabolized extracellularly by cell ectoenzymes with a profile similar to ATP. eATP decayed with a half-life of approximately 15 min, generating as by-products eADP, eAMP, and eADO (Figure 4A); moreover, 1–1,000 nM clodronate did not interfere with the eATP metabolic degradation nor affected its half-life (Figure 4A). The inset of Figure 4A depicts the effect of 10 nM clodronate and its statistical analysis compared to the first minute of eATP addition. During the 30-min protocol, eADO increased 2–3 fold (Figure 4B, inset shows 10 nM clodronate effect). Total extracellular etheno purines, (the addition of eATP plus eADP, eAMP, and eADO) did not change over time

(Figure 4C), suggesting no significant intracellular etheno derivative transport.

In contrast to eATP, eADO is not an ADA substrate nor apparently transported intracellularly, explaining that extracellular eADO remained intact during the 30-min incubation protocol (Figure 4D). In addition, 1–1,000 nM clodronate did not significantly modify eADO in the extracellular media (Figure 4D).

Endothelial cell ADA activity

To directly evaluate whether clodronate interferes with the enzymatic ADO conversion to inosine, a subset of 24-well plate endothelial cells was incubated with exogenous ADO as a substrate in the absence or presence of varying clodronate concentrations. Clodronate failed to modify ADA activity, except for 10 nM, a concentration that slightly, but consistently reduced enzyme activity ($15.5 \pm 4.3\%$, unpaired t-test, $p = .0128$, Figure 5A).

As positive controls, the cells were incubated with either 10 or 30 μM quercetin, which elicited a 5 ± 6.0 (unpaired t-test, $p = .6833$) and $41.8 \pm 2.4\%$ (unpaired t-test, $p < .0001$) reduction of ADA activity, respectively.

Crude extract ADA activity

To ascertain more directly the effect of clodronate on the enzyme activity, we used a commercial crude enzyme extract and examined whether clodronate reduced the activity of ADA. In this enzyme preparation, 10 nM clodronate caused a modest but significant $12.8 \pm 4.8\%$ ($p = .049$, Figure 5B) inhibition of the enzyme activity a result consistent with the observation of clodronate-induced inhibition of cell enzyme protocols (Figure 5A). Enzyme activity was examined using .3 mM exogenous ADO and 6.25 mU/mL ADA. Two positive controls were used in this protocol, one was .7 mM adenine, which inhibited $28.6 \pm 6.2\%$ ($n = 9$, $p = .001$); likewise, 1 mM quercetin inhibited ADA activity $13.9 \pm 4.7\%$ ($n = 9$, $p = .0283$), results compatible with the 10 nM clodronate-induced inhibition.

Discussion

Perfusion of the rat mesentery with clodronate did not reduce the outflow of ATP/metabolites and NA induced by electrical stimulation of perivascular sympathetic nerve endings from the rat mesentery vascular bed, an unexpected result considering clodronate's alleged VNUT inhibitor profile. On the contrary, a modest increase in purine overflow was shown. Notwithstanding, in matched parallel control studies, mesentery bed perfusion with EB or DIDS evidenced a significant reduction in the ATP outflow, raising doubts that clodronate is a VNUT inhibitor in sympathetic nerve endings. EB is a symmetric azo dye, currently recognized as the most potent VNUT inhibitor available (Moriyama et al., 2017); DIDS also inhibited VNUT but with markedly less potency than EB, agreeing with current findings. We are aware that neither EB nor DIDS are VNUT selective since a variety of non-VNUT effects have been consistently described, including VGLUT inhibition documented by Hartinger and Jahn, (1993), Roseth et al. (1995) and revised by Eriksen et al. (2016). In addition, EB has long been used for clinical purposes such as the estimation of human blood volume, vascular permeability,

and lymph node detection as recently reviewed by Yao et al. (2018), revealing multiple targets. The precise mechanism of how EB or DIDS elicit VNUT inhibition remains unclear. Sawada et al. (2008) observed that both EB and DIDS inhibited concentration-dependently the ATP uptake activity and also reported that the transporter is chloride-dependent. In addition, Zalk and Shoshan-Barmatz, (2006) reported that the ATP uptake observed in isolated brain synaptic vesicles was DIDS-sensitive; hence, whether this effect is due to VNUT activity remains to be determined.

We are aware that the use of a perfused vascular bed to detect the outflow of ATP and co-transmitters from the perivascular sympathetic nerve endings has limitations. Notwithstanding, this preparation was used extensively by autonomic investigators to examine the neurochemistry of the adrenergic and purinergic synapses and to quantify the outflow of these transmitters (Donoso et al., 2006; Donoso et al., 2018b). The present results do not allow the characterization of clodronate, EB, or DIDS as VNUT inhibitors, even though both EB and DIDS reduced concentration-dependently the outflow of ATP and NA from the mesentery bed, a profile expected of VNUT inhibitors. Only clodronate increased ADO outflow, suggesting a separate target, which we deem could be related to ADA inhibition. EB concentrations used in the current experiments are within reported VGLUT IC₅₀ values (Roseth et al., 1995; Thompson et al., 2005) or the purified VNUT SLC17A9 assay in the synthetic *in vitro* liposomes of the Sawada et al. (2008) study. Higher DIDS concentrations were required to inhibit VNUT in the liposome reconstituted bioassay or VGLUT (Hartertinger and Jahn 1993), a finding substantiated by current data. Moreover, in cultured mesentery-derived endothelial cells, Donoso et al. (2018a) reported that EB decreased the spontaneous extracellular cell medium ATP. This latter effect is apparently due to inhibition of vesicular ATP release mediated by an EB-sensitive mechanism, an action not observed in similar protocols using clodronate.

To account for the consistent clodronate-evoked ADO accumulation observed in the perfusion studies, we examined whether clodronate interferes directly or indirectly, with purine metabolism or transport both in the mesenteric bed or isolated endothelial cells and the crude calf intestine ADA preparation. ADO accumulation must result from either lack of its metabolism or cellular transport by these cells. Following this reasoning, we next examined whether clodronate induced inhibition of ADA activity in endothelial cells, a finding that may explain the increase in ADO following clodronate mesentery perfusion or in isolated endothelial cells. A modest yet reproducible and significant reduction in ADA activity was consistently observed only with 10 nM clodronate. The mechanism of inhibition was not further addressed, except we confirmed that plant polyphenols such as quercetin inhibited ADA activity at micromolar concentrations, in agreement with Melzig, (1996). Interestingly, only 10 nM clodronate, but not other concentrations, consistently inhibited the enzyme closely mimicking the observation in mesentery endothelial cells. Although we do not understand why the inhibition is exclusively observed with 10 nM clodronate, three separate observations support our contention that 10 nM clodronate elicits this effect: 1. in the perfused mesentery preparation, 10 nM clodronate elicited an ADO increase paralleled by a decreased neuroeffector motor response induced by transmural nerve depolarization, 2. this concentration increases extracellular ADO in endothelial cells upon mechanical stimulation, and 3. 10 nM clodronate inhibits ADA activity in a commercial crude

enzyme preparation. Moreover, in the Moriyama assay, 15 nM clodronate is the half median concentration required to inhibit VNUT activity.

In addition, current findings are consistent with previous findings that both quercetin and adenine inhibit ADA activity, apparently by a competitive mechanism (Melzing, 1996; and Alunni et al., 2008), which supports and highlights the clodronate findings. We are certain that clodronate does not interfere with ATP or eATP metabolism, except it modestly inhibits ADO degradation to inosine. The present results do not allow discarding that clodronate could eventually reduce ADO transport, but eADO results do not support this proposal. It should be emphasized that eADO is neither an ADA substrate nor an ADA inhibitor (Jamal et al., 1988); therefore, since eADO remains constant in the enzyme incubation protocol, we infer that eADO is not an ADO transporter substrate (Figure 4D). To directly support this hypothesis, we are open to further investigations. Notwithstanding, we infer that the bisphosphonate-induced ADO increase in the perfused mesentery is of functional relevance since 10 nM clodronate elicited a reduction in the increase in perfusion pressure evoked by electrical stimulation of sympathetic nerve endings. Curiously, larger clodronate concentrations did not follow this inhibitory pattern. Increasing clodronate to 100 nM not only increased ADO but also ADP and AMP, which may hinder the ADO-induced vasodilatation since ADP may constrict the mesentery vessels, causing a physiological antagonism of the ADO-evoked vasorelaxation. In this vascular bed, endogenous ADO has a strong vasodilator efficacy. Neither EB nor DIDS modified the increase in perfusion pressure elicited by electrical nerve endings depolarization, even though both chemicals reduced electrically evoked co-transmitter outflow. ATP is known to elicit a mixed dual contractile and relaxant effects related to P2X and P2Y receptor activation (Ralevic and Burnstock, 1998). Furthermore, endothelial cell P2Y receptor activation induces nitric oxide production (Donoso et al., 2018b), which may add to the ADO-induced vasodilatation. Since we are fully aware that the 40-min clodronate mesentery perfusion might not be enough to elicit a significant VNUT inhibition, the duration of the 10 nM clodronate perfusion was extended for 180 min. Notwithstanding, we did not observe a reduction in nucleotide overflow nor a further decrement in the increase of the perfusion pressure induced by electrical stimulation. On the contrary, the ADO outcome was reduced, suggesting that the increase in ADO overflow, elicited by nerve terminal depolarization, occurred within the 40-min clodronate mesentery perfusion. In contrast to 10 nM clodronate, EB which decreased the outflow of ATP and NA did not reduce the increase in mesentery perfusion pressure elicited by perivascular electrical nerve stimulation. This observation allows us to deduce that the response is clodronate-specific and that the vasomotor effect elicited by perivascular nerve stimulation must be caused by a small fraction of the released transmitters since it was not observed after 1,000 nM EB. We are conscious that transmitter outflow is the result of compounded and balanced effects between transmitter release, degradation, uptake, and transmitter diffusion through the smooth muscle and endothelium to finally reach the vascular lumen, where ATP/metabolites and NA were determined. Although EB markedly reduced the release of sympathetic co-transmitters, the fraction that reaches the neuroeffector junction

must suffice to cause a full vasomotor response elicited by perivascular nerve terminal stimulation.

To further investigate why the EB-induced reduction in the outflow of ATP/metabolites and NA was not paralleled by a reduction of the mesentery perfusion pressure, additional experiments were conducted in reserpinized rats. Reserpine elicited a concentration-dependent reduction in the increase in perfusion pressure associated with a marked decrease in ATP and NA outflow to levels comparable to those elicited by 1,000 nM EB. We are aware that the effect of reserpine was examined after 2 days of treatment (Huidobro-Toro, 1985), where adaptive mechanisms may occur such as a reduction in other sympathetic co-transmitters involved in the vasomotor response. Reserpine is used as a NA vesicular transporter marker (VMAT), in analogy to EB, a VNUT marker. This concept may help identify whether the same synaptic vesicle stores both ATP and NA or whether separate vesicle pools store independently sympathetic co-transmitters. This is an ongoing debate for several decades without a firm final demonstration. An exciting immunohistochemical study using selective color labeled antibodies for the vesicular NA transporter and VNUT recently concluded that in the rat tail artery, the NA and ATP transporter storage vesicles may be distinct and associated each with voltage-dependent calcium channel subtypes (Mojard Kalkhoran et al., 2019). These findings highlight the notion of apparently separate storage vesicles for each co-transmitter. Notwithstanding, ATP is required for NA storage (Estevez-Herrera et al., 2016), a result at variance with this structural contention, an issue that needs further research. Moreover, extracellular ATP regulates chromaffin vesicular content (Larsson et al., 2019), a finding that augments the complexity of co-transmitter storage, a fact that is not disputed for a single transmitter. Independent of the synaptic vesicle's dynamics in sympathetic nerve endings, selective vesicular transporter inhibitors such as reserpine for VMAT, or EB for VNUT, are valuable neuroscience tools for further clarifying multi-transmitter vesicular storage in sympathetic nerve terminals. An exciting venue that supports the physiological role of VNUT in purinergic transmission derives from transgenic VNUT knockout mice (VNUT^{-/-}). Transgenic mice are phenotypically apparently normal (Sakamoto et al., 2014), but several experimental lines using these animals demonstrate that VNUT-mediated vesicular ATP release is key for the storage and release of ATP. Moreover, gene silencing results in purinergic transmission impairment (Moriyama et al., 2017; Miras-Portugal et al., 2019; Tatsushima et al., 2021). The relevance of VNUT in chronic neuropathic pain, glaucoma, and other sympathetic nerve system-related diseases poses the opportunity of targeting drugs to ATP transporters, as a novel therapeutic goal of future medical applications.

Is it plausible that the mechanism of the analgesic effect of clodronate in chronic pain may be related to the observed ADO accumulation? This observation may be of clinical relevance since clodronate has a chronic pain analgesic profile (Kato et al., 2017) and ADO elicits analgesia (Sollevi, 1997; Jung et al., 2022). As to whether

our finding of ADO accumulation, likely due to nanomolar clodronate-induced reduction in the ADA activity, is somehow involved in the analgesic effect of clodronate remains to be better examined.

Clodronate is a pyrophosphate analog of biomedical relevance used for over 60 years in the treatment of bone-related diseases. Clodronate, due to its two phosphates, likely chelates calcium, with a low permeability coefficient. In Caco-2 cells, the clodronate transport value was $.25 \times 10^{-7}$ cm/s (Raiman et al., 2001), a non-favorable physicochemical variable to freely cross cell membranes, favoring our view that clodronate likely interacts with an extracellular site of action, unless it is mobilized intracellularly by phosphate transporters. In chondrocytes, a cell model used to study articular cartilage degeneration and improve arthritis management, clodronate is claimed to enter cells by pinocytosis, rather than simply diffusing or using a transporter (Rosa et al., 2014). An observation we have not fully resolved is the lack of consistent concentration-dependence of the clodronate effects. This issue likely indicates that clodronate has complex pharmacokinetics and may target several mechanisms simultaneously, indicative of compounded pharmacodynamics as well.

In summary, present findings highlight a minor, though consistent ADA inhibition which might account for the observed ADO accumulation as well as the reduction in the vasomotor effect elicited by nerve endings stimulation observed with 10 nM clodronate. The role of clodronate as a nanomolar ADA inhibitor may play a relevant role *in vivo* as an ADO modulator. Moreover, the present results do not allow characterizing clodronate as a VNUT inhibitor. Drugs which target vesicular transporters are valuable neuroscience tools to solve the dynamics of transmitter storage and recycling plus the compounded complexities of multiple co-transmitter storage mechanisms and release in sympathetic co-transmission, an exciting venue for future research.

Data availability statement

The original contributions presented in the study are included in the article/Supplementary Material; further inquiries can be directed to the corresponding author.

Ethics statement

The animal study was reviewed and approved by 121/2017-USACH.

Author contributions

MVD performed the cell culture experiments in collaboration with FH. MVD, FH, and RB performed the mesentery perfusion experiments. MVD and JH-T designed the research and drafted the

manuscript. MVD performed all statistical analyses. JH-T was the recipient of grant awards and allocated research funds.

Funding

This research was partially funded by FONDECYT grant 117-0842, CEDENNA program project, grant AFB 180001 and DICYT 2021- 022143GHT.

Conflict of interest

The authors declare that the research was conducted in the absence of any commercial or financial relationships that could be construed as a potential conflict of interest.

References

- Alunni, S., Orrù, M., and Ottavi, L. (2008). A study on the inhibition of adenosine deaminase. *J. Enzyme Inhib. Med. Chem.* 23, 182–189. doi:10.1080/14756360701475233
- Burnstock, G. (2018). Purine and purinergic receptors. *Brain Neurosci. Adv.* 2 (2), 2398212818817494. doi:10.1177/2398212818817494
- Buvinic, S., Bravo-Zender, M., Boyer, J. L., Huidobro-Toro, J. P., and Gonzalez, A. (2007). Nucleotide P2Y1 receptor regulates EGF receptor mitogenic signaling and expression in epithelial cells. *J. Cell Sci.* 120, 4289–4301. doi:10.1242/jcs.03490
- Donoso, M. V., Aedo, F., and Huidobro-Toro, J. P. (2006). The role of adenosine A2A and A3 receptors on the differential modulation of norepinephrine and neuropeptide Y release from peripheral sympathetic nerve terminals. *J. Neurochem.* 96, 1680–1695. doi:10.1111/j.1471-4159.2006.03671.x
- Donoso, M. V., Hernández, F., Villalón, T., Acuña-Castillo, C., and Huidobro-Toro, J. P. (2018a). Pharmacological dissection of the cellular mechanisms associated to the spontaneous and the mechanically stimulated ATP release by mesentery endothelial cells: Roles of thrombin and TRPV. *Purinergic Signal* 14, 121–139. doi:10.1007/s11302-017-9599-7
- Donoso, M. V., Mascayano, M. J., Poblete, I. M., and Huidobro-Toro, J. P. (2018b). Increased ATP and ADO overflow from sympathetic nerve endings and mesentery endothelial cells plus reduced nitric oxide are involved in diabetic neurovascular dysfunction. *Front. Pharmacol.* 9, 546. doi:10.3389/fphar.2018.00546
- El-Said, K. S., Atta, A., Mobasher, M. A., Germoush, M. O., Mohamed, T. M., and Salem, M. M. (2022). Quercetin mitigates rheumatoid arthritis by inhibiting adenosine deaminase in rats. *Mol. Med.* 28, 24. doi:10.1186/s10020-022-00432-5
- Eriksen, J., Chang, R., McGregor, M., Silm, K., Suzuki, T., and Edwards, R. H. (2016). Protons regulate vesicular glutamate transporters through an allosteric mechanism. *Neuron* 90 (4), 768–780. doi:10.1016/j.neuron.2016.03.026
- Estevez-Herrera, J., Domínguez, N., Pardo, M., Gonzalez-Santana, A., Westhead, E. W., Borges, R., et al. (2016). ATP: The crucial component of secretory vesicles. *Proc. Natl. Acad. Sci. (USA)* 113, E4098–E4106. doi:10.1073/pnas.1600690113
- Giusti, G., and Galanti, B. (1984). “Colorimetric method,” in *Methods of enzymatic analysis*. Editor H. U. Bergmeyer 1st edition (Weinheim, Germany: Verlag Chemie), 315–333.
- Hartertinger, J., and Jahn, R. (1993). An anion binding site that regulates the glutamate transporter of synaptic vesicles. *J. Biol. Chem.* 268, 23122–23127. doi:10.1016/s0021-9258(19)49435-0
- Hillarp, N. A. (1960). Effect of reserpine on the nucleotide and catecholamine content of the denervated adrenal medulla of the rat. *Nature* 187, 1032. doi:10.1038/1871032a0
- Huidobro-Toro, J. P. (1985). Reserpine-induced potentiation of the inhibitory action of neuropeptide Y on the rat vas deferens neurotransmission. *Neurosci. Lett.* 59, 247–252. doi:10.1016/0304-3940(85)90139-9
- Jackson, E. K., Gillespie, D. G., Cheng, D., Mi, Z., and Menshikova, E. V. (2020). Characterization of the N⁶-etheno-bridge method to assess extracellular metabolism of adenine nucleotides: Detection of a possible role for purine nucleoside phosphorylase in adenosine metabolism. *Purinergic Signal* 16 (2), 187–211. doi:10.1007/s11302-020-09699-x
- Jamal, Z., Afkham-Ebrahimi, A., and Saggerson, E. D. (1988). A novel assay for 5'-nucleotidase using 1,N⁶-etheno-AMP as substrate, and comments on the properties of the reaction product, ethenoadenosine. *Biochem. J.* 250 (2), 369–373. doi:10.1042/bj2500369
- Jung, S. M., Peyton, L., Essa, H., and Choi, D. S. (2022). Adenosine receptors: Emerging non-opioids targets for pain medications. *Neurobiol. Pain* 11, 100087. doi:10.1016/j.nypai.2022.100087
- Kato, Y., Hiasa, M., Ichikawa, R., Hasuzawa, N., Kadowaki, A., Iwatsuki, K., et al. (2017). Identification of a vesicular ATP release inhibitor for the treatment of neuropathic and inflammatory pain. *Proc. Natl. Acad. Sci. U. S. A.* pii 114, E6297–E6305. doi:10.1073/pnas.1704847114
- Larsson, A., Majdi, S., Borges, R., and Ewing, A. (2019). Vesicular transmitter content in chromaffin cells can be regulated via extracellular ATP. *ACS Chem. Neurosci.* 10, 4735–4740. doi:10.1021/acscchemneuro.9b00494
- Mandela, P., Chandley, M., Xu, Y. Y., Zhu, M. Y., and Ordway, G. A. (2010). Reserpine-induced reduction in norepinephrine transporter function requires catecholamine storage vesicles. *Neurochem. Int.* 56, 760–767. doi:10.1016/j.neuint.2010.02.011
- McGregor, D. D. (1965). The effects of sympathetic nerve stimulation on vasoconstrictor responses in perfused mesenteric blood vessels of the rat. *J. Physiol. Lond.* 177, 21–30. doi:10.1113/jphysiol.1965.sp007572
- Melzig, M. F. (1996). Inhibition of adenosine deaminase activity of aortic endothelial cells by selected flavonoids. *Planta Med.* 62 (1), 20–21. doi:10.1055/s-2006-957788
- Miras-Portugal, M. T., Menéndez-Méndez, A., Gómez-Villafuertes, R., Ortega, F., Delicado, E. G., Pérez-Sen, R., et al. (2019). Physiopathological role of the vesicular nucleotide transporter (VNUT) in the central nervous system: Relevance of the vesicular nucleotide release as a potential therapeutic target. *Front. Cell Neurosci.* 13, 224. doi:10.3389/fncel.2019.00224
- Mojard Kalkhoran, S., Chow, S. H. J., Walia, J. S., Gershome, C., Saraev, N., Kim, B., et al. (2019). VNUT and VMAT2 segregate within sympathetic varicosities and localize near preferred Cav2 isoforms in the rat tail artery. *Am. J. Physiol. Heart Circ. Physiol.* 316, H89–H105. doi:10.1152/ajpheart.00560.2018
- Moriyama, Y., Hiasa, M., Sakamoto, S., Omote, H., and Nomura, M. (2017). Vesicular nucleotide transporter (VNUT): Appearance of an actress on the stage of purinergic signaling. *Purinergic Signal* 13, 387–404. doi:10.1007/s11302-017-9568-1
- Moriyama, Y., and Nomura, M. (2018). Clodronate: A vesicular ATP release blocker. *Trends Pharmacol. Sci.* 39, 13–23. doi:10.1016/j.tips.2017.10.007
- Navarrete, L. C., Barrera, N. P., and Huidobro-Toro, J. P. (2014). Vas deferens neuro-effector junction: From kymographic tracings to structural biology principles. *Auton. Neurosci.* 185, 8–28. doi:10.1016/j.autneu.2014.05.010
- Raiman, J., Niemi, R., Vepsäläinen, J., Yritys, K., Järvinen, T., and Mönkkönen, J. (2001). Effects of calcium and lipophilicity on transport of clodronate and its esters through Caco-2 cells. *Int. J. Pharm.* 213, 135–142. doi:10.1016/s0378-5173(00)00655-4
- Ralevic, V., and Burnstock, G. (1998). Receptors for purines and pyrimidines. *Pharmacol. Rev.* 50, 413–492.
- Rosa, R. G., Collavino, K., Lakhani, A., Delve, E., Weber, J. F., Rosenthal, A. K., et al. (2014). Clodronate exerts an anabolic effect on articular chondrocytes mediated through the purinergic receptor pathway. *Osteoarthritis Cartil.* 22, 1327–1336. doi:10.1016/j.joca.2014.07.009
- Roseth, S., Fykse, E. M., and Fonnum, F. (1995). Uptake of L-glutamate into rat brain synaptic vesicles: Effect of inhibitors that bind specifically to the glutamate transporter. *J. Neurochem.* 65, 96–103. doi:10.1046/j.1471-4159.1995.65010096.x

Publisher's note

All claims expressed in this article are solely those of the authors and do not necessarily represent those of their affiliated organizations, or those of the publisher, the editors, and the reviewers. Any product that may be evaluated in this article, or claim that may be made by its manufacturer, is not guaranteed or endorsed by the publisher.

Supplementary material

The Supplementary Material for this article can be found online at: <https://www.frontiersin.org/articles/10.3389/fphar.2022.1031223/full#supplementary-material>

- Sakamoto, S., Miyaji, T., Hiasa, M., Ichikawa, R., Uematsu, A., Iwatsuki, K., et al. (2014). Impairment of vesicular ATP release affects glucose metabolism and increases insulin sensitivity. *Sci. Rep.* 4, 6689. doi:10.1038/srep06689
- Sawada, K., Echigo, N., Juge, N., Miyaji, T., Otsuka, M., Omote, H., et al. (2008). Identification of a vesicular nucleotide transporter. *Proc. Natl. Acad. Sci. U. S. A.* 105, 5683–5686. doi:10.1073/pnas.0800141105
- Sollevi, A. (1997). Adenosine for pain control. *Acta Anaesthesiol. Scand. Suppl.* 110, 135–136. doi:10.1111/j.1399-6576.1997.tb05532.x
- Tatsushima, K., Hasuzawa, N., Wang, L., Hiasa, M., Sakamoto, S., Ashida, K., et al. (2021). Vesicular ATP release from hepatocytes plays a role in the progression of nonalcoholic steatohepatitis. *Biochimica Biophysica Acta Mol. Basis Dis.* 1867, 166013. doi:10.1016/j.bbadis.2020.166013
- Thompson, C. M., Davis, E., Carrigan, C. N., Cox, H. D., Bridges, R. J., and Gerdes, J. M. (2005). Inhibitor of the glutamate vesicular transporter (VGLUT). *Curr. Med. Chem.* 12, 2041–2056. doi:10.2174/0929867054637635
- Yao, L., Xue, X., Yu, P., Ni, Y., and Chen, F. (2018). Evans blue dye: A revisit of its applications in biomedicine. *Contrast Media Mol. Imaging* 2018, 7628037. doi:10.1155/2018/7628037
- Zalk, R., and Shoshan-Barmatz, V. (2006). Characterization of DIDS-sensitive ATP accumulation in brain synaptic vesicles. *FEBS Lett.* 580, 5894–5898. doi:10.1016/j.febslet.2006.09.055



OPEN ACCESS

EDITED BY

Kenneth A. Jacobson,
National Institutes of Health (NIH),
United States

REVIEWED BY

Philippe Séguéla,
McGill University, Canada
Samuel J. Fountain,
University of East Anglia, United Kingdom
Anna Junker,
University of Münster, Germany

*CORRESPONDENCE

Mark T. Young,
✉ youngmt@cardiff.ac.uk

SPECIALTY SECTION

This article was submitted to Experimental Pharmacology and Drug Discovery, a section of the journal Frontiers in Pharmacology

RECEIVED 17 November 2022

ACCEPTED 31 January 2023

PUBLISHED 09 February 2023

CITATION

Pasqualetto G, Zuanon M, Brancale A and Young MT (2023), Identification of the molecular determinants of antagonist potency in the allosteric binding pocket of human P2X4.

Front. Pharmacol. 14:1101023.

doi: 10.3389/fphar.2023.1101023

COPYRIGHT

© 2023 Pasqualetto, Zuanon, Brancale and Young. This is an open-access article distributed under the terms of the [Creative Commons Attribution License \(CC BY\)](https://creativecommons.org/licenses/by/4.0/). The use, distribution or reproduction in other forums is permitted, provided the original author(s) and the copyright owner(s) are credited and that the original publication in this journal is cited, in accordance with accepted academic practice. No use, distribution or reproduction is permitted which does not comply with these terms.

Identification of the molecular determinants of antagonist potency in the allosteric binding pocket of human P2X4

Gaia Pasqualetto¹, Marika Zuanon¹, Andrea Brancale^{2,3} and Mark T. Young^{1*}

¹School of Biosciences, Cardiff University, Cardiff, United Kingdom, ²School of Pharmacy and Pharmaceutical Sciences, Cardiff University, Cardiff, United Kingdom, ³Department of Organic Chemistry, Vysoká škola chemicko-technologická v Praze, Prague, Czechia

P2X receptors are a family of ATP-gated cation channels comprising seven subtypes in mammals, which play key roles in nerve transmission, pain sensation and inflammation. The P2X4 receptor in particular has attracted significant interest from pharmaceutical companies due to its physiological roles in neuropathic pain and modulation of vascular tone. A number of potent small-molecule P2X4 receptor antagonists have been developed, including the allosteric P2X4 receptor antagonist BX430, which is approximately 30-fold more potent at human P2X4 compared with the rat isoform. A single amino-acid difference between human and rat P2X4 (I312T), located in an allosteric pocket, has previously been identified as critical for BX430 sensitivity, implying that BX430 binds in this pocket. Using a combination of mutagenesis, functional assay in mammalian cells and *in silico* docking we confirmed these findings. Induced-fit docking, permitting the sidechains of the amino-acids of P2X4 to move, showed that BX430 could access a deeper portion of the allosteric pocket, and that the sidechain of Lys-298 was important for shaping the cavity. We then performed blind docking of 12 additional P2X4 antagonists into the receptor extracellular domain, finding that many of these compounds favored the same pocket as BX430 from their calculated binding energies. Induced-fit docking of these compounds in the allosteric pocket enabled us to show that antagonists with high potency ($IC_{50} \leq 100$ nM) bind deep in the allosteric pocket, disrupting a network of interacting amino acids including Asp-85, Ala-87, Asp-88, and Ala-297, which are vital for transmitting the conformational change following ATP binding to channel gating. Our work confirms the importance of Ile-312 for BX430 sensitivity, demonstrates that the allosteric pocket where BX430 binds is a plausible binding pocket for a series of P2X4 antagonists, and suggests a mode of action for these allosteric antagonists involving disruption of a key structural motif required for the conformational change induced in P2X4 when ATP binds.

KEYWORDS

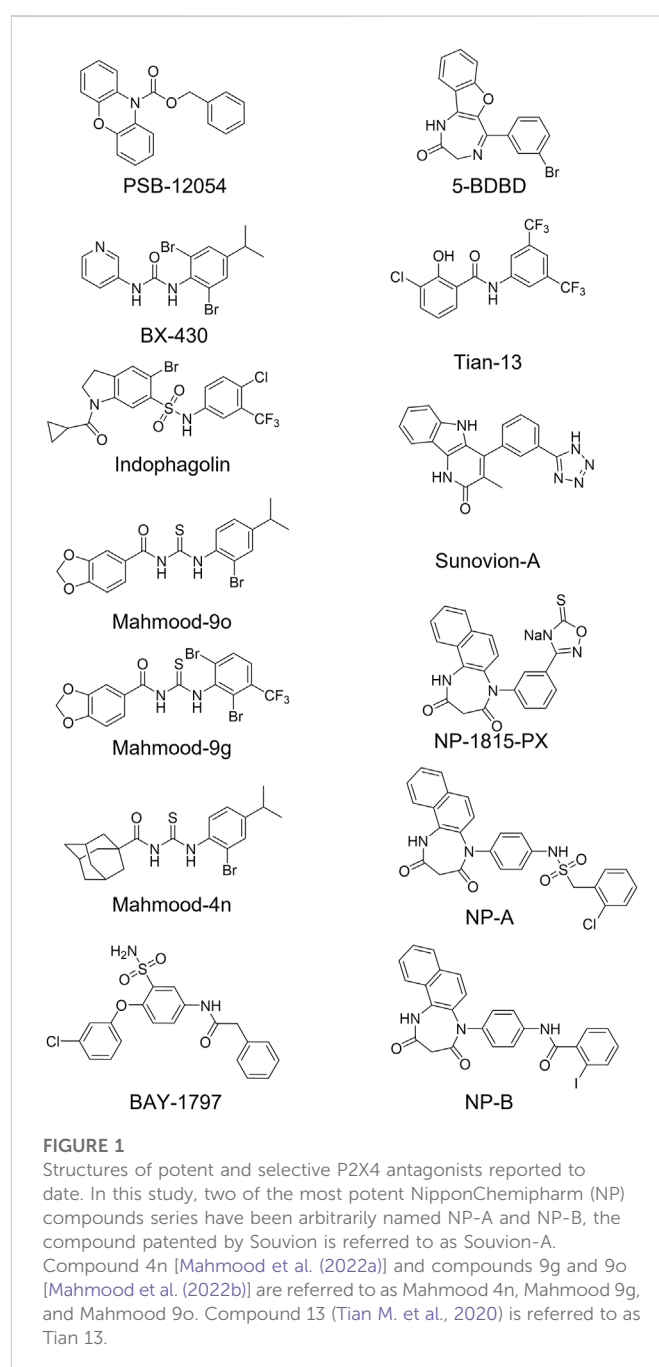
P2X4, BX430, allosteric antagonist, structure-function, calcium channel

1 Introduction

P2X receptors are eukaryotic ligand-gated cation channels activated by extracellular ATP. There are seven receptor subtypes in mammals, which combine into homo- or heterotrimers, with differing tissue expression and pharmacological properties (North, 2016). P2X receptors play numerous important physiological roles in mammals, including nerve transmission, pain sensation, inflammation, and higher neural functions, and as such are important drug targets (North and Jarvis, 2013). There is a significant body of evidence from animal models that implicates the P2X4 receptor in neuropathic pain (Tsuda et al., 2003; Matsumura et al., 2016). Furthermore, evidence from both animal models and human mutation studies link P2X4 to the regulation of vascular tone and blood pressure (Yamamoto et al., 2006; Stokes et al., 2011). Due to their roles in human disease, there has been significant interest in developing potent P2X4 receptor modulators and the determination of the crystal structures of a series of P2X receptors including zebrafish P2X4 (Hattori and Gouaux, 2012) and giant panda P2X7 (Karasawa and Kawate, 2016) has proven pivotal in the understanding of ligand binding and receptor activation. In particular, the recent and surprising discovery that a series of P2X7 antagonists (previously thought to be competitive) bound to a site distinct from the ATP binding site delineated an important allosteric binding pocket in P2X receptors.

Among the P2X4 antagonists, some are reportedly allosteric, including 5-BDBD, which displays an IC_{50} of 0.5 μ M at human P2X4 (Fischer et al., 2004). Other reported antagonists with potencies in the low micromolar range are PSB-12054 and PSB-12062 (Hernandez-Olmos et al., 2012) although these compounds only display partial solubility. In 2013, Sunovion Pharmaceutical Inc. patented a series of compounds (including the compound herein arbitrarily named Sunovion-A, Figure 1) displaying high potencies (IC_{50} < 100 nM) (Newcom and Spear, 2013). Two years later, Ase et al. (2015) reported the characterization of BX430, which displayed interesting and unexpected P2X4 species-selective potencies. Despite a lower amino acid sequence similarity between human P2X4 and zebrafish P2X4 receptor, BX430 potency was similar at human P2X4 and zebrafish P2X4 (IC_{50} values of 0.5 and 1.89 μ M, respectively) compared to its very weak activity against the rat and mouse orthologues (IC_{50} values both >10 μ M).

Other potent antagonists have been reported since, including a series developed by Nippon Chemipharm (NP-1815-PX, NP-A and NP-B) with submicromolar potency (IC_{50} values approx. 0.25 μ M at human, rat and mouse) that displayed an anti-allodynic effect in an *in vivo* rodent model of injury-induced allodynia (Matsumura et al., 2016; Ushioda et al., 2020). In 2019, BAY-1797 was identified as a P2X4 antagonist with a similar potency across human, rat and mouse P2X4 orthologues (IC_{50} of 100 nM at rat and human and 200 nM at mouse) (Werner et al., 2019). Whilst designing P2X1 antagonists, (Tian M. et al., 2020) synthesized a series of compounds (including the compound with structure reported in Figure 1, here referred to as “Tian-13”) with nanomolar potency at P2X4 but with only partial selectivity across the receptor family (P2X1 IC_{50} 58 \pm 21.9 nM; P2X4 IC_{50} 48.8 \pm 11 nM and P2X7 IC_{50} 177 \pm 11 nM). Furthermore, an interesting approach was employed by Carnero Corrales et al.



(2021), who identified, *via* thermal proteome profiling, P2X4 as potential target of indophagolin. Finally, Mahmood et al. (2022a); Mahmood et al. (2022b) recently reported several series of compounds (including series 4 and 9) with submicromolar potency at human P2X4. Figure 1; Table 1 summarize the chemical structures and reported IC_{50} values of the P2X4 antagonists considered in this study.

We initially hypothesized that BX430 might bind to the equivalent site on P2X4 to that recently identified in P2X7. We constructed a molecular model of human P2X4 based on the zebrafish P2X4 crystal structure (Hattori and Gouaux, 2012), used molecular docking to ascertain that BX430 was able to bind to the allosteric pocket, and identified a single amino-acid difference between human and rat P2X4 in the allosteric pocket

TABLE 1 Reported potencies for known P2X4 antagonists. n.r, Not reported. ^aFischer et al. (2004); ^bAbdelrahman et al. (2017); ^cSophocleous et al. (2020); ^dCoddou et al. (2019); ^eWerner et al. (2019); ^fAse et al. (2015); ^gCarnero Corrales et al. (2021); ^hMahmood et al. (2022a); ⁱMahmood et al. (2022b); ^jHernandez-Olmost et al. (2012); ^kMatsumura et al. (2016), and ^lUshioda et al. (2020) ^mNewcom and Spear (2013); ⁿTian et al. (2020).

Compound	hP2X4 IC ₅₀	rP2X4 IC ₅₀	mP2X4 IC ₅₀
5-BDBD	0.5 μM ^a ; 0.348 μM ^b ; 5.24 μM ^c	3.47 μM ^b ; 0.75 μM ^d	2.04 μM ^b
BAY-1797	0.1 μM ^e	0.1 μM ^e	0.2 μM ^e
BX-430	0.54 μM ^f ; 1.94 μM ^c	>10 μM ^f	>10 μM ^f
Indophagolin	0.140 μM ^g	n.a	n.a
Mahmood-4n	0.04 μM ^h	n.r	n.r
Mahmood-9g	0.055 μM ⁱ	n.r	n.r
Mahmood-9o	0.039 μM ⁱ	n.r	n.r
NP-1815-PX	0.26 μM ^{k, l}	n.r	n.r
NP-A	0.064 μM ^{k, l}	n.r	n.r
NP-B	0.43 μM ^{k, l}	n.r	n.r
PSB-12054	0.19 μM ^j	2.1 μM ^j	1.8 μM ^j
Sunovion-A	<0.1 μM ^m	n.r	n.r
Tian-13	0.049 μM ⁿ	n.r	n.r

(I312T) previously reported to be responsible for differential BX430 potency (Ase et al., 2019). Functional assays using calcium influx in stably transfected 1321N1 astrocytoma cells confirmed the difference between BX430 potency at human P2X4 wild type and rat P2X4 wild type, whilst the single amino-acid mutation of either human P2X4 (I312T) or rat P2X4 (T312I) was sufficient to confer the BX430 sensitivity of the other receptor orthologue, demonstrating that BX430 binds at this allosteric site in the receptor. Our results are in very close agreement with those of Ase et al. (2019) who used patch clamp electrophysiology and molecular docking studies, and reinforce their findings using an independent assay. The work of Ase et al. (2019) and our data demonstrate that BX430 binds to the equivalent allosteric site in P2X4 to that accessed by several allosteric P2X7 antagonists.

We next hypothesized that other P2X4 antagonists may bind in the same allosteric pocket as BX430 and employed *in silico* induced-fit docking approaches (where the amino-acid sidechains of the pocket are allowed to move) with a total of 12 compounds, identifying the ligand-protein interactions within the allosteric pocket important for high-potency antagonism. Using this approach, we were able to show that a network of interactions with Arg-82, Asp-85, Ala-87, Asp-88, Trp-164, Ala-297, Glu-307, and Arg-309, deep within the allosteric pocket and critical for efficient P2X4 gating, are likely to be disrupted by antagonist binding. This data will be useful for the design and development of potent P2X4 antagonists in future.

2 Materials and methods

2.1 Plasmid generation

Plasmid encoding rat P2X4 (r4-WT) (Royle et al., 2005) was a kind gift from Ruth Murrell-Lagnado, whilst that encoding human

P2X4 with a C-terminal (His)₁₀ tag has been reported previously (Young et al., 2008). Plasmids containing rat P2X4 T312I (r4-T312I) and human P2X4 I312T mutants (h4-I312T) were generated using the QuikChange Lightning site-directed mutagenesis kit (Agilent) according to manufacturer's instructions. Sequencing of the constructs and of the genomic DNA from stably transfected cells confirmed correct full coding sequences.

2.2 Development and selection of 1321N1 cell lines stably expressing human and rat P2X4 receptors

1321N1 astrocytoma cells were cultured (at 37°C, 5% CO₂) in Dulbecco's modified Eagle's medium (DMEM/F-12 with Glutamax) supplemented with 10% foetal bovine serum (FBS) and 200 unit/mL of penicillin and streptomycin antibiotics (Fisher Scientific). Stably transfected clones were grown in DMEM/F-12 with Glutamax medium supplemented with G-418 (Geneticin[®], Fisher Scientific), 600 μg/mL and 150 μg/mL during selection and maintenance, respectively. FuGene HD Transfection Reagent (Promega) was used according to the manufacturer's protocol for the generation of stable cell line expressing h4-WT, r4-WT, h4-I312T, and r4-T312I. Each cell line was then tested for P2X4 receptor expression by Western blot and for functionality using the Ca²⁺ influx assay.

2.3 Calcium influx measurements

Cells were plated the day before assay into poly-lysine-coated 96-well plates at 40–55,000 cells/mL. To load cells with calcium-sensitive fluorescent dye, culture medium was replaced with modified Ringer's buffer (140 mM NaCl, 10 mM HEPES, 10 mM Glucose, 1 mM MgCl₂,

1 mM CaCl₂, 2.5 mM KCl, 0.5% BSA, pH = 7.4) containing 2.6 μ M FLUO4-AM (Fisher Scientific) and 250 μ M probenecid (Sigma), and cells were incubated for 20–30 min. Prior to assay, buffer was replaced with fresh modified Ringer's buffer containing probenecid but not the dye. BX430 was incubated at increasing concentrations (0.03 μ M–100 μ M) for approximately 30 min prior to eliciting ATP responses. The final DMSO concentration did not exceed 0.1%. A Fluoroskan Ascent FL plate reader (Fisher Scientific) equipped with a solution dispenser and an appropriate filter pair (excitation: 485 nm, emission: 538 nm) was used to record 5-s baseline followed by P2X₄-mediated calcium influx measurements for 20–25 s after ATP stimulation (final concentration ranging between 0.03 and 100 μ M in buffered solution, pH = 7.4). The collected responses were normalized to the first data-point recorded after ATP injection. The amplitude of ATP responses was calculated as $\Delta F/F_0$, where $\Delta F = F_1 - F_0$, subtracting the fluorescent background as suggested by Bootman et al. (2013).

2.4 Homology modelling and ligand docking

In silico simulations were performed on a MAC pro 2.80 GHz Quad-core Intel Xeon running Ubuntu 12.04 LTS. Graphical representations of molecular structures were generated using MOE (Molecular Operating Environment (MOE), 2019.01; Chemical Computing Group ULC, Montreal, Canada). All crystal structure files used were retrieved from the RCSB Protein Data Bank (<http://www.rcsb.org>) as PDB file format and protonated with MOE. The human P2X₄ receptor homology model was generated using MOE 2019.01 using AMBER10:EHT force field and standard parameters for the single template mode. The model was checked visually and via PROCHECK (Laskowski et al., 1993) to exclude gross errors in protein geometry. Blind docking simulations were performed on the extracellular domain using Achilles Blind Docking Server (<https://bio-hpc.ucam.edu/achilles/>) (Sanchez-Linares et al., 2012) and ligand MOL2 files pre-generated using MOE. Docking with Glide involved pre-processing of the receptor structure via the built-in Schrodinger tools Prep Wiz, Epik, Impact and Prime (Schrodinger, New York). Ligands were prepared with LigPrep using the OPLS₂₀₀₅ force field. In simulations where the protein was treated as rigid body, a docking grid was generated with set coordinates corresponding to the mid-point of the cavity and box size of 18 Å³ and docking simulations were run with Glide Extra Precision (XP) protocol using standard parameters. In induced-fit docking simulations, Glide Standard Precision (SP) was applied generating 20 poses in the first stage before sidechain optimization within 5 Å from the ligand using Prime, followed by Glide re-docking into structures within 30.0 kcal/mol of the best structures (top 20) with SP precision.

2.5 Data analysis and statistics

Data processing and data analysis were carried out using Graphpad Prism version 6 for Mac. Figures are presented as Mean \pm SEM. Statistical significance of any difference observed between samples was calculated through one-way ANOVA

followed by Dunnett's multiple comparisons test with a single pooled variance (control, unless otherwise specified) or, when comparing only two sets of data, using an unpaired *t*-test with Welch's correction. When comparing data obtained from multiple independent experiments (N), each dataset was normalized to the mean value obtained for the vehicle control. A non-linear regression (curve fit) with four parameters (constraints to Bottom = 0 and Top = 100 were applied when considering normalized ATP concentration-response curves) was used to determine dose-response correlation and calculate EC₅₀ and IC₅₀ values.

3 Results

3.1 Docking of BX430 and analysis of human and rat P2X₄ sequences in the putative BX430 binding site reveals I312 as a key interacting residue

To perform ligand docking studies, we first generated a molecular model of human P2X₄ based upon the crystal structure of *Danio rerio* (zebrafish) P2X₄ in the closed state [PDB ID; 4DW0 (Hattori and Gouaux, 2012)]. By comparison of our model with the panda P2X₇ crystal structures in complex with allosteric antagonists (Karasawa and Kawate, 2016), we identified the corresponding putative allosteric pocket in human P2X₄ (Figure 2A). When compared to panda P2X₇ and the rat P2X₇ cryo-EM structure in the closed state [no ligand bound, PDB ID; 6U9V (McCarthy et al., 2019)], the pocket in zebrafish P2X₄ (4DW0) and in our model (Figure 2B) presents a narrower tunnel. In addition, in both the zebrafish structure and in our model, residues such as Lys-298 formed a "bottleneck" in the cavity.

Our initial molecular docking simulations with BX430 (using a rigid protein structure model) showed that the dibromo-(methylethyl)phenyl moiety was stabilized by hydrophobic interactions including with residue Ile-312, whilst the urea moiety lay in a polar region potentially making H-bond interactions with adjacent residues (Figure 2B). Based on the position of Lys-298 in the crystal structures of panda P2X₇ with the antagonists bound, it was reasonable to consider that Lys-298 could be highly flexible, especially when in presence of a ligand binding in proximity. Therefore, we performed induced-fit docking, with initial docking of the ligand with pocket residues as reference (20 ligand poses), followed by minimization of the residues 5 Å around the ligand, re-docking of the ligand in the induced-fit pocket and scoring of the poses. The induced fit protocol resulted in a substantially different conformation of Lys-298 (Figure 2C) with a wider opening of the bottleneck. The obtained BX430 conformation was similar to that reported by Ase et al. (2019) with BX430 buried deeper and the urea moiety establishing interactions with Asp-88 (backbone, Figure 2B). This may indicate an important role of the Lys-298 sidechain in the shaping of the allosteric pocket.

We then took advantage of the reported differential potency of BX430 at human and rat P2X₄ [IC₅₀ values of 0.54 μ M and >10 μ M, respectively (Ase et al., 2015)] and aligned the amino-acid sequences of human and rat P2X₄ in the region of the putative BX430 binding site to look for any major residue difference. Strikingly, there was only

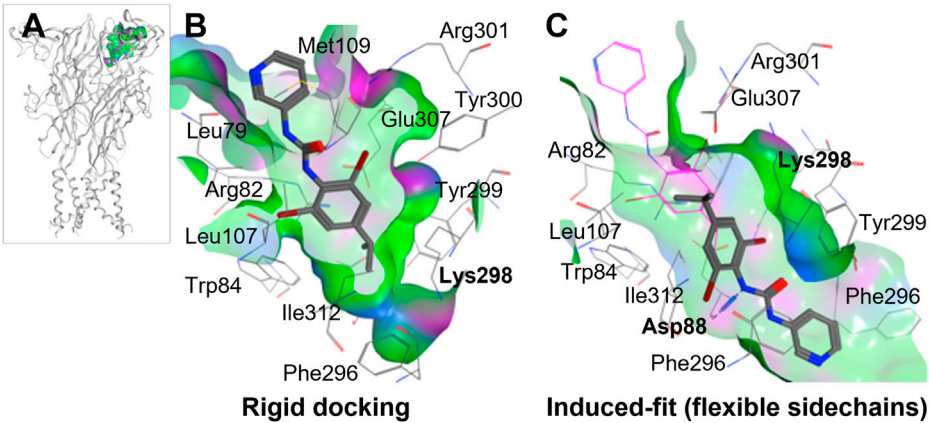


FIGURE 2
Molecular docking of BX430 into the allosteric pocket of human P2X4. **(A)**. Molecular model of human P2X4 showing the position of the pocket in the extracellular domain. **(B–C)**. Alternate binding poses of BX430 modelled into the allosteric pocket of human P2X4 using rigid **(B)** or induced-fit **(C)** docking.

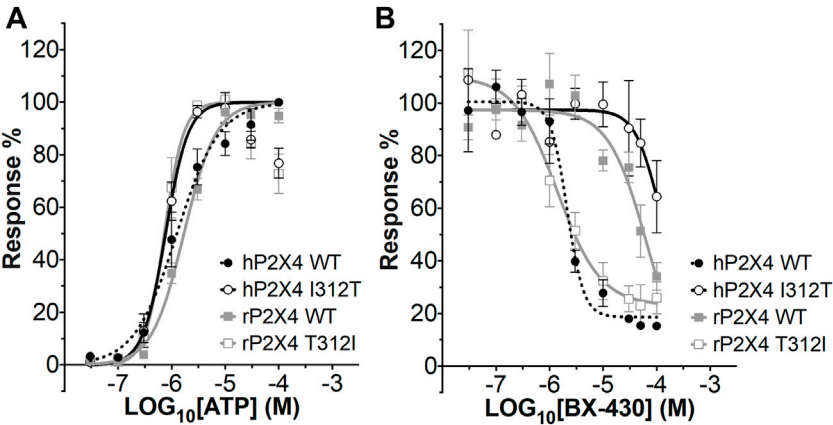


FIGURE 3
ATP concentration-response and BX430 concentration-inhibition curves for human and rat P2X4 (wild type and mutant) receptors. **(A)**. Mean ATP concentration-response curves of rat P2X4 wild type (rP2X4 WT, grey full squares), rat P2X4 T312I mutant (rP2X4 T312I, grey empty squares), human P2X4 wild type (hP2X4 WT, black full circles), human P2X4 I312T (hP2X4 WT, black empty circles). Responses represent fluorescence increase following ATP addition and were normalized to the maximum response mean value recorded among the concentrations tested. Data merged from 3 or more independent experiments (4–6 technical repeats per experiment). Error bars are SEM. EC₅₀ and Hill coefficient values are reported in Table 2. **(B)**. Mean BX430 inhibition curves of rat P2X4 wild type (rP2X4 WT, grey full squares), rat P2X4 T312I mutant (rP2X4 T312I, grey empty squares), human P2X4 wild type (hP2X4 WT, black full circles), human P2X4 I312T (hP2X4 WT, black empty circles). Responses represent fluorescence increase elicited by 1 μM ATP addition after incubation with increasing concentrations of BX430. Data points were normalized to the response obtained with vehicle-only (0.1% DMSO) and are presented as mean ± SEM. Data merged from 2 (for hP2X4 WT) or more independent experiments (3–5 technical repeats per experiment). IC₅₀ and Hill coefficient values are reported in Table 3.

TABLE 2 ATP EC₅₀, pEC₅₀, and Hill Coefficient values for wild type (WT) and mutant rat and human P2X4 receptors. SEM, standard error of the mean. *indicates a statistically significant difference between rat P2X4 WT and human P2X4 I312T (*p* ≤ 0.05).

Cell line	ATP EC ₅₀ (μM)	ATP pEC ₅₀ (± SEM)	Hill coefficient
Human P2X4 WT	1.26	5.901 (± 0.0577)	1.098
Rat P2X4 WT	1.70	5.770 (± 0.0507)*	1.441
Human P2X4 I312T	0.77	6.112 (± 0.028)*	2.057
Rat P2X4 T312I	0.73	6.136 (± 0.0645)	2.475

TABLE 3 BX430 IC₅₀ values for wild type and mutant rat and human P2X4 receptors. SEM, standard error of the mean. *indicates values significantly different to human P2X4 wild type (WT) ($p \leq 0.05$).

Cell line	BX-430 IC ₅₀ (μM)	BX-430 pIC ₅₀ (± SEM)	Hill coefficient
Human P2X4 WT	2.12	5.673 (± 0.0696)	1.098
Rat P2X4 WT	66.1	4.180 (± 0.6884)*	1.441
Human P2X4 I312T	102.4	3.990 (± 2.641)*	2.057
Rat P2X4 T312I	1.4	5.858 (± 0.1575)	2.475

one significant difference at position 312, which is an isoleucine in human P2X4 and a threonine in rat P2X4. Since our docking studies indicated that this amino-acid residue might be involved in BX430 binding, we made the reciprocal mutations, human P2X4 I312T and rat P2X4 T312I, to assess their effect on BX430 potency.

3.2 Exchange of residues at position Ile-312 is sufficient to mediate the differential potency of BX430 at human and rat P2X4 in a calcium-influx assay

We first measured ATP-induced calcium uptake using Fluo-4 in 1321N1 astrocytoma cells stably expressing either wild type human P2X4 (h4-WT), wild type rat P2X4 (r4-WT), human P2X4 I312T (h4-I312T) or rat P2X4 T312I (r4-T312I) receptors (Figure 3A; Table 2). We observed ATP EC₅₀ values for h4WT and r4WT of 1.26 ± 0.16 and 1.70 ± 0.30 μM, respectively, consistent with previous studies (Soto et al., 1996; Garcia-Guzman et al., 1997). We also found that the mutations h4-I312T and r4-T312I did not significantly affect ATP peak calcium responses and their EC₅₀ was 0.77 ± 0.52 and 0.73 ± 0.61 μM (Table 2), implying that the mutations did not affect the ability of the P2X4 receptors to respond to ATP.

We next assessed the potency of BX430 in our wild type and mutant cell lines by generating concentration-inhibition curves using EC₅₀ concentrations of ATP and estimating the BX-430 IC₅₀ at each receptor (Figure 3B; Table 3). We observed IC₅₀ values for h4-WT and r4-WT of 2.12 ± 0.60 and 66.1 ± 20 μM (ambiguous fit due to low potency), respectively, consistent with previously published values (Ase et al., 2015). Strikingly, the single point mutation of I312T in human P2X4 was responsible alone for >48-fold decrease in BX-430 potency to a similar value to that of rat P2X4 (IC₅₀ 102.4 μM). Conversely, the mutation of T312I in rat P2X4 conferred a BX430 potency similar to that of human P2X4 (IC₅₀ 1.4 μM, approx. 47-fold increase), suggesting that the residue at position 312 is sufficient to mediate the differential potency of BX430 at human and rat P2X4 and confirming the results obtained by Ase et al. (2019) obtained *via* patch clamp electrophysiology.

3.3 Docking of known allosteric antagonists in the allosteric pocket

We initially explored the hypothesis that some of the recently reported antagonists may bind to the same allosteric pocket, by

performing a blind docking simulation. A total of 12 antagonists with low micromolar to nanomolar potencies were docked, including antagonists with biological data demonstrating their binding to the allosteric pocket [BX-430 (Ase et al., 2019) and 5-BDBD (Bidula et al., 2022), which served as benchmark], ligands with previously reported inferred docking [Tian-13 (Tian, M., et al. (2020) and Mahmood 4n and Mahmood 9o (Mahmood et al., 2022a; Mahmood et al., 2022b)] and ligands with no binding information [BAY-1797 (Werner et al., 2019), Mahmood 9g (Mahmood et al., 2022b), NP-1815-PX, NP-A, NP-B (Matsumura et al., 2016; Ushioda et al., 2020) Sunovion-A (Newcom and Spear, 2013), PSB-12054 (Hernandez-Olmos et al., 2012) and indophagolin (Carnero Corrales et al., 2021)]. The Achilles Server simulation estimated binding energies of -6.00 and -7.40 kcal/mol for BX430 and 5-BDBD, respectively for the allosteric pocket. Interestingly, the cavity corresponding to the allosteric pocket was ranked in the Top-5 of favorable cavities for the majority of the ligands (Table 4). Importantly, the allosteric pocket was ranked the Top-1 and Top-5 most favorable cavity for BAY-1797 and NP-A, respectively, with estimated binding energies of -9.50 and -9.30 kcal/mol, suggesting a high probability of binding at this site. Overall, the estimated binding energies showed a good correlation with the respective calculated antagonist IC₅₀ with lower values for the more potent compounds (Table 4). Indophagolin and PSB-12054 were the ligands whose blind docking cluster poses scored lowest in the allosteric pocket. These findings suggested that most ligands considered in this study are likely to bind to the same allosteric pocket as BX-430.

Induced-fit docking was then used to dock each ligand into the allosteric pocket and investigate the nature of the ligand-target interactions (Figure 4; Supplementary Figure S1). Interestingly, no docking poses within the allosteric pocket were obtained for PSB-12054 *via* the induced fit protocol, suggesting that is unlikely that PSB-12054 and its analogues bind in the same pocket as BX430, at least in the closed state of the receptor. Several key interactions are observed in the allosteric pocket of the zebrafish P2X4 closed-state crystal structure (Figure 4A), including an ionic interaction between Glu-310 and Arg-85 (zebrafish P2X4 numbering). The docking pose of 5-BDBD (Supplementary Figure S1B), was remarkably similar to that previously reported (Bidula et al., 2022), with the amide of the dihydro-2H-benzofuro [3,2-e]-1,4-diazepin-2-one interacting with Arg-301 and Glu-307, such that the interaction between Glu-307 and Arg-82 observed in zebrafish P2X4 was disrupted [Glu-310 and Arg-85, zfp2X4 numbering; compare Supplementary Figure S1B to Figure 4A). Conversely, in our induced-fit docking of Tian-13 (Figure 4C), the molecule is

TABLE 4 Computed binding energies of P2X4 antagonists docked into the human P2X4 allosteric pocket in a blind docking simulation run using the AchillesDock Server. Ranking of the cluster of poses docked in the allosteric pocket (pocket where Ile-312 lies, investigated in this work).

Compound	Binding energy of the cluster (kcal/mol) in hP2X4 allosteric pocket	Rank	Rank after removing redundant clusters
5-BDBD	−7.40	16	8
BAY-1797	−9.50	1	1
BX-430	−6.00	11	5
Mahmood-4n	−7.40	3	3
Mahmood-9g	−7.50	9	8
Mahmood-9o	−7.30	8	5
NP-1815-PX	−9.30	6	6
NP-A	−9.30	6	5
NP-B	−8.70	8	7
PSB-12054	−7.60	13	12
Sunovion-A	−8.90	4	4
Tian-13	n.d	n.d	n.d

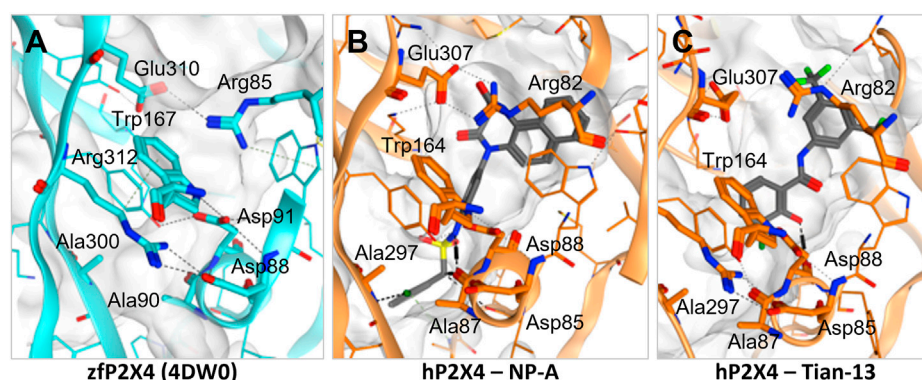


FIGURE 4

Disruption of the inter-residue protein network by P2X4 antagonists. (A). Crystal structure of zebrafish P2X4 (4DW0) with key residues involved in receptor structural stability and activation (in thick lines). (B–C). Induced-fit docking of NP-A (B) and Tian-13 (C) into a model of human P2X4. Dashed lines indicate polar interactions.

flipped compared with what was previously reported (Tian et al. (2020)]. Our docking positioned Tian-13 deeper in the pocket where the hydroxyl group of the chlorophenyl moiety established a hydrogen bond with Asp-88, modifying its orientation, whilst the 2,4-trifluoromethyl-phenyl moiety acted as a “wedge” at the top of the pocket (Figure 4C). Strikingly, our docking shows how NP-A, one of the most potent antagonists discovered to date, may occupy nearly the full length of the allosteric pocket, with the di-benzo scaffold making a potential interaction at the top of the pocket, disrupting the interaction between Glu-307 and Arg-82 (Figure 4B). The chlorophenyl moiety was positioned at the base of the pocket with the chloride making a polar interaction with the Ala-297 backbone, whilst the phenyl sulphonamide linker made further multiple interactions with the Ala-87 backbone and Tyr-299 (Figure 4B). Overall, we obtained poses fitting deeper in the

allosteric pocket for most of the ligands with the highest potency (e.g., Mahmood-9g, Mahmood-9o, NP-1815-PX, NP-A, Tian-13; Figure 4; Supplementary Figure S1) which suggests that interaction with residues located at the bottom of the pocket (Asp-85, Ala-87, Asp-88, and Ala-297) is favorable for higher potency. Furthermore, the induced-fit dock allowed us to observe how the binding of the ligand might disrupt the complex hydrogen bond and ionic interaction network that stabilizes the protein and allows channel activation.

4 Discussion

In this work, we conjectured that the binding site in human P2X4 for allosteric antagonists may be the same pocket as that

recently demonstrated in panda P2X7 (Karasawa & Kawate, 2016) and docked BX430 into this pocket in molecular models of human and rat P2X4. We demonstrated by mutagenesis and functional assay that exchange of a residue within this pocket, 312, by mutation, confers rat-like BX430 potency onto human P2X4 and *vice versa*, results that strongly support those of (Ase et al., 2019). The simplest interpretation of our data is that BX430 binds to this allosteric pocket and that amino-acid residue 312 is directly involved in BX430 binding.

Ase et al. (2019) were also able to dock BX430 into the putative allosteric pocket in which residue 312 resides, producing a binding pose similar to that which we obtained shown in Figure 2. However, in our docking studies, we found that the conformation of Lys-298 was very important in governing the overall conformation of the pocket. When applying an induced-fit docking protocol, which simulates pocket amino acid sidechain flexibility, we observed a binding pose situated deeper within the pocket (shown in Figure 2B) with Asp-88 as key residue for interactions. While our data and that of (Ase et al., 2019) are in very close agreement, an alternative potential binding pocket for BX430 on the dorsal fin region (forming interactions with Asn-208, Ile-209, and Asp-224), based on mutagenesis studies using receptor chimeras, has recently been reported (Weinhausen et al., 2022). This data may indicate more than one potential binding site for BX430, although we did not observe BX430 occupying this region of the protein in our blind docking simulations.

Recent work by Bidula et al. (2022) has also investigated the allosteric pocket in human P2X4, discovering key amino acid residues involved in the binding of the negative allosteric antagonist 5-BDBD, and docking 5-BDBD into the pocket. The authors found evidence for 5-BDBD occupying a hydrophobic pocket (similar to that occupied by the isopropyl phenyl moiety of BX430 in our docking study), with additional interactions between the sidechains of Arg-301 and Tyr-300 and the carbonyl and amide groups of 5-BDBD. Our docking produced a similar conformation when the induced fit protocol was employed; however, the amide group of 5-BDBD was stabilised by Arg-301 and Glu-307 (Supplementary Figure S1B). Bidula et al. (2022) were unable to dock 5-BDBD into a molecular model of the open human P2X4 receptor, and when comparing the antagonist effects of 5-BDBD and BX430, found that BX430, but not 5-BDBD, was capable of blocking the open channel. The authors interpreted this finding to mean that in the open channel, access to the allosteric pocket is restricted for 5-BDBD. Our docking was performed with models of the closed state, but the extensive interactions that we suggest BX430 makes deep within the pocket may explain its continued ability to access the pocket in the open channel state.

Our analysis of the docking of other known P2X4 antagonists into the receptor extracellular domain using blind docking simulations indicated the BX430 binding pocket as a highly favoured cavity for many of the antagonists, and in addition there was a good correlation between the estimated binding energy of the blind docking and the potency of the compounds. This data suggests that many of the antagonists bind in the BX430 allosteric pocket. It is important to state here that our *in silico* findings have not been experimentally validated using receptors bearing mutations within the

allosteric pocket. Strikingly, we were unable to successfully dock PSB-12054 into the allosteric pocket, suggesting that PSB-12054 (and the related PSB-12062) may bind to a different pocket on human P2X4, or only be able to bind to the open conformation of the receptor.

In our induced fit docking analysis, we found that all the ligands interacted with one or more of a network comprised of Arg-82, Asp-85, Ala-87, Asp-88, Trp-164, Ala-297, Glu-307, and Arg-309. This network of amino-acids forms critical interactions important for the structure and activity of human P2X4 (Zhao et al., 2016), particularly the salt bridge formed between Asp-88 and Arg-309, which is stabilised by Trp-164. We observed in several instances that the interactions among this amino-acid network were substantially disrupted. This was particularly true for compounds which display high potency, where we obtained poses of the ligands where they were positioned deeper into the allosteric pocket. In the case of Mahmood 4n and Tian-13, we obtained docking poses that are flipped compared to what has been published [Mahmood et al. (2022a); Tian et al. (2020)]. In these cases, the hydrophobic moieties (adamantine and the 2,4-trifluoromethyl group for Mahmood 4n and Tian-13, respectively) were positioned deeper in the pocket, indicating that there may be a need for conformational rearrangement in order to accommodate such a hindering group, and that this might cause the disruption of the key amino acid interaction network. We would expect that these disruptions would substantially impair the ability of human P2X4 to undergo ATP-induced conformational change when ligands are bound in the allosteric pocket.

It is difficult to infer information about the selectivity of the P2X4 antagonists from our studies, as we focused solely on modelling binding to the allosteric pocket of a molecular model of human P2X4. However, in their structure-activity relationship studies, Tian et al. (2020) showed that the hydroxyl of the chlorophenol moiety of Tian-13 is essential for antagonist activity but not responsible for selectivity (Figure 4C). A number of compounds developed by Tian et al. (2020) show submicromolar potency to P2X1, P2X4, and P2X7 [Tian et al. (2020)]. From our docking of Tian-13, we observe that the hydroxyl group in question interacts with the backbone of Asp-88, and we interpret this to mean that an interaction with Asp-88 is desirable for antagonist activity. As Asp-88 is conserved across the P2X receptor family, and forms a critical salt bridge interaction, this may partially explain why this series of compounds also has activity at P2X1 and P2X7, and means that the selectivity of Tian-13 will need to be developed *via* interaction with non-conserved residues.

It is interesting to note that, even though it is not among the most potent P2X4 antagonist, in our docking BX430 occupies a position deep within the allosteric pocket. This may suggest that not only deep positioning within the pocket, but also some more bulky or hindering moiety might be necessary to efficiently disrupt the key structural network.

In summary, we have used a combination of molecular docking, mutagenesis and functional assay to demonstrate the likely binding pocket for the allosteric antagonist BX430 in human P2X4, which confirms the work of (Ase et al., 2019), but also suggests a distinct, deeper positioning of BX430 where it forms key interactions including with Asp-88. Furthermore, we have performed molecular docking on a series of potent P2X4 antagonists in the allosteric pocket, enabling us to

estimate binding energies and identify disruption to a key structural network of amino acids as a main determinant of high antagonist potency. Our findings will be useful for the future design and development of allosteric P2X4 antagonists with increased potency.

Data availability statement

The raw data supporting the conclusion of this article will be made available by the authors, without undue reservation.

Author contributions

All authors participated in research design. GP and MZ conducted experiments; GP, MZ, and MY performed data analysis and GP and MY wrote the manuscript.

Funding

GP was supported by a Life Sciences Research Network Wales Ph.D. studentship. MZ was supported by a Sight Research United Kingdom Ph.D. studentship (RES013).

References

- Abdelrahman, A., Namasivayam, V., Hinz, S., Schiedel, A. C., Köse, M., Burton, M., et al. (2017). Characterization of P2X4 receptor agonists and antagonists by calcium influx and radioligand binding studies. *Biochem. Pharmacol.* 125, 41–54. doi:10.1016/j.bcp.2016.11.016
- Ase, A. R., Honson, N. S., Zaghdane, H., Pfeifer, T. A., and Seguela, P. (2015). Identification and characterization of a selective allosteric antagonist of human P2X4 receptor channels. *Mol. Pharmacol.* 87, 606–616. doi:10.1124/mol.114.096222
- Ase, A. R., Therrien, E., and Seguela, P. (2019). An allosteric inhibitory site conserved in the ectodomain of P2X receptor channels. *Front. Cell Neurosci.* 13, 121. doi:10.3389/fncel.2019.00121
- Bidula, S., Nadzirin, I. B., Cominetti, M., Hickey, H., Cullum, S. A., Searcey, M., et al. (2022). Structural basis of the negative allosteric modulation of 5-BDBD at human P2X4 receptors. *Mol. Pharmacol.* 101, 33–44. doi:10.1124/molpharm.121.000402
- Bootman, M. D., Rietdorf, K., Collins, T., Walker, S., and Sanderson, M. (2013). Ca²⁺-sensitive fluorescent dyes and intracellular Ca²⁺ imaging. *Cold Spring Harb. Protoc.* 2013, 83–99. doi:10.1101/pdb.top066050
- Carnero Corrales, M. A., Zinken, S., Konstantinidis, G., Rafehi, M., Abdelrahman, A., Wu, Y., et al. (2021). Thermal proteome profiling identifies the membrane-bound purinergic receptor P2X4 as a target of the autophagy inhibitor indophagolin. *Cell Chem. Biol.* 28, 1750–1757.e5. doi:10.1016/j.chembiol.2021.02.017
- Coddou, C., Sandoval, R., Hevia, M. J., and Stojilkovic, S. S. (2019). Characterization of the antagonist actions of 5-BDBD at the rat P2X4 receptor. *Neurosci. Lett.* 690, 219–224. doi:10.1016/j.neulet.2018.10.047
- Fischer, R., Kalthof, B., Grützmann, R., Woltering, E., Stelte-Ludwig, B., and Wuttke, M. (2004). *Benzofuro-1,4-diazepin-2-one derivatives*. Patent No WO2004085440A1. Geneva, Switzerland: World Intellectual Property Organisation.
- Garcia-Guzman, M., Soto, F., Gomez-Hernandez, J. M., Lund, P. E., and Stuhmer, W. (1997). Characterization of recombinant human P2X4 receptor reveals pharmacological differences to the rat homologue. *Mol. Pharmacol.* 51, 109–118. doi:10.1124/mol.51.1.109
- Hattori, M., and Gouaux, E. (2012). Molecular mechanism of ATP binding and ion channel activation in P2X receptors. *Nature* 485, 207–212. doi:10.1038/nature11010
- Hernandez-Olmos, V., Abdelrahman, A., El-Tayeb, A., Freudendahl, D., Weinhausen, S., and Muller, C. E. (2012). N-Substituted phenoxazine and acridone derivatives: Structure-activity relationships of potent P2X4 receptor antagonists. *J. Med. Chem.* 55, 9576–9588. doi:10.1021/jm300845v
- Karasawa, A., and Kawate, T. (2016). Structural basis for subtype-specific inhibition of the P2X7 receptor. *Elife* 5, e22153. doi:10.7554/eLife.22153
- Laskowski, R. A., Macarthur, M. W., Moss, D. S., and Thornton, J. M. (1993). Procheck: A program to check the stereochemical quality of protein structures. *J. Appl. Crystallogr.* 26, 283–291. doi:10.1107/s0021889892000944
- Mahmood, A., Ali Shah, S. J., and Iqbal, J. (2022a). Design and synthesis of adamantane-1-carbonyl thiourea derivatives as potent and selective inhibitors of h-P2X4 and h-P2X7 receptors: An Emerging therapeutic tool for treatment of inflammation and neurological disorders. *Eur. J. Med. Chem.* 231, 114162. doi:10.1016/j.ejmech.2022.114162
- Mahmood, A., Villinger, A., and Iqbal, J. (2022b). Therapeutic potentials and structure-activity relationship of 1,3-benzodioxole N-carbamothioyl carboxamide derivatives as selective and potent antagonists of P2X4 and P2X7 receptors. *Eur. J. Med. Chem.* 238, 114491. doi:10.1016/j.ejmech.2022.114491
- Matsumura, Y., Yamashita, T., Sasaki, A., Nakata, E., Kohno, K., Masuda, T., et al. (2016). A novel P2X4 receptor-selective antagonist produces anti-allodynic effect in a mouse model of herpetic pain. *Sci. Rep.* 6, 32461. doi:10.1038/srep32461
- Mccarthy, A. E., Yoshioka, C., and Mansoor, S. E. (2019). Full-length P2X7 structures reveal how palmitoylation prevents channel desensitization. *Cell* 179, 659–670. doi:10.1016/j.cell.2019.09.017
- Newcom, J. S., and Spear, K. L. (2013). *P2x4 receptor modulating compounds*. Patent No WO2015088564A1. Geneva, Switzerland: World Intellectual Property Organisation.
- North, R. A., and Jarvis, M. F. (2013). P2X receptors as drug targets. *Mol. Pharmacol.* 83, 759–769. doi:10.1124/mol.112.083758
- North, R. A. (2016). P2X receptors. *Philos. Trans. R. Soc. Lond B Biol. Sci.* 371, 20150427. doi:10.1098/rstb.2015.0427
- Royle, S. J., Qureshi, O. S., Bobanovic, L. K., Evans, P. R., Owen, D. J., and Murrell-Lagnado, R. D. (2005). Non-canonical YXXGPhi endocytic motifs: Recognition by AP2 and preferential utilization in P2X4 receptors. *J. Cell Sci.* 118, 3073–3080. doi:10.1242/jcs.02451
- Sanchez-Linares, I., Perez-Sanchez, H., Cecilia, J. M., and Garcia, J. M. (2012). High-Throughput parallel blind Virtual Screening using BINDSURF. *BMC Bioinforma.* 13 (14), S13. doi:10.1186/1471-2105-13-S14-S13
- Sophocleous, R. A., Miles, N. A., Ooi, L., and Sluyter, R. (2020). P2Y2 and P2X4 receptors mediate Ca²⁺ mobilization in DH82 canine macrophage cells. *Int. J. Mol. Sci.* 21, 8572. doi:10.3390/ijms21228572
- Soto, F., Garcia-Guzman, M., Gomez-Hernandez, J. M., Hollmann, M., Karschin, C., and Stuhmer, W. (1996). P2X4: An ATP-activated ionotropic receptor cloned from rat brain. *Proc. Natl. Acad. Sci. U. S. A.* 93, 3684–3688. doi:10.1073/pnas.93.8.3684

Acknowledgments

The authors would like to thank Dr. Marcella Bassetto for helpful comments on the manuscript.

Conflict of interest

The authors declare that the research was conducted in the absence of any commercial or financial relationships that could be construed as a potential conflict of interest.

Publisher's note

All claims expressed in this article are solely those of the authors and do not necessarily represent those of their affiliated organizations, or those of the publisher, the editors and the reviewers. Any product that may be evaluated in this article, or claim that may be made by its manufacturer, is not guaranteed or endorsed by the publisher.

Supplementary material

The Supplementary Material for this article can be found online at: <https://www.frontiersin.org/articles/10.3389/fphar.2023.1101023/full#supplementary-material>

- Stokes, L., Scurrah, K., Ellis, J. A., Cromer, B. A., Skarratt, K. K., Gu, B. J., et al. (2011). A loss-of-function polymorphism in the human P2X₄ receptor is associated with increased pulse pressure. *Hypertension* 58, 1086–1092. doi:10.1161/HYPERTENSIONAHA.111.176180
- Tian, M., Abdelrahman, A., Baqi, Y., Fuentes, E., Azazna, D., Spanier, C., et al. (2020). Discovery and structure relationships of salicylanilide derivatives as potent, non-acidic P2X₁ receptor antagonists. *J. Med. Chem.* 63, 6164–6178. doi:10.1021/acs.jmedchem.0c00435
- Tsuda, M., Shigemoto-Mogami, Y., Koizumi, S., Mizokoshi, A., Kohsaka, S., Salter, M. W., et al. (2003). P2X₄ receptors induced in spinal microglia gate tactile allodynia after nerve injury. *Nature* 424, 778–783. doi:10.1038/nature01786
- Ushioda, M., Kobayashi, K., Saito, D., Sakuma, S., Imai, T., and Inoue, K. (2020). *P2X₄ receptor antagonist*. Patent No US11434207B2. United States: Patent.
- Weinhausen, S., Nagel, J., Namasivayam, V., Spanier, C., Abdelrahman, A., Hanck, T., et al. (2022). Extracellular binding sites of positive and negative allosteric P2X₄ receptor modulators. *Life Sci.* 31, 121143. doi:10.1016/j.lfs.2022.121143
- Werner, S., Mesch, S., Hillig, R. C., Ter Laak, A., Klint, J., Neagoe, I., et al. (2019). Discovery and characterization of the potent and selective P2X₄ inhibitor N-[4-(3-Chlorophenoxy)-3-sulfamoylphenyl]-2-phenylacetamide (BAY-1797) and structure-guided amelioration of its CYP3A4 induction profile. *J. Med. Chem.* 62, 11194–11217. doi:10.1021/acs.jmedchem.9b01304
- Yamamoto, K., Sokabe, T., Matsumoto, T., Yoshimura, K., Shibata, M., Ohura, N., et al. (2006). Impaired flow-dependent control of vascular tone and remodeling in P2X₄-deficient mice. *Nat. Med.* 12, 133–137. doi:10.1038/nm1338
- Young, M. T., Fisher, J. A., Fountain, S. J., Ford, R. C., North, R. A., and Khakh, B. S. (2008). Molecular shape, architecture, and size of P2X₄ receptors determined using fluorescence resonance energy transfer and electron microscopy. *J. Biol. Chem.* 283, 26241–26251. doi:10.1074/jbc.M804458200
- Zhao, W. S., Sun, M. Y., Sun, L. F., Liu, Y., Yang, Y., Huang, L. D., et al. (2016). A highly conserved salt bridge stabilizes the kinked conformation of β 2,3-sheet essential for channel function of P2X₄ receptors. *J. Biol. Chem.* 291, 7990–8003. doi:10.1074/jbc.M115.711127

Frontiers in Pharmacology

Explores the interactions between chemicals and living beings

The most cited journal in its field, which advances access to pharmacological discoveries to prevent and treat human disease.

Discover the latest Research Topics

[See more →](#)

Frontiers

Avenue du Tribunal-Fédéral 34
1005 Lausanne, Switzerland
frontiersin.org

Contact us

+41 (0)21 510 17 00
frontiersin.org/about/contact



Frontiers in Pharmacology

